PROCEEDINGS

ORAL PRESENTATIONS

TOPIC 2:
PROCESS ANALYSIS AS A BASIS OF FLOOD MODELLING

PAPERS:
COLLECTED AND ARRANGED BY JUDITH DOBMANN AND SIMONE HUNZIKER.
PLEASE NOTE THAT AUTHORS ARE RESPONSIBLE FOR CONSISTENCY IN SPELLING.

INVESTIGATIONS ON THE INFLUENCE OF STORM CAUSED DAMAGE ON THE RUN-OFF FORMATION AND EROSION IN SMALL TORRENT CATCHMENTS

Alexandre Badoux[1], Christoph Hegg[1], Hans Kienholz[2], Rolf Weingartner[2]

[1] WSL Swiss Federal Research Institute, Zürcherstrasse 111, CH-8903 Birmensdorf
badoux@wsl.ch, hegg@wsl.ch

[2] Institute of Geography University of Berne, Hallerstrasse 12, CH-3012 Bern
kienholz@giub.unibe.ch, wein@giub.unibe.ch

SUMMARY

On the 26th of December 1999 the storm Lothar has caused great damage to the forest in Switzerland. The influence of deforestation on the processes of the water cycle and the sediment budget is investigated within the project "Lothar and Mountain Torrents" of the Swiss Federal Research Institute WSL and the Institute of Geography of the University of Berne (GIUB). The analysis of the described measurements will also help to improve the understanding of flood runoff generation and runoff propagation in forested areas.
The investigation area lies within the watershed of the Sperbelgraben in the Emmental region (Swiss prealps). Two neighbouring sub-catchments feature an area of circa 2 ha each and were variously affected by the storm Lothar. The two sub-catchments have been equipped with a gauging station at their outlets. Furthermore, in the sector between the two test areas, a precipitation gauge has been installed. Supplementary information will be acquired by the installation of selected test plots (40 to 80 m^2). Thereby several storm-affected areas as well as unaffected areas with different characteristics will be compared with each other regarding surface runoff formation and erosion.
In the present paper, the measurement installations within the two sub-catchments and the testplots are described in detail. Moreover, future activities as well as the objectives of the project are discussed.

Keywords: forest hydrology, runoff generation, storm damage, erosion, forest coverage

1 INTRODUCTION

The influence of the forest coverage on the runoff behaviour in river basins of various type represents a fundamental question in the field of forest hydrology since its beginnings.
In Switzerland, the devastating flood event of 1868 in the mountainous cantons of Ticino, Graubünden, St. Gallen, Uri and Valais implicated an important turning point in flood protection. Based on the event analysis conducted by experts, representatives of the Swiss Forestry Society publicly linked the flood event mainly to man-made deforestation and bad maintenance of wide forested areas in alpine regions. In the years following the natural disaster of 1868, structural measures were carried out in many rivers and torrents and large areas were afforested. These interventions were believed to provide a long lasting security (Schmid, 2001).
The first scientific measurements to investigate the influence of the forest on runoff in Switzerland were carried out by Engler (1919) in the early 20th century. Based on comparative measurements in two very differently forested catchments in the Emmental region (Swiss prealps, canton of Berne), his statements revealed an important attenuating impact of the forest on intensive short-time flood events. This effect relates to both runoff volume and peak discharge. During persistent rainfall a slight or no effect at all was observed, depending on the water content of the soil before the event. Furthermore, an explicit influence of forest coverage on the mean annual water balance was demonstrated. The findings of this study strongly influenced the ideas in forest hydrology for several decades.
It was only in the 1990ies that the discussion around this topic was resumed when Burch et al. (1996) carried out a study within the Alptal investigation area (Swiss prealps, canton of Schwyz) of the Federal Research Institute WSL. The influence of forest coverage on runoff coefficient and peak discharge was investigated in three forested catchments as well as on three smaller experimental plots, all located in the prealpine flysch region. On the shallow flysch soils, it was statistically impossible to demonstrate an overall effect of the forest on flood discharge. Nevertheless, the influence of the forest on the mean water balance (increased evapotranspiration and decreased snowmelt runoff) could also be shown in this study.

In a geographically widespread summary and review of 94 catchment experiments (that all pursued the objective of the quantification of the forest coverage influence) Bosch and Hewlett (1982) evaluated the effect of vegetation changes on the water balance. Following forest operations with reductions in cover, almost every experiment showed a decrease in evapotranspiration and an increase in annual runoff while an increase in cover led to the opposite. It is important to mention though that these results present a considerable variation. No statements about the runoff behaviour during single rainfall events were made in this investigation.
In two experimental catchments of the Draix investigation site (south-eastern France), a large difference in forest cover leaded to substantially diverse peak discharge as well as runoff volume during short-time flood events (Mathys et al., 1996). Moreover, after a forest fire in one of the two catchments of the Réal Collobrier test site (south-eastern France) in 1990, peak discharges increased explicitly for a few years (Martin, Lavabre, 1997). Whereas a catchment within the Mont-Lozère investigation area (south-central France) featured no clear modification in peak discharge values after clear cutting (Lavabre et al., 1999), annual runoff increased slightly (Cosandey, 1993). In the western Cascades (Oregon, USA), Jones and Grant (1996) quantified long-term changes in streamflows associated with clear cutting and road construction. Forest harvesting has increased peak discharges by as much as 50 % in relatively small basins (60 to 101 ha) and 100 % in large basins (60 to 600 km^2) over 50 years. In the studies reported above, mainly catchments in the order of magnitude of one and more square kilometres were observed. In test areas larger than a few hectares it is generally more difficult to keep apart the effect of forest coverage from the impact of differences in other catchment characteristics.
On the 26th of December 1999 the storm Lothar has caused great damage in several countries of Central Europe. In Switzerland, it has overthrown or broken numberless trees with a total wood volume of 12.7 million m^3 on an area of approximately 46'000 ha (WSL and BUWAL, 2001). In numerous regions, large-scale damage to the forests occurred. The affected areas thereby provide a good basis to investigate the influence of deforestation respectively of the forest in general on the processes of the water cycle and the sediment budget in small torrential sub-catchments.

2 ORGANISATION AND LOCATION

2.1 The Project "Lothar and Mountain Torrents"

The research on "Hydrologic Studies in Sub-Catchments" presented in this paper is part of the overall project "Lothar and Mountain Torrents" of the Swiss Federal Research Institute WSL and the Institute of Geography of the University of Berne (GIUB). Besides the question about the influence of deforestation on the water cycle and the sediment budget, the effect of storm damage on root penetration and soil structure is studied within the overall project. The field investigations on this topic have also been carried out in the Sperbelgraben test area. The overall project "Lothar and Mountain Torrents" is financed by the Swiss Agency for the Environment, Forests and Landscape BUWAL and includes the following sub-projects:

- "Hydrologic Studies in Sub-Catchments" (WSL and GIUB)
- "Vegetation Effects on Superficial Soil Movements" (WSL)
- "Forest development, root penetration and distribution, soil structure" (WSL)
- "Slope - Channel Interactions" (GIUB)

The overall project started in January 2001 and will last until early 2004. While in the year 2001 the emphasis within the sub-project "Hydrologic Studies in Sub-Catchments" was mainly put in the installation work, efforts in the year 2002 will be focussed on the analysis of the different data collected in the test area.

2.2 Investigation Area

As an investigation area, two neighbouring sub-catchments have been chosen within the torrential catchment of the Sperbelgraben. In one sub-catchment virtually no damage has been registered, whereas in the other one the majority of the trees has been overthrown by the storm. The damaged sub-catchment has been partially cleared with afforestation machinery. Figure 2-1 gives an overview of the location of the investigation area.

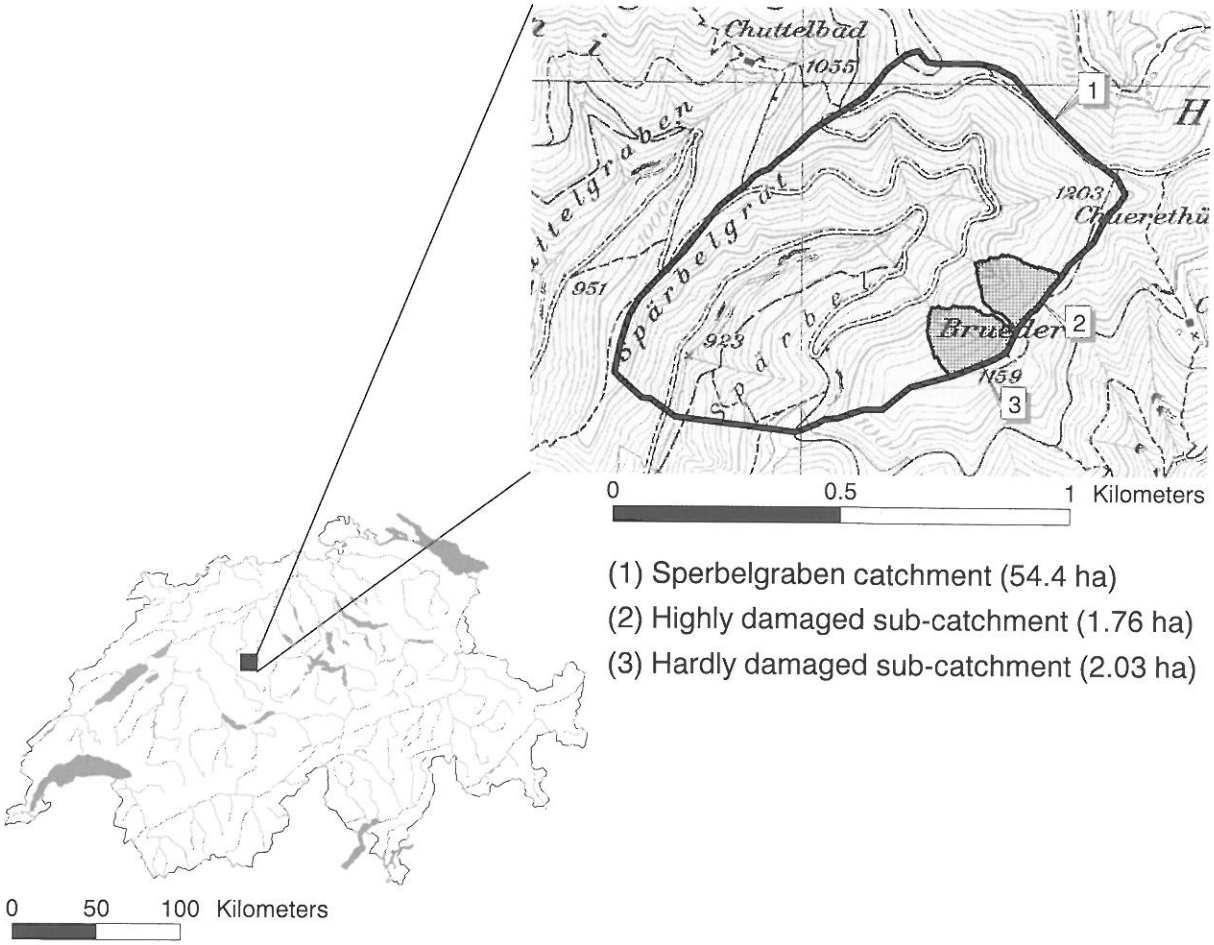

Figure 2-1: Location of the investigation area within the catchment of the Sperbelgraben. Reproduced by permission of the Swiss Federal Office of Topography (BA024351).

The Sperbelgraben transversal valley is situated in the hilly Emmental region in the Swiss prealps. It has an area of 54,4 ha and ranges from 911 m a.s.l. at the gauging station to 1203 m a.s.l. at its highest point. Geologically, the Sperbelgraben is located in the molasse zone and features mainly conglomerate layers crossed by marl layers. The variable susceptibility to weathering of the two different layer types led to the terrace shapes that can be observed all around the investigation area. The small and deep channels within the Sperbelgraben catchment show cuttings with very steep slopes and are generally flowing directly on bedrock.

The small sub-catchments feature an area of 1,76 (damaged) and 2,03 (undamaged) ha and are located in the south-east zone of the ridge of the Sperbelgraben catchment in an altitude between 1070 and 1150 m a.s.l. (Figure 2-1). Apart from some soaked zones with nearly impermeable gley soils, the investigation area is principally characterised by cambisols with partly limited and partly unlimited permeability. The mean annual precipitation (measured in immediate proximity of the gauging station of the Sperbelgraben catchment) for the period from 1961 to 1999 amounts to 1660 mm.

Hydrological measurements and studies have a history of nearly 100 years in the Sperbelgraben. The predecessor-institution of the WSL (Eidg. Centralanstalt für das forstliche Versuchswesen) started measuring runoff under the direction of Arnold Engler in 1903. Since 1958, the station is operated by the Swiss Hydrological Survey (Landeshydrologie). Full particulars about the torrential catchment of the Sperbelgraben are given in Engler (1919) and Burger (1934, 1943, 1954).

3 OBJECTIVES OF THE STUDY

The main aim of this study is to assess the effects of storm caused damage through the comparison of two neighbouring sub-catchments differently affected by Lothar. The influence of deforestation will be investigated on different levels. First, the water balance of the two sub-catchments will be compared. A slightly higher mean annual runoff is expected in the heavily damaged sub-catchment due to a decrease in evapotranspiration following the storm.
Thereafter, the peak discharge (specific runoff) as well as the discharge volume produced in the two sub-catchments during different flood events will be investigated. Possible differences in these values will be analysed and an approach will be made to explain them. The occurrence of cambisol with partly unlimited permeability, especially in the undamaged sub-catchment, rather indicates attenuated peak discharge and fair discharge volume due to an average water storage capacity. The condition of the soils within the damaged sub-catchment is not well identified though. How strongly has the water storage capacity there been affected by the storm and the removing operations, if at all?
This question points out the importance of the data acquisition from small-scale measurement sites (so-called testplots). Generally, during short flood events in small torrent catchments, the surface runoff component comes up for a substantial amount of the total runoff. Flood discharge will therefore be observed and differentiated from small areas with diverse forest characteristics as well as from small areas with different damage types respectively undamaged areas. Thus, explanations with regard to the runoff behaviour of the two sub-catchments will be searched for on the basis of the known spatial distribution of forest characteristics and elements of damage.

4 METHODS

In the following section the installed measuring equipment within and around the two sub-catchments as well as the carried out surveying and mapping projects will briefly be reviewed. The different installations have been built successively since January 2001.

4.1 Surveying and Mapping

A sector including the two sub-catchments and their close surroundings was surveyed using a global-positioning system GPS between July and September 2001. The main objective of the survey was to create a digital terrain model (DTM) with a resolution of 2 metres that meets the requirements of the small and varying area investigated. On the basis of this DTM, the morphologic parameters (e.g. size, slope) can be determined with a sufficient accuracy and subsequently be compared between the two test-areas. This is a requirement to be able to assess potential differences of the sub-catchments regarding runoff behaviour. Another objective of the survey campaign was to quantify deforestation due to the storm Lothar. Therefore damaged (broken or overthrown) as well as healthy trees with a diameter of at least 20 cm were singly surveyed.
The GPS-method using a reference station which generates differential GPS corrections proved itself to be a suitable tool for the purpose described above. The accuracy of the measurements varied between 0,5 and 5 metres (mean-value x-, y- and z axis); single measurements with an uncertainty greater than 2 metres were not taken in account. Trees, the morphology and other relevant terrain characteristics were specifically surveyed, instead of recording points randomly or following a systematic pattern. The type of a surveyed object can be read into the GPS-unit together with possible attributes (such as tree type and diameter in case of a standing tree). This enables the user to collect different information on the area at the same time as topographical data.
At some locations in the field with an obstructed view of the sky (namely in the forest), the reception of the satellite frequencies was insufficient and thus the accuracy of the measurements worse than on other locations. While this fact appeared to be very time-consuming during fieldwork, it became a serious problem in the following GIS-analysis. Surveyed points with a bad accuracy along the z-axis had to be removed manually. A map of the investigation area as well as the morphologic parameters derived from the DTM are now available and seem to be realistic.
Further investigations around the two sub-catchments include a forest characteristics map which has been established by a professional company within the sub-project "Forest development, root penetration and distribution, soil structure". This map gives an overview of the prevalent forest vegetation types that can be found in the investigation area. Additional maps on the geomorphologic and hydrological characterisation of the investigation area are being established as a part of two diploma theses within the sub-project "Hydrologic Studies in Sub-Catchments".

4.2 Runoff measuring stations

At the outlet of each of the two creeks that drain the sub-catchments, a gauging station was built. It consists of a three metre long, one metre wide and one metre deep channel made of plywood that features an aluminium V-notch at its front (Figure 4-1).

Figure 4-1: View from downstream on the gauging station at the outlet of the heavily damaged sub-catchment.

Figure 4-2: View in flow direction on the gauging station of the hardly damaged sub-catchment (grid in the foreground).

The gauging stations have been equipped with a water level recorder (micropulse transducer) and an instrument measuring electrical conductivity as well as water temperature. Collected data is stored in a local logger mounted on the side of the station. During winter, the proper operating of the gauging stations is ensured by the use of a gas heating which prevents the water surface within the channel from freezing. A frozen surface would obstruct the water level measurements in any case (floater frozen on rod) and the measuring of the electrical conductivity in extreme situations (totally frozen probe head). The heating switches on periodically when the air temperature drops below 0 °C. Maintenance of the stations is carried out weekly, including a manual runoff measurement to verify the zero mark of the gauge and the runoff-water level relationship (determined during calibration at the WSL).
The sediment transport of the two small creeks is observed and registered periodically. Coarse material and wood are detained by the means of a simply disposed but efficient grid, located a few metres above the station (Figure 4-2). Fine-grained debris as well as suspended sediment are deposited in the channel which can be cleared due to an aperture on its underside.

4.3 Precipitation registration

In the zone between the two sub-catchments, a precipitation gauge (weighing principle) with an integrated data logger was installed and is operated since April 2001. The use of a device based on the weighing principle also allows the registration of the precipitation in the form of snow (without integrated heating in the instrument). In addition, snow height and density are observed weekly on four measuring sections during the winter season.

4.4 Testplots

Surface runoff plays an important part in flood generation and in shallow erosion processes. Within the scope of the overall project "Lothar and Mountain Torrents" which deals with the influence of deforestation on runoff and erosion in general, the effect of storm damage (respectively forest coverage) on this specific runoff component will thoroughly be investigated. In the first place, the degree and the cause of a potential difference in surface runoff between the two sub-catchments will be studied. For this purpose 15 testplots have yet been installed in the zone of the test area.
In order to compare surface runoff in different manners, the location of these plots is very important. First, the impact of the diverse damage types (e.g. overthrown tree, stump, traces of logging such as drag traces etc.) on the surface runoff will be assessed. Furthermore, the runoff behaviour in the different forest types compiled in the forest characteristics map will be compared, their contribution to the total runoff in the sub-catchments analysed. To this end, testplots were placed in as many different forest types as possible, preferably in a damaged and non damaged site per type. Moreover, a plot group will be laid out as a so-called cascade (three to four plots arranged one upon the other) in each of the two test areas with the objective to learn more about the development of surface runoff on a slope.

Figure 4-3: View from below on a single testplot located within the heavily damaged sub-catchment.

Figure 4-3 shows an almost completely installed testplot within the heavily damaged sub-catchment where only the gauging box has not been disposed yet. The plots feature a size of 40 to 80 m^2 and are delimited with rigid PVC plates at the top and laterally. At the bottom of a testplot, the surface runoff component is measured in a small gauging station. The water that drains off on or close to the surface of the area flows along PVC plates laid out parallel to the slope and is conducted into a gully which leads it into the station. This gauging station consists of a plastic box (1*0,4*0,4 m) provided with a V-notch made of aluminium and a water level transmitter (pressure capsule) as shown in Figure 4-4. The installation of the testplots will be completed in spring 2002, whereon the actual measurements will begin.

Figure 4-4: Small gauging box that is placed at the bottom of a testplot.

4.5 Data transfer

Close to the precipitation gauge, the transfer station of the test area was installed. The data of the testplots as well as the precipitation data are stored there in a logger. The two runoff gauging stations are connected with the transfer station by means of a network and thus the access to runoff data is also ensured. Eventually, all collected data are linked to the WSL by mobile phone.

5 STATUS OF WORK

After an intensive period of field work during the year 2001 (installing, surveying and mapping, measuring, maintenance) the status of work appears as follows:

- Acquisition of runoff and precipitation data since April 2001
- Installation of 15 (of the planned 20) testplots so far
- Survey and mapping campaign completed
- Online data transfer installed

With the return of better weather conditions in spring 2002, the few outstanding testplots will be completed. At the same time the permanent measurement of surface runoff from the plots will begin. Suspended sediment measurements (by means of a sampler) are scheduled to be carried out in the two sub-catchments from spring 2002.

6 OUTLOOK

Studying the influence of deforestation in a single investigation area can raise the question of the transferability of the findings. An important relevance of the overall project "Lothar and Mountain Torrents" is to provide fundamentals for the evaluation in practice of the effect of forest on floods, erosion and landslides. Based on the resulting assessment, statements on the measures regarding forest maintenance shall be deduced for the practitioners. Hence, a way must be found to apply the results obtained in a specific environment to any other environment where considerations are made. A possible means to this end could be the use of a model approach that most importantly takes into account the spatial distribution of the different forest characteristic types. The surveying and mapping of the forest types being a process that can be realised within a reasonable period of time.

An important input for the calibration of such a modelling attempt would be the information on surface runoff from the testplots measurements as well as the findings from irrigation experiments carried out as a part of two diploma theses within the sub-project "Forest development, root penetration and distribution, soil structure".
In summary, the results of this research should give an answer to the question: "How does the water reach from the slope into the channel?". In case of heavy rainfall events, the measurements described in this paper can thus be analysed to learn more about flood runoff generation and runoff propagation in forested areas.

ACKNOWLEDGEMENTS

This project is financially supported by the Swiss Agency for the Environment, Forests and Landscape BUWAL. Hydrological data are provided by the Swiss hydrological survey (Federal Office for Water and Geology BWG). We would like to thank the diploma students Eva Gertsch, Harry Ilg and Philippe Marti for their contribution. Furthermore we are very grateful to Bruno Fritschi, Karl Steiner and Eva Frick whose dedication in the field has provided the basis for our research.

REFERENCES

Bosch, J. M., Hewlett, J. D. (1982): A review of catchment experiments to determine the effect of vegetation changes on water yield and evapotranspiration. Journal of Hydrology. 55, 3-23.

Burch, H., Forster, F. and Schleppi, P. (1996): Zum Einfluss des Waldes auf die Hydrologie der Flysch-Einzugsgebiete des Alptals. Schweizerische Zeitschrift für Forstwesen. 147(12), 925-937. Zürich

Burger, H. (1934): Einfluss des Waldes auf den Stand der Gewässer; 2. Mitteilung; Der Wasserhaushalt im Sperbel- und Rappengraben von 1915/16 bis 1926/27. Mitteilungen der Schweizerischen Anstalt für das forstliche Versuchswesen. 18. Band, 2. Heft, 311-416. Zürich

Burger, H. (1943): Einfluss des Waldes auf den Stand der Gewässer; 3. Mitteilung; Der Wasserhaushalt im Sperbel- und Rappengraben von 1927/28 bis 1941/42. Mitteilungen der Schweizerischen Anstalt für das forstliche Versuchswesen. 23. Band, 1. Heft, 167-222. Zürich

Burger, H. (1954): Einfluss des Waldes auf den Stand der Gewässer; 5. Mitteilung; Der Wasserhaushalt im Sperbel- und Rappengraben von 1942/43 bis 1951/52. Mitteilungen der Schweizerischen Anstalt für das forstliche Versuchswesen. 31. Band, 1. Heft, 9-58. Zürich

Cosandey, C. (1993): Conséquences hydrologiques d'une coupe forestière. Le cas du bassin de la Latte (Mont-Lozère, France). L'eau, la terre et les hommes, Hommage à René Frécaut, Griselin M. édit., Presses Universitaires de Nancy. 355-363.

Engler, A. (1919): Einfluss des Waldes auf den Stand der Gewässer. Mitteilungen der Schweizerischen Anstalt für das forstliche Versuchswesen. 12. Band, 1-626. Zürich

Jones, J. A., Grant, G. E. (1996): Peak flow responses to clear-cutting and roads in small and large basins, western Cascades, Oregon. Water Resources Research. 32(4), 959-974.

Lavabre, J., Martin, C., Didon-Lescot, J. F. (1999): Appréciation de l'impact des coupes forestières sur l'hydrologie et l'érosion des sols. Cas de la forêt d'Altefage (commune du Pont-de-Montvert - 48). Rapport à la DDAF de Lozère, Edit. Cemagref, Aix-en-Provence. 28p.

Martin, C., Lavabre, J. (1997): Estimation de la part du ruissellement sur les versants dans les crues du ruisseau du Rimbaud (massif des Maures, Var, France) après l'incendie de forêt d'août 1990. Hydrological Sciences Journal. 42(6), 893-907.

Mathys, N., Meunier, M., Brochot, S. (1997): The forest effect on floods in small mountainous catchments: some results from experimental catchments of Draix, France. Conference on Eco-hydrological Processes in Small Basins. Strasbourg, France, September 24-26, 1996. IHP-V Technical documents in Hydrology, no 14, UNESCO, Paris. 123-128.

Schmid, F. (2001): Politische Konsequenzen aus dem Unwetterereignis von 1868 - Anfänge des eidgenössischen Hochwasserschutzes. Schweizerische Zeitschrift für Forstwesen. 152(12), 521-526. Zürich

WSL and BUWAL (Hrsg.) (2001): Lothar. Der Orkan 1999. Ereignisanalyse, Eidgenössische Forschungsanstalt WSL und Bundesamt für Umwelt, Wald und Landschaft BUWAL; Birmensdorf, Bern. 365 S.

THE ROLE OF SNOW'S ACCUMULATION CAUSED BY AVALANCHE IN THE GENERATION OF FLOOD AND SOLID TRANSPORT IN SMALL ALPINE WATERSHEDS

Eric Bardou[1], François-Xavier Marquis[2], Markus Niggli[3], André Musy[3]

[1] IDEALP ingénieurs sàrl, 8 r. Majorie, 1950, SION; info@idealp.ch

[2] bureau P. Tissières, 2 Pré-de-la-Scie, 1920, MARTIGNY

[3] Land and Water Use and Management Laboratory (IATE/HYDRAM), EPFL, LAUSANNE

SUMMARY

The main goal of this paper is to analyse in a rigorous way the effect of the snow from avalanche in the generation of floods in small alpine watersheds. This effect was of evidence in field observation. To investigate this process we use two statistical approaches. A global one based on comparison between number of floods and avalanche activity of previous winter, and a more detailed approach based on a discriminant analysis which shows parameters linked with snow. This process is quite well described by statistics, but natural variability and quality of data preclude a little the analysis.

Keywords: flood generation, debris flow, snow, avalanche

1 INTRODUCTION

Floods in mountainous areas and especially in small watersheds involve always solid transport. This solid material could be mobilized either as bed load transport or as debris flow. Our observations show that sometimes floods could occur partially, or completely, due to the melting of snow accumulated by avalanche. Taking into account of this process is of importance for forecast of the flood's impact in late spring and summer.
In this paper we will try to investigate this process of flood generation. For that purpose, we are first reporting our field observations. Then we use statistical approaches, at two levels of details, to show the importance of snow in the process of flood generation in a small alpine watershed.

2 FIRST OBSERVATIONS

The first observations were made in the Illgraben (wood of Fynges area, VS). There, snow layer of about 2 meters was lying under approximately 30 centimetres of rock debris. This snow stayed in the main gully where debris flows start. During the last weeks of June to middle of July 1998, we observed many debris flows by sunny weather. Tracks and scars in scree indicated to us that snow acts as gliding plane and as supply of water. Further field observations showed us that this process was not a particular case in Illgraben (one of the most productive torrent of Switzerland). We collected more indices during summer 1999 and 2000. At this time field survey showed that rests of avalanches

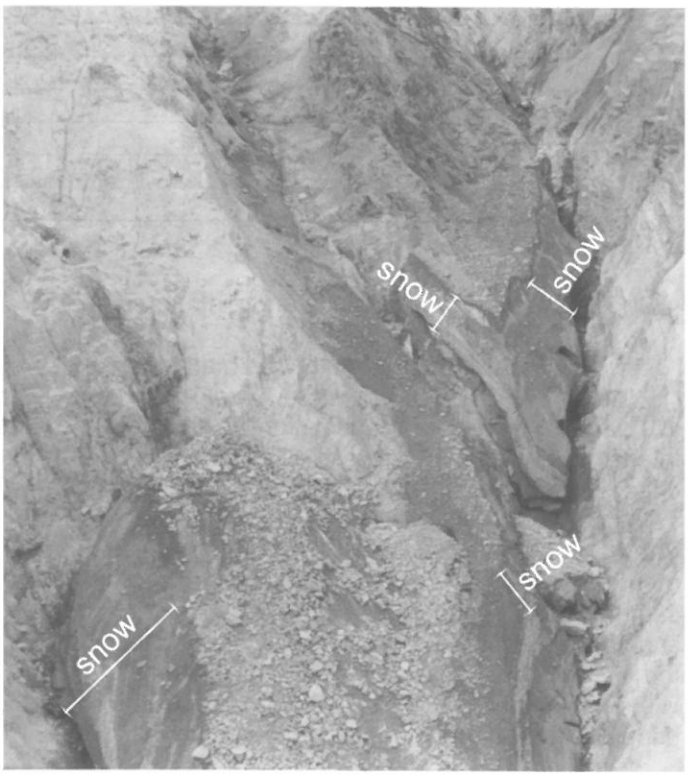

Figure 2-1: Snow accumulation in gullies due to winter avalanche activities. Note the rock debris on the snow's sheet top. Case of Illgraben (VS). Photography E. Bardou.

(from the February 1999 avalanche's events) were lying in many torrents. Our observations indicated a slight increase in solid transport events during this period (this explains the major part of the floating woods in October 2000 flood too). More observations were made: on the 18th of July 2000, snow accumulation covered by schist debris was observed in the torrent of Batsoule, Val Ferret (Bardou 2002). Six days after, a major debris flow (e.g. deposits which reach the road) occurred during not very hard precipitation events (10.7 mm/h at La Fouly rain gauge, Emosson S.A.). This event (and some of the past) was correlated with popular saying, which said: "debris flows occur only after very dry weather". This statement could be transformed in: debris flows occur only after days hot enough to cause massive snow melting.

3 DATA

3.1 Floods data

All data come from Swiss watersheds (Schipfenbach, Illgraben) observed for a long time and from well documented chronicles (right bank of Val Ferret). On these watersheds flood reports go back to XIXth century. The Table 3-1 resumes floods information. All events reported involve sediment transport (bed load or debris flows).

Table 3-1: Flood's chronicle for the 3 area of this study.

ILLGRABEN*	SCHIPFENBACH**	VAL FERRET***
1932	1834	1943
1944	1929	1962 (2 time)
1945 (3 time)	1933	1963 (2 time)
1948	1937 (3 time)	1964 (2 time)
1953	1938	1979
1961 (3 time)	1939	1981
1962 (2 time)	1945 (6 time)	1987 (5 time)
1963 (4 time)	1954	1988 (4 time)
1964 (4 time)	1960 (4 time)	1991 (2 time)
1965 (5 time)	1967 (3 time)	1992 (2 time)
1982	1968 (3 time)	1996 (2 time)
1985	1977	2000 (2 time)
1987	1987 (2 time)	
1988	1989	
1990	1990	
1991	1991	
1995	1993	
1997	1994	
1998	2000	
1999		
2000 (8 time)		

* data from this study and Zimmermann 2000
** Rickenmann et al. 2001
*** data from this study and Marquis 2001

We want to make the reader attentive that these events concern only sediments floods sufficiently intense to be noted by witness. Like often, number of events increases when present time is approached. Even in well instrumented watersheds, it is very difficult to catch every event, like shown in the Table 3-2. The lack of homogeneous data is a difficulty to analyse the process of flood generation. The data of Table 3-2 depict the chronicle of the year 2001 in Illgraben's catchments. In this catchment measurements are done with 3 geophones (velocity estimation, camera's triggering), 1 video camera (velocity and flow's height estimation), 1 radar (flow height's measurement). The left's column shows events that were detected by geophone. The right's column shows events that were not detected by instruments but were observed by authors.
We can see that only 62% of events were detected by the geophone. This observation shows that we underestimate the number of flood events.

Table 3-2: Detected and non detected events in Illgraben during the year 2001.

	Detected by geophone	Non detected (field observations)
07.04		X
29.04	X	
03.05	X	
17.05		X
03.06	X	
06.06	X	
08.06	X	
15.06	X	
28.06	X	
07.07	X	
15.06		X
03.08		X
15.10		X

3.2 Snow and avalanche data

Melting of snow is influenced by the density of snow mass. Compacted snow (e.g. snow which has been moved down by avalanche) could remain up to 3 summers in the gully before it melts totally (observations made in this study). Furthermore our field observations indicate that snow masses, which are involved, come from big avalanche events. To select years with high avalanches intensity, we extract from the historical records (SLF, 2000) all years with more than 12 deceases in building were registered (it is assumed that this number of fatalities is due to the avalanche's amount and intensity and not from random process). To take in account the fact that protection works had begun in the fifties we artificially increase the number of fatalities (in a linear way). For this purpose we assume that if there is no protection works the number of fatalities in winter 1999 will be the double and that the effect of protection works began in 1955.

3.3 Meteorological data

All meteorological and climatic data come from stations of the Swiss Meteorological Institute of Orsière (922 m^{asl}) and the Grand-Saint-Bernard (2472 m^{asl}, abbreviated GSB). The data of La Fouly (1593 m^{asl}) station comes from Electricité d'Emosson S.A.
Rainfalls are measured on an hourly basis and are given in mm.
Antecedent precipitation indexes are computed by the sum of all rain fallen in a given period, without decreasing ratio and are given in mm.
Temperatures are the daily mean and are given in degree Celsius

4 GLOBAL STATISTICAL ANALYSIS

4.1 Comparison between avalanche activity and floods occurrence

In a first approach we try to compare the number of debris flows occurring during a period of 3 summers (e.g. years) which follow a year with a high avalanche activity with a period of the same length for years not considered to have an abnormal avalanche activity. We do this comparison for the Schipfenbach and the Illgraben. Years without very high avalanche activity are chosen randomly on the all set of years with a few avalanche activity. These years are considered as non-event years.

4.2 Results

As we can see in Table 4-1 and Figure 4-1, there is a tendency to observe more flood events during the three summers that follow a year with high avalanche activity. Meanwhile, the difference on the two numbers of debris flow means between year with big avalanche and year without, is not statistically significant.

Table 4-1: Comparison between avalanche activity and floods occurrence.

Schipfenbach

year with big avalanches

	nb. of debris flows		
	year 0	year+1	year+2
1945	6	0	0
1951	0	0	0
1968	3	0	0
1970	0	0	0
1975	0	0	1
1984	0	0	0
1999	0	1	0

year without big avalanche

	nb. of debris flows		
	year 0	year+1	year+2
1946	0	0	0
1982	0	0	0
1937	3	1	1
1973	0	0	0
1940	0	0	0
1990	1	1	0
1969	0	0	0
1996	0	0	0

Illgraben

year with big avalanches

	nb. of debris flows		
	year 0	year+1	year+2
1945	3	0	0
1951	0	0	1
1968	0	0	0
1970	0	0	0
1975	0	0	0
1984	0	1	1
1999	1	6	8

year without big avalanche

	nb. of debris flows		
	year 0	year+1	year+2
1946	0	0	1
1982	1	0	1
1937	0	0	0
1973	0	0	0
1940	0	0	0
1990	0	0	0
1969	0	0	0
1996	0	1	1

This situation could be explained by the inhomogeneity in flood event's data (there are events not big enough to be reported) and the complexity of the flood generation's process (not all events are due to snow melt).

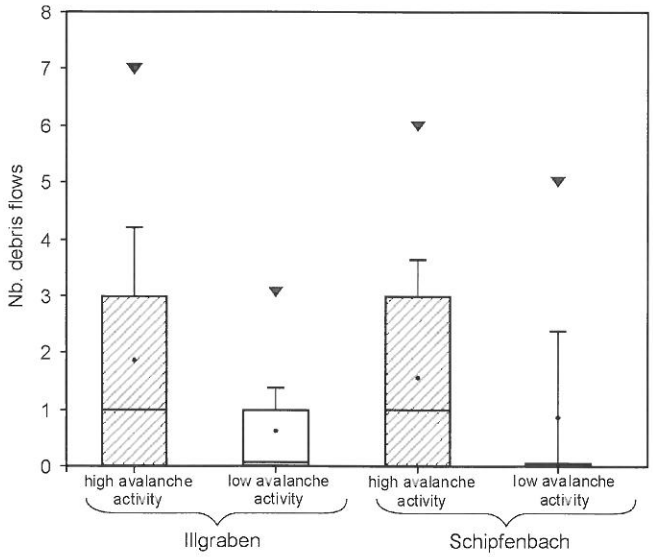

Figure 4-1: Boxplots of the number of flood events after particular year for the Illgraben and the Schipfenbach.

To go further we try to analyse the chronicle of Val Ferret on the basis of detailed meteorological parameters.

5 MORE DETAILED ANALYSIS

To match our field observations and comprehension of the mechanism of flood generation we concentrate our work on the right bank of Val Ferret (VS). Availability of rain data, a good cadastre of events, and knowledge of frequent floods guide this choice.
The Val Ferret is located near the main ridge of the Alps as we can see on Figure 5-1. This situation exposes the area to two major climatic influences: Atlantic low pressure from the west and humid ascent from the Mediterranean from the south.
Altitudes go from 1'000 to more than 3'800 $m^{as.l}$ on the west border. This allows precipitation on two forms, liquid and solid.
From a geological point of view this valley is very contrasted. The west part of the valley belongs to the Mont-Blanc massif (with mostly granite and glacier substratum). The east side belongs to the zone Sion-Courmayeur (mostly schist and wooded area).

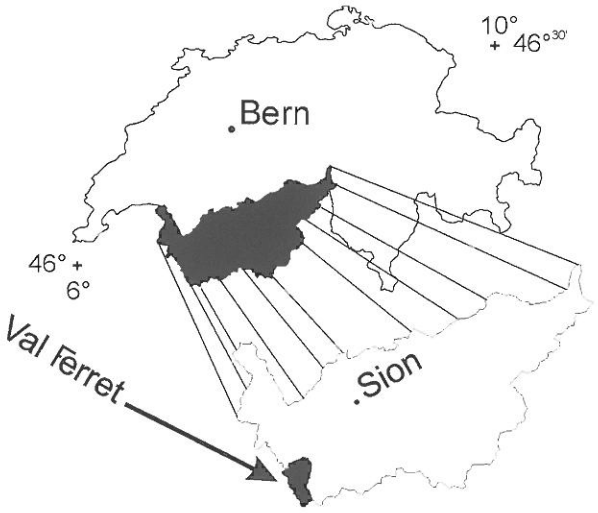

Figure 5-1: Geographical location of the study basin.

5.1 Sampling of non-events rainfall

The population's distribution of rainfalls, which generate debris flow, follows an uniform law. To select the non-event's rainfalls, we pick 30 rainfalls (in a set of 635) in a random way that follows an identical law. This work permits us to constitute two sub-populations, one of debris flows events (13 statistical units) and one of non-events (30 statistical units).

5.2 Choice of meteorological parameters

Nine meteorological parameters were observed. These are :
- Antecedent precipitation index on 5 days in La Fouly (API 5d, in mm).
- Antecedent precipitation index on 10 days in La Fouly (API 10d, in mm).
- Antecedent precipitation index on 15 months in GSB (API 15m, in mm).
- Daily rainfall in la Fouly (in mm)
- Daily rainfall in Orsières (in mm)
- The maximal hourly rainfall in la Fouly (max. hour. rain, in mm)
- The maximal hourly rainfall in GSB (max. hour. rain, in mm)
- The daily mean temperature in la Fouly (mean temp., in °C)
- The daily mean temperature in GSB (mean temp., in °C)

For all these parameters we compare the distribution of the two sub-populations (see Figure 5-2).
To know if differences seen in boxplots of the Figure 5-2 are statistically significant we do hypothesis test. As not all parameters follow a normal distribution, we use the non-parametrical Wilcoxon test. The null hypothesis is: the events sample come from the same population as the non-event sample. If the p-value calculated is inferior at *0.05* we reject the null hypothesis (bolded parameters in Table 5-1).
As we can see all parameters are significantly different between events and non-event population apart from *API 10days* in la Fouly and the maximal hourly rainfall in G^{d}-S^{t}-Bernard. These two parameters were then discarded from the multivariate analysis.

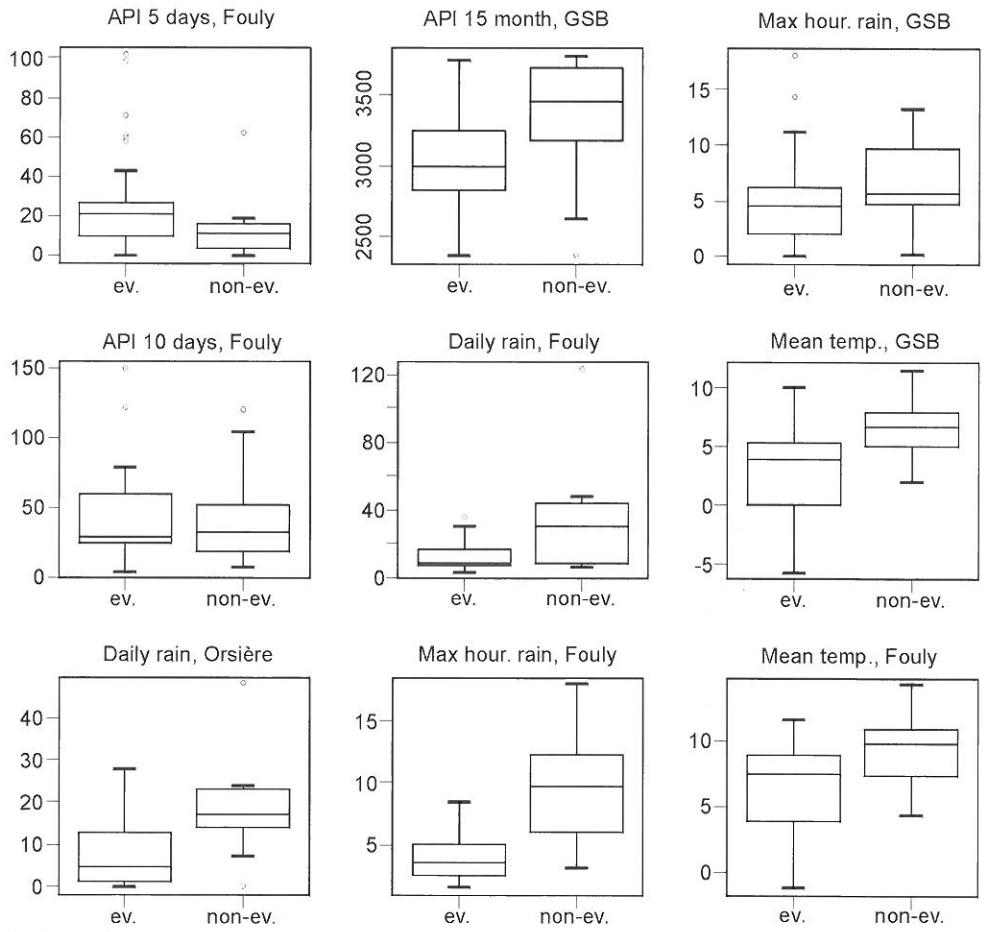

Figure 5-2: Boxplots for each parameters and for the event's population and the non-event's population (Marquis, 2001).

Table 5-1: Median for each parameters and p-value correspondent.

	Event's median	Non-event's median	p-value [-]
API 5d Fouly	**11**	**21.5**	**0.025**
API 10d Fouly	32	29	0.73
API 15m GSB	**3464**	**2991**	**0.042**
Daily rain Fouly	**31**	**8.5**	**0.005**
Daily rain Orsières	**18**	**4.5**	**0.01**
max. hour. Rain Fouly	**9.8**	**3.5**	**0.00007**
max. hour. Rain GSB	5.8	4.5	0.16
mean temp Fouly	**9.9**	**7.5**	**0.011**
mean temp GSB	**6.7**	**3.8**	**0.002**

6 MULTIVARIATE ANALYSIS

For this study we use a discriminant function analysis. The goal is to separate the two sub-populations (events and non-event) on the basis of the meteorological parameters available. The model established could be transformed into a prediction model for debris flows triggering (all mechanisms together) in Val Ferret (Marquis, 2001).

6.1 The canonical discriminant function

We determine the dependant function of the n explicative variables X_1, X_2, ..., X_n, which separates the two groups as well as possible. For that purpose, we take a linear combination of the variables:

(1) $$Z = a_1X_1 + a_2X_2 + \ldots + a_nX_n$$

The groups are well separate if the mean value of Z changes considerably between the two sub-populations and if the intra-group's values are near constant. To do this, we calculate the coefficients $a_1, a_2, \ldots, a_n$ which maximize the Fischer's ratio.

6.2 Results

With the supposition of same covariance matrix for each parameter (which is not totally true in our case) we perform on our dataset the discriminant analysis. We use the moment estimation method (or quasi-natural method) to compute the function:

(2) $$z1 = -0.006\ Y1 + 0.001\ Y2 + 0.014\ Y3 + 0.005\ Y4 + 0.233\ Y5 + 0.046\ Y6 + 0.102\ Y7$$

where Y_1= API 5 days in La Fouly; Y_2= API 15 months in GSB; Y_3= daily rainfall in Orsières; Y_4= daily rainfall in la Fouly; Y_5= maximal hourly rainfall in la Fouly; Y_6= daily mean temperature in GSB; Y_7= daily mean temperature in la Fouly.
From the established model it is possible to classify the individuals of the two sub-populations as function of their meteorological parameters in two groups. The allocation's error on the individuals, which belongs to another group (e.g. an event which is attributed to the non-event's group) shows that the established model describes satisfactorily the phenomenon of floods generation in alpine watersheds (see table 6-2).

Table 6-2: Results of the attribution by the discriminant function.

Sub-population	Number attributed to the group		Total
	Non events	Events	
Non events	28	2	30
Events	4	9	13

This result signifies that 7 times on 100 we do error in the attribution for the non-events. For the events this error raise to 31 times on 100. The distinction between these two families of complex meteorological effects is quite well described.

6.3 Discussion

However the covariance matrix is not identical for all parameters, thus we can see that 4 groups of parameters are used to describe the initiation of debris flows. There are rainfall parameters, short time antecedent precipitation index, long time antecedent precipitation index and temperature. If the two first groups are of evidence to describe flood generation, the last two groups (temperature and API 15 months)are more marginal.
The long time antecedent precipitation index includes precipitations of previous winter (but not only snow). The temperature reflects the melting potential during the period (temperature in G^d-S^t-Bernard is recorded at the same altitude than the upper part of the catchments).
Discriminant function analysis shows that meteorological factors, linked with the possibility of implication of snow in the generation of sediment transport flood, are necessary to discriminate the two populations.
The need of seven parameters (on which only 2 could be linked to snow) could be due to the fact that not all floods with solid transport are due to the presence of old snow in the gully.

7 CONCLUSIONS

Field observations give evidence that snow, actually avalanche deposits, have an influence on the generation of floods with solid transport in alpine watersheds. To determine more rigorously this influence we try to do statistical analysis at two levels of details.
If global analysis shows tendencies, no clear statistical evidences are demonstrated. A more detailed analysis done with a discriminant function is performed on a small area. The established model to predict debris flows triggering needs two parameters, on a total of seven, linked with quantities and melting of snow. This model shows that we cannot explain generation of floods in small alpine watersheds with only one mechanism.
Statistics can help to investigate these processes, but they are now diminished by the quality of data. More accurate prediction could be done in the future if statistical dataset would be recorded with separation of generation's mechanisms and if homogeneity of data (e.g. occurrence of event) could be assured.
Amelioration of the mechanism's comprehension is of great importance to increase the capabilities of model to give good prediction of floods generation on the basis of meteorological parameters.
These results should push us to establish detailed databases on debris flows where triggering mode is one of the field. This database is the only way to ameliorate our capacity to give prealerts on torrents.

ACKNOWLEDGEMENTS

We wish to thank the *Canton du Valais* and the Federal office for water and geology for funding in the Illgraben project. We also thank Mr. F. Dufour of Snow & Avalanche Research Institute for helping us with avalanche data.

REFERENCES

Bardou, E. (2002): Méthodologie de diagnostic du danger lave torrentielle sur un bassin versant alpin. Thèse de doctorat EPFL, Lausanne

SLF. (2000): Der Lawinenwinter 1999, Ereignisanalyse. Davos.

Manly, B.F.J. (1994): Multivariate statistical methods : a primer. Chapman & Hall, 2nd ed

Marquis, F.-X. (2001): Essai de détermination des conditions météorologiques et géologiques prépondérantes dans le déclenchement des laves torrentielles sur le versant droit du val Ferret. Diplôme postgrade en hydrologie EPFL, Lausanne

Rickenmann, D. et al. (2001): Murgang-Beobachtungsstationen der Schweiz. Wasser, Energie, Luft - eau, énergie, air, vol. 93, issue 1/2, pp. 1-8

Zimmermann, M. (2000): Geomorphologische Analyse des Illgrabens, GEO 7, Bern

WOLFHYDRO
A SPATIALLY DISTRIBUTED HYDROLOGICAL MODEL

Niki Beyer Portner[1], Michel Pirotton[2], Pierre Archambeau[2], Jérôme Dubois[1]

[1] HydroCosmos SA, numerical modelling in hydraulic engineering, Rue de l'Industrie 35, CH - 1030 Bussigny, Switzerland

[2] Department of Applied Hydrodynamics and Hydraulic Constructions of the University of Liege, Sart Tilman, B – 4000 Liege, Belgium

SUMMARY

WOLF is an integrated package of hydrological and hydrodynamic software entirely developed in the Department of Applied Hydrodynamics and Hydraulic Constructions (HACH) of the University of Liege. A spatial finite volume scheme was coupled with an explicit temporal discretisation for each models integrated in the WOLF package. This adaptation to the hydraulic equations is ideal for the numerical treatment and implementation. It provides a complete mass conservation of the propagated volumes and a great reliability for the momentum balance. A second order precision is assumed for both spatial and temporal discretisation. An original splitting of the convective terms was developed in order to treat any transient free surface flow discontinuities.
All the software shares the same Windows original end-users interface for pre- and post-processing. It ensures fast implementation of any complex problems, handles a wide choice of parameters and suggests various real-time representations of the flow field (water height, speed, discharge, Froude number ...) with zooms and videos.
WOLFHYDRO described in the present paper is the physically based hydrological model integrated in the WOLF package. The first advantage of this method is that it allows the fitting of parameters to any watershed. In fact, the physical meaning of the parameters limits the range of potential values. Besides, the approach is useful for impact studies since all modifications of soil use have a direct impact on the value of the different coefficients. With the tremendous increase of hardware and storage capabilities, it seems obvious to capitalize the potentiality of digital elevation model (DEM) and general satellite information.
The actual version of the hydrological software, WOLFHYDRO, resolves the conservative equations of 2-D diffusive wave model with a finite volume method for two specific vertically distributed layers. Different roughness laws (Manning, Darcy-Weissbach, Bathurst ...) are implemented to take into account the macroscopic roughness of the hydrological propagation and various flow regimes.
An application example shows the potentiality of the hydrological model of WOLFHYDRO.

Keywords: Numerical model, hydrology, finite volume method, Saint Venant equations, river network propagation, discharge capacity.

1 INTRODUCTION

The modern human society and its globalization also influence the evolution of the problems incident to it. Nevertheless, water is still a challenge which has become even greater. From flood routing to granting a low-water flow, from the growing demand of water for industrial use in a large sense to the maintenance of the ecological characteristics for consumption, the sustainable management of the scarce resource water is on of the major challenges of the 21st century.
The modern water resource management, whether interested in the origins of the water, in its consumption or in its use, or even in the possible consequences of human activity on the water cycle, can not neglect the new potentialities issued from the fast development of numerical methods. Based on the theoretical knowledge in fluid mechanics of the past centuries, these methods can be used for the development of decision aiding tools for real situations of a large scale.
Among the domains in hydraulics concerned by numerical methods, the interest of the Department of Applied Hydrodynamics and Hydraulic Constructions (HACH) of the University of Liege in modelling free surface flows is simply due to there preoccupation for all hydrodynamic phenomena human beings try to act on. Seen in relation with the global hydrologic system, the effort to manage and therefore to anticipate natural phenomena and natural hazards leads to establishing physically based approaches for modelling the course of a water droplet from the moment when it touches the surface

of the earth, through the sheet flow and the rising of the runs, rivulets and retention surfaces on to the large rivers and inland waterways.
Without going into the details of the mathematical formulations and numerical solutions, the present paper describes the numerical model representing the first part of the water droplet's course. An application to a real case shows the power of the numerical hydrological model WOLFHYDRO.

2 THE WOLF PACKAGE

2.1 Introduction

The integrated suite of software Wolf has been entirely developed in the Department of Applied Hydrodynamics and Hydraulic Constructions (HACH) of the University of Liege (http://www.ulg.ac.be/hach/). HydroCosmos SA is the owner of the unique license for the Wolf package in Switzerland.

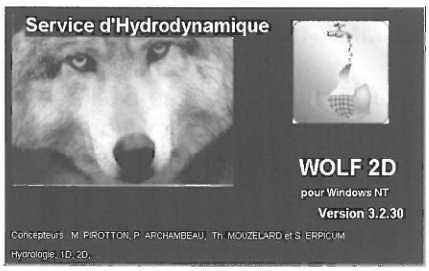

Figure 2-1: Start-up window.

2.2 Unicity of numerical resolution methods

A spatial finite volume scheme was coupled with an explicit temporal discretisation for each models integrated in the Wolf package. This adaptation to the hydraulic equations is ideal for the numerical treatment and implementation. It provides a complete mass conservation of the propagated volumes and a great reliability for the momentum balance. A second order precision is assumed for both spatial and temporal discretisation. An original splitting of the convective terms was developed in order to treat any transient free surface flow discontinuities.

2.3 End user interface

All the software shares the same Windows original end-users interface for pre- and post-processing. It ensures fast implementation of any complex problems, handles a wide choice of parameters and suggests various real-time representations of the flow field (water height, speed, discharge, Froude ...) with zooms and videos.
On the one hand, the interface has been written in Visual Basic language (Figure 2-2) to capitalise the whole Windows environment capacity and instinctive use. On the other hand, the intensive computation is performed by Fortran95 software for the uncontested scientific accuracy and computations.
This set defines the WOLF package and offers a unified and comfortable work environment.

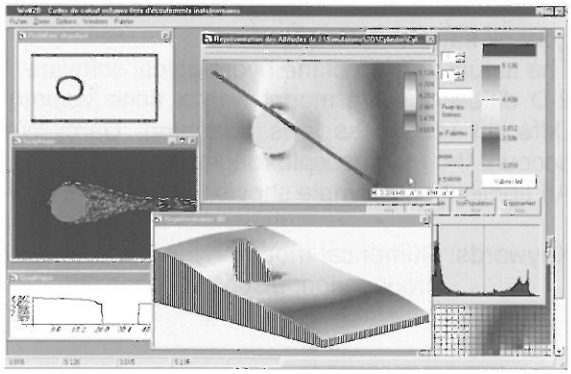
Figure 2-2: Screen capture of a WOLF window interface.

It permits for example:
- automatic generation of structured or unstructured grid for complex geometries,
- quick definition of all boundaries conditions,
- internal edition of all used matrix with a simplified spreadsheet (multi-selection, importation of external values, exportation to Excel, numerical treatment, smoothing, shading operation, cut and paste ...),
- raster representation for the two-dimensional problems,
- vectors representation of velocity and flux,
- curved representation,
- three dimensional representation with OpenGL technique,
- computation and visualization of particles tracking (LaGrangian view),
- true colours gradation (24 bits)...
- zooming in all windows,
- creation and animation of videos,
- superimposing two drawings of raster and vectorial information as a GIS based software.

3 WOLFHYDRO

WOLFHYDRO is a physically based hydrological model. The first advantage of this method is that it allows the fitting of parameters to any watershed. In fact, the physical meaning of the parameters limits the range of potential values. Besides, the approach is useful for impact studies since all modifications of soil use have a direct impact on the value of the different coefficients.
With the tremendous increase of hardware and storage capabilities, it seems obvious to capitalize the potentiality of digital elevation model (DEM) and general satellite information.
In fact, for several years, the HACH has developed some numerical hydrological software. Each model resolves a partial or the full set of Euler or Navier Stokes equations.
The actual version of the hydrological software, WOLFHYDRO, resolves the conservative equations of 2-D diffusive wave model with a finite volume method for three specific vertically distributed layers. Different roughness law (Manning, Darcy-Weissbach, Bathurst ...) are implemented to take into account the macroscopic roughness of the hydrological propagation and various flow regimes.
Originating from the well-known Saint Venant equations describing the flows:

(1) $$\frac{\partial h}{\partial t}+\frac{\partial (uh)}{\partial x}+\frac{\partial (vh)}{\partial y}=q$$

(2) $$\frac{\partial (uh)}{\partial t}+\frac{\partial \left(u^2h\right)}{\partial x}+\frac{\partial (uvh)}{\partial y}+gh\left(S_{fx}+\frac{\partial H}{\partial x}\right)=0$$

(3) $$\frac{\partial (vh)}{\partial t}+\frac{\partial (uvh)}{\partial x}+\frac{\partial \left(v^2h\right)}{\partial y}+gh\left(S_{fy}+\frac{\partial H}{\partial y}\right)=0$$

where H(x,y,t) is the water surface elevation above an horizontal datum, h(x,y,t) is the local water depth, t is the time, x, y are horizontal Cartesian coordinates, u(x,y,t), v(x,y,t) are depth averaged flows velocities in x and y directions, $S_{fx}(x,y,t)$, $S_{fy}(x,y,t)$ are friction slopes in x and y directions and g is acceleration due to gravity.
The diffusion approach can be obtained by ignoring the inertial terms compared with the gravitational terms, friction and pressure heads. Eqs (2) and (3) can then be replaced by the following system of parabolic differential equations:

(4) $$\left(S_{fx}+\frac{\partial H}{\partial x}\right)=0$$

(5) $$\left(S_{fy}+\frac{\partial H}{\partial y}\right)=0$$

In addition and for example, applying the Manning-Strickler law to the description of the friction slopes that appears in the preceding equations, the relation between the velocity and water depth components can be obtained as

(6) $$S_{fx}=\frac{n_x^2}{h^{\frac{4}{3}}}|w|wxi=\frac{n_x^2}{h^{\frac{4}{3}}}u\sqrt{\left(u^2+v^2\right)}$$

(7) $$S_{fy}=\frac{n_y^2}{h^{\frac{4}{3}}}|w|wxj=\frac{n_y^2}{h^{\frac{4}{3}}}v\sqrt{\left(u^2+v^2\right)}$$

where $w=u_i + v_j$ is the velocity vector, n_x, n_y are the Manning roughness coefficients in the directions x and y, respectively, and therefore

(8) $$|w|^2 = u^2 + v^2 = h^{\frac{4}{3}} \sqrt{\frac{S_{fx}^2}{n_x^4} + \frac{S_{fy}^2}{n_y^4}}$$

Lastly, the replacement of the preceding relation in the expression for S_{fx} (6) and S_{fy} (7) determines the following expressions for the components of the velocity vector:

(9) $$u = -\frac{\partial H}{\partial x} \frac{h^{\frac{2}{3}}}{n_x^2} \frac{1}{\left[\left(\frac{\partial H}{\partial x}\right)^2 \frac{1}{n_x^4} + \left(\frac{\partial H}{\partial y}\right)^2 \frac{1}{n_y^4}\right]^{\frac{1}{4}}}$$

(10) $$v = -\frac{\partial H}{\partial y} \frac{h^{\frac{2}{3}}}{n_y^2} \frac{1}{\left[\left(\frac{\partial H}{\partial x}\right)^2 \frac{1}{n_x^4} + \left(\frac{\partial H}{\partial y}\right)^2 \frac{1}{n_y^4}\right]^{\frac{1}{4}}}$$

A 2D multilayer model handles the rainfall propagation, spatially and temporally variable according to the cloudy fronts, on the DEM and a complete 1D model propagates the lateral floods components in the drainage path.

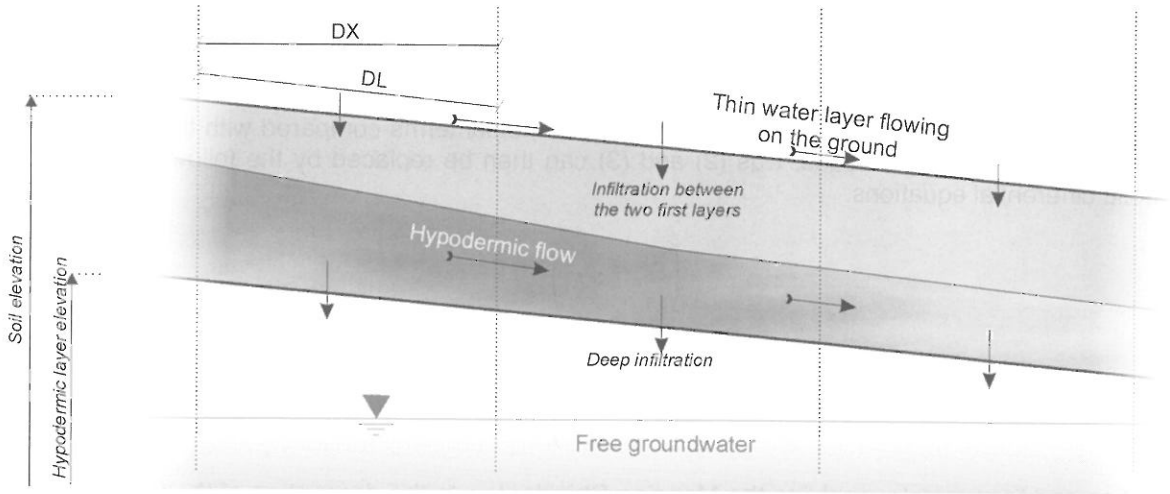

Figure 3-1: Representation of the three layers and the related flows.

The model has three bunk layers to simulate respectively the thin runoff, the hypodermic propagation and the transfer to the groundwater. The unsteady infiltration law permits the reforming of the soil capacity after the rain stopping. The calculation of long periods is possible without stopping the software.

4 EXAMPLES OF REAL CATCHMENTS

4.1 Krasnodar Dam Rehabilitation Project, Russia

The authors have participated in the hydrological study for the Krasnodar Dam Rehabilitation in Russia. This study is described by Goulpié et al. (2002) and presented at the conference. Therefore, the present paper describes other application examples of WOLFHYDRO.

4.2 Amblève watershed, Belgium

Belgium has a digital elevation model with a mean spatial discretisation of 30 m.
WOLFHYDRO ensures a suitable modification of this information to fit with the hypotheses of the hydrological propagation code. It induces slight local topographic modifications to prevent local depressions or flat areas and to create continuous slope paths.
After this fundamental and interactive stage, the hydrographical network is automatically delineated. A click on a point of this net induces an iterative automatic process to determine the limits of the watershed.
River network propagation brings out to another specific hydrodynamic process ensured with WOLF1D, hereafter presented.
The Amblève watershed covers a global surface of 976 km² at the Targnon outlet. The total number of nodes is 1'085'000 and the river network contains 9'000 segments of discretisation.
The hydrologic modelisation permits to determine the discharge evolutions into the river network and the management optimization of relevant dams.

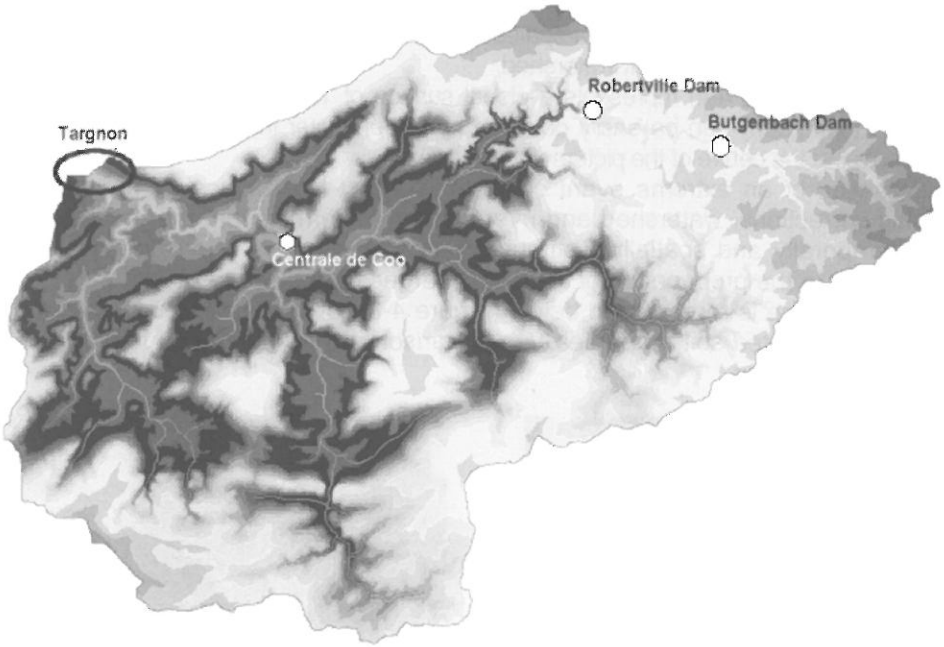

Figure 4-1: Topography of Amblève watershed (Belgium).

Figure 4-2: Hydraulic convergences – Amblève (Belgium).

4.3 Mattmark dam, Switzerland

Another application is the verification of the discharge capacity of large hydraulic constructions around the world due to likely climatic evolution and availability of hydrological numerical data on the concerned sites. In this way and to prevent extreme events, Switzerland is interested in the development and application of distributed physically based models. A study of the discharge capacity of the overflow structure of the Mattmark dam in Switzerland was conducted by Jérôme Dubois for the Laboratory of Hydraulic Construction of the Swiss Federal Institute of Technology in Lausanne (Boillat and Dubois, 1998; Boillat et al., 2000).

Figure 4-3: Dam of Mattmark (Switzerland).

Switzerland has a digital elevation model with a spatial resolution of 25 m. In the case of Mattmark watershed, the part of general map (Figure 4-4) represents a global surface of 150 km² (raster of +- 200.000 nodes). A shading view of this topography can be easily obtained by the end-user interface of Wolf. The dam and the reservoir clearly appear at the centre of the picture (Figure 4-5).

Complete modelisation of an extreme event consists in a first hydrological computation. After automatic topographic corrections, watershed and river network determination, the results of the hydrological stage are temporally and spatially distributed lateral flows poured into the river network. The second stage consists in the propagation of these discharges right down the outlet with Wolf1D.

The result of this sequence is represented below (Figure 4-8) for an extreme uniform rain, temporally variable, with safety saturated soil properties. A comparison with an observed hydrograph completes the validation of the simulation.

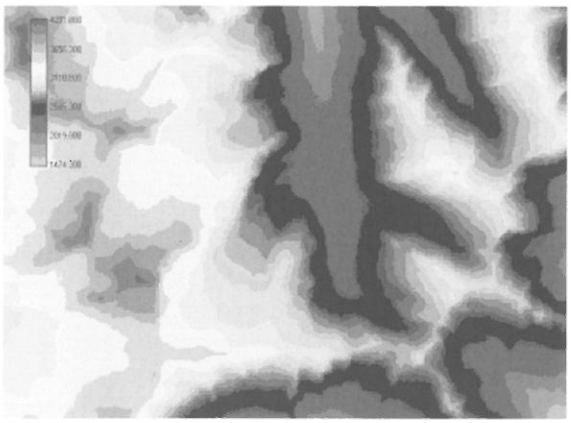

Figure 4-4: DEM of Mattmark (Switzerland) at 25 m.

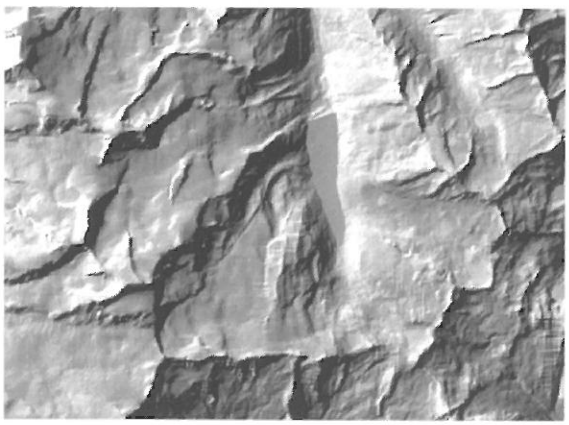

Figure 4-5: Shading view of the DEM - Mattmark (Switzerland).

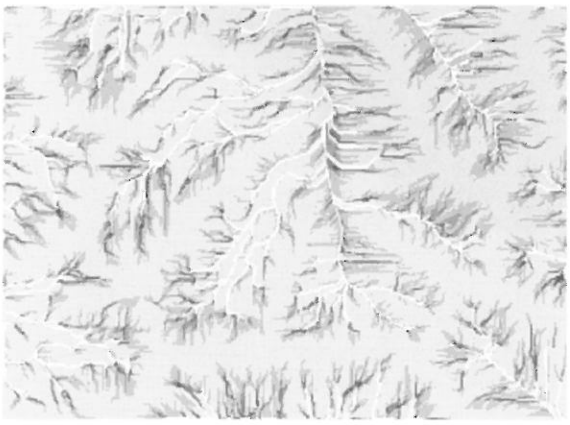

Figure 4-6: Convergences – Mattmark (Switzerland).

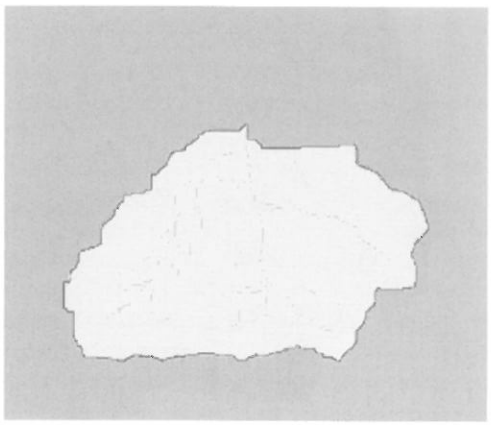

Figure 4-7: Determination of the Mattmark's watershed (Switzerland).

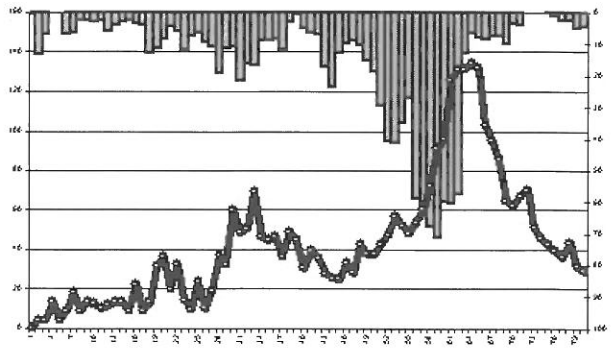

Figure 4-8: Extreme rain and observed hydrograph- Mattmark (Switzerland).

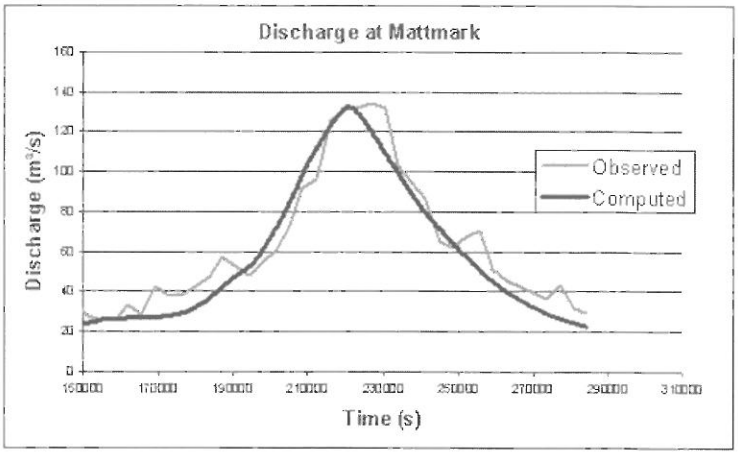

Figure 4-9: comparison between observed and computed hydrograph- Mattmark (Switzerland).

5 WOLF1D: FLOOD ROUTING IN RIVER NETWORKS

To propagate lateral inflow, coming from WOLFHYDRO, along the rivers network and, generally, to compute unsteady floods taking into account floodplains, the HACH has developed an original method of flood routing in compound channels. Propagation is ensured with a correct estimation of water height and discharge in any rivers network with any transversal sections and flow regime. This software, called WOLF1D, is implemented in the interface described before.
The system of equations below represents the 1D conservation of mass and momentum:

(11)
$$\frac{\partial}{\partial t}\begin{bmatrix}\omega\\ q\end{bmatrix}+\frac{\partial}{\partial x}\begin{bmatrix}q\\ qu+gp_{\omega}\end{bmatrix}+\begin{bmatrix}-q_L\\ -g\omega\sin\theta+n^2\dfrac{gu|q|}{R_m^{\frac{4}{3}}}+qp_x+2\left(v\omega\dfrac{\partial u}{\partial x}\right)\end{bmatrix}=\begin{bmatrix}0\\ 0\end{bmatrix}$$

(12)
$$p_{\omega}(h)=\int_0^h(h-\xi)\ell(c,\xi)d\xi$$
$$p_x(h)=\int_0^h(h-\xi)\frac{\partial\ell(x,\xi)}{\partial x}d\xi$$
$$\ell=\ell_g+\ell_d$$

where ω is the wet section, q is the discharge, u is the average speed, q_L is the lateral inflow, g is the gravitational acceleration, θ is the bed slope, n is the roughness Manning's coefficient, R is the hydraulic radius and ν is the water viscosity.
The river arms have a variable longitudinal discretisation with automatic adaptative time-step according to numerical stability conditions (Courant Number).

The numerical scheme reaches a second order precision for spatial and temporal discretisation with an original splitting of the convective terms. That ensures shock capturing properties to handle mixed regimes with unsteady hydraulic jumps and general resolution of any confluence.
For large network, statistic laws can be employed to generate an automatic rectangular minor bed to face the gap of information and ensure propagation of the floods.
To go over the limitations of the classical methods as conveyance and to numerically manage longitudinal free surface flows, the software separates computation of the hydrodynamic behaviour of each riverbed. An explicit evaluation of the lateral exchanges is performed according to the instantaneous state of each river components (water head gradients) (Figure 5-1).
To take into account the lag effect of the floodplains on the main channel and the accelerator effect of the main channel on the floodplains, it computes the interactions between longitudinal flows by the introduction of fluid-fluid friction between each channel (Figure 5-2).

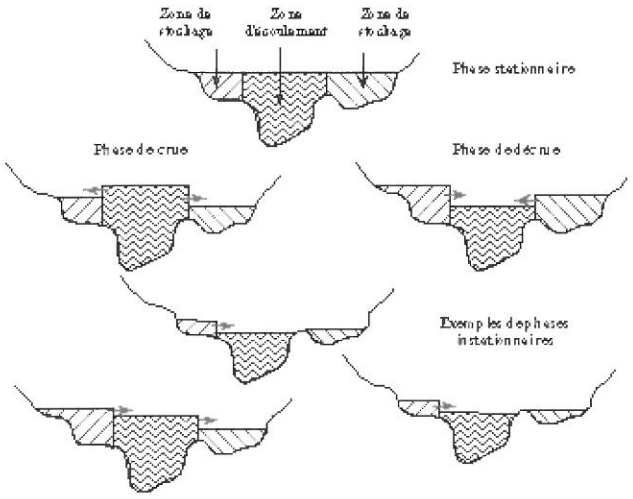

Figure 5-1: Lateral exchanges between each riverbed.

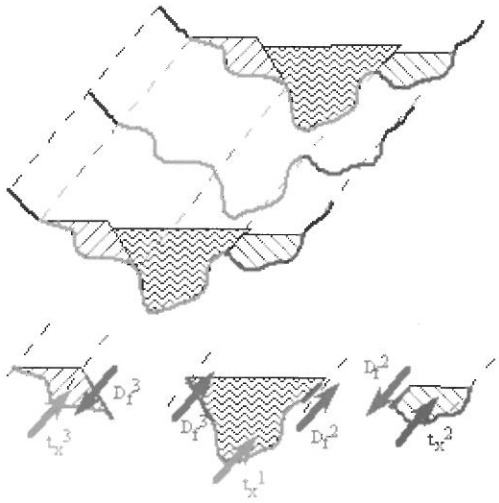

Figure 5-2: Fluid-fluid friction.

REFERENCES

Boillat J.-L., J. Dubois, J. (1998): Application of PMP-PMF methodology to the Mattmark scheme. *In*: L. Berga (ed.): Proceedings of the International Symposium on New Trends and Guidelines on Dam Safety, Barcelona, Spain. A.A. Balkema. Rotterdam.

Boillat J.-L., Dubois, J., Schleiss, A. (2000): Utilisation possible de la retenue de Mattmark pour la protection contre les crues et la production d'énergie. Actes du XX Congrès des Grands Barrages, CIGB/ICOLD, Q.77- R.23. Beijing.

Goulpié P., Hertig, J. A., Hug, Chr. (2002): Numerical modelling of probable maximum flood. Application case on the Krasnodar watershed in Russia. Proceedings of the International Conference on Flood Estimation. Berne, Switzerland.

PHYSICALLY BASED MODELLING OF RUNOFF GENERATION

Wolfgang Bott, Thilo Hofmann, Dietmar Schenk

Johannes Gutenberg University Mainz, Institute of Geocience, Division of Applied Geology
Becherweg 21, 55099 Mainz, Germany, wbott@mail.uni-mainz.de

SUMMARY

The occurrence of floods with their economic damages has forced hydrological research to take steps which decrease their impacts. In a current research project the effects of different forestal and hydrological measures on water dynamics are examined and subsequently modelled by the physically based, two dimensional precipitation-runoff-model CATFLOW (Maurer, 1997a,b; Zehe, 1999). Research is focusing on the influence of different wood-types, plant density, road construction and density, soil degradation, and drainage network. The objective is to get an applicable tool to predict runoff as a fact of land use changes in forests. For that purpose two different forest sites were chosen to yield survey input and validation data for the simulation model. Results show a dominant influence of soil hydraulic parameters. Thus, the management of the forestry is of major importance for the runoff characteristic of forested hillsides. Besides there is a distinct dependence of water dynamics within the ecosystem on field morphology, canopy cover and climate, especially on precipitation.
Accordingly, model predictions of runoff based on measured input parameters are possible and will contribute to a sustainable catchment area management and can help to decease the number of floods. Consequently the manner of forestry operation will directly affect runoff quantity.

Keywords: precipitation-runoff-model, runoff generation, subsurface flow, road density, landuse

1 INTRODUCTION

The significance of forest ecosystems with their high water retention potentials has been investigated by several authors (e.g. de Haar & Hoffmann, 1982; Mitscherlich, 1971). Rhineland-Palatinate is the state with the largest forest coverage (41%) in Germany (Leonhard, 1999). However, there are frequent floods resulting in high economic damages at the major rivers Rhine, Mosel and Nahe. To counteract these risks of flood events it is necessary to understand and improve water retention capabilities in forested catchments. In a current research project, the possibilities to decrease floods by an adjusted forestry regarding suitable rationing methods are in the scope of investigation.

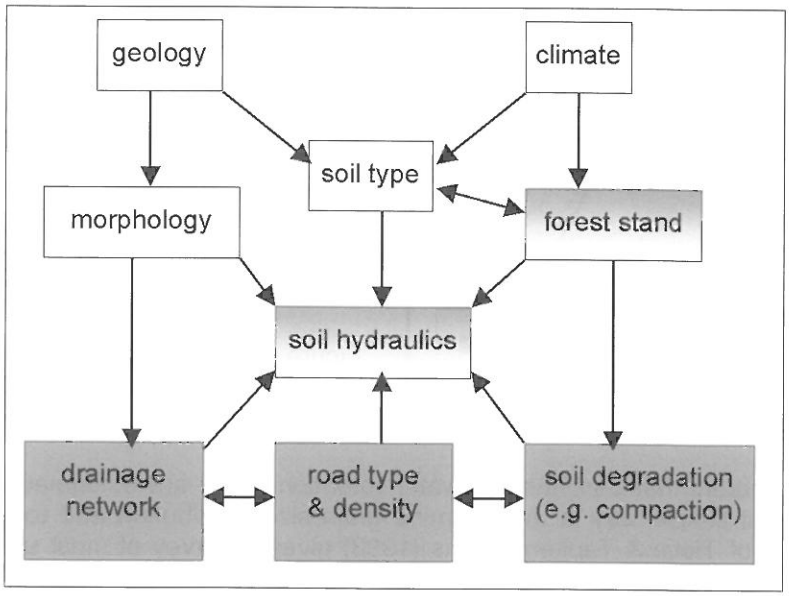

Figure 1-1: Controlling factors of water transport under forest stands and their interactions: white = naturally given factors, grey = anthropogenic factors, grey/white = influenced by natural and anthropogenic factors.

Water transport under forested areas is influenced by multifarious factors and their interactions (Figure 1-1). There are natural given like geology, morphology, soil type and climate, which can't be affected by human activities and anthropogenic factors like drainage network, road type, road density and soil degradation. Soil hydraulics, as the most important value of water transport and forest stand, are influenced by both, by natural and as well by man-made factors.
To perform that problem, water transport under two forest sites in Rhineland-Palatinate with different hydrologic properties is modelled with the physically based, two dimensional precipitation-runoff-model CATFLOW (Maurer, 1997a,b; Zehe, 1999).

2 MODEL DESCRIPTION

CATFLOW is a physically based, distributed model for the dynamics of water in the upper soil layer of small catchments including channel network and vegetation cover on the event and season time scale (Maurer, 1997a). The model is based on the idea of subdividing the 3D-landscape in patches of 2D-hillslopes. Modelling is realised by the assignment of distinct parameters at vertical sections along an idealised hillslope line (Figure 2-1). Each discrete point along the hillslope line is connected to a set of parameters, which represents a complete hill segment (Figure 2-2). This geometry is described under consideration of digital elevation model, channel profiles and elevation, soil hydraulic functions, macro-porosity, surface and channel roughness, and plant parameters. The drainage network is incorporated by combination of more than one different hill slope and information on channel geometry and determination of the stream order after Strahler (1964).

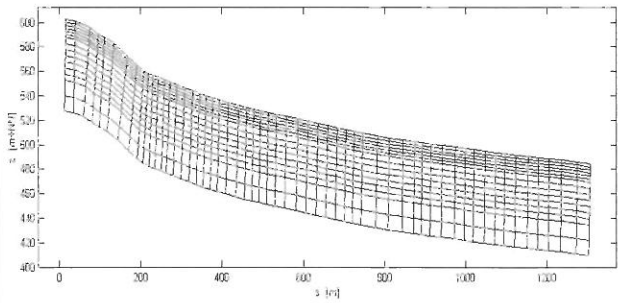

Figure 2-1: Example of a hillslope discretization along the slope line (Bott et al. 2001).

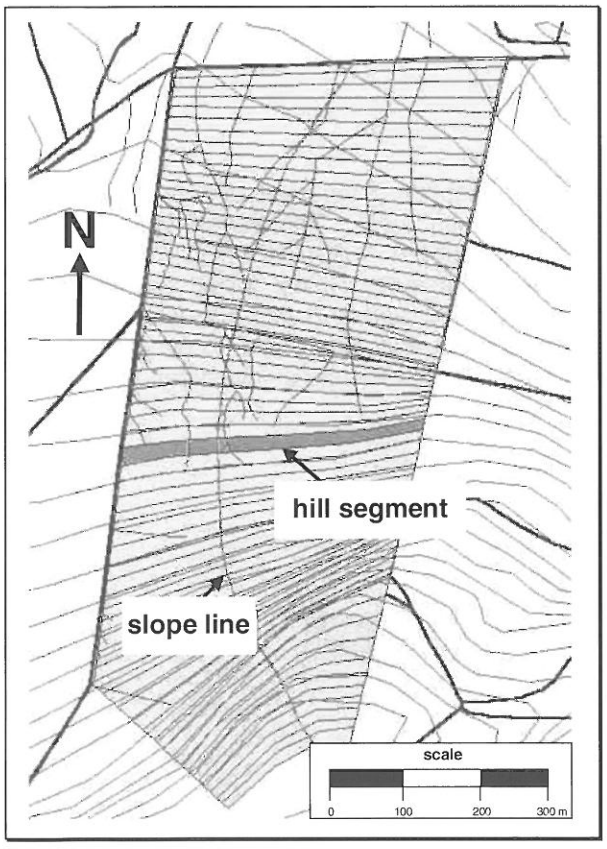

Figure 2-2: Illustration of a model hillside with hill segments (grey) and the slope line.

Soil hydraulic parameters that describe the water retention curve are estimated with two different approaches. The first simple way is to determine grain size distribution and to use pedo-transfer functions. The work of Tietje & Tapkenhinrichs (1993) gives a survey of most used functions. The other approach is laboratory measurements of undisturbed soil samples. In our investigation we used both alternatives. The measured water retention curves were compared to data obtained by the used model of van Genuchten (1980) and Mualem (1976) together with the pedo-transfer function of Carsel & Parrish (1988).

The following equation (1) determine the soil water retention curve in this model:

(1) $$\Theta^* = \left(\frac{1}{1+(\alpha \cdot \psi)^n} \right)^m = \frac{\Theta - \Theta_r}{\Theta_s - \Theta_r}$$

where

ψ = matrix potential
Θ^* = degree of saturation (effective water content)
Θ_r = residual water content
Θ_s = saturated water content
α = specifies state of poresize maximum; reciprocal value $1/\alpha$ is called air entry point
n = specifies width of poresize distribution
m = constant (m=1- 1/n)

Soil water potential, surface water depth and interception storage are calculated state variables to simulate various processes of water transport as runoff, infiltration in soil matrix and macropores, interflow, groundwater recharge, interception, evapotranspiration and changes in soil water content. State of system is changing by these processes under the influence of the controlling boundary factors mentioned in Chapter 1.

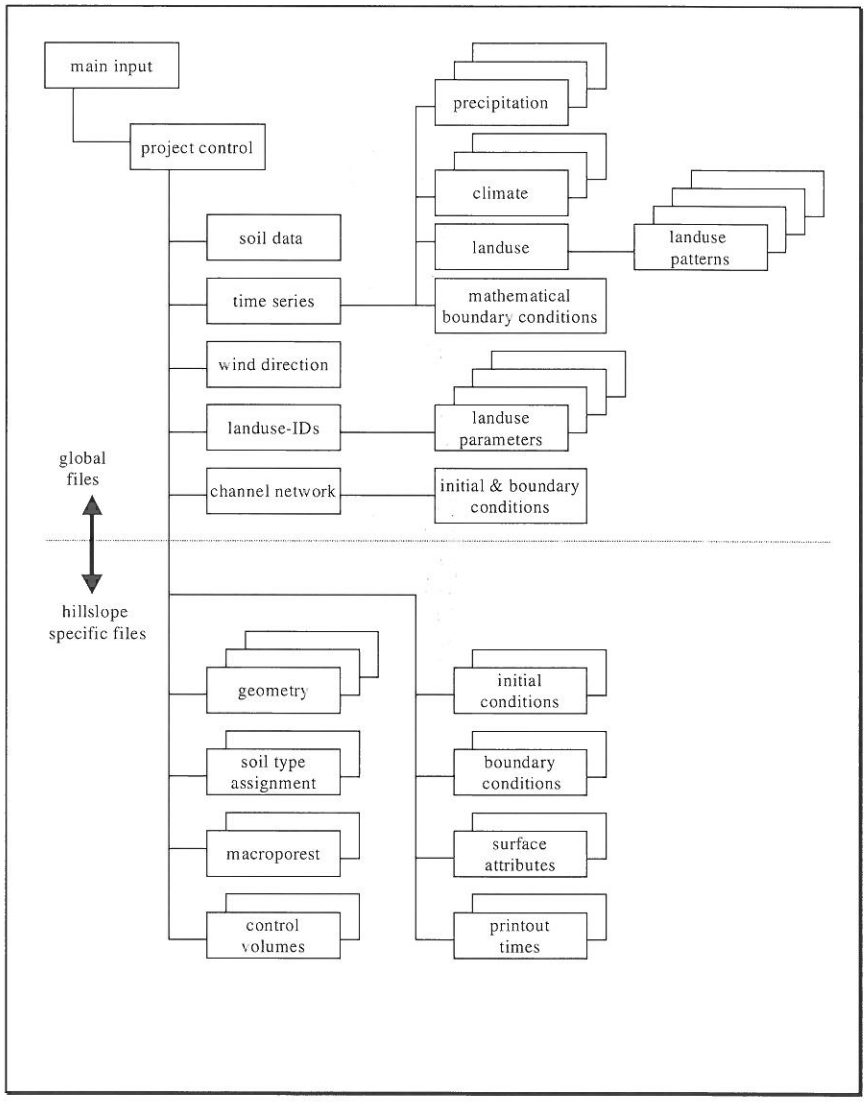

Figure 2-3: Hierarchy of input files in CATFLOW (after Maurer, 1997a, b).

Unsaturated and saturated flow in matrix is modelled by potential based solution of RICHARDS equation using Picard iteration and Taylor series expansion of the moisture content with respect to the potential as described by Hornung & Messing (1984) and Celia et al. (1990). The model allows to account for anisotrophy. Surface flow as well as channel flow is calculated by the kinematic wave approach of ST. VENANt equation (Mahmood & Yevjevich, 1975). Calculation of transpiration is based on PENMAN-MONTEITH equation. A detailed description of the mathematical approaches in CATFLOW is given in the work of Maurer (1997b).
All these data with its high spatio-temporal resolution is executed in CATFLOW by a number of specified files connected in project control files. Files are organized in a hierarchical way. Figure 2-3 gives an idea of that relational data structure.

3 TEST SITE DESCRIPTION

To yield survey input and validation data for the simulation model, two different representative forest sites were chosen. Figure 3-1 shows an overview map of Rhineland-Palatinate with the two test sites and the associated geological units.
The first area is a hillside of about 0,5 km^2 in the eastern Soonwald, which is a part of the Hunsrueck, Germany. The loamy clay soil has developed from quaternary solifluction debris overlaying a tertiary weathered surface layer, which consists of Palaeozoic schist and quarzite. According to the US-Soil-Taxonomy these soils are classified as loamy clay soils or as dystric gleysols (FAO-System, Scheffer & Schachtschabel, 1992). The forest consists of deciduous trees and conifers of all ages. The annual mean temperature is about 8.5 °C and the precipitation has a value of 750 mm/a.
The second area, also about 0,5 km^2, is situated in the Pfälzer-Wald (Germany), geologically consisting of Mesozoic sandstone. The substratum consists of sandy loam soil (US-Soil-Taxonomy) respectivley podsolic cambisols (FAO-System, Scheffer & Schachtschabel, 1992). The forest stand is mainly composed of old deciduous trees with some conifers. Mean annual temperature ranges from 7.5 to 8 °C and precipitation is about 950 mm/a.

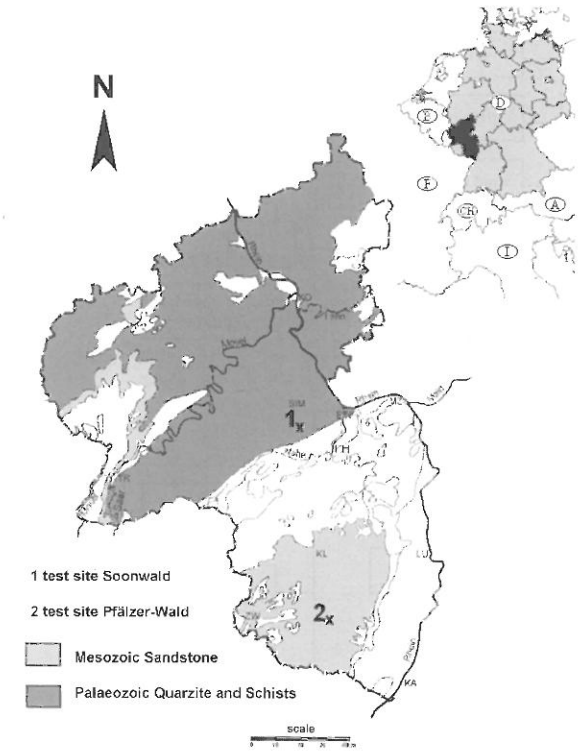

Figure 3-1: Overview of Rhineland-Palatinate indicating the test sites and the associated geological units.

4 RESULTS

4.1 General results

Results verify the obvious difference in water dynamics of the two test sites. For the Soonwald test site the simulations indicate low to medium infiltration rates. Replenishment of soil moisture storage is reached frequently and quickly. Therefore saturation is reached often and leads to surface and subsurface runoff. Groundwater recharge is low (about 10 to 15 % of precipitation). So we get here fast runoff generation, which means there is a relatively high endangerment of flood formation.
In contrast we have high infiltration and percolation rates for the Pfälzer-Wald. Replenishment of soil moisture storage is hardly reached and saturation occurs rarely. So there is no or seldomly surface runoff. Interflow doesn't play a role. Groundwater recharge in this region is up to 50 % of precipitation. Consequently there is no risk of flooding fed by runoff from the receiving overland flow from the forests of Pfälzer-Wald. Runoff is dampened by the system. These simulation results match with the results of Hahn & Friedrich (1996), who have investigated the runoff behaviour of several brooks in the south of Rhineland-Palatinate.

4.2 Influence of soil hydraulic parameters

Soil hydraulic parameters play the most important role in water transport. Figure 4-1 shows the influence of different soils and slope gradients on surface runoff at a heavy summer rain event. Sandy loam soil represents Pfälzer-Wald and silty clay loam and loam belongs to Soonwald soil types.

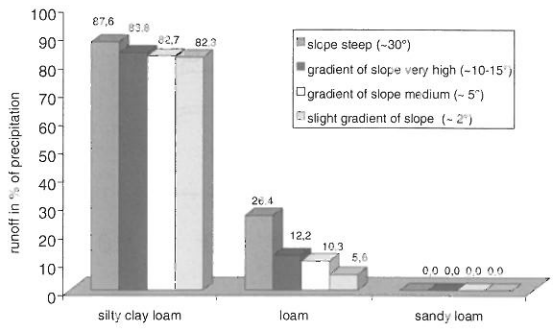

Figure 4-1: Influence of different slope gradients and soil types on simulated runoff generation during a heavy summer rain event.

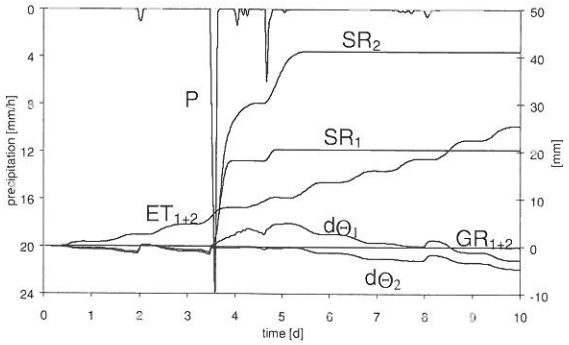

Figure 4-2: Simulation Soonwald: Decrease of saturated permeability; run 1: Ks = 0,5 m/d; run 2: Ks = 0,05 m/d; $\Theta_{initial}$ in both cases = 30%; P = precipitation; GR = groundwater recharge; ET = evapotranspiration SR = surface runoff; dΘ = changes in soil moisture.

The impact of a decrease in saturated permeability (Ks) for the soils at Soonwald is shown in Figure 4-2. The simulated decrease in one order of magnitude is thought to be realistic because of soil degradation by heavy machines used in forest cultivation (Hildebrand, 1983). The illustration represents the same intensive rainfall event mentioned in Figure 4-1. Precipitation P reaches more than 20 mm/h. Resulting changes in soil moisture dΘ, groundwater recharge GR, evapotranspiration ET and surface runoff SR are shown cumulatively.
In both cases evapotranspiration reaches the same values. There is no groundwater recharge. Instead, surface runoff becomes more important mainly fed by fast subsurface components and overland flow from forest roads. The first precipitation event on the second day was intercepted by soil moisture storage. The high incidents on the third day and the rainfall 1 ½ days later lead to surface runoff. This effect is more pronounced in simulation 2 with its lower saturated permeability. Even the small rainfall intensities between day three and five lead to a higher runoff amount. Overall surface runoff in case 2 is twice as high than in case 1. Modification of permeability due to soil compaction causes much higher surface runoff than intact forest soil.

4.3 Influence of vegetation cover

Results of modelling impact of different landuse are given in Figure 4-3. The three chosen vegetation canopies are grassland (index G), deciduous trees (index D) and conifers (index C). Under grassland surface runoff SR is higher and evapotranspiration ET is lower than under forest sites. In contrast, different kinds of trees only have a small impact on water dynamics.
The main factor in terms of forest stands is the high interception capacity compared to non-forestal landuse. Interception rates for deciduous tree reach values between 30 to 40 % and for conifers they are about 25 to 75 % (Mitscherlich, 1977). But the large difference in interception rates decreases with increasing precipitation. That means, in case of flood endangering precipitation events, there is nearly no difference between the different wood types.

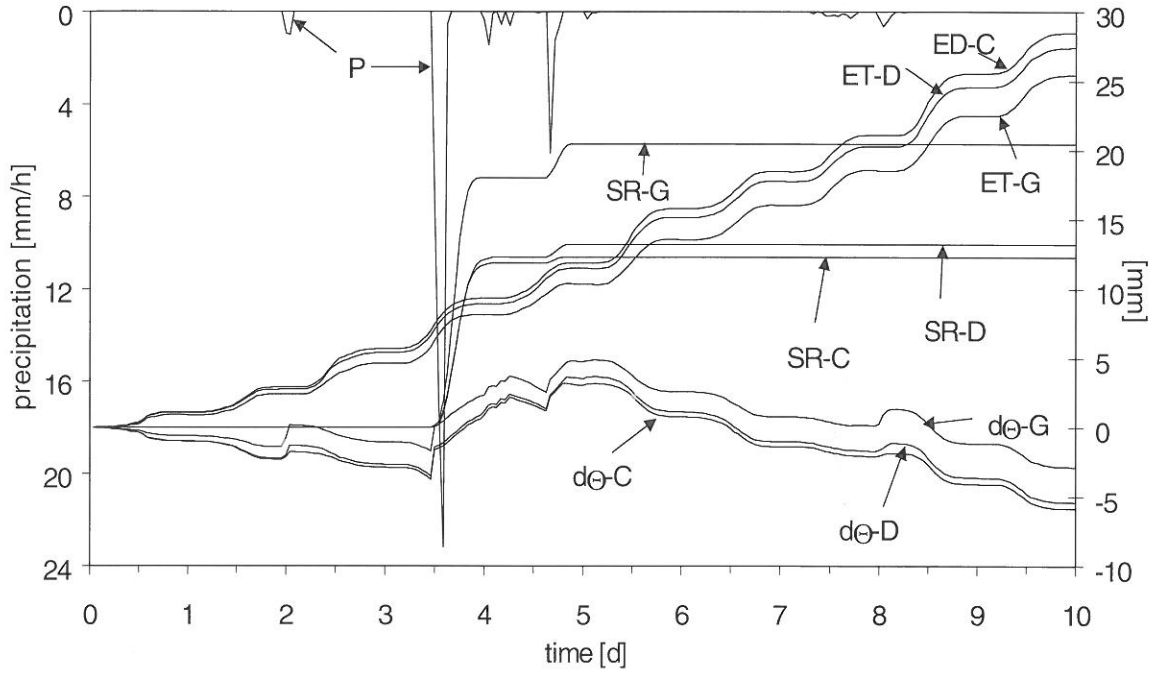

Figure 4-3: Simulation results of modelling three different vegetation canopies (grassland G, deciduous D and conifer forest C) at Soonwald test site. Ks = 0,5 m/d; $\Theta_{initial}$ = 30 %; precipitation = P; changes in soil moisture = dΘ; surface runoff = SR; evapotranspiration = ET.

4.4 Influence of roads and drainage network

The influence of road network is given on the on hand by road density and on the other hand in the kind of road construction. Based on own field measurements of infiltration capacities of different road types at forests, only two categories were distinguished; full impermeable and half permeable. Therefore, in the model the road type has only an ancillary importance. But between density of road construction and amount of runoff, there is a obvious direct relation. The influence of inclination of linear features like roads and drainage trenches, is the same like for the influence of the inclination of slopes. The higher the inclination, the faster runoff generation. Besides there is a direct relation between runoff velocity and geometry of receiving channels. This means in general, with a decreasing of trench area but same surface roughness, runoff velocity increases. This means, preferably natural rested, rough drainage systems deflates runoff generation.
In Figures 4-4 and 4-5 the runoff quantity in percent of precipitation is plotted in relation of different stages of forest development in a deciduous wood. (I) deciduous forest without any roads, log trails, skid tracks or drainage trenches, (II) 3% roads with trenches at both sides, 14% log trails and skid tracks, (III) 6% roads with trenches at both sides, 14% log trails and skid tracks, (IV) 6% roads without trenches, 14% log trails and skid tracks, re-infiltration of drainage water into forest stand, (V) 2,5% roads with trenches at both sides, 7% cable-lines, (VI) 5% roads with trenches at both sides, 7% cable-lines, (VII) 5% roads without trenches, 7% cable-lines, re-infiltration of drainage water into forest stand. Results show overland runoff in a heavy summer rainfall with a precipitation of 70 mm within 4 hours for dry (in grey) and saturated (in black) initial soil conditions. Independent from the absolute

runoff values at the different test sites, there is a obvious increase in runoff with an increasing degree of forest development by roads with attendant trenches. Forest rationing with cable-lane method instead of log trails and skid tracks, conducts to a decrease of overland runoff. A re-infiltration of drainage water into forested area leads to an additional decrease of runoff generation. But this possibility depends on soil types an their infiltration capacity. At the Pfälzer-Wald with its sandy loam soils, this could be much better realized than at Soonwald with its loamy clay soils.

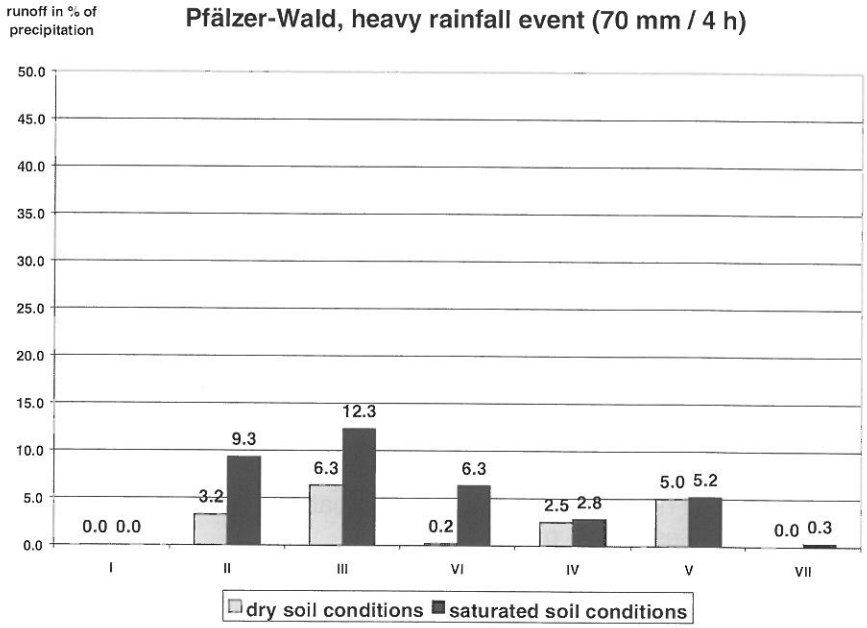

Figure 4-4: Simulation results of overland runoff during a heavy rainfall at Pfälzer-Wald for a deciduous forest with different stages of development (for specification of level I to VII see text above).

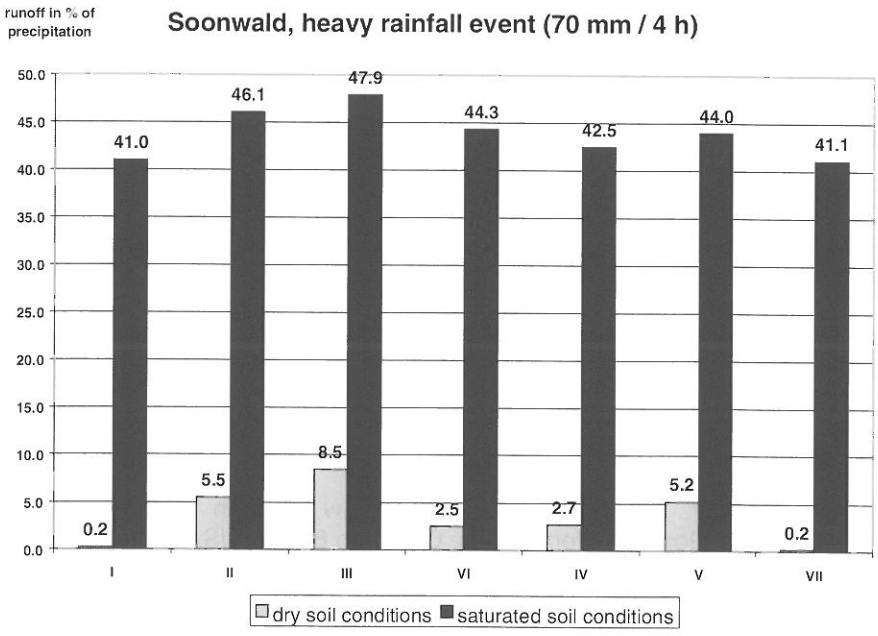

Figure 4-5: Simulation results of overland runoff during a heavy rainfall at Soonwald for a deciduous forest with different stages of development (for specification of level I to VII see text above).

5 CONCLUSIONS

The modelling results reflect the expected differences in water transport of the two investigated areas at Soonwald and Pfälzer-Wald. They demonstrate a dominant influence of natural given factors like geology, morphology, soil properties and climate on runoff generation. Especially pedological parameters, such as initial soil moisture, grain size distribution and density of soils as well as all factors controlling these parameters play a mayor role. Anthropogenic factors have lower influence on water transport, but they contain a high potential to improve retention capacity at forested catchments. Consequently the manner of forestry operation, especially the kind of road and lane construction and the density of road and drainage network, will directly affect runoff quantity. This means, a decrease of floods by an adjusted forestry is possible regarding suitable rationing methods, especially the avoidance of unregulated soil compaction and a minimum of forest development is suitable.
Simulation results are very encouraging and show that modelling runoff generation in dependence of forestry and hydrological measures is successful and can be used to contribute to a sustainable catchment area management.

REFERENCES

Bott, W et al. (2001): Modelling water retention at forest sites as a tool for water management. In C. Leibundgut, S. Uhlenbrook & J. McDonnell (eds), Runoff Generation and Implications for River Basin Modelling, Freiburg, 9-13 October 2000. Freiburger Schriften zur Hydrologie 13, S. 313-317, Freiburg

Carsel, R.F. & Parrish, R.S. (1988): Developing joint probability distribution of soil water retention characteristics. Wat. Resour. Res. 24(5), p. 755-769

Celia, M.A. et al. (1990): A general mass conservative numerical solution for the unsaturated flow equation. Wat. Resour. Res. 26(7), p. 1483-1496

Genuchten van, M.T. (1980): A closed form equation for predicting the hydraulic conductivity of unsaturated soils. Soil Sci. Soc. Am. J. 44, p. 892-898

Haar de, U. & Hoffmann, D. (ed.) (1982): Wasser aus dem Wald - Wasser für den Wald. Beiträge zur Hydrologie, Sonderheft 4, Kirchzarten

Hahn, H.J. & Friedrich, E. (1996): Die Gebirgsrandbäche: Abflußverhalten und Hochwasserschutz - Dargestellt am Beispiel der Queich. In M. Geiger (ed), Haardtrand und Weinstraße - Beiträge zur Landeskunde. Pfälzische Gesellschaft zur Föderung der Wissenschaften, p. 145-158, Speyer

Hildebrand, E.E. (1983): Der Einfluß der Bodenverdichtung auf die Bodenfunktionen im forstlichen Standort. Forstw. Cbl., 102, p. 111-125

Hornung, U. & Messing, W. (1984): Poröse Medien – Methoden und Simulation. Beiträge zur Hydrologie, Kirchzarten

Leonhard, J. (1999): Waldland Rheinland-Pfalz – Zahlen, Fakten, Übersichten. Lebendiges Rheinland-Pfalz, Heft 1/1999, Jahrg. 34/35, Mainz

Mahmood, K. & Yevjevich, V. (ed.) (1975): Unsteady flow in open channels. Vol. 1,2,3, Water Resources Publications, P.O. Box 303, Fort Collins, Colorado 80522, USA

Maurer, T. (1997a): Catflow - A physically based and distributed hydrological model for continuous simulation of catchment water dynamics, User Guide. Institute for Hydrology and Water Resources Planning (IHW), University of Karlsruhe

Maurer, T. (1997b): Physikalisch begründete, zeitkontinuierliche Modellierung des Wassertransports in kleinen ländlichen Einzugsgebieten. Mitteilungen des IHW 61, Universität Karlsruhe (TH)

Mitscherlich, G. (1971): Wald, Wachstum und Umwelt. Bd.2, Waldklima und Wasserhaushalt, 1. ed. J. D. Sauerländer's Verlag, Frankfurt am Main

Mitscherlich, G. (1977): Wald, Wachstum und Umwelt. Bd.1, Form und Wachstum von Baum und Bestand, 2. ed. J. D. Sauerländer's Verlag, Frankfurt am Main

Mualem, Y. (1976): A new model for predicting the hydraulic conductivity of unsaturated porous media. Wat. Resour. Res. 12(3), p. 513-522

Scheffer, F. & Schachtschabel, P. (1992): Lehrbuch der Bodenkunde, 12. ed. Enke, Stuttgart

Strahler, A.N. (1964): Qualitative geomorphology of drainage basins and channel networks. In Chow, van te: Handbook of applied hydrology, New-York

Tietje, O. & Tapkenhinrichs, M. (1993): Evaluation of pedo-transfer functions. Soil Sci. Soc. Am. J., 57, p. 1088-1095

Zehe, E. (1999): Stofftransport in der ungesättigten Bodenzone auf verschiedenen Skalen. Mitteilungen des IHW 64, Universität Karlsruhe (TH)

ASSESSMENT OF EXTREME FLOOD PRODUCTION MECHANISMS THROUGH POT ANALYSIS OF DAILY DATA

Pierluigi Claps[1], Francesco Laio[1] and Paolo Villani[2]

[1] Dipartimento di Idraulica, Trasporti e Infrastrutture Civili, Politecnico di Torino, C.so Duca degli Abruzzi 24, 10129 Torino, Italy, claps@polito.it; laio@polito.it

[2] Dipartimento di Ingegneria Civile – Università di Salerno, Via Ponte Don Melillo, 84084 Fisciano (SA), Italy, villani@bridge.diima.unisa.it

SUMMARY

As an attempt to improve flood risk prediction we investigate the relations between the stochastic processes of daily rainfall and runoff. We consider a simple stochastic model of the extreme precipitation in which the occurrences are mutually independent and the distribution of marks can be derived through the analysis of the Peak Over Threshold (POT) process. Our initial interest concentrates on the relationships between the mean annual number of rainfall and runoff peak events (Λ_p and Λ_q) at various thresholds: the mechanism of flood production and its changes are investigated by analysing the nature of these relationships. To this aim we consider that the watershed operates as a stochastic filter on the rainfall process, producing a filtered point process that reproduces occurrence and magnitude of floods. The analysis of the filter mechanism provides the relationships between stochastic parameters of maximum rainfall and discharge. Particularly, we consider a simple filter wherein the runoff peaks are produced after a volume abstraction on precipitation, which essentially limits the number of runoff events. Since Λ_p and Λ_q are parameters playing a significant role in Poisson-derived flood frequency distributions, we investigate the possible dependence of the obtained results on the hypothesis of Poissonian occurrences and on the distribution of marks.
We derived relations between the frequency of rainfall and flood events at varying thresholds for several observed series of rainfall and runoff. The different patterns of the basin transformation found seem to confirm the stochastic nature of the basin filter and its strong relations with the hydro-geologic and climatic characteristics of the basin.

Keywords: Floods, Rainfall, Extreme Events, POT Analysis.

1 INTRODUCTION

The research and application aspects related to regional flood frequency analysis have reached very good standards, but several controversial points still prevent the agreement on universally recognised procedures (see e.g. Bobée et al., 1993). Recent approaches agree on the necessity to maximise geomorphoclimatic information behind the flood formation mechanisms, either through models based on derived distributions (e.g. Iacobellis and Fiorentino, 2000) or by derivation of the flood curve by simulation (e.g. Hashemi et al., 2000).
Less attention has been given to the possibility of a direct statistical analysis of continuous rainfall and runoff time series, which can provide greater detail on the transformation mechanisms with respect to annual maximum series. In fact, additional information deriving from continuous daily records improves the knowledge of the base rainfall process and increases the number of observed flood peaks. This procedure therefore augments the possibilities of a data-based assessment of the hypotheses underlying the definition of a flood frequency distribution within a geomorphoclimatic framework.
The mentioned analysis can be carried out through the application of Peak Over Threshold (POT) techniques on daily rainfall and runoff records. Lang et al. (1999) recently pointed out pros and cons of POT-based flood frequency estimation. Main drawback of the technique is the difficulty to set objective criteria for the choice of the threshold values which, on the other hand, is a crucial point of the procedure. In this paper, analysis of continuous data is presented with a POT approach that allows one to naturally and objectively consider the threshold values. To this end, relations between the number of rainfall and runoff event over a given threshold have been linked to the magnitude of the events themselves, investigating the attenuation provided by the basin over the entire range of runoff peak values.

This data-based approach utilises statistical relations between rainfall and runoff peaks to explore the interaction between the empirical distributions of the two variables in different classes of drainage basins. The envisaged statistical structure is compatible with the estimation of parameters related to the geomorphoclimatic configuration of the basin and the consequent transfer of hydrologic information towards ungauged basins.

2 POT ANALYSIS

2.1 Procedures of peak selection

For a given catchment we consider the time series of daily rainfall and discharge: since both variables vary randomly in time, they can be represented as continuous stochastic processes (sampled at the daily time scale). The first step towards an analysis of the relationship between extreme rain and flood events is to select, from the continuous time series, those values that can reasonably be considered as peak events. The usual procedure for peaks selection is to retain only those peaks that exceed a certain threshold value s_0, with a procedure known as Peak Over Threshold, or POT (e.g., Todorovic, 1978; Madsen et al. ,1997; Lang et al., 1999). Each peak event is considered to last for the whole time period the discharge (or rainfall) remains above the threshold (see Figure 2-1).
This procedure of peaks selection presents some well-known difficulties in the definition of the base level s_0 (e.g., Lang et al., 1999; Robson, Reed, 1999). With low s_0 values nearly the whole time series is above the base level and only very few peaks are identified (in fact, if the discharge never downcrosses s_0 a unique peak is found) while with large s_0 only few very high peaks are retained. To have available a significant number of peaks, s_0 should be taken at intermediate values, but this arises problems of lack of mutual independence among the peaks (that is a prerequisite to any statistical frequency analysis). In the usual POT procedure it is often imposed that a peak is retained only if it is separated from the previous one by a given number of days and if the discharge before the event drops well below s_0. In addition, actual use of these criteria varies from one case to the other, with the result that a degree of subjectivity is added to the procedure.

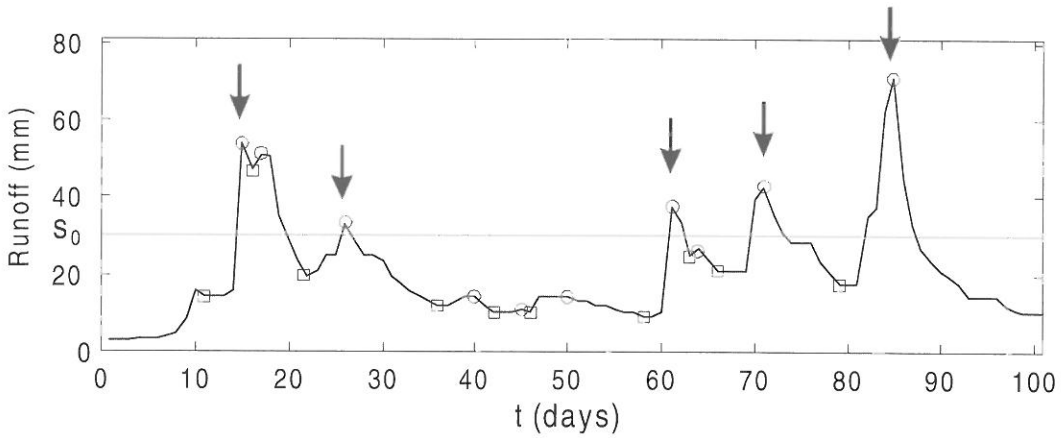

Figure 2-1: Sketch of the procedure for peaks selection from the time series of daily runoff. Arrows represent the peaks selected with the usual POT procedure; open circles and squares are the local maxima and minima used in the alternative procedure for peaks selection.

To limit the subjective characters of the procedure, we decided to adopt an alternative two-steps method: (i) the events are identified in correspondence to all the local maxima of the time series (open circles in Figure 2-1); (ii) the magnitude of each event is then assigned in two alternative ways: (a) the actual ordinate of the maximum (method M1, gray bars in Figure 2-2), or (b) the difference between the maximum and the first minimum preceding the event (method M2, black bars in Figure 2-2). The first choice has the advantage that the actual value of the discharge is preserved, while with the second method the mutual dependence of subsequent peaks is reduced. For example, consider two peaks very close in time (e.g. the first and the second in Figure 2-2): the magnitude of the second peak can result artificially increased by a value that depends on the intensity of the previous event, which has not yet exhausted its effects on the basin. Alternatively, if the ordinate of the minimum were subtracted, the mutual dependence would be eliminated (however, other sources of correlation, due for example to rainfall persistency, can still remain). As such, M2 events do not strictly represent the

real discharge; rather, they approximate the effective rainfall component, i.e. the fraction of rainfall that becomes runoff within one day. Both M1 and M2 methods will be employed in the following of the paper.

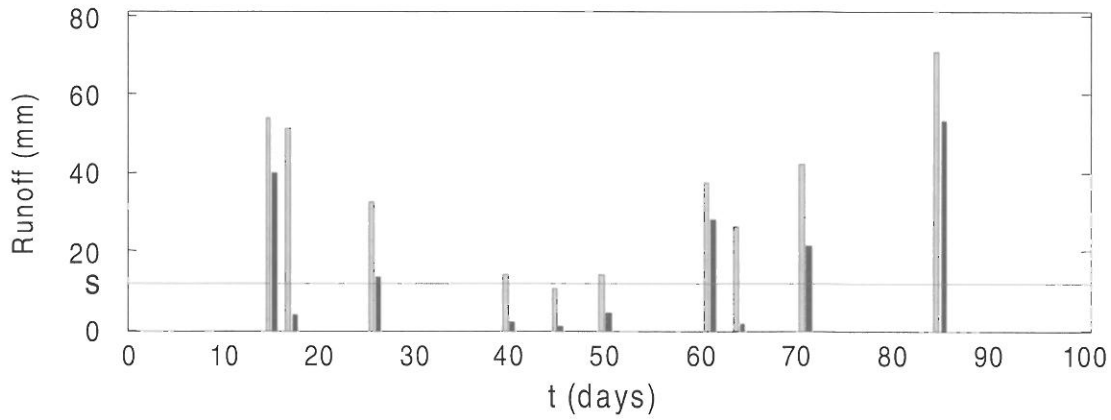

Figure 2-2: Marked point procss obtained after peak selection from the discharge time series shown in Figure 2-1. Gray bars: method M1; black bars: method M2.

2.2 Basic statistical relationships and their conditions of validity

Whatever procedure of peak selection is chosen, the continuous stochastic process of daily runoff is transformed into a marked point process (Figure 2-2), defined by the two random variables $n_0(\Delta t)$ (number of peaks in an arbitrary time interval of fixed length Δt) and x (magnitude of the event of discharge or rainfall). We will show that all the information necessary for an analysis of the flood and rainfall extremes is contained in these two variables.
Consider the probability distribution of the magnitude x of the peaks, $F_X(x)$: this distribution can be related to the frequency of occurrence of the peak values. We define first the reference frequency of the flood or rain events, as the expected value of the number of peaks occurring in one year:

(1) $$\Lambda_0 = \mathrm{E}(n_0(\Delta t = 1 \text{ year}))$$

where E( ) indicates expectation. It is then possible to retain only those peaks of the marked point process that exceed a threshold s (see Figure 2-2), and consider their average number in one year, defined as $\Lambda(s)$. Using the same definition given in Equation (1), $\Lambda(s)$ can be denoted as

(2) $$\Lambda(s) = \mathrm{E}(n_s(\Delta t = 1 \text{ year}))$$

where $n_s(\Delta t)$ is the number of marks in Δt with magnitude $x \geq s$. Notice that the $\Lambda(s)$ value in Figure relevant when low thresholds are considered, because the flow component eliminated with the method M2 can represent a significant portion of the measured runoff (see Figure 2-1, peaks between days 30 and 50).
There exist a simple explicit relationship between the frequencies $\Lambda(s)$ and the correspondent CDF's of the magnitudes x: in fact, for time-discrete processes, as in our case, the probability $1- F_X(s)$ that a given event is greater than s is given, by definition, by the number of events exceeding the threshold s divided by the total number of events:

(3) $$\frac{\Lambda(s)}{\Lambda_0} = 1 - F_X(s) = \frac{1}{T(s)}$$

where $T(s)$ is the return period of s in years. This relationship is fairly general under some basic requirements that are the same as those implying the uniqueness of the CDF: 1) independent mark values; 2) stationary marked point process; 3) identically distributed marks.
The necessity of the third condition is understandable, and requires due care, while the sense of the first two deserve specific attention. The independency issue is crucial, since some confusion may derive from the bivariate nature (i.e. marks and occurrence) of the marked point process defined with the POT procedure.

Consider first the counting process by itself, without consideration of the presence of the marks. A possible representation of the process is as a sequence of experiments (e.g., one for each day when a daily time scale is considered) classified as successes when an event occurs and as failures when it does not. Independency in the occurrences requires that the experiments are independent, i.e. that the probability of success of the n-th experiment is not affected from the successes or failures of the previous (n-1) experiments. This is called *memoryless property*. However, Equation (3) is valid also for processes that do not possess the memoryless property, because it strictly derives from the definition of the CDF of a time-discrete process. It follows that, even though only few distributions of the number of occurrences $n_0(\Delta t)$ (or $n_s(\Delta t)$) possess the memoryless property (for example the Poisson and the binomial distributions), Equation (3) is valid for any distribution of $n_0(\Delta t)$. For example, in a point process where a success and a failure regularly alternate the occurrences are far from independent, but, provided that the magnitude of the events are independent, Equation (3) is easily seen to be valid. In short, the hyphothesis that the occurrences are Poisson distributed is not necessary for the validity of Equation (3), but it can still be very important for relating the POT distribution, $F_X(x)$, to the corresponding annual maxima distribution, $G_{AM}(x)$. In fact, in case of Poisson distributed occurrences the following relationship holds (e.g., Todorovic, 1978)

$$G_{AM}(x) = e^{-\Lambda_0(1-F_X(x))} \tag{4}$$

From Equation (4) derives that an exponential distribution of the marks produces Gumbel-distributed annual maxima, while the GEV distribution is obtained with Pareto-distributed magnitudes of the events (e.g. Madsen et al., 1997).
Even more important for validity of Equation (3) is the independence among the magnitudes of the events: we clarified in Section 2.1 possible methods to minimize the chance of selecting correlated peaks.
Given independency, the stationarity requirement is not fundamental to the definition of (3), since an analogous equation accounting for the time dependency can be easily written as

$$\frac{\lambda(s,t)}{\lambda_0(t)} = 1 - F_X(s,t) \tag{5}$$

where $\lambda_0(t)$ represents the rate of occurrences of the events, i.e. the mean number of events in the time interval $[t,t+\Delta t]$, with $\Delta t \to 0$, while $\lambda(s,t)$ is the correspondent rate for the events with magnitude exceeding s. The relationship between the rates λ and the frequencies Λ is

$$\Lambda(s,t) = \int_t^{t+\Delta t} \lambda(s,u)du \tag{6}$$

When the stationarity condition holds, one has $\Lambda(s)=\lambda(s)\Delta t$ and $\Lambda_0=\lambda_0 \Delta t$, and Δt cancels out from the ratio on the left hand side of Equation (5), giving Equation (3). At a first instance we have assumed stationarity, using Equation (3) at a yearly time scale even in presence of different climatic regimes for the italian rivers (see e.g. Claps and Villani, 2001). Otherwise, one may divide the dataset in m parts representing the different climatic regimes and apply Equation (5) to each subset of data: In this second case one ends up with m different CDF's of the magnitudes of the peaks. Typically m=4 is sufficient even for climates with strong seasonalities: in an application to daily rainfall in Southern Italy, Sirangelo and Iiritano (1999) show that m=2 could be a good compromise between detailed time series description and practical calibration. However, when the method M2 is used for peaks selection, a strong seasonal component of the discharges, due for example to snow melting baseflow, is eliminated.

3 ANALYSIS OF FLOOD PRODUCTION MECHANISMS

Peak selection procedures detailed in Section 2.1 are applied in the following to the time series of rainfall p and runoff q (expressed in *mm*). The average number of rain events in one year defines the value of Λ_{0p} while Λ_{0q} defines the average number of flood events. It is then possible to find the number of rain and flood events with magnitude exceeding s, obtaining two different relationships between s and the frequencies of occurrence, $\Lambda_p(s)$ and $\Lambda_q(s)$. These relationships, along with the Λ_{0p} and Λ_{0q} values, completely define the empirical CDF's of rainfall and discharge peaks by means of Equation (3). An example of the possible shapes of the above relationships is given in Figure 3-1, where a logarithmic scale is used for the vertical axis to allow a greater detail in the low frequencies

zone, more representative for the extreme events, and also to easily recognise if the probability distributions of the magnitudes are exponential, in which case they would plot as straight lines. The two frequency-threshold relations for rainfall and discharge are then compared in order to analyse if there are changes in the flood production mechanisms that can be related to the frequency of occurrence of the events. First, a value λ for the frequency of the events is set; then the corresponding thresholds, s_q and s_p are found for rainfall and runoff (see Figure 3-1).

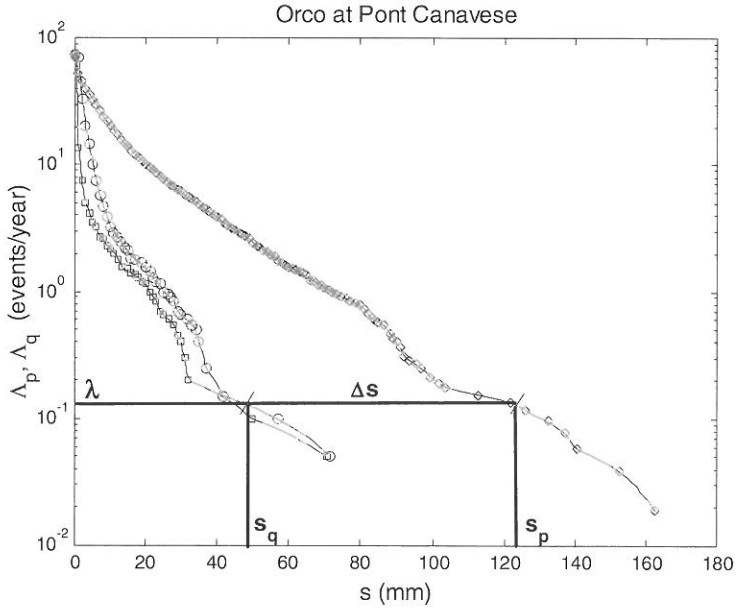

Figure 3-1: Graphical representation of the procedure adopted for obtaining the $\Delta s(\lambda)$ relationship. Diamonds represent the frequency-threshold relation for the rainfall events; circles and squares are related to runoff events obtained with methods M1 and M2 for peaks selection, respectively.

The difference between s_p and s_q represents the rainfall loss for that given frequency, namely

(7) $$\Delta s(\lambda) = s_p(\lambda) - s_q(\lambda)$$

The meaning of $\Delta s(\lambda)$ can be more clear if one considers a simple mechanism of runoff production. Introducing Φ as an abstraction term ($P - Q$), it can be demonstrated that Φ equals Δs for each λ, provided the rainfall-runoff transformation is deterministic. For this reason, Δs is assumed as a meaningful control variable in the comparison of rainfall and runoff frequency distributions. In addition, consideration of Δs makes it possible the above comparison even when the time series of the two variables (P and Q) are measured in non-overlapping years, which often happens when short time series of daily rainfall and runoff are available. This is actually the case of the application presented in the following section. Another important advantage of this procedure is that it works at the coarse level of average values (see Equation (2)), thus eliminating the problem of correctly matching the single rainfall and discharge peaks working at the scale of the event.
Working at equal frequency values λ hampers the usage of an analogous of this procedure with annual maximum data, because in that case the actual frequencies of occurrences are found only in an indirect manner using relations valid in special cases (e.g., Equation (3) and (4) when the occurrences are Poisson distributed).

4 CASE STUDY

35 time series of daily data of runoff and areal rainfall are analysed to evaluate the possibility of highlighting different flood production mechanisms. Drainage basins are mostly located in the North-West of Italy, in the Piemonte region. The Alps influence the majority of basins in the considered group, but some basins are located in a different (Apennine) context. Although not really covering the

entire climatic and geologic variety available in Italy, this datasets represent a significant starting point with regard to the mechanisms of flood formation they show.
In some cases, available datasets are not sufficiently long to rely on the resulting information. We decided that reliable data should present a $\Lambda(s)$ relationship comparable in shape to that obtained from the analysis of the annual maxima of rainfall and runoff, as resulting from an independent, and tested, dataset (SIVAPI, 1999).
Evaluating the frequency-threshold diagram ($\Lambda(s),s$) and the corresponding loss-frequency plot (Δs, $\Lambda(s)$), we found basin responses which can be grouped as follows:
i. the loss Δs increases steadily with decreasing frequencies (Figure 4-1b);
ii. Δs reaches a maximum for rare events and then decreases (or reaches a plateau) (Figure 4-1d);
iii. the relationship between Δs and frequency presents multiple curvatures (Figure 4-1f).

Trying to understand more quantitatively the physical mechanisms underlying these different patterns, one may analyse simple theoretical models of the rainfall-runoff transformation. The simpler possibility is to consider the flood amount (in mm over a day) produced by a constant abstraction Φ on the rainfall depth P, namely $Q = P - \Phi$. In this case the loss Δs coincides with the abstraction Φ, and remains constants with varying frequencies. This model seems to be able to interpret only small portions of the loss-frequencies relations (e.g., the plateau for intermediate frequencies in Figure 4-1f).
A somewhat more general model considers a linear relationship between rainfall and runoff: $Q = \alpha (P - \Phi)$, where α is a routing coefficient, to be taken in the range [0,1], that depends on climate, size and geomorphological characteristics of the basin. In this case the abstraction Φ does not correspond to the actual loss Δs, and the latter increases with decreasing frequencies, because the difference is proportional to P. All patterns showing increasing Δs up to low frequencies are compatible with such simple model, but the variety of curves found require further analyses on the actual role of the coefficient α.
To discriminate among the above patterns one can also compare the mutual shape of the $\Lambda(s)$ curves for the rainfall and runoff processes. The point is to evaluate if and how these curves follow different patterns and to relate them to the cases described above. We will refer to type **a** curves for those showing a linear shape in the semilog $\Lambda(s)$ diagram, to type **b** for those presenting a marked upward curvature in the diagram (high skewness) and to type **c** curves for the case of downward curvature. Examples of **a** and **b** curves are given by the relationships for precipitation in Figure 4-1a and 4-1e, respectively.
The differences in basin response (i to iii above) can therefore be referred to three main categories of rainfall and runoff curves:
i) Almost-linear response, with both rainfall and runoff following the type **a** pattern. A typical example is given in Figures 4-1a and 4-1b for river Rutor, in Nortwestern Italy, having area of 49 km^2 and average elevation of 2616 m a.s.l. The behaviour here can be interpreted with a linear relationship between precipitation and discharge. Many high-elevation basins among those considered seem to belong to this category. Note the marked difference on the low peaks between curves produced by the M1 and M2 procedures, due to the removal of the glacial baseflow in summer. The case of rainfall and runoff both of type **b** is also present but does not necessarily reflects simple linearity in the response.
ii) "parabolic" response, with type **a** rainfalls and type **b** runoff. An example is given by river Grana (Figures 4-1c and 4-1d), again in Northwestern Italy (area of 109 km^2 and average elevation of 1540 m a.s.l.). A marked change in the floods generation mechanism seems to occur here, with the magnitude of the rare floods that results strongly increased by the reduced absorption of rainfall by the soil. Possible causes for this behaviour are changes in the runoff production mechanism (from an infiltration capacity to a saturation from below mechanism) or differences in the areal coverage of precipitation when "normal" or rare events are considered. The geomorphological and climatic characteristics of the basins belonging to this category are currently under investigation with data from additional basins.
iii) "mixed" nonlinear response, with type **b** rainfalls and type **a** runoff. An example is river Agri (area of 174 km^2 and average elevation of 933 m a.s.l.) in Southern Italy (Figures 4-1e and 4-1f). In this case the loss-frequency relation tends to assume one of the shapes described above, but then deviates upward due to the greater intensity of the extreme rain events. The fact that Δs increases again after it has reached stability shows that the capacity of the soil was not exhausted yet notwithstanding the downward curvature of the $\Delta s(\lambda)$ relationship. This requires a very high absorption capacity of the soil, which is found on highly permeable basins (the river Agri basin, for example, is mainly constituted by fractured limestone).

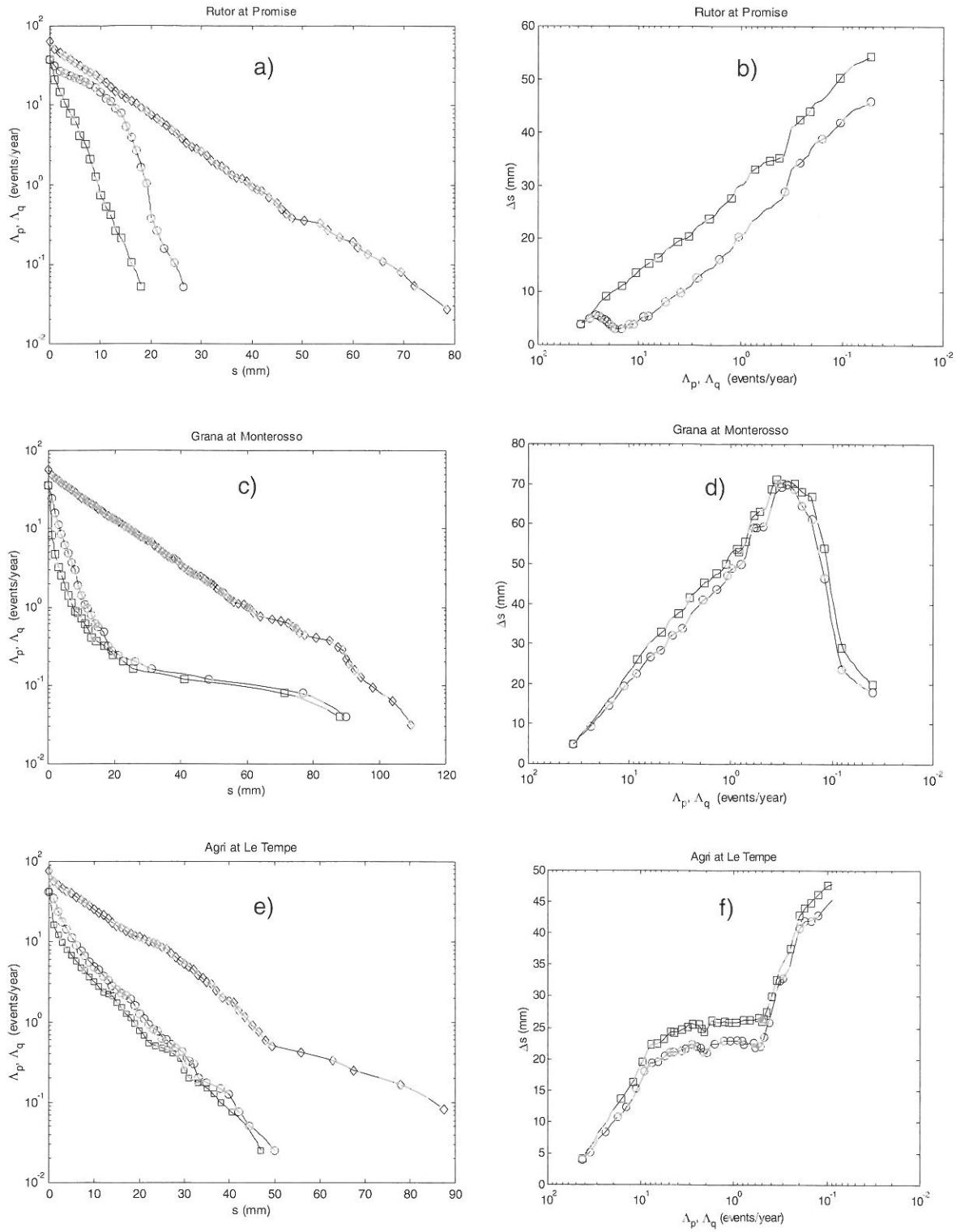

Figure 4-1: Left panels report examples of the frequency-threshold relationships for rainfall (diamonds) and runoff; right panels show relations between the current loss and the discharge frequency (in all cases, circles correspond to method M1 for peaks selection, squares to method M2). Note the reversed scale in the diagrams on the right.

Figure 4-1 deserves further comments. Notice how the shape of the relationships in the right panels tends to be insensitive to the choice of the peak selection procedure (method M1 or M2). This is common to all of the data analysed and is quite important. In fact, we have seen that method M2 minimises the problems deriving from seasonal components and from the possible lack of independence among the marks. The fact that the relations found with method M1 are very similar to those obtained with method M2 demonstrates that, in all the series considered here, seasonality and mutual depen-

dence do not really influence the results. The case of river Rutor, for instance, shows that a marked seasonality in the runoff can produce a deviation only in the lower part of the relationship (Figure 4-1b). The method adopted in this paper seems therefore rather robust.
A second important comment regards the fact that only part of the diagrams in Figures 4-1b, 4-1d and 4-1f are actually meaningful in terms of design floods. In other words, the left part of the diagrams concerns very frequent events, in which the increase of the loss at decreasing frequencies corresponds to the increasing absorption capacity of the soil with not very intense rainfalls. The interesting part of the figures, in terms of annual maxima, are instead on the side of low frequency events (right side). This fact must be carefully considered when using models of transformation that look unsuitable in the side of low frequencies.

5 CONCLUSIONS

The Peak Over Threshold analysis of continuous rainfall and runoff daily data presented in this paper aims to highlight phenomenological mechanisms dominating the flood formation in different physiographic and climatic contexts. An objective procedure was devised for identification of the rainfall and runoff peaks and a simple method for removal of runoff dependence and baseflow effects was proposed. Scope of the analysis is to demonstrate that the relation between the number of flood and rain events exceeding different thresholds can provide meaningful information on the basin transformation. Qualitative information is deduced by drawing diagrams of loss variation versus the frequency of the observed events; quantitative information can be deduced using simple models of the transformation and estimating relevant parameters. The latter step is currently being investigated and is only quickly sketched here.
Markedly different patterns of runoff formation were found on a set of 35 rainfall and runoff time series recorded in Italian rivers, and exploratory justification were provided for their shapes, using also rainfall and runoff frequency curves. These patterns show differences in the mechanisms of basin transformation not easily recognisable from observation of the annual maximum frequency curve. Simple models of constant and proportional abstraction were preliminarily suggested for partial explanation of the observed patterns; derivation of analytical curves from these models under different hypotheses is currently under way.
In view of a thorough specification of the patterns of non-linearity in the rainfall-runoff transformation presented in this paper, climatic issues also require to be integrated in the procedure, being the climatic regime an important source of dissimilarity among basins. Seasonal analyses performed on the same class of data (e.g. Merz et al., 1999; Claps and Villani, 2001) can possibly provide a significant added value to the results shown here.

REFERENCES

Bobée, G. et al. (1993): Towards a systematic approach to comparing distribution used in flood frequency analysis, J. Hydrol., 142, 121-136.

Claps, P., Villani, P. (2001): Using rainfall and runoff peaks over threshold in the analysis of flood generation mechanisms, Proceedings of the 3rd EGS Plinius Conference, held at Baja Sardinia, Italy, October 2001 (in press).

Hashemi, A. M. et al. (2000): Climatic and basin factors affecting the flood frequency curve: PART I -A simple sensitivity analysis based on the continuous simulation approach, Hydrology and Earth System Sciences, vol. 4, no. 3, pp. 463-482.

Iacobellis, V., Fiorentino, M. (2000): Derived distribution of floods based on the concept of partial area coverage with a climatic appeal, Water Resour. Res., 36(2), 469-482.

Lang, M. et al. (1999): Towards operational guidelines for over-threshold modeling, J. Hydrol., 225, 103-117.

Madsen, H. et al. (1997): Comparison of annual maximum series and partial duration series methods for modeling extreme hydrologic events. 1. At-site modeling, Water Resour. Res., 33(4), 747-757.

Merz, R. et al. (1999): Seasonality of flood processes in Austria. In: "Hydrological Extremes". Proceedings of the IUGG 99 Symposium, Birmingham. IAHS Publ. No. 255, pp. 273-278.

Robson, A., Reed, D.W. (1999): Flood estimation Handbook. Vol. 3: Statistical procedures for flood frequency estimation, Institute of Hydrology, Wallingford, UK.

Sirangelo, B., Iritano G. (1999): I processi puntuali nello studio delle occorrenze delle precipitazioni intense, L'Acqua, 6, 35-60 (in italian).

SIVAPI (1999): Sistema Informativo per la Valutazione delle piene in Italia, http://www.cs.cnr.it/ GNDCI/ SivapiNew.htm (date of access, Mar. 2002).

Todorovic, P. (1978): Stochastic models of floods, Water Resour. Res., 14(2), 345-356.

FLOOD GENERATION IN THE MIDDLE MOUNTAINS OF NEPAL

Pradeep M. Dangol[1], Juerg Merz[1/2], Rolf Weingartner[2]

[1] *PARDYP*/International Centre for Integrated Mountain Development, Kathmandu, Nepal

[2] *PARDYP*/Department of Geography, University of Bern, Switzerland

SUMMARY

Flooding in Bangladesh and the plains of Northern India has often been accredited to the land management practices of the Himalayan farmers and deforestation in the populated areas of the highest mountain range. These arguments however are mainly based on myths and many authors showed, that other causes are more important in the generation of floods in these areas. The mentioned studies were mostly conducted in the plains themselves and hardly any studies in this respect from the mountainous areas of the Himalayas exist. The People and Resource Dynamics of Mountain Watersheds in the Hindu Kush-Himalayas (PARDYP) project is focusing on process analyses in order to understand flood generation on different land use and under the present conditions and land management practices of the heavily populated areas of the Middle Mountains in the Himalayas.
The presented paper is giving an introduction to the measurement network setup and discusses preliminary results on flood generation in the Middle Mountains in Nepal. It focuses on event analysis on the different spatial scales according to the principle of the nested approach. The attempt of establishing valid relationships between rainfall and runoff generation for the prevailing conditions is discussed. This investigations form the basis for the estimation of floods in a region where there is a considerable lack of data.

Keywords: Flood generation, scale, event analysis, Nepal Middle Mountains

1 INTRODUCTION

Flooding and subsequent stream bank erosion is a severe problem in the foothills and the adjacent plane areas of the Himalayas. To what extent these processes are accelerated and enhanced by human interference is still a major point of discussion (Ives and Messerli, 1989). Although different authors have stressed the importance of the practices of the Himalayan farmers in the generation of flood events, opinions about the importance of these practices in this process differ widely. Deforestation in the populated areas of the Himalayas is often blamed to be the main cause for flooding downstream, e.g. Bangladesh (Hossain et al., 1987; Choudhury, 1989). Other authors (e.g. Agarwal and Narain, 1991) argue that the conversion of forest to terraced land actually decreases the effect on flooding and the impact of the conversion of forest to grazing land is minimal on a larger scale. The main point of disagreement is the effect of these changes at a large scale. Kiersch (2000) reviewed a number of studies and concluded that a change of land use at the micro scale may only affect lower meso-scale catchments, but may be undetectable on a macro scale. Hofer (1998a) showed that the flooding in Bangladesh is a regional effect and may not be attributed to the practices of the Himalayan farmers. Rowe et al. (1997) concluded that there is evidence of effects of land use change on small watersheds. However, for larger scale this relationship has to be established. Agarwal and Narain (1991) further argue that the effect of land use change is only evident on small to medium events. Large events are inevitable and people have to learn to cope with it. The same was shown by Merz et al. (2000a) in a watershed of the Nepal Middle Mountains where during large events land use did not play a major role in flood generation.
This paper is showing some preliminary results on the generation of high flow events at the watershed scale. The contribution from different spatial levels (sub-catchments and plots) is determined and compared with the flow events at the main hydrological station. It is of interest to determine to what extent interventions at plot level are successful in prevention of flooding. The question of the influence of different land use is addressed and thus the influence of different farming practices investigated.
The key questions in this paper are
- under what conditions runoff is generated at the plot scale;
- under what conditions are larger floods generated at the outlet of the watershed.

2 THE STUDY AREA

The Jhikhu Khola watershed with a size of 111.4 km^2 is located about 45 km east of Kathmandu on the Araniko Highway in Kavrepalanchowk District, Nepal. A network of meteorological and hydrological stations was established during 1992 and continuously upgraded and reviewed (Figure 2-1).

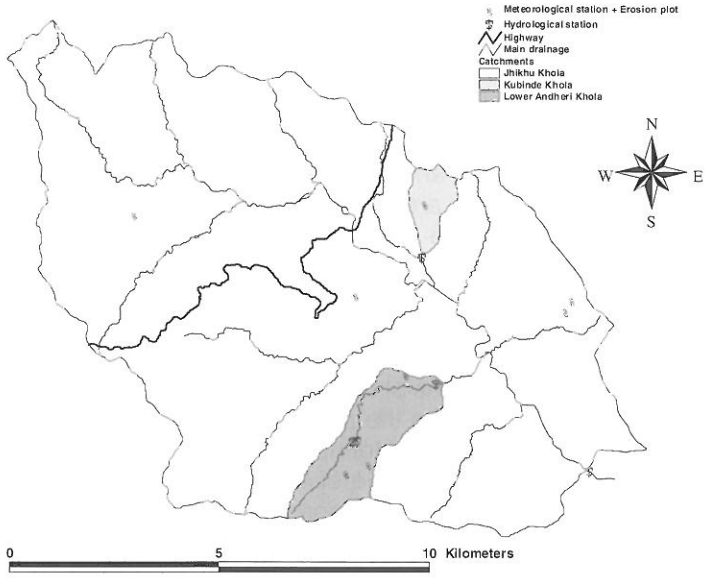

Figure 2-1: Measurement Network of Jhikhu Khola Watershed.

The network was set up according to nested approach principles as described in detail in Hofer (1998b). A total of 5 hydrological, 11 meteorological and 8 erosion plots are monitored regularly. For purposes of this study, the sub-catchments on the north-facing slope, the Lower Andheri Khola sub-catchment (site 2) and the Kubinde Khola sub-catchment (site 13) were chosen.

Table 2-1: Characteristics of Monitored Sub-catchments in the Jhikhu Khola Watershed.

Site No.	Catchment (Site Name)	Catchment Size [km^2]	Alt. Range [m asl]	Land cover [%]	
1	Jhikhu Khola watershed (Main Hydro Station)	111.4	790-2200	Khet: 17 Bari: 38 Forest: 30	Grass: 6 Shrub: 7 Other: 3
2	Andheri Khola sub-catchment (Lower Andheri Khola)	5.4	850-1700	Khet: 7 Bari: 37 Forest: 40	Grass: 8 Other: 8
13	Kubinde Khola sub-catchment (Kubinde)	1.5	850-1000	Khet: 14 Bari: 38 Forest: 34	Grass: 3 Other: 10

Note: Khet = irrigated agricultural land Bari = rainfed agricultural land

Table 2-1 shows the key characteristics of the entire watershed and the sub-catchments. Erosion plots, each monitoring between 50 to 100m^2 of either degraded or rainfed agricultural land, have been established within the sub-catchments. For this study all plots with complete data series since 1997 were chosen for comparison. Table 2-2 records the important physical aspects of the Jhikhu Khola erosion plots.

Table 2-2: Characteristics of Erosion Plots in the Jhikhu Khola Watershed.

Site No.	Site Name	Land cover	Soil Type	General Slope [deg]
4	Baghkhor	degraded grazing	red	11.5
6	Bela	rainfed agriculture	red	20.4
14a	Kubindegaun	degraded	red	15.0
16	Bhetwalthok	rainfed agriculture	non-red	6.7

Discharge from the sub-catchments was determined indirectly by measuring water level and subsequent calculation of discharge by using a rating curve. At the main station, water level is measured digitally by means of a pressure transducer and logger (a Kern FL-2) which is recording values at 5 minute intervals during monsoon (June to September) and at 15 minute intervals during the rest of the year. The other stations are equipped with pressure sensors connected to SmartReader loggers recording data at a 2 minute interval. Readings from the equipment are cross-checked with daily readings of staff gauges by local readers. Discharge measurements for the establishment of the rating curves are done by means of current metering.
Rainfall data is derived from 8" diameter tipping buckets of 0.2mm capacity per tip. Each event of ≥0.2mm is recorded on a HOBO logger. This data is cross-checked with the data from ordinary daily 8" diameter storage rain gauges.

3 HYDROLOGICAL CONDITIONS DURING THE PERIOD OF INVESTIGATION 1997 TO 2000

For the purpose of this study data from the period 1997 to 2000 was used. Figure 3-1 shows a comparison of the four years in terms of rainfall at the main meteorological station and in terms of discharge at the main hydrological station.

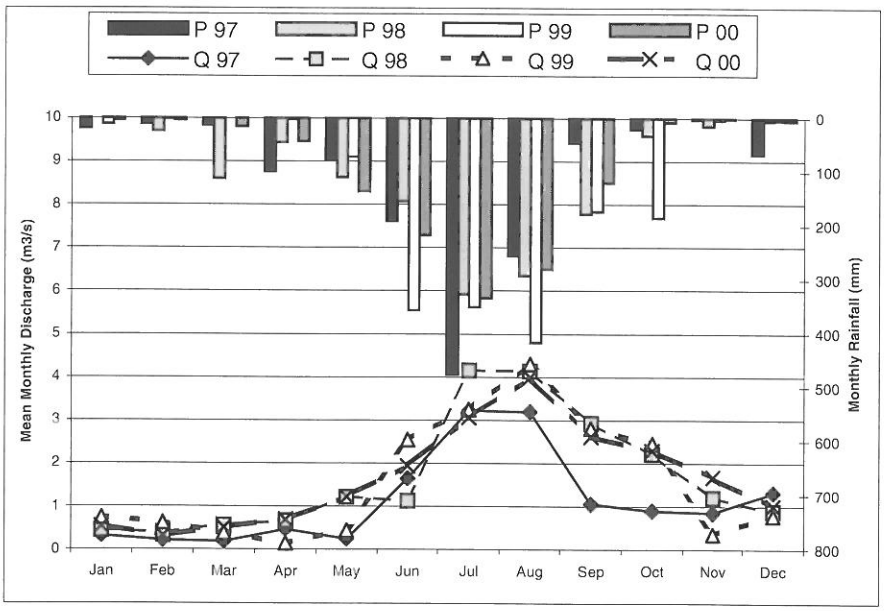

Figure 3-1: Comparison of monthly discharge for 1997 to 2000 at Main Hydrological Station and monthly rainfall at Main Meteorological station in Tamaghat.

The rainfall and discharge patterns show a distinct monsoonal pattern with maximum rainfall/discharge during July and August. About 80% of the annual precipitation is expected in the monsoon season lasting from June to September (Merz et al., 2000b). The time of pre-monsoon between March and May is very dynamic with heavy downpours and often destructive effects in terms of surface soil loss. 50 – 90 % of the annual surface soil loss occurs during this season (Carver and Nakarmi, 1995).

4 RUNOFF EVENTS IN EROSION PLOTS

The main land use in the Jhikhu Khola watershed is rainfed agricultural land (38% of the total area) with outward sloping terraces followed by forest (30%) and irrigated agricultural land (17%) (Table 2-1). The remaining is grassland (6%), shrub (7%) and other land use, e.g. settlements, roads and land slides (3%). 7 % of the watershed area is degraded. From the point of view of runoff generation the most likely contributors to flooding are rainfed agriculture, grazing and degraded lands. Irrigated land with inwards sloping terraces accumulate water (Agarwal and Narain, 1991) and act as deposition zone for sediment (Carver, 1997). Herewith they are less likely to contribute to runoff generation. Well-managed forests likewise reduce peak flows at the micro and lower meso scale (Bruijnzeel and Bremmer, 1989).
In the following the results from the erosion plots on rainfed agricultural land and degraded areas, which used to be grazing land, are discussed. Figure 4-1 shows the seasonally disaggregated data from four erosion plots on daily basis.

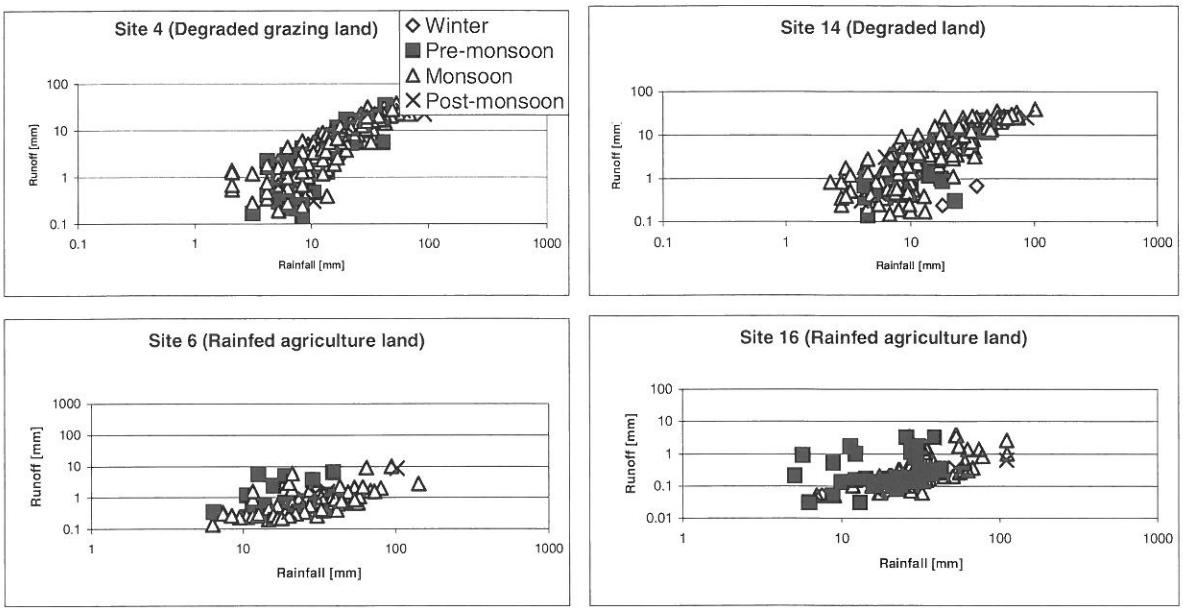

Figure 4-1: Daily rainfall versus daily runoff on degraded plots (sites 4 and 14) and on rainfed agricultural land (sites 6 and 16). Note: graphs are in log-log scale.

In all plots a distinct relationship between the daily amounts of rainfall with the daily runoff can be established. Runoff rates on degraded plots are generally higher with the highest events well over 10 mm. On agricultural land the highest measured rates were between 8 and 10 mm. Thresholds of rainfall to produce runoff are lower on degraded land than on rainfed agricultural land. It is estimated to be 2 mm rainfall on degraded sites and 5 mm on rainfed agricultural land. It may surprise that as large events as 141mm (28 june1999) produced only 3.2 mm runoff at site 6. This particular case can be attributed to the afact that two days earlier on 26 june 1999, the farmer weeded and hewed the plot, which resulted in decreased runoff.This can be observed in many case. In general runoff coefficients are very low on agriculture land, between 0.01and 0.44, on degraded land the runoff coefficient up to 0.74.
While in degraded sites seasonality does not seem to have any effect, on rainfed agricultural plots pre-monsoon rainfall events seem to yield higher runoff rates than events of the remainder of the year. The seasonality can be explained with land management practices (field preparation and maize planting) and changes of vegetation cover. Typically the fields are prepared after the first pre-monsoon rains at the end of April to early May.

It can be summarized that the
- degraded lands are more prone to runoff generation than rainfed agricultural land
- degraded lands yield higher runoff rates than rainfed agricultural lands
- degraded lands do not show seasonal effects
- rainfed agricultural lands are more prone to high rates of direct runoff during pre-monsoon than during the remainder of the year

5 INITIAL IDEAS ON FLOOD GENERATION AT THE MAIN HYDROLOGICAL STATION

For the purpose of investigating the connection between the processes on the plot scale and the processes at the watershed scale only the 20 largest events at the outlet of the watershed at site 1 (hydrological station) were chosen (Figure 5-1). The selection of the cutoff point at $10m^3/s$ is arbitrary.

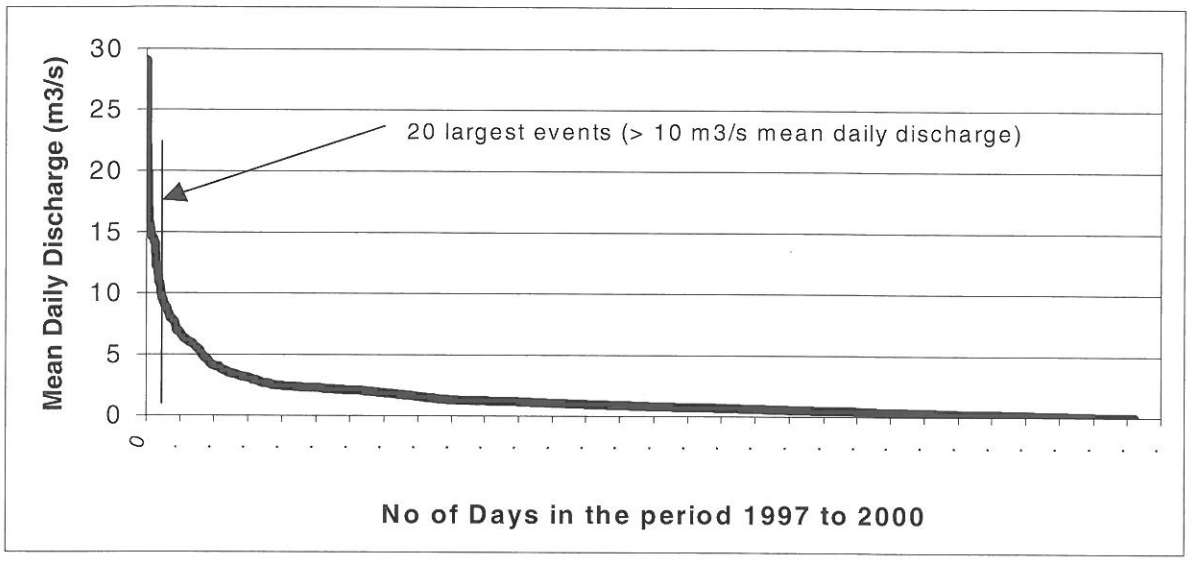

Figure 5-1: Daily discharge at the main hydrological station, Jhikhu Khola watershed.

Only two sub-catchments on the north and the south facing slopes of the watershed are intensively monitored, while the entire western part of the watershed is not instrumented. For investigations of processes at different scale therefore only these events at site 1 (outlet of the watershed) were selected with a clear contribution from the intensively monitored areas. Certain events have watershed-covering rainfall, while others only have intense rainfall in certain sub-catchments. Figure 5-2 shows the rainfall distribution over the entire watershed of two large events at the outlet of the watershed. Event A on September 8, 1998, the 6th largest event at the main station was triggered by rainfall in the upper and northwestern parts of the watershed. In the intensively monitored areas there was only around about 20mm of rainfall during this event. During event B on July 1st, 1997, there was heavy rainfall mainly on the north facing slopes including the monitored sub-catchments. This led to large contribution of this area to the largest flood at the main hydrological station.

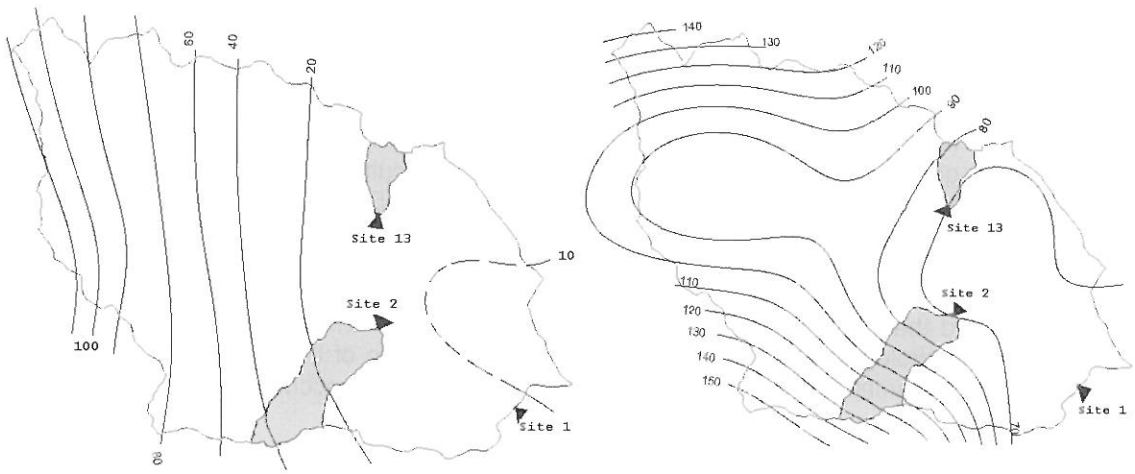

Figure 5-2: Rainfall distribution over the Jhikhu Khola watershed on A) September 8, 1998 and B) July 1, 1997.

For the purpose of this study from all flood events in the watershed only the events, which could be identified in the monitored sub-catchments at site 13 and 2 were selected. From the 20 largest events at site 1, a number of eleven events was selected for further analysis (Table 5-1). Four events had an impact on the south facing slopes and were mainly measured at site 13 in the Kubinde Khola sub-catchment. Seven events were detected at site 2 in the Lower Andheri Khola sub-catchments.

Table 5-1: Daily mean discharge (m^3/s) at hydrological stations 1, 2 and 13.

	Daily discharge (m^3/s)		
	Site#1	Site#2	Site#13
01/07/97	29.033	3.288	na
21/10/99	20.258	2.328	0.096
09/07/98	19.890	2.174	0.133
21/07/98	16.386	0.995	0.102
21/08/98	15.669	1.227	0.094
08/09/98	15.458	1.048	0.076
25/07/00	14.989	1.215	0.196
06/09/98	14.603	1.361	0.185
20/10/99	14.553	1.482	0.363
07/09/98	14.492	1.060	0.099
29/07/97	14.154	1.370	0.088
28/06/99	14.085	2.024	0.552
11/07/97	12.224	1.897	0.079
28/07/99	12.184	1.216	0.161
18/08/97	12.166	1.069	0.136
19/08/98	11.176	1.451	0.113
25/08/99	10.859	0.665	0.182
02/08/99	10.826	0.303	0.178
19/08/97	10.536	0.860	0.095
13/08/97	10.058	1.189	0.114
26/08/99	9.590	2.279	0.083
03/07/99	9.573	0.988	0.271

Note: highlighted are not selected for further analysis.

These events are generally the largest or amongst the largest events on the respective plots (Figure 5-3).
The comparison of the selected 11 events with the remaining erosion plot events shows that they can be classified as the largest rainfall events often triggering highest amount of runoff. There is a clear difference of runoff generation between degraded areas and agricultural land. During the selected events degraded plots yielded all more than 15 mm and up to 45 mm. On agricultural land the maximum runoff rate recorded was 10 mm.
A major impact on the flood generation seems to have the duration of the rainfall event. On all plots the relationship between the rainfall duration and the runoff rates is positive.
It can be summarised that the runoff generation on the erosion plots shows the same behaviour for large events as the hydrological stations. Therefore the understanding of the runoff generation at the plot scale during large events will help to understand and predict the occurrences of floods at the outlet of the watershed.

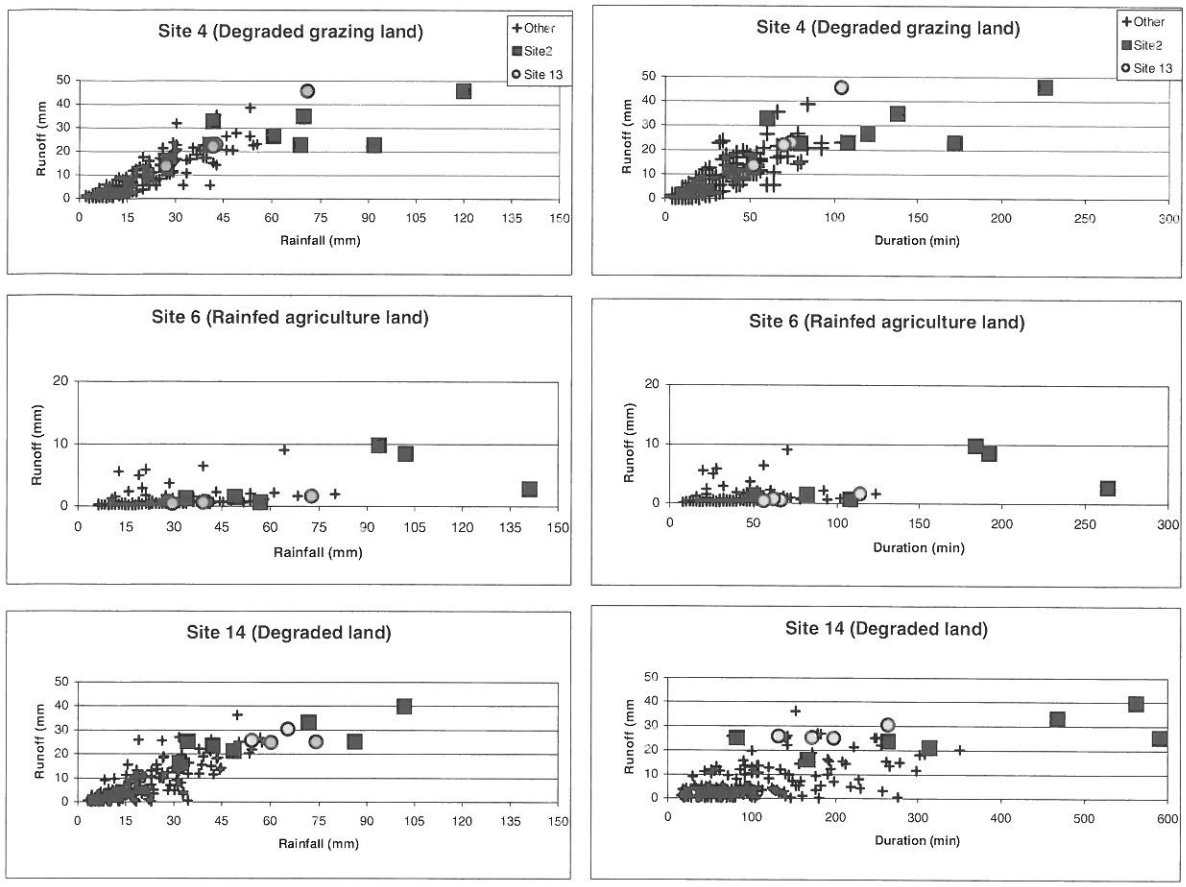

Figure 5-3: Daily rainfall and rainfall duration versus runoff on the erosion plots. Note: y-axis in degraded plots is maximal 50 mm, on agricultural plots 20 mm.

6 CONCLUSION

The comparative analyses above have shown that there is a distinct difference of runoff generation on degraded lands and rainfed agricultural areas. Degraded areas typically yield runoff at a threshold of 2 mm of rainfall. On agricultural land runoff is only triggered after 5 mm of rainfall. Runoff rates are typically higher on degraded land and therefore contribute more to the floods at the main hydrological station. However, for the generation of major events all areas are contributing including the agricultural fields.
Mitigation of floods and prevention of runoff generation is therefore only possible to the extent of intermediate events. The large events with high return periods have to be accepted and managed. With the above analyses no answers to the scale issue has been given yet. The preliminary results will have to be further substantiated with in-depth event analysis. However, the understanding of the generation of large events at the plot scale may well be crucial for understanding of floods at the meso scale catchment level.
For surface runoff harvesting degraded sites are more appropriate than agricultural sites due to their high runoff rates. Recharge of groundwater is reduced on degraded areas due to the immediate runoff from the surface. Mitigation measures such as contour trenches and eyebrow terraces both help to reduce the runoff and increase the recharge capacity. Infiltration on agricultural land is limited during early pre-monsoon season (March to early May) before planting of the monsoon crop. This is also the time of highest soil losses as shown by Carver and Nakarmi (1995). With the planting activities surface roughness and infiltration capacity are increased and runoff rates decrease.
Further analyses to identify the important parameters for flood generation and their impact on possible mitigation measures are planned in near future.

ACKNOWLEDGEMENTS

The authors would like to acknowledge the financial support of the Swiss Agency for Development and Cooperation (SDC), the International Development Research Centre (IDRC) and the International Centre for Integrated Mountain Development (ICIMOD) for the PARDYP project. Furthermore without the support of the PARDYP Nepal team, Pravakar B. Shah, Madhav P. Dhakal, Bhawani S. Dongol and Gopal Nakarmi in particular this paper would not have been possible. The continuous efforts of the field assistants and the local readers who maintain the stations and read the data every day is highly appreciated. Pradeep M. Dangol's visit to the Bern 2002 Conference was made possible through the financial support of the Max and Elsa Beer-Brawand Foundation. This support is herewith highly acknowledged.

REFERENCES

Agarwal, A., Narain S. (1991): Floods, flood plains and environmental myths. Centre for Science and Environment, India.

Anderson, M.G.; Burt, T.P. (1990): Subsurface runoff. In: Anderson, M.G.; Burt, T.P. (eds.), Process studies in hillslope hydrology. John Wiley & Sons, Chichester.

Bruijnzeel, L.A.; Bremmer, C.N. (1989): Highland-lowland interactions in the Ganges Brahmaputra river basin. ICIMOD Occasional Paper No. 11. International Centre for Integrated Mountain Development, Kathmandu.

Carver, M., Nakarmi, N. (1995): The effect of surface conditions on the surface erosion and stream suspended sediments, In Schreier, H., Shah, P. and Brown, S., J. (eds.) Challenges in Mountain resource Management in Nepal: Processes, trends and dynamic in middle mountain watershed. Kathmandu: ICIMOD.

Carver, M. (1997): Diagnosis of headwater sediment dynamics in Nepal's middle mountains: Implications for land management. Unpublished PhD Thesis at University of the British Columbia, Canada.

Choudhury, A.M. (1989): Flood 1988. In: Ahmand, M. (ed.): Flood in Bangladesh. Community Development Library, Dhaka.

Hofer, T. (1998a): Flood in Bangladesh: A highland-lowland interaction? Geographica Bernensia G48, Bern.

Hofer, T. (1998b): Hydrometeorological Measurements and Analysis in Interdisciplinary Watershed Projects. Discussion Paper No. MNR 98/3. International Centre for Integrated Mountain Development, Kathmandu.

Hossain, M. et. al. (1987) Floods in Bangladesh.: Recurrent disaster and people's survival. Universities Research Centre, Dhaka.

Merz, J., et. al. (2000): Impact of land use on generation of high flows in the Yarsha Khola watershed, Nepal. In: Allen, R.; Schreier, H., Shah, P.B.; Brown, S.J. (eds.) PARDYP –research for development in the HKH – the first three years (1996-1999). International Centre for Integrated Mountain Development, Kathmandu.

Merz, J. et. al. (2000): Calculation and Comparison of Climatological Balances in the Jhikhu Khola and the Yarsha Khola Watersheds. In: Allen, R.; Schreier, H., Shah, P.B.; Brown, S.J. (eds.) PARDYP – research for development in the HKH – the first three years (1996-1999). International Centre for Integrated Mountain Development, Kathmandu.

Rowe, L. et. al. (1997): Effects of land use on floods and low flow. In: Mosley, M.; Pearson, C. (eds.) Floods and Droughts: the New Zealand experience. New Zealand Hydrological Society, Wellington.

MODELLING OF FLOOD INUNDATION AND EFFECT OF DEM ON MODEL OUTPUTS

Dushmanta Dutta[1], Srikantha Herath[2]

[1] International Center for Urban Safety Engineering, Institute of Industrial Science, The University of Tokyo, 4-6-1 Komaba, Meguro-ku, Tokyo 153-8505, Japan, dutta@iis.u-tokyo.ac.jp

[2] Institute of Industrial Science, The University of Tokyo, 4-6-1 Komaba, Meguro-ku, Tokyo 153-8505, Japan, herath@iis.u-tokyo.ac.jp

SUMMARY

Mathematical models play an important role in flood disaster mitigation. Physically based distributed hydrological modelling is a technique, which can be effectively used for simulation of flood inundation in a river basin as it can provide us with necessary information of floods both in temporal and spatial scales in real-time as well as for future events. A high level of accuracy of outputs of such models is of utmost importance for any decision making process in flood risk management. Assuming that the mathematical formulation and solving process of governing equations of flow in different hydrologic processes are considered properly, the level of accuracy of model outputs will entirely depend on the accuracy of the spatial and temporal input datasets. In flood inundation modeling, topography is one of the spatial datasets that affect the accuracy of model outputs to a great extent. Topographic data are the primary data source to delineate drainage network used for flood modeling. Input elevation data in raster format of specific resolution known as digital elevation model (DEM) is generated from the existing topography data available in the form of contour or spot elevations. Based on the steepest slope direction, drainage networks are generated from the DEM for any watershed. In steep and sloping terrain, generated drainage network agrees well with actual flow paths. However in flat areas, generated stream channels often deviate from the actual path of drainage, the deviations ranging from few meters to several kilometres depending on the DEM data resolution. In nature, truly flat landscapes with zero slope seldom occur, however, when a landscape is represented by a DEM, very flat areas are averaged into flat surfaces. These flat surfaces typically are the result of inadequate vertical resolution of DEM, which can be further worsened by a lack of horizontal resolution. Such surfaces are also generated when depressions in the digital landscape are removed by raising the elevations within the depressions to the level of their lowest flow. A variety of methods have been proposed to address the problem of drainage analysis over flat surfaces. Methods range from simple DEM smoothing to arbitrary flow direction assignment.
One of the widely adopted methods to improve a DEM is based on an algorithm in which the DEM is hydrologically improved with the aid of actual drainage paths such that improved DEM can produce the drainage network very close to the actual one. In this study, this methodology for hydrological improvement of DEM based on actual flow paths was analysed to evaluate its impacts in flood inundation modeling. A physically based distributed hydrological model was used to carry out this study in a river catchment in Japan. The simulated results show that the hydrologically improved DEM with the influence of the actual drainage information enhances the performance of the flood inundation simulation model to a great extent.

Keywords: Drainage-enforced DEM, distributed hydrological model, flood inundation modelling

1 INTRODUCTION

A typical physically based distributed hydrological model considers the various components of hydrologic cycles, including (but not restricted to) evapotranspiration, unsaturated zone flow, saturated zone flow and overland flow, in the modelling process using the physically based governing equations of each component to simulate water movement. The overland flow components, which includes flow in surface and in streams, lakes, wetlands and reservoirs, is the most complex of all the phases of the hydrologic cycle, because it interacts with the other three phases, namely atmospheric water, soil water and groundwater, because of the flow velocity is large compared to the velocity of groundwater, and because the flow environment is complicated, and depending in part on the characteristics of the land surface and in part on the characteristics of the stream system. For application of such distributed hydrologic model for any purpose, it is necessary to prepare a huge amount of input spatial and temporal datasets for each process. The importance of various datasets varies according to the

application purpose. In flood inundation simulation, topography dataset is one of the most important spatial datasets, which governs the flow behaviour in overland flow. In any application of distributed model, the stream network is delineated from the topography data. As stream network is the most critical item in surface flood modelling, it is important that stream network is delineated accurately.
A standardized way of delineating watersheds and stream networks is the following: construct the stream network in the standard way by choosing a drainage area threshold; divide the stream network so created into individual stream links; find the outlet cell at the lower end of each link; delineate the watershed for each of these outlet cells. This method works relatively well in hillslopes, however it fails in flat areas, the errors in delineation sometimes becoming critically large. Truly flat landscapes (with zero slope) seldom occur in nature. In nature, truly flat landscapes with zero slope seldom occur, however, when a landscape is represented by a DEM, very flat areas are averaged into flat surfaces. These flat surfaces typically are the result of inadequate vertical resolution of DEM, which can be further worsened by a lack of horizontal resolution. Such surfaces are also generated when depressions in the digital landscape are removed by raising the elevations within the depressions to the level of their lowest flow.
A variety of methods have been proposed to address the problem of drainage analysis over flat surfaces. Methods range from simple DEM smoothing to flow direction assignment (Maidment, 1996; Tribe, 1992; Garbrecht et al. 1995 and 1997). TOPAZ was one of such methods in which a new way of treating the flat surface problem was addressed. This method performed well in creating consistent flow direction for the entire catchment including flat areas with one single outlet, however, there was no approach to match the delineated drainage path with actual ones. The most satisfactory method addressing the issue of accurate drainage network was developed at CRES, Australian National University (Hutchinson, 1989 and 1991). The principal innovation of the procedure is a drainage enforcement algorithm which automatically removes spurious sinks or pits from the fitted grid. The algorithm is adopted in popular GIS software ARC/INFO for interpolation of topography data for creation of hydrologically improved DEM.
This paper presents a study that was carried out to analyse the effect of the hydrologically improved DEM in the outputs of flood inundation model in comparison with the existing DEM.

2 DEM RESOLUTION AND DRAINAGE NETWORK

DEM resolution has a direct influence on the total drainage area, length and slope. Too coarse resolution causes an undersampling of the hillslopes and valleys where hilltops are cut off and valley filled. Two principal effects result: drainage length is shortened by short-circuiting; and slope is flattened. DEMs commonly contain localized depressions and flat surfaces, most of which are artifacts of the horizontal and vertical DEM resolution, DEM generation method, and elevation data noise. These features are problematic for the downslope flow routing concept on which many DEM processing models are based. Depressions are sinks at the bottom of which drainage terminates, and flat surfaces have indeterminate drainage. In standard methods of delineation of drainage network, sinks of DEMs are first filled to the level of the lowest elevation of the surrounding eight neighboring grids. However, due to low vertical and horizontal resolution, delineated drainage networks in low land flat terrain are not representative of the actual drainage paths.
To illustrate the variation of accuracy of delineated drainage networks with horizontal and vertical resolutions of DEM, analyses were carried out in several Asian river catchments, which have vast low land areas with very mild slopes and are frequently flooded. Figure 2-1 shows the delineated river network from 1 km resolution DEM together with actual flow paths in the Chao Phraya river basin (up to Nakhon Sawan: area 110,500 km^2). In this case, the

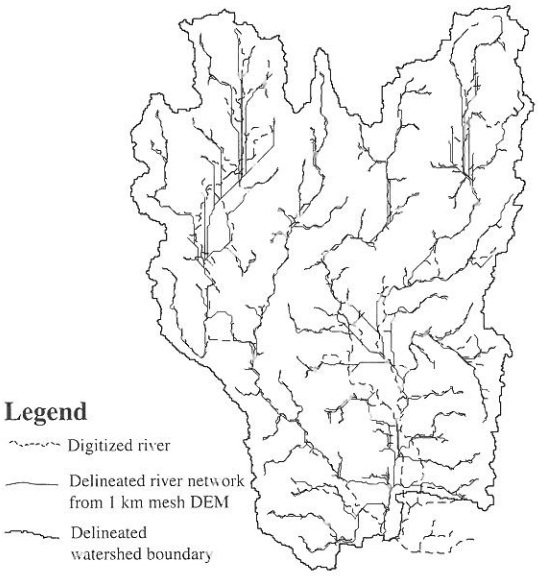

Figure 2-1: Comparison of delineated river network from 1km mesh DEM with actual flow paths in Chao Phraya river basin (upto Nakhon Sawan).

source of the DEM is GTOPO30 global dataset of USGS, which was developed from 1:1,000,000 scale base topography map. Due to poor resolution, the generated river network deviates up to several kilometers from the actual drainage paths in flat terrain. The delineated watershed boundary also does not agree well with the actual one. Similar results can be observed in other river basins also where the same resolution DEMs from this global dataset are used. With the increase of horizontal and vertical resolutions, how delineated river networks from DEM become closer to the actual flow paths are shown through the examples in three river basins: Agno, Tsurumi and Ichinomiya river basins. Agno river basin is located in the Luzon Island of the Philippines (Figure 2-2) and Tsurumi and Ichinomiya river basins are located in the Kanto region of Japan (Figure 2-3). In the Agno river basin (considered up to Carmen: area 1,700 km^2), topographic data were obtained from 1:50,000 scale contour maps, and a 100m mesh-size DEM was generated from it. The drainage network generated from this DEM is shown in Figure 2-4 together with the actual drainage paths. The agreement was satisfactory in upstream hillslopes, but in the downstream part of the basin with very mild slopes, the agreement is not good. Some improvement of the vertical resolution of the DEM was achieved by spatial interpolation of spot elevation data (at 216 locations in downstream) using kriging technique and it enhanced the delineated river network to some extent although not to the level of the requirement for flood modelling (Figure 2-5). Figure 2-6 shows the comparison of the generated drainage network from 50m mesh topographic data (origin: 1:25,000 scale map) and actual flow paths in the Tsurumi river catchment. It can be observed that with the increase of vertical and horizontal resolution of the DEM, the delineated river networks come to close agreement with the observation particularly in hillslopes, but results of 50m mesh data are not satisfactory in flat urban areas, where river networks are human controlled. Figures 2-7 through 2-9 show the improvement of delineated river networks in the Ichinomiya river network through the improvement of the 50m mesh topographic data with contours of 1m interval from 1:2,500 scale in flat areas. A tremendous improvement of the delineated river network with the increased precision of vertical resolution of topographic data can be seen. This delineated river network may be not still useful when it comes to flood inundation simulation. Where is the end and is it possible for us to obtain such high resolution datasets for our application? In most of cases, for hydrologic modelling in the areas of our interest (that is Asian region), it is not possible to obtain DEM of even 1:100,000 scale contour maps. In this case, we need alternative ways to improve DEM such that delineated river network agrees well with the observation.

Figure 2-2: Agno river basin.

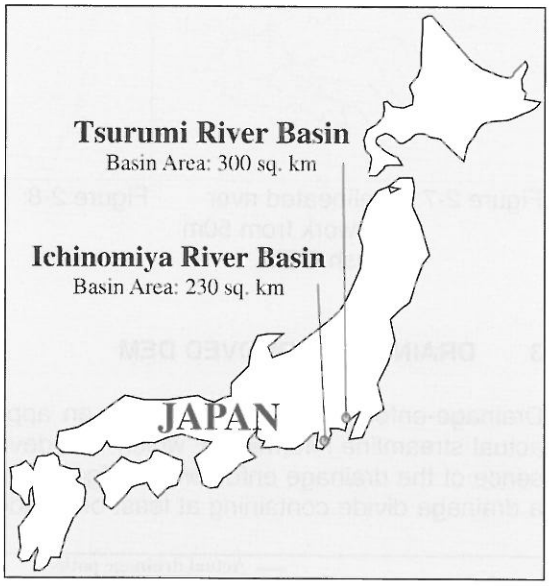

Figure 2-3: Locations of Tsurumi river and Ichinomiya river basins.

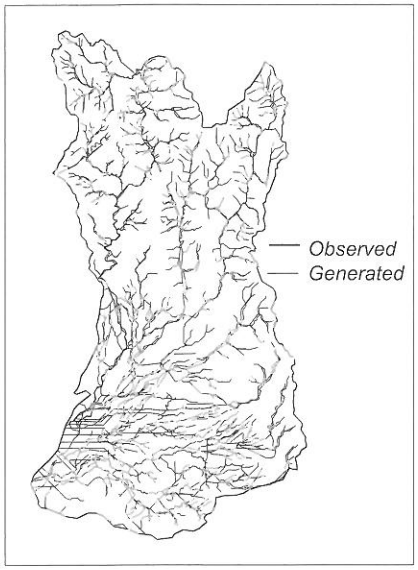

Figure 2-4: Delineated river network from 100m mesh DEM in Agno.

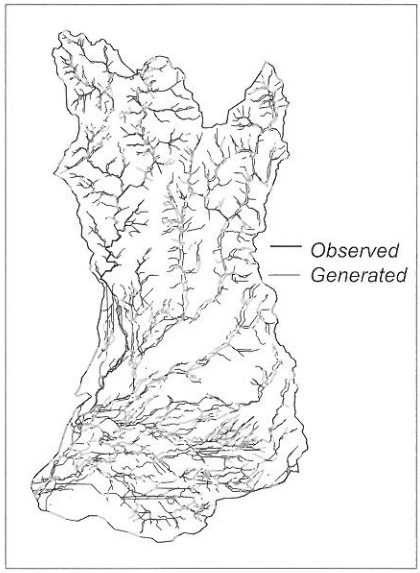

Figure 2-5: Delineated river network from improved 100m mesh DEM.

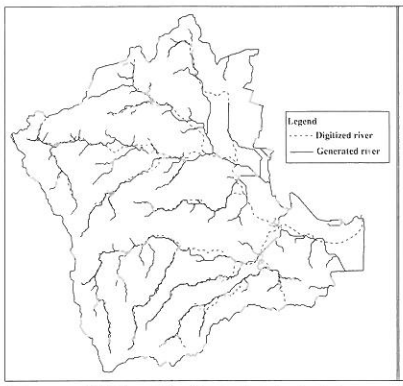

Figure 2-7: Delineated river network from 50m mesh DEM.

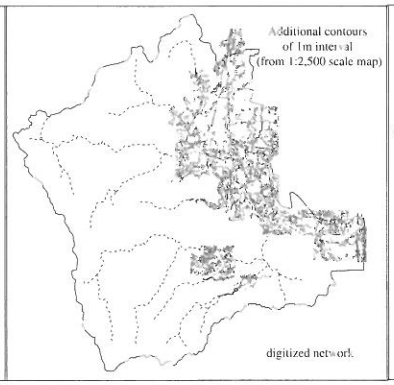

Figure 2-8: Locations of added 1m interval contours.

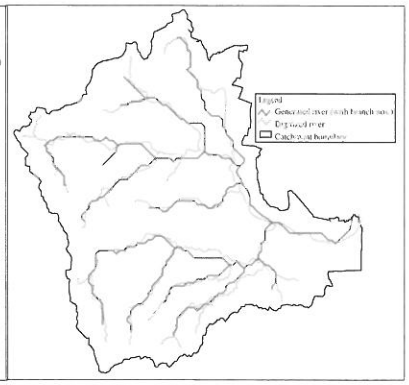

Figure 2-9: Delineated river network from improved 50 mesh DEM.

3 DRAINAGE-IMPROVED DEM

Drainage-enforced DEM algorithm is an approach to improve the DEM hydrologically based on the actual streamline information, which was developed at CRES, Australian National University. The essence of the drainage enforcement algorithm is to recognize that each spurious sink is surrounded by a drainage divide containing at least one saddle point. If the sink is associated with an elevation data

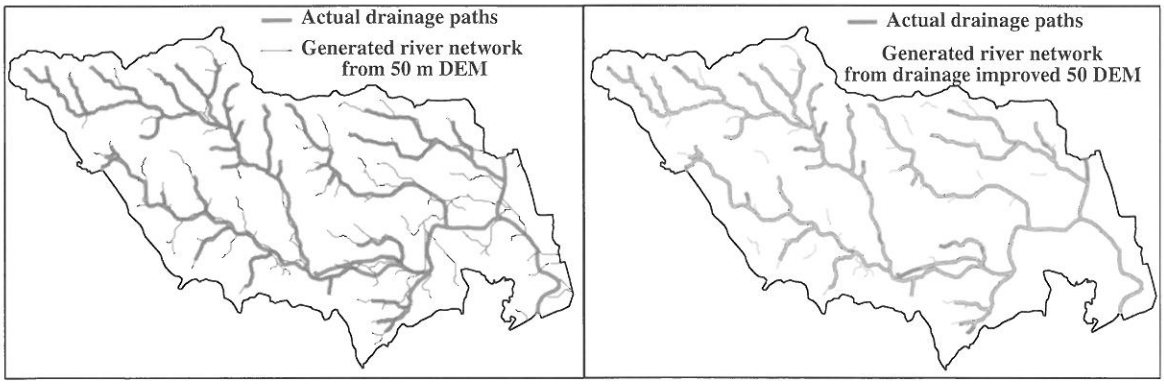

Figure 3-1: Delineated river networks of Tsurumi basin from 50m DEM and drainage-enforced DEM.

point then the lowest such saddle, provided it is not also associated with an elevation data point, identifies the region of grid, which is modified in order to remove the spurious sink. If on the other hand the lowest saddle point is associated with an elevation data point but the sink is not, then the sink and its immediate neighbors are raised above the height of the data point saddle. If neither the sink nor the lowest saddle are associated with elevation data points then grid points in the neighborhood of both the sink and the lowest saddle are modified to ensure drainage. Finally, if both sink point and saddle point are associated with elevation data points, then a choice is made, depending on the a user-supplied tolerance, between enforcing drainage and maintaining fidelity to the data (Hutchinson, 1989, 1991, 1996) .

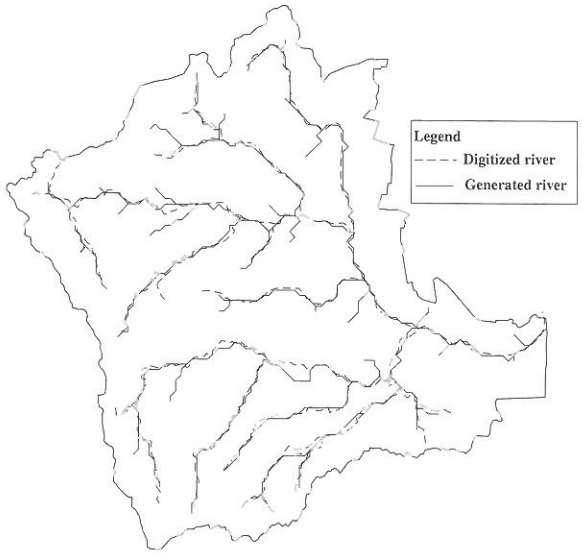

Figure 3-2: Delineated rivers for Ichinomiya Basin using drainage-enforced 50m DEM.

The generated river network from the drainage-enforced DEM using the above mentioned algorithm is compared with the actual river networks for the Tsurumi and Ichinomiya river basins in Figures 3-1 and 3-2. From the figure it can be seen that generated river networks for all these cases follow the actual river networks from upstream to downstream very closely compared to the previous two generated networks. This demonstrates that his methodology is able to provide hydrological improved DEM which can be used to delineate sufficiently accurate drainage network in terms of the flow paths.

4 EFFECT OF DEM IMPROVEMENT IN FLOOD INUNDATION MODELING

The flood inundation model used in this study is a physically based distributed hydrological model. The model consists of various hydrological components and governing equations for flow propagation in different components are solved using finite difference schemes. The model is designed to simulate flood inundations including urban flooding taking into consideration of boundary conditions of existing river embankments. The detailed description of the model was given elsewhere (Jha et al., 1997; Dutta et al., 2000).

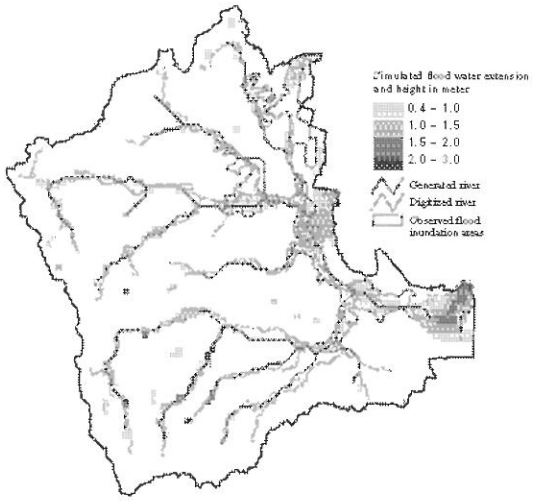

Figure 4-1: Simulated flood inundation map using 50m mesh DEM data and delineated river network from it.

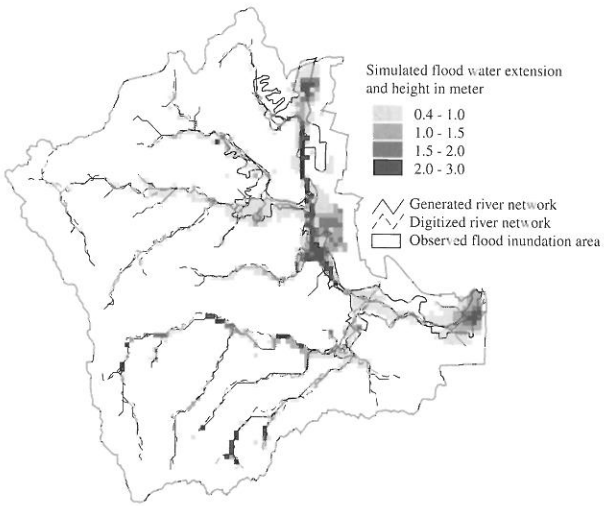

Figure 4-2: Simulated flood inundation map using drainage-enforced DEM data and delineated river network from it.

For the model application, the flood event of September 1996 was considered when the basin suffered from a big flood disaster due to the heavy rainfall. During a span of 24 hours the basin received about 360mm rainfall and was under flooding for about two days. Using the available temporal and spatial input parameters obtained from different sources, the flood event was simulated by the model twice, first with the DEM of the study area derived by conventional methods and the secondly with the drainage-enforced DEM. For these two cases, the generated river networks from the respective DEMs were used (refer to Figures 2-9 and 3-2), all other input data were kept the same. Figure 4-1 shows the simulated maximum flood inundation maps for the first case. It can be observed that although the general simulated inundation pattern is similar to the actual flooding as represented by the surveyed map, there was a clear shifting of the inundation areas in all locations where generated river network deviated from the actual flow paths. This mirrors the fact that the flooding mainly occurs due to the overflow of river banks.
The simulated flood inundation areas using the drainage-enforced DEM are shown in Figure 4-2. From this figure it can be seen that there was no shift of the inundation areas from the actual inundation areas in this case as there was either no shift of the generated river network. Also, it can be observed that the simulated inundation areas in upper part of the basin agree well with the surveyed one compared to the previous simulation, where the inundated area was much less when compared with the survey map. As in the first case also, here much more areas were shown as inundated areas in the simulation in several locations as compared to the surveyed inundation map. This was due to the negligence of the locally elevated lands such as highways, etc in the model, which actually block the movement of flooding from the riverside to the other side. However, in a simulation based on the 200m resolution DEM data such local elevations of few meter widths could not captured, which affected the simulation results.

5 CONCLUSIONS

A study to analyse the impact of DEM model accuracy in a flood inundation simulation is presented in this paper. The accuracy of the DEM is viewed in hydrological context requiring that the generated drainage networks from the DEM model represents the actual flow paths adequately. It can be seen from the analysis that with the improvement of the DEM also an improvement occurs in the generated drainage network. As with the existing topographic data, it was not possible to improve the DEM beyond a certain extent, an algorithm is used to improve the DEM hydrologically using the existing streamlines. The simulated results of the flood inundation model show that flood inundation simulation can be improved by hydrologically improving the DEM model. Such an approach of DEM improvement is required for large catchments where existing DEM data are not adequate to generate a drainage network that can represent the actual flow paths.

REFERENCES

Dutta, D. et al. (2000): Flood Inundation Simulation in a River Basin Using a Physically Based Distributed Hydrologic Model, Hydrological Processes, 14(3), 497-520, USA.

Garbrecht, J., Martz, L.W. (1995): TOPAZ: an automated digital landscape analysis tool for topographic evaluation, drainage identification, watershed segmentation and subcatchment parameterization; overview, USDA, Agricultural Research Service, National Agricultural Water Quality Laboratory, Oklahama, NAWQL 95-1, 17pp.

Garbrecht, J., Martz, L.W. (1997): The assignment of drainage direction over flat surfaces in raster digital elevation models, Journal of Hydrology 193, 204-213, Amsterdam.

Hutchinson, M.F. (1989): A new procedure for gridding elevation and stream line data with automatic removal of pits, Journal of hydrology 106, 211-232, Amsterdam.

Hutchinson, M.F. (1991): A continental hydrological assessment of a new grid-based digital elevation model of Australia, Hydrological Processes, 5, 455-458, USA.

Hutchinson, M.F. (1996): A locally adaptive approach to the interpolation of digital elevation models Proceedings of the Third International Conference on GIS and Environmental Modeling, Santa Fe, New Mexico, USA.

Jha, R. et al. (1997): Development of IIS Distributed Hydrological Model (IISDHM) and Its Application in Chao Phraya River Basin, Thailand, Annual Journal of Hydraulic Engineering, JSCE, 41, 227-232, Japan.

Maidment, D.R. (1996): GIS and Hydrologic Modeling – an Assessment of Progress, Proceedings of the Third International Conference on GIS and Environmental Modeling, Santa Fe, New Mexico, USA.

Tribe, A. (1992): Automated recognition of valley lines and drainage networks from grid digital elevation models: a review and a new method, Journal of Hydrology, 139(3), 263-293, Amsterdam.

NUMERICAL MODELLING OF PROBABLE MAXIMUM FLOOD FOR THE WATERSHED OF THE KRASNODAR DAM IN RUSSIA

P. Goulpié[1]; Dr. J.-A. Hertig[1]; F. Reinhardt[1]; Ch. Hug[1]; J.M. Fallot[1]; O.F. Stirnimann[1], Dr.J. Dubois[2]

[1] LASEN-DGC EPFL CH-1015 Lausanne

[2] Hydrocosmos S.A., Rue de l'Industrie 35 CH-1030 Bussigny

SUMMARY

The research objective is to develop a numerical tool for the modeling of precipitation over complex topography at a regional scale. This paper deals with the presentation of the calculation of the Probable Maximum Flood (PMF) for the large Kuban river watershed (about 41 000 km^2) in the South of Russia. A three dimensional hydrodynamic solver, CFX4, adapted by the LASEN laboratory to atmospheric flows is used to calculate wind fields in the stratified atmosphere and the ensuing precipitation over complex terrain. This model is time dependent and includes the energy equation expressed in terms of potential temperature. The equations are solved on a non-staggered grid, with variable mesh size, by means of a finite volume approach. The closure of the turbulent equation set is provided by a modified k-ε turbulence model in order to take into account thermal stratification of the atmosphere.
The methodology consists in identifying by a meteorological analysis of the considered region what are typical meteorological events which would lead to severe precipitation and floods. According to LASEN method, precipitation occurs under three main modes of generation: orographic, convective and opposition of pressure system, for each a dedicated maximization procedure has to be applied. Numerical simulations of selected events are carried out by initializing calculation and setting boundary condition with theoretical profile of atmospheric variables (geostrophic wind speed, geostrophic wind direction, ground temperature, thermal stratification and relative humidity). These idealized representations of atmospheric flows allow reproduction of events even with a sparse set of data. A chapter concerns sensitive studies which have been performed on atmospheric parameters which lead to heavy precipitation for orographic regime. Among selected events, following the appropriate maximization methodology, atmospheric critical situations are modeled and routed on the watershed. Among them, the PMF is identified and consequently the Probable Maximum Precipitation.

Keywords: Probable Maximum Flood, Probable Maximum Precipitation, atmospheric microphysics, complex terrain, numerical modeling

1 INTRODUCTION

The engineering company Stucky Ingénieurs-Conseil S.A. has been contracted to design the spillways of the Krasnodar dam in Russia and to check the security conditions for the inhabitants in case of an intense precipitation event and a consequent flood. For this purpose, Stucky has contracted LASEN for the calculation of the Probable Maximum Flood (PMF) for the Kuban river watershed. The atmospheric numerical model developed by the LASEN group calculates wind and precipitation fields in the whole domain for a given atmospheric situation. The methodology leads to evaluate the highest Probable Maximum Precipitation (PMP) as well as the most unfavourable spatio-temporal distribution.To achieve PMF calculation, several extreme precipitation fields have to be modelled. These PMP have to be routed in order to determine which precipitation event leads to the PMF. The flood modelling is being carried out by the company HydroCosmos. A spatially and temporally distributed hydrologic model WolfHydro developed at the University of Liege was applied to the calculated precipitation field. The method employed for the estimation of the PMP is based on the numerical modelling of air masses and precipitation. The steps of the methodology used for the Kuban watershed are:

- Analysis of meteorological situations and hydrological measurements in the watershed in order to identify reference flood events to be numerically modelled;
- Creation of a numerical representation of topography;
- Numerical simulation of the selected flood events to determine the hydrological parameters of the watershed;
- Analysis of the meteorological and geographical conditions of the area in order to determine which meteorological situation is likely to generate extreme precipitation;

- Numerical calculation of extreme precipitation for selected sectors and identification of the most critical situation;
- Sensitivity study of PMP with respect to the CRUEX method (Hertig 1997);
- PMP is routed across the complete watershed to determine the discharge and the extreme flood;
- Calculation of the PMP-PMF for the considered watershed.

2 THE KUBAN RIVER WATERSHED

The Kuban river watershed is in South Occidental Russia. Krasnodar town is at the output of the basin at the geographical coordinates 45°2 N and 39°0 E. Simulation domain (Figure 2-2) covers southwest part of Russia which presents a very flat area in the north part of the watershed and a rapid change of altitude in the south direction, up to a height of 5'600m in the Caucasus Massif (Figure 2-1). This highest point does not appear on the next graph since it does not belong to the considered watershed.

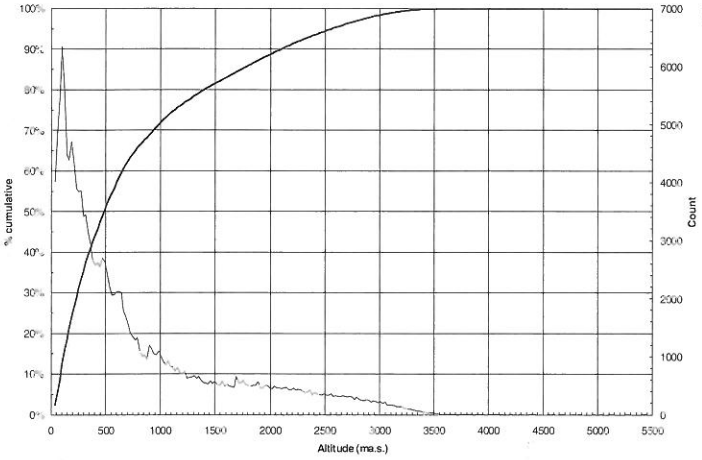

Figure 2-1: Hypsometric curve (bold, legend on right axis) and altitude histogram (thin, legend on left axis) of the Kuban river watershed; it shows the strong altitude variations limited in space across the basin.

Calculation domain covers 410 km by 310 km and extends to 12 km in the vertical. Next figure shows domain topography:

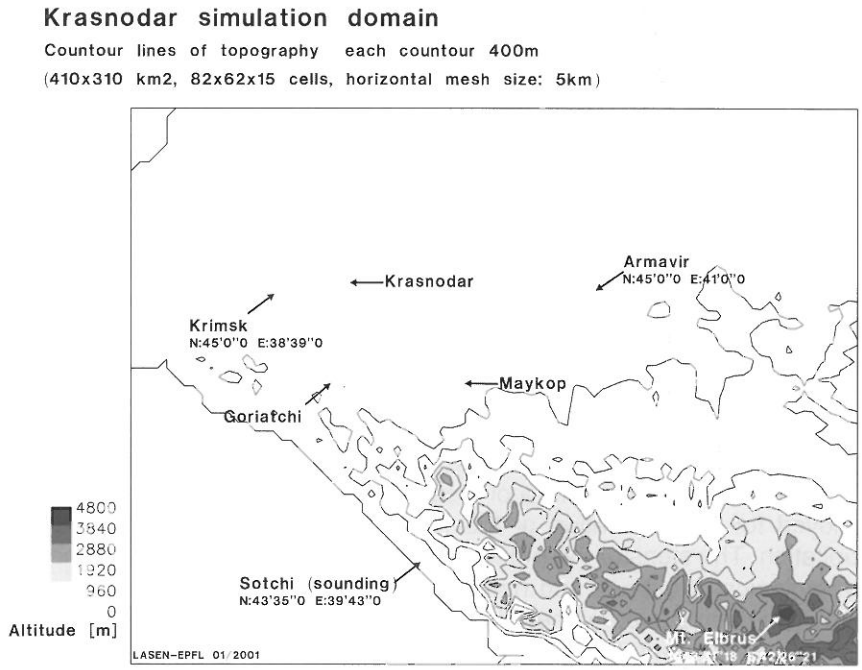

Figure 2-2: Surface contours for the calculation domain. Topographical data from the Digital Chart of the World.

3 METEOROLOGICAL SURVEY

A report of Hydrography and Hydrology prepared by Kuban Vod Project (KVP) and several sets of measurements of the flow rate of the Kuban River during severe flood events have been transmitted to LASEN. From these documents date of severe events have been selected. The meteorological survey has consisted in consulting the European Meteorological Bulletin collection available at LASEN and to select and analyse the most representative situations.
The main characteristics of the climatology of precipitation in the south of Russia are the following: Flood events generally occur under meteorological conditions with an opposition of a hot air mass coming from the southwest and a cold one coming from the north. On the other hand, wind sectors, which are able to bring large amounts of humidity, are from sector 270° to 360°.
Convective storms are associated with high intensity precipitation and their intensity can be of higher magnitude (20% in average) than orographic precipitation, but due to their small spatial extent and their short duration (from 20 minutes to 1 hour), their effect is not critical for the size of the Kuban watershed (almost 41'000 km^2). Thus, only orographic contributions have been taken into account.

4 DESCRIPTION OF THE REFERENCE FLOOD EVENT

The heaviest precipitations over the whole of the basin were measured from July 6 to 8, 1987 and the Kuban river flow reached a maximum value of 1850 m^3/s on July 10, 1987, which represents the highest value measured during the 1980s. Precipitation accumulated from July 6 to 8, 1987, ranges between 50 and 110 mm according to the five measurement stations (Table 4-1) in the Kuban river basin (high for this region). For this period, a cold front coming from the Northwest waved for 2 days on the northern slopes of the Caucasus. This situation could become critical for precipitation in this region, when rain falls on the same area along the front during these days, the length of such a situation becoming the main factor for PMP. Thus, opposition of air masses with a stationary front and wind shear need to be reproduced by the meteorological mesoscale model of LASEN for a correct simulation of rainfalls in the Kuban river basin during this period.

Table 4-1: Daily precipitation and flow measured at some locations in the Kuban river basin in May-June 1984 and June-July 1987.

Date	Krasnodar mm/day	Maïkop mm/day	Krimsk mm/day	Goriatchi mm/day	Arnavir Mm/day	Kuban M^3/s
3.6.1984	0.3	-	0.6	-	0.3	1077
4.6.1984	3.8	25.2	35.5	5.9	2.3	1039
5.6.1984	8.5	8.9	2.0	5.3	25.8	966
7.6.1987	23.9	6.0	2.9	5.3	2.1	1220
8.6.1987	-	2.9	0.5	0.3	30.1	1008
9.6.1987	-	25.4	0.1	2.2	7.5	853
29.6.1987	7.6	103.0	3.8	15.6	3.5	1357
30.6.1987	1.7	24.3	-	13.8	12.2	1815
1.7.1987	-	-	-	-	-	1705
6.7.1987	10.9	49.3	23.2	42.0	66.3	916
7.7.1987	14.4	19.9	19.8	10.8	1.0	907
8.7.1987	35.8	22.5	6.5	45.6	44.6	908
9.7.1987	-	1.5	-	0.6	-	1515
10.7.1987	-	-	-	-	-	1851
11.7.1987	-	-	-	-	-	1444
13.7.1987	-	-	-	-	22.0	1446
14.7.1987	-	37.7	0.9	-	38.7	1193
15.7.1987	1.9	-	0.1	-	-	1281
29.7.1987	-	-	-	-	-	508
30.7.1987	5.0	10.4	-	46.8	18.4	472
31.7.1987	-	-	-	-	-	495

For the considered area, a unique vertical sounding is available at Sotchi (Table 6-1). The data used to initialise the model (humidity, ground temperature, and vertical gradient, geostrophic wind speed and direction) were calculated from the following table 4-2.

Table 4-2: Parameters measured from atmospheric soundings over Sotchi (southern slopes of the Caucasus) from July 6 to 9, 1987, at 0 GMT.

July 6, 1987 Level	Altitude (m ASL)	Temperature (°C)	Dew Point (°C)	Wind Direction	Wind Velocity (m/s)
Surface	0	21-26	19-21	E	3
850 hPa	1440	14	11	S	3
700 hPa	3060	5	0	S	8
500 hPa	5710	-14	-15	SW	10
300 hPa	9390	-42	-44	WSW	15
200 hPa	12170	-48	-55	WSW	25
100 hPa	16620	-60	-69	W	10
July 7, 1987 Level	Altitude (m ASL)	Temperature (°C)	Dew Point (°C)	Wind Direction	Wind Velocity (m/s)
Surface	0	18-25	14-20	S	3
850 hPa	1450	14	10	E	3
700 hPa	3070	4	0	S	3
500 hPa	5730	-10	-16	SSW	8
300 hPa	9470	-39	-48	SW	18
200 hPa	12180	-48	-55	WSW	35
100 hPa	16670	-58	-65	SW	23
July 8, 1987 Level	Altitude (m ASL)	Temperature (°C)	Dew Point (°C)	Wind Direction	Wind Velocity (m/s)
Surface	0	20-21	18-20	ENE	3
850 hPa	143	13	9	NE	10
700 hPa	303	3	2	NE	10
500 hPa	5690	-11	-12	SW	8
300 hPa	9420	-39	-42	S	22
200 hPa	12120	-48	-52	WSW	30
100 hPa	16630	-56	-63	WSW	10
July 9, 1987 Level	Altitude (m ASL)	Temperature (°C)	Dew Point (°C)	Wind Direction	Wind Velocity (m/s)
Surface	0	17-25	14-16	SW	3
850 hPa	1480	11	4	ENE	10
700 hPa	3060	1	-1	ESE	10
500 hPa	5720	-14	-22	NE	10
300 hPa	9370	-42	-47	NNE	8
200 hPa	12050	-47	-55	W	13
100 hPa	16560	-55	-66	WSW	10

5 NUMERICAL SIMULATIONS

The numerical simulation of precipitation is carried out in two steps: simulation of the wind field and simulation of precipitation with a stationary wind field.
The parameters used in the simulation of the wind and precipitation fields are geostrophic wind speed, geostrophic wind direction, ground temperature, thermal stratification and relative humidity. Depending on the wind direction, the calculations for the wind field simulation were initialised with a different geostrophic speed and a different vertical temperature gradient. Main features of the wind model are: velocity profile of the Planetary Boundary Layer (according to Harris and Deaves, 1981), parameterisation of the Eckmann spiral (according to Zilitinkevich et al., 1998), turbulent flow depending on thermal stratification, transient flow, with boundary conditions stationary in time.
The wind fields calculated in the first step have been used as initial conditions for the calculation of precipitation. The model solves the Kessler equations for the precipitation variables. The simulation conditions are: initial and boundary conditions: relative humidity of 100%, no cloud water (m=0), no precipitation (M=0), stationary boundary conditions and three dimensional and transient flow. As it was done for the wind fields, here too, the convergence of the solution and of the internal iterations is checked at each time step.
Solutions are obtained for the distribution of cloud water m and precipitation M in three dimensional space and for the ground distribution of precipitation intensity in mm/h.
Routing of the precipitation has been performed using the Wolf software (from the University of Liege). The physical processes taken into account are the run-off and the subsurface flow. A base flow, derived from the measured hydrograph of the 1980 flood, has to be added to the simulated

hydrograph. The watershed of the Krasnodar dam has been described by a digital elevation model (mesh size 1km) and the Wolf software automatically generates the river network. Wolf Hydro resolves the conservative equations of 2-D diffusive wave model with a finite volume method for three specific vertically distributed layers. Different roughness law (Manning, Darcy-Weissbach, Bathurst ...) are implemented to take into account the macroscopic roughness of the hydrological propagation and various flow regimes. The model has three bunk layers to simulate respectively the thin runoff, the hypodermic propagation and the transfer to the groundwater. The unsteady infiltration law permits the reforming of the soil capacity after the rain stopping. Using this routing model, it is possible to determine the travel time of the flood to the dam site in the whole network.

6 NUMERICAL MODELLING OF THE REFERENCE SITUATION

To reproduce the convergence of the two air masses, the numerical wind field was generated in two steps: Firstly, a numerical simulation was performed that was aimed at reproducing the cold air masses coming from the North. This run was initialized through an atmospheric vertical profile similar to the ones measured at Sotchi from 6th to 8th July 1987 (Table 4-2). The pseudo stationary solution of the first run was used as initial condition for a second run that aimed at reproducing the advection of hot wind from Southwest. The result of the second simulation is the wind field which corresponds to the meteorological situation to be reproduced (Figures 6-1 and 6-2). The reproduction of the main characteristic of the frontal meteorological situation compares well with the observed situation from the Europe Meteorological Bulletin of the day. The meteorological sounding performed at Sotchi (see Table 4-2) is also well reproduced.

Table 6-1: Coordinates of the five ground based stations in the watershed (and Sotchi sounding and Elbrus Mountain for indication).

	Latitude ° N	Longitude ° E	X [km]	Y [km]
Goriatchi	44'30"0	39'10"0	123.208	155.000
Krimsk	45'0"0	38'39"0	84.200	208.000
Maïkop	44'30"0	40'0"0	186.125	155.000
Arnavir	45'0"0	41'0"0	261.625	208.000
Krasnodar	45'2"0	39'9"0	121.950	211.533
Sotchi	*43'35"0*	*39'43"0*	*164.733*	*57.833*
Elbrus	*43'21"18*	*42'26"21*	*374.246*	*38.400*

The routing of these reference case has been carried out with the following value of the different parameters for the hydrologic model: Manning coefficient of the surface: 1 $s/m^{1/3}$; Darcy coefficient of the subsurface layer: 0.007 m/s, depth of the subsurface layer: 1.5 m, initial infiltration capacity: 140 mm/h, deep infiltration: 0.72 mm/h and porosity of the subsurface layer: 0.3. These values are very "standard" in reference to the specialised literature. All the values tested have changed the peak discharge for a maximum of 16% only. Unless the Manning coefficient is extremely high. But several studies achieved on alpine watersheds have shown that Manning coefficient lies between 0.5 and 5 $s/m^{1/3}$.
Finally, the daily precipitation field for the 6, 7 and 8 July are respectively given in Figures 6-3 (a,b and c) where the plots have been restricted to the watershed. 6-3 (d) shows the measured and simulated hydrographs for this reference case. Considering the fact that the available data is restricted to daily discharge, this result is very encouraging.

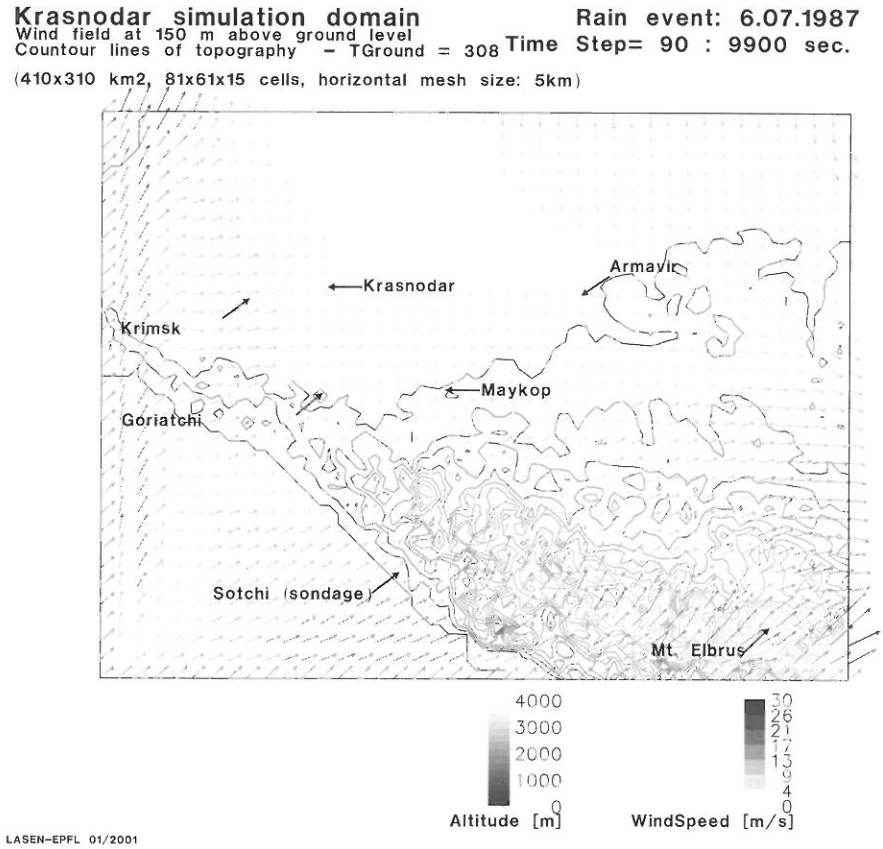

Figure 6-1: Simulated wind field at 150 m above ground level corresponding to the 6 July 1987 atmospheric conditions.

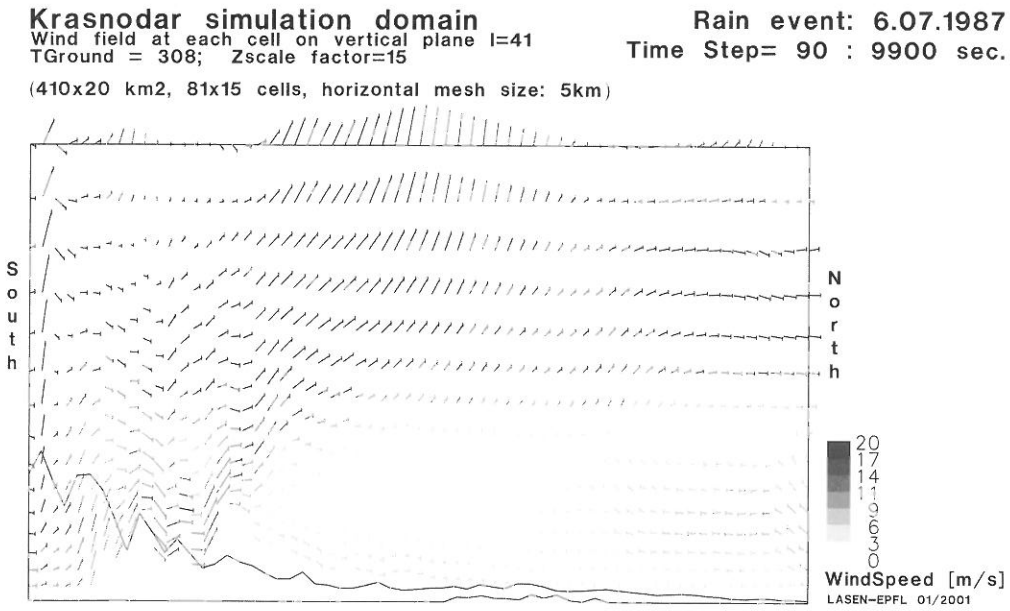

Figure 6-2: Vertical plane of wind field corresponding to the 6 July 1987 atmospheric condition.

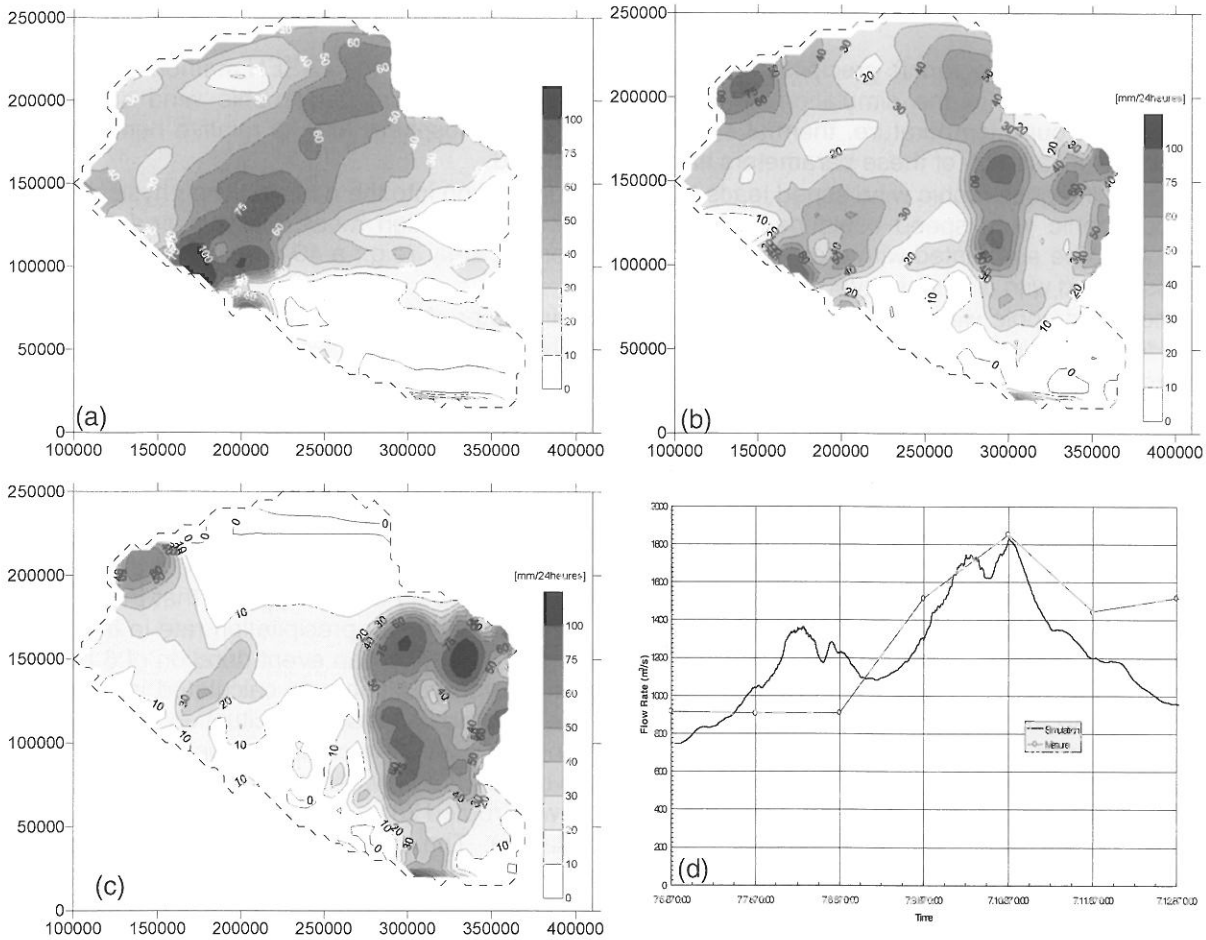

Figure 6-3: Simulated accumulated precipitation field at ground level (a,b,c) for the reference case of 6,7 and 8.07.1987. Simulated and measured flow rate (d) at Krasnodar from 6-12.07.1987.

7 SCENARIOS OF MAXIMISATION

- Precipitation is produced either by non-orographic mechanisms e.g. the passage of a front, convergence of air masses, convection which are responsible for precipitation over flat terrain, or orographic mechanisms in which the presence of mountains, hills etc. is paramount. Orographic precipitation is associated with the passage of air masses over the topography, and their intensity will depend on the wind speed. The stronger the advection at high altitude is, the heavier the precipitations are. A complete analysis of orographic precipitation has been achieved at the LASEN and the main conclusions are given in chapter 7.1.
- According to the performed meteorological survey, convergence of air masses is prevailing in the generation of intense showers for this watershed. The simulated wind field, and consequently the precipitation field, results in this case from the opposition of the advection of hot air coming from south west and a pre-existent cold air pool localized at the north of the Caucasus massif. Increasing the geostrophic wind speed or stabilizing the vertical thermal stratification would unbalance the dynamics of the meteorological situation and would deplete the convergence effect. The maximisation method has consisted for this case in considering what could be the worst temporal evolution of this situation, without acting on the atmospheric parameters which characterize the frontal situation.
- Considering the highly mountainous terrain formed by the Caucasus Massif, the winter PMP (including the melting of snow) is also to be explored in order to quantify what would be the maximum contribution from the snow cover in the case of severe warm precipitation during winter season.

7.1 Orographic

Maximisation of orographic precipitation has been achieved following the LASEN method. It concerns parameters used in the simulation of wind and precipitation fields: geostrophic wind speed and direction, ground temperature, thermal stratification of the atmosphere and its relative humidity. The influence of variation of these parameters has been explored:

- Increasing geostrophic wind speed leads to higher precipitation into the domain. The physical limit of geostrophic wind speed could be estimated from weather station measurements and has been found to be associated with a given event duration for the area. (e.g.: a 40 m/s geostrophic wind is associated with a 6 hours event duration).
- The geostrophic wind direction is an independent parameter. All directions have to be explored in order to take into account the specific topography of the area.
- Ground temperature is related with the acceptable quantity to humidity in the atmosphere. Increasing ground temperature leads to higher precipitation.
- An increase in atmospheric stability enhances precipitation on the foremost mountains.
- In the perspective of maximisation it has been assumed that air is saturated throughout the whole of the troposphere

The maximisation method consists in combining these parameters (applied through the boundary conditions) in order to maximise the rainfall rate in the watershed. From an analysis of the 12 wind field simulations (one chart for each geostrophic wind direction every 30°), it appears that the situation with a northern geostrophic wind (sector 0° or 360°) generates a higher precipitation rate in the watershed than any other wind direction. The simulated precipitation field for an event duration of 6 hours is given in Figure 7-1. Here, the maximum catchment-wide averaged rain rate calculated is 39 mm/h. According to the meteorological study of the region, the assumed atmospheric situation is able to last 6 hours giving a maximum daily rain rate of 240 mm in the basin. This compares well with the maximum precipitation recorded of 175 mm during 24 hours in the area between 1891 and 1965.

The full temporal evolution of the precipitation result was routed (8 rain maps of 30 minutes each, corresponding to the temporal evolution of the simulation). The precipitation distribution shown in Figure 7-1 is then maintained for 6 hours (corresponding to the 40 m/s geostrophic wind speed) and finally relative humidity at the boundary conditions of the domain is dropped to 80 % and precipitation in the watershed stop. Thus, entire event duration is 10 hours.

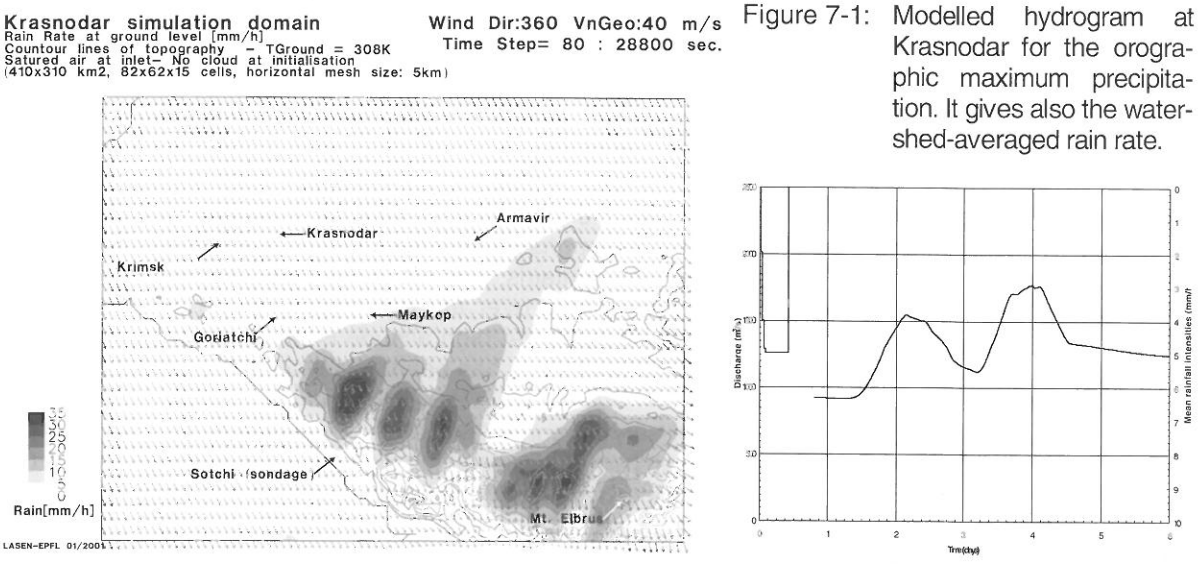

Figure 7-1: Modelled hydrogram at Krasnodar for the orographic maximum precipitation. It gives also the watershed-averaged rain rate.

The simulated hydrograms show two peaks which can be explained by the very different transfer times between the Kuban River and the tributary located at the south of the Krasnodar dam.

7.2 Frontal

The frontal meteorological situation results from the convergence of two different air masses. The method consists in maximising the precipitation field by keeping the same boundary conditions as in the reference case and by determining the most unfavourable chronology for the depletion of the frontal situation.

The solution consists in adding an extreme event after the sequence of the flood event recorded on 6-8 July 1987. According to the distribution of the pressure field for this situation, a severe precipitation event characterized by a strong and humid advection would occur from the southwest. This situation has been simulated by a saturated air mass advected from sector 210 with a 40 m/s geostrophic wind of 4 hours duration on the pre existent cold air mass. The time between the rain episode and the following extreme event was reduced to the minimum in order to prevent the soil from drying too much between the two events. The results of the routing for the frontal probable maximum precipitation and the watershed-averaged rain rate for these 4-day events are given in this figure.

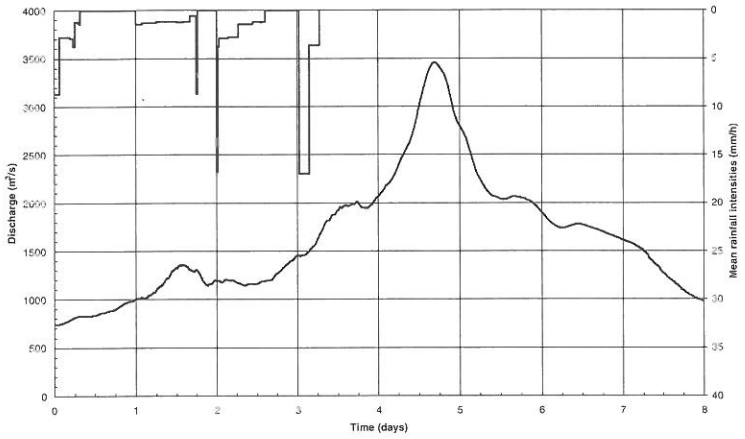

Figure 7-2: Modelled hydrogram at Krasnodar for the frontal maximum precipitation.

7.3 Melting snow

To determine the **winter PMP** the case of warm precipitation on a previous snow cover is considered with the aim to determine the volume of melting snow which could be generated. To maximise this volume, a sequence of two melt periods has been assumed: a sunny snow melt period just follows the melting of the snow cover by the rain. The initial snow cover extends vertically from 100 m above sea level to the top of the culminating point and the winter PMP situation consists of a relative warm humidity field coming from the North. Figure 7-3 shows the simulated hydrograph, the bold line is obtained with a frozen ground (lower infiltration coefficient) while the thin line results from the calculation on a summer ground. For the same reasons than the orographic PMF, precipitation on melting snow shows two distinct peaks.

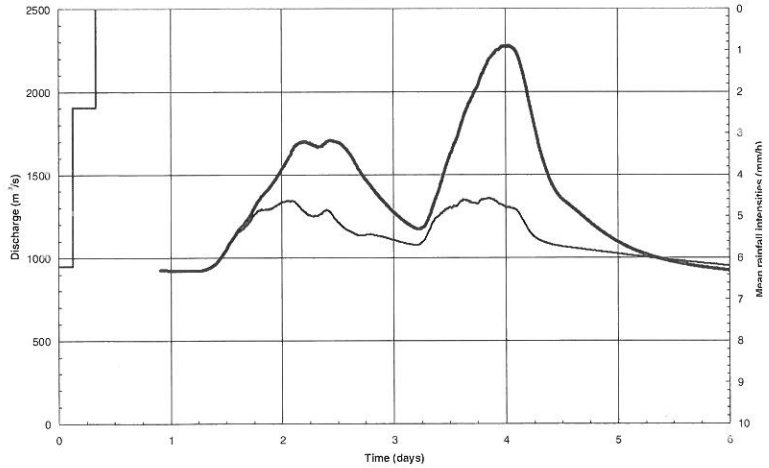

Figure 7-3: Modelled hydrogram at Krasnodar for the winter maximum precipitation (incl. melting of snow).

8 COMPARISON OF THE NUMERICAL RESULTS WITH THE CLASSICAL PMP APPROACH

The WMO recommendation leads to a PMP of 310 mm / 24 h, which is 40 % greater than those calculated through numerical modelling. The classical PMP estimation relies only on the properties of the atmosphere and in particular on the value of the dew point. It does not take into account neither the influence of topography nor the origin of the air masses. The calculated PMP is the same for all the region of the same latitude and with a same dew point. It is well known that the Northern region of the Caucasus is less exposed to humid air masses than other regions at the same latitude. Thus, numerical modelling which takes into account the origin of the air masses provides a lower PMP value. Since the numerical approach is based on physical models which also take into account the particular characteristics of the meteorological and hydrological parameters, the results obtained appear to be more representative of the region of interest and thus more physically convincing. This is particularly important for such a large watershed which presents a lot of inhomogeneity in soil and atmospheric features.

9 CONCLUSIONS

The first part of the study has lead to the description on one hand of the meteorological and climatological characteristics and of the other one of the topographical and hydrological properties of the Kuban River watershed.
In the North hemisphere, the humid air masses responsible of heavy precipitation are coming from the west to southwest. For the considered area, they arrive on the south slope of the Caucasus Massif. Analyses of meteorological maps have shown that orographic precipitations are not predominant in the PMP study of the area. Modelling the critical situation has also shown this. Concerning orographic precipitation, the most critical event corresponds to an advection from the North, which is not able to bring large amount of warm air and humidity. This case is concerned by polar air masses.
Climatological analysis of severe events has pointed out the frontal meteorological situation for which a humid air masse coming from south to southwest is up-lifted above the Kuban River plain over a pre-existent cold air mass. With regards to the meteorological simulation, the frontal atmospheric case is able to generate the most extreme floods in the basin.
Maximisation of this frontal extreme event leads to the determination of the Probable Maximum Flood for the considered basin (see Figure 7-2). The winter case has been taken into consideration. The flow rate calculated by the models in the case of melting of the snow cover first by a severe rain event and followed by a sunny period does not lead to a discharge as important as in the frontal case event by considering frozen ground conditions.
Considering the large spatial extend of the watershed, convective precipitation on flat terrain has not been taken into consideration. Indeed convective events generate very local precipitation short in duration which could not lead to a strong flood in this basin. Meteorological convergence situations contain dry continental air masses. Thus, they have not been modelled either.
Analyses of the hydrological behaviour of the basin show that the hydrograms present two peaks because the flood is composed of the contribution of two distinct geographical areas. The time between the contribution from the mountain and the contribution from the plain is around 1 day and a half.

REFERENCES

Cotton, W.R., Anthes, R.A. (1989): Storm and Cloud Dynamics, Int. Geophys.Series, 44, Academic Press, San Diego, 883 pp.

Hertig, J.-A. Goulpié, P. CRUEX (1997): Septième rapport intermédiaire, LASEN/LCH/IATE EPFL avril 97

Duynkerke, P.G. (1988): An application of the k-e turbulence closure model to the neutral and stable atmospheric boundary layer. J. Atmos. Sci., 43, 2527-2543.

Geiger, H., Zeller, J., Röthlisberger, G. (1991): Starkniederschläge des schweizerischen Alpen und Alpenrandgebietes. Eidgenössische Anstalt für das forstliche Versuchswessen, Birmensdorf

Goulpié, P., Montavon, C. (1996): Simulation de l'Atmosphère dans le projet CRUEX, Rapport interne LASEN-EPFL No 547.110, Décembre 96

Grebner, D. (1993): Meteorologische Analyse des Unwetters von Brig und Saas-Almagell vom 24. September 1993.Wasser, energie,luft-eau,energie *air*, 86. Jahrgang, Heft1/2, CH-5401 Baden.

Haiden, T., Kerschbaum, M., Kahlig, P., Nobilis, F. (1992): A refined model of the influence of orography on the mesoscale distribution of extreme precipitation. *Hydrol. Sci. J.*, 37 (5), 417-427.

Harris, R. I., Deaves, D. M. (1981): The structure of strong winds. Proceedings of the CIRIA conference held on 12/13 Nov 1989 CIRIA

Hertig, J., Goulpié, P., Reinhardt, F.: "Estimation numérique de la PMP pour le basin versant du barrage Deriner en Turquie" Rapport LASEN n 546 100

Kessler, E. (1969): On the precipitation distribution and continuity of water substance in atmospheric circulations. *Meteor. Monogr.*, 10 (32), *Am. Meteor. Soc.*, 84pp.

Montavon, C. (1997): Validation Of A Non-Hydrostatic Numerical Model To Simulate Stratified Wind Fields Over Complex Topography, in Proceedings of the 2nd European & African Conference on Wind Engineering, Geneva, Italy, June 22-27, 1997, pp. 357-364

Montavon, C., Alexandrou, C., Hertig, J.-A. (1995): Simulation of Extreme Precipitation Events in the Swiss Alps, Symposium 'Research and Developments in the Field of Dams' (Crans-Montana, September 1995

WMO (1986): Manual for estimation of probable maximum precipitation. *Operational Hydrology Rep. No.1*, 2nd ed., Geneva, 269 pp.

Zilitinkevich S. S., Johansson P.-E., Mironov D. V., Baklanov A. (1998): An analytical similarity-theory model for wind profile and resistance law in stably stratified Planetary Boundary Layers. JWEIA in press.

FLOOD FORECASTING EXPERIENCES IN ASIAN RIVER BASINS

S. Herath[1], R. Jha[2] and D. Dutta[1]

[1] Institute of Industrial Science, The University of Tokyo, 4-6-1 Komaba, Meguro-ku, Tokyo 153-8505, Japan, herath@iis.u-tokyo.ac.jp, dutta@iis.u-tokyo.ac.jp

[2] Institute of Engineering, Tribhuwan University, Pulchowk, Lalitpur, Nepal, raghunathjha@hotmail.com

SUMMARY

The paper describes flood forecasting experiences in Chao Phraya River basin, Thailand and Agno River basin, Philippines using a physically based distributed hydrological model for early warning purposes. An implicit solution of the dynamic form of the Saint Venant equations for the river network has been carried out with downstream forecasting to find the feasible lead times in the catchments. To set up practical and computationally feasible forecasting schemes, sub catchments are delineated that range from about 600 km^2 to 2000 km^2. Real time river discharge monitoring provides the upstream boundary conditions. The studies show that lead times around 12-14 hours are feasible in Thailand whereas movement of rainfall, and large flow from the tributaries in Agno River basin in the Philippines makes it difficult to forecast floods without adequate monitoring of rainfall distribution and tributaries.

Keywords: Flood forecasting, distributed hydrological model, river network solution, lag time, diffusive wave model

1 INTRODUCTION

The Asian region experiences the highest casualty rates as well as the highest economic damage from floods among the different regions in the world (Herath, 1996). Growing population and consequent population migration to vulnerable areas exacerbate the problem in the future. Competing investment demands make it difficult for developing economies in the region to commit funds for mitigation measures. With this rather unpromising future, early warning is extremely important in reducing flood damage and avoiding loss of life. This paper discusses flood forecasting modeling experiences in two Asian catchments for early warning purposes.

Traditionally conceptual and time series models have been used in flood forecasting. These models are effective if enough historical observations are available for model calibration and verification as well as when continuous monitoring is carried out for modification and upgrading of the models to reflect catchment changes. Japan is an example where flood forecasting is carried out successfully with simple conceptual models supported by more than 2400 telemetered river discharge gauges and close to 2800 telemetered rainfall stations in addition to a complete country coverage by 26 weather radars. Unfortunately, most of the Asian countries lack historical data and similar monitoring infrastructure. Physically based hydrological modeling is an alternative solution to forecast floods adequately in such locations where model parameters can be estimated using physical characteristics of the catchment and calibration can be carried out with a small number of observations.

Most Asian countries have limited logistical support for evacuation and mitigation measures. This calls for long lead times in the forecasts and also realistic assessments in feasible lead times. For example, many flood warning authorities in Japan are content with a 6 hour lead time, where as in Thailand or Viet Nam, authorities wish for lead times of one to few days, which can be achieved only in large catchments. Secondly, past flood experiences suggest the need to anticipate downstream effects, especially temporary blockades at bridges by fallen trees, etc., on the increase of upstream flood risk. In order to set up downstream boundary conditions, either the diffusive form or the dynamic form of Saint Venant equations should be used in the solution scheme. Distributed hydrologic models with implicit river network solutions make heavy demands in computational time if applied at high spatial resolution over large areas and are not very suited for operational flood forecasting. In order to over come this difficulty, small sub catchments above the locations of interest and bounded by a suitable boundary condition point, such as a dam or a gauging station, are modeled. Three case studies, two in Chao Phraya River basin, Thailand and one in Agno River basin, Philippines are modeled using a distributed hydrological model with a river network model which solves the dynamic form of Saint Venant equations. Global data sets of elevation, landuse and soil properties are used to set up the models.

2 MATHEMATICAL MODEL

2.1 Hydrological model

The system used in the modeling is a grid based distributed hydrological model developed at the Institute of Industrial Science, University of Tokyo, which is a coupled system for modeling different components of the hydrological cycle. For flood forecasting studies outlined in the present study, it is convenient to consider the flow generation components separately from the flow transport, i.e. river network modeling component. The flow generation, or the hydrological modeling system consists of interception, evaporation, surface flow, sub surface flow and ground water modeling components. Spatial distribution of catchment parameters, rainfall input and hydrological response are represented in the horizontal plane by an orthogonal grid network and in the vertical plane by a column of horizontal layers at each grid. Only the model components directly relevant to flood modeling are described here. A complete description of the model is described in detail elsewhere. (Herath et al., 1997; Jha et al., 1997)

2.1.1 Interception

The interception component calculates net rainfall reaching the ground through the canopy, the amount of water stored on the canopy and evaporation from the canopy. The interception process is modeled as in BATS (Dickinson et al. 1993).

2.1.2 Evapotranspiration

The actual evapotranspiration is calculated on the basis of potential evapotranspiration (directly input to the model) and the actual soil moisture status in the root zone. The model adopted is the one described by Kristensen and Jensen (1971).

2.1.3 Subsurface Flow

The subsurface flow component connects the surface flow and the ground water flow components. Soil moisture distribution in the unsaturated zone is calculated by solving three-dimensional Richards' equation. The X and Y components of the Richards' equation are solved explicitly for previous time step. Soil moisture flux due to X and Y components, extraction of moisture for transpiration and soil evaporation are introduced as sink terms at the node points in the root zone. Infiltration rates are determined by surface boundary conditions that may be either flux controlled i.e. net rainfall or head controlled, in the case of ponding. The subsurface zone is modeled by an adaptive finite difference grid scheme where the lowest node coincides with the phreatic surface.

2.1.4 Ground water flow

The ground water level is modeled as multi layered two-dimensional system where each layer could be either a confined or unconfined aquifer. The spatial and temporal variation of hydraulic head is calculated by non-linear Boussinesq equation for multi-layer leaky aquifers and is solved by implicit finite difference approximation using successive over relaxation (SOR) scheme. The interaction of the aquifer with the river system is calculated on the basis of the difference in river water levels and ground water table elevation.

2.1.5 Overland Flow

Overland flow is generated when the rainfall rate exceeds the infiltration rate and ponding occurs or when the ground water level rises up to the ground surface. Overland flow is simulated in each grid square by solving the two-dimensional diffusive wave approximation of St. Venant equation. When the Manning equation is substituted in diffusive wave equation the resulting equation becomes non linear and obtaining a stable solution is difficult. To overcome this difficulty, following simplifications are adopted.

The diffusive wave equation is written as;

(1) $$\frac{\partial h}{\partial t}+U\frac{\partial h}{\partial x}+V\frac{\partial h}{\partial y}=q$$

where U and V are calculated in the previous time step. The implicit finite difference form equations are written for all nodes and solved by SOR using Chebysher acceleration.

2.1.6 Coupling

The above processes are computed by independent numerical schemes that are coupled by flux and head boundary conditions. A coupling module coordinates the coupling process where each process is simulated with different time steps and is finally coupled at a common coupling time steps. Additionally, the coupling module carries out the update of the boundary conditions as well as the reading of meteorological inputs at appropriate times.

2.2 River network model

2.2.1 River Routing

In the river routing scheme both the Kinematic approximation and the dynamic version of the Saint Venant equations are implemented.
The equations are solved explicitly to get the river discharge at next point. The river routing starts from a far upstream point and proceeds downstream to the mouth of the river.

2.2.2 Dynamic River Routing

Algorithms have been developed (Fread, 1976; Amein, 1970) to use full dynamic equation to simulate the floods. The Weighted four point finite difference approximation (Chow et al., 1988) are written for each point of river network, which produce (2N-2) non-linear equations. Where N is number of points in river network. For each branch there are two boundary conditions (upstream and down stream). Two junction boundary conditions are employed. They are the continuity equation and the equality of water head in each branch in the junction. With these boundary conditions 2N nonlinear equations and 2N unknowns result, which are solved for each time step, using the Newton Raphon method (Fread, 1976). The details of the solution scheme for a river network is given in Jha et al. (2000).

2.2.3 Initial and Boundary conditions

To apply the river modules it is necessary to know the initial depth and discharge at each simulation node. In the case of flood forecasting these values may not be available at the start of the computations as the modeling might start from an arbitrary point in time. When the initial river discharge information is not available, it is estimated from an equilibrium discharge computed using the following formula,

(2) $$Q=\Delta A.rlf$$

where Q is the discharge, ΔA is the catchment area for the channel and rlf is the regional low flow factor. The upstream boundary condition of each stream link is provided as a water depth or discharge time series, and Q = 0 is assigned if there are no inputs to the starting node of a stream. For flood forecasting, there are occasions where upstream boundary condition has to be estimated for the future predictions. A simple model of the following form was used to estimate the future upstream boundary condition.

(3) $$Q[t]=Q[t-1]+\alpha\frac{\partial Q}{\partial t}n\Delta t$$

where α is a regression constant, Q[t] and Q[t-1] refers to current and previous time steps, Δt is the simulation time step and n is the forecasting time step. The downstream boundary condition is not required in the Kinematic wave solution as the backwater effects are neglected in the scheme, whereas it is required in the dynamic solution. While this could be available for simulating past events, it has to be estimated when flood forecasting is carried out. For forecasting purposes, downstream discharge is estimated using the following equation,

$$Q_{ds} = Q_n - \left(\frac{Q_n - Q_{n-1}}{\Delta X_n}\right)\left(\frac{v_n + v_{n-1}}{2}\right)\Delta t \tag{4}$$

where v_n and v_{n-1} are velocities in the previous time step at locations n and n-1 respectively, Δt is the time step and ΔX_n is the distance between points n and n-1. Q_{ds} is the required discharge at the downstream point and Q_n and Q_{n-1} are the discharges at n and n-1 points at the previous time step. This formulation also makes it possible to estimate the water level changes if the downstream river capacity gets reduced due to debris, etc.

3 CASE STUDIES

Flood forecasting studies were carried out in two locations in the Chao Phraya basin in Thailand (Figure 3-1) and the Agno basin in the Philippines. The catchment characteristics modeling results are outlined below.

3.1 Chiang Mai City, Ping River basin, Thailand

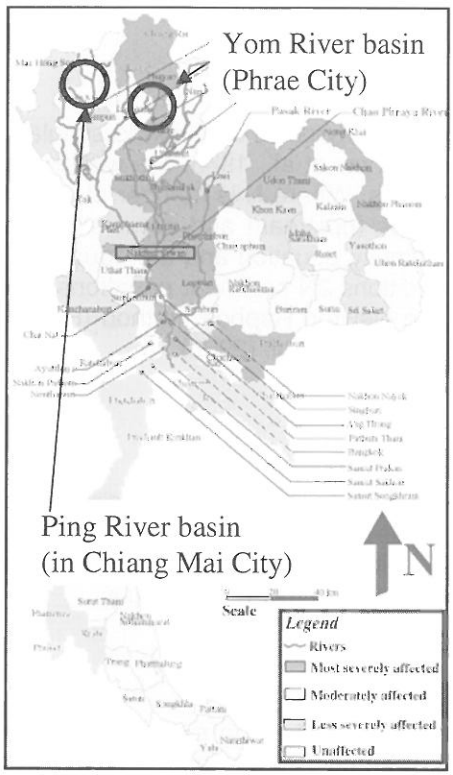

Figure 3-1: Locations of flood forecasting studies with a map of flood affected areas in Thailand, 1995.

Ping river basin, a sub-catchment of Chao Phraya river basin, is located at north-western part of Thailand between 18°45'N to 19°45'N latitude and 99°45'E to 100°15'E longitude with a drainage area of 6,300 km^2 (Figure 3-2). The average rainfall in this catchment is 1,250 mm. In 1995, the upper Chao Phraya river basin experienced severe flooding as a result of rain from tropical storm Lois, which was generated in the South China Sea, passed over Nan province on August 27 and moved towards Phrae and Pha Yao on 31st August reaching finally Lam Pang on September 1. The storm caused intense rainfall in north, northeastern and eastern regions of Thailand (*INCEDE Newsletter, 1995*). The Chiang Mai city (Ping river basin) was hard hit and flooding in the city was severe and extensive with peak inundation lasting for several hours and general inundation for much longer. Flood forecasting in the city is presently carried out using a regression relation, which correlates upstream gauging water level to the water level at the station nearest to the city.

A subcatchment of the Ping basin at Chiang Mai was selected for flood forecasting studies. The river network for the selected area is shown in Figure 3-3. At first, several simulation studies were carried out to investigate whether it is possible to carry out flood forecasting in the basin and whether sufficient lag time exists between the upstream and downstream gauges. The Mae Faek station was considered as uppermost boundary condition (refer to Figure 3-3) while two other gauging stations, P21 and P4a too are used as boundary conditions where observed discharge data are used as input boundary condition. The catchment areas at P.4A, P.21 and Mae Faek are 1902km^2, 515 km^2 and 3583 km^2 respectively. While the catchment area upstream of P1 station is around 6600 km^2, the selected sub catchment area covers an area of about 600 km^2 or less than 10% of the total area. Figures 3-4 and 3-5 show the observed hydrograph at Mae Faek station

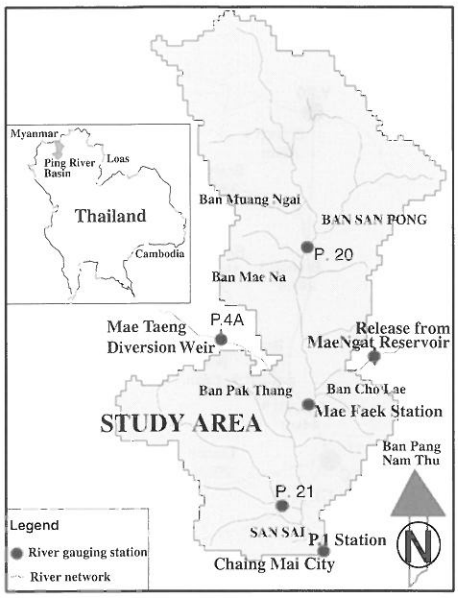

Figure 3-2: Ping River basin, Thailand.

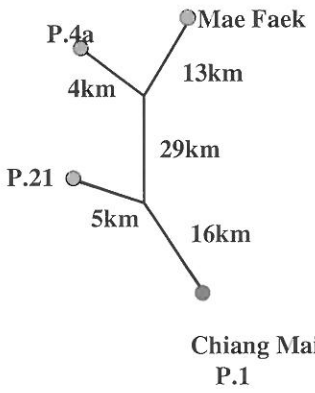

Figure 3-3: Schematic River network for Chaing Mai forecasting.

and simulated hydrograph at P1 station without rain and with rain for a period of 110 hours starting from 4 hr. of September 4 to 18 hr. of September 8, 1995, the distance from Mae Faek station to P1 station is approximately 60 km. From the Figure 3-4, it is seen that flow wave propagation from the Mae Faek station to P1 station takes about 20 hours under no rain conditions and that it reduces to about 17 hours when rainfall is added to the system (Figure 3-5). This significant lag time implies the possibility of real time flood forecasting using the upstream river discharges. The reduction in lag time in the presence of rainfall is due to increased flow velocities and lateral inflow to the river, which implies that during flood times the lead-time would get reduced more. Further, the inputs from P4a and P21 alter the quantity as well as the time to peak.

As an example, a flood-forecasting event is described in Figure 3-6, for a flood event that took place from the 30th of August to 05th of September 1995. The dynamic form of the river routing model is used in this example. The simulated and actual discharges match well for practical forecasting purposes. The forecasts up to about 12 hours in advance do not deviate from the simulation accuracy which suggest that it is feasible to use dynamic form of river network solution for forecasting flood peaks with estimates of the downstream and upstream conditions using equations (3) and (4) for this sub catchment for about 12 hours. After that numerical instability occurs, which is most likely triggered by the downstream boundary condition forecasts.

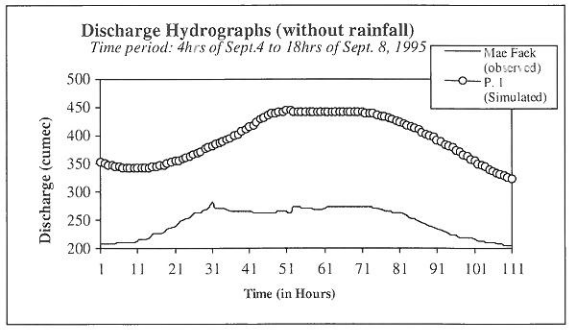

Figure 3-4: Upstream and downstream hydrographs without rainfall.

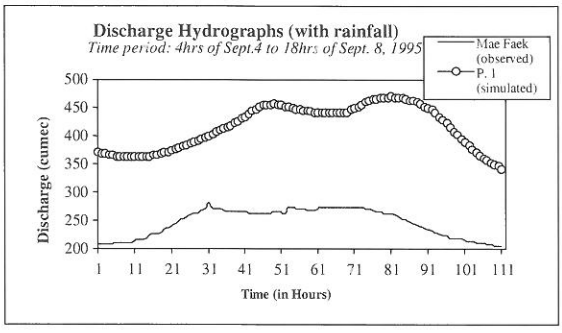

Figure 3-5: Upstream and downstream hydrographs with rainfall.

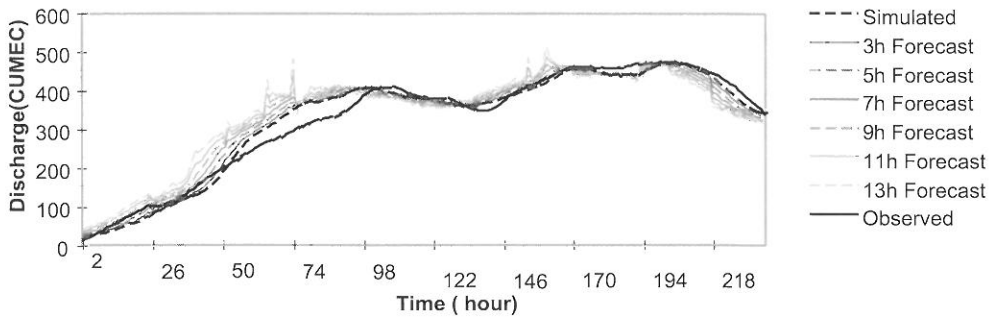

Figure 3-6: Flood forecasts for the Ping River basin at Chiang Mai city.

3.2 Phrae City, Yom River basin, Thailand

Phrae city with a population of about 20,000 in the municipal area covers an area about 9 km^2 and is located at the bank of the Yom River. The city experiences flooding 3 to 5 times a year, with inundated area going up to about 50% of the city. During the heavy rain in 1995, the whole city was flooded and the economical loss was estimated at around 16 million US$. Generally, the inundation starts approximately about 3 km upstream of the city by bank over topping. There is a gauging station (Y1C) near the city and the catchment area at this location is 7624 km^2

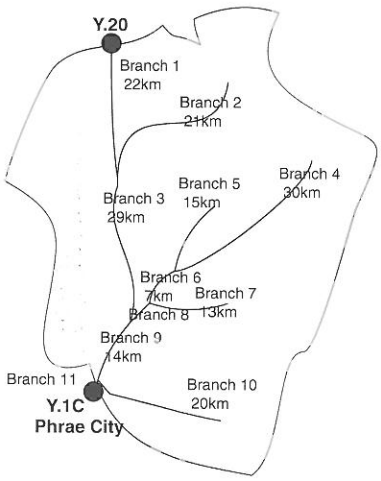

Figure 3-7: Location of Phrae City in the Yom River basin.

Two events, one a moderate flood from 5 August to 10 August 1995 and a large flood event from 30 August to 6 September were selected for flood forecasting. The maximum flow for event one is 1183 m^3/s for the first event and 2205 m^3/s for the second event at Y1C station. For forecasting purposes, the sub catchment and the river network shown as in Figure 3-7 is adopted. The forecasted and observed hydrographs for the event 1 is shown in Figure 3-8. For this case the rainfall data at the beginning of the storm was not available, and hence there is some discrepancy between the observed and simulated hydrographs can be seen at the hydrograph initiation. Further, we do not expect the estimation of the downstream hydrograph to match very accurately with the observations, as the single available rain gauge is not expected to capture the spatial and temporal variation of rainfall adequately. Rather we look at the forecasting lead times by comparing the forecasted hydrograph with the simulated hydrograph. As can be seen, the methodology adopted makes it possible to carry out 10-12 hour forecasts with good accuracy. Similar results were obtained for the case 2 indicating applicability for high floods too, with a lead-time of about 12-14 hours.

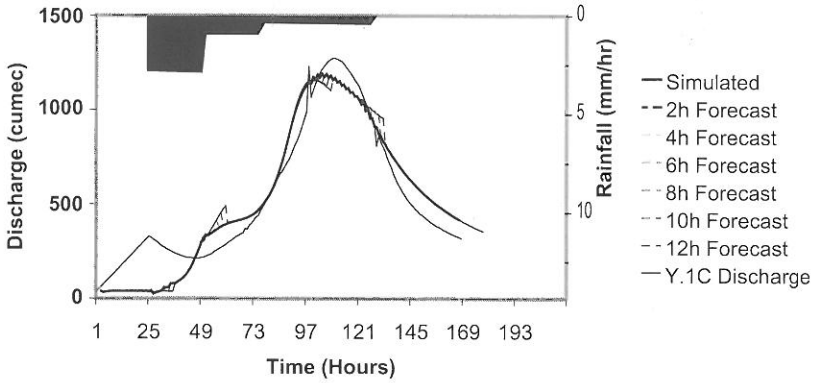

Figure 3-8: Flood forecasting in Yom River basin, case 1, from 5-10 August, 1995.

3.3 San Roque, Agno River basin, Philippines

The Agno river basin, which lies in the western portion of the central part of Luzon island, is the fifth largest river basin of the Philippines with a drainage area of 5,952 km^2 (Figure 3-9) Severe typhoons and consequent floods frequently affect the basin many times a year. In September 1989 torrential rains associated with typhoon Angela caused severe floods in Agno river basin, which took lives of 119 people, destroyed over 14,000 houses and left nearly 85,000 people homeless. PAGASA (Philippine Atmospheric, Geophysical and Astronomical Services Administration) has been working on flood forecasting in the basin. Telemetric system is used to obtain hourly rainfall and water level data in different locations of the basin. However, due to technical problems, datasets in many gauging stations are not available for continuous long periods. In this study, depending on the availability of required data, a sub catchment of the basin with an area of 1,700 km^2 is selected (Figure 3-10). The annual average rainfall varies from 2,000 mm in the southeastern part to more than 4,000 mm in the northern mountainous part of the study area. The northern mountains rise to a maximum evaluation of 2100 m from mean sea level (msl) whereas the lower part is rather flat (around 40 m from msl). The

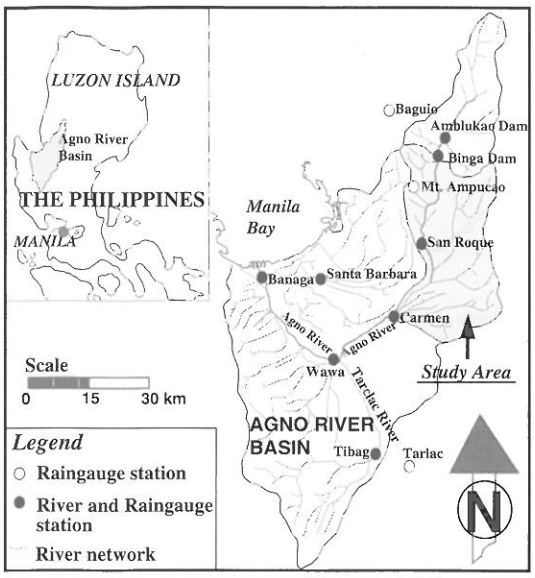

Figure 3-9: Location of Agno River basin.

Figure 3-10: Sub catchment of Agno basin selected for study.

vegetation of the upper mountainous area includes dense and light forest areas, whereas agricultural fields and grasslands cover lower flat area (Dutta and Herath, 1996). In the lower part, along the Agno River, residential areas are located.

Simulation of river flows in the Agno basin has showed that it is possible to model the river flows adequately with the distributed hydrological model using the available rainfall and upstream inflow data. For the forecasting purposes, water levels at Binga dam (upstream boundary condition), San Roque (mid point) and the rainfall data are available in real time. Thessen polygons corresponding to each of the 3 rain gauges are shown in the background of Figure 3-10. The flow characteristics of the Agno River are demonstrated with the simulation results of two river flow events. The Figure 3-11 shows the propagation of the river flows associated with a dam release. As can be seen in the figure, the lag time between the peak at San Roque and Binga dam is about 4 hours, and that between Carmen and San Roque is about 6 hours. However, during the event from 11 hour of October 19 to 23 hour of October 21 shown in Figure 3-12, the flood volume at Carmen is mostly contributed from the rivers flowing from east side of the catchment. The contribution from the main river, as shown by the flood hydrograph at San Roque station, is substantially small compared to the discharge hydrograph at Carmen. Further the as shown in the rainfall distribution in Figure 3-13, the rainfall in the downstream and mid stream areas of the basin are higher than the rain recorded in the mountainous areas. In order to forecast the floods in this catchment, it is important to estimate the flows from the tributaries to the east of the catchment accurately. It would be possible to increase the forecast lead time by installing rainfall monitoring stations on the east side so that rainfall movement can be incorporated in the forecasting process.

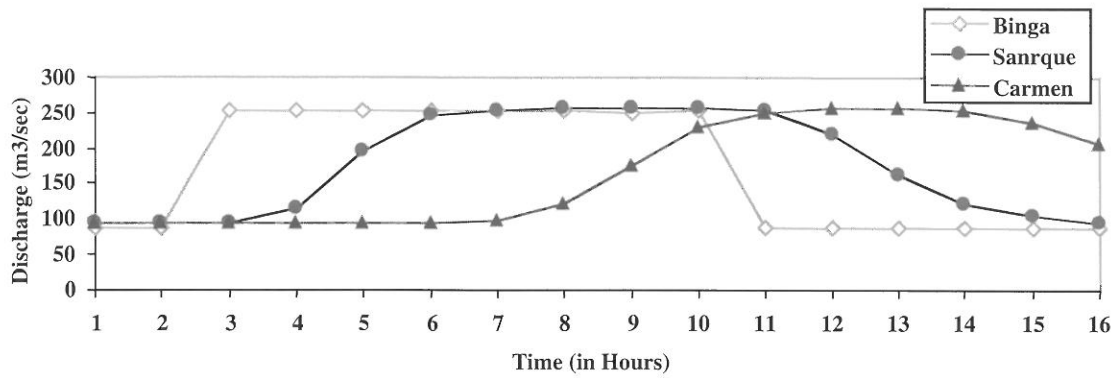

Figure 3-11: Binga Dam Release and Simulated flood hydrograph (Period:12hrs. of August 13 to 4hrs. of August 14, 1989).

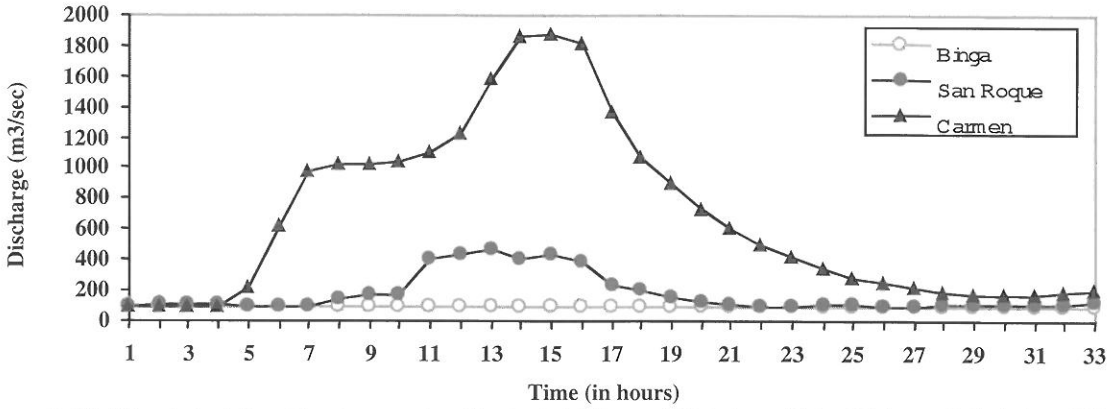

Figure 3-12: Simulated flood hydrographs (Period: 11 hrs. of October 19 to 23 hrs. of October 21).

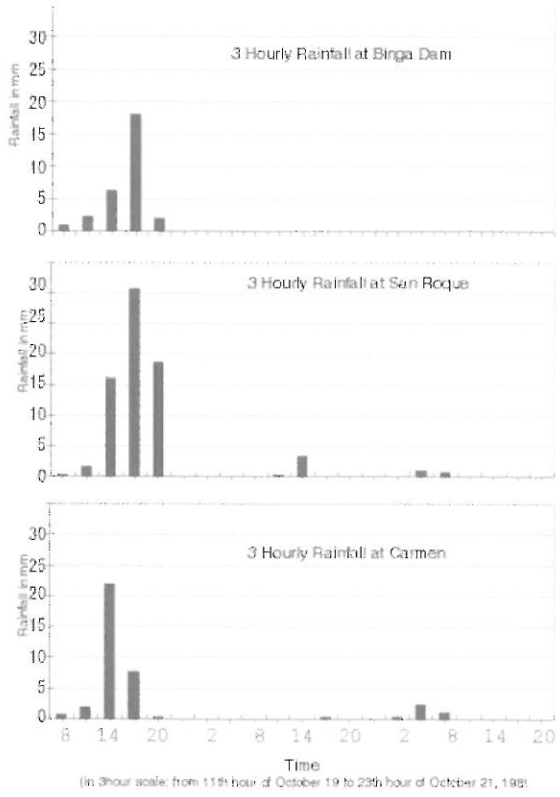

Figure 3-13: 3 hourly rainfall distribution for the event 2 from 11 hrs. October 19 to 23 hrs. October 21, 1989.

4 CONCLUSIONS

Flood forecasting studies carried out with a physically based distributed hydrological model and readily available catchment physical data has demonstrated that it is a practically viable method for flood forecasting where calibration of conceptual models is difficult due to lack of historical data. The physically based approach gives insight in to the flood mechanism and helps in determining what monitoring equipments are necessary to improve accuracy and lead-time of forecasts. From the modeling experiences it is recognized that rainfall distribution and movement have the largest impact on the flood forecasting ability.

In the present study the dynamic form of the river network solution scheme was used, in order to model accurately the backwater effects such as overflow from tributaries and blockades of river sections, which often causes river floods. In order to use the dynamic form for forecasting, it is necessary to anticipate or forecast the downstream boundary conditions. This could be either controlled by river discharge capacity under blocking conditions or by downstream water head in case of fixed downstream boundary conditions. In the absence of such boundary conditions, the discharge

conditions would be determined by the flow characteristics. In steep terrain as in the cases investigated in the present study, the flow of the main stream could be closer to Kinematic assumptions, where the friction slope nearly equals the bed slope. As shown by the Thailand case studies, forecasting lead-time in the present simulations are limited by numerical dispersions, most likely associated with the downstream boundary conditions that are estimated from equation 4. This solution stability probably can be improved by estimating downstream boundary conditions by Kinematic wave model, before iterative dynamic wave solution for the river network is carried out. The use of dynamic form provides a more realistic assessment of the forecasting possibilities, as in most flood situations, the down stream conditions, such as temporary blocking at the bridges could create backwater conditions that exacerbate the severity of floods. However, further studies are required for optimal incorporation of anticipated downstream conditions in forecasting situations.

REFERENCES

Amien, M and Chang, C. S. (1970): Implicit Flood Routing in Natural Channels, J. Hydraulic Div., ASCE, 96 (HY12), USA pp. 2481-2500.

Chow, V.T. et al. (1988): Applied Hydrology; McGraw-Hill International Editions; Civil Engineering Series, USA

Diskinson, R.E. et al. (1993): Biosphere Atmosphere Transfer Schemes (BATS) version 1e, as coupled to the Community Climate Model. NCAR Technical Note NCAR/TN-387+STR, National Center for Atmospheric Research, Boulder, CO., USA

Dutta, D. and Herath, S. (1996): Development of A GIS For The Hydrologic Analysis of Agno River Basin, Proc. Annual Conf. of Japan Society of Civil Engineers, Tokyo, Japan, pp. 334-335.

Kristensen, K.J. and Jensen, S.E. (1975): A Model for Estimating Actual Evaporation from Potential Evaporation, Nordic Hydrology, Denmark, Vol. 6. pp. 70-88.

Fread, D.L. (1976): Theoretical Development of Implicit Dynamic Routing Model, Dynamic Routing Seminar at Lower Mississippi River Forecast Center, National Weather Service, NOAA, Silver Spring, Md., December 1976b, USA

Herath, S. (1996): Floods in Asia: characteristics and mitigating issues; Proceedings of International Seminar on Recent Trends of Floods and Their Preventive Measures, Sapporo, Japan, pp. 107-120

Herath, S. et al. (1997): Application of IISDHM in Northern Chao Phraya, Thailand, The Third Intl. Study Conference on GEWEX in Asia and GAME, Korea, GAME International Science Panel, pp.125-133.

INCEDE Newsletter (1995): 1995 Floods in Thailand; INCEDE, IIS, University of Tokyo, Vol. 4, No. 4, pp. 13-14

Jha, R. et al. (1997): Development of IIS Distributed Hydrological Model (IISDHM) and its Application in Chao Phraya River Basin, Thailand; Annual Journal of Hydraulic Engineering, JSCE, Japan, Vol. 41, pp. 227-232

Jha, R. et al. (2000) River Network Solution for a Distributed Hydrological Model and Applications, Journal of Hydrological Processes, John Wiley & Sons, USA, Vol.14, No. 3, pp. 575-592

STUDY OF HYDROLOGICAL PROCESSES FOR BETTER MODELS AND FLOOD ESTIMATIONS

C. Joerin [1], A. Musy [2], D. Talamba[2]

[1] Federal Office for Water and Geology, 3003 Bern, Switzerland, christophe.joerin@bwg.admin.ch

[2] Institute of Soil and Water Management, Swiss Federal Institute of Technology, 1015 Lausanne, Switzerland, andre.musy@epfl.ch, daniela.talamba@epfl.ch

SUMMARY

The objective of this research is to improve the comprehension of the hydrological behavior of natural catchments. The main originality of this work is to associate different types of measurements in order to obtain a better vision of hydrological processes. First, the hydrological behavior is studied at the catchment scale by the application of environmental tracing. The temporal variability of hydrological responses seems essentially controlled by the catchment moisture. Soil contribution increases with the rise of the basin humidity. The soil water dominates the generation of major floods, which occur in wet conditions. In order to discover the processes responsible for the important soil water contributions, a large-scale Time Domain Reflectometry (TDR) experiment (64 probes) was conducted. On the whole, this experiment indicates that the water flow processes are spatially quite heterogeneous and depend on local properties. During a rainfall simulator experimentation macropore flows were clearly identified. This mechanism may be responsible for the important contribution of soil water and the heterogeneity of the soil moisture. In order to test this hypothesis a dye tracing experiment was done. This new investigation confirms that an important part of soil water reaches the stream by preferential flows. This process is certainly at the origin of the important contribution of soil water to flood. Finally a conceptual model, based on the extension of contributing areas and on the role of preferential flows, is proposed to explain the hydrological and chemical.

Keywords: Haute-Mentue watershed, hydrological processes, association of measurements, hydrograph separation, time domain reflectometry, rainfall simulator, dye tracing.

1 INTRODUCTION

In the actual context, where the preoccupation for the climatic hazard is increasingly important, it is fundamental that hydrologists have efficient models to estimate and forecast the consequence of extreme events. The quality of these previsions depends on the adequacy of hydrological models. It is essential that models reproduce correctly the processes and the hydrological responses observed in the watersheds, but despite the complexity of some (e.g. physically based models), it is not the case for many of them. It seems that the improvement of forecast can be reached only with a better conceptualization of hydrological models. This observation is at the origin of this research. Its objective is to improve the comprehension of the hydrological behavior of natural catchments. More particularly this study aims to identify which processes are responsible for flood generation.

During the last decades, an important number of case studies has been made with the aim of identifying hydrological processes and physical factors, which control them. In this area environmental tracing has perhaps yielded the most interesting results. In general, applications of environmental tracing in the regions with humid and temperate climate demonstrate that floods are mostly generated by subsurface water which is present in the watershed before the beginning of the rainfall-runoff event (Buttle, 1994). At present the principal concern of the fundamental hydrological research is certainly the explanation, in processes terms, how the pre-event water achieves to contribute so strongly and quickly to the flood generation.

The environmental tracing is particularly important because it allows the study of hydrological processes at the catchment scale. Nevertheless its application does not allows the identification of the mechanisms responsible for flows through hill slopes. In fact the hydrograph decomposition identifies the origin of flows but the mechanisms responsible for the stream flow generation cannot be determined from it (Elsenbeer et al., 1995). Indeed, water following different pathways can present the same tracer concentration or a mechanism can involve different kinds of water (chemical characteristics) (McDonnell, 1990). More generally, because of the equifinality problem (Buttle, 1994) it is not possible to identify the combination of hydrological processes from the application of only one

observation method (Ambroise, 1998). Then in order to identify the water pathways and the mechanisms which are at the origin of flood formation, it seems necessary to associate hydrochemical observations to others type of measurements (Jenkins et al., 1994).

2 STUDY AREA

Jordan (1994) gives a fully detailed description of the Haute-Mentue basin. Here only a brief description is given in order to introduce the geographical, geological and meteorological context of this study. The basin is in the Swiss Plateau about 20 km north of Lausanne. The climate is humid temperate with slight continental characteristics. Mean annual precipitation is around 1280 mm and mean potential evapotranspiration is around 600 mm. Annual average runoff at the outlet of the Haute-Mentue basin is 680 mm. The hydrological regime has a seasonal cycle with a discharge minimum at the end of summer and maximum during winter. The bedrock is composed of low permeability sedimentary deposits (sandstone and siltstone) called "molasse". A variable layer of basal moraine overlies this substratum, which is almost impermeable. Soils are sandy loams or loamy sands and are classified as dystric cambisoils and luvic cambisoils. They have an average depth of one meter and are moderately permeable. The investigations reported here are concentrated essentially on the Bois-Vuacoz subbasin (24 ha) situated in the upper and forested part of the Haute-Mentue. The altitude ranges between 900 and 927 m and the average slope is about 7.5%.

3 METHOD

This study proposes an approach for the identification of hydrological processes, which associates environmental tracing and hill slope measurements. First, hydrological behavior is studied at a large scale by the application of environmental tracing. Next, hydrometric measurements are conducted to identify contributing areas to study specific mechanisms and to discover the controlling parameters. The different experiments conducted in the Haute-Mentue are briefly presented below.

3.1 Environmental tracing

According to the pedological, geological and hydrochemical conditions of the Haute-Mentue watershed, a three-component mixing model based on silica (SiO_2) and calcium (Ca^{2+}) concentrations was developed (Iorgulescu, 1997; Joerin et al., 2002). The calcium concentration is on the one hand low in acid soil water (150-650 µeq/l) and on the other hand high in groundwater (1650-2900 µeq/l). So, calcium is a good tracer in order to distinguish groundwater from superficial waters (soil water and rainfalls). Silica allows to distinguish water, which has had contact with the mineral matrix (acid soil water and groundwater) from rainfalls. In fact, silica concentration in acid soil water (5-14 mg/l) and in groundwater (8-14 mg/l) differs considerably from concentrations in direct precipitation (0-1 mg/l).
By hypothesis, the catchment outflow is considered as a mixture of n flow sources which are characterized geochemically by m tracers. In the particular case of the Haute-Mentue's mixing model $n = 3$ and $m = 2$. It is then possible to express the mass conservation of water and tracers with the following expressions:

$$Q_t = \sum_{i=1}^{n} Q_i$$

$$Q_t \cdot C_t^j = \sum_{i=1}^{n} Q_i \cdot C_i^j \qquad j = 1,...,m \tag{1}$$

In summary, this model can differentiate in the hydrograph the following components: direct precipitation, soil water (acid soils) and groundwater (in contact with the carbonate bedrock).

3.2 Time domain reflectometry

According to previous studies conducted in the Haute-Mentue (Jordan, 1994; Iorgulescu, 1997), the hydrological behavior seems to depend strongly on wet antecedent conditions. So it was chosen to conduct a large-scale time domain reflectometry (TDR) experiment. The utilization of TDR has been proven to be a reliable method for the determination of soil moisture. The TDR equipment covered an area of approximately 500 m^2 located in the Bois-Vuacoz sub-basin. Thanks to multiplexing, the system records hourly the apparent length of 64 probes computed from the plotted pulse with the software Pc208e from Campbell Scientific. Each probe is composed of two wires, which are 30 cm long. The soil moisture is calculated from the measurement of the apparent dielectric constant of the soil ε_r and applying the three-phase (solid, liquid and gas) model of Tinga et al. (1973):

$$\varepsilon_r = \left[\theta \cdot \varepsilon_w^{\beta} + (1-\phi)\cdot \varepsilon_s^{\beta} + (\phi-\theta)\cdot \varepsilon_g^{\beta}\right]^{1/\beta} \quad (2)$$

where ε_W, ε_S and ε_G are the dielectric constants of water, solid and gas phases, respectively, ϕ the soil porosity, and θ the soil volumetric water content. Coefficient β depends on the spatial structure of the mixture and its orientation with respect to the outer electric field.

3.3 Rainfall simulator

For this experiment, a rainfall simulator (ORSTOM type, cf. Asseline and Valentin (1978)) was used. With this equipment it is possible to apply rainfalls with intensity varying between 25 and 150 mm/h on an experimental area of 1 m^2. This area is delimited by square of metallic plates, which are knocked in the soil at a depth of 5 cm. The lowest plate is pierced; the holes come up to ground level. A duct collects the surface flow which transits through these holes. An automatic system composed of pressure sensor and a datalogger measures continuously the water level of surface flow accumulated in a container. The infiltration is deducted from the difference between the surface flow and the applied rainfall intensity. Next to the collecting area three TDR probes (10, 20, 30 cm) were vertically inserted in the soil. These probes were used to follow the evolution of water content during the simulated rainfall.

3.4 Dye tracing

The dye tracing experiment aimed to estimate the ability of soil to transmit a water lateral flow. It was conducted in the Bois-Vuacoz sub-basin. For the injection of tracers three long (100 cm) and three short piezometers (40 cm) were inserted in the soil near the main stream. The distance between the injection points and the stream was about 12.8 meters (Figure 3-1).
In order to determine directly in the field the tracer concentration, a fluorimeter GGUN (Schnegg and Doerfliger, 1997) was installed in the river (Figure 3-1). For this experiment two tracers were used the sulforhodamin G and the uranin. This choice was done according to the possibilities offered by the fluorimeter and the particular conditions of this experiment. The use of these two tracers to follow the water flow in the soil and the aquifer is not ideal.

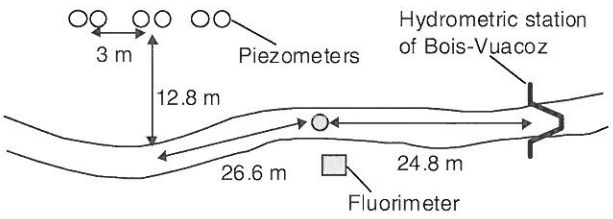

Figure 3-1: Position of the equipment used in the context of the dye tracing experiment.

The uranin can be partially retained in clays or in organic soils. The use of the sulforhodamin G is not recommended in aquifers with interstice porosity. The principal consequence of the behavior of these tracers is a low recovery rate. Since the aim of the experimentation was only to determine the transit velocity of water in the soil, this limit of application does not constitute a big disadvantage. A solution of sulforhodamin G (90 g sulforhodamin G diluted in 1 liter of water) was dumped in each piezometer

of 40 cm. In tubes of 100 centimeters, a solution of uranin (50 g of uranin diluted in 1.5 liter of water) was injected. With these two tracers it was possible to follow simultaneously the water flows at two different depths.

4 RESULTS

4.1 Environmental tracing

The hydrograph separation of main floods observed in four Haute-Mentue sub-basins between 1997 and 1999 allowed the study of the spatial and temporal variability of hydrological responses characterized by the contribution of the three components (Joerin, 2000). The spatial variability of the hydrological response seems mainly due to the catchment morphology and geology. In view of the complexity and the heterogeneity of basins, it is highly probable that the water flows are controlled by a combination of processes. This set of processes depends certainly on the physical properties of the basins. The relative importance of one process in comparison with the others varies in time with the wet conditions. Despite the spatial variability, a common trend was observed among the four sub-basins. The hydrograph separations presented in Figure 4-1 for the rainfall-runoff events which occurred in Bois-Vuacoz between the 5 November 1997 and 2 December 1997 illustrate well this common trend (Figure 4-1).
The study period presents relatively wet antecedent conditions. In October it rained 76.3 mm. Nevertheless, a relatively long period without rain occured between 24 October and 3 November. Initially storm flow can be explained as a mixture of pre-event base flow and precipitation. As the basin becomes wetter, the contribution of soil water increases. Finally, in wet conditions soil water dominates storm flow. The most relevant observations are that the groundwater dominates the flow almost all the time (GW 36% - 99%) and that the soil water contribution increases during the series of four events between the 8 and 13 November (Figure 4-1). Moreover, during the 13 November peak flow soil water dominates the flood (SW 46%, GW 41% and DP 13%).

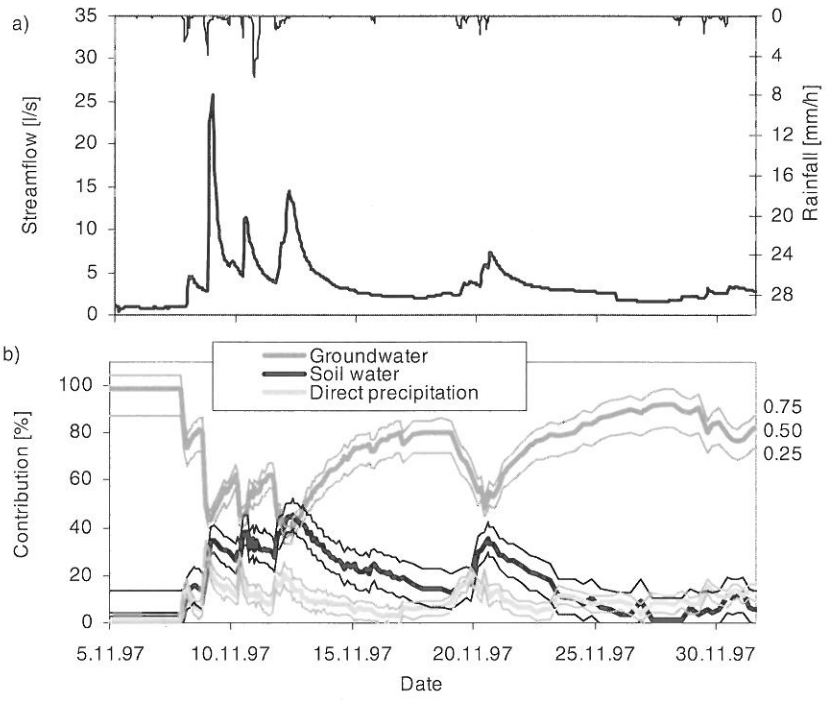

Figure 4-1: Hydrological responses in Bois-Vuacoz sub-basin a) Rainfall and runoff b) Hydrograph separation and representation of component contribution in quartile form (0.75, 0.50, and 0.25).

In general all the results presented in this article concern events observed in the sub-basin of Bois-Vuacoz during the wet period, which stretches from the autumn to the spring. The highest soil water contributions were observed for this particular case. This example was chosen, because in view of the environmental tracing results this study aims precisely to explain the important contribution of subsurface flows and more particularly of the soil water.

4.2 Time domain reflectometry

The soil water content was recorded during two periods October - November 1997 and May - October 1998 (Joerin, 2000). The TDR experiments showed that the soil moisture varies strongly in time and in space. During the dry months, between June and August, the evapotranspiration is the principal process which controls the soil water content. Since the evapotranspiration is very strong during this period, the drying dynamics of soil is spatially very homogeneous. At the opposite the soil drainage during the wet period is spatially very heterogeneous. Two observation points a few meters apart can present completely different dynamics of soil water discharge. For example the different behaviors highlighted in Figure 4-2 are observed between probes, which are 1-8 meters apart.

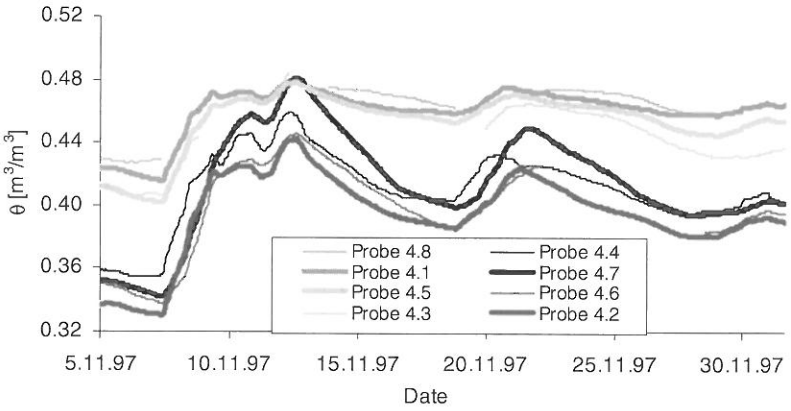

Figure 4-2: Continuous soil moisture measurements at 8 vertical probes (length 30 cm).

In wet conditions it is possible to distinguish two patterns. In the first case (e.g. probes 4.4, 4.7, 4.6, 4.2 in Figure 4-2), the soil moisture increases more strongly than in the second one (e.g. probes 4.8, 4.1, 4.5, 4.3 in Figure 4-2). In the first case the initial soil water content is clearly lower than in the second, but the soil moisture maximums of both series are very close. Nevertheless the time taken to reach soil moisture maximum is similar in both cases varying between 15 and 17 hours. The decrease of soil moisture is also completely different. In the first case this dynamic is clearly stronger and quicker than in the second.
It is interesting to compare the soil moisture dynamic with the hydrograph separation. The series of soil water content presented in Figure 4-2 were recorded during the same period as the hydrograph separation from Figure 4-1. The soil water dynamic is similar to the soil moisture dynamic. In fact these two series follow the same evolution, and they reach their maximum virtually at the same time on 13 November (lag of one hour). Overall TDR observations confirm partially the relative importance of the soil water component. After important precipitation, the soil water content increases strongly (Figure 4-2) and can reach a moisture level close to saturation (the soil porosity at Bois-Vuacoz is around 50 m^3/m^3). This context, which occurs at the same time as the streamflow increases, seems to be favorable for subsurface flows. According to environmental tracing and TDR results it seems possible to confirm the importance of the soil water contribution and the one of subsurface flows to the flood generation in wet conditions. Furthermore, the TDR experiment indicates clearly that conditions of subsurface flows are not homogeneous within hill slopes. Consequently, hydrological processes such as soil moisture depend probably on very local characteristics. Concerning the form of the subsurface flows, they are probably lateral rather than vertical. In fact during the studied period (Figure 4-2) the evaporation was negligible and the soil was almost saturated. At about 1 meter there is a soil layer which has a low permeability. The water could not seep vertically so the soil should be drained by lateral flows. With regard to the strong spatial variability of soil drainage, it seems that groundwater flow is controlled by local processes rather than by water flows at the hill slope scale. This hypothesis is also coherent with TDR. Preferential flows could explain the spatial variability of soil humidity and differences of saturated areas' drainage. Nevertheless with the available information, it is difficult to confirm this hypothesis and to associate these subsurface flows with particular hydrological processes.

4.3 Rainfall simulator

Again to explain the important contribution of soil water highlighted by the environmental tracing application the soil infiltration capacity was explored during the rainfall simulation experiment. The experiment was conducted in five locations where several (3-4) rainfall simulations were applied. Here only the results of two simulations conducted in the Bois-Vuacoz sub-basin on the same area as the large TDR experiment is presented and discussed. These simulations were done at two different plots which were about 20 meters apart. In both cases the simulated rainfall had an intensity of 60 mm/h and a duration of 30 minutes. The soil moisture was high before the two simulations.
At site 1, the surface flow starts 5 minutes after the beginning of the rain and it reaches the maximum flow (52.9 mm/h) after about 14 minutes (Figure 4-3). The surface flow is very important and the infiltration is very low. The soil moisture increases also very quickly and reaches its maximum almost at the same time as the maximum surface flow. The first 30 centimeters of soil is almost saturated. After the end of the simulated rainfall the soil is drained very slowly. Twenty minutes after the end of the precipitation the soil water content does not decrease (Figure 4-3b).

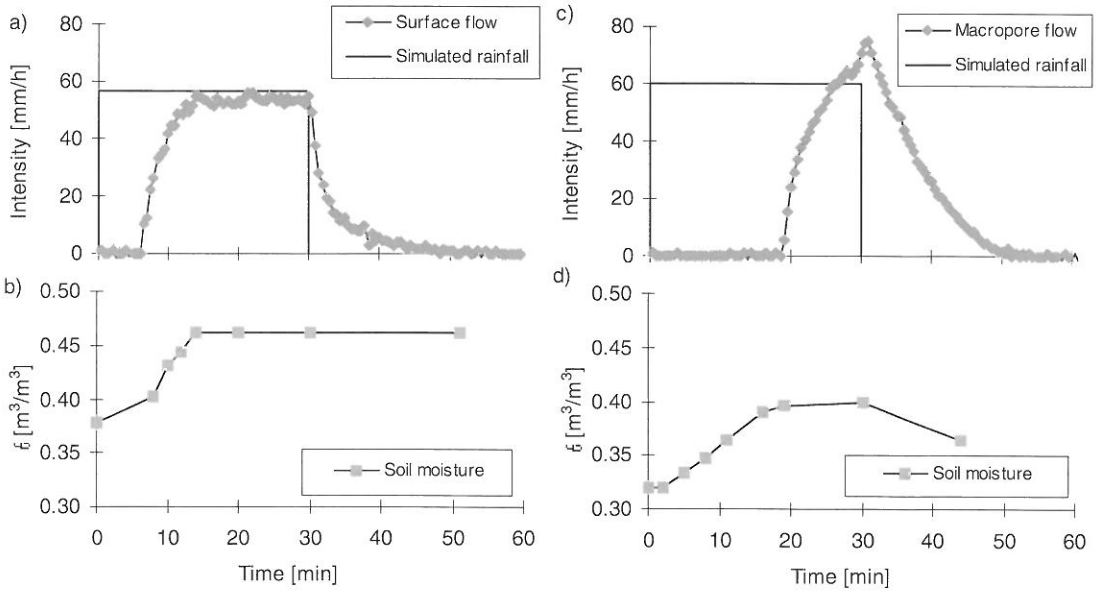

Figure 4-3: Results of both rainfall simulations in the Bois-Vuacoz sub-basin. a) Surface flow and simulated rainfall observed at site 1. b) Soil water content recorded during the rainfall simulation at site. 1 c) Macropore flow and simulated rainfall observed at site 2. d) Soil water content recorded during the rainfall simulation at site 2.

Despite the proximity of both plots, the hydrodynamic behavior observed at site 2 is completely different. During the rainfall simulation no surface flow was observed. All the water infiltrates in the soil. Initially this difference of behavior between both sites was inexplicable, but fortunately a macropore (diameter: 1-2 centimeter), which drained all the experimental area, was identified. Then the measurement system was adapted in order to collect the macropore flow rather than the surface flow. The macropore flow is represented in Figure 4-3c. The water comes out the macropore about 17 minutes after the beginning of the simulated rainfall. Then the flow increases very quickly and reaches the maximum value of 75 mm/h. The macropore drains an area larger than the experimental plot. In fact the volume drained by the macropore is larger than the volume of rain which was applied on the experimental plot. When the rain was stopped the macropore flow was still increasing, so it seems that it may be more important. In order to estimate the draining capacity of this macropore a rain with an intensity of 120 mm/h was applied during one hour. In this particular case the maximum macropore flow was estimated equal to 103 mm/h. Concerning the soil water content, it is interesting to observe that it increases very quickly until the macropore flow starts (Figure 4-3d). This flow begins only when the soil is almost saturated. At the end of the simulated rain the soil moisture decreases quickly. It seems that the macropore drains the first centimeters of the soil.
It is particularly interesting to compare the variations of soil moisture observed in one hand during the rainfall simulator experiment (Figure 4-3) and in other hand during the large TDR experiment (Figure 4-2). According to the results of the rainfall simulator experiment, the important spatial variability of soil water content highlighted during the TDR experiment could be due to macropore flows.

Several active macropores were observed in the watershed. The origin of the macropores is certainly due to the presence of old tree roofs. In reality the macropore flows seem active in the Haute-Mentue watershed. However on basis of the previous experiments, it is not possible to assess the role of macropore flows in flood generation.

4.4 Dye tracing

The objective of the dye tracing experiment was to discover if the soil water located in the hill slope can reach the stream fast enough to contribute to the flood generation. The estimation of the water flow through the soil should give an additional indication concerning the nature of flows and of hydrological processes.
In order to make the relation between the results of the dye tracing and the environmental tracing, these two experiments were conducted simultaneously in the Bois-Vuacoz sub-basin.
The initial soil moisture was relatively high but the soil in the studied hill slope was not saturated. There was no water in the six piezometers the day of the injection (20th October 1999). Since the soil was not saturated, it seems reasonable to suppose that the tracers were retained in the soil by capillarity force and they were concentrated around the injection point. During the study period three floods occurred (Figure 4-4).

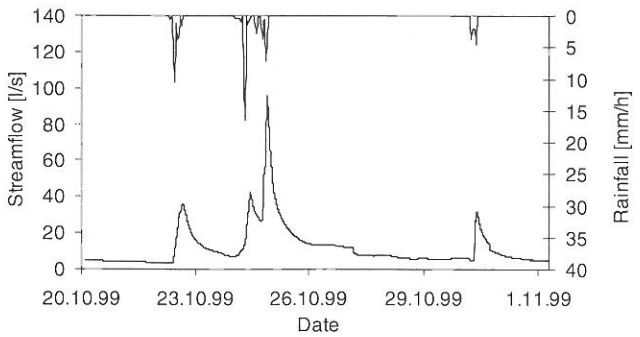

Figure 4-4: Rainfall-runoff events observed at Bois-Vuacoz during the dye tracing experiment.

On the whole the dynamic of the uranin signal is different of the sulforhodamin G one (Figure 4-5). Following the beginning of the rain, the concentration of sulforhodamin G increases faster than the uranin one. While the stream flow decreases, the sulforhodamin G concentration decreases also much faster than the uranin one. So it seems possible to distinguish two flow patterns in the soil according to the depth. The flows next to the surface, traced by sulforhodamin G, contribute rapidly to the flood generation but they stop quickly after the end of the precipitation. At the opposite the deep flows, characterized by the uranin signal, start later but they contribute much longer to the stream flow. Despite these differences of behavior, the velocity of the water transit through the soil is high in both cases and exceeds largely the theoretical hydraulic conductivity deduced from the Darcy law. In fact, according to a laboratory experiment conducted on soil probes of 100 cm^3 with a constant charge permeameter, the saturated hydraulic conductivity of soil in the sub-basin of Bois-Vuacoz varies between 35 and 116 mm/h.
During the first rainfall-runoff event occurring between the 22 and the 23 October 1999, the peaks of sulforhodamin G and uranin concentrations occurre respectively 8h46 and 10h50 after the beginning of the precipitation. Subtracting the distance done in the stream from the down slope to the fluorimeter (Figure 3-1), the mean velocity of the sulforhodamin G and uranin through the soil is respectively about $1.5 \cdot 10^{-3}$ and $4.6 \cdot 10^{-4}$ m/s, which is very high. This result is surprising given the physical properties of the soil in presence. These velocities seem to be explained only by preferential flows. These flows may be responsible for the important and rapid contribution of soil water during the flood generation. In order to analyze this hypothesis, the signals of the dye tracers is compared with the temporal variation of soil water contribution determined during the hydrograph decomposition (Figure 4-5).

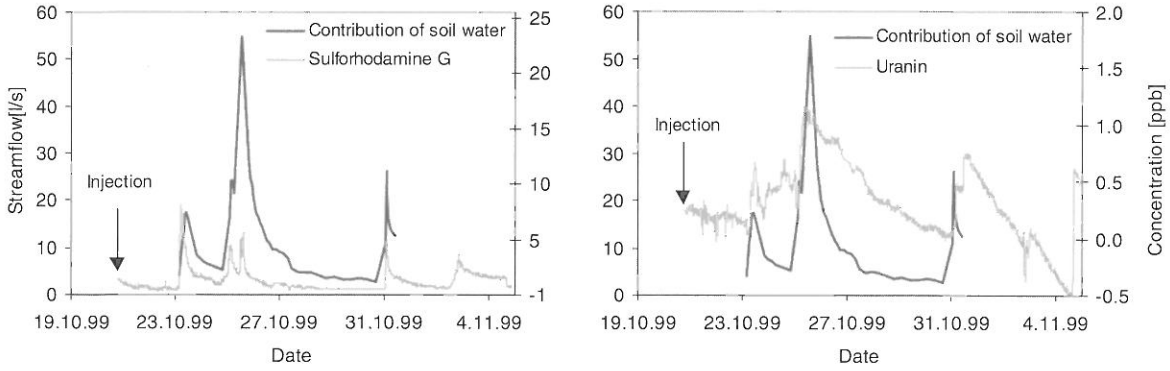

Figure 4-5: Concentrations of sulforhodamin G and uranin recorded in the stream water compared with the soil water contribution obtained by the hydrograph separation.

According to this comparison, it seems that the soil water contribution can be explained by the water flow going through the hill slope next to the stream. In fact, the temporal dynamics of both dye tracers are similar to the soil water contribution ones. The time lags between the series of dye tracers and the soil water contribution are relatively limited. According to the reaction velocities of the sulforhodamin G, it seems that the soil water contribution during the rising part is due essentially to near subsurface flows. In wet conditions, the velocity of the uranin signal, or in other words of deep flows, can be also very fast.
In summary the transit speeds highlighted during this experiment are quick enough to conclude that the water contained in hill slopes contributes to the stormflow generation. Considering the physical and hydrodynamic properties of soils, only preferential flows can explain such transit velocities. On the basis of only this experiment, it is not possible to determine the nature of these preferential flows, but according to previous results it seems due to a macropore network.

5 DISCUSSION

According to the above results, the macropore flows could be at the origin of the important contribution of soil water highlighted by the application of environmental tracing. In order to validate this hypothesis we have to characterize the chemical signature of water going through macropores and to verify if this flow is enough to explain the volume of soil water observed during the hydrograph decompositions.
The chemical signature of the water contained in the soil before the runoff event of the 23 October 1999 (Figure 4-4) was certainly similar to the signature of the soil water component defined for the hydrograph decomposition (median concentrations: silica 8 mg/l and calcium 300 µeq/l). The last rain before this event occurred the 20 October 1999. The time between these two events (58 hours) was large enough so that the rain (median silica concentration = 0.1 mg/l) took the silica signature of soil water. The dynamic of silica enrichment was estimated in laboratory using soil probes of the Haute-Mentue. It was approached by a kinematics of the first order. The median of the reaction constant of silica enrichment was estimated equal to $0.05h^{-1}$. According to the theory only a small part of the water contained in the soil before the beginning of the rainfall of the 22 October 1999 could reach the stream during the flood. In fact, before this event the soil was not saturated, thus water was captured mainly in capillary pores. Only the fraction over the water-retaining capacity could be mobilized. The tracing with the sulforhodamin G indicates that a part of this prevent soil water was mobilized and reached the stream during the flood event. Is this fraction of water enough to explain the volume of soil water contributing to the flood generation?
During the event of the 23 October 1999 which lasted about 42 hours, the volume of soil water contribution was 222 m^3. According to the experiment with the sulforhodamin G, the water next to the soil surface had a mean velocity of $1.5 \cdot 10^{-3}$ m/s. So during these 42 hours the soil water coming from a distance of 227 m could reach the stream. In other words a volume of 131'206 m^3 (total stream length = 289 m; mean soil depth = 1 m) could be potentially drained by preferential flows during the studied flood. If we consider that the soil was just over its water-retaining capacity (30%), only a small fraction (0.57%) of the water contained initially in the soil is enough to explain the total volume of soil water ($0.30 \times 0.00566 \times 131206 \approx 223\,m^3$).
On the basis of this rough calculation, it seems that the macropore flows can explain the volume of soil water determined by the hydrograph decomposition. On the other hand this mechanism does not achieve to explain the maximum flow of soil water observed during the flood of the 23 October 1999.

The peak of soil water flow is close to 18 l/s (Figure 4-5). Knowing the macropore flow velocity ($1.5 \cdot 10^{-3}$ m/s) and supposing as first approximation that macropore flows are composed only of soil water, it is possible to calculate the total surface of macropores; it is equal to $12m^2$. This value is very high in comparison with the total length of the stream (289 m). In fact it corresponds to a surface of 208 cm^2 per unit meter. This surface is even bigger because in reality the macropore flow is composed of a mixture of soil water and precipitation water. In conclusion the macropore flows are not enough to explain the generation of the soil water peak flow. At this stage, we have to find new explanations. Other processes completing the macropore flows should be involved in the generation of soil water.
Iorgulescu (1997), who conducted a study in the same experimental catchment, supposed that the temporal and spatial variability of the hydrological responses highlighted by the decomposition of hydrograph is due to the extension of the hydrographic network and the contributive area. This phenomenon, which was clearly observed in the field observations and respects the physical sense, has the effect of increasing the surface contact between the river and the bank and more particularly the total macropores surface. So the combination of the macropore flows with the extension of hydrographic network could explain the peaks of soil water contribution.
In order to explain the hydrological behavior of the Bois-Vuacoz sub-basin highlighted by the field experiments and observations, a conceptual model is proposed. This model summarizes the notions and the hypotheses which were presented above. In dry conditions, the streamflow is composed only by groundwater flows, which have an extended contact with the carbonated substratum. With the precipitation the soil water content increases rapidly under the impact of rain infiltration. If the soil texture is fine enough, so that a capillary fringe can be formed, the groundwater level may raise at the velocity of kinematic waves (Beven, 1982). This velocity is even higher if the water deficit of the soil in comparison with its saturation is small. Thus the soil becomes rapidly saturated. As soon as the saturation conditions are reached in the upper soil horizons, where the roof network is well developed, the macropore flows start. In this condition, the soil water flows are essentially horizontally since the soil is saturated and its permeability is low in depth. The chemical signature of these flows is a mixture of precipitation and soil water. The proportion between these two components depends on the wet antecedent conditions. The water retained in the soil between the hydrological events takes rapidly the chemical signature of the soil water component. The macropore system may drain an important surface. In fact, the macropore flow velocity is apparently very high. The contribution of the macropore flows is probably increased by the extension of the hydrographic network during the rainfall-runoff events. With this association of processes, it is possible to explain the peak flows of soil water. The maintaining of the soil water contribution, during long rainfall events or when the rain follows one another, could be explained by the extension of contributive area and the silica enrichment of rain water having an extended contact with the soil. A part of the rain reaches also the stream by surface runoff on the saturated areas. The groundwater contributes to the flood generation, too. The quick rise of its contribution is certainly due to the saturation of deep horizon and the start of lateral flows (kinematic wave, transmissivity feed-back, groundwater ridging). Preferential flows may also appear at the interface soil-bedrock (e.g. fissures in the bedrock). Moreover, the macropore system in the lower part of hill slopes may also drain a part of the groundwater. This conceptual model must be considered as a general hypothesis concerning the hydrological behavior of the Bois-Vuacoz sub-basin. Despite the good concordance between this model and the field observations, it should be validated with additional observations done in the rest of the Haute-Mentue catchment.

6 CONCLUSIONS AND PERSPECTIVES

The main originality of this work is to associate different types of measurements (e.g. environmental tracing, TDR, rainfall simulator, dye tracing) in order to obtain a better vision of hydrological processes. Each measurement technique has an area of application and consequently result interpretation. For example the environmental tracing gives an image of the hydrological behavior at the catchment scale, but it can not identify precisely which mechanisms are responsible for the streamflow generation. On the other hand the punctual measurements like the TDR ones furnish a very incomplete spatial vision of the hydrological processes. The combination of information coming from different scales allowed to identify and understand the hydrological behavior of the Bois-Vuacoz sub-basin. So it was possible to propose a conceptual model for this particular basin. This model is based essentially on the concept of the contributive area extension and on the central role of macropore flows. This result is particularly interesting because it explains in terms of mechanisms the hydrological and chemical responses highlighted by the hydrograph decomposition. Furthermore it is coherent with results of TDR, rainfall simulator and dye tracing experiments.

Generally the information concerning the hydrological processes, as presented in this study, should be considered to develop or control the physical concept of hydrological models. It is essential that models reproduce the real processes in order to deliver realistic forecasts and to evaluate the effects of modifications, like climate changes or new soil occupations, on the hydrological cycle. In this context, it would be interesting to couple the environmental tracing with the hydrological models. In fact, the environmental tracing gives an integrated information at the catchment scale about the hydrological processes. Ideally the structure of models should be adapted in order to reproduce both the hydrological and the tracer responses. This combination should conduct to a better conceptualization of the hydrological processes in models. Nevertheless the consideration of environmental tracing in the models would not conduct necessarily to an improvement of streamflow simulations. In fact, the adaptation of the model structure, which considers the environmental tracing, will need the introduction of new parameters, this will affect consequently the quality, the representativeness of simulations.

ACKNOWLEDGEMENTS

This research was conducted at the EPFL in the framework of the Ph.D. thesis of Christophe Joerin. It was supported in part by the Swiss National Research Foundation (Grant # 21-43308.95) and by OFES (Grant # 95.00449) in the framework of the EU funded Project VAHMPIRE.

REFERENCES

Ambroise, B. (1998): Genèse des débits dans les petits bassins versants ruraux en milieu tempéré: 1 - Processus et facteurs. Revue des Sciences de l'Eau, 11: 471-495.

Asseline, J., Valentin, C. (1978): Construction et mise au point d'un infiltromètre à aspersion. Cah. ORSTOM, série Hydrol., XV(4): 321-349.

Beven, K. (1982): On subsurface stormflow: Prediction with simple kinematic theory for saturated and unsaturated flows. Water Resources Research, 18(6): 1627-1633.

Buttle, J.M. (1994): Isotope hydrograph separations and rapid delivery of pre-event water from drainage basins. Progress in Physical Geography, 18(1): 16-41.

Elsenbeer, H. et al. (1995): Mixing model approaches to estimate storm flow sources in an overland flow-dominated tropical rain forest catchment. Water Resources Research, 31(9): 2267-2278.

Iorgulescu, I. (1997): Analyse du comportement hydrologique par une approche intégrée à l'échelle du bassin versant. Application au bassin versant de la Haute-Mentue. Thèse No 1613, Ecole Polytechnique Fédérale de Lausanne, 216 pp.

Jenkins, A. et al. (1994): A case study in catchment hydrochemistry: conflicting interpretations from hydrological and chemical observations. Hydrological Processes, 8: 335-349.

Joerin, C. (2000): Etude des processus hydrologiques par l'application du traçage environnemental. Association à des mesures effectuées à l'échelle locale et analyse d'incertitude. Thèse No 2165, Ecole Polytechnique Fédérale de Lausanne, 224 pp.

Joerin, C. et al. (2002): Uncertainty in hydrograph separations based on geochemical mixing model. Journal of Hydrology, 255(1-4): 90-106.

Jordan, J.-P. (1994): Spatial and temporal variability of stormflow generation processes on a Swiss catchment. Journal of Hydrology, 153: 357-382.

McDonnell, J.J. (1990): A rationale for old water discharge through macropores in a steep, humid catchment. Water Resources Research, 26: 2821-2832.

Schnegg, P.-A., Doerfliger, N. (1997): An inexpensive flow-through field fluorometer, 6e Colloque d'hydrologie en pays calcaire et milieu fissuré, La Chaux-de-Fonds.

Tinga, W.R. et al. (1973): Generalised approach to multiphase dielectric mixture theory. Journal Applied Physics, 44: 3897.

CLIMATE CHANGE AND RUNOFF STATISTICS: A PROCESS STUDY FOR THE RHINE BASIN USING A COUPLED CLIMATE-RUNOFF MODEL

Jan Kleinn, Christoph Frei, Joachim Gurtz, Pier Luigi Vidale, Christoph Schär

Institute for Atmospheric and Climate Science, ETH Zurich, Winterthurerstrasse 190, 8057 Zürich, Switzerland, kleinn@geo.umnw.ethz.ch

SUMMARY

To asses the influence of a warmer climate on the hydrological cycle, a regional climate model is coupled to a distributed runoff model. The regional climate model is driven by ECMWF reanalysis and is run in a nested mode with 56 km and 14 km horizontal grid spacing, respectively. The distributed runoff model is operated at a horizontal gridspacing of 1 km for the Rhine basin down to Cologne. Five winters (1989/90 - 1993/94), each from November until January, are considered in the analysis. The precipitation fields simulated by the regional climate model show good correspondance with observed precipitation fields regarding the spatial distribution and the interannual variability. The finescale and altitudinal distribution of precipitation and the precipitation frequency are however more critical. The simulated runoff does nevertheless correspond well with the observed.
The simulations of a warmer climate show an increase in precipitation, especially in strong precipitation events and in liquid precipitation, for all winter months. The number of high runoff events rises consequently, between 15% and 30% for daily runoff events with an amplitude of a few mm/day.

Keywords: climate change, regional climate modelling, distributed runoff modelling, precipitation frequency, flood frequency.

1 INTRODUCTION

The consequences of extreme runoff and extreme water levels are within the most important natural hazards induced by weather. The question about the impact of global climate change on the runoff regime, especially on the frequency of floods, is of utmost importance.
In winter-time, two possible climate effects could influence the runoff statistics of large Central European rivers: the shift from snowfall to rain as a consequence of higher temperatures (Grabs, 1997) and the increase of heavy precipitation events due to an intensification of the hydrological cycle (e.g. Frei et al., 2000; IPCC, 2001; Trenberth, 1999). The combined effect on the runoff statistics is examined in this study for the river Rhine. To this end, sensitivity experiments with a model chain including a regional climate model and a distributed runoff model are presented. The experiments are based on an idealized surrogate climate change scenario (Schär et al., 1996). It should be stressed that this approach does not provide a full climate change scenario but merely an analysis of relevant nonlinearities and sensitivities. In addition to these sensitivities, climate change would also imply changes in synoptic climatology that are not considered in this study.

2 MODEL CHAIN AND EXPERIMENT SETUP

The model suite consists of the regional climate model CHRM and the distributed runoff model WaSiM. The regional climate model CHRM is based on the mesoscale weather prediction model HRM of the German Weather Service (DWD) and has been adapted for climate simulations (Vidale et al., 2002). The CHRM is being used in a nested mode with horizontal grid spacings of 56 km and 14 km, respectively (hereafter called CHRM56 and CHRM14). The model domains are depicted in Figure 2-1.
The distributed runoff model WaSiM is operated at a horizontal grid spacing of 1 km for the whole Rhine basin down to Cologne, covering approx. 145'000 km^2. WaSiM is a distributed, gridbased runoff model using physically based algorithms like the Richard's equation (Schulla, 1997). The entire model suite covers scales of more than two orders of magnitude (Figure 2-1).
The boundary conditions for the regional climate model are taken from the original ECMWF reanalysis and from a modified version representing the surrogate scenario, both at a horizontal resolution of approx. 120 km (T106). The scenario of a warmer climate consists of driving fields with a uniformly increased temperature of 2 Kelvin and associated an increased atmospheric humidity of approx. 15%. Such a temperature shift can be formulated consistently with the governing equations (Schär et al.,

1996), and the methodology has earlier been applied by Frei et al. (1998). The simulations cover the five winter seasons 1989/90 till 1993/94, each from November until January. The control simulation is hereafter referred to CTRL and the scenario of a warmer climate is referred to WARM.

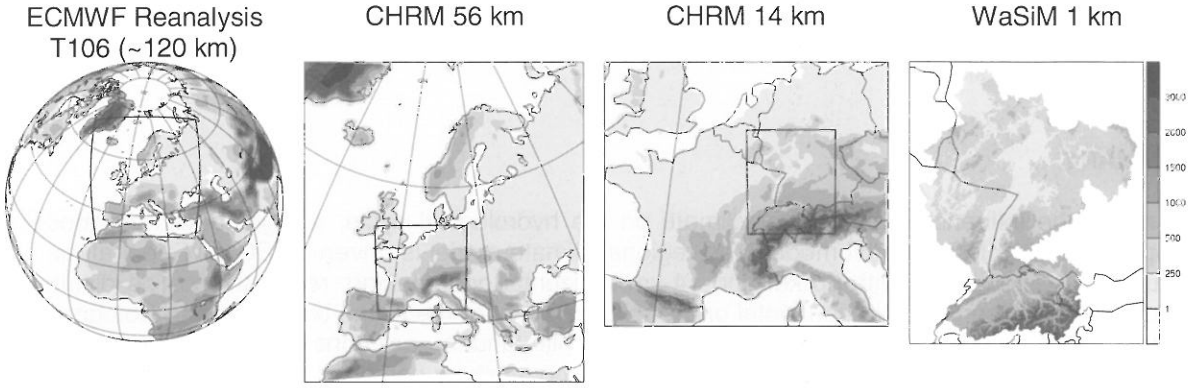

Figure 2-1: Domains and topography of the ECMWF Reanalysis, the CHRM with 56 and with 14 km horizontal resolution, respectively, and the distributed runoff model WaSiM.

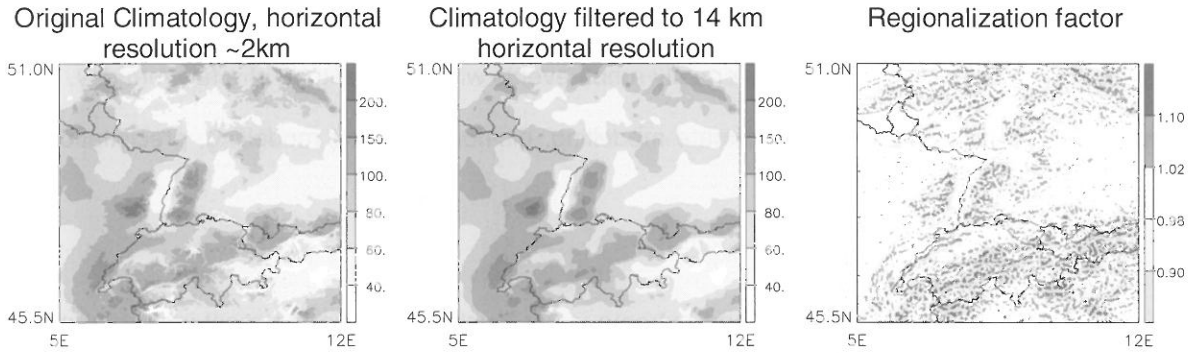

Figure 2-2: Downscaling of precipitation fields using a high resolution precipitation climatology.

The coupling of the models is purely one-way, i.e. from the large to the small scale. It is provided by the downscaling of the climate model fields (precipitation, temperature, radiation, humidity, and wind) to the resolution of the distributed runoff model. Downscaling of precipitation fields from CHRM14 to WaSiM (Figure 2-2) is done according to Widmann and Bretherton (2000) using a high resolution precipitation climatology by Schwarb et al. (2001) and the downscaling of temperature fields is done using the vertical temperature gradient provided by the climate model and the fine-scale topography.

3 VALIDATION OF THE MODEL CHAIN

A detailed validation of the model precipitation is done using the precipitation climatology of Frei and Schär (1998), that uses approx. 6000 daily precipitation measurements. The validation of the control simulation shows a good correspondence of the precipitation fields from the regional climate model with measured fields regarding the distribution of precipitation at the scale of the Rhine basin. The CHRM14 shows the ability to generate fine-scale precipitation features not represented by the CHRM56 (Figure 3-1). It also shows an overestimation (of approx. 10%) of precipitation in the Alps and a slight upstream shift (~20 km) of the precipitation anomalies along the Black Forest and the Vosges Mountains (Figure 3-1). Consideration of monthly mean precipitation (Figure 3-2) demonstrates the ability of simulating the inter-annual precipitation variability in response to large-scale forcing. In particular the root mean square (RMS) difference of the CHRM14 monthly means against observations is significantly smaller than the standard deviation of the observations. The simulated precipitation has systematic errors on the scale of subcatchments, concerning the distribution with height and the frequency distribution. The number of small precipitation events is slightly underestimated in most catchments (Figure 3-3) whereas the number of strong precipitation events is usually overestimated. Nevertheless, the characteristics of the different catchments are well represented. The previously mentioned overestimation of precipitation in the Alps can be seen in Figure 3-4: Precipitation is overestimated between altitudes of 1000 to 2000 m a.s.l. and underestimated between 200 and 1000 m a.s.l.

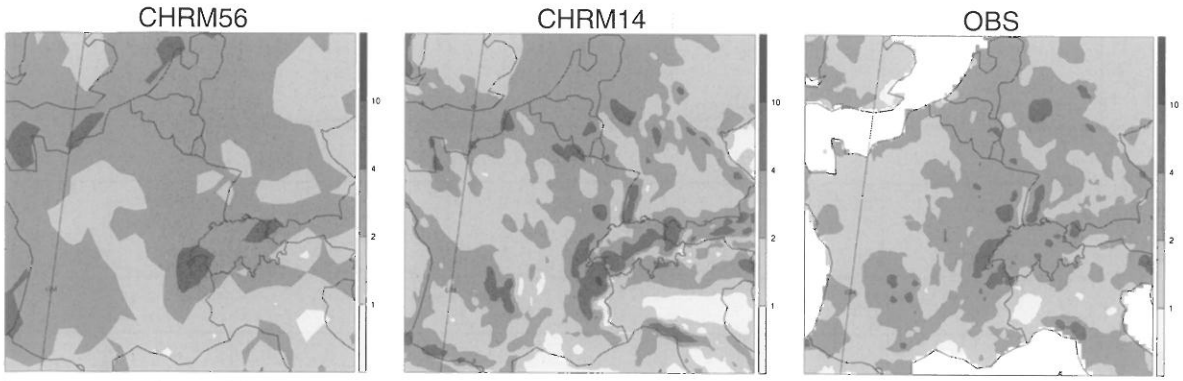

Figure 3-1: Mean daily precipitation in mm averaged over the winters 1989/90 to 1993/94, each winter consisting of November till January.

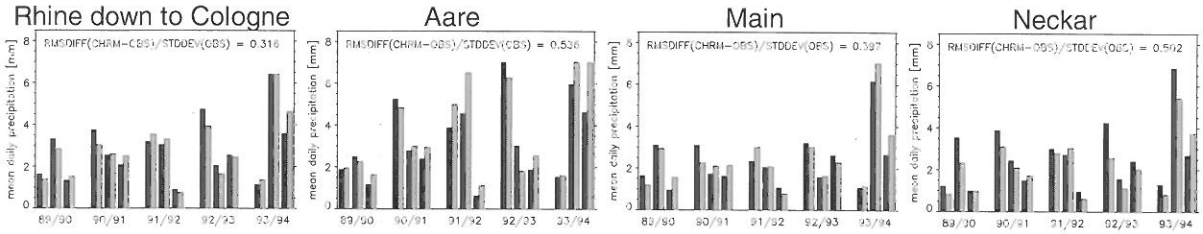

Figure 3-2: Monthly (Nov, Dec, Jan) mean daily precipitation for the Rhine basin down to Cologne, the Aare, the Main, and the Neckar, observed (black) and CHRM14 (gray).

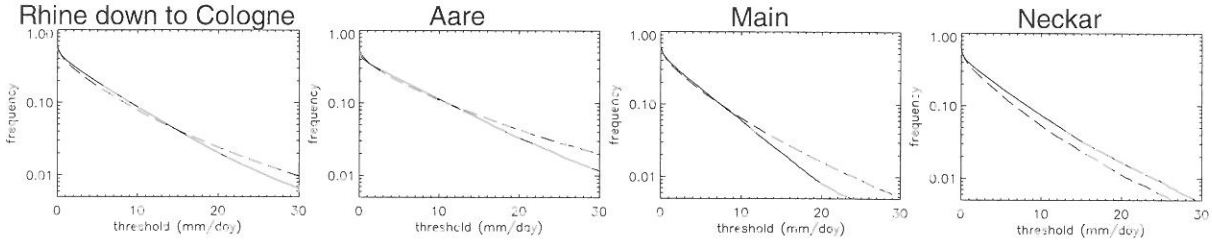

Figure 3-3: Precipitation frequency of daily precipitation according to observations (solid line) and the CHRM14 (dashed line).

Despite the errors in the simulated precipitation, the simulated runoff shows good correspondence with the observations (Figure 3-5). Looking at the runoff from a climatological point of view in terms of the frequency distribution of daily runoff events (Figure 3-6), a net improvement in the simulation of high runoff events can be seen due to the increased resolution of the CHRM14 compared to the CHRM56.

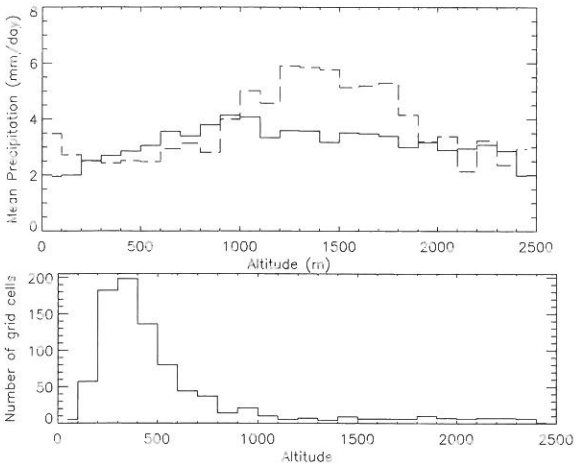

Figure 3-4: Altitudinal distribution of precipitation. Mean daily precipitation and number of CHRM14 grid points per altitude bin of 100 meters.

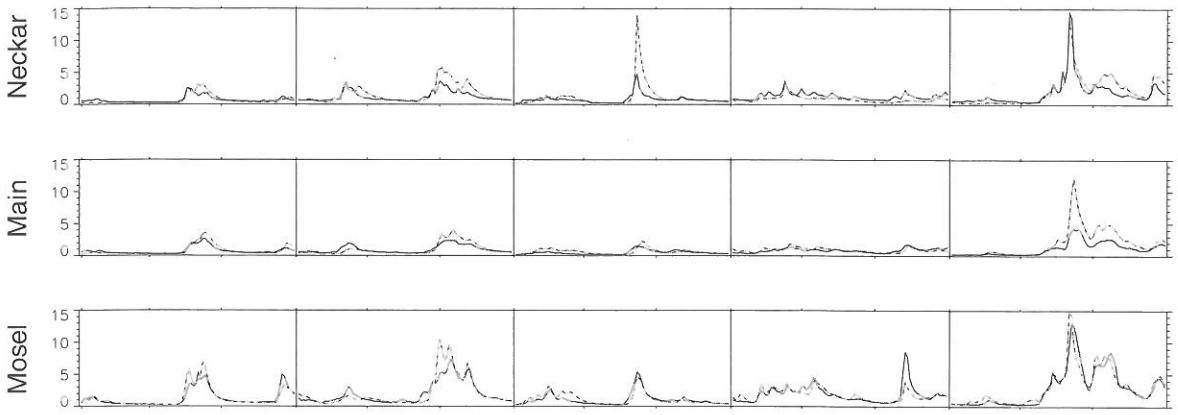

Figure 3-5: Daily runoff in mm/day for 5 winters, 1989/90 until 1993/94, from Nov till Jan. Each winter is shown in a subpanel. Curves show observed (solid) and WaSiM simulated (dashed) runoff.

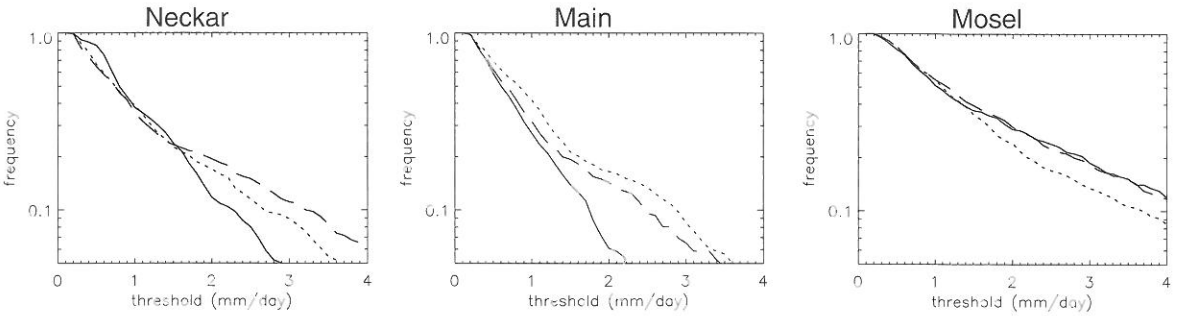

Figure 3-6: Runoff frequency of the Neckar, the Main, and the Mosel basin, observed (solid) and the hydrologic simulations driven by the CHRM14 (dashed) and by the CHRM56 (dotted).

4 SCENARIO OF A WARMER CLIMATE

Simulations of a warmer climate show an increase in precipitation amounts by more than 10% in most parts of Europe (Figure 4-1). The increase in liquid precipitation is even stronger (Figure 4-2), with increases as high as 50% in large parts of the Alps, as a shift from snowfall to rain occurs in warmer winter months. The increase in precipitation mostly comes from an increase in the heavy precipitation events. While the number of days with precipitation hardly changes, the frequency of days with more than 20 mm precipitation increases by approx. 25% (Figure 4-3).
As a result of stronger precipitation and higher snowline the mean winter runoff increases by 10% to 25%, depending on the catchment (Table 4-1). An increase of strong events can also be seen in the runoff statistics, where the number strong runoff events increases (Figure 4-4).

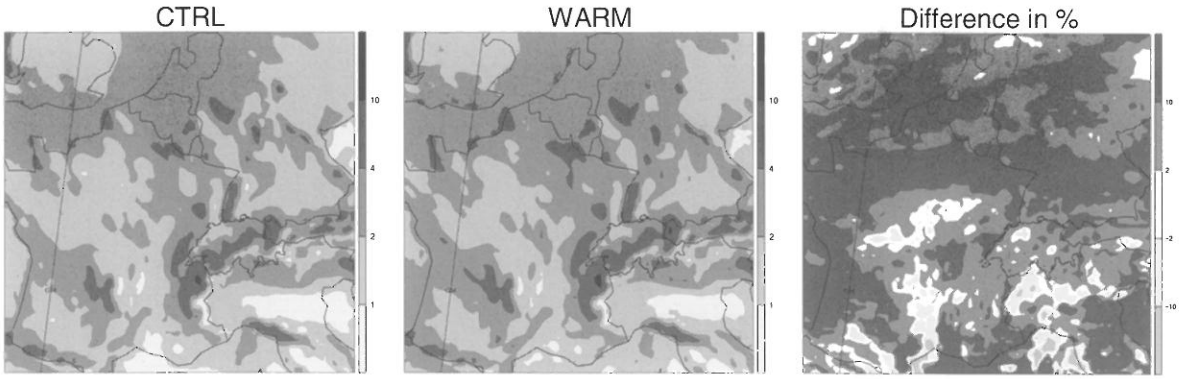

Figure 4-1: Mean daily precipitation in mm, control run (CTRL), warmer climate (WARM), and difference in %.

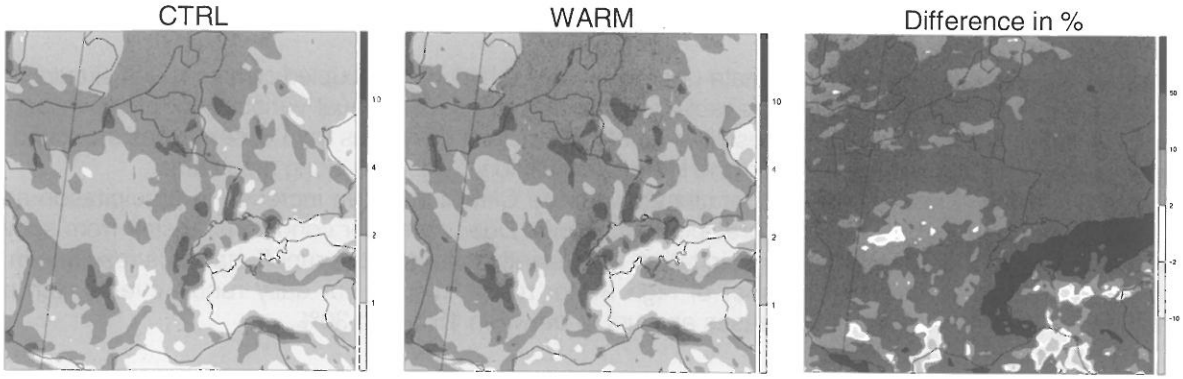

Figure 4-2: Mean daily liquid precipitation in mm, control run (CTRL), warmer climate (WARM), and difference in %.

Basin	CTRL	WARM	Diff in %
Neckar	1.14	1.44	26.3
Main	0.96	1.07	11.9
Mosel	1.69	1.98	17.1

Table 4-1: Mean runoff in the control and warm simulation (mm/day) and difference in %.

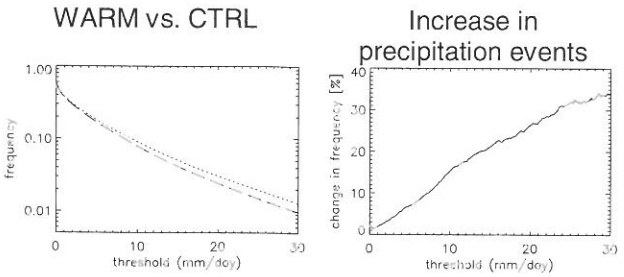

Figure 4-3: Mean change in precipitation intensity in a warmer climate for CHRM14 grid points in the Rhine basin, WARM (dotted) vs. CTRL (dashed), difference in %.

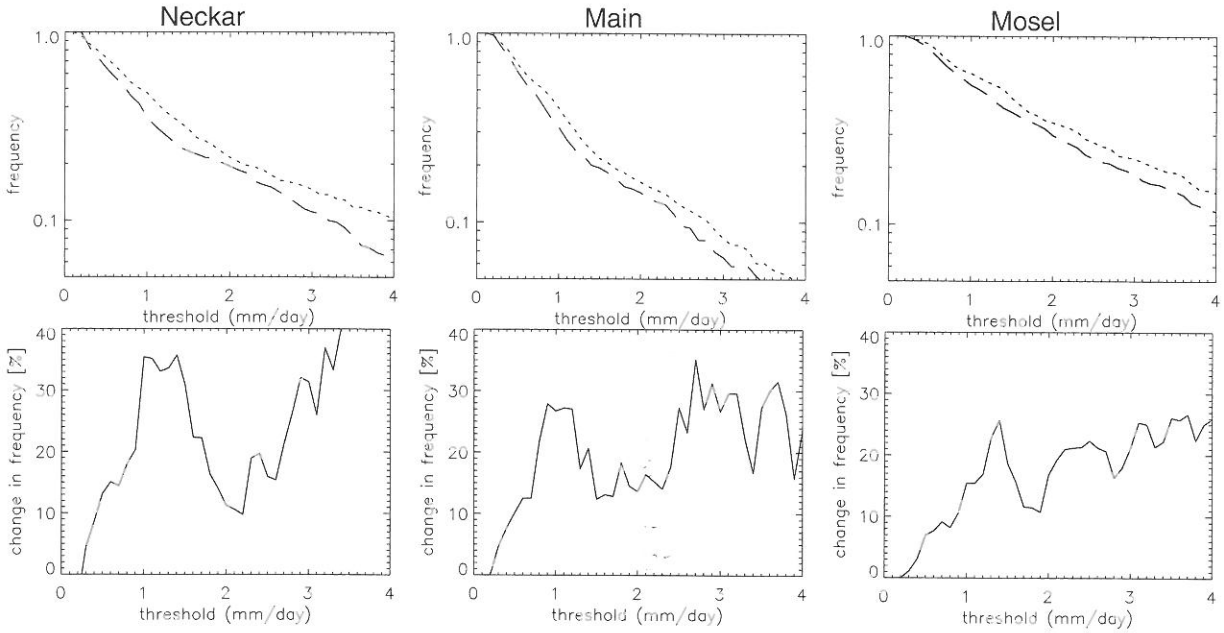

Figure 4-4: Change in runoff intensity in a warmer climate in the Neckar and Main basins, WARM (dotted) vs. CTRL (dashed), difference in %.

5 CONCLUSION

To asses the influence of a warmer climate upon the regional hydrology, coupled climate-runoff simulations were performed. The model chain is capable of reproducing the interannual variability of precipitation as well as its spacial distribution and the resulting runoff. Substantial deviations from observations are found in the altitudinal distribution of precipitation and in the precipitation distribution along mountains.
The sensitivity experiments of a warmer climate with the CHRM show an increase in precipitation and an increase in the number of strong precipitation events. Due to warmer conditions, a shift from snowfall to rain occurs. These signals in precipitation significantly influence the runoff statistics resulting in a longer duration and/or a larger number of high winter runoff events. For daily runoff events with an amplitude of a few mm/day, the increases amount to between 15% and 30%.

ACKNOWLEDGEMENTS

Special thanks are due to the International Commission for the Hydrology of the Rhine basin (CHR) for providing the surface data for the runoff modelling and to the Swiss Federal Office for Water and Geology and the German Federal Institute of Hydrology for providing the runoff data.

REFERENCES

Frei, C. and Schär, C. (1998): A precipitation climatology of the Alps from high-resolution raingauge observations. Int. J. Climatol., 18, 878-900.

Frei, C., Schär, C., Lüthi, D. and Davies, H.C. (1998): Heavy precipitation processes in a warmer climate. Geophys. Res. Lett., 25, 1431-1434.

Frei, C., Davies, H.C., Gurtz, J., and Schär, C. (2000): Climate dynamics and extreme precipitation and flood events in Central Europe. Integrated Assessment, 1, 281-299.

Grabs, W. (Ed.) (1997): Impact of Climate Change on Hydrological Regimes and Water Resources Management in the Rhine Basin. International Commission for the Hydrology of the Rhine Basin (CHR), CHR-Report no. I-16, Lelystad, The Netherlands.

IPCC (2001): Climate Change 2001: The Scientific Basis, Contribution of Working Group I to the Third Assessment Report of the Intergovernmental Panel on Climate Change, Cambridge University Press.

Schär, C., Frei, C., Lüthi, D., and Davies, H.C. (1996): Surrogate climate-change scenarios for regional climate models. Geophys. Res. Lett., 23, 669-672.

Schulla, J. (1997): Hydrologische Modellierung von Flussgebieten zur Abschätzung der Folgen von Klimaänderung. PhD thesis. Swiss Federal Institute of Technology (ETH). Dissertation No. 12'018. Zurich, Switzerland.

Schwarb, M., Daly, C., Frei, C., and Schär, C. (2001): Mean Annual Precipitation throughout the European Alps 1971-1990. Hydrological Atlas of Switzerland, Plates 2.6 and 2.7.

Trenberth, K. (1999): Conceptual Framework for changes of Extremes of the Hydrological Cycle with Climate Change. Climatic Change, 42, 327-339.

Vidale, P.L., Lüthi, D., Frei, C., Seneviratne, S., and Schär, C. (2002, in preparation): Physical processes affecting the seasonal and interannual variations of the European water cycle: lessons from a regional climate model.

Widmann, M. and Bretherton, C.S. (2000): Validation of Mesoscale Precipitation in the NCEP Reanalysis Using a New Gridcell Dataset for the Northwestern United States. J. Climate, 13, 1936-1950.

DEPENDENCE OF SURFACE RUNOFF ON RAIN INTENSITY – RESULTS OF RAIN SIMULATION EXPERIMENTS

Bernhard Kohl, Gerhard Markart

Austrian Institute for Avalanche and Torrent Research, Hofburg-Rennweg 1; A-6020 Innsbruck, Austria, bernhard.kohl@uibk.ac.at

SUMMARY

A data set of rain simulation experiments carried out within the last ten years at the Austrian Institute for Avalanche and Torrent Research was used to challenge runoff coefficient as a constant value. Repeated sprinkling tests with different rain intensities showed a moderate increase of surface runoff coefficients between 30 and 100 mm h^{-1}. Within this rainfall intensity range the appropriation of runoff coefficient classes to different soil / vegetation units can be accounted as constant. Below 30 mm h^{-1} the runoff coefficient changes rapidly with decreasing precipitation. Seasonal effects such as grazing can rise runoff coefficients to a bigger extent as it varies with increasing rainfall (above 30 mm h^{-1}).

Keywords: Surface runoff, runoff coefficient, rain intensity, rain simulation

1 INTRODUCTION

The dimensionless runoff coefficient C, although an old concept, remains a practical tool in engineering hydrology (Gottschalk, Weingartner, 1998). This C-value, the ratio of runoff depth A to precipitation depth i can be estimated from tables available in the literature (e.g. Zeller, 1981; Chow et al., 1988; Browne, 1990; Pilgrim and Cordery, 1993). All these tables presuppose this parameter as a constant factor, that is assigned to a certain vegetation or land use. Only rarely, restrictions of the validity of the runoff coefficients are declared. For example, a runoff coefficient between 0.25 - 0.35 is assigned for lawns on heavy soil with an inclination over 7 percent. This value should be applied to smallest surfaces, stormy rain of short duration and return periods of 5 to 10 years. For longer return periods the runoff coefficient should be chosen greater than stated, but however the amount is uncertain. The practitioner must use experience and judgement to select the appropriate runoff coefficient within the given ranges.
Runoff coefficients are used in a lot of formulas and models. The Rational Method is one of the simplest and best known methods often routinely applied in hydrology. The Rational Method formula (Dooge, 1957) expresses the estimated peak rate (of storm runoff) as the product of the catchment area, a peak rate of rainfall, and a runoff coefficient,

$$Q = k\,C\,i\,A \tag{1}$$

where: Q - Peak flow, k - conversion factor, C - Runoff coefficient, i - Rainfall intensity, and A - Catchment area). The formulas take into account that the runoff coefficient is a constant value.
The Soil Conservation Service (SCS) Curve Number (CN) method is used widely to estimate runoff, water recharge, stream flow, infiltration, soil moisture content, and landfill leachate production from precipitation (Mack, 1995). The SCS method calculates runoff coefficients from soil properties and land use. SCS Curve Numbers are selected by using a table relating land use to hydrologic soil type. For each land use type there is a corresponding curve number for each of the SCS hydrologic soil types (A, B, C, and D). A rain intensity dependent runoff coefficient is derived from this CN values. From experience, this procedure delivers too small C values for rain intensities smaller than 50 mm (DVWK, 1984).
A transportable spray irrigation installation for large plots (50 up to more than 100 m^2) was constructed at the Austrian Institute for Avalanche and Torrent Research (AIATR) in Innsbruck/Tyrol with the aim to characterise and define the different runoff producing areas in torrent catchments. In the last ten years 123 different soil / vegetation units were irrigated and about 200 rain simulation experiments were carried out. To allow comparison with irrigation experiments done by other research institutions the applied water intensities were 100 mm h^{-1}. Additionally, several rain simulations were carried out by the use of lower rain intensities in order to observe surface runoff in dependence on rain intensity.

2 METHODS

The AIATR irrigation installation allows a very good adaptation to the terrain-morphology. A U-form pipe system with 5 m width and a variable length from 10 to more than 20 m is the frame of the rain simulator. The irrigated surface amounts from 50 m² in the minimal case up to more than 100 m², according to terrain conditions and water availability. A standard size of 80 m² was chosen for most experiments. The amount of rainfall can be adjusted by number and type of the rain nozzles (quarter -, half - and full-circle). An automatic pressure regulation prevents from too high flow rates in the inclined terrain at the ulterior nozzles. By reduction of the number of nozzles, starting from a standard precipitation intensity of 100 mm h^{-1} also lower rain amounts can be simulated. Due to the rain pattern of this nozzle type intensities lower than 30 mm h^{-1} do not make sense, because a homogeneous distribution of the rain could no longer be achieved.
Lateral losses often are a major problem of rain simulation installations. In order to prevent the lateral displacement of the precipitation on the surface and in the soil as well as losses by wind drift, the two outsides of the research plot are also irrigated. Observations as well as measurements of rain distribution on the research plot confirm the usefulness of this method, the precipitation loss is reduced to a minimum. The applied amount of rainfall is controlled by means of a water counter. For quantification of appearing surface runoff and interflow a trench is prepared directly below the irrigation plot,. Steel plates and/or a plastic foil drain the water into a runoff channel and further in calibrated tanks (300 l). The collected runoff is measured temporal and quantitative. Usually, a time span of one hour is chosen for the duration of the rain simulation experiment. In the case, that the balance between infiltration and runoff has not yet appeared, the duration of the rainfall simulation experiment is extended up to this time.
Markart and Kohl (1995) as well as Markart (2000) give an elaborate description of the rain simulation installation used at the Austrian Institute for Avalanche and Torrent Research.
In Figure 2-1, a typical hydrograph of a rain simulation experiment is represented. After a certain acceleration time, which is essentially depending on the initial conditions (interception, evaporation, initial moisture situation, etc.), the runoff increases till a constant rainfall loss rate is reached. The C_{max} value, where infiltration and runoff are in balance, therefore describes a constant system status. The total surface runoff C_{tot}, as ratio of total runoff to total precipitation, includes in contrast to C_{max} the whole acceleration time, and is therefore also dependent from the initial conditions.

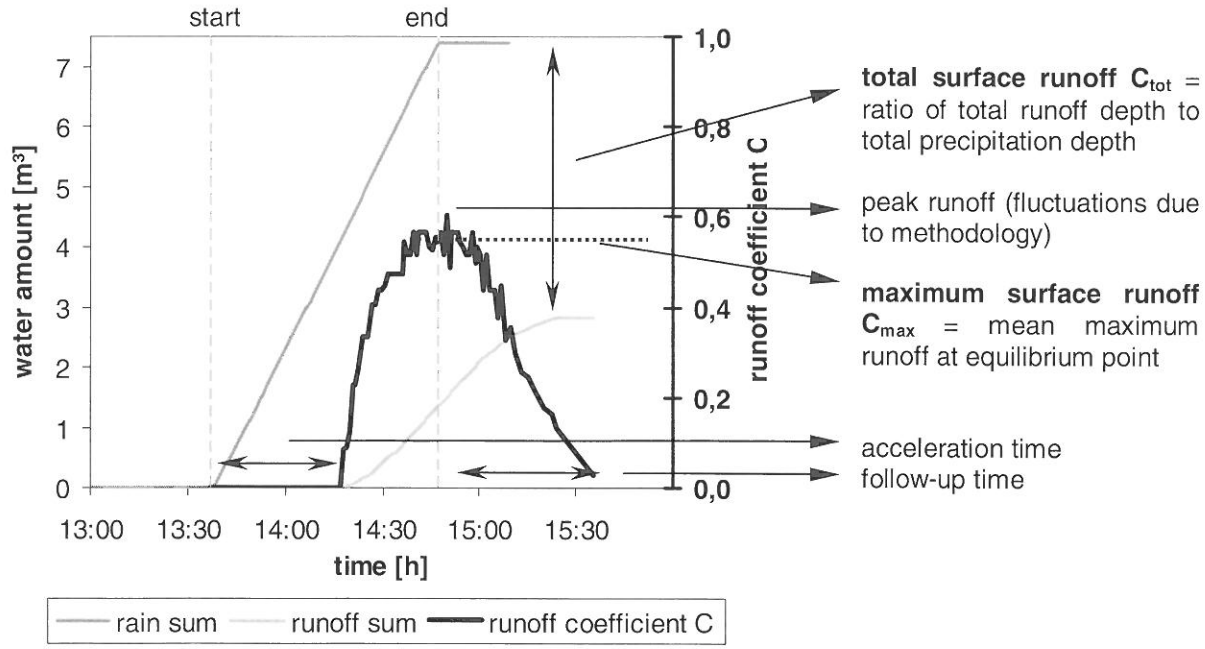

Figure 2-1: A typical rain simulation hydrograph showing different runoff coefficients (total surface runoff C_{tot}, maximum surface runoff C_{max}, peak runoff).

Due to the variable initial system status of the experiments C_{tot}, (the value of total surface runoff) is no good comparative value for different soil / vegetation units. Assessing runoff characteristics of different soil / vegetation units in torrent catchment areas we presuppose a realistic "worst case scenario". For such a scenario we assume that preceding precipitations have already moisturised vegetation and soil. In such a case the initial losses (interception, evaporation) of a storm event become very small.

As mentioned C_{tot} does not describe surface runoff sufficiently. Thus maximum surface runoff C_{max} is used to describe and compare the runoff disposition of different plots.
From 123 runoff plots with about 200 experiments carried out within the last ten years 26 plots remain, where more than one rain intensities were applied (see Table 2-1). In addition there are ten more plots that were irrigated at different seasons at each case.

Table 2-1: Rain simulations conducted by the Austrian Institute for Avalanche and Torrent Research (Innsbruck, Tyrol) 1992 – 2001.

rain simulation database	plots	experiments	catchments
rain simulations	123	197	19
repeated simulations with different intensities	26	65	10
repeated simulations at different seasons	10	27	4

3 RESULTS

Runoff coefficient values from the experiments treated cover the entire potential sample space $0 \leq C \leq 1$. Two locations from the collective show higher coefficients than 1. Those two stands are inclined swamps with a permanent downpour before, during and after the rain simulation experiment. Due to this effect of permanent running water drain reaches more than 100 percent. The resulting maximum runoff coefficients from the different rain simulation plots are shown in Figure 3-1. The distribution function of this runoff coefficients is just similar to the function of runoff coefficients from different drainage basins, that Gottschalk and Weingartner (1998) presented for Swiss pre-alpine basins. They describe such pre-alpine catchments as a response class of basins with steep slopes and high river network density, giving rise to quick drainage and thus relatively high runoff coefficients. Our data sets, derived from 10 Austrian torrent catchments, can be assigned to this pre-alpine response class of basins.

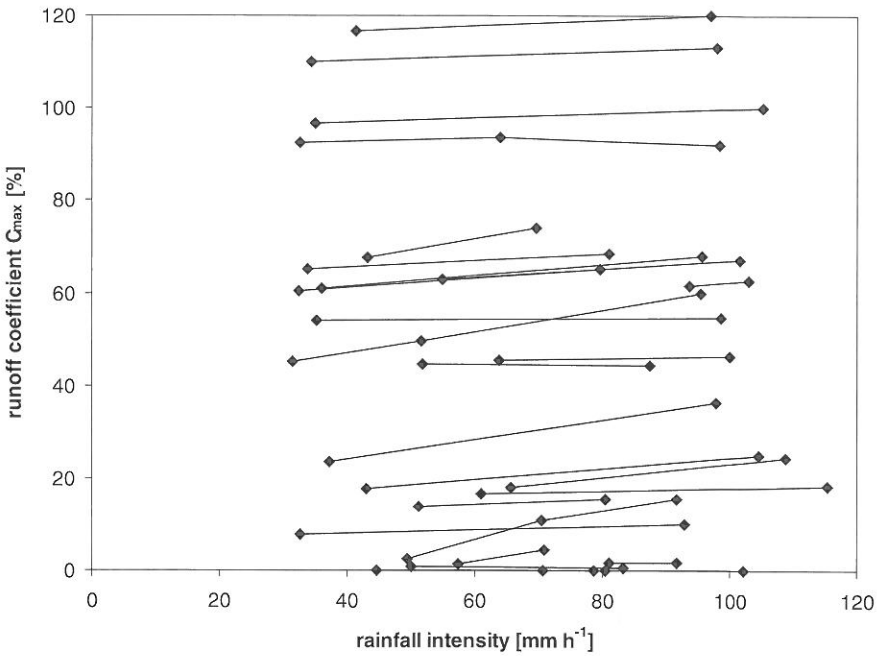

Figure 3-1: Rainfall intensity i versus runoff coefficient C for rain simulation experiments from 26 rain simulation plots within 10 small Austrian drainage basins.

In the classical rational formula the runoff coefficient is considered to be a constant, differing in value between diverse types of surface cover of a catchment. Since decades it is a controversial question, whether or not the runoff coefficient can be considered as a constant value. Lütschg-Löetscher (1945, cited in Gottschalk, Weingartner, 1998) sums up the problem as follows: "In spite of the fact that Karl Fischer and Walter Wundt have expressed their opinion repeatedly and in depth, the erroneous opinion is at hand still here and there that the value of this relation (the runoff coefficient) for a certain drainage basin is a hydrographic constant, so that by changing precipitation runoff can be determined in advance or, vice versa, the precipitation can be determined from the runoff." If the runoff coefficient

C is not a constant but rather a stochastic variable, with a distribution function that is a reflection of the physical characteristics of a catchment and its climate, this should also apply to smaller areas within the catchment like the representative soil / vegetation units chosen for the rain simulation experiments. Therefore we should find a surface runoff dependence on rain intensity within our data set. In Figure 3-2 runoff coefficient C_{max} is plotted against rainfall intensity i as a linear function with a mean gradient of 0.09 within the intensity space of 30 and 100 mm h^{-1}. For example, with a given runoff rate of 50 % at a precipitation intensity of 30 mm h^{-1} we can expect an average increase of the drain of 6.3 percent (for a 100 mm h^{-1} rainfall event). C_{max} = 0.5 resulting from a rain simulation experiment at 100 mm h^{-1} would decrease to 0.44 with rain intensity decreasing to 30 mm h^{-1}. But within this intensity range also a constant runoff coefficient value (gradient = 0) is inside the standard deviation.

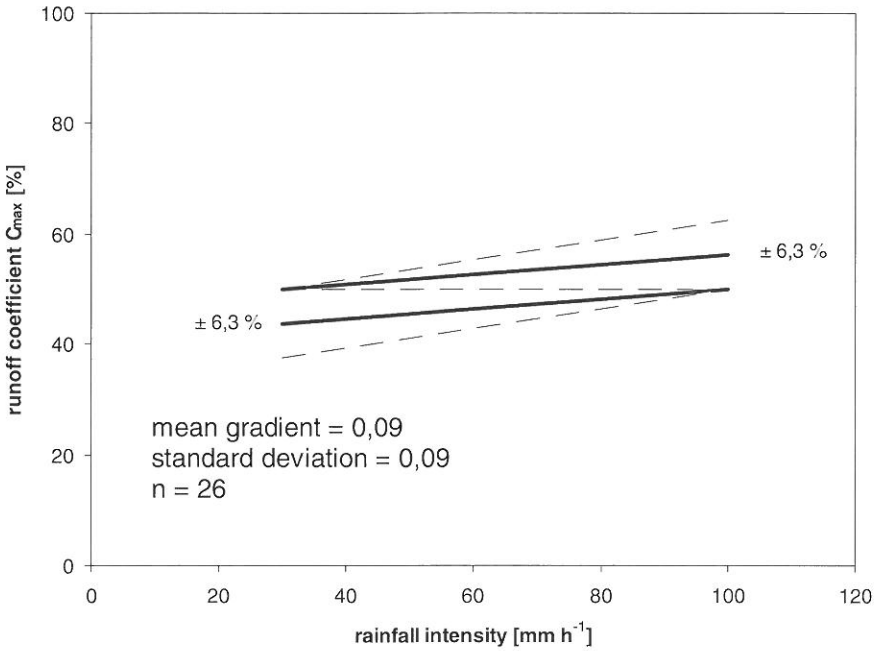

Figure 3-2: Mean gradient of the relationship of rainfall intensity (between 30 and 100 mm h^{-1}) and runoff coefficient for rain simulation experiments from 26 rain simulation plots within 10 Austrian small drainage basins.

Due to the rain pattern of the nozzle type of the used rain simulator it does not make sense to produce rain intensities lower than 30 mm h^{-1}, because a homogeneous distribution of the rain could no longer be achieved. While we have seen a quite moderate decrease of the runoff coefficient within the intensity space of 100 and 30 mm h^{-1}, a significant decrease down to zero is to be expected for lower rain intensities. A new sprinkling equipment (installation No.2) was constructed 2001 at the Austrian Institute for Avalanche and Torrent Research (AIATR) in order to investigate runoff characteristics long running rainfall with low intensities (duration > 24 h, i = 5 - 20 mm h^{-1}). Wending rain nozzles, which irrigate a half cycle in about 30 s, allow simulation of an area-wide rainfall event. Size of the experimental plot can be extended up to more than 400 m^2 for irrigation of whole slope segments. One first result of such a long-lasting rain simulation experiment with low intensity is shown in Figure 3-3 (Koralpe BF1). While the measuring points at 65 and 100 mm h^{-1} are derived from irrigation installation No.1, two measurements were made with the new rain simulator (installation No.2). According to the described relationship above a runoff coefficient C_{max} = 0.4 for a rain intensity of 30 mm h^{-1} was calculated. The curve shows a probably distribution of the increase of the runoff coefficient with rising amount of rainfall. The second rain simulation plot presented in this figure (Löhnersbach BF4) is the one with the nethermost simulated rain intensity of the older spray irrigation system. A similar run of the C_{max} – curve is imaginable.

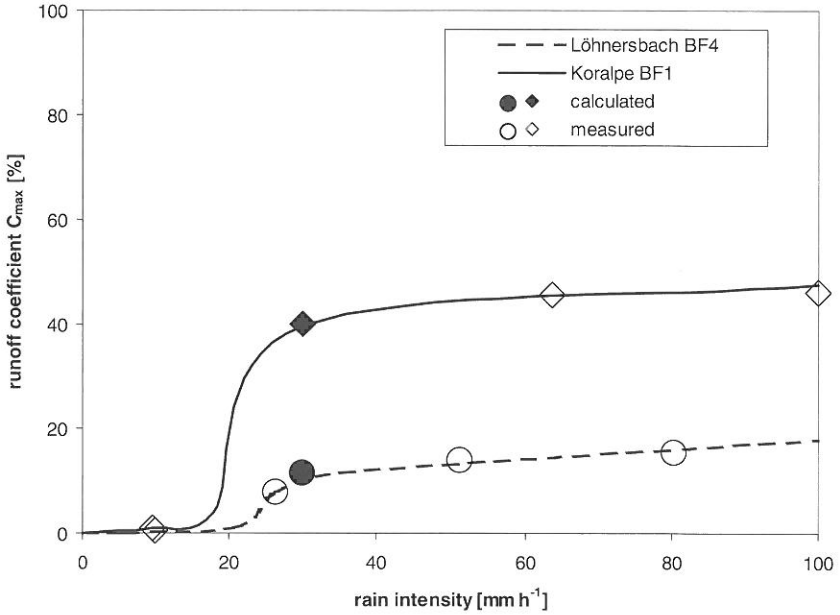

Figure 3-3: Rainfall intensity i versus runoff coefficient C for rain simulation experiments of different rain intensities from two rain simulation plots.

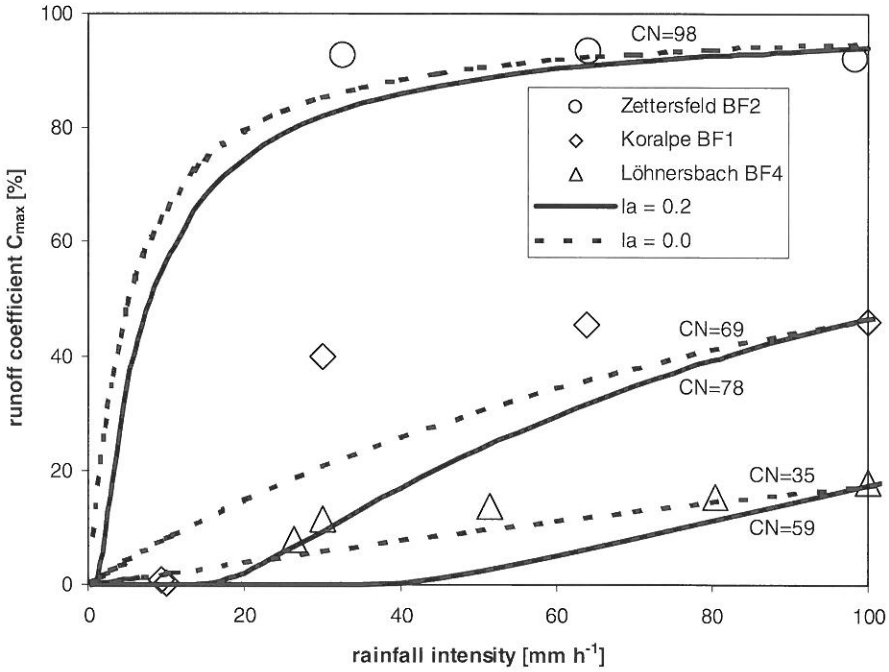

Figure 3-4: Relation between rainfall intensity i and runoff coefficient C for different CN-values (with original SCS method: initial abstraction I_a = 0.2; full line, and initial abstraction I_a = 0.0; dashed line) in comparison with rain simulation experiments from three rain simulation plots.

A rain intensity dependent runoff coefficient can be derived from curves of the Soil Conservation Service (SCS) Curve Number (CN) method. For almost impermeable soils (see Figure 3-4, Zettersfeld BF2) a proper CN can be found to explain the runoff behaviour. For plots with a minor tendency to produce surface runoff no curve numbers can be found that fit to our investigations. The dashed lines in Figure 3-4 show curve numbers where the initial abstraction I_a (the accumulated loss up to time of ponding) is set to zero. Since the initial losses (interception, evaporation, initial moisture situation, etc.) for the calculation of C_{max} are almost negligible, as mentioned in the methods part, the modified curve numbers show a better approach to our data, but they still remain unsatisfactory.
Seasonal changes of the infiltration rate and thus changes of the runoff coefficient are well known from regions where wet and dry seasons change cyclic (Cerdà, 1997; Mollenhauer et al., 1999). Rain simulation experiments in the Mediterranean region on heavy soils as well as on sandy soils show a

conspicuous dynamic in surface runoff due to high seasonal differences in soil moisture situation. Such great differences are more seldom in Central Europe and the Alps. Schwarz (1986) describes variations in runoff coefficient caused by dry-rifts in cohesive soils. Within the database of rain simulation experiments of the Austrian Institute for Avalanche and Torrent Research there are nine pasture plots and one forest stand where irrigation tests were repeated at different seasons (see Table 2-1 and Figure 3-5). All sites show an increase in runoff in summer even though mean soil moisture conditions are higher in spring. From the factors responsible for these observations, mainly the influence of grazing and soil frost on surface runoff have to be mentioned. While grazing impact causes soil compaction leading to higher runoff rates (Schauer, 2000), soil frost effects regeneration of the infiltration capacity. Whereas very cohesive stands and wet stands show little differences, more coarse textured soils feature a regeneration capacity of up to more than fifty percent.

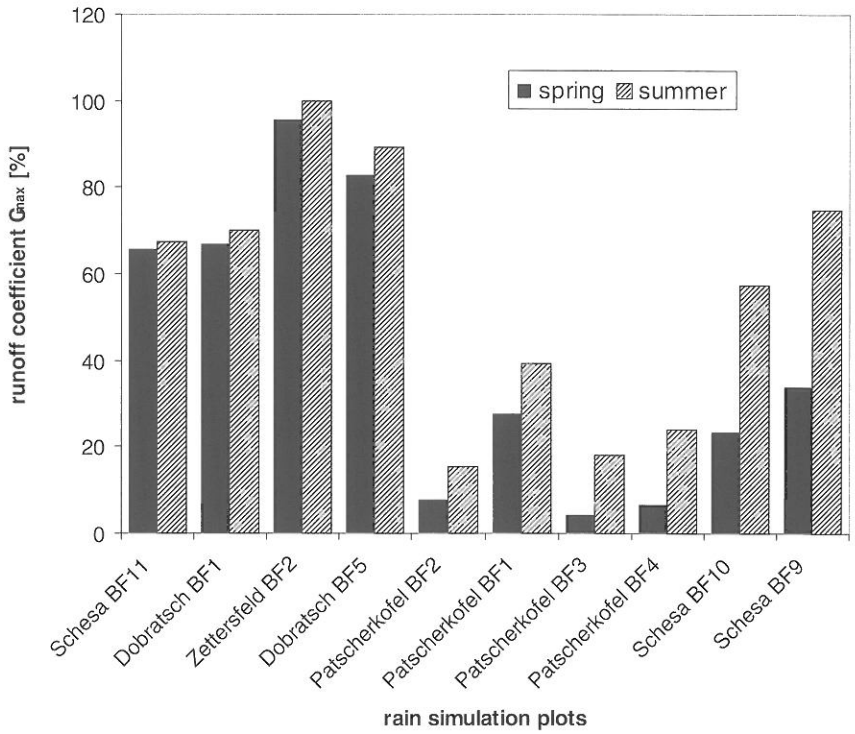

Figure 3-5: Seasonal changes of runoff coefficient C_{max} at 10 rain simulation plots.

4 CONCLUSION

For the implementation of runoff coefficient concept in practice it is often recommended to assign not exact runoff values but rather runoff classes to different soil / vegetation units (Löhmannsröben et al., 2000; Markart et al., 2001). Table 4-1 shows a possible runoff coefficient classification, which can be used for runoff coefficient mapping. Such kind of maps are an important basis for precipitation / runoff calculations and modelling as shown by Angerer et al. (2000), Markart et al. (2000) and others. Repetitions of rain simulation experiments with different rain intensities show between the range of 30 and 100 mm h^{-1} only a moderate increase of the runoff coefficient. The appropriation of runoff coefficient classes to different soil / vegetation units can therefore be accounted as constant within this rainfall intensity range.

Table 4-1: Runoff coefficient classes.

Runoff coefficient classes	range C	range C%	colour
Class C1	0 – 0.1	0 - 10	dark green
Class C2	0.1 – 0.3	10 - 30	light green
Class C3	0.3 – 0.5	30 - 50	yellow
Class C4	0.5 – 0.75	50 – 75	orange
Class C5	0.75 - 1	75 - 100	red

While we have seen a quite moderate decrease of the runoff coefficient within the intensity space of 100 to 30 mm h^{-1}, a significant decrease down to zero is to be expected for lower rain intensities. This assumption can be confirmed by first results of long-lasting, low intensity rain simulation experiments. Further investigations in the future will help to describe the relations between rain intensity and runoff coefficient more accurately at the intensity range lower than 30 mm h^{-1}.
When searching for a proper curve number of the Soil Conservation Service method to explain the runoff behaviour of our data no satisfactory approach could be found. One reason of delivering too small runoff values for rain intensities lower than 50 mm using the SCS method (DVWK, 1984), is that the rainfall events producing peak flows have lower or negligible initial abstractions ("worst case scenario"). In such a case, when initial conditions are bad (interception and evaporation almost zero, initial moisture situation high, etc.) total runoff coefficient C_{tot} gets very close to maximum runoff coefficient C_{max}.
As exposed variability of runoff with precipitation is high at the intensity range up to 30 mm h^{-1} and only a moderate increase of runoff is to predict for rising intensities up to 100 mm h^{-1}. For estimation of infiltration characteristics of different soil / vegetation units in torrent catchments and runoff coefficients respectively the influence of land use, especially grazing becomes very important. Such influences can more than double the runoff rate within months.

REFERENCES

Angerer, H. et al. (2000): Multidisziplinäre Prozeßanalyse in einem Wildbacheinzugsgebiet am Beispiel des Wartschenbaches in Osttirol. Intern. Symposion Interpraevent 2000 – Villach/Österreich. Tagungspublikation. 3, pp. 3-17.

Browne, F.X. (1990): Stormwater Management. in Standard Handbook of Environmental Engineering, ed. by R.A. Corbitt, McGraw-Hill Inc., New York. pp. 7.1-7.135,.

Cerdà, A. (1997): Seasonal changes of the infiltration rate in a Mediterranean scrubland on limestone. Journal of Hydrology. Amsterdam. 198, pp. 209-225.

Chow, V.T et al. (1988): Applied Hydrology. McGraw-Hill Inc., New York

Dooge, J.C.I. (1957): The rational method for estimating flood peaks. Engineering. London. 184, pp. 311-377.

DVWK, (1984): Arbeitsanleitung zur Anwendung von Niederschlag-Abfluß-Modellen in kleinen Einzugsgebieten. DVWK-Regeln zur Wasserwirtschaft. Deutscher Verband für Wasserwirtschaft und Kulturbau. Bonn. 113, p. 34.

Gottschalk, L., Weingartner, R. (1998): Distribution of peak flow derived from a distribution of rainfall volume and runoff coefficient, and a unit hydrograph. Journal of Hydrology. Amsterdam. 208, pp. 148-162.

Löhmannsröben, R. et al. (2000): Geländeanleitung zur Abschätzung des Abfluß- und Abtragsgeschehens in Wildbacheinzugsgebieten. Bayerisches Landesamt für Wasserwirtschaft. München. Materialien Nr. 87, p. 111.

Mack, M.J. (1995): HER-hydrologic evaluation of runoff; the soil conservation service curve number technique as an interactive computer model. Computers & Geosciences. Oxford. 21, 8, pp. 929-935.

Markart, G., Kohl, B. (1995): Starkregensimulation und bodenphysikalische Kennwerte als Grundlage der Abschätzung von Abfluß- und Infiltrationseigenschaften alpiner Boden-/ Vegetationseinheiten. Ergebnisse der Beregnungsversuche im Mustereinzugsgebiet Löhnersbach bei Saalbach in Sbg. Berichte der Forstlichen Bundesversuchsanstalt. Wien. 89, p. 38.

Markart, G. (2000): Der Wasserhaushalt von Hochlagenaufforstungen. Dargestellt am Beispiel der Aufforstung von Haggen bei St. Sigmund im Sellrain. Berichte der Forstlichen Bundesversuchsanstalt. Wien. 117, p. 126.

Markart, G. et al. (2000): From point data and cartography to the analysis of runoff and mass-movement processes in torrent catchment areas. In: Proceedings of the Workshop on Advanced techniques for the Assessment of Natural Hazards in Mountain Areas. 5 – 7 June 2000, Igls, Austria. 72–73.

Markart, G. et al. (2001): Provisorische Geländeanleitung zur Anschätzung des Oberflächenabflusses auf alpinen Boden-/Vegetationseinheiten bei Starkregen (Version 1.0). Interner Bericht der Forstlichen Bundesversuchsanstalt, Wien.

Mollenhauer, K. et al. (1999): Die Saisonalität der Erodierbarkeit von Böden, dargestellt am Beispiel von sandgeprägten Standorten im westlichen Anatolien. J. Plant Nutr. Soil Science. Weinheim. 162, pp. 631-636.

Pilgrim, D.H., Cordery, I. (1993): Flood Runoff. in Handbook of Hydrology, ed. by D.R. Maidment, McGraw-Hill Inc., New York, pp. 9.1-9.42.

Schauer, Th. (2000): Der Einfluss der Schafbeweidung auf das Abfluss- und Abtragsgeschehen. Intern. Symposion Interpraevent 2000 – Villach/Österreich. Tagungspublikation. 2, pp. 65-74.

Schwarz, O. (1986): Zum Abflußverhalten von Waldböden bei künstlicher Beregnung. in Das landschaftsökologische Forschungsprojekt Naturpark Schönbuch. Hrsg. G. Einsele. Dt. Forschungsgemeinschaft DFG. Forschungsbericht. Weinheim. pp. 161-180.

Zeller, J. (1981): Starkniederschläge und ihr Einfluß auf Hochwasserereignisse. Bericht Nr. 126 der Eidg. Anstalt für das forstliche Versuchswesen. 2. Auflage. p. 109.

GENETIC AND STATISTICAL ANALYSIS OF THE MAXIMUM RIVER RUN-OFF IN EAST SIBERIA AS THE GROUND FOR MODELING AND FORECASTING INUNDATIONS

L.M.Korytny[1], N.V.Abasov[2], T.V.Berezhnykh[2], N.V.Kichygina[1]

[1]Institute of Geography, Siberian Branch, Russian Academy of Sciences, Laboratory of natural resources, 1, Ulan-Batorsky st., 664033, Irkutsk, Russia, korytny@irigs.irk.ru

[2]Energy Systems Institute, Siberian Branch, Russian Academy of Sciences, Laboratory of risk problems in energetics, 132, Lermontov st., 664033, Irkutsk, Russia, berejn@isem.sei.irk.ru

SUMMARY

The paper discusses analysis of genesis and repeatability of inundations in one of the largest regions of Russia – East Siberia. Zoning (and regional differentiation) of the territory with respect to the danger of inundations has been conducted. Variants of computation of maxima of river run-offs are considered. Techniques of forecasting extreme situations on rivers and lakes are proposed.

Keywords: Inundations, maximum river run-off, distribution curves, super long-term forecasting

1 INTRODUCTION

In East Siberia, as well as everywhere in the world, inundations dominate among natural calamities with regard to such factors as repeatability and real impact. Flooding of territories in case of inundations has substantial social consequences as well as exceedingly negative impact on the regional economy. Mathematical modeling of the maximum run-off, after which long-term forecasting may be made, could substantially reduce risks of inundations. Revealing regularities in the genesis, distribution, repeatability as well as finding out causes (of both earthly and space origin) of formation of large spring floods is an important stage, which follows before the stage of prediction of inundations. This problem is solved by the authors of the paper for the territory of East Siberia in the investigations supported by Russian Foundation for Fundamental Research, Project No. 00-05-64345.

2 GENESIS AND REPEATABILITY OF INUNDATIONS

East Siberia is characterized by inundations, caused by spring (spring-summer) floods and summer precipitation floods; elevations of water levels due to spring ice jams (gorges) and ice dams; anthropogenic activity, in particular, by discharges of excessive water masses through the dams of integrated systems of water power development; wind pileups and tides in mouths of rivers. Uplifts of water levels in small rivers of East Siberia are often caused by melting ice mounds formed as a result of freezing the beds of these rivers. Sometimes inundations are caused by several factors simultaneously (by spring floods and blockages on the valleys, by melting snow and intensive precipitation in the mountains).

In East Siberia, inundations most frequently take place during precipitation floods and spring floods. Analysis of the relation between maximum flood discharges of these important hydrological phases reveals the following principal regularities: maxima of precipitation floods dominate in mountain areas of the West and East Sayan, the Khamar-Daban, the North-Baikal and the Pathomsky mountain ranges; as far as the Mid-Siberian plateau is concerned, the largest water discharges and levels relate to the phases of spring or spring-summer floods; valleys near mountains are characterized by combinations of the factors. Spring floods take place in May and June, precipitation floods - in July or less frequently in August. Cases of superposition of precipitation and spring floods (mixed inundations) are rather seldom.

More frequently spring-flood and ice-jam inundations are superimposed, but ice jams often cause inundations by themselves. In East Siberia, the number of ice-jam inundations and the detriment caused by them are very large since main rivers of East Siberia flow in the submeridional direction, what, as experts know, provokes ice jams.

Ice jams constitute up to one third part and more than all other causes of inundations. Noteworthy, the basins of such rivers as the Lena, the Yana, the Indigirka and the Kolyma run the danger of ice-jam inundations more than other basins. On the whole, there are about 447 ice-jam areas of total length of

744 km on the territory of East Siberia, inundations taking place on 62 (or 14%) of them. On many rivers, which carry waters south to north, ice jams make over one third and more than all other causes of inundations.

Ice-dam inundations are more frequent in the region under scrutiny. Before hydroelectric power plants (HEPPs) were erected, even Irkutsk suffered from inundations caused by ice-dam inundations. But even when HEPPs exist, the danger of such inundations appear in the boundary between the unfrozen patch of water in the midst of ice and the edge of ice in the tail race. In particular, this is characteristic of the section of the Yenissey between the mouths of the Angara and the Podkamennaya Tunguska. So, inundations caused by ice jams and ice dams are widely spread on rivers of East Siberia.

The danger of inundations as a result of hydrotechnical construction activity is also substantial. For example, in recent years, cases of forcing the level above the normal hydrostatic upthrust level have become more frequent in the head races of the Angara cascade of HEPPs. This, in particular, has become the cause of almost permanent flooding of low parts of Lake Baikal shores. On the other hand, discharge of additional water masses through the dam in order to prevent flooding in the head race provokes flooding over or underflooding the objects in the tail race (as it happened in Irkutsk in 1995).

Especially dangerous are the inundations, which take place in cases of damages of integrated systems of water power development, due to formation of breakage waves in tail races. They carry huge masses of water moving at high speeds. Analysis of such situations on the territory of Russia (Malik, 1995) has given evidence of such danger also for HEPPs of the Angara-Yenissey cascade: in 1988, a situation close to it happened in the tail race of the Krasnoyarsk HEPP. The fact that in this region there are several large HEPPs, which are included into the list of potentially dangerous objects of economy, should be taken into account.

In case of break of the dam of the Irkutsk HEPP a potential zone of catastrophic inundation of area of 62.4 km^2 may be formed, the population which amounts to 123600 occur in the zone of this potential inundation; for the Bratsk HEPP - 104 km^2 (33300 men); for the Ust-Ilimsk HEPP - 117 km^2 (13500 men). It is necessary to take this danger into account considering the fact that a number of HEPPs are situated in the seismic zone.

On the whole, on the hydrotransits of East Siberia rivers , during the period of instrumental monitoring we have registered 1703 inundations (Korytny, Kichygina, 1998). The largest number of hydrotransits characterized by inundations have been registered for the Lena; the number of inundations here is also the largest (Figure 2-1).

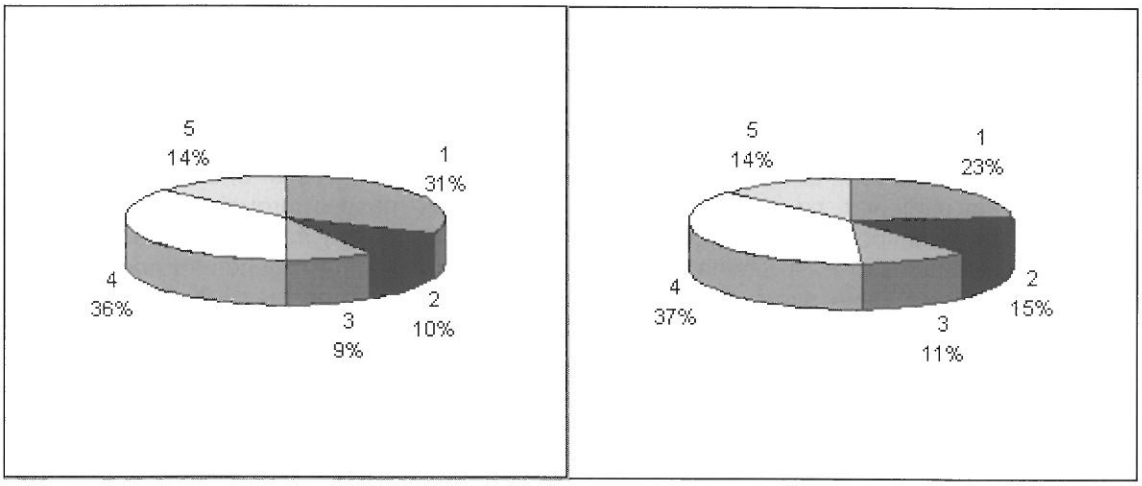

a *b*

Figure 2-1: Distribution of hydrotransits subject to inundations (a) and cases of inundations (b), % for the river basins of East Siberia. The basins of : 1 – the river Yenissey, 2 the river Angara, 3 – Lake Baikal, 4 – the river Lena, 5 – rivers the Yana and the Indigirka.

3 ZONING OF EAST SIBERIA WITH REGARD TO THE DANGER OF INUNDATIONS

In the process of zoning (Table 3-1), in addition to characteristics of danger and their integrated explication (class of danger), physico-geographical differences of regions, prevailing hydro-morphological parameters of river valleys, characteristics of their exploitation and population have been taken into account. As a result, considering the combination of all the characteristics analyzed, the following 7 regions have been differentiated.

Table 3-1: Classes of danger of inundations for some regions of East Siberia.

№	Name of the region	Genesis of inundations	Class of danger of inundations
I	East-Sayan	Precipitation	III-IV
II	Zabaikalsky	Precipitation Pileup	II-III I
III	Vitim-Olekmisky	Precipitation Ice-jams and ice-dams Spring-floods	II
IV	Upper-Yenisseysky	Spring-floods Precipitation	II-III
V	Mid-Siberian	Spring-floods Spring ice-jams	I-II III-IV
VI	North-East	Precipitation Spring ice-jams Spring-flood	II-III
VII	North-Siberian	Spring-flood Pileup and Tides	I-II

4 ANALYSIS OF EFFICIENCY OF SCHEMES FOR COMPURING MAXIMUM RUN-OFF

Computations of the maximum run-off for the periods of spring flood and precipitation floods using the two schemes - principal and alternative ones - have been performed for the hydrotransits in the south of East Siberia. The principal computational scheme employed the binomial curve (Pirson III-d type), the curve of 3-parameter gamma-distribution (Krivitsky-Menkel) and parametric techniques of approximation. For the Pirson curve, parameters were determined by the method of moments or by the graph-analytical technique; for the Krivitsky-Menkel curve, the parameters were determined by the method of moments or by the technique of the greatest plausibility of approximation. As an alternative one, Yu.B.Vinogradov's computational technique (1988), which is based on application of a family of functionally-normal curves (the lognormal curve and the curve C-3), as well as nonparametric techniques of approximation have been considered.

Using the results of the computations, we have conducted the comparative estimation of efficiency of both the principal and the alternative computational techniques. B.I.Gartsman's (1996) approach has been chosen as the technique for comparative estimation. For the purpose of estimating the quality of approximation of the empirical curve by the analytical curves we used the following 4 estimating criteria. Criterion 1 is the relation of 1% of the computed analytical distribution to the maximum value in the sequence, which characterizes the safety factor of the decision made. Criterion 2 defines the value of the factor of convergence for empirical and analytical distributions of probability (i.e. reliability of approximation). Criterion 3 characterizes the value of discrepancy (with respect to the absolute values of the ordinates) between the empirical points and the points of the analytical curve; the minimum of this value corresponds to the most close correspondence of the curves with respect to the absolute value, i.e. the maximum accuracy of approximation. Criterion 4 is equal to the lower boundary of the analytical curve and is physically possible only when the value lies between zero and the minimum value of the analytical sequence.

The comparison has been conducted within the frames of geographical analysis (basins, areas) and genetic analysis (spring floods, precipitation floods) on account of the dimension of the water catchment area as well as the length of observations.

The analysis has given evidence of obvious general preference of the alternative technique in the aspects to both quality of results and computations. The advantage of techniques based on both functional-normal distribution curves and nonparametric approximation is more explicit in computations of

sequences of precipitation flood maxima and for small rivers, furthermore, this advantage is obvious for long and shirt sequences. Above advantages are especially explicit in estimating with respect to the two quite important characteristics: correctness and reliability. For example, the segments for the lognormal curve and curve C-3 include 44% and 48% of best computational results with respect to correctness, respectively; 40% and 45% with respect to reliability, respectively; and 24% and 26% with respect to precision, respectively. The advantage of the lognormal curve and the curve C-3 the respect to precision is not very obvious. Computations of the control curves with the aid of Krivitsky-Menkel's and Pirson III-d kind curves as well as with the aid of the techniques of determination of their parameters, which form the principal technique, are more applicable in computations of the spring flood run off and - for medium-size and large rivers.

5 METHODS OF SUPER LONG-TERM FORECASTING OF EXTREMUM RUN-OFF

A methodology of long-term forecasting of natural-climatic processes has been developed. It employs some ideas of research schools of academican I.P.Druzhinin and Prof. A.P.Reznikhov and consists in detailed investigation of cause-effect relations, finding out physical analogs and their application in formalized methods of long-term forecasting (Abasov, Berezhnykh, 1999; Abasov et al., 2000; Berezhnykh et al., 2000), which are subdivided into qualitative (background method; method of analogs with respect to solar activity), probabilistic and approximation methods (analog-similarity relations; a discrete-continuous model). These methods of forecasting have been implemented in the form of analytical aids of the information-forecasting software GYPSAR, which provides for some elements of artificial intelligence.

5.1 Background forecasts of the South Siberian rivers (the Ob, the Yenissey, the Angara)

They are grounded on space-temporal regularities revealed after taking account of the phase shifts in occurrence of secular maxima and minima on integral-difference curves of many-year hydrological processes in objects under comparison, have given the possibility to estimate the water content of these rivers for the perspective of 10, 15 and 25 years. The decrease of water content of Lake Baikal expected in the forthcoming quarter of a century may provoke - in some periods - the conditions which are unfavorable especially for energetics. These conditions cannot be ignored.

5.2 The Method of analogs with respect to indices of solar activity

Solar activity plays substantial role in investigations of global variations of climatic processes. Its account in *the method of superimposed epochs* (Figure 5-1) has allowed us to draw a conclusion on increased probability of the low-water period in the useful inflow of Lake Baikal, which takes place on the branch of increase in solar activity of the 11-year solar cycle. This period starts a year before the minimum of solar activity and ends a year after its maximum for practically every other solar cycle. Increased probability of high-water period on the branch of solar activity decrease from the 2^{nd} to the 5^{th} year after the maximum of solar activity. The low-water period on Lake Baikal, which started in 1996, will - in accordance with our estimates - be over in 2000-2001.

5.3 The probabilistic method of forecasting

It is based on the property of alternation of series of years of increased and decreased observed indicators (characteristic indices) of natural processes. The main mass of the series (98,4-99,6%) is represented by series of one to three years, furthermore, relative frequencies of occurrence of series of varied durations are rather stable, and for the generalized indices of the run-off for the rivers are distributed as follows: 0.68 (for 1-year series), 0.24 (for 2-year series), 0.065 (for 3-year series), 0.014 (for 4-year series), 0.008 (for 5-year series), 0.001 (for 6-year series).
The problem of forecasting is subdivided into the two parts: 1) qualitative forecasting of probability of either continuation of a started series or its noncontinuation (appearance of a new one) during the next year (this forecasting is formed of frequency characteristics for series of years of increase or decrease of the prognosticated sequence); 2) obtaining the qualitative estimate of the prognosticated quantify in the form of a curve of conditional provisions, which is based on intra-sequence interdependences

between hydrometeoelements on account of their differentiation with respect to series of years of increase or decrease, by constructing particular curves of conditional provisions of the run-off for each of expected variants of development of the series and subsequent constructing of a generalized curve.

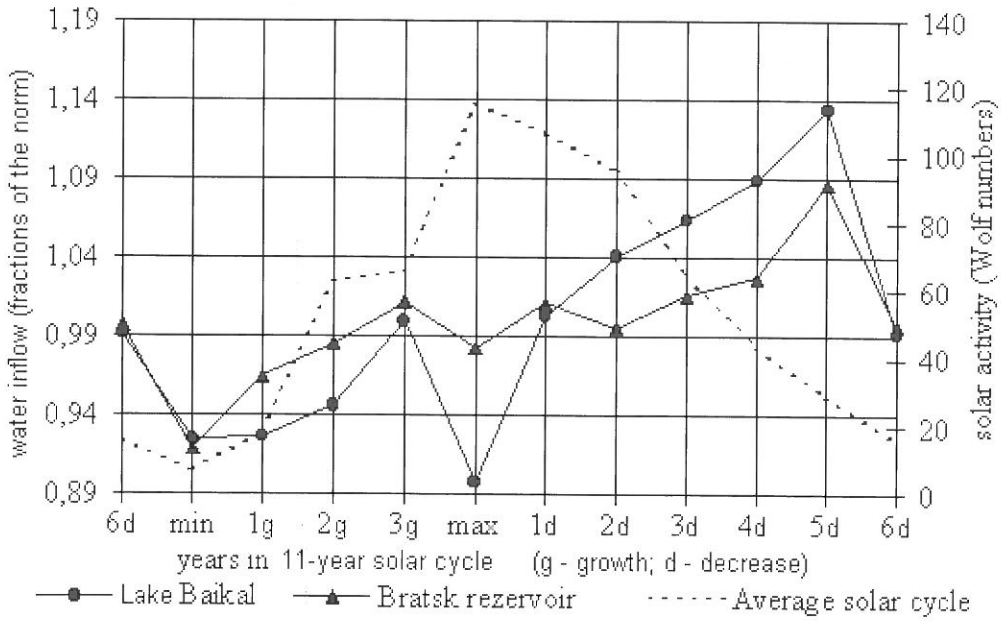

Figure 5-1: The relationship between water inflow to Lake Baikal and to the Bratsk artificial reservoir and the solar activity.

5.4 Approximative learning methods

They form prognostic trajectories of behavior for a long perspective. These methods constitute the formalized part of the methodology.
The method of analog-similarity relations is grounded on the fact that some similarities in the character of variability of indices for some fragments of the sequence $x(t)$ with respect to definite criteria can appear (and have been revealed) during a long period of observations. The idea of the method consists in estimating of the similarity of such fragments of the series, which have been called the analogs. Multistage optimization of both external parameters (e.g. the number of iterations of the sliding averaging needed for the purpose of decomposition of the sequence into two components: the smoothed one containing individuated periodic oscillations and the residual one - arbitrary). The method may be applied to current advancements of forecasting up to the double solar cycle. Using a special procedure of complexing, it separates only those of them, which give the best results for the given optimization subsample. A few optimal vectors of parameters obtained undergo verification on the verifying subsample. If the latter procedure was successful then the prediction is immediately obtained by combining (complexing) several best solutions.
The computed prognostic trajectory of the river run-off for two to three 5-year periods obtained by this method in the process of multiple averaging, which is needed to increase reliability of forecasting, reduces the indices of extreme events, more precise estimation of which requires additional procedures.

5.5 Details of forecasting extreme processes

Methods of long-term forecasting allow to obtain sufficiently reliable predictions within the interval of $x_{min}+\Delta_1$, $x_{max}-\Delta_2$ (i.e. within the interval of medium values of indices). Meanwhile, in the bands close to extreme ones, reliability of predictions is substantially lower. While for medium values the statistics for the interval of 100 years gives acceptable results at the expense of a sufficiently large number of necessary analogies which correspond to prognostic samples - for extreme values the situation is quite different, first of all in virtue of poverty of statistical data.

Decreasing the values of Δ_1,Δ_2: $\Delta_1,\Delta_2 \rightarrow 0$ (by including them into optimization parameters of forecasting methods under scrutiny) could be one of the ways of increasing reliability of forecasts. Partially, such an approach has been realized in the method of analog-similarity relations, what gives the possibility to form the interval of possible prognostic trajectories in the two variants - from the minimum possible trajectory to the maximum possible one.

5.6 Provision of reliability of long-term forecasting

Both the methodology and the methods considered above have been implemented in the form of the information-forecasting software system GIPSAR, which includes some tools implementing several methods of forecasting, some tools for analysis of initial and prognostic information, a developed database, a set of tools for verification of algorithms, additional information bound up with algorithms of statistical processing of sequences (sliding averaging, integral-difference curves, etc.), aids to organize output of initial information (in its various forms) as well as the aids of formation of output prognostic documents.
The systemic part of GIPSAR is formed by the programming environment ZIRUS, which includes several software tool packages: the system's kernel, which supports the model of data; packages of "man-machine" dialog interaction; a hypertabular editor combined with an editor of forms (needed for preparing as well as scanning and viewing complex hierarchical and network models of data); packages of support of interfaces needed for data exchange; etc.
In virtue of multifactor character and variability of regularities, which are characteristic of natural processes, forecasts obtained by different methods undergo verification and then complexing on account of forecasts of other processes (solar activity, atmospheric precipitation, air temperature drifts, etc.).
To the end of increase of reliability in prediction of extreme figures of water content we have proposed an approach in the form of correction of probability-like prognostic distributions in the direction of expected extreme figures. For example, the distribution of the prognostic index $P(x)$ is replaced with

$$P'(x) = P(x) \cdot \xi(x), \tag{1}$$

where $\xi(x)$ is the distribution of damages under the conditions of expected larger water content. On account of some given threshold value of P^*, the most probable prognostic interval is replaced with a wider one.

6 CONCLUSION

As the most dangerous forms of inundations for East Siberia we consider precipitation inundations, mixed ones (spring-flood ones with superimposed precipitation floods or ice-jams) and inundations resulting from ice-jams. Furthermore, there exists a danger of catastrophic damage inundations in cases damages of integrated systems of water power development. Distribution of territories with different danger of inundations can be obviously explicated by zoning.
Estimation of applicability of statistical methods for computing the maximum run-off for the rivers of south of East Siberia gives evidence of marked preference of the alternative computational technique with regard to both the technique of computations and the qualitative of results.
Our approach to long-term forecasting and its implementation in the form a forecasting system GIPSAR give the possibility to develop existing methods of forecasting further, add new ones, adapt them for the needs of prediction of extreme figures and indices, while including different heuristic techniques of estimation employing the aids of artificial intelligence, which are available in the tool-kit of the software GIPSAR.

REFERENCES

Abasov, N.V. et al. (2000): Long-term forecasting of naturally conditioned factors in energetics // Systems Investigations of Energetic Problems. - Novosibirsk: Nauka Publ., 2000, -pp.415-429.

Abasov, N.V., Berezhnikh, T.V. (1999): Reliability of long-term forecasting of the river run-off as a factor reducing the risk for natural economy // Proc. 4-th All-Russian Symposium "Risk and Insurance".- Irkutsk: ISEM Publ., 1999. – pp. 216-228.

Berezhnikh, T.V. et al. (2000): The role of forecasting of water inflow into reservoirs of hydroelectric power plants of the Angara cascade in the management of water-economic and ecological risks // Proc. 4-th Research and Methodological Symposium "The Problems of Complex Usage of Resources of the Angara cascade Reservoirs". Moscow: Moscow Social Research Foundation, 2000. pp.. 52-68.

Vinogradov, Yu.B. (1988): Mathematical Modeling of Processes of Formation of the River Run-off. - Leningrad: Hydrometeoizdat, 1988. – 312 p.

Gartsman, B.I., Stepanova, M.V. (1996): Techniques of hydrological computations of the maximum river run-off for the Russian Far East // Geography and Natural Resources. - No.4. - pp. 103-110. - Novosibirsk

Korytny, L.M., Kichygina, N.V. (1998): Inundations in river valleys of East Siberia // Water Resources. . -No.2. - pp. 161-165. - Moscow

Malik, L.K. (1995): Natural and anthropogenic factors of damage of hydrotechnical constructions // Izvestiya of Russian Academy of Sciences: Geography.- No. 1. - Novosibirsk

DEVELOPMENT OF METHODOLOGIES FOR THE ANALYSIS OF THE EFFICIENCY OF FLOOD REDUCTION MEASURES IN THE RHINE BASIN ON THE BASIS OF REFERENCE FLOODS (DEFLOOD)

P. Krahe[1]; D. Herpertz[1]; H. Buiteveld[2]; N. Busch[1]; M. Eberle[1], H. Engel[1]; A. Helbig[4]; F. Naef[3]; K. Wilke[1]

[1] Federal Institute of Hydrology (BfG), Kaiserin-Augusta-Anlagen 15-17, 56068 Koblenz, Germany, krahe@bafg.de / herpertz@bafg.de / busch@bafg.de / eberle@bafg.de / engel@bafg.de / wilke@bafg.de

[2] Institute of Inland Water Management and Waste Water Treatment (RIZA), P.O. Box 9072, 6800 ED Arnhem, The Netherlands, h.buiteveld@riza.rws.minvenw.nl

[3] Institute of Hydromechanics and Water Resources Management, Swiss Federal Institute of Technology (ETH Hönggerberg), 8093 Zürich, Switzerland, naef@ihw.baug.ethz.ch

[4] Department Climatology of University of Trier /FB VI, 54286 Trier, Germany, helbig@uni-trier.de

SUMMARY

After some years of extreme flooding in the 1990s extended efforts were made to improve flood protection by means of an integrated river basin management. Part of this strategy is the implementation of decentralised flood reduction measures (FRM). With this in mind, the CHR/IRMA-SPONGE Project DEFLOOD was initiated. By establishing a set of methodological tools this project aims at making a step further towards a quantitative hydrological evaluation of the effects of local FRM on flood generation in large river basins. The basin of the River Mosel and in particular, the basins of its tributaries Saar and Sauer served as case study areas for testing the methodological approach.
In large river basins the hydrological efficiency of FRM strongly depends on the spatial and temporal distribution of precipitation. Classified hydrometeorological conditions were established for the study area and extreme flood events were estimated with respect to an area related distribution of maximum possible precipitation (ADMP).
An integrated modelling approach based on both precipitation-runoff and flood routing procedures was set up. In the defined Framework for Integrated River Basin Modelling (FIRM) scenarios of land use and soil related measures as well as for retention of water along rivers were taken into account in an appropriate manner.
The integration of regional flood reduction measures into the modelling approach and their local effects on downstream flooding is demonstrated for a meso-scale sub-basin in the Moselle/Saar river basin.

Keywords: Flood simulation, flood reduction measure, hydrometeorological reference condition, integrated river basin modelling, framework

1 INTRODUCTION

In response to recent extreme flooding events in the River Rhine basin, revised integrated management strategies were initiated which aim at improving the protection against high water by taking into account hydraulic, ecological and socio-economic functions of the entire river system on a transnational level. From the perspective of a long-term sustainable and resilient river basin development, hydrological studies related to flood risk management have become an important issue especially with regard to the spatial planning processes. In order to reduce flood risk along affected river reaches, (inter)national action plans on flood defence were elaborated for the River Rhine basin. A set of measures was defined to tackle the various problems and issues raised by flooding disasters. One category of measures is the implementation of decentralised flood reduction and retention measures, which aim at enhancing water storage capacities within the river basin.
There is a number of recent studies within the River Rhine basin which examine the local and regional effects of basin related measures. Results from these studies allow to quantify the effect of measures for the particular river (sub-)basin under consideration. However, extended to larger river basins, evaluations could only be made in a qualitative way. Applied to the River Rhine, it is well known that measures do not have the same effect in all cases of flooding and along the entire river. The effects of the different measures cannot simply be added, but the range of local and spatial effects must be combined in order to obtain the precise sum of effects for a specific flooding event at a particular place.

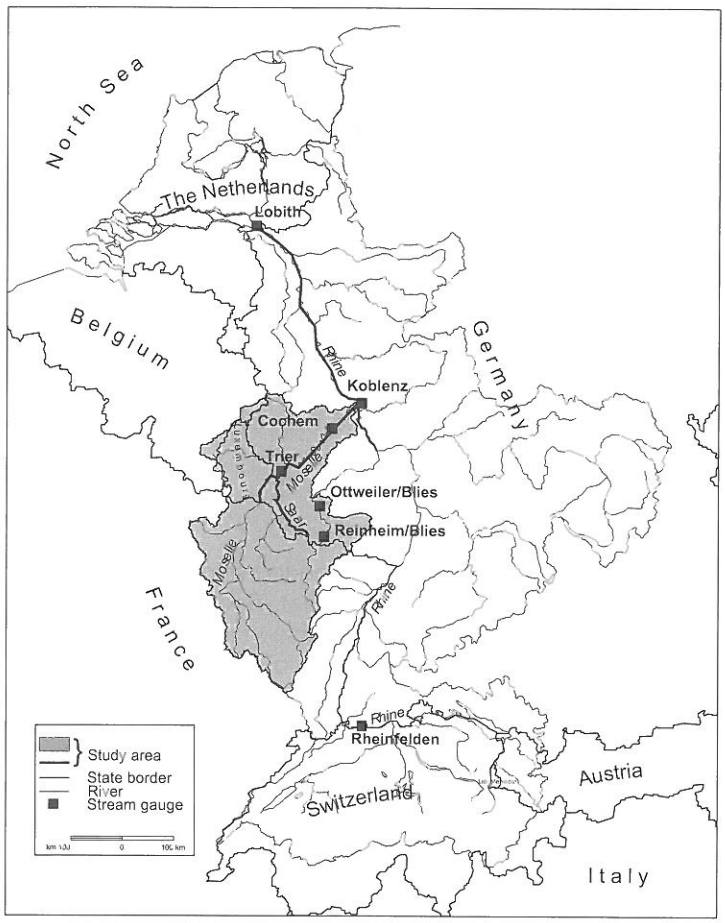

Figure 1-1: The River Rhine basin with the River Moselle basin and flood routing stretches for the River Rhine

A quantification of the impact of flood reduction measures (FRM) in the basin area has yet to be carried out for flood generation in large river basins. Within the DEFLOOD project a methodology is proposed which allows an assessment of the effect of decentralised measures. Apart from the supra-regional hydrological evaluation of the measures, the procedures developed can also be used as a planning instrument. Furthermore, the methodology should help to compare and evaluate the levels of past and probable future flood events.

Basic assumptions of the approach are: Firstly, the varied spatial/temporal precipitation distribution particularly in large river basins causes the occurrence of flood events with varying peaks, quantities and duration. Secondly, the efficiency of decentralised FRM depends - to a great extent - on the ratio of the spatial/temporal precipitation distribution to the type and location of the flood reduction measure in question. Furthermore, when discussing the potential of decentralised FRM for flood reduction, natural catchment characteristics as well as land use and potential inundation areas along rivers and creeks need to be taken into account.

Owing to its large catchment area of about 28 000 km² and its exposition to the predominantly westerly drift of cyclonic cells, the River Moselle plays a major role in flood formation of the Middle Rhine downstream of Koblenz and the Lower Rhine. Therefore, the River Moselle basin was selected as the pilot study area for demonstrating the methodologies developed. Figure 1-1 illustrates the River Moselle basin and flood routing stretches within the River Rhine basin.

Recently elaborated international action plans on flood defence define - among others – a number of flood reduction and retention measures that tackle the flooding problem by focusing on runoff formation in the river basin areas (ICPR, 1998; IKSMS, 1999). These basin related measures are often termed decentralised flood reduction measures and do basically aim at enhancing water storage capacities of soils and along affluents. Three main categories of decentralised flood reduction can be distinguished.

1) Activation and enhancement of natural storage capacities of soils (e.g. unsealing, seepage of rainwater);
2) Measures for protection and reactivation of flood zones along affluents (e.g. renaturation measures, relocation of dikes, protection of flood zones against further sealing);
3) Technical flood reduction (e.g. reservoirs, flood retention areas, technical storages along affluents, technical storage at a small scale).

Basin related measures focus on enhancing the storage capacities of soils and the local retention of rainfall excess water. Accordingly, they predominantly affect the runoff generation process. Runoff concentration and flood routing processes, however, are influenced by stormwater management practices and retention measures implemented along river stretches and affluents. Land use and landscape management play a major role for the efficiency of implemented measures.

2 GOALS AND STRATEGY OF THE DEFLOOD APPROACH

2.1 General strategy

According to the lessons learnt by studying the results of the recent studies focussing on the effect on land use changes on discharge the following key actions were identified which provide the methodological basis for assessing the efficiency of decentralised flood reduction measures in large river basins:

- Application of methodologies for identifying the potential of flood reduction measures in a river basin;
- Definition of scenarios of flood reduction measures realisable form a technical and political point of view;
- Collection of information about realised measures;
- Assessment of the efficiency of flood reduction measures by means of integrated river basin modelling.

Methods for identifying the potential of flood reduction measures are available (e.g. Faeh et al., 1997; Haider,1994) and form the basis for the definition of realistic flood reduction scenarios for a river basin. By means of integrated river basin modelling the potential effects of measures can be quantified and demonstrated by scenario runs. Following this strategic line, valuation of hydrological quantities are enabled which can be employed in Decision Support Systems or overall River Basin Management Systems dealing with flood hazard and flood risk.

Besides the application and testing of methodologies for identifying the potential of flood reduction in selected meso-scale river basins of Switzerland within the DEFLOOD project, most of the work is focussing on the appropriate set-up and implementation of an integrated river basin modelling tool for the River Rhine basin. The integrated river basin modelling tool is required in order to enable the determination of the potential of local/regional measures for supra-regional flood reduction as well as realistic flood reduction scenarios since for this purpose many hydrological characteristics have to be taken into account in each sub-basin and along several river reaches down to a certain spatial scale. The application of the integrated river basin modelling approach leads to the generation of so-called standardised (i.e. reference) hydrographs which have to be used in an appropriate manner for assessing the downstream efficiency of decentral flood reduction measures in large river basins.

Floods in central European main rivers are caused by extreme rainfall events in combination with unfavourable soil and snow conditions. Accordingly, the generation of reference floods has to be based on these flood inducing hydrometeorological conditions. It therefore is an important task of this project to develop and apply procedures for defining thoroughly derived standardised hydrometeorological boundary conditions. These conditions are termed hydrometeorological reference conditions (HRC), which are based on classified historical and synthetic time series of precipitation and temperature as well as on antecedent storage conditions. In addition, methods are studied that facilitate the estimation of a maximum possible precipitation distribution. By means of combined watershed modelling and flood routing procedures as well as under consideration of various hydrometeorological constellations reference floods can be generated . In addition, estimates of the maximum possible floods (MPF) are given. The methodologies developed are applied for the River Moselle basin and are described in chapter 3.

2.2 A framework for integrated river basin modelling

For carrying out all the necessary studies in large river basins a technical framework needs to be provided. Therefore the *FIRM-Flood Reduction* (Framework for Integrated River basin Modelling) concept is set-up as the main methodological feature of the DEFLOOD project. The main elements of *FIRM-Flood Reduction* are:

- Standardised flood events;
- Set up and linkage of different models corresponding to different scales;
- Integration of flood reduction scenarios;
- Interpretation of scenario runs.

Main procedures of the versatile methodological *FIRM* approach developed within DEFLOOD are the generation of hydrometeorological reference conditions, macro-scale precipitation-runoff modelling and linked flood routing tools. The idea behind the *FIRM* concept is to avoid redundant efforts in data aquisition and pre-processing and to optimise the use of existing modelling tools by providing a pool of standardised input data, feasible methodological procedures as well as interfaces between existing models.

The elements of the concept regarding the optimisation of the spatial and temporal modelling scale, a suggestion of the kind of hydrological and hydrodynamical models to be used and three different procedures for the generation of the Hydrometeorological Reference Conditions (HRC) are described in more detail in Krahe et al. (2002).

An important result considering the spatial and temporal discretisation for modelling is the zoning of the area under study. For the River Rhine basin Level 1 encompasses the total large river basin under consideration, e.g. the River Moselle or Rhine basin. According to literature studies hydrological sub-basins of $A_{E0} = \pm 1000$ km^2 basin area are identified as appropriate computational units for hydrological applications in large river basins (Level 2). All sub-units of this level of disaggregation ought to be linked by hydrological flood routing models.

Table 2-1: Proposed models at different spatial levels.

Level	Basin	Basin area [km²]	Models
1	Rhine and major Tributaries of the River Rhine	5000-150000	Hydrological or hydrodynamic flood-routing models; e.g. SYNHP, SOBEK
2	Sub-basins of major tributaries	~1000	Macro-scale precipitation-runoff modelling; e.g. HBV-SMHI
3a	Minor tributaries	~1000	Flood-routing including flood plain inundation; e.g. FPSIM
3b	Affluents of minor tributaries	~100-300	Meso-scale precipitation-runoff models e.g. HBV/BfG

In order to standardise the time series for model input, hydrometeorological reference conditions are defined. Based on these and the proposed modelling approach, calculations of standardised, i.e. reference floods as well as maximum possible floods can be carried out.

Hydrometeorological reference conditions are defined as standardised event based time series of precipitation and air temperature which are adapted to the spatial modelling structure under consideration. Furthermore, initial storage conditions for the hydrological system have to be determined and taken into account for establishing HRC. According to statistical analyses of observed flood producing rainfall events a time frame of 61 days (30 days before and after the flood peak and the peak day itself) was identified as an appropriate period (Helbig, 2001).

Three procedures were developed and applied in order to create the required meteorological time series:

- Classified historical rainfall fields;
- The set-up of a rainfall simulator for designing typical flood producing rainfall events;
- The application of a rainfall generator for generating synthetic 1000 years time series of multi-site precipitation and air temperature (Wojcik et al., 2000).

All procedures for interpolating and classifying as well as for generating and simulating precipitation and air temperature data are based on daily values which were disaggregated to the required hourly modelling time step.

The definition of standardised initial storage conditions of the hydrological system ought to be made independently of the hydrological model and of the spatial modelling structure employed. Storage components under consideration are the water contents of snow and soils. In the context of the DEFLOOD project a grid based definition of initial conditions is made. Generally, within *FIRM-Flood Reduction* the use of climatological initial conditions is recommended, which are based on the long term mean of storage contents at the first day of the month for the period October to April. In order to calculate these data sets water balance models working on a decade or monthly basis can be employed. For the River Rhine basin the water balance models RHINEFLOW - developed at the

University of Utrecht (Kwadijk, 1993) - and the WABIMON model - developed at BfG (Ulmen, 2000) - are available. Since these well known water balance models are available for the River Rhine basin these issues are not considered in more detail within the DEFLOOD project. Table 2-2 summarises the procedures for generating HRC related to their products available for the River Moselle basin.

Table 2-2: Procedures for generating HRC and their products available for the Moselle basin

	Procedure	Basic data	Products
Meteorological time series	Classification procedures	Observed historical precipitation series	Classes of typical precipitation fields
	Rainfall simulator	Classified historical precipitation data	Characteristic precipitation distribution types (temporal/spatial)
	Rainfall generator	Statistical distributions of historical precipitation and temperature series	1000-years synthetic rainfall and temperature series
Initial storage conditions	GIS based definition (grid)	Spatial basin information on soils, routing depth and rainfall	Output fields on storage conditions
	RHINEFLOW	Long term mean of storage contents at the first day of the month for the period October to April	
	WABIMON		

In the course of the DEFLOOD project an international workshop on the "Generation of Hydrometeorological Reference Conditions for the Assessment of Flood Hazard in Large River Basins" was organised. Problems and methods were presented and discussed. The workshop papers are compiled in a CHR-report by Krahe and Herpertz (2001).

2.3 Methodology for generating flood reduction scenarios in the River Rhine basin

In order to generate flood reduction scenarios in the River Rhine basin the steps defined in the *FIRM-Flood Reduction* need to be applied systematically. This concerns especially the identification of the potential of flood reduction measures with respect to basin and river characteristics in the river basin under study as well as the definition of realistic flood reduction scenarios for large river basins require a very high input of manpower and must therefore be beyond the scope of the current project. Realistic measures have also to be defined in cooperation with the water administration authorities responsible within the river basins under consideration. In this study, however, an exemplified virtual implementation of flood reduction measures is carried out and scenarios of their quantified effects are established for the upper part of the River Blies (tributary of the River Saar).
By means of the integrated river basin modelling tool *FIRM – Flood Reduction*, input, spatial modelling structures and interfaces can be provided for

- generating flood hydrograph scenarios within the River Moselle basin with regard to flood reduction measures and HRC,
- generating flood scenarios for the Rivers Moselle, Lower and Middle Rhine,
- generating worst case scenarios.

3 GENERATION OF EXEMPLIFIED REFERENCE FLOODS IN THE RIVER MOSELLE BASIN

Reference floods are simulated hydrographs based on standardised precipitation input and initial soil and snow storage conditions. The definition of these hydrometeorological reference conditions (HRC) is described in chapter 2.2. The reference floods allow a standardised analysis of the effect of flood reduction measures (FRM). The generation of exemplified reference floods based on the hydrometeorological reference conditions generated by three different methods is carried out for the River Moselle basin.
Corresponding to the respective scale different modelling approaches are applied. An example for the meso-scale is the Upper Blies at gauge Ottweiler (A_{Eo} = 160 km^2), for which discharge is simulated with the HBV/BfG model. Discharges of all macro-scale sub-basins in the Moselle basin, e.g. the whole River Blies at gauge Reinheim (A_{Eo} = 1910 km^2), are computed with the macro-scale precipita-

tion-runoff model HBV/SMHI. The results of this macro-scale watershed modelling are used in combination with the flood-routing model SYNHP to calculate the discharge at the outlet of the River Moselle basin at gauge Cochem. The resulting reference floods can be used as input for the hydrodynamic modelling of the River Rhine downstream of Koblenz up to Lobith in the Netherlands. The applied macro-scale modelling approach and the underlying spatial model structure are described in Eberle et al. (2001). Precipitation-runoff modelling is carried out with an hourly time step.

3.1 Hydrometeorological reference conditions

Beside the precipitation input, discharge formation depends on initial conditions, especially snow storage and antecedent water content of the soil. Concerning all three generated reference floods, the storage conditions on the 30th day before the 1993/94 flood peak at the River Moselle gauge Trier are defined as a standardised initial stage. The gauge Trier was chosen For the generation of reference floods a period of 61 days is chosen which describes the 30 days before and after the peak at gauging station Trier.
The first simulated flood event is the historic 1993/94 flood event. This event is regarded representative of several historic events and therefore chosen as reference flood. For the period in question, grid based daily precipitation data are available that have been computed at the University of Trier as part of the DEFLOOD project. For macro-scale precipitation-runoff modelling, these have been combined with hourly data in order to calculate hourly area related precipitation values. Further model input are historic temperature data and daily values of the grass reference evapotranspiration after the FAO standard (Wendling, 1995).

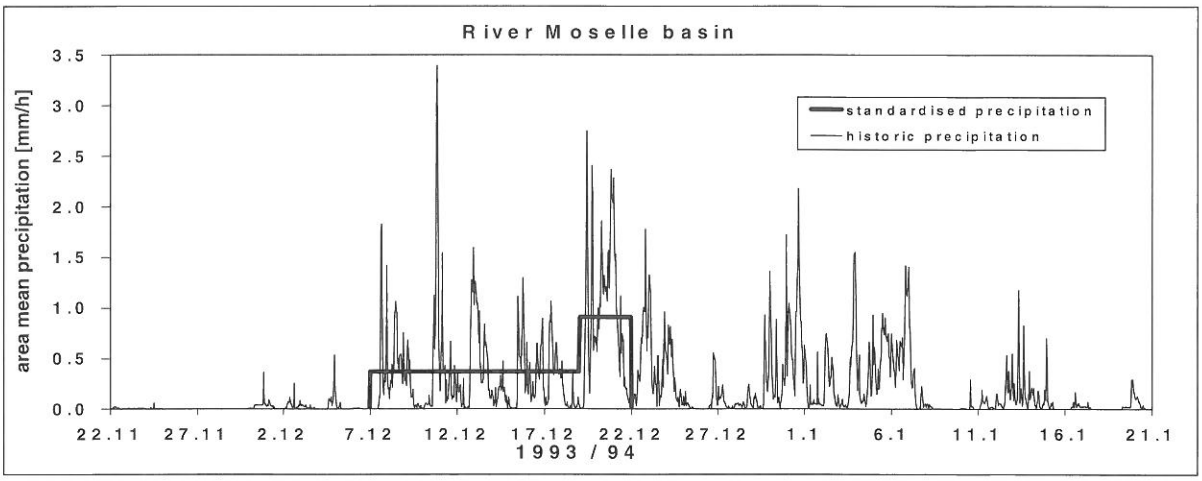

Figure 3-1: Precipitation event created by the rainfall simulator based on the 1993/94 flood producing precipitation.

Input for the second reference flood is precipitation from a precipitation simulator, i.e. standardised precipitation reflecting the typical features of a class of events. The current example depicts the class Type 2 the 1993/94 flood event belongs to. In the example, the precipitation data are standardised with respect to the distribution in time. The spatial distribution and total amount of precipitation during the 30 days before the peak discharge are equal to the historic data. The class of the 1993/94 flood event is defined by high precipitation during the last 15 days previous to the peak discharge and a final precipitation peak inducing the flood peak. To reflect this, the discharge amount of each macro-scale sub-unit on *day 1* to *day 27* (*day 31* is the day of the discharge peak) is distributed equally on *day 16* to *day 27* and precipitation of the *days 28 to 30* is distributed equally on these last three days before the peak. Beginning with *day 31* no more precipitation is assumed in the standardised event. Figure 3-1 shows the standardised area average precipitation of the Moselle basin that has been derived from the precipitation event that induced the 1993/94 flood.

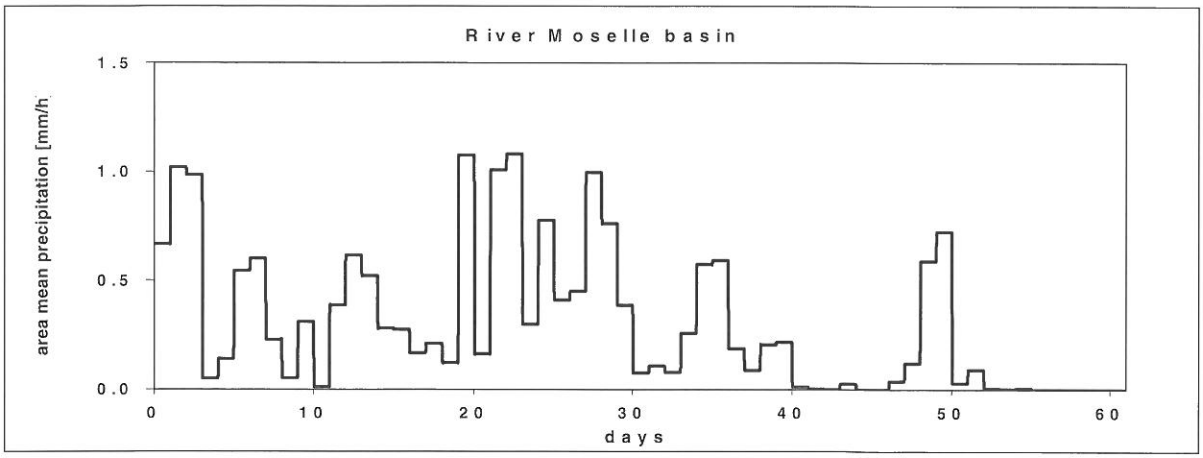

Figure. 3-2: Precipitation event with the maximum 30-day precipitation sum selected out of 1000 generated model years.

The third reference flood is based on synthetic precipitation from a stochastic rainfall generator based on nearest neighbour resampling that has been developed at the Royal Netherlands Meteorological Institute (KNMI) by Wójcik et al. (2000). For the Moselle basin a 1000-years time series of daily precipitation for 42 sub-basins and of daily temperature values at eight climate stations are generated. The generated precipitation values are used to estimate maximum possible precipitation and subsequently maximum possible floods (MPF). Out of the 1000-years time series the maximum 30-day precipitation sum for the total Moselle basin is selected supposing this precipitation should cause an extreme flood event. This precipitation event is depicted in Figure 3-2. In the chosen period, the daily values are distributed equally to hourly values to allow hourly precipitation-runoff modelling. For macro-scale modelling, area average precipitation for the 26 macro-scale sub-basins are computed out of the 42 available time series. Evapotranspiration is simulated in the HBV modelling system based on long-term mean monthly values.

3.2 Results and discussion

Figures 3-3 to 3-5 show the simulated reference floods for three river basins reflecting the different spatial scales. The hydrographs based on the maximum generated 30-day precipitation sum (Q_max_0199) illustrate once more that extreme floods in large rivers, as the River Moselle, are not necessarily extraordinary high floods in the smaller tributaries. The generated event exceeds the 1993 peak at Cochem, and the volume of the flood can be considered as an estimation of the maximum possible volume of a flood event in the Moselle basin.
The two other simulated floods are the historic 1993/94 flood event (Q_93_base) and discharge from standardised simulated precipitation (Q_93_synt) based on this event. For the total Moselle basin discharge dynamics based on the simulated precipitation are comparable to the historic event. In the smaller sub-units the two hydrographs correspond less.

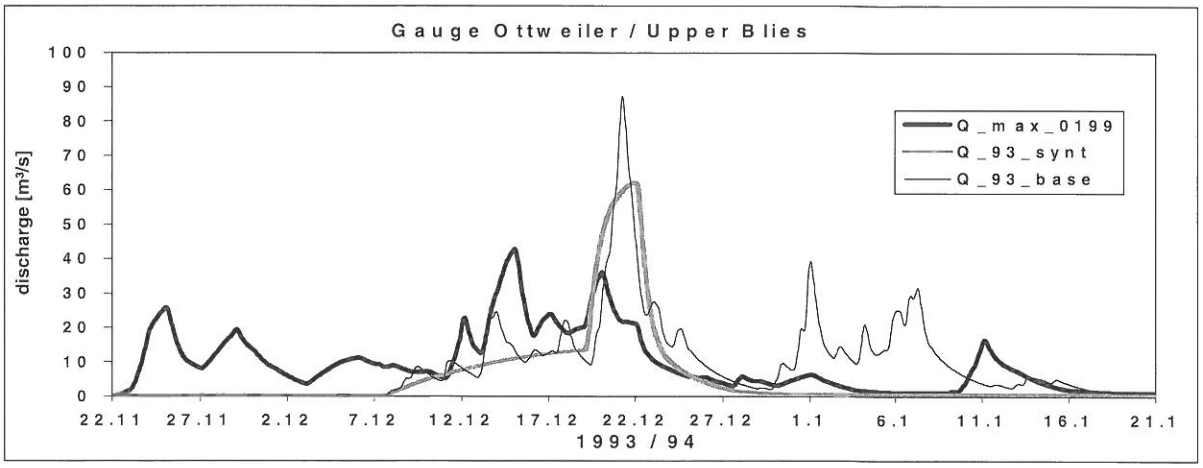

Figure 3-3: Reference floods for the Upper River Blies basin (meso-scale).

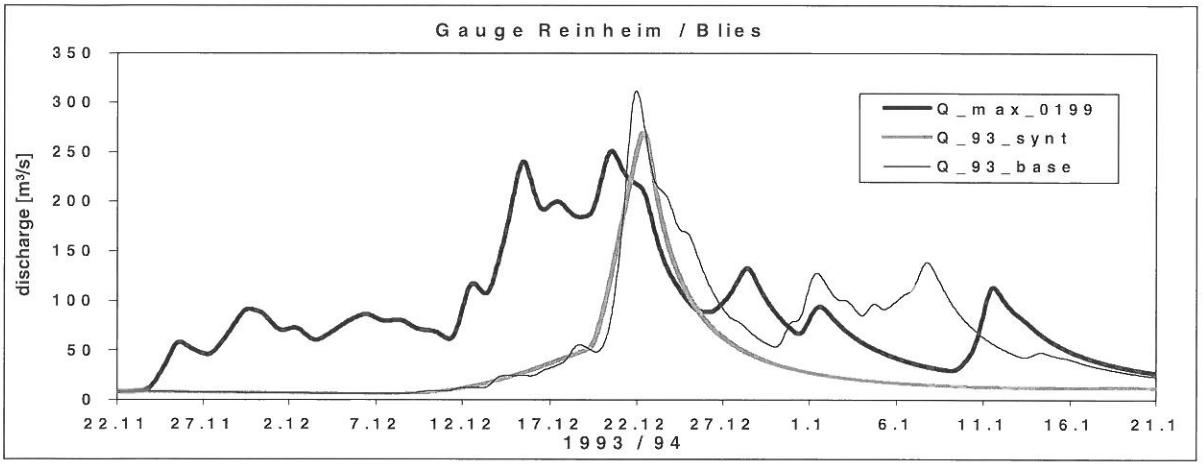

Figure 3-4: Reference floods for the River Blies basin (macro-scale).

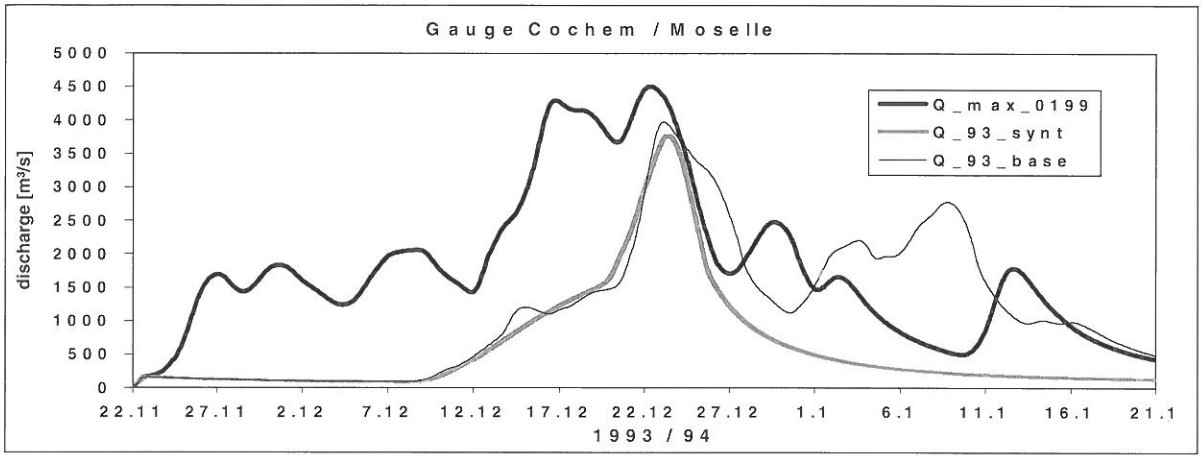

Figure 3-5: Reference floods for the River Moselle basin.

4 CONCLUSIONS AND RECOMMENDATIONS

With the present study methods and procedures are developed that allow to evaluate the effect of decentral FRM's in large river basins taking into account the effect of basin related and river related FRM's on the flood hydrographs of meso-scale catchments. Owing to the standardised spatial structures, interfaces, applications and pre-processed data provided by the *FIRM – Flood Reduction* concept, the approach may form the basis for various future studies on the quantifícation of the efficiency of decentral FRM's, which are currently undertaken by water management authorities. Time and money consuming redundant data aquisition, pre-processing and model calibrations as well as model linkages can be avoided by employing the available FIRM structures.
With the DEFLOOD project, progress was made towards the assessment of possible effects of decentral FRM's in large river basins. Nevertheless, there is a need for further refinement of some procedures proposed within the framework. Furthermore, beside progress in hydrological modelling a base of knowledge needs to be built up and administered which encompasses hydrologically relevant information on the actual state and prospected developments in the River Rhine basin. Additionally, problem-oriented hydrological process studies in selected small-scale river basins ought to be carried out. Based on these studies conceptual meso-scale modelling approaches can be improved and validated in terms of reducing the uncertainty factor, which is inherent in all scenario calculations. In order to identify the potential of decentral measures for flood reduction in entire large river systems, the existing methodologies for identifying different types of runoff generation in meso-scale watersheds have to be enhanced for applications in larger basins.
Statements on future developments of the climate as well as the efficiency of flood reduction measures always inhere uncertainties. The development of methodologies for the estimation of these uncertainties and the incorporation of uncertainty measures into the decision making process have to be put forward. In order to reduce uncertainty – either related to the modelling approaches involved or

to the scenario building and calculation - case studies within the Rhine/Meuse basins have to be undertaken and monitored over several years.
When elaborating action plans for flood reduction in the River Rhine (basin) the establishment of an integrated modelling approach and a pool of basin related information is recommended. This ought to be realised by means of an open system software and standardised catchment and time series data. Features and instructions for realisation of such a system are provided by the *FIRM-Flood Reduction* approach. An example for such a system was initiated within the European Union funded project "European River Flood Occurrence and Total Risk Assessment System" (EUROTAS) (Samuels, 2000).

ACKNOWLEDGEMENT

This study was carried out as project Nr. 1 within the EU funded IRMA-SPONGE Umbrella Program. The program was financed partly by the European INTERREG Rhine-Meuse Activities (IRMA), managed by the Netherlands Centre for River Studies (NCR) and partly by national funds. More detailed information on the IRMA-SPONGE Umbrella Program can be found on the website: *www.irma-sponge.org*. The work within the DEFLOOD project was coordinated by the International Commission for the Hydrology of the Rhine Basin (CHR). The authors thank all parties involved for their support.

REFERENCES

Eberle, M. et al. (2001): Hydrological Modelling in the River Rhine Basin, Part II. Report on Hourly Modelling. BfG - Report 1338. Bundesanstalt für Gewässerkunde. Koblenz

Faeh, A. et al. (1997): A combined field and numerical approach to investigate flow processes in natural macroporous soils under extreme precipitation. Hydrology and Earth System Sciences, pp.797-800

Haider, S. (1994): Der Beitrag von Vorlandüberflutungen zur Verformung von Hochwasserwellen. Mitteilungen der Versuchsanstalt für Wasserbau, Hydrologie und Glaziologie der ETH Zürich Nr. 128. Zürich

Helbig, A. (2001): Spatio-Temporal Structure of Precipitation during Flood Events in the Moselle Basin. In: Generation of Hydrometeorological Reference Conditions for the Assessment of Flood Hazard in Large River Basins (Workshop papers). CHR/KHR-Report I-20. Lelystad

ICPR – Internationale Commission for the Protection of the Rhine (1998): Action Plan on Flood Defence. Koblenz

IKSMS – Internationale Kommissionen zum Schutze der Mosel und der Saar (1999): Aktionsplan Hochwasser im Einzugsgebiet der Mosel und Saar. Trier

Krahe, P., D. Herpertz (2001): Generation of Hydrometeorological Reference Conditions for the Assessment of Flood Hazard in Large River Basins (Workshop papers). CHR/KHR-Report I-20. Lelystad

Krahe, P. et al. (2002): Development of Methodologies for the Analysis of the Efficiency of Flood Reduction Measures in the Rhine Basin on the Basis of Reference Floods. Final report of the IRMA-SPONGE Project 1, CHR/KHR. Lelystad

Kwadijk, J.C.J. (1993): The impact of climate change on the discharge of the River Rhine. PhD-thesis University of Utrecht, (Nederlandse geografische studies, 168). Utrecht

Samuels, P.G. (2000): A new tool for sustainable flood defence planning- An overview of the EUROTAS research project. In: Proceedings of the 'European Conference on Advances in Flood Research', Vol.1; PIK Report No.65. Potsdam

Ulmen, C. (2000): Modelling raster-based monthly water balance components for Europe. GRDC Report No. 26, Bundesanstalt für Gewässerkunde. Koblenz

Wendling, U. (1995): Berechnung der Gras-Referenzverdunstung mit der FAO Penman-Monteith-Beziehung. Wasserwirtschaft 85, pp.602-604

Wójcik, R. et al. (2000): Rainfall generator for the Rhine basin: Multi-site generation of weather variables for the entire drainage area. KNMI-publication 186-IV. KNMI. De Bilt

THE DYNAMICS OF CONTAMINANT TRANSPORT AT DIFFERENT SCALES DURING NATURAL AND ARTIFICIAL FLOOD EVENTS

Andreas Kurtenbach, Andreas Krein, Wolfhard Symader

University of Trier, Department of Hydrology, Germany-54286 Trier, kurt6101@uni-trier.de

SUMMARY

Natural flood events have been investigated in four heterogeneous river basins of different size (3, 35, 238, 4,259 km^2) in order to find similar and reproducible reaction patterns of dissolved and particle bound contaminant transport. In addition to the detailed analyses of chemographs and hydrographs during natural flood events, artificial flood events have been investigated in two of the basins. The differentiation in artificial and natural events provides a good insight in channel erosion processes in contrast to natural events controlled by numerous factors outside the river system.
Beyond catchment specific reaction patterns during natural flood events, similarities of contaminant transport could be identified in all river basins. Especially dissolved iron and manganese are suited as tracers for delayed runoff components which are composed of ground- and soil water during floods following short intensive storm events. A quick response of dissolved copper, zinc, manganese and phosphate during the first stages of the flood events is caused by the influence of waste water and flush effects from streets, sewer systems and settlement areas. Additional anthropogenic tracers are particle bound zinc, copper and polycyclic aromatic hydrocarbons. While relationships between particle bound heavy metals and grain size could be observed during artificial flood waves, an allochthonous input of material masks these relationships during natural events. The dynamics of dissolved and particulate contaminant transport during the investigated floods are strongly dependent on the spatial and temporal activation and exhaustion of sources. These processes are decisive for a strong variability of the chemographs in all basins.

Keywords: Contaminant transport, runoff generation, flood events, scale effects

1 INTRODUCTION AND OBJECTIVES

Natural flood events are complex hydrological and chemical responses of the river basin to a precipitation event. The dynamics of contaminant transport and runoff generation during these events depend on numerous factors such as antecedent climatic conditions, precipitation amount and intensity, morphology and size of the basin, hydraulic properties of the channel, vegetation cover and anthropogenic influences. Beyond autochthonous activation of sources in the river itself an allochthonous input from the basin is responsible for a high variability in contaminant transport (Burt, 1989; Diekkrüger et al., 2001; Droppo, Jaskot, 1995; Krein, Bierl, 1999; Pilgrim et al., 1982).
Due to complex reaction patterns, case studies are often carried out in small, homogeneous river basins (Caissie et al., 1996; Ladouche et al., 2001; Pilgrim et al., 1982). The transferability of results to larger, heterogeneous river basins is impeded (Pilgrim et al., 1982; Symader et al., 1999).
This study aims at finding similar and reproducible patterns of dissolved and particle associated pollutant transport during flood events in order to transfer the results to other basins. We investigated four heterogeneous river basins of different size (3, 35, 238, 4,259 km^2) and looked for similar transport patterns during the flood waves. The heterogeneity helps to discriminate and identify flow components from various parts of the basin and different solute and particle sources. The measurement program consists of a wide array of parameters enabling multivariate evaluation.

2 THE INVESTIGATED RIVER BASINS

The four investigated basins are typical of the middle mountain ranges around the city of Trier, South-West Germany (Figure 2-1). They are characterised by intense anthropogenic influences and heterogeneous land use as well as different basin size, geology and topography (Table 2-1).
The bedrock in the drainage basin of the Kartelbornsbach (3 km^2) consists mainly of triassic limestone and marls. The mixed land use is characterised by arable land, pastures and small patches of scrub and

wood. An inadequate sewage treatment plant has a considerable impact on the water quality of the Kartelbornsbach.

The Olewiger Bach (35 km^2) and Ruwer (238 km^2) basins are situated in the northern Hunsrück mountains near the city of Trier. Their bedrock is dominated by quartzite and Devonian schist. The land use is a complex pattern of arable land on the broad ridges and pasture on the valley bottoms. The steep, south facing slopes in the lower reaches of the Ruwer basin and small parts of the Olewiger Bach basin are planted with vineyards. North- and east facing slopes are predominantly forested. The water quality of both basins is influenced by waste water treatment plants, several villages with minor industrial settlements and some major streets (Krein, 2000; Udelhoven, 1998).

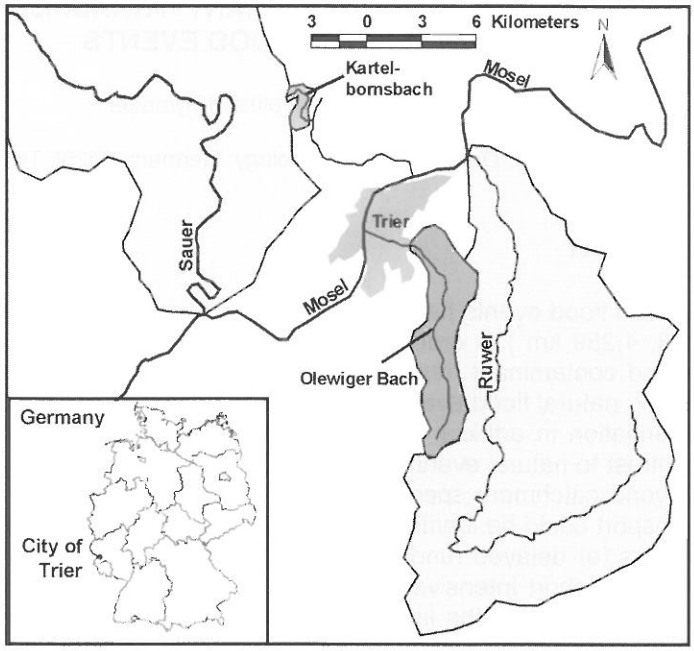

Figure 2-1: Map of the investigated river basins.

The Sauer river basin with an area of 4,259 km^2 covers almost the entire territory of Luxembourg, partially western Germany and small parts of Belgium and France. The river basin is subdivided in a northern part with altitudes generally above 450 m and a southern region with altitudes normally under 350 m. The northern part consists of older Palaeozoic, mainly Devonian rocks. Mesozoic, mainly Triassic and Lower Jurassic sediments are typical of the southern part of the Sauer basin (Umweltbundesamt, 1995). The southern region is, in contrast to the northern part, characterised by intensive land use and considerable anthropogenic influences, for instance Luxembourg-city and the steel industry in the south of Luxembourg. The Alzette river, which mainly drains this southern part of the Sauer basin carries the effluents of about 60 sewage treatment plants.

Table 2-1: Characteristics of the investigated basins ([a,b]Krein, 2000; Udelhoven, 1998; [c]Vohland et al. 2000; [d]Umweltbundesamt, 1995; Su, 1996).

	Kartelbornsbach[a]	Olewiger Bach[b]	Ruwer[c]	Sauer[d]
catchment size [km^2]	3	35	238.5	4,259
geology	mainly triassic bedrocks	quartzite and devonian schist	quartzite and devonian schist	northern part: quarzite and devonian schist southern part: mainly mesozoic bedrocks
altitude [m]: lowest / highest	293.1 / 392.6	153.5 / 508.3	125.2 / 707.3	132 / 699
slope [°]: mean / maximum	5.7 / 25.2	9.9 / 46.1	9.1 / 51.5	7 / 85
mean annual temperature [°C]	8.6[1]	8 (higher ridges)[2]	6 (higher ridges)[3]	6.9 (higher ridges)[4b]
		9.1 (lower river valley)[2]	10 (lower Ruwer valley)[3]	8.9 (lower Sauer valley)[4a]
mean annual precipitation [mm]	841[1]	784 (lower river valley)[2]	700 (lower Ruwer valley)[3]	745 (lower Sauer valley)[4a]
		791 (higher ridges)[2]	1100 (higher ridges)[3]	966 (higher ridges)[4b]
land use [%][5]				
crop land	41.8	47.2	15.8	22.6
green land	34.6	14.4	19.4	32.2
vine yards		4.9	1.6	
forest	13.4	23.6	57.0	36.5
built-up area	10.2	9.9	3.8	8.6
water			0.2	0.1
deforested areas			2.2	

[1]Krein, 2000: time period 1961-1990
[2]Krein, 2000: time period 1961-1990
[3]Vohland et al., 2000: time period not specified
[4]Su, 1996: time period 4a: 1970-1992; 4b: 1970-1991
[5]year of land use classification: Kartelbornsbach: 2000; Olewiger Bach: 1990; Ruwer: 1989; Sauer: 1989

3 SAMPLING STRATEGY AND METHODS

The characterisation of contaminant transport and runoff generation during natural events requires a high sampling density and an analysis of a wide array of contaminants to realise multivariate evaluation. The sampling and analysing programme during natural and artificial flood events cover the aspects hydrological conditions, conductivity, dissolved nutrients and heavy metals, particle characteristics and particle associated contaminants. In co-operation with the municipal water works of Trier the artificial flood flows were generated by an upstream drinking water reservoir (Ruwer basin) and a water works inlet (Olewiger Bach). Beyond the investigation of natural and artificial flood events, daily water samples (Kartelbornsbach, Olewiger Bach, Ruwer) respectively weekly samples (Sauer) have been taken for the characterisation of antecedent conditions and seasonal variations. To distinguish among different origins of water, additional samples of sewage treatment plant outflows, street flushes and soil water were analysed. Water samples have been taken midstream with two litre polyethylen bottles. Suspended matter concentrations were determined gravimetrically by filtering the sample over a WHATMAN GF/F glass fibre filter. During the sampling procedure, conductivity and temperature were measured in situ. The dissolved anions (NO_3, SO_4, Cl) have been analysed by ion chromatography (METROHM 690 IC). Dissolved ortho-phosphate and ammonium have been analysed with a photometer using standard methods. Suspended matter was sampled with 20 litre containers, separated by centrifugation and freeze dried. The suspended matter was digested with concentrated nitric acid for 6 hours under pressure at 170° before analysis. Dissolved and particle bound metals (K, Ca, Mg, Fe, Mn, Zn, Cu, Pb) were analysed with atomic absorption spectroscopy (VARIAN-SpectrAA-10 and VARIAN-SpectrAA-640 GTA100). The effective particle size distributions without pre-treatment (Walling, Woodward, 2000) were performed by a stream laser technique using the GALAI CIS-1 system. The Clay content is the integral of particles < 2 µm. Nitrogen and total carbon in suspended matter were determined with a LECO CHN 1000, the TOC(total organic carbon)-content with the LECO RC-412 element analyser. The polycyclic aromatic hydrocarbons (PAHs; 16 US-EPA) were enhanced solvent extracted and measured with gas chromatography/mass-spectrometry (GC HP5890II - MSD HP5970-B) in SIM Mode. Reference materials have been analysed for both inorganic and organic substances to meet analytical quality assurance standards. For interpretation purposes, discharge dynamic and precipitation variability have been taken into account.

4 RESULTS AND DISCUSSION

4.1 Transport dynamics of contaminants during natural flood events

Despite the growing importance of spatial variability of rainfall and diverging transport times from tributaries with increasing catchment size similarities of dissolved and particle-bound transport were found in all river basins. The following examples of flood events in the Kartelbornsbach, Olewiger Bach and Ruwer basins exhibit typical reaction patterns of contaminants during natural flood waves following short convective storm events.
Figure 4-1 illustrates the dynamic of conductivity, dissolved calcium, zinc, copper, iron and manganese during two flood events in the Kartelbornsbach basin (3 km^2) and Ruwer basin (238 km^2). Despite their heterogeneous geology and land use (Table 2-1), similar reaction patterns occur in both basins. Dilution effects shown by the conductivity could be observed during both flood events. This dilution is caused by a fast input of electrolyte poor runoff components e.g. street flushes (Table 4-1) following the onset of precipitation and a shift of the dissolved phase from the upper basin. A relative quick mobilisation of dissolved calcium during both events is supposed to be a subsurface component released from the upper soil horizons.
A quick response of dissolved copper and zinc following the onset of rainfall is observable in both basins. This is typical for a fast runoff component composed of sewage water and flushes from road surfaces and sewer systems. Street surface runoff and waste water are typically contaminated with copper and zinc in comparison to river water (Table 4-1). This flow component is short-lived, dominates the chemographs only at the beginning and becomes less important in the chronological development of the flood wave. Dissolved ortho-phosphate shows high concentration levels during the first stages of numerous flood events analogous to copper and zinc. Potential sources for this nutrient are waste water and an additional diffuse input due to surface erosion from agricultural areas. Apart from these three hydrochemical tracers an increasing ammonium amount during the rising limb can be attributed to anthropogenic influences such as drainage and sewer systems (Symader et al., 1999).

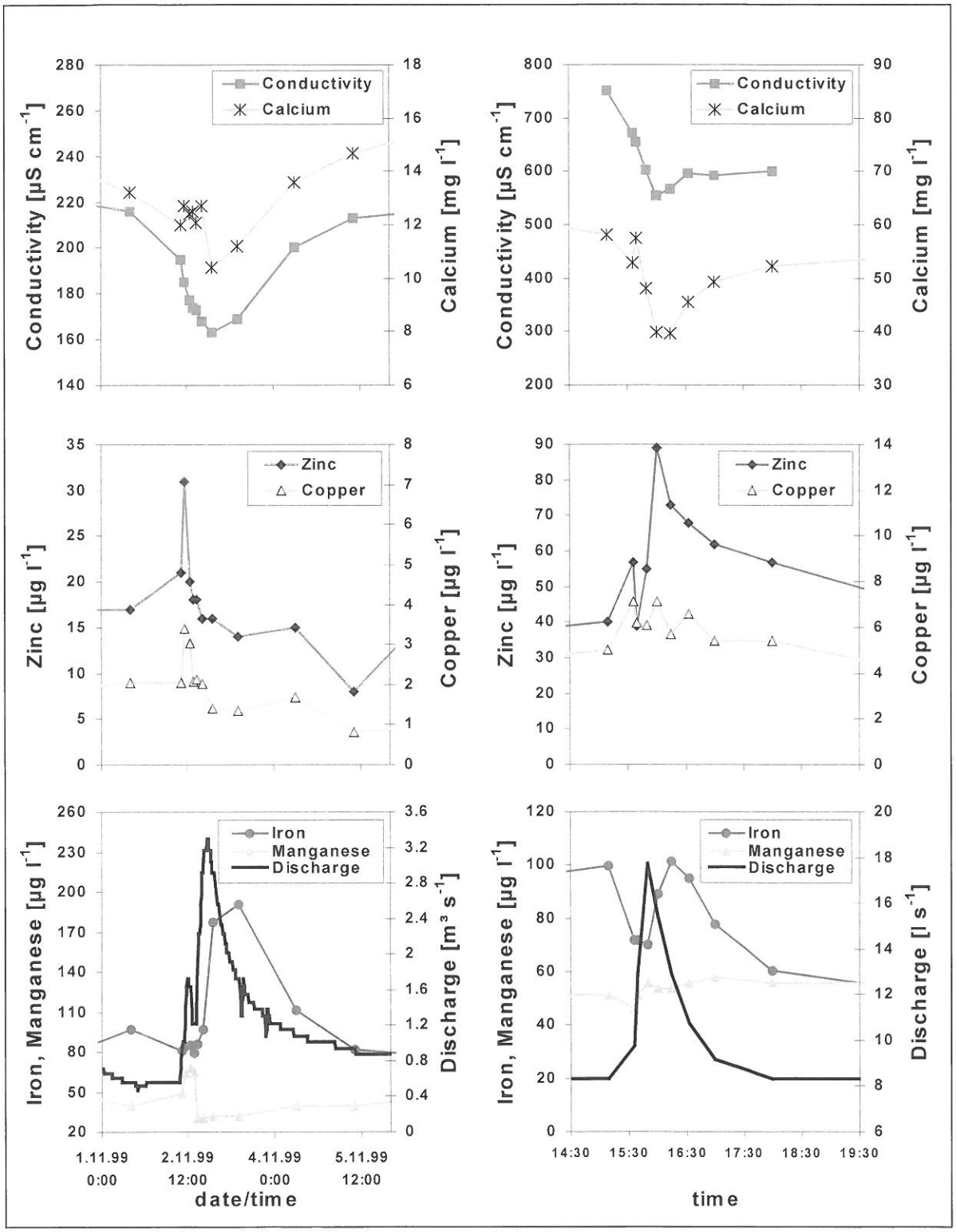

Figure 4-1: Flood events in the Ruwer basin (left side, 02.11.99) and in the Kartelbornsbach basin (right side, 29.08.96).

Manganese increases at the beginning of both floods (Figure 4-1). For this heavy metal, three main input pathways are conceivable: waste water (Table 4-1), a release out of interstitial water due to remobilization of sediments (Krein, Bierl, 1999) and a soil water component (Krein, 2000).

Table 4-1: Chemical composition of different matrices in the Ruwer and Sauer basin.

	rivers	suspended matter mg l^{-1}	conductivity µS cm^{-1}	iron µg l^{-1}	manganese µg l^{-1}	zinc µg l^{-1}	copper µg l^{-1}
sampling point RUWER VILLAGE*	RUWER	17.1	147.7	58.7	19.5	8.6	0.6
waste water plant - outflow*	⟶ ↑	4.5	380.5	9.0	70.7	24.6	1.2
sampling point KASEL*	RUWER	14.1	132.6	61.1	16.5	8.1	0.7
street flush Ruwer basin 03.01.01	RUWER	69.1	64.0	11.6	2.9	13.2	2.7
river sample Ruwer 03.01.01	RUWER	12.6	156.0	69.0	20.9	9.4	0.6
street flush Sauer basin 19.12.00	SAUER	934.0	197.0	103.8	157.4	17.3	3.0
river sample Sauer 19.12.00	SAUER	14.9	309.0	31.8	13.3	< d.l.	< d.l.
street flush Sauer basin 04.01.01	SAUER	74.3	92.0	83.1	39.4	12.4	4.5
river sample Sauer 04.01.01	SAUER	37.0	290.0	99.5	8.2	< d.l.	2.1

d.l.: determination limit

*weekly samples, mean values, each sampling point n = 22

The chronological occurrence of the dissolved substances is traceable to the attendance of different runoff components and the activation of various sources. First, zinc and copper react due to a fast input of waste water and flushes from streets and settlement areas near around the sampling point. Dissolved calcium also increases at the beginning of the event which is explainable by an additional contribution of surface near soil water. The maximum of dissolved manganese is delayed in comparison to zinc, copper and calcium which is induced by an influence of a soil water component released out of intermediate soil horizons. Dissolved iron exhibits the most distinct delay (Figure 4-1). The maximum concentrations of this heavy metal occur after the hydrograph peak of the flood waves. The differing response of iron and manganese depends on redox processes, lead to a delayed reaction of iron and is linked to an influence of deeper soil water or groundwater.

The distinct succession of the described metals could be verified with sprinkling experiments in riparian zones of the Kartelbornsbach basin (Krein, 2000). With increasing experiment duration a successive activation of soil layers in different depths was observed. First, the upper soil horizon reacts and releases water characterised by the highest calcium-concentrations. Second, the delayed dissolved phase delivered out of the intermediate soil horizons was marked by calcium and manganese and third, the water released out of the deepest soil layers shows the most distinct delay and was composed of calcium, manganese and maximum iron concentrations.

The dynamic of particle bound pollutants during natural flood events is, similar to the dissolved contaminants, strongly connected to the activation and exhaustion of sources. Figure 4-2 depicts the dynamic of a flood event in the Ruwer basin induced by an intensive rainfall event with an amount of 80 mm d^{-1} and maximum intensity of 42,4 mm h^{-1}. Again, as shown in Figure 4-1, dissolved copper and zinc as well as phosphate show high concentrations at the beginning of the event. This combination of characteristics reveals anthropogenic influences. In comparison to the event on 02.11.1999 (Figure 4-1) in the Ruwer basin, which is induced by a rainfall event with an amount of 18 mm d^{-1} and maximum intensity of 8 mm h^{-1}, the increase of dissolved copper, zinc and the suspended matter amount is much more intensive.

The activation of particle sources close to the measurement point during this intensive precipitation event lead to an extreme increase of the particle amount from 122 mg/l up to maximum measured 5.926 mg/l (Figure 4-2). This high suspended matter input originates from quick street flushes, which are marked by high particle contents (Table 4-1), strong erosion processes from steep, vineyard planted slopes close to the measurement point as well as a remobilization of channel sediments (Figure 4-5; Bierl et al. 1996). During the recession phase of the wave the transport capacity decreases and the particle sources are exhausted respectively could not be activated any further due to decreasing rainfall intensity. This results in sharply reduced suspended matter amounts.

The first suspended matter sample is characterised by high concentrations of particle associated copper and zinc. Fluoranthene as an example of polycyclic aromatic hydrocarbons equally exhibit highest concentrations in this sample, which suggests an activation of similar sources for these organic pollutants and heavy metals e.g. flushes from traffic areas and settlements (Bierl et al., 1996). The very high content of particle bound copper is basin specific and related to a short time input of eroded

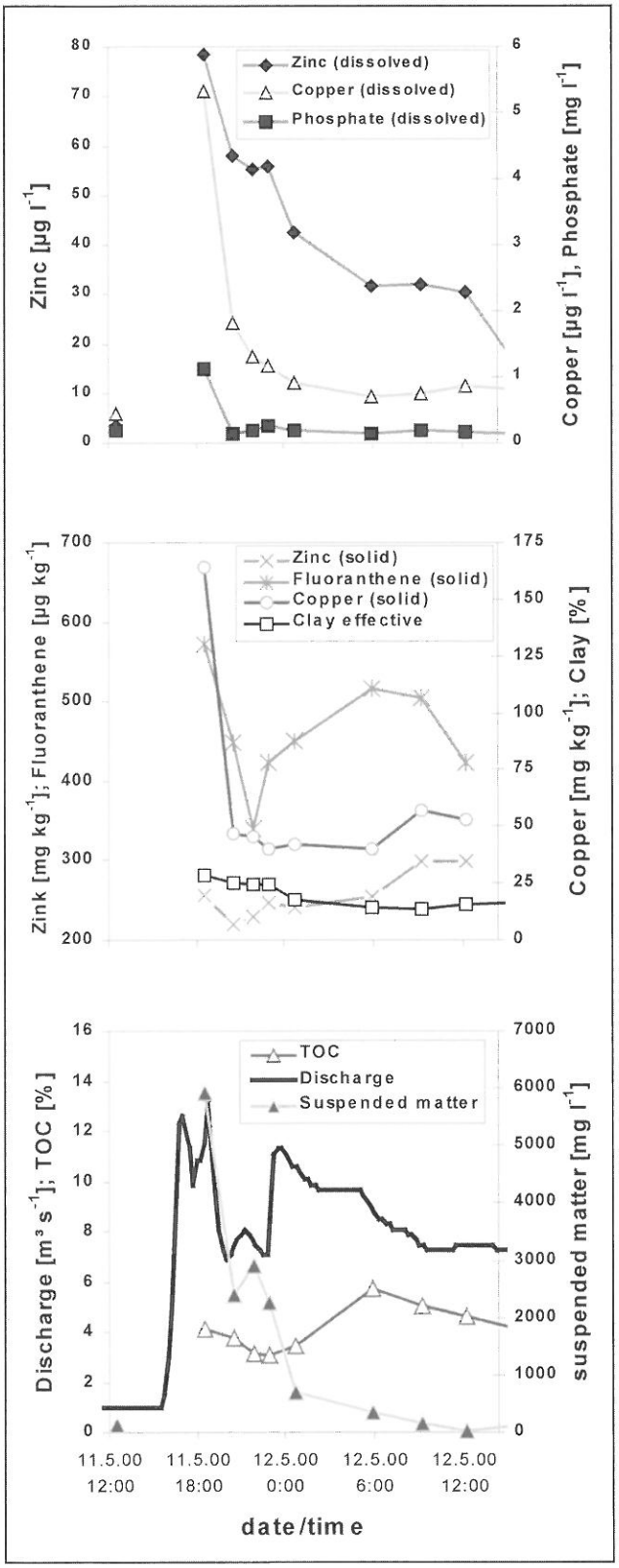

Figure 4-2: Flood event in the Ruwer basin, 11.05.2000.

material from steep vineyard areas located near around the sampling station. Thus, the particle bound transport during the first stages is dominated by an input of polluted particles from waste water plants, sewer systems and surface runoff from settlements and streets. During the further development of the wave the transport of eroded, uncontaminated top soil material from the river basin cause a decreasing of heavy metal and PAH concentrations. A renewed rise of particle bound copper and zinc in the last two samples is not related to the dynamic of the effective clay content, which remains similar during this flood stage. A relative enrichment of contaminated waste water particles is responsible for this new increase of the zinc and copper chemographs. The input of eroded material and the transport from upper parts of the basin are also responsible for the minima of the TOC-content. Increasing contents of waste water particles and low water suspended particles characterised by high TOC-contents (Udelhoven, 1998) are responsible for rising TOC-contents in the last samples.

The response of the Olewiger Bach to a precipitation event is similar to the Ruwer basin. The particle composition and variability during flood events in both basins are dominated by the activation of sources. Figure 4-3 illustrates a flood event in the Olewiger Bach. At the beginning, high concentrations of dissolved phosphate, particle bound copper and fluoranthene are caused by an input of polluted material from settlement areas and sewage water (Figure 4-3). Decreasing concentration levels are also observable induced by an input of unpolluted soil material from the basin. During the falling limb the particle bound copper increases again. Parallel, a high dissolved phosphate concentration occurs which indicates an influence of polluted material from settlement areas and a sewage treatment plant in the upper parts of the Olewiger Bach basin.

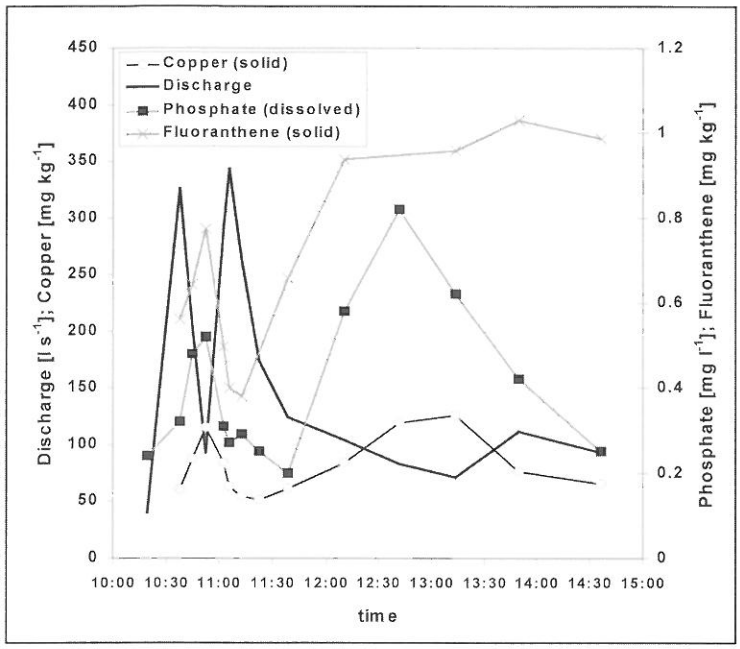

Figure 4-3: Natural flood event in the Olewiger Bach basin, 16.05.1997.

4.2 Transport dynamics of contaminants during artificial flood events

Hydraulic effects during artificial flood events are responsible for remobilization and erosion processes in the river channel and represent additional autochthonous sources of suspended particles, associated contaminants and dissolved substances. Figure 4-5 shows an artificial flood event generated by an upstream drinking water reservoir in the Riveris (Figure 4-4), a small tributary of the Ruwer. The discharge amount during this event released from the drinking water reservoir was about 1500 l/s for one hour.

The sampling station 1 is typical of the reaction of the tributary Riveris. Station 2 is situated further downstream and characterises transport patterns in the Ruwer (Figure 4-4). The distance between Station 1, Station 2 and the drinking water reservoir is about 4.5 kilometres respectively 7.8 kilometres. At Station 1, suspended sediment increases and conductivity decreases simultaneously to water rise (Figure 4-5). The time lag between the onset of water rise and the first recognisable change of conductivity at this station is about 2 minutes. In comparison to antecedent conditions, the mobilised particles are characterised by lower zinc concentrations. The dynamic of zinc shows an intense relationship to the effective clay content. This could be explained by the mobilisation of coarser particles and a grain size effect (Droppo, Jaskot, 1995). At Station 2, a disconnection of the water rise and the arrival of the event water released by the drinking water reservoir occur. The first water rise (Figure 4-5, a) is composed of old Ruwer base flow. The time lag between the onset of water rise and the first recognisable change of conductivity at this station is about 94 minutes. The disconnection is strongly related to discharge amount and antecedent conditions in the river basins. A clearly defined mobilisation of river bed sediment during the first stage of the artificial flood event at station 2 lead to a suspended matter amount up to 32.4 mg/l (Figure 4-5,

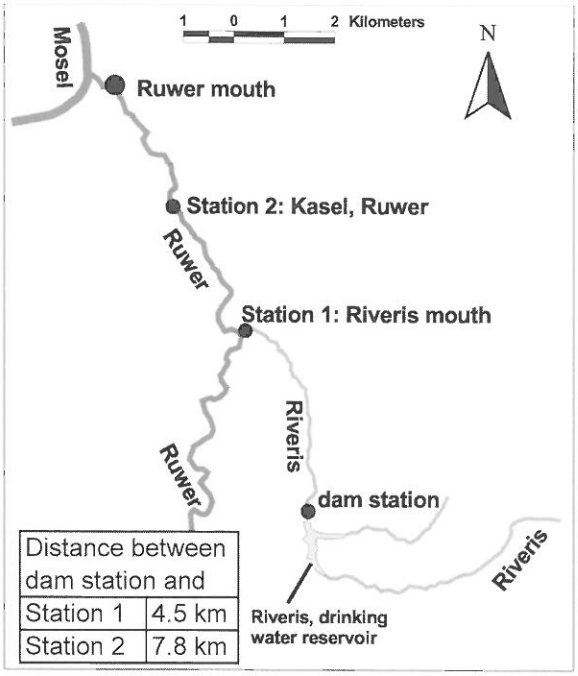

Figure 4-4: Locations of the sampling stations 1 & 2 during the artificial flood events in the Ruwer basin.

a). The second maximum of the suspended sediment amount after the hydrograph peak is caused by the influence of the new water and suspended sediment from the drinking water reservoir (Figure 4-5, b). Dilution effects in the Ruwer and sedimentation processes due to decreasing transport capacity cause the lower increase of the particle content up to 22.7 mg/l. During the first water rise at station 2 coarse material has been mobilised with lower particle bound zinc concentrations (Figure 4-5, a) in comparison to antecedent conditions. As described for station 1, the dynamic of particle associated zinc is strongly related to the effective clay content. Similar relationships between grain size and heavy metals and transport patterns were found during artificial flood flows in the Olewiger Bach basin. The autochthonous remobilization of sediments is an important source that has to be considered during natural flood events. The lower contents of particle bound heavy metals during these artificial flood flows in comparison to antecedent conditions emphasise the importance of allochthonous sources of polluted material during natural events.

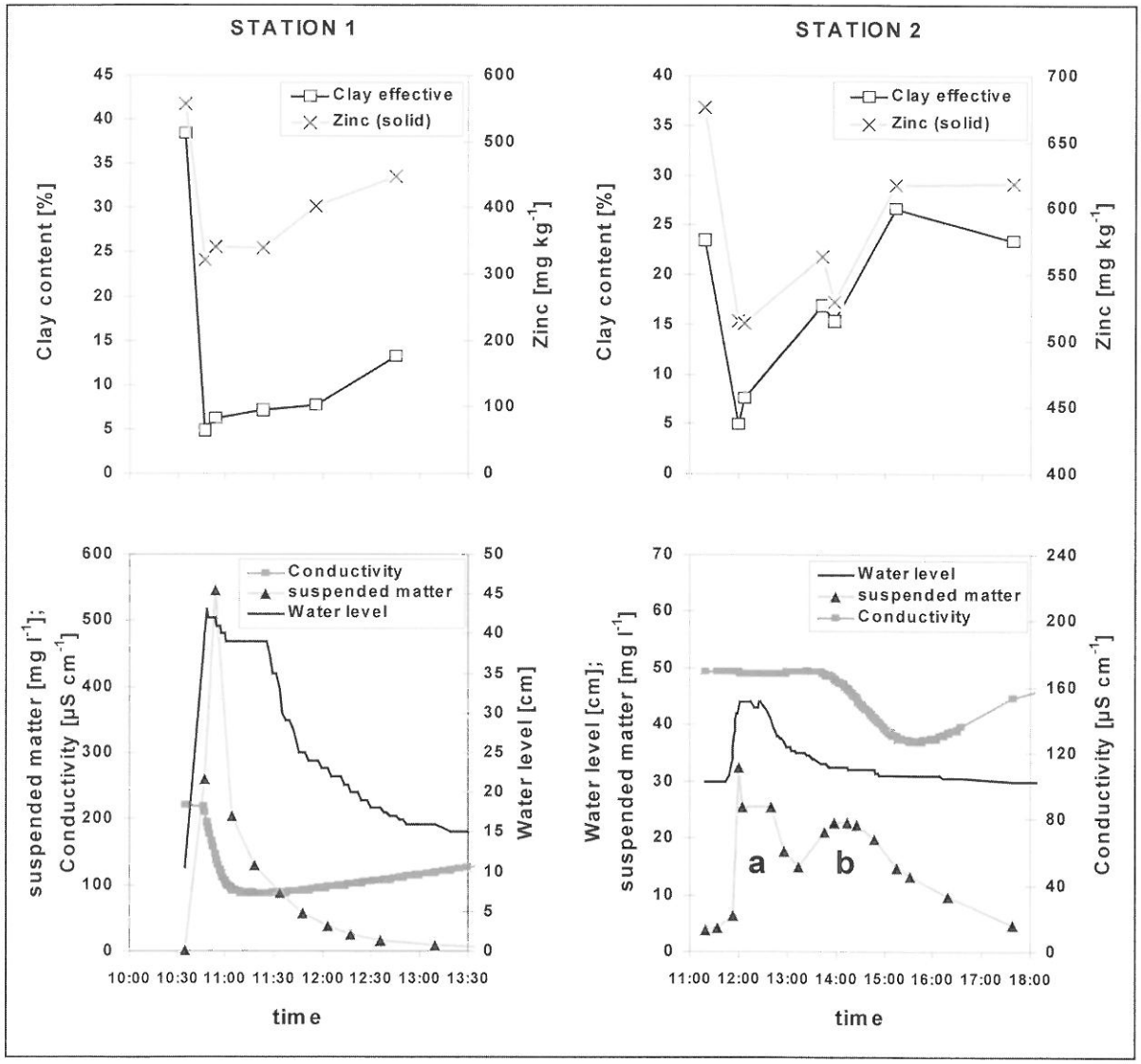

Figure 4-5: Artificial flood event in the Ruwer basin, 30.07.2001 at station 1 (left side) and station 2 (right side) along the brook axis.

5 CONCLUSIONS

Despite the growing importance of spatial variability of rainfall and diverging transport times from tributaries with increasing catchment size similarities of dissolved and particle-bound transport were found in all investigated river basins. Especially iron and manganese are suited as tracers for delayed runoff components which are characterised by influences of ground- and soil water during floods following short and strong precipitation events. A quick response of dissolved and particle bound copper and zinc, dissolved manganese and phosphate and particle associated polycyclic aromatic hydrocarbons is typical of anthopogenic influences such as waste water sewage plants and flush effects from traffic areas and sewer systems.
Hydraulic effects during artificial flood events are responsible for remobilization and erosion processes in the river channel. Clearly defined mobilisation of old sediment during the first stage of water rise have been determined as well as a delayed transport of the new water and suspended sediment cloud from the upper basin. The remobilization of sediments is an important source that has to be considered during natural flood events. The lower contents of particle bound heavy metals due to remobilization of coarser particles during these artificial flood flows in comparison to antecedent conditions emphasise the importance of allochthonous sources of polluted material during natural events.
The load of aquatic particles with pollutants and the suspended matter properties during natural flood events are strongly supply controlled in all basins and connected to spatial and temporal activation of autochthonous and allochthonous sources.

ACKNOWLEDGEMENTS

This research project is part of the collaborative research centre 522 „environment & region“ at the University of Trier. The research centre has been funded by the „Deutsche Forschungsgemeinschaft“. The authors wish to thank the municipal water works of Trier for generating the artificial flood events. Additionally, the authors wish to thank the „Landesamt für Wasserwirtschaft Rheinland-Pfalz“ for providing discharge and precipitation data sets for the Ruwer and Sauer basins and the „Landesanstalt für Pflanzenbau und Pflanzenschutz Rheinland-Pfalz“ as well as the „Deutscher Wetterdienst“ for providing precipitation data sets.

REFERENCES

Bierl, R. et al. (1996): Particle associated contaminants in flowing waters - the role of sources. Arch. Hydrobiol. Spec. Issues Advanc. Limnol., 47, 229-234, Stuttgart

Burt, T.P. (1989): Storm runoff generation in small catchments in relation to the flood response of large basins. In: Beven, K., Carling, P. [Ed.]: Floods – Hydrological, sedimentological and geomorphological implications. 11-35, Chichester

Caissie, D. et al. (1996): Variation in stream water chemistry and hydrograph separation in a small drainage basin. Journal of Hydrology 178, 137-157, Amsterdam

Diekkrüger, B. et al. (2001): Spatial variability and scale dependent runoff generation. – Leibundgut, C. et al. [Ed.]: Runoff generation and implications for river basins modelling. Freiburger Schriften zur Hydrologie, Issue 13, 17-27, Freiburg

Droppo, I.G., Jaskot, C. (1995): Impact of river transport characteristics on contaminant sampling error and design. Environ. Sci. Technol., 29, 161-170, Washington, D.C.

Krein, A., Bierl, R. (1999): Identifying major sources of organic micropollutants and heavy metals during flood events in a partly urbanised headwater catchment. IAHS Publ., 259, 263-268, Wallingford

Krein, A. (2000): Stofftransportbezogene Varianzen zwischen Hochwasserwellen in kleinen Einzugsgebieten unter Berücksichtigung partikelgebundener toxischer Umweltchemikalien.Ph.D thesis, University of Trier, Aachen

Ladouche, B. et al. (2001): Hydrograph separation using isotopic, chemical and hydrological approaches (Strengbach catchment, France). Journal of Hydrology 242, 255-274, Amsterdam

Pilgrim, D.H. et al. (1982): Effects of catchment size on runoff relationships. Journal of Hydrology, 58, 205-221, Amsterdam

Su, Z. (1996): Remote sensing applied to Hydrology: The Sauer river basin study. - Ph.D thesis, University of Bochum, Schriftenreihe Hydrologie/Wasserwirtschaft, Bochum

Symader, W. et al. (1999): Abflußereignisse, eine skalenabhängige, multiple Antwort von Einzugsgebieten auf Niederschläge. Acta hydrochim. Hydrobiol. 27, 2, 87-93, Weinheim

Udelhoven, T. (1998): Die raumzeitliche Dynamik des partikelgebundenen Schadstofftransportes bei Trockenwetterbedingungen in kleinen heterogenen Einzugsgebieten. Ph.D thesis, Trierer Geographische Studien, Heft 19, Trier

Umweltbundesamt [Ed.] (1995): Entwicklung eines mathematischen Modells zur Untersuchung des Einflusses von Klima- und Landnutzungsänderungen auf den Hoch- und Niedrigwasserabfluß im Einzugsgebiet der Mosel sowie zur Echtzeitvorhersage unter Verwendung von Fernerkundungstechniken. Research Report Water 102 01 304, Berlin

Vohland, M. et al. (2000): Landnutzungsbezogene Modellierung hochwassergenetisch relevanter Abflusskomponenten im Ruwer - Einzugsgebiet. Hydrologie und Wasserbewirtschaftung 44, 4, 190- 200, Koblenz

Walling, D.E., Woodward, J.C. (2000): Effective particle size characteristics of fluvial suspended sediment transported by lowland British rivers. IAHS Publ., 263, 129-139, Wallingford

SIMULATING THE EFFECTS OF FLOOD REDUCING MEASURES ON THE FLOOD CONDITIONS OF THE RIVER RHINE

R. Lammersen[1], N. Ritter[2], H. Buiteveld[1], M. Disse[2], H. Engel[2], Y, Hundecha[3]

[1] Institute for Inland Water Management and Waste Water Treatment (RIZA), P.O. box 9072, 6800 ED Arnhem, The Netherlands, R.Lammersen@riza.rws.minvenw.nl; H.Buiteveld@riza.rws.minvenw.nl

[2] Federal Institute of Hydrology (BfG), Kaiserin-Augusta-Anlagen 15-17, Postfach 200253, 65002 Koblenz, Germany, Disse@bafg.de; Engel@bafg.de; N.Ritter@wsa-hd.wsv.de

[3] Institute of Hydraulic Engineering, University of Stuttgart, Pfaffenwaldring 61, 70550 Stuttgart, Germany, hundecha@iws.uni-stuttgart.de

SUMMARY

In the frame of the IRMA (INTERREG Rhine-Maas activities) program of the EU the project LAHoR was carried out in order to quantify the influence of land surface and river training on flood conditions in the Rhine basin. Therefore a modelling tool was developed, which makes a combined simulation of rainfall runoff processes and flood propagation processes possible, taking into account land use changes and flood retention measures along the Rhine. These models are briefly introduced and simulation results are shown.

Keywords: flood propagation, flood retention, land use change, rainfall runoff modelling, retention polder

1 INTRODUCTION

The frequent occurrence of several extreme flood events like the winter floods in 1993/1994 and 1995 in the Rhine river basin, which caused severe damage in Germany and the Netherlands, have brought up an ongoing debate about the human impact on this phenomenon. There is no doubt that changes of land use as well as river training activities in great parts of Central Europe have lead to an altered flood situation in this region. The magnitude of these effects however can not be quantified, leading to two main questions:

- To what degree do environmental changes (land cover, climatic boundary conditions and river training) influence the flood situation in the Rhine basin,
- To what degree can flooding be mitigated by water retention measures both in the landscape and along the river courses.

Therefore the project LAHoR (Quantification of the influence of the land surface and river training on flood conditions in the Rhine basin) was set up to quantify the impact of landscape hydrology and river network hydraulics on flooding conditions in the Rhine basin.

2 METHOD

In order to reach the aim hydrological rainfall runoff modelling for the river basin of the Rhine was coupled with the hydrodynamic modelling of the Rhine and its main tributaries Neckar, Main and Saar/Mosel, both covering the German part of the river basin between Maxau and Lobith (Figure 2-1).

2.1 Hydrological rainfall runoff model HBV

The rainfall runoff processes was modelled using the hydrological model HBV. HBV, originally developed by the Swedish Meteorological and Hydrological Institute (Bergström, 1995), is a semi-distributed conceptual model. The model uses subcatchments as primary hydrological units. Based on elevation, soil types and land use classes these subcatchments can further be subdivided into zones. The model has conceptual routines that compute snow accumulation, snow melt, soil moisture and runoff generation. At the Institute of Hydraulic Engineering of the University of Stuttgart (IWS) some components of the original version of the model were modified and new components were added to

take into account the interception storage of different land use classes as well as the effects of sealed areas. Thus it is possible to simulate the effects of land use change (Bárdossy et al., 2001).
On the base of land use and other catchment characteristics as well as measured discharge data available for different subcatchments this HBV-IWS model was calibrated for the Rhine basin between Maxau and Lobith (Figure 2-1a). To derive the model parameters, a transfer function of the catchment caracteristics was used (Bárdossy et al., 2002).

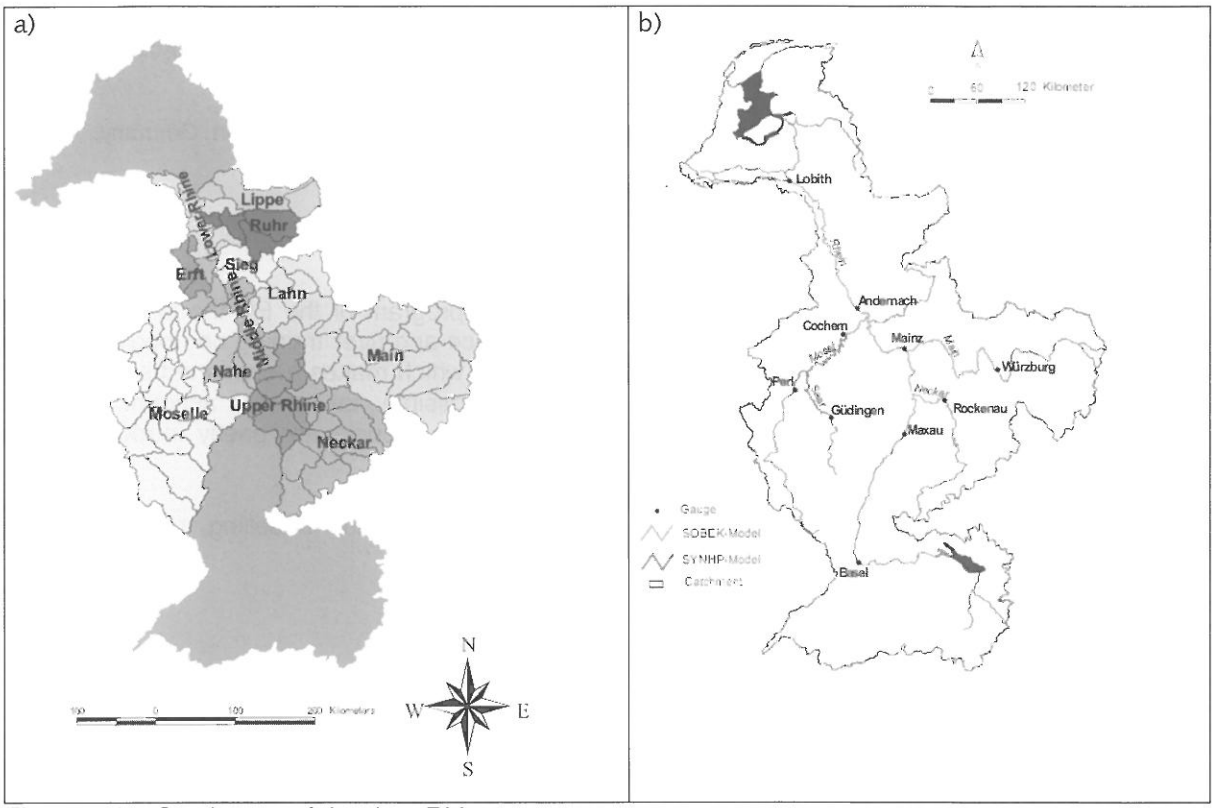

Figure 2-1: Catchment of the river Rhine
a) sub catchments in order to simulate rainfall runoff processes and
b) river stretches for the flood routing modelling (further explanation see text).

2.2 Hydrodynamic Models SYNHP und SOBEK

The river stretches of the Mosel between Perl and Cochem and the Saar downstream Güdingen were simulated using the hydrological model SYNHP (Figure 2-1b). Based on a model of the BfG SYNHP was developed by the Landesanstalt für Umweltschutz (LfU) in Baden-Württemberg in the 1980-ies and was applied to evaluate the effects of retention measures (dike relocation, controlled and non-controlled retention polders) along the Upper Rhine. Based on the river geometry it simplifies the flood routing processes in the river by linear stores (Homagk, 1985).
For the Rhine between Maxau and Lobith, the Neckar downstream Rockenau, the Main downstream Würzburg and the Mosel downstream Cochem (Figure 2-1b) calculations were carried out using the hydraulic model SOBEK. SOBEK was developed by Delft|Hydraulics and RIZA for one-dimensional modeling of river flow (Delft Hydraulics, The Ministry of Transport, Public Works and Water Management, 1997). It is based on the Saint-Venant equations and considers different physical processes that influence the flow. This model is able to simulate measures in the river bed as well as flood retention measures (dike relocation, controlled and non-controlled retention polders). Since there is a substantial exchange between river and ground water in the Lower Rhine area, the model SOBEK was combined with a simple ground water model based on the equation of Darcy (Barneveld, Meijer, 1997). On the base of geometrical data the SOBEK Model for the River Rhine, the Neckar, Main and Mosel was built up and calibrated using measured discharges and water levels (BfG, RIZA, 2002). For the river stretches, which were simulated using SYNHP, models already were available.

2.3 Change of boundary conditions

To simulate the combined effects of land use change and flood reducing measures along the river scenarios were defined, taking into account different land use and retention measures as well as rainfall events, which further were called model events.

2.3.1 Model events

The model events M83, M88, M93 and M95 were derived from four historical rainfall events, which resulted in the floods of 1983, 1988, 1993 and 1995. They assume historical precipitation data. Increasing the historical precipitation data of M95 with an additional 20% rainfall resulted in the model event $M95^{+}$. Based on $M95^{+}$ the model event $M95^{++}$ was derived by adding a snow cover of 20 mm water equivalent, which melts during the flood event.

2.3.2 Changes in land use

Five land use scenarios were used called IST92, LN1, LN2, LN100 and LNW.
The land use scenario IST92 is based on the land use conditions from 1992, as defined in the dataset from the CHR, where 8 landuse classes are distinguished. In order to estimate the effects of land use changes, scenario IST92 was used as reference-scenario.
Based on IST92 LN1 was derived by linear enlarging the urbanized areas, thus an average growth of urbanized area of 2% (based on the whole area) was reached (Table 2-1). This number was derived from the results from Dosch and Beckmann (1999), where a growth of urbanized areas over the whole catchment was calculated with an average increase over the whole catchment area from 18% to around 20% in 2010.
Land use scenario LN2 is a scenario, which considers the growth of the urban areas as described in scenario LN1, but additionally applies an reduction of the degree of sealing of the urbanized areas from 35,0 % to 27,03 %. Thus the aim of the ICPR (1998), to reduce the sealed area in the Rhine-catchment with 2500 km^2 (1,3 % from 190 000 km^2 Rhine river basin) from 1998 to 2020, is simulated in this scenario.
Based on IST92 land use scenario LN100 implies an doubling of the urban area, and LNW a Rhine catchment entirely covered with forest.
Table 2-1 gives an overview of the mean values of the land use distribution over the whole Rhine catchment.

Table 2-1: mean values of the land use distribution over the whole Rhine catchment.

Land use scenario	Percentage land use area				Percentage sealed area	
	forest	water	Agricultural area	Urbanized area	Sealed area	Sealed area
	% of whole area	% of whole area	% of whole area	% of whole area	% of urbanized area	% of whole area
IST 92	40.38	0.57	43.77	15.28	35.00	5.35
LN1	40.29	0.57	41.90	17.24	35.00	6.03
LN2	40.29	0.57	41.90	17.24	27.03	4.66
LN100	38.80	0.57	30.34	30.29	35.01	10.61
LNW	100.00	0.00	0.00	0.00	0.00	0.00

2.3.3 Retention measures

In order to reduce flooding along the Rhine, retention facilities with a total volume of 288 million m^3 are planned along the Upper Rhine (ICPR, 1997). Of these a capacity of 208 million m^3 is located upstream Maxau, leaving 80 million m^3 in the Rhine stretch covered by the hydrodynamic model. Along the Lower Rhine a retention volume of 65 million m^3 is modelled based on recent planning documents. These retention facilities along the Rhine are partly retention polders with controllable and non-controllable inlets and partly relocations of dikes. An overview is given in Table 2-2. There were two retention scenarios simulated, one without any retention measures and one considering all retention measures mentioned in Table 2-2.

Table 2-2: Retention facilities along the River Rhine downstream of gauge Maxau.

Retention facility [Name]	Location [Rhine-km]	Mode of operation	Volume [million m³]
Upper Rhine downstream Maxau			
Elisabethenwört	381,3 - 383,0	Polder*	11,9
Rheinschanzinsel	390,4	Polder *	6,2
Wörth/Jockgrim/Neupotz	368	Dike relocation & Polder *	16,2 (12 +4,2)
Mechtersheim	388,4	Polder *	7,4
Flotzgrün	392,6	Polder *	5,0
Kollerinsel	409,9	Polder *	6,1
Waldsee/Altrip/Neuhofen	411,5	Dike relocation & Polder *	9,1 (7,9 +1,2)
Petersau/Bannen	436	Dike relocation	1,4
Mittlerer Busch	440	Dike relocation	2,3
Worms Bürgerweide	438	Dike relocation	3,4
Bodenheim/Laubenheim	490	Polder *	6,4
Ingelheim	517	Polder	3,8
Sum Upper Rhine downstream gauge Maxau			**79,2**
Lower Rhine			
Köln-Langel	668,5 - 673,5	Polder	4,5
Worringer Bruch	705,5 - 708,5	Polder	8
Monheim	707,5 - 713,5	Dike relocation	6,9
Itter-Himmelgeist	723,5 - 727,5	Dike relocation	2
Ilvericher Bruch	750,5 - 754,5	Polder	8,1
Mündelheim	760,5 - 769,5	Dike relocation	3
Orsoy Land	797,5 - 803,5	Dike relocation	10
Bislicher Insel	818,5 - 823,5	Dike heightening	-
Lohrwardt	832,5 - 833,5	Dike relocation & Polder	12,9 (10,3 +1,6)
Grietherbusch	837,5 - 847,5	Dike alignment	-
Bylerward	845,5 - 854,5	Polder*	10
Sum Lower Rhine			**65,4**
Total sum of all facilities (polders,dike relocations etc.) considered in the model			***about 145***
Sumof Polders			***about 108***
**)* controlled Polder			

2.3.4 Simulation - scenarios

In order to simulate the combined effects of land use change and retention measures scenarios were composed by combining model events with land use scenarios and retention scenarios along the Rhine. Table 2-3 gives an overview over the simulated scenarios.

Table 2-3: Flood scenarios modelled by combined hydrological and flood routing computations.

Model events	Land use scenarios									
	IST92		LN1		LN2		LN100		LNW	
	oR	mR	oR	mR	oR	mR	oR	mR	oR	mR
M83	x	-	x	-	x	-	x	-	x	-
M88	x	-	x	-	x	-	x	-	x	-
M93	x	-	x	-	x	-	x	-	x	-
M95	x	x	x	x	x	x	x	x	x	-
M95^{+}	x	x	x	x	x	x	x	x	x	-
M95^{++}	x	x	x	x	x	x	x	x	x	-

oR: without retention in and along the Rhine
mR: with retention in and along the Rhine
x: simulated
-: not simulated

IST92 Reference scenario state 1992
LN1: Urbanization according to Dosch and Beckmann, 1999 (reference year 2010)
LN2: same as LN1, reduced according to ICPR Action Plan (reference year 2020)
LN100: IST92 + 100% additional impervious land surface
LNW: All land surfaces assumed to be forested.

The model waves were generated from rainfall patterns like those determined for the historical events.

- The model waves without "+" were generated from rainfall patterns like those determined for the historical events.
- For M95^{+}, the historical precipitation of the flood 1995 was increased by 20%.
- For 1995^{++}, additionally to 1995+ an snow cover of 20 mm was assumed.

3 RESULTS

Simulations were carried out using the scenarios described above. It turned out, that the model events caused floods of different magnitudes along the Rhine (Table 3-1).

Table 3-1: return periods of peak discharges for land use scenario IST 92 without retention measures.

	return period [years] (flood series 1901 – 2000)					
gauging station	Maxau	Worms	Kaub	Andernach	Köln	Rees (Lobith)
M83	20	50	20	20	25	25
M88	10	50	100	20	20	40
M93/94	2	20	30	50	50	70
M95	10	5	40	40	50	80
$M95^{+}$	10	40	400	300	400	600
$M95^{++}$	10	70	500	400	500	800

It is obvious, that a great range of flood events is covered, where
- rainfall was quite evenly distributed over the whole catchment (M83),
- high discharges from the tributaries Nahe and Main caused high peak discharges at Kaub (M88),
- extreme high discharges from the Mosel (the highest since 1784) caused the highest discharges downstream Koblenz, visible also in Köln and Rees (M93) and
- extreme high discharges in the Mosel and the tributaries of the Middle Rhine and the Lower Rhine causing the highest flood discharges along the Lower Rhine (M95).

With the model floods $M95^{+}$ and $M95^{++}$ extreme floods had been produced for the Lower Rhine. The fact that the return periods at Maxau and Worms are much lower is due to the fact, that these simulations were done using the historical flood wave at Maxau (without enlarging the discharge at Maxau).

3.1 Effect of land use change

Comparative analysis of the hydrographs show in general, that the effects of the more realistic scenarios LN1 and LN2 are of minor magnitude, followed by the scenario LN100 (doubling the impervious area), while the biggest effects obviously can be seen at the quite fictive scenario LNW (river basin being covered totally with forest) (Figure 3-1). As a rule both the increases of stream flow due to additional impervious land surfaces (LN1, LN100) and the decreases of stream flow following the removal of impervious surfaces (LN2) and afforestation (LNW) are effective in the rising limb of the floods and their maximum effects occur distinctly before the flood peaks. In the falling limb the effects are the other way round with decreasing stream flow due to additional impervious land surfaces and increasing stream flow following the removal of impervious surfaces and afforestation. For the selected model floods the maximum increases result for LN100 (with 200 to 300 m^3/s at Worms and 500 to 1000 m^3/s at Lobith). The maximum decreases can be observed for the forest-scenario LNW with 500 to 1000 m^3/s at Worms and 1000 to 1700 m^3/s at Lobith.
For the model floods M83, M88, M93 and M95 the waterlevels during the flood peak are effected relatively little by the realistic land use changes LN1 (growth of urbanization) and LN2 (reduction of the impervious area following ICPR, 1998). They range from 5 cm higher waterlevels to no effect for LN1 and 2 cm higher levels to 1 cm lower levels for LN2 (Table 3-2). For the less realistic land use scenario LN100 the effects on the flood peaks are slightly higher due to the remarkable growth of urbanization, which lead to larger storing capacities. Caused by afforestation and therefore missing impervious areas, the irrealistic scenario LNW leads to a remarkable lower peak water level. In both cases the effects on peak water levels are the highest along the Middle Rhine (Kaub, Andernach) and are decreasing further downstream in the Lower Rhine (Köln, Lobith). In contradiction in most of the cases the peak discharge increases downstream. Due to the stream geometry of the Lower Rhine an increasing difference in stream discharge downstream does not result in a increasing difference in water level.
As it also can be seen in Table 3-2, the effects are varying from place to place and from flood to flood due to the genesis of the flood. Thus the effects of land use is dependent on the flood event. In all scenarios the model flood M93 shows the highest effects, showing that the flood pattern remains even with changing land use.

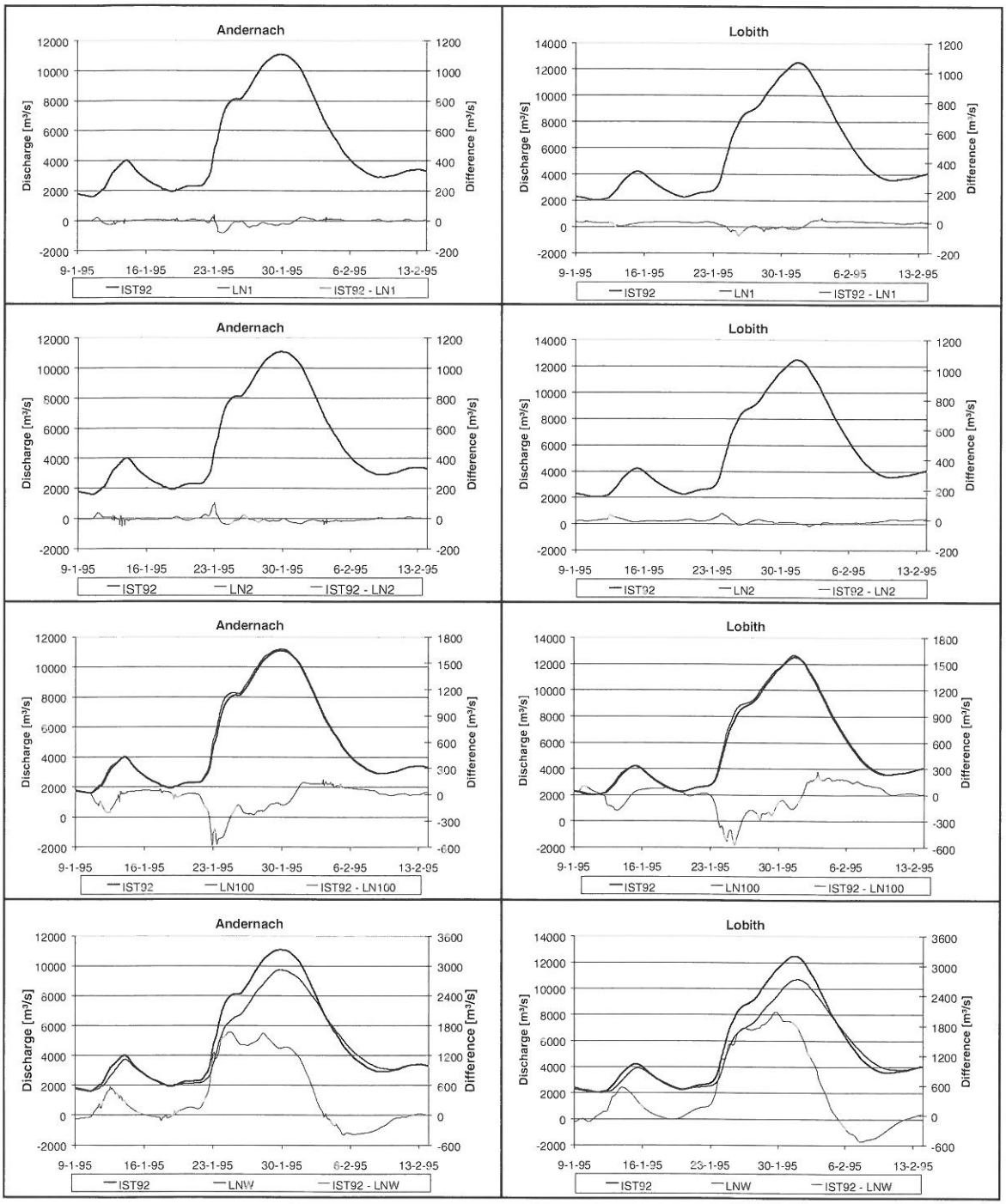

Figure 3-1: Impact of land use changes on flood waves at Andernach and Lobith.

Although the up graded model events M95^{+} and M95^{++} are characterized by higher rainfalls, the effects of changing land use on peak discharge (and water level) is of the same magnitude as for the historical based model flood (M95). Only for the scenario LNW it is obvious, that the flood reducing effects of the afforestation is smaller with increasing rainfall (M95 compared with M95^{+}). Although this is also the case for the model flood M95^{++}, the effects are slightly higher than for the model flood M95^{+}. This is caused by the relative high interception capacity of the forest for snow.

Table 3-2: Changes in peak discharges and peak water levels due to land use changes.

	Differences in peak flow [m^3/s]						Difference peak water level [cm]					
Model event	M83	M88	M93	M95	$M95^+$	$M95^{++}$	M83	M88	M93	M95	$M95^+$	$M95^{++}$
Worms												
D1	-4	-6	-42	0	2	0	0	-1	-5	0	0	0
D2	-7	-3	-17	-5	-4	-5	0	0	-2	-1	0	-1
D3	-27	-43	-278	-3	13	-1	-2	-3	-32	1	-1	-1
D4	392	365	962	298	113	182	38	38	51	23	14	23
Kaub												
D1	-15	-8	-49	-16	-14	-22	-1	-1	-4	-1	-1	-2
D2	-10	-5	-18	-7	-10	-16	-1	0	-2	-1	-1	-1
D3	-92	-40	-281	-89	-75	-115	-7	-3	-23	-7	-6	-9
D4	658	628	1353	942	513	694	54	50	116	77	41	54
Andernach												
D1	-20	-14	-24	-23	-18	-25	-1	-1	-2	-1	-1	-1
D2	-21	-8	-24	-8	-10	-15	-1	0	-2	0	-1	-1
D3	-107	-70	-290	-112	-89	-105	-6	-4	-17	-7	-5	-6
D4	932	877	2327	1349	645	831	54	57	145	89	37	47
Köln												
D1	-20	-12	-26	-29	-24	-36	-1	-1	-1	-2	-1	-2
D2	-21	-6	-26	-8	-14	-19	-1	0	1	0	-1	-1
D3	-111	-66	-290	-172	-139	-188	-7	-4	-15	-9	-7	-9
D4	954	909	2359	1487	717	879	60	57	138	88	37	45
Lobith												
D1	-22	-14	-38	-38	-32	-46	-1	0	-1	-1	-1	-1
D2	-28	-6	-34	-18	-20	-24	-1	0	-1	-1	-1	-1
D3	-85	-61	-244	-151	-180	-267	-3	-2	-8	-5	-6	-8
D4	985	1077	2326	1805	834	1030	41	41	84	61	26	32

D1 = IST 92 – LN1 D2 = IST 92 – LN2 D3 = IST 92 – LN100 D4 = IST 92 - LNW
Negative differences are increasing, positive differences are decreasing values in comparison to scenario IST92

There are also effects on the arrival of the flood peaks. In general an increase of impervious area (LN1, LN100) causes an earlier arrival of the flood peak with up to 1 hour for LN1 and up to 5 hours for LN100. A decrease of impervious areas causes the flood peak arriving later, with remarkable 39 hours at Worms for the scenario LNW / model flood M93. The effects of the scenario LN2 are much smaller, due to the smaller amount of reduction of impervious area. In all cases time lags are very different in dependency of the model event and the place along the river course. This is very obvious for the scenarios LN2 and LNW.

3.2 Effect of retention measures

To evaluate the efficiency of the retention measures, the flood waves calculated for the model events M95, $M95^+$ and $M95^{++}$ for scenario IST92 with retention measures were compared to those calculated without retention measures. Figure 3-2 shows results for Kaub and Lobith.

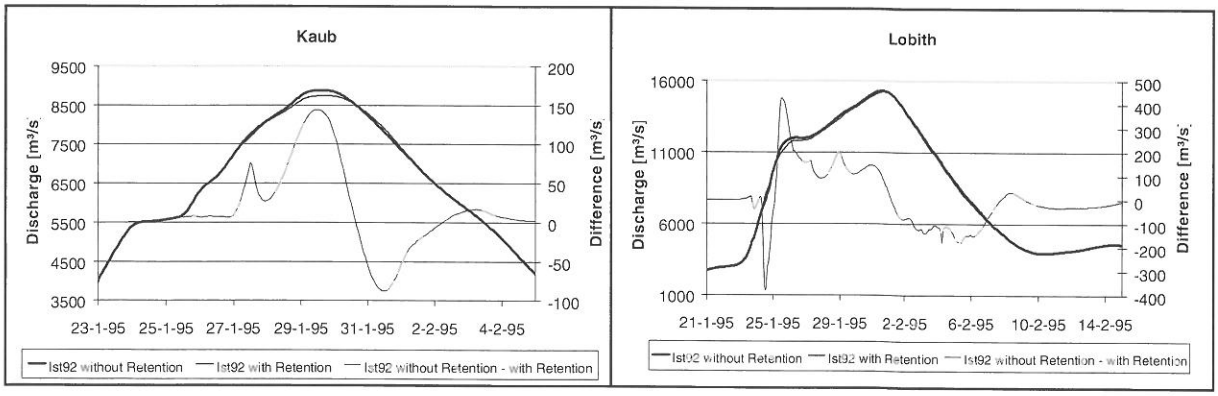

Figure 3-2: Impact of retention measures on flood waves at Kaub and Lobith, model flood $M95^{++}$, IST 92.

Table 3-3 gives an overview over the effects on peak water levels along the Rhine. It can be seen, that there are only minor effects on peak discharge and resulting water levels even for the greater model floods. The detailed analysis of the results for the three model floods shows, that the peaks of the model floods M95, M95^{+} and M95^{++} are too low to activate (M95) or completely fill (M95^{+}, M95^{++}) the polders at the Upper Rhine until Mainz. Therefore for the model flood M95 the floodwaves in Mainz were only influenced by the dike relocations with maximum effects during the rising limb of the flood wave by up to 15 m³/s (1 cm). At the model floods M95^{+} and M95^{++} the polders along the Upper Rhine between Maxau and Kaub were partly filled, causing a reduction of 118 m³/s (9 cm) or 142 m³/s (11 cm) at Kaub. Here the flood reducing effects coincide with the flood peak (Figure 3-2, Kaub).

Table 3-3: Impact of retention measures on peak water level and peak discharge along the Rhine.

Gauging station	Maximum difference of discharge [m³/s]	Maximum difference of water level [cm]	Difference of peak discharge [m³/s]	Difference of peak water level [cm]	Difference of peak time [h]
Model event M95, IST92					
Worms	24	1	5	0	-1
Mainz	15	1	0	0	-1
Kaub	22	2	21	2	1
Andernach	21	1	21	1	0
Köln	76	5	21	1	0
Rees	137	7	52	4	0
Lobith	277	10	95	3	-5
Model event M95^{+}, IST92					
Worms	194	18	79	10	5
Mainz	142	7	129	8	5
Kaub	130	10	118	9	2
Andernach	123	7	110	6	-1
Köln	122	6	114	6	-1
Rees	228	9	101	3	-1
Lobith	300	10	101	3	-1
Model event M95^{++}, IST92					
Worms	183	19	150	17	6
Mainz	150	8	145	7	-2
Kaub	144	11	142	11	-3
Andernach	139	8	139	8	0
Köln	139	7	115	6	-1
Rees	248	12	94	3	-2
Lobith	428	15	93	3	-2

In contradiction to the Upper Rhine the retention polders along the Lower Rhine were also activated by the model flood M95, retaining a volume of 35 million m³ (32% of the retention volume available between Maxau and Lobith). At Lobith the maximum reduction of 277 m³/s (10 cm) is reached during the rising limb of the flood wave, in the peak still reaching 95 m³/s (3 cm). The peak arrives 5 hours later at Lobith.
In addition to the partly filled retention polders along the Upper Rhine, for both model floods M95^{+} and M95^{++} all retention polders at the Lower Rhine were filled completely leading to a maximum reduction of stream flow of 300 m³/s (10 cm) and 428 m³/s (15 cm) respectively at Lobith. At both model floods this took place during the rising limb of the flood wave, while the flood reduction of the peak was smaller with 101 m³/s (3 cm) and 93 m³/s (3 cm) respectively (Figure 3-2, Lobith). During the model flood M95^{+} a volume of 83 million m³ was retained in the retention polders, and during the flood M95^{++} 88 million m³. The main reason for not gaining the maximum effects of the retention polders along the Lower Rhine during the peak flow must be seen in the fact, that for the model floods M95^{+} and M95^{++} the polders are nearly or completely full when the peak arrives the polder inlet (Figure 3-3).
In comparison to simulations based on model floods with return periods of 200 years at Andernach and 400 years at Rees/Lobith, the flood peak reductions at Lobith calculated earlier (Schieder, 2001) are higher than those calculated here. This shows that the efficiency of the retention measures along the river are highly dependent on the flood magnitude. Therefore when constructing effective flood retention polders it is very important to take into account the discharge in the river where the highest effect of flood reducing is needed, as well as the interaction of the retention measures.

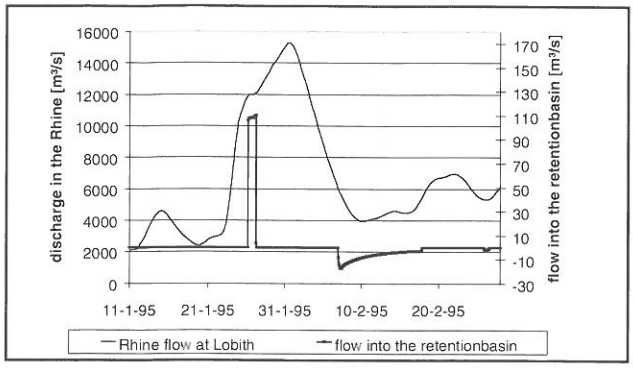

Figure 3-3: Discharge in the Rhine at Lobith and filling/emptying of retention polder Bylerward, model flood $M95^{++}$, IST92.

The combined effects of different land uses and retention capacities can be quantified simply by adding the differences that were caused by land use changes and retention measures individually. This clearly is the case, since the effects of the land use scenarios LN1, LN2 and LN100 on magnitude and form of the flood waves are very small, thus not causing a change in the reaction of the retention measures. For LNW the combined effect of land use change and retention measures on peak water level only can be derived by adding the single effects, since most of the polders were not activated. It must be expected however, that with hydrographs, which might be changed into a magnitude, which derives flood peak values where the retention measures are more effective, the combined effects of land use changes and retention measures can not be quantified simply by adding the single effects.

4 CONCLUSIONS

With the developed numerical models a tool is available, for simulating the hydrological rainfall-runoff processes in the catchment in combination with the hydrodynamic modelling of flood wave propagation, thus making a combined simulation of land use scenarios and retention measures along the river possible.
The analysis of the various land use scenarios reveal that, as a rule, both the increase in stream flow due to extension of impervious surfaces and the reductions of stream flow as consequence of reduced impervious land surfaces/afforestation show their effects in the rising limb of Rhine floods, and that the maximum effect occurs distinctly before the flood peaks.
The extreme scenario assuming a total forest cover in the Rhine basin (increase from presently 30% to 100%) produces for the considered model events in the rising flood wave a mean maximum reduction of 1 m at Lobith. The peak is reduced on average by approximately half a meter. The estimated effect of a realistic increase in forest cover (e.g. from 30% to 40%) lets expect peak reductions up to 10 cm at Lobith.
Concerning the hight of the flood wave other findings are:

- The size of the impervious area loses significance when rainfall increases.
- The reduction effect of forest cover decreases in case of extreme rainfall.

When water retention is practiced along the Upper and Lower Rhine, under the given boundary conditions positive effects (including reduced flood peaks) occur along the Rhine downstream to Lobith amounting to about 3 cm in the peak. Other investigation with boundary conditions leading to floods reaching a magnitude of values between 200 and 400 year return period at Andernach and Lobith respectively (which is higher than the values of the model events M83, M88, M93 and M95 but lower than $M95^{+}$ and $M95^{++}$) however show, that the effects of the retention measures can be higher. This shows the necessity to optimise the present activation criteria with view to their effect on flood peaks in the Rhine.
Up to now, the modelling area is restricted to the Rhine catchment downstream Maxau. Thus the effect of land use change and retention measures in the Rhine catchment upstream Maxau can only be estimated using the results from former investigations (e.g. Lammersen et al., 1999). In dependency on the flood genesis flood retention measures can lead to flood reductions of a magnitude from 100 to (in exceptions) 900 m^3/s. It is obvious that further development should be done to enlarge the model area in order to overcome the problem of not simulating the whole Rhine catchment.

ACKNOWLEDGEMENT

In the frame of the IRMA (INTERREG Rhine-Maas activities) program of the EU the project LAHoR (Quantification of the influence of the land surface and river training on flood conditions in the Rhine basin) was carried out by the PIK (Potsdam Institute for Climate Impact Research e.V.), the IWS, the BfG and the RIZA. Detailed information over the Project and its results can be found in Bárdossy et al. (2001), in Bárdossy et al. (2002) and in BfG and RIZA (2002).

REFERENCES

Bárdossy, A. et al. (2001): LAHoR, Quantification of the influence of land cover and river training measures on the flood condition at the Rhine river basin, final report IRMA-Code3/DU/1/002, Potsdam Institute for Climate Impact Research, Potsdam 2001, 34 pp.

Bárdossy, A. et al. (2002): LAHoR, Quantifizierung des Einflusses der Landoberfläche und der Ausbaumaßnahmen am Gewässer auf die Hochwasserbedingungen im Rheingebiet, Report IRMA-Code3/DU/1/002, CHR report II-17, Lelystad 2002, 70 pp, in preparation.

Barneveld, H. J., Meijer, D. G. (1997): SOBEK-Model Andernach-Lobith, Model construction, calibration and verification, Final report of a cooperative project RIZA-BfG; Lelystad 1997, 46pp., annexes.

Bergström, S. (1995): The HBV model. In: Computer models of watershed Hydrology (ed. by V.P. Singh), Water Resources Publications, Littleton, Colorado, USA, 1995, pp 443-476.

BfG, RIZA (2002): Wellenablauf in den bedeutenden Nebengewässern des Rheins und im Rhein zwischen Maxau und Lobith, Aufgabe 3 des Projektes LAHoR, Quantifizierung des Einflusses der Landoberfläche und der Ausbaumaßnahmen am Gewässer auf die Hochwasserbedingungen im Rheingebiet, IRMA-Code3/DU/1/002. BfG-report, Koblenz 2002, in preparation

Delft Hydraulics, The Ministry of Transport, Puplic Works and Water Management (1997): SOBEK, Technical Reference Manual, Delft 1997.

Dosch, F., Beckman, G. (1999): Trends und Szenarien der Siedlungsflächenentwicklung bis 2010. In Bundesamt für Bauwesen und Raumordnung (Ed.): Perspektiven der zukünftigen Raum- und Stadtentwicklung, 11, Berlin 1999, pp. 827-842.

Homagk, P. (1985): Ermittlung von Steuerreglements für die Rückhaltemaßnahmen am Oberrhein mit Hilfe von mathematischen Modellen. In: 1. Wissenschaftliche Tagung „Hydrologie und Wasserwirtschaft, Planung und Betrieb wasserwirtschaftlicher Maßnahmen", 18. – 20. März 1985. Institut für Hydrologie und Wasserwirtschaft (IHW) Universität Karlsruhe. S. H6-1 – H6-10.

ICPR (1997): Hochwasserschutz am Rhein, Bestandsaufnahme, International Commission for the Protection of the Rhine, Koblenz 1997, 62 pp.

ICPR (1998): Action Plan on Flood Defense, International Commission for the Protection of the Rhine, Koblenz 1998, 30 pp.

Lammersen, R. et al. (1999): Einfuss der geplanten Retentionsmaßnahmen an Ober- und Niederrhein auf extreme Abflüsse am Niederrhein; BfG-report-1221, Koblenz 1999, 36 pp., Annex

Schieder, T. (2001): Auswirkungen der Hochwasserrückhaltemaßnahmen am Niederrhein auf den Wellenablauf im Rhein zwischen Andernach und Lobith - Kalibrierung und Anwendung eines hydrodynamischen Modells-; Diplomarbeit, Geographische Institute der Rheinischen Friedrich-Wilhelms-Universität Bonn

ANALYSIS OF FLOOD EVENTS IN A STEEP MOUNTAIN TORRENT

Serena Liener Hegg[1,2], Hans Kienholz[1], Rolf Weingartner[1]

[1] Institute of Geography University of Berne, Hallerstrasse 12, 3012 Bern, Switzerland, kienholz@giub.unibe.ch, wein@giub.unibe.ch

[2] GEOTEST AG, Birkenstrasse 15, 3052 Zollikofen, Switzerland, serena.liener@geotest.ch

SUMMARY

The paper analyses and describes the major one hour and longterm rainfall-runoff events of the Spissibach catchment at different scales. Special attention is given to the comparison of the two most important sub-catchments ("Baachli" and "Fulwasser") with quite different landscape features.

Keywords: Flood runoff analyses, measuring system, mountain torrent

1 INTRODUCTION

Mountain torrents are conspicuous phenomena in the alpine environment. The steep slopes and the fan are origin and result of a number of individual as well as interdependent geomorphological processes, triggered and controlled by geological, hydro-meteorological, and hydraulic conditions. Torrents have to be regarded as open and complex systems, which require an interdisciplinary approach.
The mountain torrent systems project in the Spissibach catchment (Lake Thun area, Switzerland; 2.6 km^2) aims to measure, analyze and model runoff and bedload transport in a very steep mountain torrent. Since ten years precipitation, runoff and bedload transport have been permanently monitored at different stations of several sub-catchments as well as at the main station (following a nested approach). Additional measurements include changes in soil water storage. Special investigations (e.g. sprinkling tests) deepen the knowledge of runoff generation.
In the European Alps, only a few micro-scale torrential basins are systematically measured and investigated. Besides, the Spissibach catchment is one of the steepest instrumented research catchments with its average slope gradient of 28°. Therefore, the results of the Spissibach project provide an essential contribution to the understanding of flood processes in alpine torrents. However ten years of measuring under difficult conditions do not allow many final conclusions. Therefore this paper presents first analyses and results of the ongoing research in the Spissibach catchment.

2 THE SPISSIBACH CATCHMENT

The research area belongs to the Bernese alps and is situated at the border of lake Thun above the village Leissigen. The highest point of the catchment is the Morgenberghorn at 2250m a. s. l. The Spissibach catchment has a surface of about 2.6 km^2 and an average slope gradient of 28°. 45% of the catchment area is covered by forest and 43% by pasture. The remaining 12% are formed by outcrops of bedrock or covered with debris.
The geology is dominated by the Helvetic Wildhorn nappe in the peak area of the Morgenberghorn and by an Ultrahelvetic melange mainly composed of marls and sandstones in the lower part of the catchment (Hunziker, 1992). These rocks are highly erodable and therefore about 2/3 of the catchment area are affected by mass movements (mainly landslides and rockfall).

2.1 The measuring system

The first measurements in the Spissibach catchment were carried out in 1991. Since then a measuring system for registering meteorological, hydrological and geomorphological parameters has been established (Hegg, 1997).

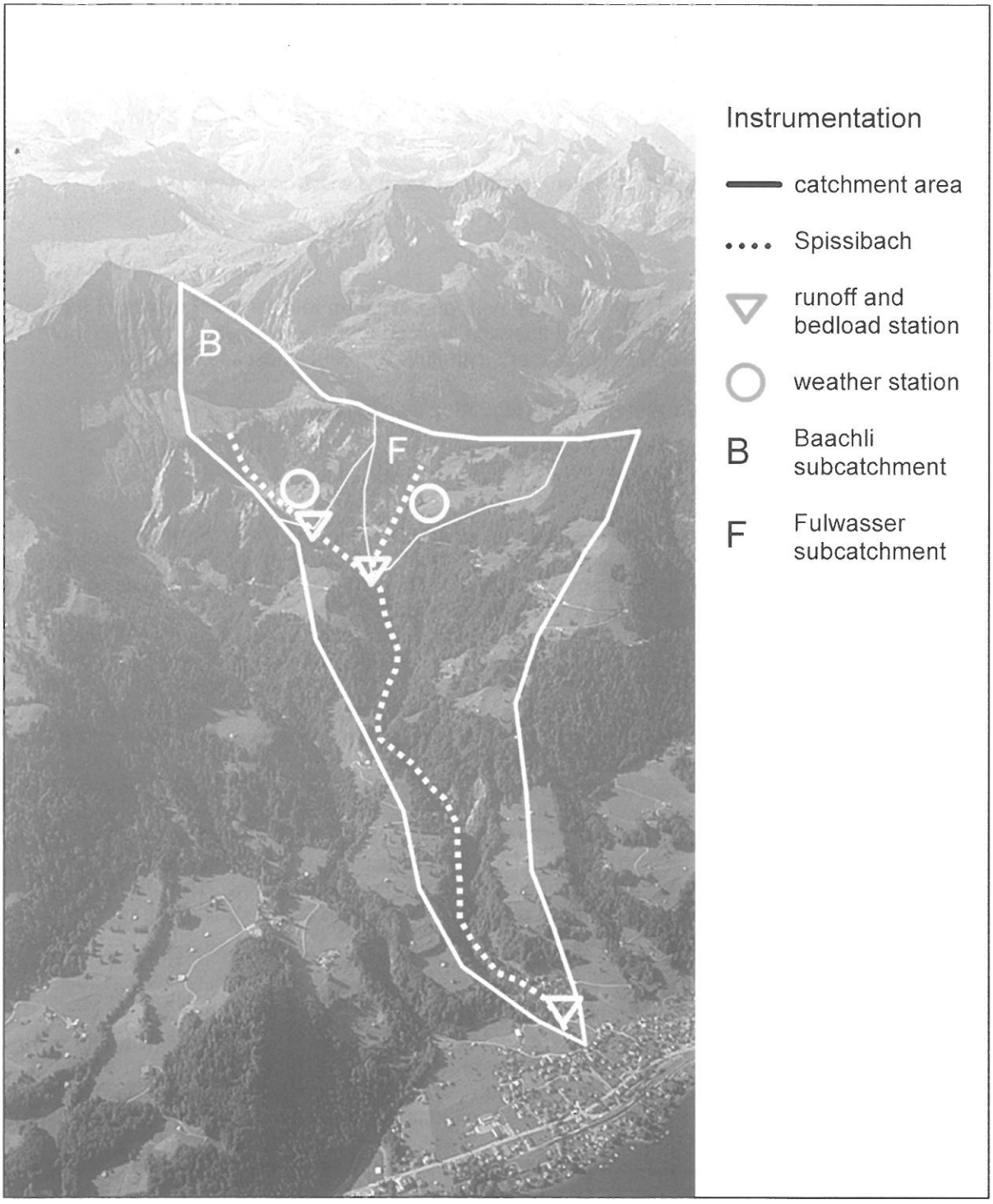

Figure 2-1: Situation and Instrumentation of the Spissibach catchment.

Precipitation and Evaporation are important parameters of the hydrological system. Therefore two weather stations measure precipitation, temperature, relative humidity, global and net radiation, wind direction and wind speed with a temporal resolution of 10 minutes. Both weather stations are situated approximatly in the centre of the catchment area at Fulwasser and Baachli (Figures 2-1). Additionally 5 storage gauges have been installed to observe the spatial distribution of precipitation.
The runoff of the Spissibach catchment and of some sub catchments is gauged by totally 5 stations, measuring water level, electric conductivity and water temperature with a temporal resolution of 10 minutes. The network design is based on a nested approach.
Measuring the bedload in a mountain torrent has been so far a difficult task. Nevertheless in 1999 a measuring system for bedload transport has been constructed above the village of Leissigen (Figures 2-1). The measuring station consists of a balance to weigh the transported bedload during a flood

event. The bedload balance is supported by so called ‚Hydrophones', which register the vibrations caused by bedload transport (Rickenmann et al., 1997). The station is completed with a radar system for measuring the water level.

2.2 The sub catchments Baachli and Fulwasser

The upper part of the Spissibach catchment consists of the two sub catchments „Baachli" and „Fulwasser" (Figure 2-1) with quite different landscape features as shown in Table 2-1.

Table 2-1: Properties of the sub catchments Baachli und Fulwasser.

Sub catchment	Baachli	Fulwasser
Area	0.62 km^2	0.26 km^2
Mean altitute	1610 m a.s.l	1429 m a.s.l
Mean slope angle	33°	25°
Channel density	2.6 km/km^2	3.65 km/km^2
Forest	11 %	42 %
Bedrock	27 %	2 %
Rockfall debris	15 %	0 %

The "Baachli catchment" is very steep with a mean slope angle of 33°; it contains the steep bedrock cliffs of the Morgenberghorn, which is followed by a belt with permeable rockfall debris and a belt of pastures. The "Fulwasser catchment" is less steep than the "Baachli catchment" and contains hardly any bedrock part. The catchment starts at the steep Greberegg ridge and goes down to the flat and mainly swampy area around the alp Fulwasser, which is a main part of the catchment area. Below the alp Fulwasser follows a steeper mainly forested area.

3 FLOOD EVENTS

3.1 Rainfall

In steep mountain torrents important flood events occur mainly during thunderstorms and sometimes during long-term rainfall events. For this investigation, the flood events with the most intensive one hour rainfall and/or the highest long-term rainfall have been selected and analysed. Special attention is given to the comparison of the two most important sub-catchments ("Baachli" and "Fulwasser") with quite different landscape features (Table 2-1).
The highest one hour rainfall measured so far in the research area is 39 mm/h, which represents an event with a return period of 20 to 30 years (Geiger et al., 1992).

Table 3-1: The highest 1h rainfall events measured at the station Fulwasser and Baachli (1992-2001).

Date	1h-rainfall	
	Station Fulwasser	Station Baachli
31.7.1993	31.2 mm/h	37.8 mm/h
11.7.1995	no data available	39.2 mm/h*
7.8.1995	25.2 mm/h	33 mm/h
13.8.1995	33 mm/h	19.2 mm/h
10.6.1996	25.4 mm/h	30.4 mm/h
14.6.2000	32.6 mm/h	35.8 mm/h

Table 3-1 shows, that the rainfall is similar at both stations and high rainfall intensities normally occur on both rainfall gauges at the same time. The rainfall at the station Baachli is often a little higher than at Fulwasser. This is probably due to the topographical situation of the Baachli station, which is situated below the steep cliff of the Morgenberghorn. During thunderstorms the rainfall intensities may vary in time between the two rainfall stations.

3.2 Flood events with heavy rainfall

On 11. July 1995 the highest 1-h rainfall measured so far occurred in the Spissibach catchment. The antecedent moisture was relatively low, because the last week before the event almost no rainfall had been fallen. The total rainfall amount was 57 mm with a maximal intensity of 14 mm per 10 minutes. Both sub catchments reacted at the same time with an increasing runoff about one hour after rainfall had started. At Leissigen the runoff increased with some delay compared to the two sub catchments. The delay between the highest runoff peak at the sub catchments Baachli/ Fulwasser and Leissigen was 20 minutes. The direct runoff volume at Leissigen was 11 mm, which corresponds to 20 % of the rainfall amount (Table 3-2).
Both sub catchments reacted quite similar during the ascending part of the flood hydrograph, although their properties are completely different. The Leissigen catchment reacts with a delay of 20 to 30 minutes compared with both subcatchments. During the recession the runoff at Baachli and at Leissigen show a small second peak. This second peak can't be observed at the Fulwasser station. It's assumed, that the second peak is caused by water storage in the debris belt situated in the middle part of the Baachli catchment.

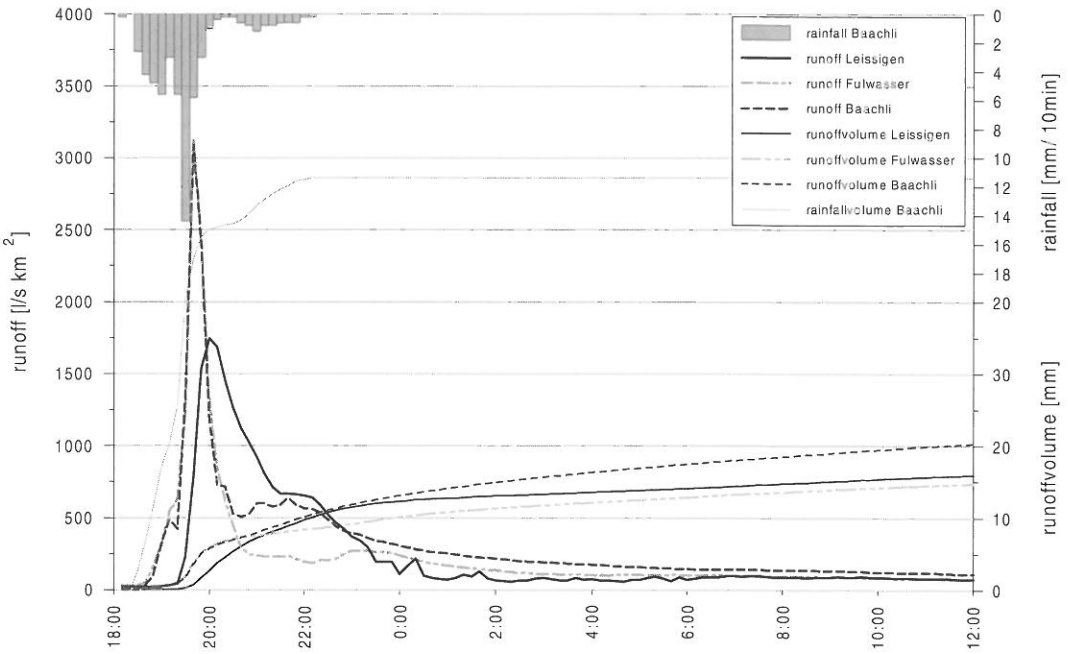

Figure 3-1: Flood event of 11.7.1995.

Table 3-2: Rainfall and runoff parameters of the 11.7.1995.

	Leissigen	Baachli	Fulwasser
Rainfall volume	-	57 mm	-
Max. 1h-rainfall	-	39 mm/h	-
Max. rainfall intensity	-	14.4 mm/10min.	-
Peak runoff	4500 m^3/s	1900 m^3/s	800 m^3/s
Specific peak runoff	1730 $m^3/s\ km^2$	3060 $m^3/s\ km^2$	3070 $m^3/s\ km^2$
Direct runoff	11.4 mm	9.1 mm	9.4 mm
Percent of direct runoff	20 %	16 %	16.5 %
Reaction time	50 minutes	30 minutes	30 minutes

On 31. July 1993 a similar runoff event with a peak runoff of almost 4000 l/s (1540 $l/s*km^2$) occured at the main station at Leissigen. The runoff stations Baachli and Fulwasser were not yet working at this time, so there are no data available. The total rainfall amount measured during that event was 65 mm with a maximal intensity of 12.6 mm per 10 minutes.

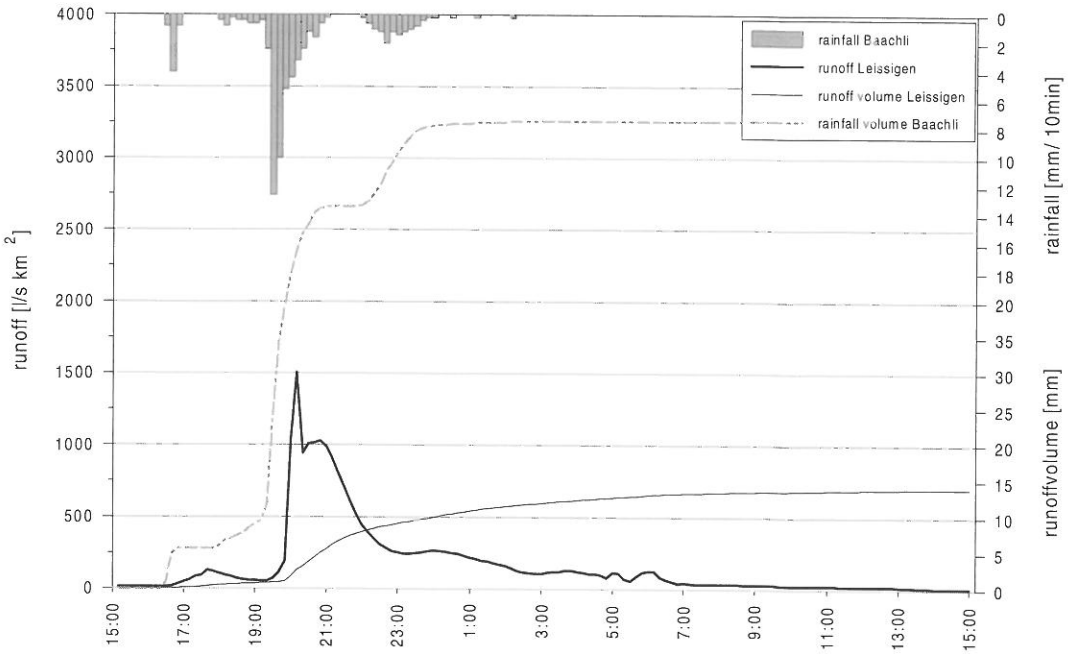

Figure 3-2: Flood event of 31.7.1993.

During the flood event of the 7.8.1995 (Figures 3-3) the Baachli and Fulwasser subcatchments had similar flood hydrographs to the event of the 11.7.95. The rainfall amounts and the rainfall intensities as well as the specific peak runoffs of the subcatchments were a little bit lower than at the 11.7.95. Although the difference of the rainfall amount of the two events is not very big, the peak runoff at Leissigen is considerably lower at the 7.8.95. Therefore we assume, that only rainfalls exceeding a critical rainfall amount and intensity can produce high peak discharges. These threshold values are lower for the smaller subcatchments than for the whole Leissigen catchment.

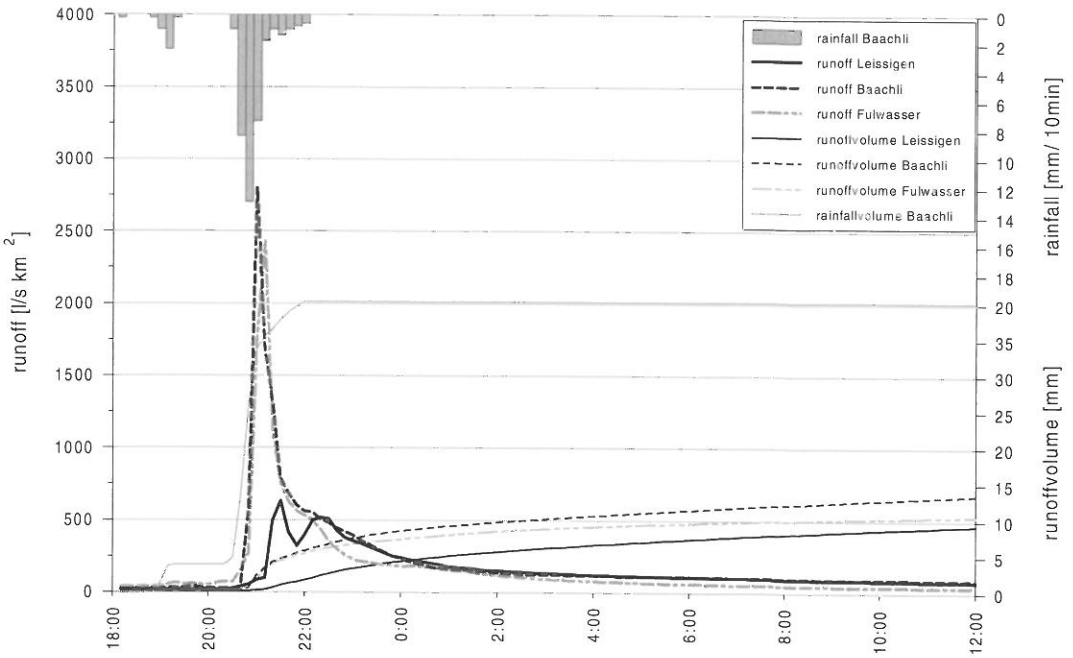

Figure 3-3: Flood event of 7.8.1995.

Table 3-3: Rainfall and runoff parameters of the 7.8.1995.

	Leissigen	Baachli	Fulwasser
Rainfall volume	-	40 mm	30 mm
Max. 1h-rainfall	-	33 mm/h	25 mm/h
Max. rainfall intensity	-	13 mm/10min.	10 mm/10min
Peak runoff	1600 m^3/s	1700 m^3/s	600 m^3/s
Specific peak runoff	630 $m^3/s\ km^2$	2440 $m^3/s\ km^2$	3070 $m^3/s\ km^2$
Direct runoff	4 mm	6.6 mm	4.9 mm
Percent of direct runoff	11 %	16.5 %	16.3 %
Reaction time	10 minutes	10 minutes	0 minutes

3.3 Longterm flood events

Some important flood events are related to longterm rainfall events. In July 1995 about 60 mm rain had fallen during 12 hours with a maximal intensity of 9 mm/ 10 min. Figure 3-4 shows, that the sub catchments react always earlier on the rainfall than the Leissigen station. During the first part of the flood the Fulwasser catchment had higher specific runoff than the Baachli station, whereas the specific peak runoff is clearly higher at the Baachli station (Baachli: 1342 l/s or 2160 l/s*km^2, Fulwasser: 289 l/s or 1110 l/s*km^2). During the first part of the event more direct runoff was contributed by the Fulwasser area. It seems that the swampy, highly saturated area reacts faster on lower rainfall than the Baachli area. The runoff reaction at Leissigen is delayed compared to the reaction of the two subcatchments. This first part of the described flood event seems to be a typical reaction on low intensity rainfall.
During the second part of the event, when the peak runoff occurred, the flood hydrographs look very similar to heavy rainfall events. The flood peak in Leissigen is less delayed compared with the sub-catchments. The Baachli area reacts more intensive than the Fulwasser area. Probably water, which has been stored in the debris belt during the first part of the event, together with more saturated soils, cause higher direct runoff and higher specific runoff in the Baachli area during the second part of the event.
At the Leissigen station a high peak runoff of 2980 l/s (1140 l/s*km^2) had been measured. The total direct runoff volume was 35 mm, which corresponds to 55% of the rainfall amount. This is considerably higher than the direct runoff percentage of the short rainfall events.

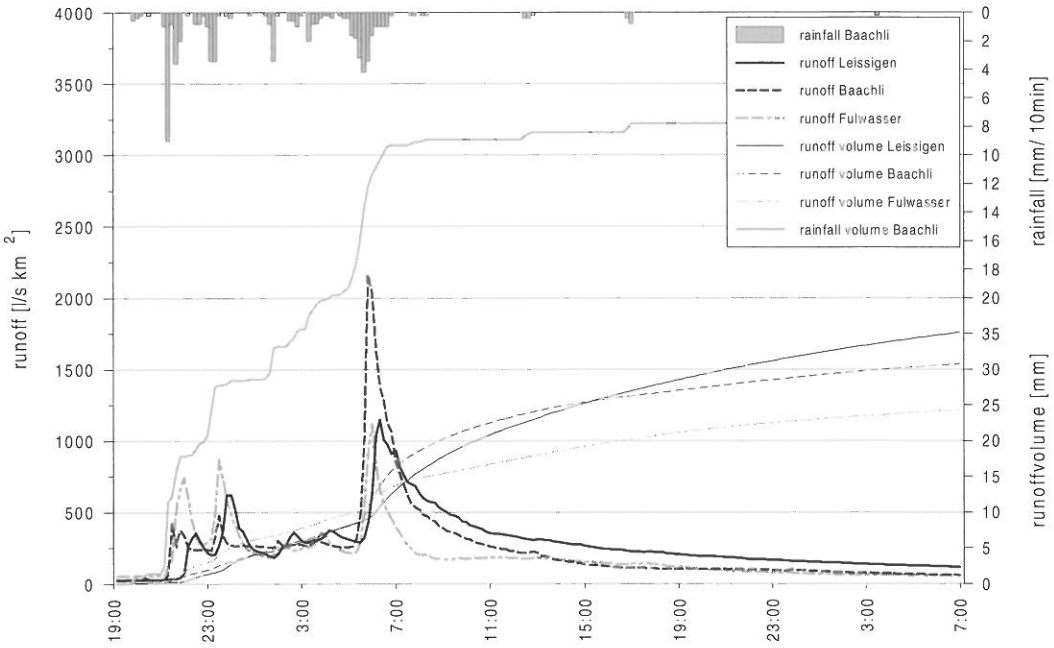

Figure 3-4: Flood event of 2.- 4. July 1995 caused by longterm rainfall.

4 COMPARISON FULWASSER WITH BAACHLI

A hydrological comparison of the two sub catchments Baachli and Fulwasser was drawn on the basis of TOPMODEL, which is a physically based semi-distributed model (Beven et al. 1995). A topographical index (topoindex), which represents the special topography of such a steep catchment, is derived from the Digital Elevation Model. It describes possible surface runoff in consequence of saturated soils. With this index the catchment can be subdivided into classes with similar runoff conditions.
For the model application the parameters precipitation, evaporation, soil water in the root zone, soil transmissivity and mean velocity of channel runoff are required. With the combination of TOPMODEL and the GIS system Arc/Info the simulation of the spatial-temporal development of surface runoff in saturated zones can be made visible. Long-term (months) as well as short-term simulations (single events) can be carried out.

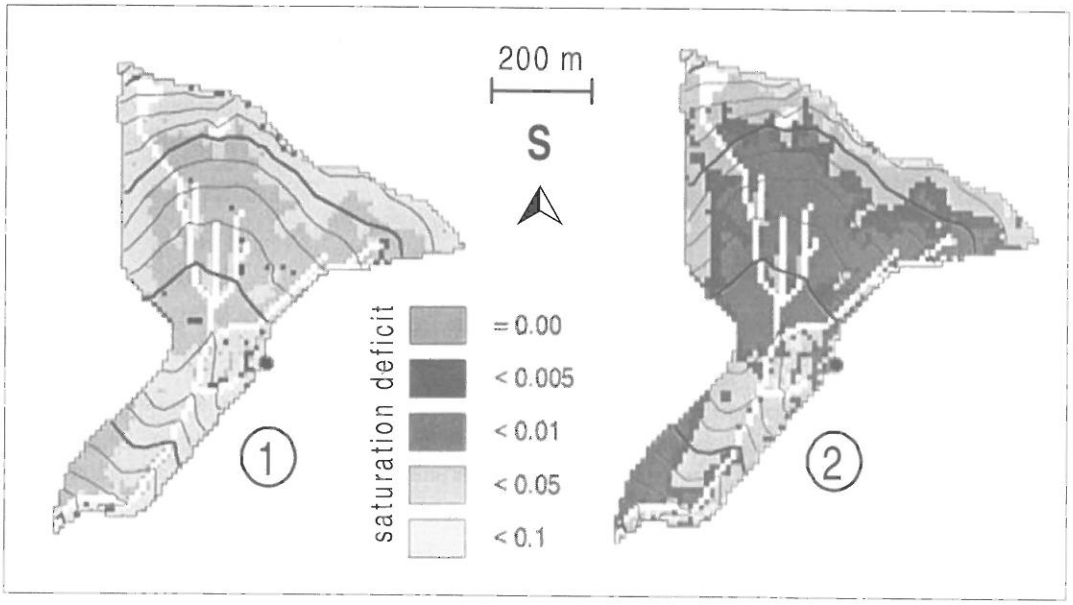

Figure 4-1: Dynamics of saturated areas in the sub-catchment Fulwasser after the rainfall event of 11 July 1995. ① shows the situation before the beginning of rainfall, ② represents the situation 7 hours later after the end of rainfall (Brünisholz 1999).

The comparison of the simulation results of Baachli and Fulwassers gives interesting insights in the differences in runoff generation, as shown by the flood event of July 11, 1995 (Figure 4-1 and Figure 3-1). After the rainfall event with a total rainfall of 60 mm within 4 hours the percentage of saturated areas in Fulwasser is much higher with a maximum of 59% than in Baachli with 23% only. The TOPMODEL simulation shows that soil saturation is quickly attained in Fulwasser, a fact that is confirmed by field observations (Lämmli 2000). In Fulwasser, the areas with less steep slopes are nearly saturated even in dry periods which however do not last very long (less than two weeks).

5 CONCLUSIONS

5.1 Measuring concept

The analyses of the events measured so far show, that the concept with measuring at different stations of several sub-catchments as well as at the main station (following a nested approach) seems suitable to carry out flood analyses in small and steep mountain torrents.
For analyses of thunderstorm events rainfall information with higher temporal and spatial resolution can be helpful. To fully understand runoff reaction in such small and steep catchments shorter measuring intervals for rainfall and runoff are necessary because these catchments can react within some minutes on rainfall events.

5.2 Flood analyses in the Spissibach catchment

The reaction of the runoff on heavy rainfall is generally very fast and the peak discharge occurs normally at the main station within 30 minutes after the most intensive rainfall. The relation between rainfall and runoff shows, that only rainfall events exceeding a critical rainfall amount and a critical rainfall intensity can produce high peak discharges. If the total rainfall amount is bigger than 50 to 60 mm and the hourly rainfall is bigger than 30 mm/h high peak runoff can occur at the Leissigen station. In general, these threshold values are lower in the sub-catchments. Direct runoff varies between 16% and 20% during heavy rainfall events producing high peak discharges.
If a rainfall event lasts longer than 40-50 minutes, a second peak discharge can often be observed at the Leissigen station, which is probably produced by the sub-catchment "Baachli", where water can be stored in a debris belt.
Further comparisons of the Baachli and Fulwasser show that both sub-catchments react quite similar to high rainfall intensities during the ascending part of the flood hydrograph, although the sub-catchment properties are completely different. During recession the Baachli area produces normally higher specific runoff than the Fulwasser area. Longterm events show, that during lower rainfall the Fulwasser catchment causes more direct runoff than the much steeper and partially rocky area of the Baachli area. Generally the influence of the catchment properties becomes less, the more intensive the rainfall is.

REFERENCES

Beven, K.J. et al. (1995): TOPMODEL. In P.P. Singh (Ed.): Models of Watershed Hydrology. Water Resources Publications, Colorado

Brünisholz, M. (1999): Zur räumlich-zeitlichen Dynamik der Hochwasser in Wildbacheinzugsgebieten – TOPMODEL-Anwendung in Kombination mit einem GIS im Testgebiet Leissigen. Diplomarbeit der Philosophisch-naturwissenschaftlichen Fakultät der Universität Bern, Publikation Gewässerkunde No. 228, Bern.

Hegg, Ch. (1997): Zur Erfassung und Modellierung von gefährlichen Prozessen in steilen Wildbacheinzugsgebieten, Geographica Bernensia G52, Universität Bern, Bern

Geiger, H. et al. (1992): Extreme Punktregen unterschiedlicher Dauer und Wiederkehrperioden 1901–1970. In: Hydrologischer Atlas der Schweiz, Tafel 2.4, Bern.

Hunziker, G. (1992): Zur Geologie im Gebiet Leissigen-Morgenberghorn, unveröff. Diplomarbeit, Geologisches Institut d. Uni Bern., Bern

Lämmli, M. (2000): Vergleichende hydrologische Untersuchungen in drei Kleinsteinzugsgebieten des Fulwasserbaches. Diplomarbeit, Universität Bern, Publikation Gewässerkunde No. 250, Bern.

Liener, S. (2000): Zur Feststofflieferung in Wildbächen, Geographica Bernensia G64, Universität Bern, Bern

Rickenmann, D. et al. (1997): Geschiebemessungen mittels Hydrophon. Oesterreich. Wasserwirtschaft, Jg. 49, Heft 11/12:219-228., Wien.

ACCURACY OF KINEMATIC WAVE AND DIFFUSION WAVE FOR FLOOD PROCESSES IN NATURAL CHANNELS

Tommaso Moramarco[1], Florisa Melone[2]

[1] Research Institute for Hydrogeological Protection in Central Italy, CNR, Via M.Alta 126, 06128 Perugia, Italy, T.Moramarco@irpi.pg.cnr.it

[2] Research Institute for Hydrogeological Protection in Central Italy, CNR, Via M.Alta 126, 06128 Perugia, Italy, F.Melone@irpi.pg.cnr.it

SUMMARY

The kinematic-wave and diffusive-wave approximations are analyzed for flood routing process in natural channels as support in flooding risk evaluation. Errors were computed by comparing the steady dimensionless profiles of the flow depth with those estimated by the dynamic-wave solution. Two types of downstream boundaries, critical-flow depth and zero-flow depth gradient, are considered together with the condition of steady state at the upstream end. The role of inertial, pressure, friction and gravity forces is investigated for sixteen test cases defined through the kinematic wave number, K, and the Froude number, F_0, whose range is assumed to be (3-30) and (0.1-1), respectively. Moreover, the accuracy of the two approximations is assessed through the mean value, ε, of the errors in magnitude computed for the channel region where the solution is not greatly influenced from the boundary conditions. For critical flow at the downstream end and for ε less than 5%, the kinematic-wave approximation (KW) was reasonably accurate for $KF_0^2 \geq 1.4$ whereas the diffusive-wave solution (DW) for $KF_0^2 > 0.6$. However, close to downstream end the KW approach gave large errors in flow depth showing that if accurate solution is needed there KW solution should not be used. For the DW approach the maximum error in flow depth occurred close to downstream end, too: for the lowest K and F_0 values it reached 13% which could be unacceptable for evaluation of flood risk. On the other hand, under the condition of zero-depth gradient both the diffusive solution and kinematic solution were found reasonably accurate for any K and F_0 values. However this boundary condition is not suitable in representing the flow depth in a natural channel because changes in the geometry or in the hydraulic characteristics could occur next to the outlet section. The involved differential equations were solved adopting a numerical scheme implemented to the purpose and based on two-step Lax-Wendroff technique coupled with the characteristic equations at the boundaries.

Keywords: Flood routing, De S.Venant equations, kinematic-wave, diffusive-wave, dynamic-wave

1 INTRODUCTION

The flood routing in natural channels is generally considered as one-dimensional flow. The flow depends on the balance among inertial, pressure, friction and gravity forces, expressed by the momentum equation (Moramarco and Singh, 2000). The relative significance of these forces is expressed through the kinematic wave number, K, and the Froude number, F_0.

Based on the analysis of these parameters the regions where the kinematic-wave and diffusive-wave approximations can be considered accurate were estimated both for channel flow (Ponce et al., 1978; Daluz Vieira, 1983) and overland flow (Woolhiser and Ligget, 1967; Singh and Aravamuthan, 1995). These regions were defined comparing the involved solutions in terms of discharge hydrographs at the outlet of the domain (Morris, 1979).

Singh and Aravamuthan (1995; 1997) deduced the accuracy of these approximations by investigating the steady state profiles of the flow depth over the plane for uniform rainfall excess. Similar analysis was carried out by Moramarco and Melone (2000) for spatial-varying rainfall excess. An interesting aspect pointed out in these latter investigations was that by comparing the steady water profiles computed by the diffusive approach with those estimated by the dynamic equation, the former underestimated the flow depth over the entire plane. This result, if also confirmed for channel flow routing, is fundamental on the choice of the approximation to be applied for the flooding area evaluation.

The aim of this paper is to investigate the accuracy of the kinematic and diffusive-wave approximations in estimating the steady dimensionless profiles of flow depth in natural channels. Using a set of K and F_0 values the solution of kinematic and diffusive-wave equations were compared with that of the dynamic equation, assuming an input hydrograph discharge which reaches the steady state while a critical flow or zero-depth gradient condition is given at the downstream end. The accuracy of the approximations is assessed by the analysis of error distribution in flow depth along the channel.

2 GOVERNING EQUATIONS

Considering a prismatic channel with rectangular cross section and the simplification of fluid incompressibility, constant density and hydrostatic pressure distribution, the conservation laws for the mass and momentum neglecting lateral inflows can be written as:

(1) $$\frac{\partial f}{\partial t}+\frac{\partial[p(f)]}{\partial x}=S$$

with:

(2) $$f=\begin{vmatrix}A\\Q\end{vmatrix} \qquad p(f)=\begin{vmatrix}Q\\\frac{Q^2}{A}+\frac{1}{2}gBh^2\end{vmatrix} \qquad S=\begin{vmatrix}0\\gA(S_0-S_f)\end{vmatrix}$$

where A is the wetted cross sectional area; Q discharge; h flow depth; B channel width; g acceleration due to gravity; t time; x distance along channel; S_0 bed slope; S_f is the friction slope which can be estimated by the Manning formula. Equation (1) is the governing equation for the dynamic-wave (DYW) representation. Neglecting the local and convective inertial terms, Eq.(1) represents the diffusive-wave (DW) approximation with (Morris and Woolhiser, 1980):

(3) $$f=\begin{vmatrix}A\\0\end{vmatrix} \qquad p(f)=\begin{vmatrix}Q\\\frac{1}{2}gBh^2\end{vmatrix} \qquad S=\begin{vmatrix}0\\gA(S_0-S_f)\end{vmatrix}$$

The kinematic-wave (KW) representation is obtained if the pressure term is also negligible, yielding:

(4) $$f=\begin{vmatrix}A\\0\end{vmatrix} \qquad p(f)=\begin{vmatrix}Q\\0\end{vmatrix} \qquad S=\begin{vmatrix}0\\gA(S_0-S_f)\end{vmatrix}$$

The initial condition assumed here is a steady discharge very close to zero along the entire channel. As regards the boundary conditions, one hydraulic variable has to be assigned at each of the channel ends for the case of sub-critical flow. At the upstream boundary, an inflow hydrograph reaching the steady state, Q_0, at time $t=t_0$ is assumed in the form:

(5) $$Q(0,t)=\begin{cases}Q_0\, t/t_0 & t\le t_0\\ Q_0 & t>t_0\end{cases}$$

At the downstream end, x=L, two different types of boundaries are considered:
a) Critical-flow depth:

(6) $$Q(L,t)=A\sqrt{gA(L,t)/B}$$

b) Zero-flow depth gradient:

$$\left.\frac{dh}{dx}\right|_{x=L} = 0 \tag{7}$$

3 SOLUTION BY THE TWO-STEP LAX WENDROFF METHOD

In order to solve Eq. (1) by a simple numerical technique, an explicit scheme based on the two-step Lax-Wendroff method was employed (Richtmyer and Morton, 1967). For purposes of completeness, a short account of the scheme as applied to channel flow is provided here. The vector f at time (n+1) Δt and at section jΔx, f_j^{n+1}, is calculated through two steps using its values at times n Δt and (n+1/2) Δt, with Δx and Δt spatial and time step, respectively. The first-step is considered for estimating $f_{j+1/2}^{n+1/2}$:

$$f_{j+1/2}^{n+1/2} = \frac{f_j^n - f_{j+1}^n}{2} - \frac{\Delta t}{2\Delta x}\left(p_{j+1}^n - p_j^n\right) + \frac{\Delta t}{4}\left(S_{j+1}^n + S_j^n\right) \tag{8}$$

An analogous expression is used for $f_{j-1/2}^{n+1/2}$. At the second step, the value of f_j^{n+1} is calculated as:

$$f_j^{n+1} = f_j^n - \frac{\Delta t}{\Delta x}\left(p_{j+1/2}^{n+1/2} - p_{j-1/2}^{n+1/2}\right) + \frac{\Delta t}{2}\left(S_{j+1/2}^{n+1/2} - S_{j-1/2}^{n+1/2}\right) \tag{9}$$

The approximations (8) and (9) are computed for all the interior grid points, j = 2,...,N-1. At the boundary grid points, j = 1 and j = N, the characteristic method was applied (Sivaloganathan, 1987). In fact, it is known that if one of the flow variables is assigned at one end of the channel, the other dependent variable is generally determined by the method of characteristics which can be expressed by:

$$\frac{dx}{dt} = \frac{Q}{A} \mp c \tag{10}$$

$$\frac{dQ}{dt} - \left(\frac{Q}{A} \pm c\right)\frac{dA}{dt} = J_S \tag{11}$$

with $J_S = gA(S_o - S_f)$ and $c = \sqrt{g\frac{A}{B}}$. The upper and lower algebraic sign in Eq.(10) refers to characteristic C^- and C^+, respectively. Equations (10) and (11), together with the relation Q = Q(t) or A = A(t) defined at the boundary, allow for calculation of the other physical condition at the end sections.

The stability of the numerical scheme is ensured by the Courant condition; for a fixed spatial grid, Δx, the value of Δt satisfying the Courant condition is determined (Hromadka and deVries, 1988; Dawdy, 1990). As the method is second-order accurate in space and time, a dissipative interface was implemented for damping numerical oscillations (Abbott, 1979).

3.1 Dynamic Waves

Equations (8) and (9) are applied for discretizing Eq.(1) with vectors defined by Eq.(2) for the interior grid points.

The solution at the upstream boundary is given by Eqs. (10) – (11) with Q(t) expressed by Eq.(5) and considering the negative characteristic, C^-, through the end point (1,n+1). The characteristic is

assumed to be a straight line with slope $\left(\frac{Q}{A}-\sqrt{g\frac{A}{B}}\right)\Big|_k$, where k is the point of intersection of the negative characteristic, C^-, through the point (1,n+1) with the time level line t=n (Sivaloganathan, 1987). Equation (11) can be written in finite difference form as:

$$\frac{Q_1^{n+1}-Q_k}{\Delta t}-\left(\frac{Q}{A}+c\right)_k\frac{A_1^{n+1}-A_k}{\Delta t}=\left(J_S\right)_k \tag{12}$$

As regard the downstream end section, x=L (j=N), the positive characteristic, C^+, is involved. Specifically:

a) For critical-flow depth condition, Eq.(6) coupled with Eq.(11) yields:

$$\frac{A_N^{n+1}\sqrt{g\frac{A_N^{n+1}}{B}}-Q_l}{\Delta t}-\left(\frac{Q}{A}-c\right)_l\frac{A_N^{n+1}-A_l}{\Delta t}=\left(J_S\right)_l \tag{13}$$

where subscript l refers to the point of intersection of the C^+ through (N,n+1) with the time level line t=n.

b) For zero-depth gradient condition applied on a rectangular channel, Eq. (7) implies $A_N^n = A_{N-1}^n$. Therefore, Eq.(11) in finite difference form can be cast as:

$$\frac{Q_N^{n+1}-Q_l}{\Delta t}-\left(\frac{Q}{A}-c\right)_l\frac{A_{N-1}^{n+1}-A_l}{\Delta t}=\left(J_S\right)_l \tag{14}$$

3.2 Diffusive Waves

Equations (8) and (9) are applied to Eq. (1) with vectors defined by Eq. (3) for interior grid points. Given the upper boundary condition (5), the water depth at x=0 can be written as:

$$h_1^{n+1}=h_2^{n+1}-\left(S_o-\frac{S_f\Big|_1^n+S_f\Big|_2^n}{2}\right)\Delta x \tag{15}$$

For the downstream boundary we have:

a) In the case of critical flow depth condition, the solution is given by Eq.(6) along with Eq.(15) applied for the grid points N and N-1.

b) Zero depth gradient condition, assuming the Manning formula for the friction slope, yields:

$$Q_N^{n+1}=\frac{\sqrt{S_o}}{n_*}\frac{\left(A_{N-1}^{n+1}\right)^m}{\left(B+2\dfrac{A_{N-1}^{n+1}}{B}\right)^{m-1}} \tag{16}$$

where n_* is the Manning coefficient and m=5/3.

3.3 Kinematic Waves

Equation (1) along with Eq. (4) can be rewritten as:

$$\frac{\partial A}{\partial t} + \frac{\sqrt{S_0}}{n_*} m R^{m-1} \left[1 - \frac{2}{B}\left(1 - \frac{1}{m}\right) R \right] \frac{\partial A}{\partial x} = 0$$

(17)

$$Q = \frac{\sqrt{S_0}}{n_*} R^{m-1} A$$

where R is the hydraulic radius. Equations (8) and (9) is applied to Eq. (17), for interior grid points. At upstream end the solution is determined by Eq.(6) with A given by Manning's formula; whereas at the downstream end the characteristic equations derived by Eq. (17) furnish the value of A:

$$\frac{dA}{dt} = 0$$

(18)

$$\frac{dx}{dt} = \frac{\sqrt{S_0}}{n_*} m R^{m-1} \left(1 - \frac{2}{B}\left(1 - \frac{1}{m}\right) R \right)$$

4 EXPERIMENTAL TESTS

For estimating the errors of the KW and DW approximation the water flow depth profiles have been investigated for different values of kinematic wave number, K, and Froude number, F_0. These parameters are usually used in literature to represent the role of each force in the momentum equation and they are defined, referring to Q_0 and H_0, as:

$$K = \frac{S_0 L}{H_0 F_0^2}$$

(19)

$$F_0 = \frac{Q_0}{A_0 \sqrt{g H_0}}$$

where H_0 is the normal depth for the steady discharge Q_0. Sixteen cases were considered for each boundary condition involving F_0 = 0.1, 0.5, 0.8, 1.0 and K=3, 5, 10 and 30. For a fixed pair (K, F_0), the geometric and hydraulic characteristics of the channel were computed in order to obtain a reasonably steady state flow value, Q_0. Table 4-1 shows these characteristics for each pair (K, F_0) along with the concentration time, T_0.

Following Singh and Aravamuthan (1995) the accuracy of kinematic-wave and diffusive-wave approximations was assessed by comparison of steady water profiles over the channel with those given by the dynamic-wave solution used as a benchmark. For a systematic comparison, the results are shown in dimensionless form with the normal flow depth:

(20)

$$H^* = \frac{h}{H_0}$$

along the dimensionless distance:

(21) $$X^* = \frac{x}{L}$$

For the numerical solution the spatial step, Δx, was fixed the same for all approximations, whereas the time step, Δt, was always given by the Courant condition (Richtmyer and Morton, 1967; Dawdy, 1990). The mass balance was checked for all test cases with a threshold for the error between the total inflow and outflow volume of 3%.
The error in the solution of an approximation (kinematic-wave or diffusion wave) in comparison with the dynamic wave solution was defined as:

(22) $$E = \frac{S - S_D}{S_D}$$

where S is the solution from the KW or DW approximation and S_D is the solution from the DYW representation, each computed in terms of flow depth.

Table 4-1: Hydraulic and geometric characteristics of the channel used for experimental tests as a function of the Froude number, F_0, and the kinematic wave number, K. For other symbols see text.

F_0	K	H_0 (m)	Q_0 (m^3s^{-1})	n, ($m^{-1/3}s$)	T_0 (s)	S_0	B (m)	L (m)
0.1	3	5.00	88	0.041	1430	$1.5x10^{-4}$	25	1000
0.5	3	1.20	82	0.011	1750	$3.0x10^{-4}$	40	3000
0.8	3	1.09	115	0.010	1140	$7.0x10^{-4}$	40	3000
1.0	3	0.80	134	0.005	2850	$3.0x10^{-4}$	60	8000
0.1	5	4.00	63	0.033	3190	$1.0x10^{-4}$	25	2000
0.5	5	1.00	78	0.011	2550	$3.1x10^{-4}$	50	4000
0.8	5	0.88	82	0.010	1710	$7.0x10^{-4}$	40	4000
1.0	5	0.84	145	0.006	4180	$3.5x10^{-4}$	60	12000
0.1	10	4.00	75	0.049	3190	$2.0x10^{-4}$	30	2000
0.5	10	1.12	93	0.017	2410	$7.0x10^{-4}$	50	4000
0.8	10	0.84	97	0.011	2610	$9.0x10^{-4}$	50	6000
1.0	10	0.91	163	0.008	4690	$6.5x10^{-4}$	60	14000
0.1	30	3.33	10	0.070	1750	$1.0x10^{-3}$	5	1000
0.5	30	1.33	96	0.029	2760	$2.0x10^{-3}$	40	5000
0.8	30	0.88	103	0.019	2990	$2.4x10^{-3}$	50	7000
1.0	30	0.85	148	0.012	5530	$1.6x10^{-3}$	60	16000

5 RESULTS

5.1 Critical Depth Downstream Boundary Condition

The shape of the dimensionless water profiles given by the KW approximation was substantially different from that derived by the DYW solution. For the KW approximation, the profile was independent of K and F_0, in accordance with the Saint Venant equation written in dimensionless form (Morris and Woolhiser, 1980), while the profiles estimated by DYW approximation exhibited a large variability in relation to these two parameters. Figure 5-1(a) and 5-1(b) show the dimensionless profiles for the DYW approximation for the case F_0=0.1 and F_0=0.5, respectively. The KW solution gave a flow depth

equal to H_0 ($H^*=1$) along the whole channel which is higher than that given by the DYW approximation, mainly for lower K and F_0 values. However for $F_0>0.5$ the KW solution was in a good accordance with the DYW solution in the upstream portion of the channel; from 70% of the channel length for $F_0=0.5$ up to 100% of the length for $F_0=1$.

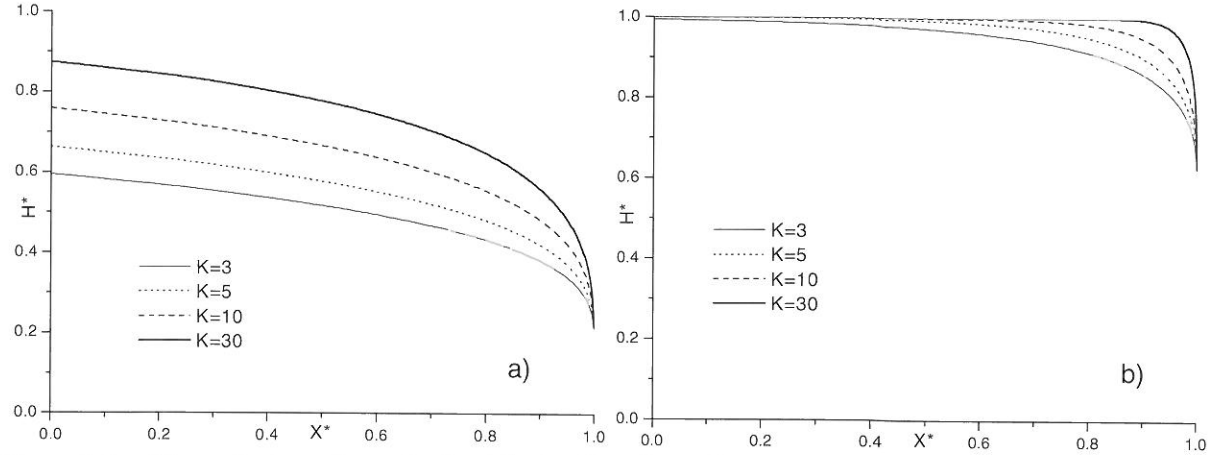

Figure 5-1: Dimensionless flow depth, H^*, by the dynamic-wave approximation as a function of dimensionless distance, X^*, for different values of kinematic wave number, K, and for Froude number, F_0, equal to (a) $F_0=0.1$ and (b) $F_0=0.5$. Upstream inflow is steady and downstream boundary is the critical flow.

The DW solution was not substantially different from that of the DYW approximation, as seen from a comparison of Figures 5-1(b) and 5-2(a) for the test cases with $F_0=0.5$. Specifically the DW solution gave a flow depth lower than that given by the DYW approximation, mainly for lower values of F_0 and K as shown in Figure 5-2(b). For $F_0>0.5$ the water profile shape was slightly different from DYW solution mainly in the region $0.5<X^*<1$. However, in accordance with the DYW solution, the dimensionless flow depth at the downstream end of the channel was independent of K and it was equal to $F_0^{2/3}$ (Pearson, 1989; Singh and Aravamuthan, 1995).

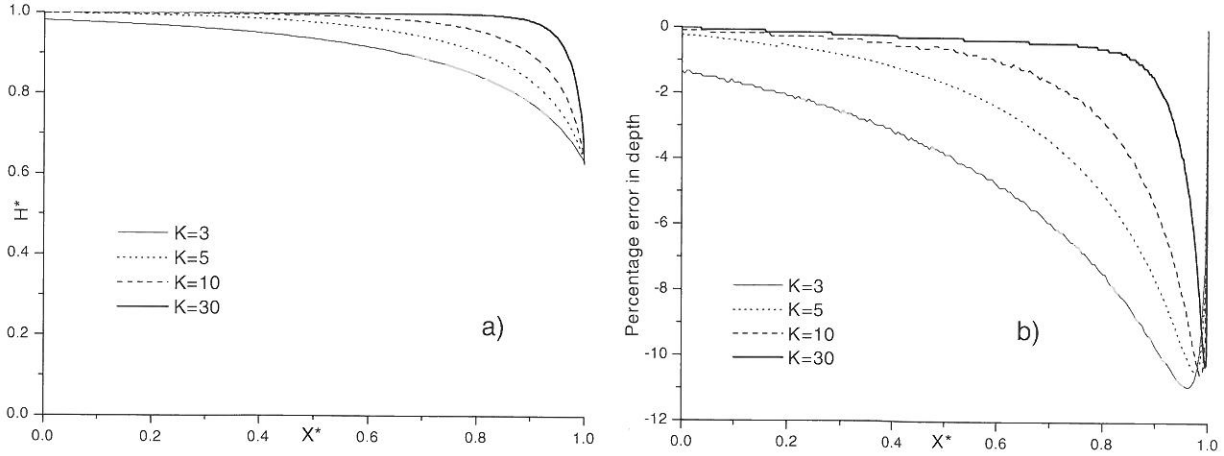

Figure 5-2: Diffusive wave solution for Froude number, F_0, equal to 0.5 and different value of kinematic wave number, K: (a) dimensionless flow depth, H^*, as a function of dimensionless distance, X^*; (b) error in flow depth compared to dynamic-wave solution. The upstream inflow is steady and downstream boundary is the critical depth.

Errors in flow depth, as defined by Eq. (22) for the KW approximation increased drastically in the region close to the downstream boundary, especially for low values of K and F_0. An overall analysis of the accuracy was done by using the mean value, ε, of the errors in magnitude within the channel region $0.05\leq X^*\leq 0.95$, where the KW approximation was not greatly influenced by the boundary

condition (Singh and Aravamuthan, 1997). The ε value was very close to zero for the pair (K, F_0)=(30, 1), whereas it increased up to 100% for (K, F_0)=(3, 0.1).
Assuming that the KW and DW solutions can be considered as an adequate approximation of the DYW solution for ε<5%, it was found that the KW accuracy increases with the Froude number. Particularly, the application field can be sketched by the rule:

$$KF_0^2 \geq 1.40 - 1.62\,(F_0 - 0.1) \qquad 0.1 \leq F_0 \leq 0.5$$

$$KF_0^2 \geq 0.75 - 2.00\,(F_0 - 0.5) \qquad 0.5 < F_0 \leq 0.8$$

$$KF_0^2 \geq 0.15 \qquad 0.8 < F_0 \leq 1$$

The DW solution furnished errors in flow depth lower than the KW approximation. They are shown in Figure 5-2(b), for the case F_0 = 0.5, where it can be seen that the maximum error occurs in the region close to the downstream end. The DW approach performed well the flow depth at the upper end with an error less than 4% for F_0 > 0.1, whereas in the region close to the downstream boundary the error increased up to 13 % for F_0 = 0.1 and K=3. The latter could be considered unacceptable for applications concerning the flooding area evaluation. Assuming for ε the threshold of 5% the DW solution can be applied by using the rule:

$$KF_0^2 \geq 0.03 + 1.42\,(F_0 - 0.1) \qquad 0.1 \leq F_0 \leq 0.5$$

$$KF_0^2 \geq 0.60 - 0.80(\,F_0 - 0.5) \qquad 0.5 < F_0 \leq 1$$

For F_0 > 0.5 the DW solution was found slightly less accurate than the KW solution This is due to the critical depth condition at downstream boundary which imposes a force balance in Eq.(1) among the convective inertial term, $\frac{\partial}{\partial x}(\frac{Q^2}{A})$, and the pressure term, $\frac{\partial}{\partial x}(\frac{1}{2}gBh^2)$, approaching zero more quickly than the only pressure force in Eq.(3). This aspect can be deduced by comparing Figures 5-3(a) and 5-3(b) where the inertial and pressure terms for the DYW solution and the pressure term for the DW solution are shown for the test cases (K, F_0)=(3, 0.1) and (K, F_0)=(3, 0.8), respectively.

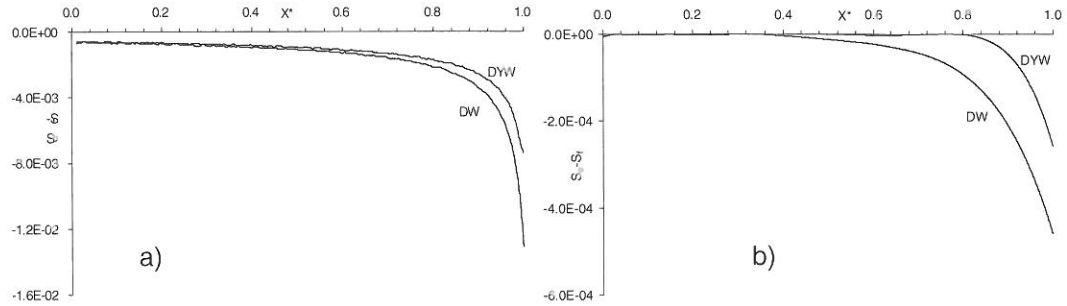

Figure 5-3: Inertial and pressure terms balance along the dimensionless distance X* expressed as the difference between channel slope and friction slope, S_0- S_f, for the dynamic solution (DYW) and diffusive solution (DW). Test cases with the kinematic wave number equal 3 and: (a) Froude number equal to 0.1; (b) Froude number equal to 0.8.

5.2 Zero-depth gradient downstream boundary condition

The shape of the dimensionless flow profiles given by both the KW approach and DW approach was found not substantially different from that of DYW solution with errors less than 2% along the whole channel. Moreover, for each F_0 and K value the water profile estimated by DYW solution was similar to that derived under the hypothesis of uniform flow. This occurs because the condition of zero depth gradient at downstream end along with a constant inflow at upstream end caused the inertial and pressure terms in the momentum equation to be negligible in comparison to the gravity force. In this context the KW solution could be applied in flooding risk evaluation studies.

However this downstream boundary condition has to be adopted carefully in natural channels because, for instance, a variation of the Manning roughness close to the downstream end of the channel is sufficient to make it not suitable for representing the water profile. In this case the boundary condition can be assigned through a rating curve yielding the KW solution unreliable. Figure 5-4 shows the dimensionless water profile estimated by the approximations considered in this analysis for the test case (K, F_0)= (3, 0.5) with the Mannning coefficient at downstream end assumed twice that of entire channel. As it can be seen the DW solution performs with a fair accuracy the DYW approach, whereas the KW solution, not depending from K and F_0, is really poor in representing the flow depth especially for low F_0 and K values.

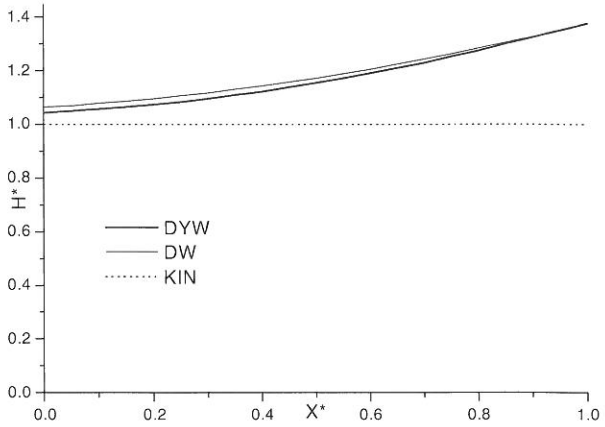

Figure 5-4: Dimensionless flow depth, H*, as a function of dimensionless distance, X*, for the dynamic (DYW), diffusive(DW) and kinematic-wave (KW) solution with Froude number F_0=0.5 and kinematic wave number K=3 and Manning roughness at downstream boundary twice that of the entire channel.

6 CONCLUSIONS

The kinematic and diffusive approximations for flow routing in natural channel have been investigated considering two different downstream boundary conditions under the hypothesis of steady state as often used in flood risk evaluation. The accuracy has been assessed using as benchmark the results given by the dynamic wave solution in the channel region not greatly influenced by the boundary conditions.

For the critical depth at downstream end, the KW solution was reasonably accurate for $KF_0^2 \geq 1.40$ and $F_0 \leq 1$. However, at the downstream end of the channel, the errors increased drastically, showing that, if accurate solutions are needed in the region close to the boundary, the KW should not be used. On the other hand, the DW approximation was almost accurate for $KF_0^2 \geq 0.6$ if $F_0 \leq 1$. Also in this case the maximum error occurred towards the downstream boundary where the flow depth was underestimated. Decreasing KF_0^2 the error increases and reaches the value of 13% that could be unacceptable for applications concerning the flooding area evaluation. Moreover, because of the convective inertial effects, the KW solution has been found slightly more accurate than the DW solution for Froude number greater than 0.6.

For the other downstream boundary investigated, zero-flow depth gradient, both the simplified approaches are found quite accurate for all cases investigated. However, this condition has to be applied carefully in natural channels where variations in the geometry and/or in the hydraulic parameters at the downstream end could occur.

ACKNOWLEDGMENTS

The authors wish to thank B. Bani, C. Fastelli and R. Rosi for their assistance. This work was supported by the National Research Council of Italy, in part under the Special Project GNDCI.

REFERENCES

Abbott, M.B. (1979): Computational Hydraulics. Pitman Publ. Ltd, London.

Daluz Vieira, J.H. (1983): Conditions governing the use of approximations for the Saint Venant equations for shallow surface water flow. J. Hydrology, 60, 43-58. Elsevier. Amsterdam.

Dawdy, D.R. (1990): Discussion on 'Kinematic wave routing and computational error'. J. Hydraulic Engineering, 114(2), 278-280. Am. Soc. Civil Engineering. Reston, VA.

Hromadka, II T.V., DeVries, J.J. (1988): Kinematic wave routing and computational error. J. Hydraulic Engineering, 114(2), 207-217. Am. Soc. Civil Engineering. Reston, VA.

Moramarco, T., Melone, F. (2000): Sull'applicabilità dell'onda cinematica e diffusiva per pioggia netta non uniforme lungo un piano. Atti XXVII Convegno di Idraulica e Costruzioni Idrauliche. Genoa University, Vol. II, 91-99.

Moramarco, T., Singh, V.P. (2000): A practical method for analysis of river waves and for kinematic wave routing in natural channel networks, Hydrological Processes, 14, 51-62. John Wiley & Sons, Ltd. Chichester, UK.

Morris, E.M. (1979): The effect of the small-slope approximation and lower boundary conditions on solutions of the Saint Venant equations. J. Hydrology, 40, 31-47. Elsevier. Amsterdam.

Morris, E.M., Woolhiser, D.A. (1980): Unsteady one-dimensional flow over a plane: partial equilibrium and recession hydrographs. Water Resources Research, 16(2), 355-360. American Geophysical Union. Washinghton.

Pearson, C.P. (1989): One-dimensional flow over a plane: criteria for kinematic wave modeling. J. Hydrology, 111, 39-48. Elsevier. Amsterdam.

Ponce, V.M., Li, R.M. and Simons, D.B. (1978): Applicability of kinematic and diffusion models. J. Hydraulic Division, 104 (HY3), 353-360. Am. Soc. Civil Engineering. Reston, VA.

Richtmyer, R.D., Morton, K.W. (1967): Difference Methods for Initial-Value Problems. John Wiley & Sons. Inc. New York.

Singh, V.P., Aravamuthan, V. (1995): Errors of kinematic-wave and diffusion-wave approximations for time-independent flows. Water Resources Management, 9, 175-202. Kluwer. Dordrecht, The Netherlands.

Singh, V.P., Aravamuthan, V. (1997): Accuracy of kinematic wave and diffusion wave approximations for time-independent flow with momentum exchange included. Hydrological Processes, 11, 511-532. John Wiley & Sons, Ltd. Chichester, UK.

Sivaloganathan, K. (1987): LAXWND - Computations for unsteady flows in open channels. Microsoftware for Engineers, 3(2), 94-100.

Woolhiser, D.A., Liggett, J.A. (1967): Unsteady, one-dimensional flow over a plane: the rising hydrograph. Water Resources Research, 3(3), 753-771. American Geophysical Union. Washinghton.

ASSESSMENT OF FLOODS IN A SMALL MOUNTAIN STREAM (SPANISH PYRENEES)

M. Rico, G. Benito

Centro de Ciencias Medioambientales-CSIC. Serrano 115 Bis, 28006 Madrid, Spain, mayte@ccma.csic.es

SUMMARY

This paper is focused on the combination of historical, palaeoflood and instrumental records applied to estimate magnitude and frequency of floods in a high-gradient small catchment in the Spanish Central Pyrenees: the Montardit basin, 15.2 km^2. Historical data corresponding to past floods occurring in the Montardit drainage basin during the 20th Century were compiled through interviews with inhabitants of villages located in the basin. The largest floods of the stream were recorded in November 1907, in August 1924 and in 1944. Palaeoflood techniques were used to estimate discharge values corresponding to seven cross-sections along the stream channel. The first four cross-sections (1-4) were located upstream of the alluvial fan in reaches where critical flow during flooding was assumed. Sections 5 to 7 were taken along the stream's final channelled reach (partially filled at the present). The methods of discharge estimation employed were (1) the critical-depth method in sections were critical flow during floods was assumed and (2) the Manning's equations using the approach proposed by Jarrett (1984, 1985). Two further methods of rainfall-runoff simulation were applied using precipitation data from gauging stations close to the basin: (1) the unit hydrograph method and (2) the modified rational method employed in Spain.
The results of the methods applied in this study suggest that for high-frequency, low-magnitude events there is a good correlation between peak discharges yielded by palaeoflood reconstruction (7 to 46 m^3 s^{-1}) and those estimated through rainfall-runoff modelling (8 to 46 m^3 s^{-1}). In contrast, high magnitude events show a higher historical frequency than that provided by rainfall-runoff methods. Bankfull discharges estimated in the cross-sections along the channelled reach on the alluvial fan (6 and 7) for the present-day channel geometry were 59 m^3 s^{-1}. Future floods surpassing that discharge would overflow the canal and inundate the topographically lower areas.

Keywords: Palaeofloods, Palaeohydrology, Rainfall-runoff methods, Mountain streams; Pyrenees, Spain

1 INTRODUCTION

Throughout the 20th century, the Montardit catchment, located in the Spanish Central Pyrenees (Figure 1-1), has suffered repeated flooding causing damage to property. In this small steep stream system flash floods are related to intense convectional thunderstorms produced during summer and autumn. However, the lack of an extensive network of precipitation gauging stations to accurately record the spatial and temporal distribution of this type of rainfall, hinders the prediction of flood events using methods based on precipitation data.
Over recent years new methods have been developed that permit the estimation of peak discharges when the use of conventional rainfall-runoff methods is unreliable. Several authors (Costa, 1987; Jarrett, 1987, 1990a; House, 1991; Martínez-Goytre et al., 1994) report the use of palaeoflood reconstruction methods to estimate the magnitude of palaeofloods in small mountain basins. Palaeoflood data may provide long term data applicable to flood frequency analysis, and may represent a more extensive record than the instrumental data sets used in rainfall-runoff methods, thus yielding much more reliable results (Stedinger and Baker, 1987).

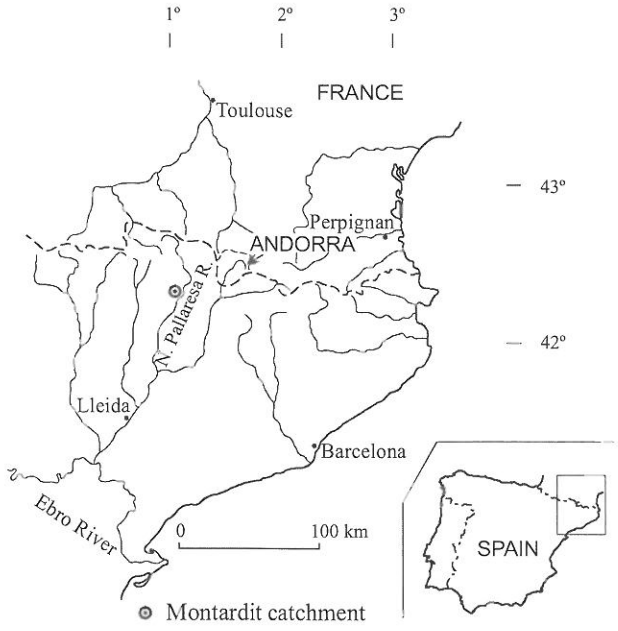

Figure 1-1: Location map of study area.

In this paper we describe the combination of historical, palaeoflood and instrumental records (through rainfall-runoff modelling) applied to estimate the magnitude and frequency of palaeofloods in a small mountain catchment and compare the results yielded by them.

2 DESCRIPTION OF THE STUDY AREA

The Montardit drainage basin (15.2 km^2) is located in the upper basin of the river Noguera Pallaresa, Spanish Central Pyrenees (Figure 1-1). The basin ranges in altitude from 2364 m to 660 m and has a mean slope of 14.9%. At its confluence with the main valley, the stream develops a wide alluvial fan of 1.8% mean slope.
The upper and middle basins are comprised of slates, shales, limestones, conglomerates and breccias, Palaeozoic in age (Zwart, 1979). The 2 km final reach flows through tuffites and andesites, Carboniferous in age, and gypsums, marls and limestones (Keuper facies) of the upper Triassic (Zwart, 1979). In this final reach lateral erosion of the main channel has lead to the development of an alluvial bed of 230 m maximum width and slopes from 3 to 5 % (Figure 3-1). The stratigraphy of infill deposits of this reach comprises coarse sediments generated by torrential flow dynamics overlain by fine sediments of homogenous grain size and spatially variable thickness (0.35-1.45 m).
Between 1925 and 1929 a canal, 900 m in length, was built along the alluvial fan reach (Figure 3-1) to prevent the overflowing and shifting of the channel during flooding and to protect the crops, the town of Ribera de Montardit and the motorway running over the fan surface (División Hidrológico-Forestal, 1925). Presently there are large amounts of deposits along the canal reach and in several places, the vegetation has colonised these deposits reducing the canal section and the stream's conveyance capacity.

3 METHODOLOGY

Information about the largest historical floods occurring in the Montardit basin during the 20th century was compiled. Thematic maps were drawn up using graphical documents (aerial photographs and historical maps) and field surveying. Finally, three methods were used for estimating flood peak discharges and flood frequency: two based on instrumental records, the modified rational and unit hydrograph methods, and a further method based on palaeoflood reconstruction.

3.1 Historical Flood Data

Written record (official documents and local chronicles) were reviewed in order to compile data corresponding to the largest historical floods in both the Montardit catchment and the reach of the river Noguera Pallaresa near the study area. The following historical floods have been recorded in the Noguera Pallaresa river: 1348, January 1433, autumn 1436, 1617, 1637, 1753, 1853, 1894, October 1907, October 1937, August 1963, November 1963, November 1967, April 1971, November 1982, September 1983 and November 1984 (Coy y Cotonat, 1906; Comisión Técnica de Inundaciones, 1985). However no significant damage was registered on any of the 20th century flood events in the Montardit basin.
Floods occurring in basins at a distance from large communities are not reported, so interviews with inhabitants were used to compile information on floods in the study area. These data reflect the direct experience of villagers or events related by the previous generation to their children and provide, especially for the Montardit basin, a detailed record of the largest floods occurring in the 20th Century and of the areas affected by these floods.
The first reference to major flooding of the Montardit stream is that of November 1907. In August 1924, a flood provoked the shifting of the channel and its waters invaded the northern side of the alluvial bed upstream the alluvial fan and flooded the village, with reports of two metres of water in some houses. In 1929, the channelisation works were completed. In 1944, a local storm caused great damage to the area as the strength of the water and transported materials broke the lateral containment wall of the canal. The stream flowed in its original natural course flooding the crops along its way. Transported materials were deposited in the middle and distal areas of the fan forming the lobe of boulders and gravel shown in the aerial photograph taken in 1957 (Figure 3-1). It is of note that the rainfall, during the 1944 event, was localised to such an extent that no substantial rainfall was recorded by any of the precipitation gauges close to the basin.

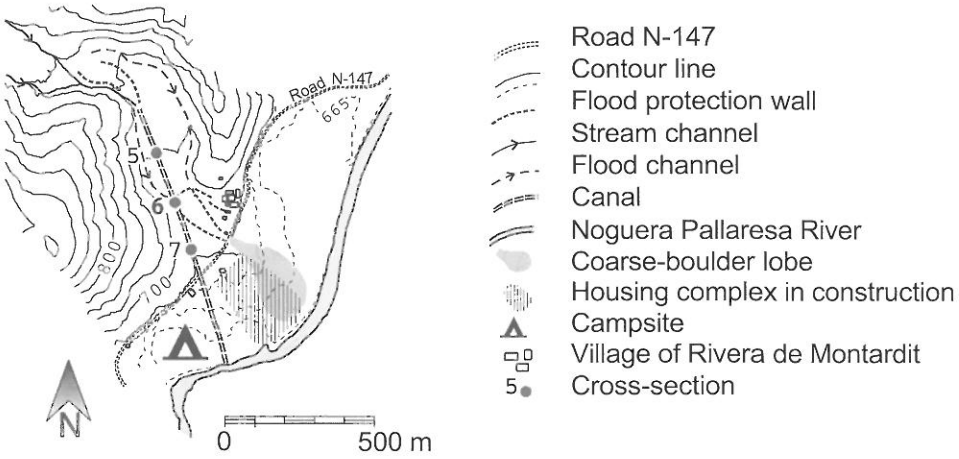

Figure 3-1: Topography of the alluvial fan and final reach of the Montardit stream.

Channel changes and areas affected by flooding were documented through the analysis of consecutive aerial photographs and historical maps, and supported by exhaustive field identification work. The 1957 aerial photograph shows the system of flood protection walls built by people living in the basin and the lobe of sediments deposited during the 1944 flood (Figure 3-1). To the north and south of this lobe there are no signs of recent (post-1957) fan activity in any of the graphical documents consulted. At the beginning of the 1990's, housing construction started on the most recently active sector of the fan (Figure 3-1). At present a campsite is located on the southernmost area of the fan, bounded to the north by the Montardit stream and to the south by the Noguera Pallaresa River and another small tributary stream.

3.2 Palaeoflood reconstruction

Palaeoflood reconstruction methods are based on the field identification of preserved palaeostage indicators and the geometric characteristics of the channel sections that can be used in standard hydraulic procedures for estimating peak discharges. In this paper two different methods were used depending on the hydraulic condition at each site: (1) the critical-depth method in sections where critical flow during floods was assumed and (2) the Manning's equations using the approach suggested by Jarrett (1984, 1985) in the estimation of Manning's n roughness coefficient for high-gradient mountain streams. In the present study, these equations were applied in sections with slope ranges from 0.028 to 0.046 (mm^{-1}).

The critical flow method (Chow, 1959) requires the field selection of sections fulfilling conditions of critical flow, but in contrast, does not depend on the arbitrary estimation of variables such as roughness or slope (O'Connor and Costa, 1993; Benito et al., 1998). For non-rectangular channel sections, critical velocity (V_c) is defined as the square root of the critical depth (y_c) multiplied by the acceleration of gravity (g = 9.8 m sec^{-2}). Stream flow (Q) through the section is calculated using the equation: $Q = A_c V_c$ (m^3 sec^{-1}), where A_c is the section area.

Using empirical data from numerous channels with slopes greater than 0.002 mm^{-1}, Jarrett (1984, 1985, 1987) developed an equation that uses energy gradient and hydraulic radius to predict the roughness coefficient, n, value. The Manning's equation may be re-formulated for estimating velocity and discharge in high-gradient natural channels as:

(1) $$V = 3.17 R^{0.83} S^{0.12}$$

(2) $$Q = 3.17 A R^{0.83} S^{0.12}$$

where V is the mean flow velocity in m sec^{-1}, Q is the discharge in m^3 sec^{-1}, A is the cross-sectional area of flow in m^2. The energy gradient (S) is either the energy gradient, or water-surface or bed slope if the channel is relatively uniform (Jarrett, 1990b). In this paper the bed slope has been used.

Seven cross-sections of the stream channel were selected and surveyed (Figures 3-1 and 3-2b) in reaches with evidence of high-water marks (HWM) or palaeostage indicators (PSI) associated with floods. The first four cross-sections (1, 2, 3 and 4) were chosen for their relatively stable geometry and due to their location a few metres upstream of a waterfall where critical flow during flooding was assumed. The most frequent flow stage indicators were drift wood and gravel bar surfaces.

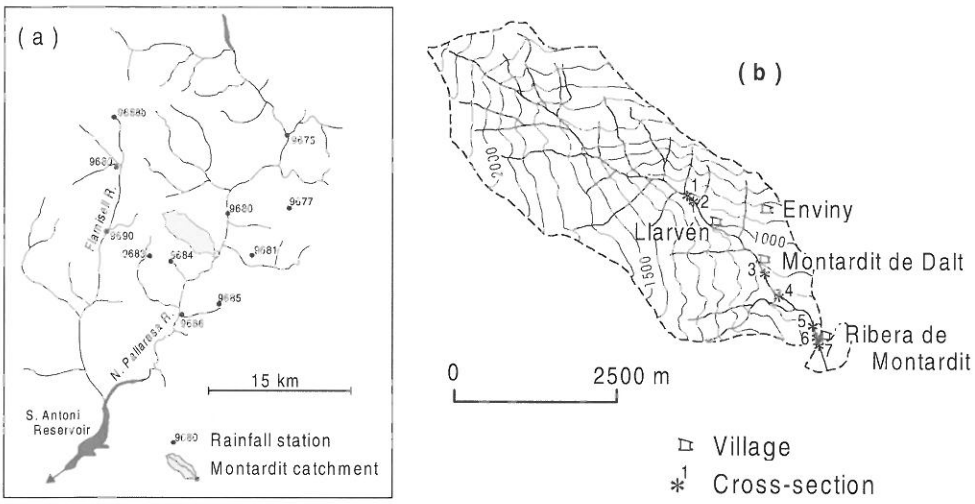

Figure 3-2: Location of the rainfall gauges (a) and cross-sections (b) (contour intervals is 100 m).

The remaining cross-sections (5, 6 and 7) are located in the lowest part of the basin and were selected for their high risk of overflowing during floods. Discharge values and bankfull peak discharges for these reaches were estimated using the Manning equation as modified by Jarrett (1984, 1985) for high-gradient streams (Equations (1) and (2)). A second discharge estimation for these cross-sections using the critical flow equation was obtained.
Sections 5 to 7 were taken along a partially filled canal reach (Figure 3-1), in stretches that are currently of smallest capacity and therefore present the greatest risk of overflowing during a flood. For each section, two possible situations were considered: (1) peak discharge flowing through the clean, deposit-free canal; and (2) peak discharge, taking into account current vegetation and canal infill.

3.3 Rainfall-runoff methods: rational and unit hydrograph

Two rainfall-runoff methods were applied: (1) the rational method which provide peak discharges for different recurrence periods and (2) the unit hydrograph method that, in addition, permits the complete reconstruction of the hydrograph. In this study a modified rational method adapted to the specific climatic conditions of Spain was used. This method, proposed and developed by Témez (1991), is extensively used in Spain for natural watersheds with surface areas up to 3000 km^2 and concentrate time (T_C) ranging from 0.25 to 24 hours (Témez, 1991; M.O.P.U., 1990). The following calculation formulas were proposed by Témez (1987, 1991):

$$Q = (1/3.6) \cdot CIAK \tag{3}$$

where Q (m^3 sec^{-1}) is the peak discharge, I (mm h^{-1}) is the maximum average intensity for the duration interval equal to concentration time, C is the runoff coefficient for the interval in which I is produced, A (km^2) is the area of the tributary watershed, and K is the uniformity coefficient. Remaining formulas for estimate these parameters can be found in Ferrer (1993) and MOPU (1990). Also the equations recommended for the modified rational method were used to calculate the concentration time (T_C).
Statistical analysis were carried out on the basis of the rainfall data (the highest rainfall value recorded within a 24 hour period for each year) sets from 11 rain gauges situated in the surrounding areas of the basin (Figure 3-2a). For the statistical analysis the two-parameter distribution SQRT-Exponential Type Distribution of Maximum (SQRT-ET$_{max}$) was applied and the parameters were estimated using Maximum Likelihood (ML) estimators. The reduction factor per area (K_A) was estimated through the following equation, $K_A = 1 - (Log_{10} A / 15)$, where A is the surface area of basin, in km^2, yielding a value of 0.92. Areal precipitation (P_A) was calculated using the modified Thiessen method.

In the modified rational method to obtain the volume of rainfall leading to surface runoff, the runoff threshold parameter (P_O) was used. This parameter has been related by Ferrer (1993) to the curve number (CN) devised by the S.C.S. (U.S. Soil Conservation Service, S.C.S., 1972), through the equation: $CN = 1000 / (10 + 0.2\ P_O)$. The value of the runoff threshold parameter, P_O, as the curve number, depends on the soil, cover and hydrologic condition of the land surface. Maps were drawn up to define soil types, vegetation and slopes using 1:33,000 aerial photographs, 1:25,000 orthophotographs and 1:250,000 land-use maps. Through fieldwork, the specific maps were completed. The maps were drawn using the different categories of soil, vegetation and land use as defined by the S.C.S. for the calculation of CN. In Spain, this parameter (P_O) needs to be adapted to the rainfall characteristics of the study area using a correction coefficient (Témez, 1991) reflecting the regional variation of background soil moisture conditions before rainfall-produced floods. Once the runoff threshold correction factor, which takes on a value of 1.8 in this area, was applied, resultant runoff thresholds were 26.2 mm.
An aggregate basin model was considered for the unit hydrograph method, due to the lack of major subcatchments. As the available precipitation gauges only record one measurement every 24 hours there are no available data for defining a historic storm, thus synthetic hyetographs were obtained using an intensity-duration curve and applied in both rational and unit hydrograph method. The lag time (T_{LAG}) was calculated according to the formula proposed by the S.C.S. for small basins with mainly overland-flow. The HEC-1 programme (U.S. Army Corps of Engineers, 1990) was used to transform the hyetograph into the hydrograph.

Table 3-1: Measured and estimated hydraulic parameters for several high-water marks and palaeostage indicators at the different cross-sections of the Montardit stream.

Site	Stage* indicators	Method**	A (m^2)	R (m)	S ($m\ m^{-1}$)	Vc*** ($m\ sec^{-1}$)	Qc ($m^3\ sec^{-1}$)	n	V**** ($m\ sec^{-1}$)	Q ($m^3\ sec^{-1}$)
1	HWM	CF	14.4	0.58	0.075	4.2	60	----	----	----
	HWM	CF	23.6	0.87	0.075	4.6	108	----	----	----
2	HWM	CF	7.6	0.84	0.152	4.1	31	----	----	----
	HWM	CF	5.7	0.72	0.152	3.8	21	----	----	----
3	HWM	CF	9.5	0.45	0.123		31	----	----	----
	HWM	CF	5.4	0.28	0.123	2.9	16	----	----	----
	HWM	CF	2.6	0.37	0.123	2.5	7	----	----	----
	PSI	CF	9.5	0.45	0.123	3.3	31	----	----	----
	HWM	CF	13.1	0.60	0.123	3.5	46	----	----	----
	PSI	CF	26.0	1.12	0.123	4.3	112	----	----	----
4	HWM	CF	2.6	0.33	0.144	2.5	7	----	----	----
	HWM	CF	6.6	0.72	0.144	3.4	22	----	----	----
5	B (1)	CF/M	19.1	1.36	0.046	5.2	99	0.095	2.8	54
	B (2)	CF/M	24.4	1.70	0.046	5.2	127	0.091	3.4	83
6	B (1)	CF/M	12.7	1.14	0.046	4.6	59	0.097	2.4	31
	B (2)	CF/M	17.0	1.32	0.046	4.6	79	0.095	2.8	47
7	PSI	CF/M	4.6	0.46	0.028	2.4	11	0.093	1.1	5
	B (1)	CF/M	14.7	1.20	0.028	4.0	59	0.080	2.4	35
	B (2)	CF/M	15.1	1.21	0.028	4.0	61	0.080	2.4	37

A: Cross-sectional flow area; R: Hydraulic radius; S: Channel slope; n: Manning coefficient according to Jarrett's equation for high-gradient streams ($n=0.32S^{0.38}R^{-0.16}$)

* HWM: High Water Marks; PSI: Palaeostage Indicators; B: Bankfull stage (1: current conditions; 2: clean conditions)

** Calculation method: M: Manning's equation; CF: Critical flow equation

*** Vc and Qc: Flow velocity and discharge assuming critical flow

**** V and Q: Mean flow velocity and discharge using Manning's equation

Table 3-2: Peak discharges estimated for the Motardit basin according to the rational, modified by Témez (1991), and unit hydrograph methods for different recurrence periods.

Method*	P_0 (mm)	T** (h)	Q2*** (m3 s-1)	Q5 (m3 s-1)	Q10 (m3 s-1)	Q25 (m3 s-1)	Q50 (m3 s-1)	Q100 (m3 s-1)
U.H.M.	26	TLAG	8	19	29	44	58	72
M.R.M.	26	TC	13	24	32	46	58	70

PO: Runoff threshold (mm)

* Calculation methods: U.H.M.: Unit Hydrograph Method; M.R.M.: Modified Rational Method

** T: Time parameters (in hours): TLAG: Lag time; TC: Concentration time

*** Q2, Q5, ...: Peak discharges (m3 sec-1) for each recurrence period: 2, 5, ... years

4 RESULTS AND CONCLUSION

The results of the different methods applied are showed in Tables 3-1 and 3-2. Palaeostage indicators and high-water marks of the recent floods within the last few decades provided peak discharges ranging from 7 to 46 m^3 s^{-1} which are similar to those obtained for rainfall events with recurrence periods of 2-25 years. The highest peak discharge estimated using palaeostage indicators (scar on tree) was 112 m^3 s^{-1} (section 3) which would correspond to recurrence periods up to 100-years according to results provided by rainfall-runoff methods.

The cross-section 6 coincides with the reach that overflowed during the 1944 flood. The maximum peak discharge estimated to flow through this section was 79 m^3 sec^{-1}, indicating that over the last 70 years, a flood of similar discharge was produced at least once. High-water marks in cross-section 1 (upstream of the channelled reach) provided discharge estimates of up to 108 m^3 sec^{-1}. This discharge may correspond to the 1944 flood which did not overflow banks in cross-section 5 (bankfull discharge of 123 m^3 sec^{-1}) but it did at cross-section 6 (bankfull discharge of 79 m^3 sec^{-1}). Discharge estimated in section 3 (112 m^3 sec^{-1}) may correspond to a previous flood (1907 or 1924). Magnitude ranking for the 20th Century floods is difficult to establish because the flood potential effects (level of perception by inhabitants) were modified by the canal construction, finished in 1929. Nevertheless, according to interviews, the 1924 flood was bigger than the 1944 one and, at least, two floods (1924 and 1944) of a similar magnitude (Q> 79 m^3 sec^{-1}) occurred in a 21-year interval, which according to hydrometeorological methods would correspond to recurrence periods of over 100-years.

Considering present-day channel geometry, bank overflow (bankfull) discharge in the stream's final channelled reach on the alluvial fan (cross-sections 6 and 7) will be attained at a discharge of 59 m^3 sec^{-1} . Future floods surpassing 59 m^3 sec^{-1} would overflow the canal and inundate the topographically lower areas, which are presently occupied by cultivated land, a housing complex and the village of Ribera de Montardit.

The results of the different models applied to the Montardit drainage basin suggest that for high-frequency, low-magnitude rainstorms there is a good correlation between peak discharge values estimated through palaeoflood reconstruction and those provided by rainfall-runoff methods. In contrast, evaluation of high magnitude rainstorms indicates a higher historical frequency than that predicted by rainfall-runoff modelling. The main reason for this discrepancy is that the extreme rainfall generating such floods in small basins is rarely monitored. Thus, only the combined use of historical information and both methods (palaeoflood reconstruction and rainfall-runoff methods) yields the necessary information to define the temporal and spatial occurrence of floods in small mountain watersheds.

REFERENCES

Benito, G. et al. (1998): The geomorphic and hydrologic impacts of the catastrophic failure of flood-control-dams during the 1996-Biescas flood (Central Pyrenees, Spain). Z. Geomorph. N. F.,42 (4): 417-437. Stuttgart

Chow, V.T. (1959): Open-channel hydraulics. McGraw Hill, New York

Comisión Técnica de Inundaciones (1985): Estudio de inundaciones históricas: mapa de riesgos potenciales, Comisión Nacional de Protección Civil, IV-VIII. Madrid

Costa, J.E. (1987): Hydraulics and basin morphometry of the largest flash flood in the conterminous United States. J. Hydrol., 93: 313-338. Amsterdam

Coy y Cotonat, A. (1906): Sort y comarca Noguera-Pallaresa. Imprenta y Litografía de la Viuda de José Cunill, Barcelona. (Reprinted 1974, Romargraf, S.A. Barcelona).

División Hidrológico-Forestal, 1ª. (1925): Proyecto de corrección del Torrente de Montardit. Encauzamiento. Memoria. Technical report, División Hidrológico-Forestal, ICONA, Madrid

Ferrer, J. (1993): Recomendaciones para el cálculo hidrometeorológico de avenidas. CEDEX M-37, Madrid

House, P.K. (1991): Paleoflood hydrology of the principal canyons of the southern Tortolita Mountains, southeastern Arizona. Arizona Geological Survey Open File Report, 91-6: 22 pp. Tucson

Jarrett, R.D. (1984): Hydraulics of high-gradient streams. J. Hydraul. Div. Am. Soc. Civ. Eng., 110: 1519-1539. New York

Jarrett, R.D. (1985): Determination of roughness coefficient for streams in Colorado. U.S. Geol. Surv. Water Resour. Invest., Report 85-4004. Washington D.C

Jarrett, R.D. (1987): Errors in slope-area computations of peak discharges in mountain streams. J. Hydrol., 96:53-67. Amsterdam

Jarrett, R.D. (1990a): Paleohydrologic techniques used to define the spatial occurrence of floods. Geomorphology, 3: 181-195. Amsterdam

Jarrett, R.D. (1990b): Hydrologic and hydraulic research in mountain rivers. Water Resources Bulletin, 26 (3): 419-429. Urbana

Martínez-Goytre, J. et al. (1994): Spatial variability of small-basin paleoflood magnitudes for a southeastern Arizona mountain range. Water Resour. Res., 30 (5): 1491-1501. Washington D.C.

M.O.P.U. (Ministerio de Obras Públicas y Urbanismo) (1990): Instrucción 5.2-IC. Drenaje superficial. Dirección General de Carreteras. M.O.P.U., Madrid

O'Connor, J.E., Costa, J.E. (1993): Geologic and hydrologic hazards in glacierized in North America resulting from 19th and 20th Century global warming. Natural Hazards, 8: 121-140. Dordrecht

Stedinger, J.R., Baker, V.R. (1987): Surface water hydrology: historical and paleoflood information. Reviews of Geophysics, 25: 119-124. Washington D.C.

Témez, J.R. (1987): Cálculo hidrometeorológico de caudales máximos en pequeñas cuencas naturales. Dirección General de Carreteras, M.O.P.U., Madrid

Témez, J.R. (1991): Extended and Improved Rational Method. Version of the Highways Administration of Spain. Proc. XXIV Congress. Madrid, Spain,. Vol A., pp. 33-40.

U.S. Army Corps of Engineers (1990): HEC-1: Flood Hydrograph Package, User's manual. U.S. Hydrologic Engineering Center, Davis, California

U.S. Soil Conservation Service (1972): National Engineering Handbook, Sec. 4, Hydrology, U.S. Department of Agriculture, Washington D.C.

Zwart, H.J. (1979): The Geology of the Central Pyrenees. Leidse Geologische Mededelingen, Leiden

ASSESSMENT ON RAINFALL EROSIVITY WITH REGARD TO THE FLOOD OCCURRENCE AT MAJOR RIVER OF PENINSULAR MALAYSIA

Roslan Zainal Abidin[1], Janmaizatulriah Jani[2]

[1] Faculty of Civil Engineering, Universiti Teknologi Mara, Shah Alam, Malaysia, drroslan@civil.engr.itm.edu.my

[2] Faculty of Civil Engineering, Universiti Teknologi Mara, Shah Alam, Malaysia, j_jan2000@yahoo.com.my

SUMMARY

In Malaysia, major flood events usually occur during the North – East Monsoon due to continuous heavy rainfall. As much as 9 % of the land areas in Malaysia, amounting to 29,000 sq. km is flood prone. Large floods had damaged properties, public utilities, cultivation, and loss of lives and also caused hindrance to social and economic activities. Average annual flood damage amounts to RM 100 millions as quoted by the Department of Irrigation and Drainage, Malaysia. In this context, rainfalls as the main agent in causing flood. Thus, the focus of this research is on analysing aspects of rainfall and particularly its erosivity with regards to flood occurrence. In order to get the idea of the erosive properties of rainfall, the intensity, duration, total rainfall and kinetic energy of the rainfall have to be considered. These properties are based on recorded flood event occurrence. By knowing all this properties, a relationship between amount of rainfall erosivity and the types of flood occurrence can be linked. The method adopted in analysing the rainfall erosivity is the R factor of the Universal Soil Loss Equation. Up to date, there is no research of this kind in creating a number with respect to the type of flood. As a result of this research finding, "ROSJAN's Numbers" has been created to relate the type of flood occurrence mainly minor, moderate and major/flash flood. It is hope that the outcome of this research can be used in forecasting the possible flood prone areas in Malaysia which depend on rainfall erosivity factor.

Keywords: Rainfall intensity, rainfall erosivity, kinetic energy, flash/major flood, Universal Soil loss Equation

1 INTRODUCTION

In Malaysia, major flood events usually occur during the North - East Monsoon due to continuous heavy rainfall. The largest floods on record occurred in 1926 and were followed by recurrence of severe floods as in 1931, 1947, 1954, 1957, 1967, 1971 and 1992. As much as 9 % of the land areas in Malaysia amounting to 29,000 sq. km are flood prone. Large floods had damaged properties, public utilities, cultivation, and loss of lives and caused hindrance to social and economic activities.
In the state of Kedah, Malacca, Negeri Sembilan, Perak, Perlis, Pulau Pinang and Negeri Selangor, no doubt that flooded areas are not widespread, since flash floods that subside quickly occur only at localised regions where considerable downpour occurred in a very short period. Nevertheless, destruction of properties in general is not at heavy losses, but subsequent interruptions such as traffic, social and economical activities are encountered. In this context, rainfall is the major important agent in causing flood. In order to get the idea of the erosive properties of rainfall, the intensity, duration, total rainfall, kinetic energy and rainfall erosivity of the rain have to be considered. Thus, the focus of this research is on analysing aspects of rainfall particularly its erosivity with regards to flood occurrence.

2 OBJECTIVE OF RESEARCH

The main objectives of this research are:

1. To record and assess cost of damage on assets property and death based on the flood occurrence
2. To determine the rainfall energy and rainfall erosivity during flood occurrence
3. To link the rainfall erosivity index in relation to flood occurrence and categorising flood type (e.g. major, moderate and flash flood)

3 SCOPE OF RESEARCH

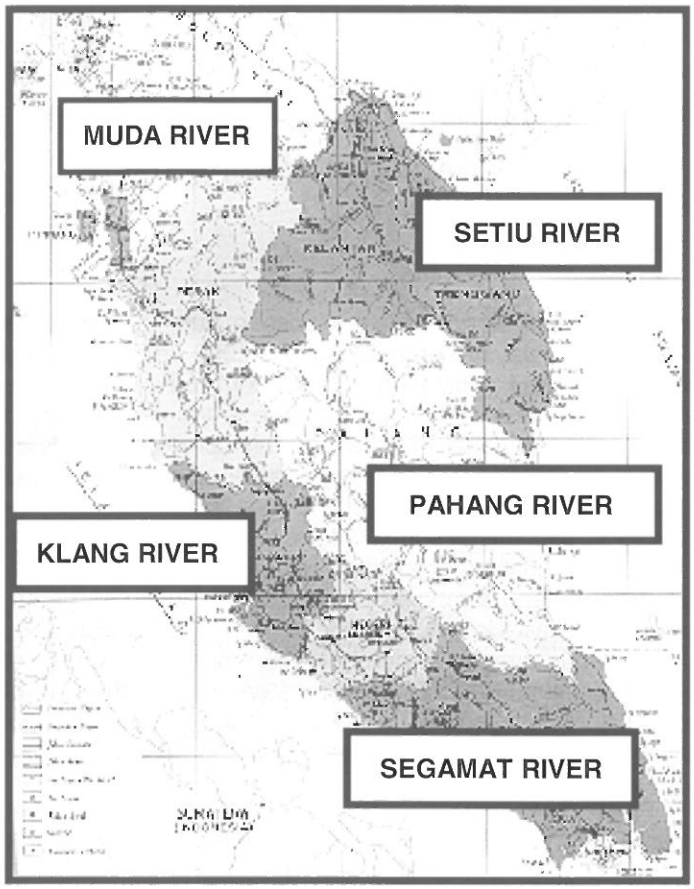

The scope of this research is on analysing aspects of rainfall particularly its erosivity with regards to flood occurrence. In order to get the idea of the erosive properties of rainfall; the intensity, duration, total rainfall and kinetic energy of the rain have to be considered. These properties are based on recorded flood event occurrence. By knowing all this properties, a relationship between degree of rainfall erosivity and the type of flood occurrence can be linked. The method adopted in analysing the rainfall erosivity is R factor of the Universal Soil Loss Equation (USLE). The outcome of this research can be used in forecasting the possible flood prone areas in Peninsular Malaysia, which depend on rainfall erosivity factor. The main study area of this research are at Muda river, Klang river, Setiu river, Pahang river and Segamat river as shown in Figure 3-1.

Figure 3-1: Study area of Main River in Peninsular Malaysia.

4 RESEARCH METHODOLOGY

The research methodology involved uses the existing information on flood occurrence for major river in Peninsular Malaysia such as rainfall and water level data. Basically, the breakdowns of the methodology adopted for the study area are as follows:

1. Thorough literature review on flood modelling system.
2. Collection of flood events from year 1997 – 1998 for each study area.
3. Collection of rainfall data and water level data based on data of flood event.
4. Analysis of rainfall data by using the USLE equation particularly the rainfall energy and erosivity.
5. Statistical analysis by using SPSS in order to prove that there is a correlation between the rainfall erosivity, type of flood and rainfall intensity.
6. Identify the link between degree of rainfall erosivity and intensity with type of flood for each main river in Peninsular Malaysia.

5 RECORDED FLOOD OCCURRENCE

In order to assess the link between the rainfall erosivity, type of flood and the rainfall intensity, five floods prone areas were identified which are located at five main states in Peninsular Malaysia. It includes of Muda river, Klang river, Setiu river, Pahang river and Segamat river. Selections of flood prone area are based on recorded flood occurrence and information with suggestion from the Department of Irrigation for each state (Department of Irrigation and Drainage, 2000).

6 RAINFALL DATA ANALYSIS

Rainfall data been analysis in order to determine the energy and how erosive the rainfall which can cause flood. Furthermore, this study will look into the relationship between the rainfall and the type of flood. At each river different rainfall station and water level station are used. These researches only take into account the increasing in water level, rainfall amount and rainfall intensity. By knowing the rainfall parameters such as the rainfall amount, duration and intensity; the rainfall erosivity can be determined by evaluating the R factor of the Universal Soil loss Equation. The rainfall data itself is collected during the time of flood event and the data are taken at every ten minutes interval. The data are taken from the time of continuous rainfall until the water level decrease. At this point, the water level being monitored so as to compares the rainfall data and the water level itself. Analysis of data differs from one study area to another because each study area has different geographical properties. Each analysis has different result on their rainfall intensity and erosivity. Whereby the amount and duration of rainfall influence the calculation. In this research, presumptions have been made which noted that the higher rainfall intensity would cause the major flood or flash flood. Table 6-1 shows the result of rainfall intensity and rainfall erosivity with respect to the date of rainfall and Table 6-2 shows the relationship between the rainfall intensity, erosivity and the type of flood for the main rivers of Peninsular Malaysia.

Table 6-1: Rainfall intensity and erosivity with respect to the date of flood among five main rivers in Peninsular Malaysia.

Rank No.	Date of rainfall	Rainfall intensity (mm/hr)	Rainfall erosivity ($J/m^2.hr$)
Klang river 1	15/7/99	13.2	142.8
2	12/7/99	14.1	387.63
3	28/3/99	15.2	590.52
4	16/5/99	16.5	188.9
5	18/5/99	17.34	199.5
6	22/3/97	19.71	437.80
7	19/11/97	19.89	728.42
8	10/11/98	25.02	931.5
9	18/5/99	26.18	528.35
10	10/7/99	26.33	701.05
Muda river 1	16/11/98	3.11	53.42
2	22/8/97	4.5	49.23
3	23/8/97	5.49	93.5
4	15/11/98	8.2	528.1
5	31/10/98	9.07	708.05
6	16/11/98	9.33	176.9
7	22/8/97	9.59	104.19
8	23/8/97	12.6	569.04
9	14/10/98	13.38	375.4
Pahang river 1	31/12/98	2.94	43.12
2	27/12/98	3.07	24.2
3	27/12/98	4.05	82.48
4	01/01/99	7.5	263.43
5	28/12/98	9.5	295.89
6	27/12/98	24.64	948.28
7	31/12/98	28.65	847.92
8	28/12/98	31.92	469.72
9	29/12/98	32	687.36
Segamat river 1	15/12-16/12	3.06	24.18
2	17/12-18/12	10	160.68
3	15/12-16/12	13.48	208.59
4	15/12-16/12	20.07	520.35
Setiu river 1	10/2/99	9.2	103.45
2	11/2/99	9.98	179.15
3	12/2/99	10.64	331.27

4	25/12/98	8.35	89.63
5	28/12/98	9.19	158.19
6	31/12/98	15	165.99
7	28/12/98	13.82	176.76
8	28/12/98	13.64	182.89
9	25/12/98	16.54	243.01
10	30/12 – 31/12/98	12.6	259.83
11	10/2/99	14.78	275.95
12	28/12/98	18.51	302.64
13	10/2/99	25.8	326.44
14	11/12/99	22.58	672.44
15	11/12/99	7.67	76.44
16	12/12/99	8.71	78.3
17	25/12/98	4.43	78.86
18	22/12/98	15.05	166.08
19	11/12/99	7.03	185.99
20	18/12/98	15.24	206.39
21	30/12/98	5.93	253.31
22	29/12/98	7.24	507.75
23	31/12/98	15.81	607.4
24	11/2/99	9.38	191.37
25	12/2/99	12.21	211.41
26	11/2/99	14.32	379.91

Table 6-2: Relationship between rainfall intensity, erosivity and type of flood among five main rivers.

DEGREE	RAINFALL INTENSITY mm/hr	RAINFALL EROSIVITY $J/m^2.hr$	TYPE OF FLOOD
STUDY AREA: KLANG RIVER BASIN			
1	< 6.5	< 100	MINOR
2	6.5 ~ 13	100 ~ 140	MODERATE
3	> 13	> 140	FLASH/MAJOR
STUDY AREA: MUDA RIVER BASIN			
1	< 6.5	< 100	MINOR
2	6.5 ~ 13	100 ~ 140	MODERATE
3	> 13	> 140	FLASH/MAJOR
STUDY AREA: PAHANG RIVER BASIN			
1	< 6.5	< 100	MINOR
2	6.5 ~ 13	100 ~ 140	MODERATE
3	> 13	> 140	FLASH/MAJOR
STUDY AREA: SEGAMAT RIVER BASIN			
1	< 6.5	< 100	MINOR
2	6.5 ~ 13	100 ~ 140	MODERATE
3	> 13	> 140	FLASH/MAJOR
STUDY AREA: SETIU RIVER BASIN			
1	< 9.0	< 100	MINOR
2	> 9.0	100 ~ 140	FLASH/ MAJOR

7 STATISTICAL ANALYSIS

In order to get the validity of results, statistical analysis was performed. Statistics deals with analysis of sample data and probability deals with the measure of chance of likelihood based on sample data. Hydrologic data could be suitable transformed into statistical parameters and can be treated with the theory of probability. It could be stated that hydrologic data are highly erratic and stochastic in nature so amenable to statistical interpretation and probability analysis.
An analysis of variance (ANOVA) was performed to determine if there were differences in the intensity and erosivity of rainfall values among the five rivers studied. An F-test did not indicate any differences in the erosivity (p value = 0.061) among the rivers studied. However, there are differences in the

intensity (p value = 0.01). Because of the differences, DUNCAN multiple comparison test was conducted. It was found that Muda, Pahang and Klang River were different in the intensity where the amount of differences of Klang River is 56.8% and Pahang River is 48% higher than Muda River respectively. In order to study the effect of intensity on the erosivity of rainfall, a regression analysis was performed. By linear regression analysis the R square value indicate that there are not very good linear relationship between the rainfall intensity and erosivity among the rivers. Since there is non-linear relationship, transformation of data was employed. In Figure 7-1 below, the value of coefficient of determination (R square) was found to be 0.6410. It is also obvious from the figure that most of the flood cases in Pahang, Klang and Setiu River lies in the zone of major / flash flood event whereas Segamat and Muda River lies in the zones of moderate and minor flood event respectively.

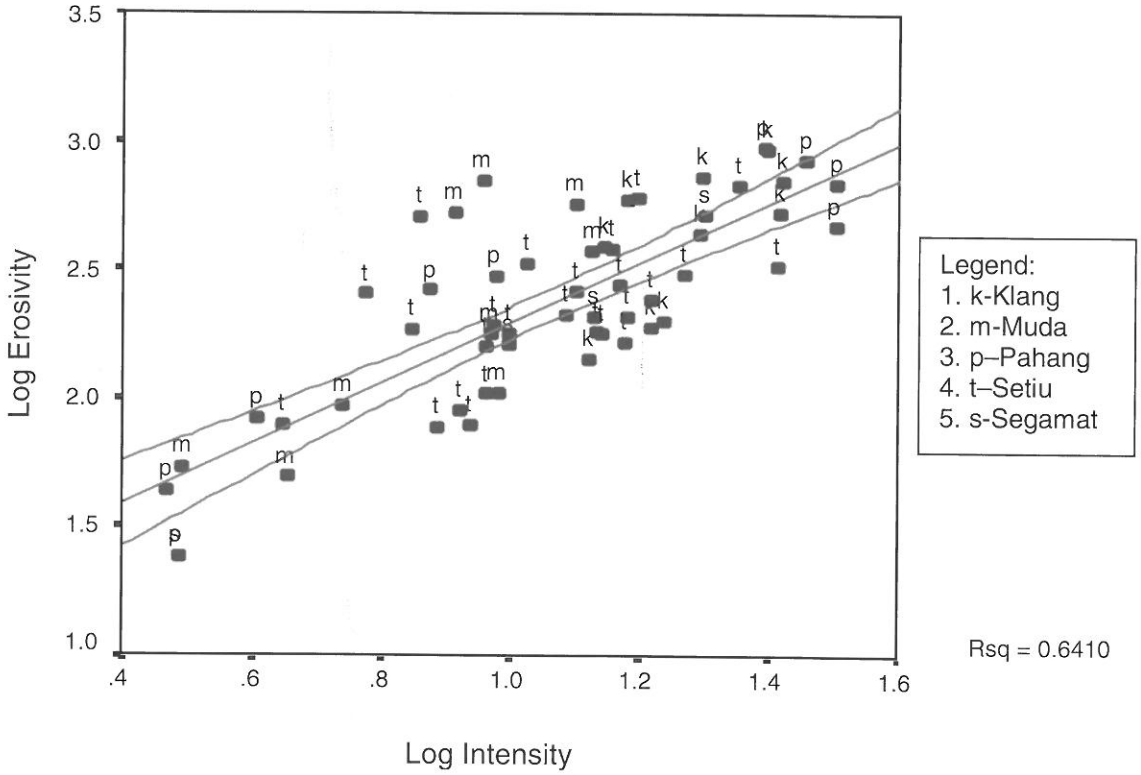

Figure 7-1: Log intensity and erosivity relationship with their respective rivers.

These indicate that only about 64% of the variation among the erosivity is encountered by the differences in intensity. The remaining 36% of the variation is due to other factors such as the geographical, flood area, soil penetration, urbanization, soil parameters and land use aspect.

8 DISCUSSIONS AND CONCLUSION

From the analysis of rainfall, it cannot be said that the rainfall intensity is proportional to rainfall erosivity. A range of values for rainfall erosivity as well as intensity has been established separately for each study area. According to Roslan (1993), there is a categorisation of rainfall intensity status that based on the amount of rainfall (i.e. low, moderate, high and critical). Based on that and from the research analysis, another relationship between the rainfall intensity and rainfall erosivity among five rivers in Peninsular Malaysia was found. Therefore, the flood categorisation was developed based on these two parameters.

An analysis of variance (ANOVA) was performed and indicates that there are differences in rainfall intensity among Klang, Muda and Pahang rivers. The differences are due to the location of the rivers and the amount of rainfall received in that area. By linear regression analysis, R square value indicates that there are not very good linear relationship in intensity and erosivity of rainfall among the five main rivers. Thus, transformation of data was employed. From the linear regression analysis, general range of values for rainfall erosivity as well as intensity to the type of flood occurrence can be finally established. This can be tabulated as follows:

Table 8-1: Establishment of relationship between RE, RI and flood type among major rivers.

Degree	Rainfall intensity (mm/hr)	Rainfall erosivity ($J/m^2.hr$)	Type of flood event
1st	< 6.5	< 135	Minor
2nd	6.5 ~ 14	135 ~ 290	Moderate
3rd	> 14	> 290	Major/Flash

9 CONCLUSION

From the research that has been carried out, there do exist relationship between the rainfall erosivity values and flood categorisation (i.e. as the value of rainfall erosivity increase, the type of flood occurred can be classified as major/flash flood event and vice versa) Nevertheless, rainfall intensity influenced the relationship between rainfall erosivity and flood categorization.
As for rainfall intensity, the relationship to the flood occurrence or categorisation can also be established (i.e. the higher the intensity, the flood occurrence can also be classified as major/flash flood event). Besides that, the maximum 30 minutes rainfall amount also influenced the value of rainfall erosivity. By statistical analysis, relationship between the rainfall erosivity and intensity was found. The basic linear equation given as:

(1) $$\log E = 1.172 \log I + 1.118$$

The outcome of this research can also leads to the creation of ROSJAN's number (after the name of researcher, Roslan and Janmaizatulriah) in terms of the type of flood categorization. This can be tabulated as shown in Table 9-2 below.

Table 9-2: ROSJAN's number.

Number	ROSJAN's	Flood categorization
1	< 27	Minor
2	27 ~ 52	Moderate
3	> 52	Flash/ major

It is hoped that this research findings can be used to predict future flood occurrence, type of flood for any area in the country and basic linear equation established can be applied and used internationally.

REFERENCES

Chow, V.T. (1975): Handbook of hydrology, Statistical and probability analysis of hydrological data, section 8-1 parts 1.

Department of Irrigation and Drainage, Ampang (1998): Flood Report For Malaysia for 1990-1997.

Department of Irrigation and Drainage, Kedah (1998): Flood Report (1997 & 1999).

Heiler T.D. and Chew H.H. (1974): Magnitude and frequency of flood in Peninsular Malaysia, DID hydrological Procedure No.4, Ministry of Agriculture and Fisheries, K.L. Malaysia.

Hosoyamada, K and Roslan, Z.A. (1991): On the calculation of rainfall erosivity factor with regards to soil erosion, Bulletin Faculty of Agriculture Miyazaki University vol. 38; pp 47 ~ 53.

Hosoyamada, K. (1981): On soil erosion by rainfall, Trans. JSIDRE 9; pp 8 ~ 14.

Hosoyamada, K. (1986): The effects of rainfall and soil properties on farmland conservation; Journal Irrigation Engineering & Rural Planning vol. 9; pp 6 ~ 10.

Department of Irrigation and Drainage, Ampang (Nov. 1993): International symposium on management of river for the future, Volume 1.

Laws, J.O Parsons, D.A. (1963): The relation of raindrop size to intensity, Transactions of geophysical union; page 452 ~ 460.

Mark L. et al.: Intermediate Statistical Methods & Applications, Prentice-Hall Inc.

M. Paul Mosley and Charles P. Pearson (1997): Flood and Droughts: The New Zealand Experience.

M. Paul Mosley (2000): Proceeding of Fresh Perspective On Hydrology And Water Resources in Southeast Asia & The Pacific.

Norman Hudson (1981): Soil Conservation - Second Editions, Cornell University Press.

"Rainfall erosivity": http://home.swipnet.se/valter/re.html

"Recent flood in Malaysia": http://agrolink.moa.my/jps/river/floodact.html

Santos A. (1970): The statistical treatment of flood flows, Water Power Vol. 22 No. 2.

"Suruhanjaya Tetap Banjir": Http ://agrolink.moa.my/jps/river/r.fww.html

Wischmeier, W.H. and Smith, D.D. (1958): Rainfall Energy And Its Relationship To Soil Loss, Trans. AM. Geophysics.

Wischemeier,W.H. & Smith, D.D. (1965): Predicting rainfall erosion from Cropland, Agri Handbook 282 USDA,

Yevjevich, Y.M. (1972): Probability and statistics in hydrology, Water Resources Publications, Fort Collins, Colorado.

Department of Irrigation & Drainage, Kuala Lumpur (2000): Flood report (1997 ~ 1999)

Department of Irrigation & Drainage, Kedah (2000): Flood report (1997 ~ 1999)

A PROCEDURE FOR THE IDENTIFICATION OF DOMINANT RUNOFF PROCESSES BY FIELD INVESTIGATIONS TO DELINEATE THE RELEVANT CONTRIBUTING AREAS FOR FLOOD MODELLING

Simon Scherrer[1], Norbert Demuth[2], Andreas Meuser[2]

[1] Scherrer AG, Hydrology and Flood Defence Strategies, Stockackerstrasse 25, 4153 Reinach, Switzerland, scherrer@scherrer-hydrol.ch

[2] Landesamt für Wasserwirtschaft Rheinland-Pfalz, Am Zollhafen 12, 55118 Mainz, Germany, Norbert.Demuth@wwv.rpl.de

SUMMARY

Intense field studies on runoff processes have been performed to improve the knowledge on flood formation. The measurements of overland, subsurface flow and soil water changes during sprinkler experiments yielded good information to identify the dominant runoff processes. Certain key-points could be recognised, which play a cardinal role in runoff formation. The combination of such key-points served to explain the runoff phenomena observed on the investigation sites. This knowledge provided the background to develop a general usable guide-line to define flood contributing areas and finally to estimate flood peak flows. The central part of this procedure consists of a process decision scheme to indicate the dominant runoff process on plot scale. First applications performed in several micro- and meso-scale catchments in Rhineland-Palatinate (Germany) confirmed the suitability of this tool for practical use.

Keywords: Dominant runoff process, overland flow, subsurface flow, process identification, field investigation, runoff formation.

1 INTRODUCTION

After every extreme flood event the question arises which are the major contributing areas in a river basin. When the extreme floods occurred in 1882/83, 1926 and 1993 in the river Rhine, groups of experts were convened to discuss this question. Besides the controversial influence of flood protection measures on flood generation (e.g. the straightening of the course of the Rhine River), the question of runoff formation in the basin is always crucial. To analyse which areas produce what quantity of discharge, the dominant runoff processes must be identified in the catchment. If in a catchment Hortonian Overland Flow, as a consequence of infiltration hindrance dominates runoff formation, generation and magnitude of a flood is influenced by a different way as if soils have first to be saturated to produce runoff and consequently Saturation Overland Flow is the relevant process. Is this question of process dominance spatially solved, it is possible to decide weather a modified land-use system can reduce the quantity of water that runs off. In addition, to estimate flood discharge in catchments where continuous and long runoff measurements are not available, such process knowledge yields substantial improvement.
In both cases, such improvements are not only of scientific interest but also are prerequisite to make a reliable decision where and how it is best to invest scarce financial resources to reduce flood damages. In this context, modelling tools to simulate the hydrological response of a basin have been available for many years. However, the quality of such simulations is often not satisfying due to the lack of understanding of fundamental hydrological processes. As a cheering prospect extensive field process studies provided progress in the last decade (e.g. Naef et al., 1998; Scherrer and Naef, 2002; Faeh, 1997). The Landesamt für Wasserwirtschaft Rheinland-Pfalz (Rhineland-Palatinate, Germany) in Mainz, responsible for flood protection measures and flood forecasts, supported efforts to adapt the new knowledge for the reconnaissance of flood formation. Thus, it was stimulated to summarise the knowledge (Leibundgut and Uhlenbrook, 1997) and to transpose the gained understanding on runoff processes in the development of a guide-line (Naef et al., 2000; Scherrer, 2001). This guide-line should enable to identify the dominant runoff processes in the field in order to define flood contributing areas.

2 PRECEDING STUDIES

Extensive field experiments have been performed to improve the understanding of runoff processes. With sprinkling tests on hill-slope plots of 60 m^2, runoff formation has been investigated by monitoring overland and subsurface flow and measuring soil water changes by field instruments installed on the plots (TDR-probes, tensio- and piezometers). This approach enabled the identification of the dominant runoff processes on 18 plots in Switzerland due to Infiltration Excess (Hortonian overland flow, HOF), due to soil saturation (Saturation Overland Flow, SOF), and Flow in lateral preferential pathways in the soil (Sub-surface Flow, SSF) and Deep Percolation (DP). Intense rainfall rates between 50 and 100 mm/h were applied for several hours which represent extreme rainfall events. The set-up of the experiment, the approach to identify the relevant runoff processes and the results are described in detail by Faeh et al. (1997), in Naef et al. (1998) and Scherrer & Naef (2002).
Big variation of runoff responses could be recognised from site to site. However, the observed runoff processes and runoff response could not be explained by usually applied parameters as antecedent soil moisture, topography (slope angle) or soil properties as texture or bulk density. Other approaches to derive runoff formation from soil type or land use also failed, since soil type classification is a qualitative assessment based on genesis and particle size distribution or stratification and typically do not consider hydrologically relevant properties. Thus, explanations were seek to bring light to the observed phenomena. Finally, criteria for every observed runoff process could be derived, which describe the conditions when the processes occurred. The 48 experiments on 18 predominantly as pasture used sites revealed that relevant factors are the vegetation-topsoil interface and the structure of the soil profile, so-called "key-points", that govern runoff formation. Figure 2-1 shows these "key-points" schematically on a soil profile.
The interface of vegetation cover, soil surface and top-soil was identified as crucial for the infiltration of water. If there is a relevant infiltration barrier in this zone, the storage capacity of the entire soil profile cannot be used. Such an infiltration hindrance is formed for example by surface sealing or soil crusts developing from splashed and dried soil aggregates. When the vegetation cover is dense enough, aggregates are protected from raindrop impact and thus aggregates do not collapse. Hydrophobic top-soil can also be responsible for infiltration hindrance. Excessively dry soils show a transient hydro-phobicity, while e.g. organic rich soils can be water repellent with persistency (Doerr et al., 2000). Macropores (earth worm channels, soil cracks, plant roots etc.) can bypass such infiltration hindrance when the initiation of macropore flow is ensured. The initiation of macropore flow and the water exchange between preferential flow paths and the soil matrix (interaction) are crucial in this context (Weiler, 2001). An extended macropore network in combination with an effective interaction with the soil matrix enables an excessive exploitation of storage volume. This volume is limited by the characteristics of soil texture, bulk density and profile depth. If the geological sub-stratum is impervious, the storage volume of water is limited by the soil profile. In contrary, the field experiments showed, that a permeable sub-stratum increases this potential, thus a macroporous soil profile hardly can be saturated. Highly permeable layers above an impeding layer or lateral soil pipes enable rapid lateral flow of water.
These process criteria served to identify the relevant runoff processes in more than 40 catchments (1 to 250 km^2). Available information on geology, vegetation, geomorphology and soils were collected and evaluated in respect to runoff processes. This information was combined with extensive field work including geomorphology, vegetation and land use and soil survey with special focus on soil profiles. Occasionally, additional field tests (infiltration tests, sprinkling tests on small plots) were performed to verify the process identification exemplary. This finally yielded the information to delineate the process areas and later flood contributing areas. The expected runoff response (runoff reaction curves) of these areas were derived from sprinkling experiments (Scherrer, 1996). Both information were used to run rainfall runoff models to simulate observed flood events and to extrapolate on extreme events. This procedure provides the model with physically based information. Consequently, the relevant model parameters are gained independently from model calibration.

3 STRUCTURE OF THE GUIDE-LINE

This guideline has been developed for the conditions (geology, soils, land use, topography) of Rhein-land-Pfalz (Germany) in central Europe (Scherrer, 2001). Nevertheless, the concept and structure of the guideline and the process identification scheme (decision tree) allows to be adapted easily to conditions in other climatic zones with different physical conditions.

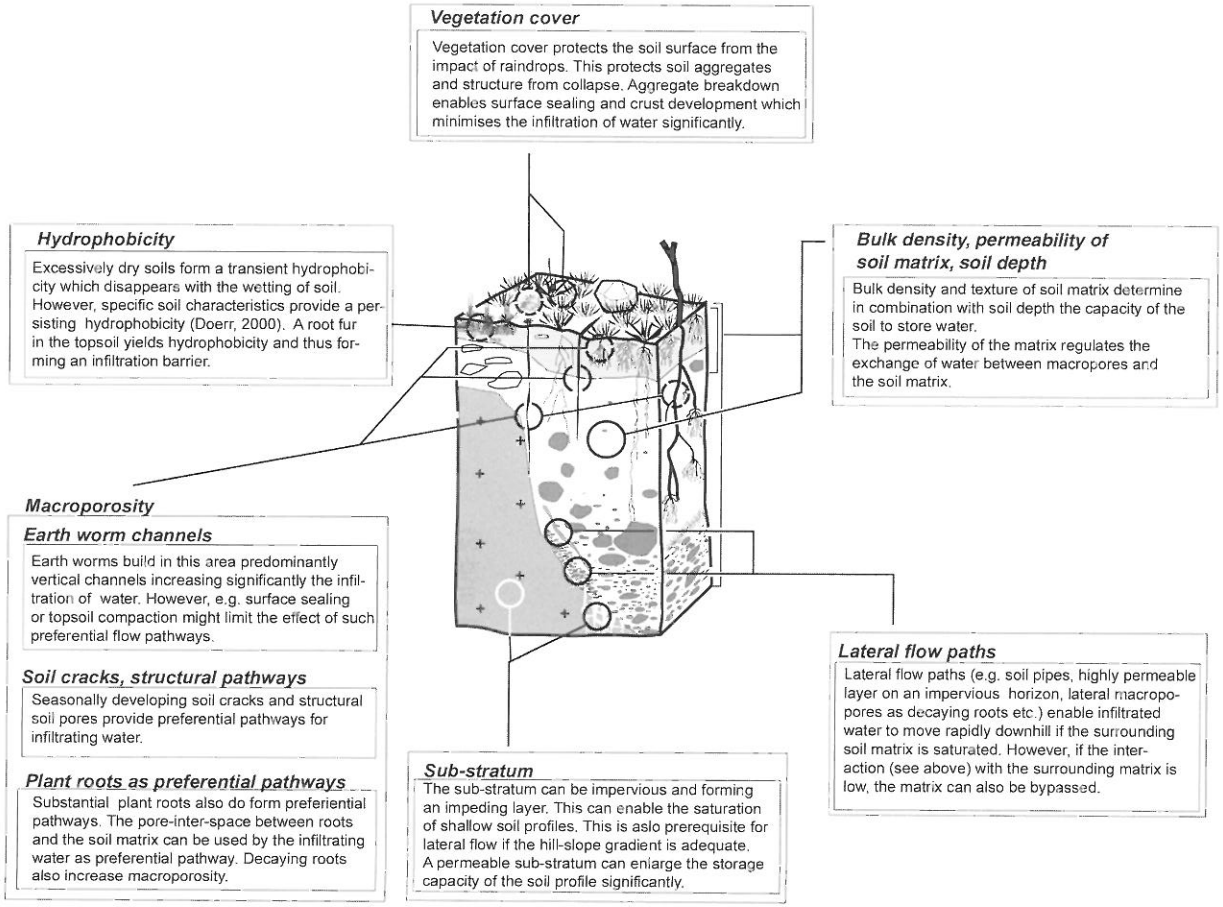

Figure 2-1: Relevant factors ("key-points") influencing infiltration of water into the soil and the movement of water across the soil, displayed as a schematic soil profile.

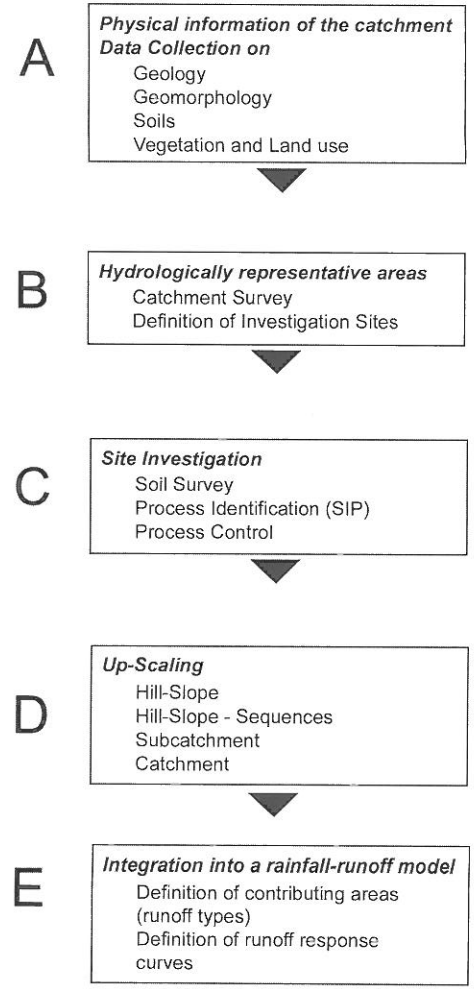

Figure 3-1: The procedure to apply the guideline for the identification of dominant runoff processes to delineate flood contributing areas.

The main steps of this guide-line to achieve a reliable process identification in catchments are illustrated in Figure 3-1. The experience of previous assessments revealed that a thorough understanding of the basins characteristics is prerequisite (A). This understanding is gained by evaluation of collected data on geology, soils, geomorphology and land-use. The survey of the catchment enables the recognition of hydrologically relevant and representative units with similar topography, geology, soils and land-use. This helps to locate the investigation sites (B). In the third step (C), at these sites soil profiles are assessed intensively due to the "key-points" outlined above. The registration of the relevant factors allows the application of the decision tree and the identification of the dominant runoff processes. The **S**cheme for the **I**dentification of dominant runoff **P**rocesses (SIP) illustrated in Figure 4-2 represents the central part of the guide-line. The structure and concept of the scheme has been described in detail by Scherrer and Naef (2002). The aim of the scheme structured as a decision tree was to adequately account for the range of processes and characteristics that can operate and interact to produce the runoff at a given site. The "key-points" evaluated in the experiments provide the framework of the scheme which corresponds to a soil column with horizons of vegetation, topsoil, subsoil and bedrock. The scheme allows the combination of different soil and site characteristics thus the wide range of variation can be considered. The scheme traces the rainfall water impacting the surface, moving vertically and horizontally into and across the topsoil, and through subsoil and bedrock. In the scheme, the user has to decide which criteria are fulfilled. At the end of a branch, a particular process is defined. The process verification is performed with additional hydrological field experiments. If, as an example, the process identification results as HOF (Hortonian Overland Flow), then infiltration tests or plot sprinkling experiments should be performed to confirm such infiltration hindrances. In contrary, if SOF3 (a very delayed Saturated Overland Flow) was evaluated, high infiltration rates are substantial. The next step (D) serves to up-scale the locally valid information of the dominant runoff process to hill-slopes, hill-slope sequences (see Figure 4-3), sub-catchments and finally to the entire catchment. Since up-scaling is still a problem to be solved in hydrology, an approach how to transpose the local information is presented in section 4.

4 PROCESS IDENTIFICATION IN THE IDARBACH CATCHMENT

In this section the process identification for rainfall events of low intensities (< 20 mm/h) is demonstrated in the Idarbach catchment. Figure 4-1 shows the topography of the catchment of 14.1 km^2 size. The annual rainfall rate is 1055 mm/a and about 20% of the catchment area are mapped as marsh or moist areas which refer to gleyic soils. The rest of the catchment area shows Cambisol soil type. The map also shows the 22 locations of field investigation (soil profile survey, infiltration and sprinkling tests) performed by Naef et al. (2000). In a first step, the identification of the dominant runoff processes is demonstrated at 2 sites located in the north eastern part of the basin used as arable land, pasture or meadow. The evaluation of the entire hill-slope sequence is shown exemplary and finally the process map is presented.

4.1 Process Identification at Plot-scale (Site 1 and 2)

4.1.1 The relevant factors

The scheme for the identification of dominant runoff processes requires data to evaluate soil and site characteristics ("key-points") outlined in Figure 2-1. Table 4-1 shows the relevant "key-points" and how to assess them in the field.
The location in the hill-slope sequence and structure of the soil profiles are shown in Figure 4-3. On site 1 (slope 5%) used as arable land (wheat), on the weathered quartzite bedrock consisting of stones and boulders, an acid sandy loam Cambisol (FAO, 1974) developed with a soil depth of 0.8 m. The topsoil (0.2 m) consists of humus with high root density but low earth worm activity. In the subsoil, fine material dominates the soil matrix, however the amount of stones and gravel increases with soil depth.

Table 4-1: The hydrologically relevant "key-points" in a soil profile. The table also gives a description of the relevant characteristics observed at site 1 and 2.

Horizon	"key-point"	Description and hydrological relevance	How to evaluate the criterion in the field	Site 1	Site 2
Vegetation	density of vegetation cover	Dense vegetation cover protects the soil surface from the mechanical impact of rain drops.	Scheme to evaluate the density of vegetation cover.	30-40%	30-40%
Soil Surface and Topsoil	aggregate's susceptibility for sealing effects and forming soil crusts	High content of humus, clay or $CaCO_3$ give stability to the aggregates and prevents aggregate collapse, surface sealing and soil crust development.	Sealing traces after intense rainfall (Römkens et al., 1990), from the quantity of clay, $CaCO_3$ or humus (AG Boden, 1994) the susceptibility for aggregate collapse and surface sealing can be estimated.	no	no
	surface roughness	Highly rough soil surface (e.g. ploughed soil) provides surface retention	estimated	smooth surface	smooth surface
	compacted soil matrix near surface	on arable land heavy machinery can compact soil matrix and infiltration of water is limited	estimated by soil profile survey.	no	no
	permeability of soil matrix	texture and bulk density of the matrix determine permeability	estimated by soil texture and bulk density (Rawls and Brakensiek, 1989) and AG Boden, 1994 adapted in Scherrer, 2001). Permeability > $5.5*10^{-6}$ m/s (ca. 20 mm/h) is evaluated as permeable in respect to low intensity rainfall events.	perme-able	perme-able
	macroporosity	An extended macropore network (e.g. earthworm channels, soil cracks, structural voids) influence the infiltration of water significantly and enable to bypass a less permeable soil matrix.	Macroporosity (macropore density) has to be assessed in different soil horizons. The number of macropores and diameter determine macroporosity (Scherrer, 2001).	few macro-pores	few macro-pores
	total soil depth increasing 0.4 m	determines besides permeability the storage volume for water	assessed by soil profile survey	yes	yes
	slope > 10%	The gradient to produce sub-surface flow e.g. on less permeable plough pans	assessed by soil profile survey	5%	15%
Subsoil	plough pan or subsoil compaction	Such a structure is a hindrance for infiltrating water.	assessed by soil profile survey	no	no
	matrix permeability	see above	see above	yes	yes
	total profile depth > 0.8 m	Profile depth determines beside other characteristics the storage volume for soil water.	assessed by soil profile survey	yes	no
Geology	permeable stratum	A permeable geology enables to expand the storage volume of the overlying soil.	estimated at profiles or from literature	no	no

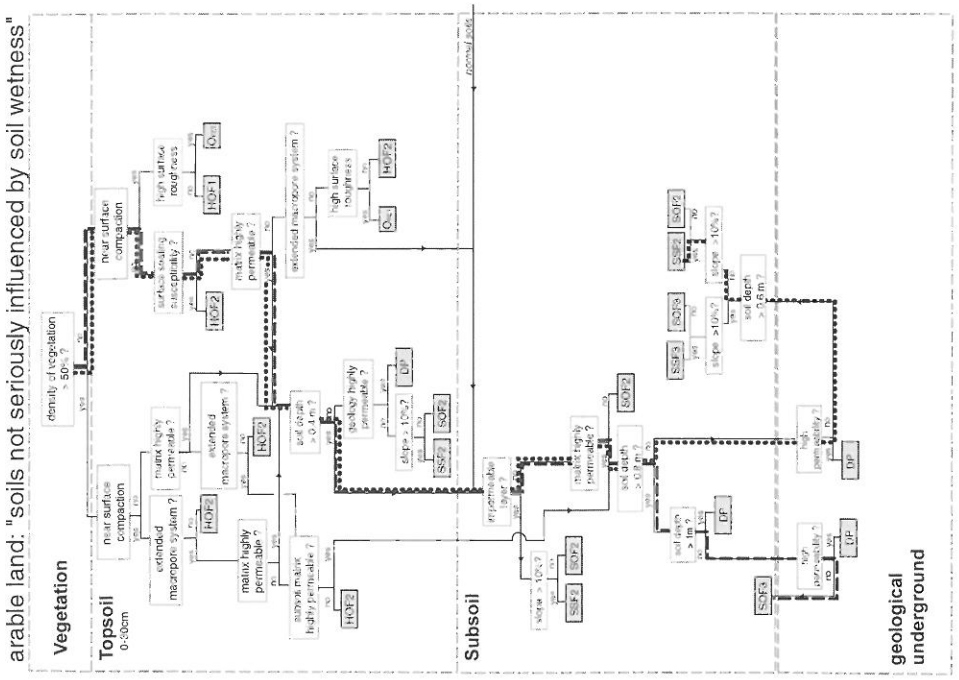

Figure 4-2: Scheme for the Identification of dominant Runoff processes (SIP) for arable land and slope 3 - 20%. The course of the process evaluation for site 1 (dashed line) and site 2 (dotted line) is also illustrated.
HOF1,2: Immediate and slightly delayed Hortonian Overland Flow,
SOF1-3: Immediate, slightly delayed and delayed Saturation Overland Flow;
SSF1-3: Slightly delayed, delayed and very delayed Sub-surface Flow.
DP: Deep Percolation, ORET: Surface retention.

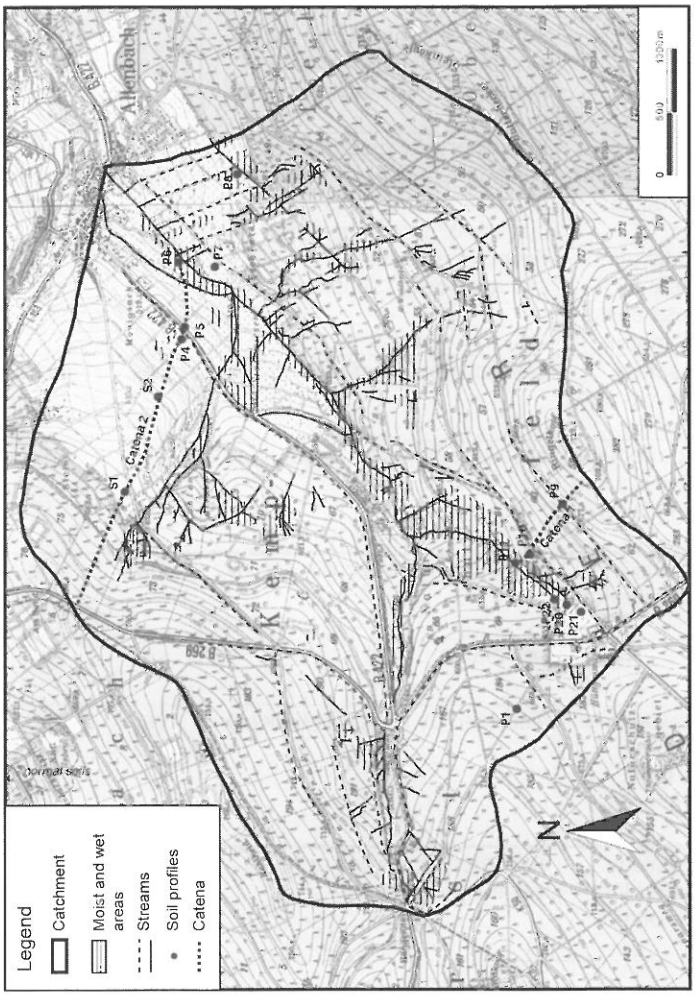

Figure 4-1: The Basin of the Idarbach (14.1 km²) in the Hundsrück mountain in Rheinland-Palatinate. The map shows the network of the creeks and ditches, the moist and wet areas mapped in the field (modified from Naef et al., 2000).

The steeper site 2 (15%) located about 500 m away from site 1 is also used as arable land. On the schist substratum a shallow soil profile (sandy loam Cambisol) of 0.8 m depth developed. The topsoil consists of an shallow A horizon and a A/B-horizon measuring 0.3 m which is influenced by ploughing impact. Both horizons are gravel rich (25%). The schist bedrock, however, is rather compact and forms an impeding layer.

4.1.2 Process Identification

To decide which runoff process is dominant at this site is supported by the process identification scheme. Figure 4-2 shows the scheme for arable land which is not influenced by soil wetness. In the decision tree the evaluated soil characteristics listed in Table 4-1 have to be assessed and consequently they determine the course of the evaluation illustrated with dashed (site 1) and dotted line (site 2). Following the lines, finally for site 1 SOF3 is evaluated and for site 2 SSF2 is reached as the dominant runoff process.

4.2 Processes at the hill-slope-scale

When the process identification is performed on the plot-scale, an up-scaling to hill-slope and hill-slope sequence is necessary. Figure 4-3 shows a schematic longitudinal section of the hill-slope where site 1 and 2 are located. In the relatively flat and forested area of the upper hills-slope permeable soils of 1 - 1.5 m depth enable deep percolation. Such a hill-slope does not contribute to flood runoff. In the subsequent forested hill-slope, after long and extensive rainfall events the infiltrating water reaches the relatively dense quarzite bedrock and flows laterally down-slope as a very delayed version of subsurface flow (SSF3). At site 1 water infiltrates in the permeable soil and a very delayed saturation of the soil profile occurs which results as SOF3. In the steeper part of the hill-slope sequence, at site 2, the combination of permeable topsoil with laterally permeable weathered bedrock and the impervious schist bedrock, provide the conditions for slightly delayed subsurface flow (SSF2). On the foot of the hill, this subsurface flow is forced to emanate to the surface due to the changing slope and nearly saturated soils building return Flow or slightly delayed SOF2. Finally, near the creek, a surface near water table produces fast reacting overland flow (SOF1).
When the local evaluation of site 1 and 2 is up-scaled, the question has to be answered how these processes influence one another. This question arises when a fast reacting process is situated upslope and might influence areas with a moderate runoff response located down-slope. In the actual hill-slope, such a situation is not present. In contrast to that, in alpine catchments fast reacting surfaces are frequently located in the periphery of a catchment as steep rocky surfaces or areas with shallow overburden. Then such influence becomes relevant and has taken into account.
In another step this thorough knowledge on runoff formation processes has to be transposed to subcatchment and catchments. Figure 4-4 shows the map of the dominating runoff process evaluated in the Idarbach catchment. In grey colour the overland flow processes are mapped, hatched surfaces refers to terrain where the dominance of subsurface flow processes is expected. On the one hand, 58% of the catchment area is dominated by subsurface flow processes and 16% of the areas do hardly contribute to flood generation due to deep percolation. Fast overland (SOF1) and subsurface flow (SSF1) is relevant for only 21% of the catchment area. Rapid runoff processes due to infiltration hindrance (HOF1, HOF2) are not relevant in this catchment.

4.3 The relevance of spatial distribution of dominant runoff processes for flood modelling

With the identification of relevant runoff processes in a catchment, the flood producing areas are assigned. The distribution of fast contributing areas in respect to delayed or non-contributing areas provides fundamental information for the model conception. Especially, when the question of dominance of infiltration excess or soil saturation processes is solved, the principal reaction of the catchment can be predicted.
From this spatial distribution of the dominant runoff processes shown in Figure 4-4 it can be concluded that the major part of the catchment has a slightly delayed or delayed runoff response (SSF1, SOF2, SOF3, DP, SSF2, SSF3). When a short thunderstorm hits the Idarbach, only the areas of SOF1 and HOF2 will be active and contribute to runoff. In contrary to this, long and extensive rainfall events will activate the bigger areas of the processes with delayed response. In this case, it can be supposed that the longer rainfall events produce the major floods. However, the question which scenario is relevant has to be solved with a rainfall runoff model taking such principle difference in runoff processes into account.

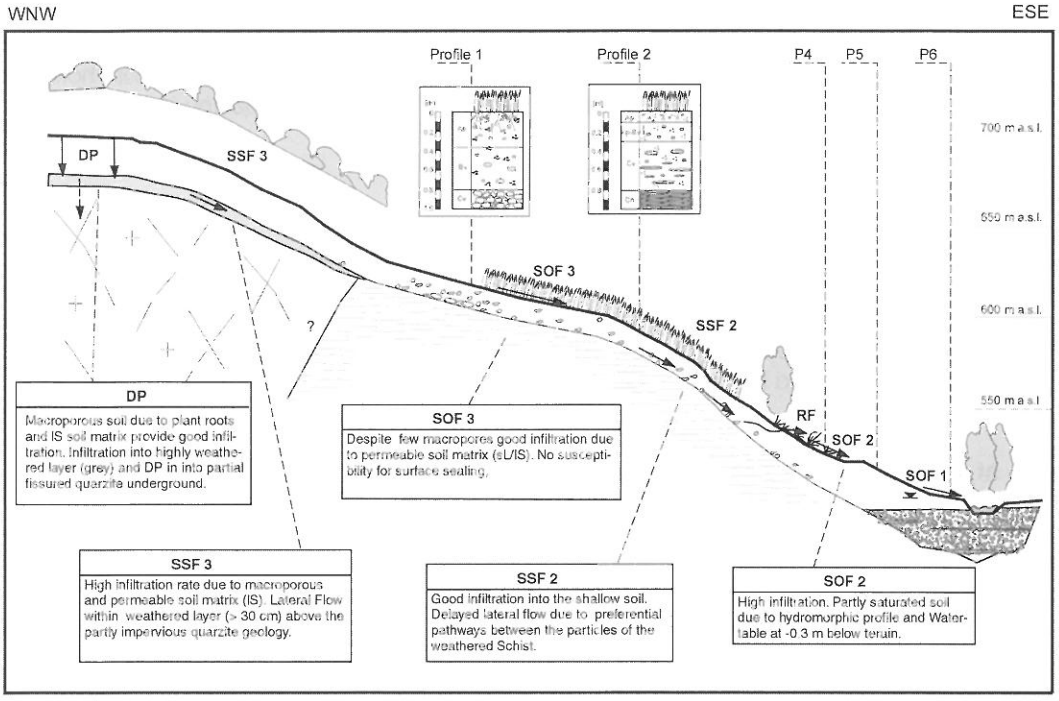

Figure 4-3: Hill-slope sequence with soil profiles of Site 1 and 2 and identified dominant runoff processes. (Abbreviations: HOF = Hortonian Overland Flow, SOF = Saturation Overland Flow, SSF = Sub-surface Flow, DP = Deep percolation; IS = loamy Sand.
Figure from Naef et al. (2000), slightly modified.

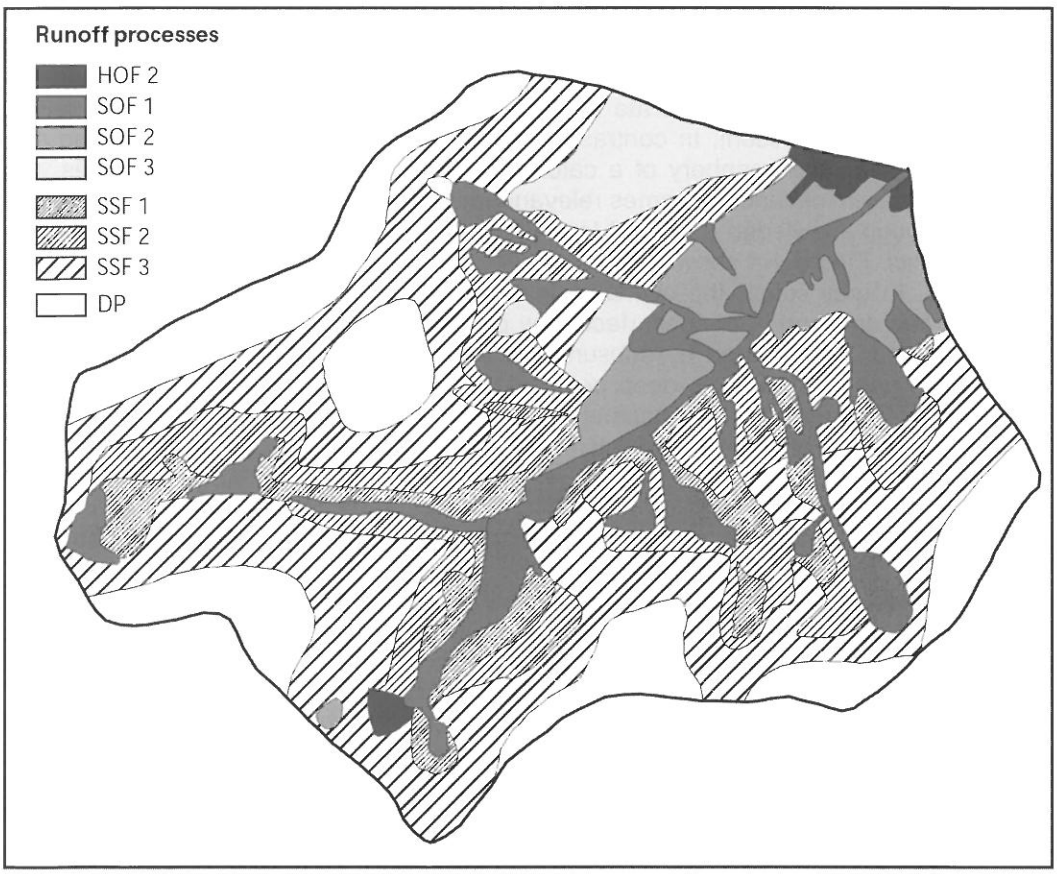

Figure 4-4: Map of the spatially distributed runoff formation as dominant runoff processes valid for extensive rainfall events (Abbreviations: see legend of Figure 4-3 above).

To integrate such process information in a model needs some simplifications if not every single process should be simulated which normally makes models dull and slow. One approach is to summarise areas of processes with similar hydrological behaviour as so-called runoff type. HOF1, HOF2 and SOF1 represent runoff type 1 with a rapid and intense runoff response. SOF2 and SSF1 form a delayed reacting runoff type 2, SSF3 corresponds to runoff type 3 and SOF3 and SSF3 are represented by runoff type 4 with a moderate and low runoff response.

5 DISCUSSION

With the presented concept the understanding of the dominant runoff process is gained in a first step at plot-scale. By means of the ideas of "hill-slope hydrology" presented by Kirkby (1978) and Anderson and Burt (1990) the point information is up-scaled to hill-slope and finally to sub-catchments and catchments-scale. These investigations revealed that the differing reactions of catchments to intense rainfall can be better explained when the dominant runoff processes are recognised (Naef et al., 1999). This necessary process knowledge and extended experience is gained by evaluation of catchments. This guide-line provides hydrologists with the necessary information to proceed and to reduce the subjectivity. First applications of this guide-line performed by hydrologists in micro- and meso-scale catchments in Rhineland-Palatinate (Germany) confirmed the suitability of this tool for practical use. However, time consuming field studies are still necessary to attain an adequate result. Therefore, methods are searched to facilitate the data collection in the field without loosing sight of the fundamentals of the runoff processes. Nevertheless, the structure of the decision schemes requires a certain data-set to perform a process identification.
The understanding of runoff processes gained by this procedure has to be integrated into rainfall-runoff models. This promising approach provides more realistic flood estimates. When the field information is integrated into models differences to "normal" model application to estimate flood flows can be assigned. The presented concept tries to define model parameters independently in the field, while with the "normal" approach parameters are calibrated within the model. Our procedure might be following the suggestions of Grayson and Blöschl, 2001 with their DPC (Dominant Process Concept), which require models that concentrate on the important processes and which are not over-parametrisised.
The mapping of the relevant runoff processes in a catchment provides information on dominant runoff processes with a spatially highly resolution and thus, the basis for a realistic delineation of flood contributing areas. Since now, about 50 catchments were investigated based on the ideas on dominant runoff processes and process information has been included into rainfall-runoff models. When this procedure is implemented into practical flood estimation studies, it yields satisfying results. However, to investigate larger (makro-scale) basins the procedure has to be modified to attain also reliable results, because only a reduced spatial resolution of field investigation is enabled. One approach to solve this problem might be to regionalise sub-catchments based on the available data on geology, soils, topography due to hydrological criteria. This allows a preliminary identification of representative catchments indicating to the dominant runoff processes. Then, the field investigations can be concentrated on some representative catchments where the dominant runoff processes are identified by the procedure described in this paper.

ACKNOWLEDGEMENT

We like to express our gratitude to the Swiss National Research Foundation and the Landesamt of Wasserwirtschaft of Rhineland-Palatinate (Germany) which supported the investigations with the sprinkling experiments and the conception of the guideline respectively. Felix Naef of the Swiss Federal Institute of Technology provided constructive criticism in the process of developing the guide-line granted the copyright for some graphics.

REFERENCES

Anderson, M.G., T.P. Burt (1990): Process studies in hill-slope hydrology, J. Wiley & Sons, Chichester

Arbeitsgemeinschaft Boden (1994): Bodenkundliche Kartieranleitung, 4. Ed., Stuttgart

Doerr, S.H. et al., (2000): Soil water repellency: its causes, characteristics and hydrogeomorphological significance. Earth-Science Review, 51. 33-65

Faeh, A.O. (1997): Understanding the processes of discharge formation under extreme precipitation. Mitteilungen der Versuchsanstalt für Wasserbau, Hydrologie und Glaziologie, D. Vischer (Ed.) Vol. 150, Swiss Federal Institute of Technology, Zürich

Food and Agricultural Organisation FAO (1974): FAO Unesco Soil map of the world, 1:5'000'000, Vol. I, Legend, Unesco, Paris

Faeh, A. O., (1997): A combined field and numerical approach to investigate flow processes in natural macroporous soils under extreme precipitation. Hydrology and Earth System Sciences, 4, 787-80, Katlenburg-Lindau

Grayson R., Blöschl G. (2001): Spatial patterns in catchment hydrology – observation and modelling. Cambridge University Press

Kirkby, M.J. (1978): Hillslope Hydrology (Ed.), John Wiley & Sons, Chichester

Leibundgut, Ch., Uhlenbrook S. (1997): Abflussbildung bei Hochwasser. Materialien zum Hochwasserschutz am Rhein. Landesamt für Wasserwirtschaft Rheinland-Pfalz (Ed.), Mainz

Naef, F. et al. (1998): Die Auswirkungen des Rückhaltevermögens natürlicher Einzugsgebiete bei extremen Niederschlagsereignissen auf die Grösse extremer Hochwasser (The influence of the retention capacity of natural basins in respect to the magnitude of extreme flood events). Final report of the National Research Programme 31, vdf, Zurich

Naef et al. (1998): Grosse Hochwasser – unterschiedliche Reaktion von Einzugsgebieten (Major Floods – Differing reactions of catchments). Hydrologischer Atlas der Schweiz, Bern

Naef, F. et al. (2000): Die Beurteilung von Einzugsgebieten und ihrer Teilflächen nach der Abflussbereitschaft unter Berücksichtigung der landwirtschaftlichen Nutzung. (Evaluation of catchments areas with respect to runoff formation considering agricultural land-use in Rheinland-Palatinate). Landesamt für Wasserwirtschaft Rheinland-P. (Ed.), Mainz

Rawls W. J., Brakensiek, D.L. (1989): Estimation of Soil Water Retention and Hydraulic Conductivity. In: Unsaturated Flow and Hydrologic Modelling, Theory and Practice, Morel-Seytoux H.J. (Ed.); Kluver Academic Publishers, Dordrecht

Römkens M.J.M. et al. (1990): Surface sealing and infiltration; In: Anderson M.G., Burt T.P. (eds.), Process studies in Hill-slope Hydrology. J. Wiley & Sons, Chichester

Scherrer, S., Naef, F. (2002): A decision scheme to indicate dominant hydrological flow processes and on temperate grassland, Hydrological Processes, New York, accepted

Naef, F. et al., (2002): A process examination of the potential to reduce flood runoff by changing land use. Submitted to: Hydrology and Earth System Sciences, Katlenburg-Lindau

Scherrer, S. (2001): Leitfaden zur Identifikation hochwasserrelevanter Flächen in Rheinland-Pfalz. Guideline to identify flood relevant contributing areas in Rheinland-Palatinate, Mainz

Scherrer, S. (1996): Abflussbildung bei Starkniederschlägen – Identifikation von Abflussprozessen mittels künstlicher Niederschläge.(Runoff generation during intense rainfall – Identification of runoff processes using sprinkling experiments). PhD Thesis No.11793 of Swiss Federal Institute of Technology ETH, Zurich

Weiler, M.H. (2001): Mechanisms controlling macropore flow during infiltration - Dye tracer experiments and simulations. Publications of Institute of Hydromechanics and water Resources Vol. 7, Swiss Federal Institute of Technology, Zurich

THE INFLUENCE OF FLOODS ON THE WATER BALANCE OF RIVER BASINS BY MEANS OF ISOTOPES OF THE WATER MOLECULE

Ulrich Schotterer[1], Willibald Stichler[2], Hansueli Bürki[1], Ronald Kozel[3], Peter Nyfeler[1], Thomas Stocker[1], Peter Trimborn[2]

[1] Climate and Environmental Physics, Physics Institute, University Berne, Sidlerstrasse 5, 3012 Berne, Switzerland, name@climate.unibe.ch

[2] GSF – Institute for Hydrology, Ingolstädter Landstraße 1, D 85764 Neuherberg, Germany, name@gsf.de

[3] Federal Office for Water and Geology, 3003 Berne, Switzerland, ronald.kozel@bwg.admin.ch

SUMMARY

The distribution of tritium, deuterium, and oxygen-18 in river waters allows the separation of different water components as surface run-off of precipitation and groundwater. Although the discharge characteristics depend on the physical boundary conditions of the respective river basin, the contribution of individual water components are also controlled by the frequency and magnitude of floods following snow melt or storm events. Isotope networks in Switzerland and Germany analyse continuously the major river systems together with the isotopic composition of precipitation. According to climate-induced changes in precipitation distribution and/or winter snow cover, the isotopic composition of river water reflects the diverse local and regional conditions of surface-groundwater interactions and recharge mechanisms on a long-term base.

Keywords: isotope, river, observation network, Switzerland, Germany

1 INTRODUCTION

Water in rivers may originate from many sources with different isotopic composition depending on precipitation distribution and infiltration characteristics, residence time, or altitude of recharge areas of the contributing ground water components. Depending on the size of the water catchment a single precipitation event or the seasonal change may determine the isotopic distribution of the run-off. In any case, the isotopic ratios of precipitation and the contributing groundwater components must differ from the river water for successfully applying isotope techniques for hydrograph separation. First attempts used fall-out tritium from nuclear weapon tests together with oxygen-18 to separate the melting winter snow cover from the groundwater base flow (Dinçer et al., 1970). In a long-term study from 1961 to 1973 the tritium pulse in 1963 with the subsequent declining tritium concentration in precipitation and in the River Rhine allowed to develop a discharge model, which considered also different residence times for the contributing water components (Weiss and Roether, 1975). A similar study was carried out for the River Danube at Vienna with additional time series of stable isotopes (Rank et al., 1998).
The difference in the mean altitude of recharge areas as expressed by differences in their stable isotope composition was applied to separate the contribution of the River Aare to local groundwater recharge (Oeschger and Siegenthaler, 1972). Numerous investigations followed and supported these early findings. Especially the application of stable isotopes to discharge studies from glaciated areas resulted in new insights to the run-off regime. Such studies are usually favoured by pronounced isotopic differences of the contributing water components like melt-water from snow cover or glaciated areas but a modification of stable isotopes during melting has to be taken into account (i.e. Fritz, 1981; Stichler and Schotterer, 2000).
Climate also changes the isotopic composition of river water. A general warming trend together with reduced winter precipitation in Europe during the late 1980ies led to a marked increase in $\delta^{18}O$ and δD in precipitation and river water as well (Schotterer et al., 1993), and recently the distribution of $\delta^{18}O$ and δD in river waters across the United States was used to classify large water catchments in terms of moisture sources and recharge compositions (Kendall and Coplen 2001).
The base of all investigations are networks that record the varying influence of precipitation distribution (and storm events and floods in particular) on the hydrology of river basins with systematic isotope measurements of river water, precipitation, and groundwater. In the Alpine region such investigations are favoured by the early build-up of isotope networks created and/or supported by government and institutions.

2 ISOTOPE NETWORKS IN SWITZERLAND AND GERMANY

The national networks have been developed from networks of individual research groups contributing to the Global Network for Isotopes in Precipitation (GNIP), which is co-ordinated and maintained by the International Atomic Energy Agency (IAEA) in Vienna. In contrast to efforts in Germany or Austria, the Swiss network for the observation of isotopes in the water cycle is supported and operated by the Federal Office for Water and Geology (FOWG). It provides not only input data for hydrological engineering but also long-term time series necessary to assess climate induced changes regarding the spatial variability in amount and seasonal distribution of precipitation, changes in evapo-transpiration, changes in snow cover and glacier melt water; this also includes flood frequency. The network started in 1992 and includes presently 11 precipitation stations, 6 river stations, and 1 ground water station (i.e. Schotterer et al., 2000). The collected samples represent monthly composites except the River Aare at Brienzwiler, Thun and Berne (twice a month) and the ground water station (once a month). Oxygen-18/tritium and deuterium in the water samples are analyses by the Climate and Environmental Physics group at the University of Berne and by the Institute of Mineralogy and Petrography at the University of Lausanne, respectively. The measurements of tritium, deuterium and oxygen-18 are published together with the necessary hydrological and meteorological background information in the Hydrological Yearbook of Switzerland (FOWG 2001). Data are also directly available from the FOWG.

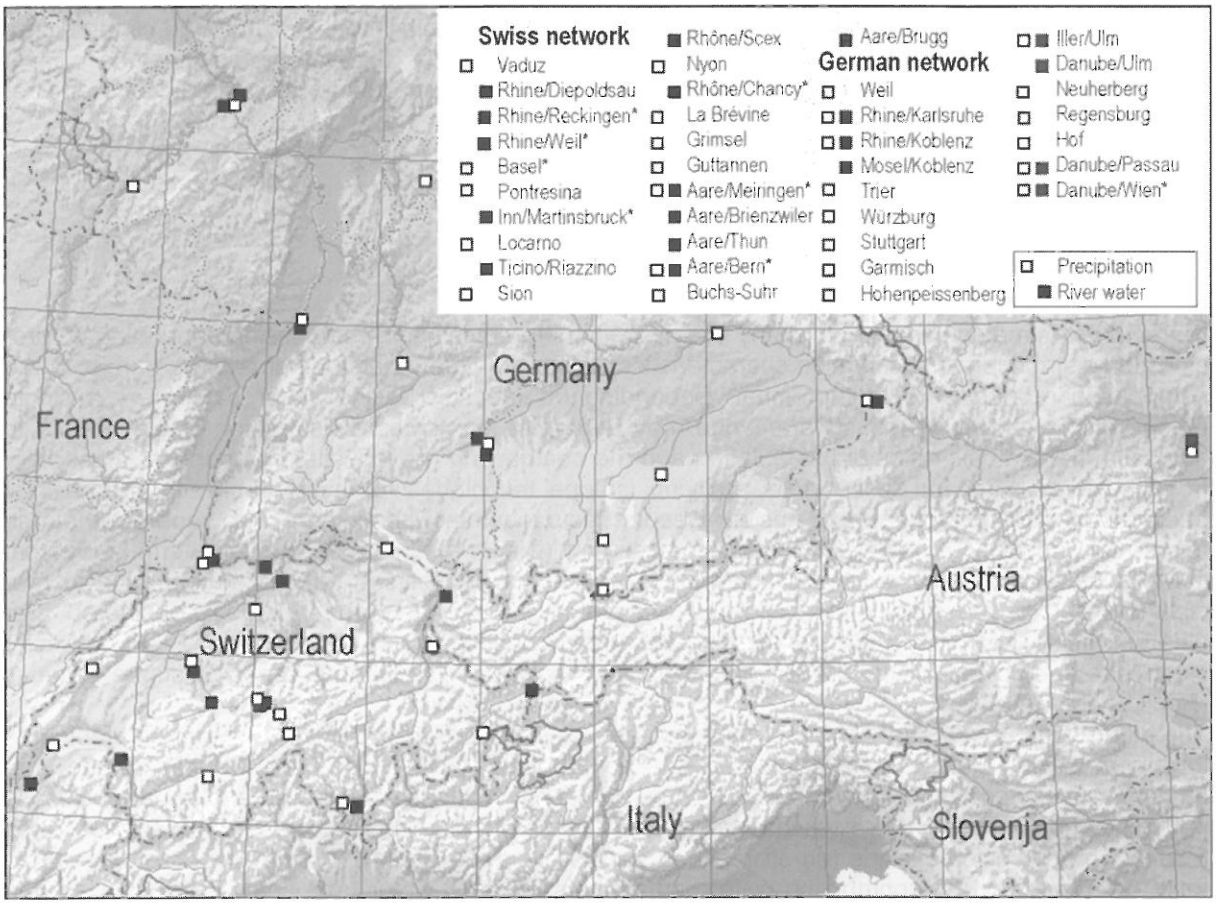

Figure 2-1: Isotope network for precipitation and river water in Switzerland and Southern Germany. Stations marked with a star are not permanently sampled or not included in the official networks.

The German network consists of 29 precipitation stations. Part of them started in 1973 in cooperation with the German Federal Institute of Hydrology (BfG). The tritium measurements are performed at BfG (Dr. W. Krause), the stable isotopes (deuterium and oxygen-18) at the GSF Institute for Hydrology. All data are published in GNIP of the IAEA. Since 1988 two river water stations have been included. In 1997 additional stations were installed in cooperation with the German Meteorological Service (DWD). At four stations stable isotopes are measured in daily precipitation.

Sampling sites in Switzerland and Southern Germany are mapped in figure 2-1. The dense network of Austrian stations is maintained by the Federal Environment Agency together with the Arsenal Research in Vienna. The network stations are not considered here except River Danube at Vienna, which is part of border-crossing projects together with Germany. The map contains also stations in Switzerland that are maintained by the Climate and Environmental Physics group at the University of Berne, which are marked with a star.
It is obvious that the often small-scaled differences in the alpine orography cannot be sampled with adequate density to reproduce local effects. The geographic coverage of the networks is designed to record the main air mass systems for determining climate-induced changes that influence isotopes in precipitation and consequently also the isotopic run-off composition of the major river systems. Some river systems are sampled at different altitudes to observe changes in the respective catchment areas.

3 SELECTED RESULTS

During the year the stable isotope distribution in river water reflects the correspondent variability of that in precipitation, but dampened. Mean winter – summer $\delta^{18}O$ differences in precipitation are in the order of 5 to 8 ‰; in river water they hardly exceed 1 to 2 ‰ depending on the size of the catchments and the turn over of lakes in between. If solid precipitation dominates during winter the negative isotope values are shifted towards the warmer season when water from snow melt is the dominating discharge component. The figure below illustrates an example where the different discharge behaviour of two river systems influences alternating local groundwater recharge.
The two rivers have different isotopic characteristics according to their different catchments. River Danube at Ulm has a lower catchment area as compared to the River Iller, which originates from the Alps in Southern Germany. The River Danube therefore has higher mean $\delta^{18}O$ values that follow the known seasonal variation of stable isotopes in precipitation with a maximum during summer. Rain in winter does not delay surface run-off considerably. The isotopic composition of the River Iller on the other hand, is altered by snow melt that shifts the more negative $\delta^{18}O$ winter values towards summer. The stable isotope content of the groundwater varies between those of the two rivers.

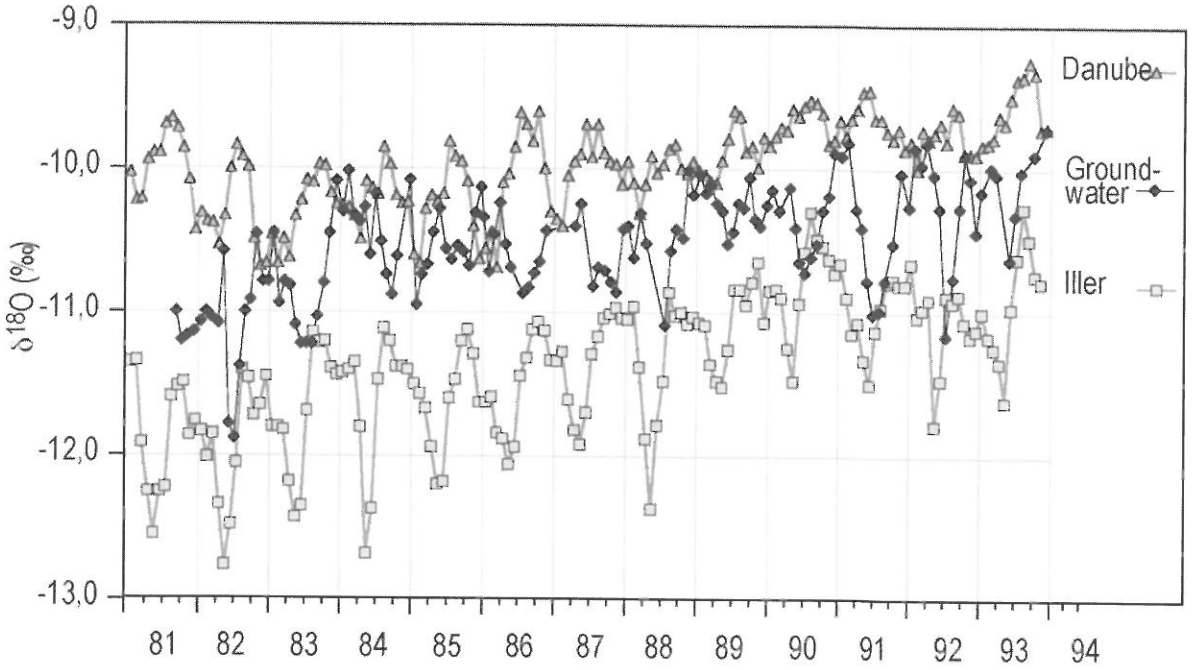

Figure 3-1: Seasonal varying influence of the rivers Iller and Danube on groundwater recharge. Depending on the differences in discharge the $\delta^{18}O$ of the ground water reflects the dominating renewal rates of the respective rivers as well as climate-induced changes in the river basins.

During late autumn and winter the local groundwater is generally renewed more directly by the River Danube. Several weeks after the negative $\delta^{18}O$ pulse of the snow melt flood of the River Iller has arrived, the $\delta^{18}O$ of the groundwater starts also to shift to more negative values. This indicates that now Iller water is preferentially recharging the groundwater. The amount varies from year to year. Following extreme floods the River Iller contribution to the renewal rate of the groundwater may be even more than 75% (Bertleff et al., 1985).
Moreover, the isotope values not only reflect the seasonally alternating influence of both rivers but also changes in the river basins with time as a result of hydro-climatic changes. Increasing temperatures and less winter snow cover cause the $\delta^{18}O$ trend towards more enriched values between 1982 and 1992. The trend is more pronounced in the alpine catchment of the River Iller than in that of the River Danube. Depending on the changes in the respective catchments, timing and percentage of the individual renewal contributions to local groundwater are influenced.
The climate and/or catchment-induced influence on the isotopic composition of river water can be distinguished more clearly, if a river is sampled not only at different altitudes but also before and after great lakes, that alter residence times, dampen short term precipitation events and may additionally modify the isotopic composition by evaporation processes. In the following we will discuss some findings from the rivers Aare and Rhine related to these influences.
The mean altitude of the catchment of the River Aare decreases from about 2200m at Meiringen and Brienzwiler to 1000m at Brugg. Between Brienzwiler and Thun, Lake Brienz and Lake Thun influence the residence time of the river water. Further downstream important tributaries discharging glaciated areas or lakes join the river. At the confluent point with the Rhine, the Aare catchment covers nearly 12'000km^2; the glaciated areas cover 2%.

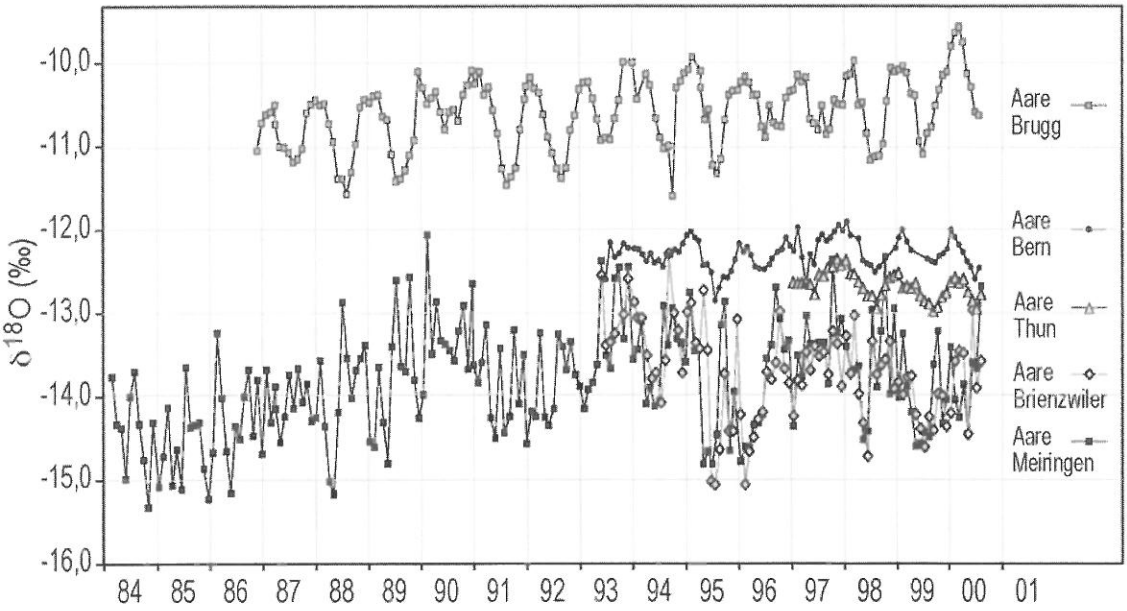

Figure 3-2: Hydro-climatic influenced $\delta^{18}O$ variability in the run-off from River Aare. $\delta^{18}O$ decreases with increasing altitude of the contributing catchments at the respective sampling sites. The seasonality depends on the magnitude of the snow melt pulse and the damping influence of lake water mixing.

The longest isotope time series exist for the River Aare at Meiringen, where the sampling started in the late sixties. Those of the FOWG-station at Brienzwiler complete these data since 1992. Although sampling takes place only once or twice a month the long-term trend as seen in the River Iller (and from the respective isotope measurements in precipitation) is clearly visible. This indicates also that climate-induced changes had regional impacts because they altered the run-off regimes of different rivers in a similar way. Of course, short-term changes or a complete snowmelt flood cannot be followed with such a sampling frequency. Moreover, the discharge of the River Aare is influenced by hydropower installations in the uppermost part of the catchment. Nevertheless, the average isotope values over several years do not differ from those of precipitation at an elevation that corresponds to the mean altitude of the River Aare catchment at Meiringen and Brienzwiler respectively.
The seasonality of the isotope content is dampened to several tenth of a per thousand in $\delta^{18}O$ as the river water mixes with lake water but the seasonality still remains (Aare at Thun and Berne) and is not

shifted. With decreasing influence of lake water the seasonality in the river water increases again and at Brugg it is more than doubled. The negative $\delta^{18}O$ values from winter precipitation are shifted towards summer indicating the still dominating influence of the melt water pulse from the winter snow cover. The shape of this pulse varies considerably. Since the isotope data at Brugg represent discharge-proportional monthly composites, the year to year storage in the regional snow cover and its contribution to the river discharge may be evaluated more quantitatively.

As the mean altitude of the river catchments decreases downstream from Meiringen to Brugg, the $\delta^{18}O$ in river water increases due to the altitude effect of stable isotopes in precipitation. Evaporation process may influence this altitude effect for example when the river flows through lakes. This overall-influence can be controlled by the $\delta D/ \delta^{18}O$ relation in the river water as compared to the corresponding relation in precipitation. The deuterium excess decreases with increasing influence of evaporation. Such an influence is measurable along the course of the River Aare: the long-term mean of the deuterium excess decreases from Brienzwiler (~10‰) to Brugg (~6‰).

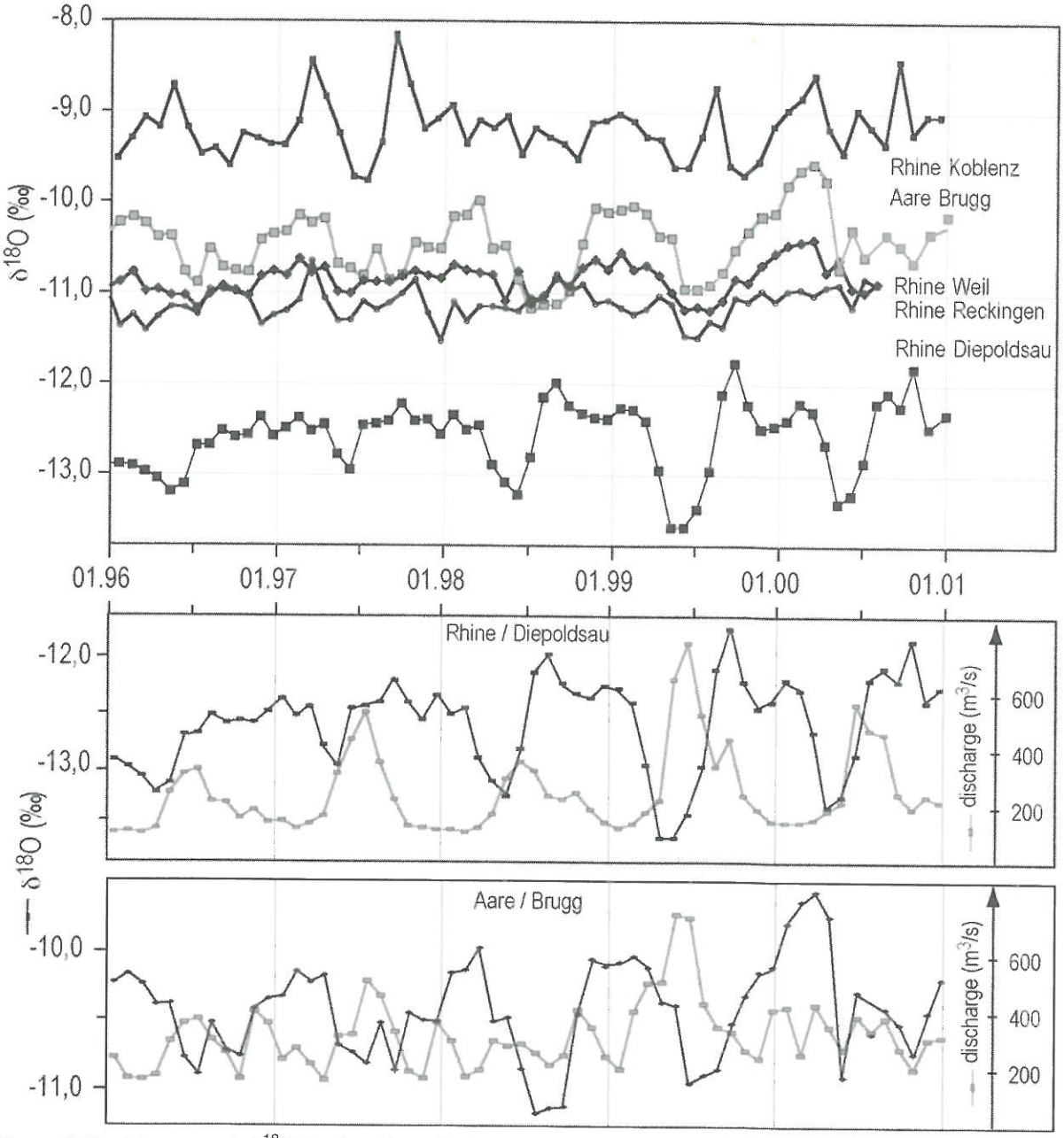

Figure 3-3: Upper part: $\delta^{18}O$ in the River Rhine at Diepoldsau and at Reckingen being upstream and downstream the Lake Constance respectively, and at Weil, downstream the confluent with River Aare. Lower part: $\delta^{18}O$ and discharge of the River Rhine at Diepoldsau and River Aare at Brugg.

The damping influence of a great lake and the changing influence of snowmelt floods on the isotopic distribution of river run-off is also seen along the River Rhine. Before entering Lake Constance the seasonality in $\delta^{18}O$ is clearly visible especially for the years 1998 through 2000. Downstream Lake Constance at Reckingen, mixing and discharge from catchments, where snow cover plays a minor role, eliminate this seasonality. Downstream the confluent with the River Aare, the snowmelt induced seasonality recovers somewhat (River Rhine at Weil). Further downstream this influence on the stable isotope content of run-off is again overprinted by local influences, which results in a more irregular behaviour of the $\delta^{18}O$ values (upper part of figure 3-3). In the lower part of figure 3-3, discharge and $\delta^{18}O$ are compared for the River Rhine at Diepoldsau and the River Aare at Brugg for the same period of time.

4 CONCLUSION

Changes in the hydrology of river basins caused by snow melt floods or climate-induced shifts of seasonal precipitation distribution are large-scale labelled by isotopes in precipitation. A successful application of tritium, $\delta^{18}O$, and δD-methods requires continuous and long-term networks for the observation of isotopes in the water cycle (precipitation and river water) at sensitive key sites where changes in the isotopic composition can be observed with the necessary degree of confidence. The examples from the Aare, Rhine, and Danube river systems demonstrated the use of isotopes as diagnostic variables for a better understanding of basic processes within river basins. Their ability to trace pathways of different water sources and changes in the composition of ground water and river run-off opens new possibilities for dynamical changes in water resources if hydrological models are developed through the combined use of hydrodynamic parameters, geochemical tracers and water isotopes.

ACKNOWLEDGEMENTS

The Swiss National Science Foundation and the Federal Office for Water and Geology who operates the Swiss Network for Isotopes in the Water Cycle supported this work. The German Federal Institute of Hydrology (BfG) in Koblenz and the German Meteorological Service (DWD) in Offenbach are acknowledged for technical support.

REFERENCES

Bertleff, B., Stichler, W., Stober, I., Strayle, G. (1985): Geohydraulische und isotopenhydrologische Untersuchungen im Mündugsbereich zwischen Donau und Iller; - Abh. Geol. Landesamt Baden-Württemberg, 11, 7-44.

Dinçer, T., Payne, B.R., Florkowski, T., Martinec, J., Tongiorgi, E. (1970): Snowmelt run-off from measurements of tritium and oxygen-188. Water Resources Research, 40, 6, 110-124.

FOWG (2001): Hydrological Yearbook of Switzerland. Federal Office for Water and Geology, Berne, Ittigen.

Fritz, P. (1981): River waters, in: *Stable Isotopic Hydrology: Deuterium and Oxygen-18 in the Water Cycle*, Gat, J. R., and R. Gonfiantini eds, IAEA Tech. Rep. Ser., 210, pp 177-210.

Kendall, C. and Coplen T. B. (2001): Distribution of oxygen-18 and deuterium in river waters across the United States, Hydrological Processes 15: 1363-1393.

Oeschger, H. and Siegenthaler, U. (1972): Umgebungsisotope im Dienste der Hydrologie, Das Gas- und Wasserfach, Heft 11, R. Oldenbourg München , 501-508.

Rank, D., Adler, A., Araguas, L.A., Froehlich, K., Rozanski, K., Stichler, W. (1998): Hydrological parameters and climatic signals derived from long term tritium and stable isotopes time-series of the river Danube, in: *Isotope Techniques in the Study of Environmental Change*, International Atomic Energy Agency, Vienna, 191-205.

Schotterer, U., Fröhlich, K., Stichler, W., Trimborn, P. (1993): Temporal Variation of ^{18}O and Deuterium Excess in Precipitation, River and Spring Waters in Alpine regions of Switzerland. In: Isotope

Techniques in the Study of Past and Current Environmental Changes in the Hydrosphere and Atmosphere IAEA, Vienna, 53-64.

Schotterer, U., Stocker, T., Bürki, H., Hunziker, H., Kozel, R., Grasso, D.A., Tripet, J.P. (2000): Das Schweizer Isotopen-Messnetz: Trends 1992-1999, Gas-Wasser-Abwasser gwa, 2000, 10, 3-11.

Stichler, W. and Schotterer U. (2000): From accumulation to discharge; Modification of stable isotopes during glacial and post-glacial processes. Hydrol. Process. 14, 1423-1438.

Weiss, W., and Roether, W. (1975): Der Tritiumabfluss des Rheins 1961-1973, Deutsche Gewässerkundliche Mitteilungen, 19. Jahrgang, Heft 1, 1-5.

DOES IMPROVED MODEL CALIBRATION LEAD TO MORE ACCURATE FLOOD ESTIMATION?

Jan Seibert

Swedish University of Agricultural Sciences, Department of Environmental Assessment, Box 7050, S-750 07 Uppsala, Sweden, jan.seibert@ma.slu.se

SUMMARY

Predictions of probabilities and magnitudes of extreme events are essential for water management. The use of extreme value statistics has been criticized, mainly because fitted distribution functions have to be extrapolated far beyond the probabilities that can be justified from the runoff observations. An alternative is the use of conceptual runoff models as tools for flood estimation. This approach, however, can be questioned for the same reason: the model has to be used for conditions far beyond those used for model development and calibration. The only reason why we should rely more on the model than on extreme value statistics is that we have confidence in the validity of the model and, thus, assume that extrapolation of the model is more reliable. In order to have more confidence in a calibrated model than in a fitted distribution function we have to ensure that the model does not only correctly simulate runoff but also does so for the right reasons. Recent studies aiming at improving the calibration of runoff models can be classified into two groups: (1) making more use out of the runoff series and (2) using additional data to constrain the model. An implicit assumption is that the improved model calibration not only will reduce parameter uncertainty and strengthen internal model consistency but also improve model predictions. The idea is that a model, which has been calibrated looking on more aspects than just the squared errors of its runoff simulations, should give more reliable model predictions. While this assertion might be reasonable, the effects of improved model calibration on prediction errors still have to be investigated. In this study the HBV model, a conceptual runoff model, which is used, for instance, to compute design floods for dam safety in Sweden, was applied to two different catchments where groundwater levels were available. Differential split-sample testing (calibration on years with lower runoff peaks and testing it on years with higher peaks) was used to evaluate model performance for the situation when the model has to be used to simulate runoff during conditions different from those observed during calibration. To assess the value of improved calibration this model performance was then compared for simulations derived from different calibration procedures such as, for instance, including groundwater-level observations. The results indicated that applying a model to conditions different from those during the calibration period might not give accurate results and that improved calibration procedures might not automatically provide more accurate flood estimations.

Keywords: model testing, multi-criteria calibration, differential split-sample test, flood estimation, Monte Carlo

1 INTRODUCTION

Predictions of probabilities and magnitudes of extreme events are essential for water management. The traditional approach of fitting distribution functions to the observed extreme values and extrapolating these functions can be criticised for different reasons (Linsley, 1986; Klemeš, 1986a, 2000a,b). The main criticism is that a distribution function of unknown shape has to be extrapolated far beyond the probabilities that can be justified from the available observations.
Alternatives to the distribution fitting are modelling approaches (*e.g.*, Bergström et al., 1992; Calver and Lamb, 1995). The basic idea is to use a runoff model, which has been calibrated against existing streamflow data, to simulate the streamflow caused by extreme meteorological conditions. Obviously the need for data on extreme circumstances is only shifted from the streamflow to the meteorological data, but it might be more likely to have suitable data on extreme conditions for meteorological data than for streamflow. Firstly, more observations are often available, both in time and space, for meteorological data, such as precipitation or temperature, than for streamflow. Secondly the modelling approach allows combining extreme conditions (e.g., a winter with much snow accumulation, a rapid rise of temperatures in spring and a large rainfall event) (Bergström et al., 1992). The use of a model to estimate extreme runoff events has certainly advantages, but this approach can be criticised in exactly the same way as the fitting of some distribution function: the model has to be applied for conditions far beyond the conditions used for development and calibration for computation of extreme

floods. The only reason why we should rely more on the model than on distribution functions is that we have confidence in the validity of the model and, thus, assume that extrapolation of the model calculations are more reliable.

A usual test of a model is a simple split-sample test, where the model is calibrated on data from one period and tested for another, independent, period. This kind of test gives an indication how the model might perform for independent period with similar conditions. Examples where the result of such a test is called 'not successful' are seldom found in literature. This may be mainly because this kind of validation is a simple task (Kirchner et al., 1996; Mroczkowski et al., 1997). Furthermore, this kind of test is not suited to test the models ability to give reasonable simulations for conditions that differ from those of the calibration period (Xu, 1999). However, models are most important for problems where we have to apply the model beyond the conditions observed before. The need to apply a model is, for instance, much larger for predicting a 1000-year flood than for predicting a 10-year flood. In the latter case enough data may be available to compute the flood from time series without any model.

In order to test how accurate model predictions might be when applying the model to different conditions a differential split-sample test is more suitable than the simple split-sample test (Klemeš, 1986b; Xu, 1999). The basic idea is to calibrate and to test the model on time periods with dissimilar hydrological conditions such as, for instance, a period with mainly small runoff events and a period with large events. Results of such a test may provide an indication on model performance when we have to extrapolate into 'really unknown' conditions. This is a more powerful test of a model, but it is only seldom applied (*e.g.*, Refsgaard and Knudsen, 1996; Donelly-Makowecki and Moore, 1999).

The issue of parameter uncertainty (e.g., Beven, 1993) has become widely recognized during the recent years. Often parameter sets, which perform equally well (according to some criteria) for a calibration period, can be found at very different locations in the parameter space. It may be argued that the problem of identifying a unique parameter set is not an issue for practical model applications, *i.e.*, if different parameter sets were equally suitable to simulate runoff during a calibration period, any one of these sets may be applied. However as shown by, for instance, Seibert (1997) and Uhlenbrook et al. (1999) these 'equally good' parameter sets may give very different predictions for individual events. Uhlenbrook et al. (1999) computed design floods using 'equally good' parameter sets and found that the predicted peak discharge of a flood with a probability of 0.01 yr^{-1} varied from 40 to almost 60 mm d^{-1}.

Others have emphasised on the need to utilize additional data for model calibration and testing in the recent years (de Grosbois et al., 1988; Ambroise et al., 1995; Refsgaard, 1997; Kuczera and Mroczkowski, 1998). Using additional data for the model calibration is one way to reduce parameter uncertainty (e.g., Franks et al., 1998; Lamb et al., 1998; Seibert, 2000). Besides the reduced parameter uncertainty, the multi-criteria calibration is assumed to provide parameter sets that are a more appropriate representation of the catchment than a calibration against only runoff. Runoff might be simulated slightly worse during the calibration period, but the internal variables come into much better agreement with the conditions in the catchment. It seems reasonable that this improved internal consistency could be associated with more reliable predictions outside the calibration domain. The idea is that, for a model that agrees with the real system in different respects (*e.g.*, with observed internal variables), extrapolation beyond the testable conditions is more reasonable than for a model that just matched runoff during some period.

In this study the HBV model (Bergström, 1995), a conceptual runoff model, which is used, among other applications, to compute design floods for dam safety in Sweden (Bergström et al., 1992; Lindström and Harlin, 1992), was applied to two different catchments where groundwater-level data were available. Differential split-sample testing, *i.e.*, calibration on years with lower runoff peaks and testing it on years with higher peaks, was used to evaluate model performance for the situation when the model has to be used to simulate runoff during conditions different from those observed during calibration. To assess the value of improved calibration the model performance was compared for simulations derived from including groundwater-level observations or an additional peak-flow criterion into the calibration.

2 MATERIALS AND METHODS

2.1 HBV model

The HBV model (Bergström, 1976; 1992) is a conceptual model that simulates daily discharge using daily rainfall and temperature, and monthly estimates of potential evaporation as input. The model consists of different routines (Figure 2-1), where snowmelt is computed by a degree-day method, groundwater recharge and actual evaporation are functions of actual water storage in a soil box, runoff formation is represented by three linear reservoir equations and channel routing is simulated by a triangular weighting function. For both the snow and the soil routine, calculations are performed for each different elevation zone, but the response routine is a lumped representation of the catchment. Further descriptions of the model can be found elsewhere (*e.g.*, Bergström, 1992; 1995; Lindström et al., 1997; Seibert, 1999).

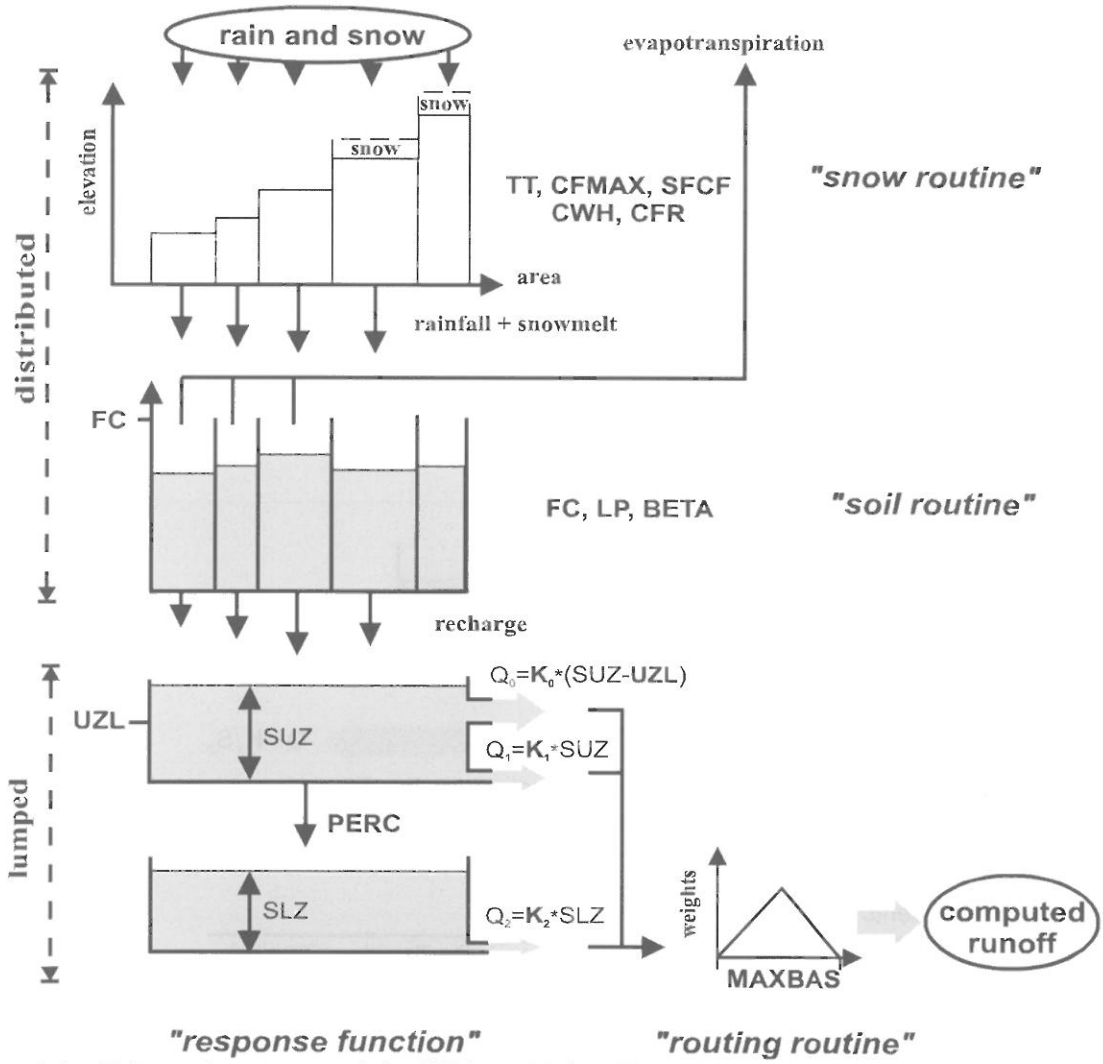

Figure 2-1: Schematic structure of the HBV model (modified after Bergström, 1992).

2.2 Study catchments

2.2.1 Lilla Tivsjön

The Lilla Tivsjön catchment (Table 2-1) is a subbasin of the former International Hydrological Decade representative basin Kassjöån (Waldenström, 1977) in central Sweden, 50 km NW of the city of Sundsvall. The landscape is hilly with elevations ranging from 250 to 440 m a.s.l.. The catchment is mainly forested and covered by till soil. Precipitation and temperature were measured close to the

catchment outlet. Almost complete data series with twice-monthly observations of groundwater levels were available from ten tubes located in different parts of the catchment.

2.2.2 Tärnsjö

The Tärnsjö catchment (Table 2-1) is located in central Sweden, 50 km NW of the city of Uppsala and about 300 km S of the Lilla Tivsjön catchment. A large esker (ridge of glaciofluvial deposits), rising up to 50 m above the surrounding land, runs through a part of the catchment. The remaining part of the mainly forested catchment is covered by till soil. Precipitation measurements were available from a station within the catchment whereas temperature was measured about 30 km away from the catchment. Groundwater levels were observed twice monthly at several tubes, from which seven tubes with almost complete data sets were used in this study. It should be noted that some of the tubes were located up to 4 km outside the water divide; however, they were assumed to correspond with the conditions within the catchment.
Previous studies indicated that the response function of the traditional HBV model might not be appropriate for the Tärnsjö catchment, and that an alternative response function may give better results (Bergström and Sandberg, 1983; Seibert, 2000). The recharge simulated by the soil routine is divided into two parts (Figure 2-2). A portion C_{PART} [-], related to the portion of the till soil area, is added directly to an linear storage whereas the remaining recharge generated on one day is added evenly distributed over a subsequent period of C_{DELAY} [d] days to another linear storage. The latter storage is thought to represent the esker in which recharge is delayed because of the large unsaturated zone.

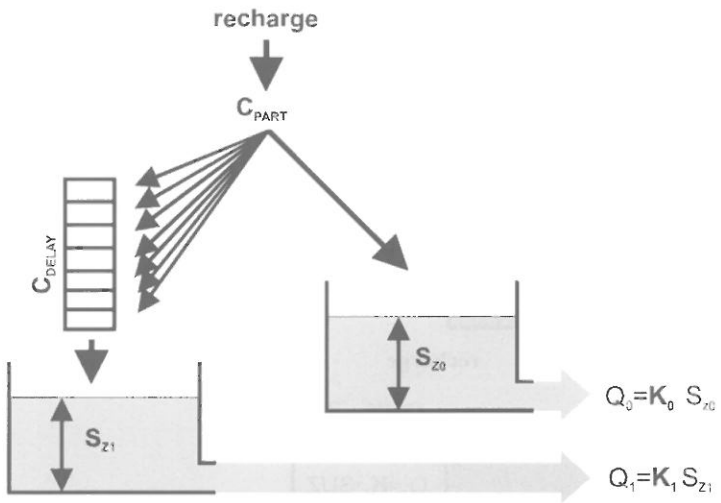

Figure 2-2: Structure of the modified response function for the Tärnsjö catchment. The new parameters control the division of the recharge between the two boxes (c_{PART}) and the delayed delivery of recharge to one box (c_{DELAY}).

Table 2-1: Catchments characteristics.

Characteristic	Lilla Tivsjön	Tärnsjö
SMHI[1] station number	42-1920	54-2299
Area [km^2]	12.8	14
Forest percentage [%]	88	85
Lake percentage [%]	2.7	1.8
Range of elevations [m a.s.l.]	246-440	55-105
Mean annual precipitation [mm]	586	729
Mean annual runoff [mm]	262	266
Mean annual temperature [°C]	2.1	5.3

[1] Swedish Meteorological and Hydrological Institute

2.3 Model application and differential split-sample test

For both catchments calibration and test periods were chosen so that the floods were significantly larger during the test period (Figure 2-3). The maximum peak flows during the calibration period corresponded to 5.3 and 3.6 mm d^{-1} for the Lilla Tivsjön and Tärnsjö catchment respectively, whereas the largest peak flow during the test period were 8.4 and 5.3 mm d^{-1}. The differential split-sample test used in this study consisted of the following steps: (1) Monte Carlo model runs with randomly generated parameter sets for the calibration period, (2) selection of an assembly of the *n* best parameter sets according to some goodness-of-fit measure, and (3) simulation of the test period with all parameter sets of the assembly. For the Monte Carlo runs ranges of possible values were specified for each model parameter based on the range of calibrated values found in previous model applications (Bergström 1990; Seibert, 1999). For each catchment 3 million parameter sets were drawn randomly using uniform distributions within these ranges. The model was run for each parameter set and the values of different objective functions were computed.
The agreement between observed (Q_{obs}) and simulated (Q_{sim}) catchment runoff was evaluated by the model efficiency (Nash and Sutcliffe, 1970), here called R_{eff} (Eq. 1).

(1) $$R_{eff} = 1 - \frac{\sum (Q_{obs} - Q_{sim})^2}{\sum (Q_{obs} - \overline{Q_{obs}})^2}$$

The model efficiency tends to focus on high flow conditions. However, since the aim was to simulate extreme floods another goodness-of-fit measure was used additionally. This measure, R_{peak}, addressed the ability of the model to reproduce peak flows directly (Eq. 2) by using the absolute differences between observed and simulated peak streamflows ($Q_{peak,\ obs}$ and $Q_{peak,\ sim}$) for all *n* peaks during the simulation period. The set of peaks was determined from the observed runoff series, to be included a peak had to exceed the long-term mean runoff by three times. Furthermore, only the largest peak within any one-month window was used. With these criteria 8 peaks were selected for the Lilla Tivsjön catchment and 7 peaks for the Tärnsjö catchment. The corresponding simulated peaks were taken as the largest runoff during a one-week window centred on the date of the observed peak.

(2) $$R_{peak} = 1 - \frac{\sum_{i=1}^{n} \left| Q_{peak,obs,i} - Q_{peak,sim,i} \right|}{\sum_{i=1}^{n} Q_{peak,obs,i}}$$

In both catchments used in this study groundwater levels were measured about fortnightly at a number of groundwater tubes. Because the HBV model simulates the groundwater lumped over the catchment local observations could not directly be compared to the simulations. The groundwater observations also were spatially averaged, *i.e.*, the arithmetic mean was computed from the observations at the different tubes. To allow comparison with the observed mean groundwater level the storage in the groundwater boxes (S_{UZ} and S_{LZ}) had to be transformed into a groundwater level, *z* [m a.s.l.]. A linear equation (Eq. 3) with a slope *m*, which corresponded to the inverse of the storage coefficient, and an offset *c* was used. The coefficients were determined by linear regression between the simulated storage and groundwater levels.

(3) $$z = m\left(S_{UZ} + S_{LZ}\right) + c$$

The performance of the groundwater level simulation was evaluated using the coefficient of determination, r^2, as objective function. For the Tärnsjö catchment, where the alternative model structure was used, the tubes where grouped according to whether they were located on the esker or not and mean time series were computed for both groups. The geometric mean of the r^2 values of the fit for the two series was computed as objective function.
Three different assemblies of 'best' parameters sets were compiled, each consisting of the 50 parameter sets which performed best according to one goodness-of-fit measure. The three measures used were: model efficiency (R_{eff}), the mean of efficiency and goodness of groundwater level simulations (R_{eff} and r^2), as well as the mean of efficiency and goodness of peak flow simulations (R_{eff} and R_{peak}).

Finally, these assemblies were used to simulate runoff for the test periods. In particular the ability to predict floods was tested based on the peak flows during the test period (12 for Lilla Tivsjön, 8 for Tärnsjön). Both median and the range of 80 percent of the predictions from the 50 parameter sets were computed.

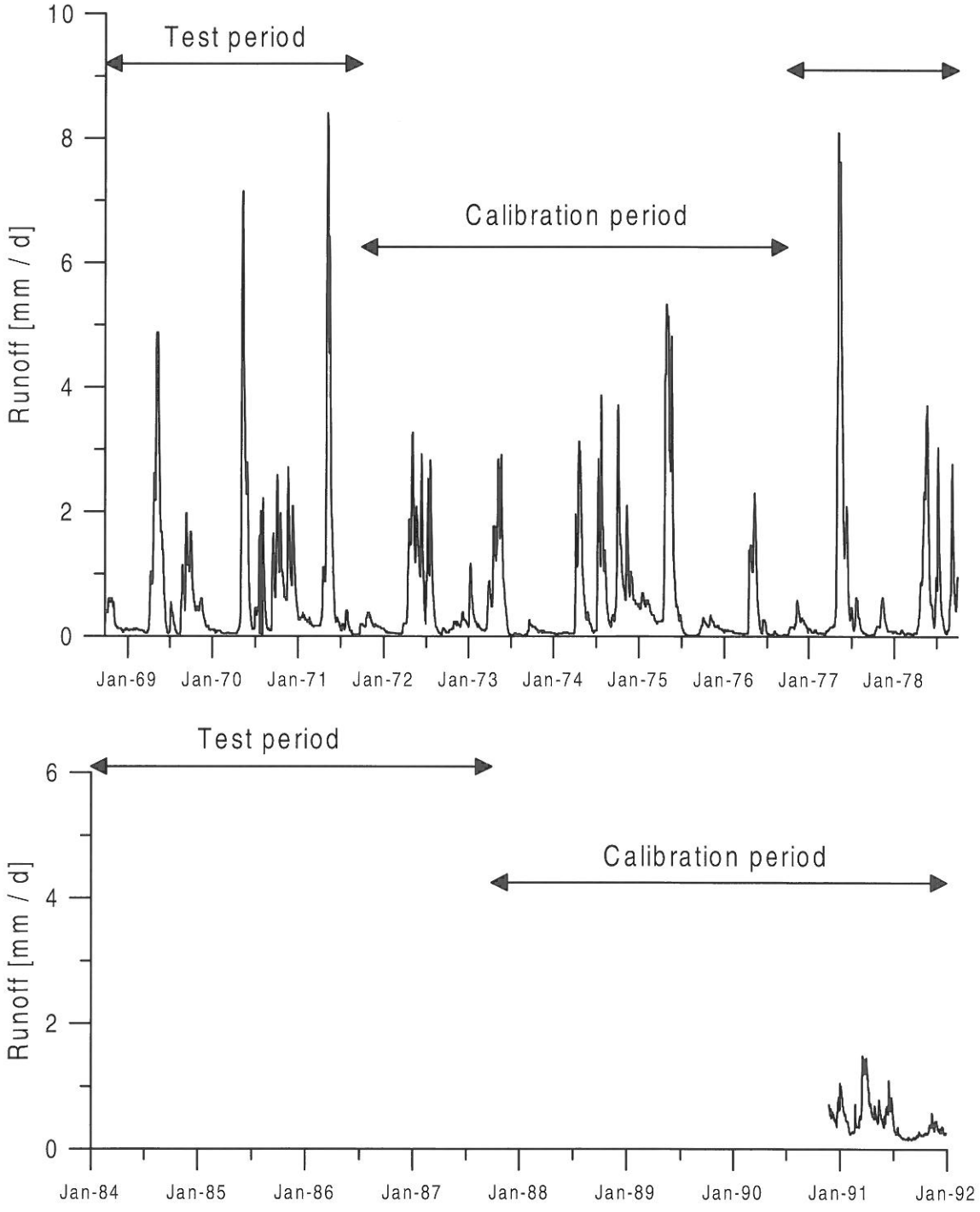

Figure 2-3: Runoff series for calibration and test periods in the two catchments Lilla Tivsjön (a) and Tärnsjö (b).

3 RESULTS

Different objective functions judge the model performance with regard to different aspects. If two criteria are highly correlated no new information is provided by the additional objective function. However, in the case of the three objective functions used in this study there was a 'trade-off' between the

objective functions (Figure 3-1). This means that the criteria provided different information, but also that it is not possible to find a solution that was optimal according to all criteria simultaneously.

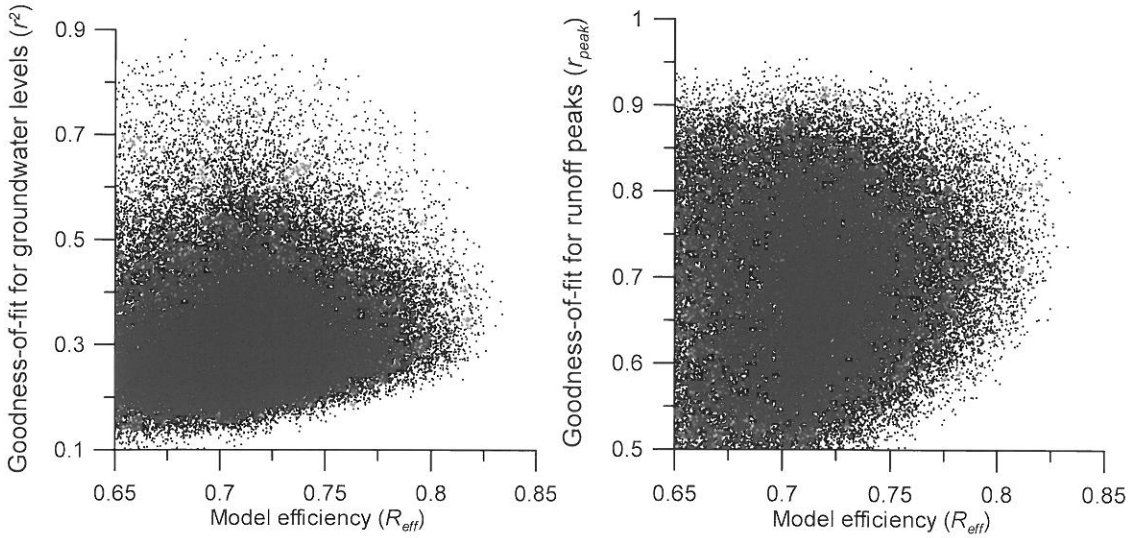

Figure 3-1: Model performance for the Monte Carlo runs according to the different criteria for the Lilla Tivsjön catchment. Each dot represents one model run with a randomly generated parameter set.

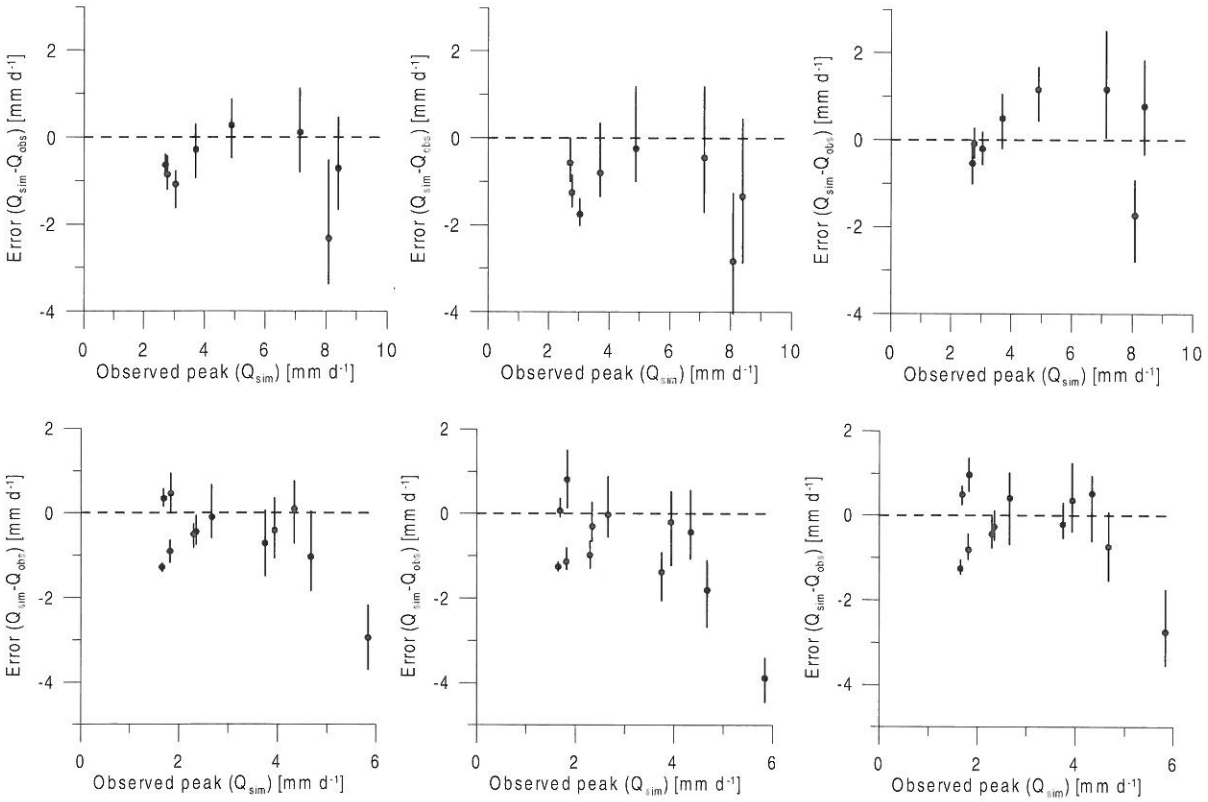

Figure 3-2: Errors of the simulated peak flows for peaks of different magnitudes during the test period (upper row Lilla Tivsjön catchment, lower row Tärnsjö catchment). Both the median and the 80-percent range of the prediction errors obtained using the 50 best parameter sets are shown. The assemblies of best parameter set were determined with regard to the model efficiency (R_{eff}, left graph), the mean of efficiency and goodness of groundwater level simulations (R_{eff} and r^2, middle), as well as the mean of efficiency and goodness of peak flow simulations (R_{eff} and R_{peak}, right).

In general good fits could be found for both catchments for the calibration period with efficiency values around 0.8 (Table 3-1). As in previous studies equally good calibration results could be obtained with very different parameter values. Most important to note is the drastic drop of efficiency values when using the 'best' parameter sets to simulate the test period (Table 3-1).
For the events during the test period, simulated peak flows were significantly erroneous for several events, in particular for the largest events (Figure 3-2). The simulated peak flows varied over rather large ranges for most events for all parameter-set assemblies.

Table 3-1: Model efficiency (R_{eff}) for the calibration and test period using assemblies of the parameter sets which performed best during the calibration period (medians of 50 simulations).

Best parameter sets according to....	Lilla Tivsjön		Tärnsjö	
	Calibration period	Test period	Calibration period	Test period
R_{eff}	0.82	0.36	0.79	0.65
$(R_{eff}+r^2)/2$	0.73	0.40	0.69	0.54
$(R_{eff}+R_{peak})/2$	0.78	0.21	0.75	0.64

4 DISCUSSION

The simulated peak flows deviated significantly from the observations. Parameter uncertainty caused considerably different predictions for the different peak flows, despite the fact that only the very best parameter sets were included in each assembly (50 best of 3 million runs!). Even more important, also the median of the 50 predictions was erroneous in many cases, especially for the largest floods. Contrary to the results of Harlin (1992), who did not find a systematic underestimation of extreme floods, the largest floods were all underestimated. There was hardly any improvement when using additional criteria for optimisation; neither the groundwater data nor the extra peak-criteria had the effect one might have hoped for (Figure 3-2). Considering the groundwater-level simulations for the selection of the best parameter sets provided the highest efficiency values for the test period in the Lilla Tivsjön catchment, however in the Tärnsjö catchment the result was opposite (Table 3-1).
Although not shown in this paper, it can be noted that the results were similar when other combinations of the objective functions, or using the volume error and the efficiency of the log-runoff values as additional criteria, were used to select the assembly of best parameter sets.

5 CONCLUDING REMARKS

There was a significant range of predictions obtained using parameter sets that behaved equally well, according to some goodness-of-fit measure, during the calibration period. This prediction uncertainty caused by parameter uncertainty has been demonstrated before (e.g., Seibert, 1997; Uhlenbrook et al., 1999). Again the results strongly suggest to consider these uncertainties and to present model predictions rather as ranges than as single values.
The results of this study indicate that extrapolations of a model, *i.e.*, the simulation of conditions not observed during the calibration period, should be interpreted with care. This is of special concern when models are to be used to predict extreme events, e.g., design floods. Furthermore, the results suggested that improved calibration procedures might not automatically provide more accurate flood estimations. The results presented in this paper are based on only two catchments and rather short calibration and test periods. Results obviously might be different in other cases, but more research is motivated on the extrapolation of models. It can be argued that more physically based models might have a greater potential to obtain predictions beyond the range of conditions during calibration. However, Refsgaard and Knudsen (1996) did not find any significant differences between a fully-distributed, physical model and a lumped, conceptual model with regard to model performance in a differential split-sample test. The assertion of the superiority of more physical models, thus, remains to be demonstrated. Differential split-sample test as used in this study provide a more powerful test on model capabilities than the usual split-sample test, because it allows testing the 'risky' predictions of a model rather than the 'safe' ones.

ACKNOWLEDGEMENT

Runoff, precipitation and temperature data were measured by SMHI (Swedish Meteorological and Hydrological Institute). The groundwater level data were provided by SGU (Swedish Geological Survey).

REFERENCES

Ambroise, B., Perrin, J.L., and Reutenauer, D. (1995): Multicriterion validation of a semidistributed conceptual model of the water cycle in the Fecht Catchment (Vosges Massif, France), Water Resources Research, 31: 1467-1481

Bergström, S. (1976): Development and application of a conceptual runoff model for Scandinavian catchments. Report No. RHO 7, Swedish Meteorological and Hydrological Institute (SMHI), Norrköping, Sweden, 134 pp.

Bergström, S. (1990): Parametervärden för HBV-modellen i Sverige, Erfarenheter från modelkalibreringar under perioden 1975-1989 (Parametervalues for the HBV model in Sweden, in Swedish), SMHI Hydrologi, No.28, Norrköping, 35 pp.

Bergström, S. (1992): The HBV model - its structure and applications. Report RH No.4, Swedish Meteorological and Hydrological Institute (SMHI), Hydrology, Norrköping, Sweden, 35 pp.

Bergström, S. (1995): The HBV model (Chapter 13, pp. 443-476), in: Singh, V.P. (ed.) Computer models of watershed hydrology, Water Resources Publications, Highlands Ranch, Colorado, U.S.A., 1130 pp.

Bergström, S., and Sandberg, G. (1983): Simulation of groundwater response by conceptual models - three case studies, Nordic Hydrology, 14: 85-92

Bergström, S., Carlsson, B., and Sandberg, G. (1985): Integrated modelling of runoff, alkalinity, and pH on a daily basis, Nordic Hydrology, 16: 89-104

Bergström, S., Harlin, J. and Lindström, G. (1992): Spillway design floods in Sweden: I. New guidelines. Hydrological Sciences Journal 37: 505-519

Beven, K.J. (1993): Prophecy, reality and uncertainty in distributed hydrological modelling. Advances in Water Resources 16: 41-51

Calver, A. and Lamb R. (1995): Flood frequency estimation using continuous rainfall-runoff modeling, Physics and Chemistry of the Earth, 20(5-6): 479-483

de Groisbois, E., Hooper, R.P., and Christophersen, N. (1988): A multisignal automatic calibration methodology for hydrochemical models: a case study of the Birkenes model, Water Resources Research, 24: 1299-1307

Donelly-Makowecki, L.M. and Moore, R.D. (1999): Hierarchical testing of three rainfall-runoff models in small forested catchments, Journal of Hydrology, 219: 136-152.

Franks, S., Gineste, Ph., Beven, K.J. and Merot, Ph. (1998): On constraining the predictions of a distributed model: The incorporation of fuzzy estimates of saturated areas into the calibration process. Water Resources Research 34: 787-797.

Harlin, J. (1992): Modelling the hydrological response of extreme floods in Sweden. Nordic Hydrology, 23: 227-244.

Kirchner, J.W., Hooper, R.P., Kendall, C., Neal, C. and Leavesley, G. (1996): Testing and validating environmental models. The Science of the Total Environment 183: 33-47

Klemeš, V. (1986a): Dilettantism in hydrology: transition or destiny. Water Resources Research 22(9): 177S-188S

Klemeš, V. (1986b): Operational testing of hydrological simulation models. Hydrological Sciences Journal 31: 13-24

Klemeš, V. (2000a): Tall Tales about Tails of Hydrological Distributions. I, Journal of Hydrologic Engineering, 5(3): 227-231

Klemeš, V. (2000b): Tall Tales about Tails of Hydrological Distributions. II, Journal of Hydrologic Engineering, 5(3): 232-239

Kuczera, G. and Mroczkowski, M. (1998): Assessment of hydrological parameter uncertainty and the worth of multiresponse data. Water Resources Research, 34: 1481-1489.

Lamb, R., Beven, K.J. and Myrabø, S. (1998): Use of spatially distributed water table observations to constrain uncertainties in a rainfall-runoff model. Advances in Water Resources, 22(4): 305-317

Lindström, G., Johansson, B., Persson, M., Gardelin, M., and Bergström, S. (1997): Development and test of the distributed HBV-96 hydrological model. Journal of Hydrology, 201: 272-288

Lindström, G., and Harlin, J. (1992): Spillway design floods in Sweden. II: Application and sensitivity analysis. Hydrological Sciences Journal, 37: 521 - 539.

Linsley, R.K. (1986): Flood estimates: how good are they?, Water Resources Research 22(9):159S-164S

Mroczkowski, M., Raper, G.P., and Kuczera, G. (1997): The quest for more powerful validation of conceptual catchment models. Water Resources Research, 33(10): 2325-2335

Nash, J.E., and Sutcliffe, J.V. (1970): River flow forecasting through conceptual models, part 1 - a discussion of principles, Journal of Hydrology, 10: 282-290

Refsgaard, J.C. (1997): Parameterisation, calibration and validation of distributed hydrological models. Journal of Hydrology, 198: 69-97.

Refsgaard, J.C., and Knudsen, J. (1996): Operational validation and intercomparison of different types of hydrological models, Water Resources Research, 32: 2189-2202.

Seibert, J. (1997): Estimation of parameter uncertainty in the HBV model. Nordic Hydrology, 28(4/5), 247-262

Seibert, J. (1999):, Regionalisation of parameters for a conceptual rainfall-runoff model, Agricultural and Forest Meteorology 98-99: 279-293

Seibert, J. (2000): Multi-criteria calibration of a conceptual runoff model using a genetic algorithm. Hydrology and Earth System Sciences, 4: 215-224.

Uhlenbrook, S., Seibert, J., Leibundgut, Ch. and Rodhe, A. (1999): Prediction uncertainty of conceptual rainfall-runoff models caused by problems to identify model parameters and structure, Hydrolgical Sciences - Journal des Sciences Hydrologiques 44(5): 779-798

Waldenström, A. (1977): Slutrapport över hydrologiska undersökningar i Kassjöåns representativa område. HB Rapport nr 29, Swedish Meteorological and Hydrological Institute (SMHI), Norrköping, Sweden (in Swedish with English description of the area, English titel: Final report on hydrological studies in the representative basin Kassjöån)

Xu, C-Y (1999): Operational testing of a water balance model for predicting climate change impacts, Agricultural and Forest Meteorology, 98-99 (1-4), 295-304.

USING SIMULATED TIME SERIES OF RAINFALL AND TEMPERATURE FOR DESIGN AND LONG TERM FLOOD WARNING

Thomas Skaugen[1,2], Marit Astrup[1], Elin G. Langsholt[1] , Christian Onof[3] and Hans-Christian Udnæs[1]

[1] Norwegian Water Resources and Energy Directorate. P.O. Box 5091, Maj, 0301 Oslo, Norway.

[2] Department of Geophysics, University of Oslo. P.O Box 1022, Blindern, 0316 Oslo, Norway.

[3] Department of Civil and Environmental Engineering, Imperial College of Science, Technology and Medicine, London SW7 2BU, UK

SUMMARY

A study has been initiated in order to determine whether simulated time series of rainfall and temperature can be used as input in a simple rainfall runoff model, so that reasonable discharge values can be obtained for long time flood warning and design purposes. In Norway, precipitation stored as snow for a significant time is of great hydrological importance both for flooding and energy assessments. This poses an additional challenge for the simulation models in that it is necessary for the precipitation model to accumulate the correct amount of precipitation at the time of the onset of the melting season and for the temperature model to correctly place the beginning of the melting period. In this study daily temperature is generated with a conventional autoregressive model and daily rainfall is generated with the rainfall model Random Parameter Bartlett Lewis Rectangular Pulse Model (RPBLRP). The temperatures are simulated with stationary daily means and standard deviations while monthly parameter sets (of 6) are determined for the RPBLRP. The rainfall runoff model used is the Swedish HBV model, which is the forecasting tool of the national flood forecasting service. The precipitation and temperature models have been calibrated for two drainage basins where the rainfall runoff model is known to produce reliable simulations. Ten time series of equal length as the historical data have been simulated and fed to the rainfall runoff model. Although the precipitation and temperature models are able to capture the statistical characteristics such as monthly mean, monthly variance, autocorrelation, probability of a dry day and the duration of dry periods, the simulated mean annual flood are not well reproduced. Deviations in the order of 20 % are found for the mean annual flood, which is obviously unsatisfactory for our purpose. Improvements of the model have been achieved by introducing rightly skewed temperature deviations. The results, however are still not of an operative quality and further analysis of the simulated time series of discharge and comparisons to the observed discharge will be performed in order to isolate possible errors in the modelling framework.

Keywords: runoff scenarios, rainfall, temperature, simulation

1 INTRODUCTION

The national flood forecasting service in Norway provides nation-wide spring flood-scenarios at the onset of each melting season. The customary way to make these scenarios is to use an updated version of the operative rainfall-runoff model (the Swedish HBV model) (Bergstrøm, 1992) and then run the model forward as many times, N, as you have years of historical data of precipitation and temperature. Updated in this context means that the most current estimates of snow coverage and snow water equivalent and discharge observations are used. This procedure provides N outcomes, scenarios, for the future melting season, and the probability of exceedance of certain critical discharge values like the mean annual- or ten-year flood can be assessed.
The problem with this method, and the motivation for this project, is that the length of the historical series of precipitation and temperature at hand is, as a rule, of insufficient length to make reliable inferences on probabilities of exceedance. To estimate such probabilities one should ideally have several hundred of years of data, but the typical situation is from one to a few decades of historical data. To remedy this situation we want to use models that generate time series of precipitation and temperature of sufficient length. In this way more reliable assessments of the probabilities of exceedance of discharge values could be obtained.If one succeeds in establishing good synthetic time series of precipitation and temperature, and good, accurate hydrological models are used, one can think of a variety of possible applications. For design purposes one can use continuous synthetic flow data and analyse the flood peaks. It is no longer necessary to make the assumptions behind the design event approach

or the simplifying assumptions of the event-based derived-distribution approach. Also, as the soil moisture accounting is automatically dealt with, antecedent wetness conditions are no longer an issue (Cameron et al., 2001; Lamb, 1999). Furthermore, if regionally calibrated rainfall runoff models are put into operation, design values and indeed the hydrological regime can be estimated at ungauged drainage basins.

2 METHODOLOGY

A precipitation model, a temperature model, and a rainfall runoff model are necessary in order to build a system for producing spring flood scenarios for Norway. The country is stressed here, because in Norway, precipitation is stored as snow for a significant time, which poses an additional challenge to the simulation system compared to more mid latitude countries. The temperatures must be simulated in such a way that precipitation is correctly accumulated in the cold months and the onset of the melting period is correctly placed in time

2.1 Precipitation model

The model chosen to simulate precipitation time series is the Poisson process based (independent and exponentially distributed inter-arrival times) Bartlett-Lewis Rectangular Pulse Model, or more specifically the Randomised Bartlett-Lewis Rectangular Pulse Model (RBLRPM) (Onof and Wheater, 1993; Onof, 2000). This model is chosen because the Bartlett-Lewis approach to the clustering of cells within larger storms is used in the current developments in spatio-temporal rainfall modelling (Onof, 2000). In the Bartlett-Lewis Rectangular Pulse Model, storms arrive according to a Poisson process with parameter λ. Each storm is followed by a Poisson process of cell arrivals with parameter β, which has a finite duration V. V is chosen as an exponentially distributed random variable with parameter γ. The precipitation is then added to this wet/dry picture in the form of precipitation pulses of exponentially distributed intensity (parameter $1/\mu_x$) and independently exponentially distributed duration with parameter η. In order to improve the reproduction of dry periods, the parameters η, β and γ are considered to be random variables, thus the *Randomised* BLRPM. The total number of parameters is now 6. The model assumes stationary precipitation data, so to take the variability across the year into account, each month is considered separately. As no significant trends were found in the annual totals, inter-annual variability was not considered for the modelling of precipitation. Analytical relations between monthly rainfall statistics such as the probability of a dry day, mean duration of a dry period, mean, variance, and autocovariance and monthly values of the above parameters can be found in Onof and Weather (1993) and Onof et al. (1994).

2.2 Temperature model

The temperature model is a standard linear time series model. The temperature time series are made stationary by considering the daily mean and standard deviation. As in the case of the precipitation modelling, inter-annual variability was not considered as no significant trends were found for the annual means. Simulated temperature values are obtained by simulating from the assumed stationary (normal) distribution of standardised deviations.

$$t(i,j) = (T(i,j) - m_T(i))/s_T(i), \tag{1}$$

where t is the standardised temperature deviation for day i in the j'th year, T is the actual temperature for day i in the j'th year and m_T and s_T are the mean and standard deviation for day i, respectively.

2.3 Rainfall-runoff model

The HBV model, originally developed at the Swedish Meteorological and Hydrological Institute (Bergstrøm, 1976), has been the dominant operative rainfall-runoff model in Scandinavia for two decades. It

can be classified as a semi-distributed conceptual model, using subbasins as primary hydrological units, area-elevation distribution and a simple classification of land use (forest, open and lakes). The model can be described consisting of three main components: subroutines for snow accumulation and melt, subroutines for soil moisture accounting and subroutines for response- and river routing (Sælthun, 1996). The Norwegian national flood forecasting service has calibrated the HBV model for 60 drainage basins to represent the different climatic- and hydrological regimes of Norway. These 60 models form the basis for the forecasting of runoff and flood warnings.

3 CASE STUDY

3.1 Study area and data

The data sets analysed are from two Norwegian drainage basins, Knappom and Gaulfoss (Figure 3-1). Knappom is an inland drainage basin (1625 km^2) situated towards the east, by the Swedish border, and drains to the largest river in Norway, Glomma. Knappom has a median altitude of 396 masl. The Gaulfoss (3085 km^2) drainage basin is situated in central Norway and drains north to the Trondheimsfjord. Gaulfoss is a highland drainage basin with median altitude of 624 masl.

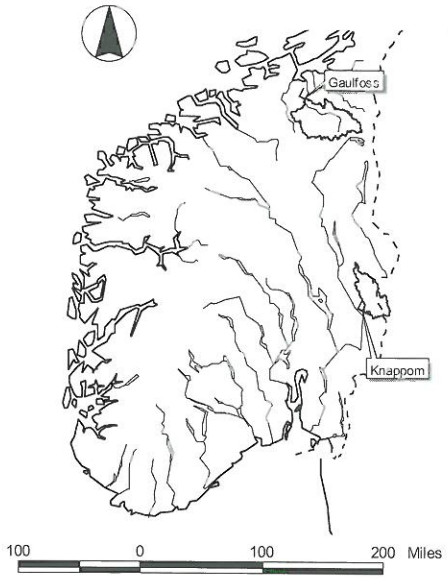

Figure 3-1: The Gaulfoss and Knappom drainage basin in Norway.

The meteorological data for the Gaulfoss drainage basin are measured at two meteorological gauging stations. 15 years of data is used for simulation (1983, 1985-1994 and 1996-1999). Runoff data exists for the periods 1958-1976 and 1988-2000.
At Knappom one meteorological station, with observations from 1976-1986, 1988 and 1990-1998 (21 years), is used. Runoff data is available from 1916.

3.2 Climate and runoff regime

The climatic- and runoff regime for the two drainage basins differs in some respect. Gaulfoss is exposed to a maritime climate, while Knappom is influenced by a more continental weather type. For both drainage basins the temperature variations are characterised by strong seasonality. A comparison of the temperature regime for Gaulfoss and Knappom shows that the former site is warmer in winter and colder in summer (Figure 3-2). This is due to a smoothing effect of humid air masses throughout the year at Gaulfoss. The figure also illustrates that the variability increases as the mean temperature decrease.

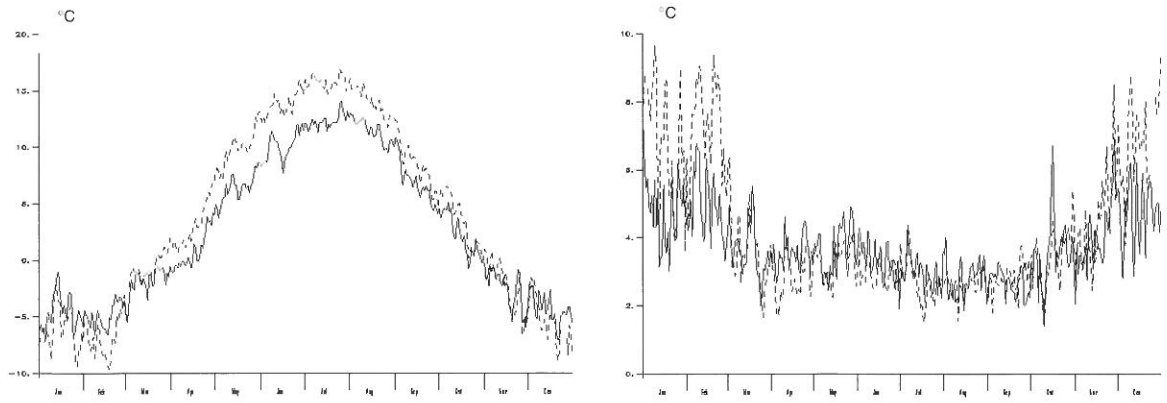

Figure 3-2: Temperature observations (mean(left) and standard deviation(right)). Solid line represents Gaulfoss, and dashed line represents Knappom.

The dominating frontal weather system at Gaulfoss also leads to more precipitation, especially in autumn and winter (Figure 3-3). The relatively high variability in summer for the Knappom drainage basin is, on the other hand, typical for summer showers. For both drainage basins the climatic conditions results in accumulation of snow in winter.

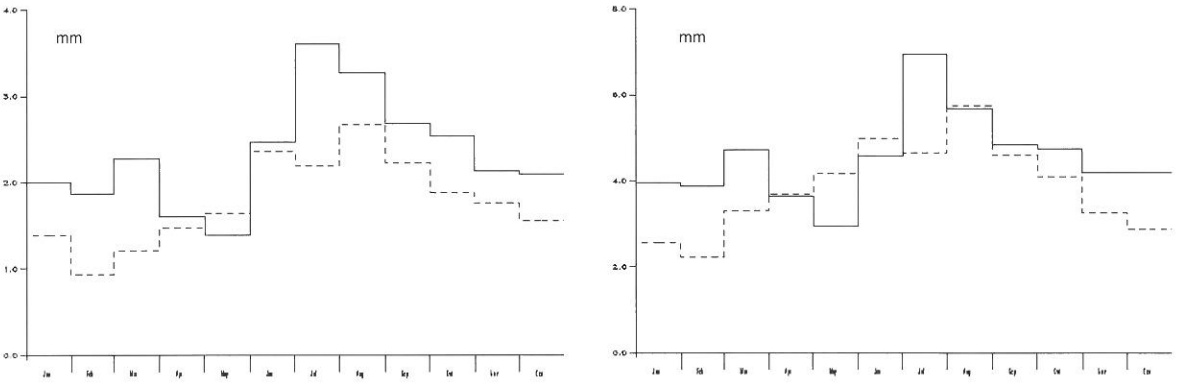

Figure 3-3: Precipitation observations (mean (left) and standard deviation (right)). Solid line represents Gaulfoss, and dashed line represents Knappom.

The annual runoff at Gaulfoss is almost twice as high as for Knappom (27 l/s km^2 and 14 l/s km^2 respectively), while the seasonality is comparable for the two drainage basins with a dominant spring flood as the most obvious feature (see Figure 3-4). Rainfall induced floods in summer and autumn occurs, typically earlier at Gaulfoss than at Knappom.

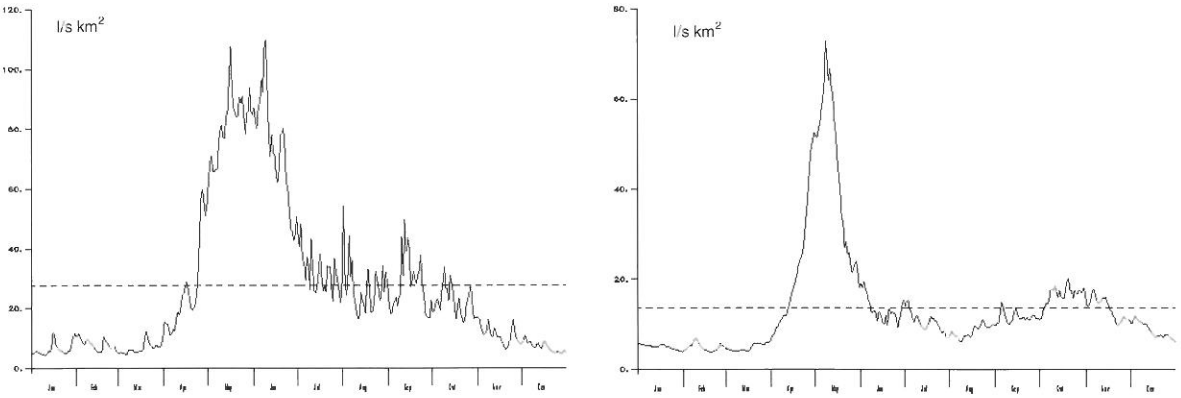

Figure 3-4: Variation of runoff over the year with Gaulfoss left and Knappom right. Solid line represents observed daily mean and dashed line represents annual runoff.

4 RESULTS

Ten temperature- and precipitation series of equal length as the historical series are simulated for the two drainage basins. A validation is performed to ensure that the simulated series correctly reproduces statistical features of the observed series. Good results were obtained for monthly values of mean and variance of precipitation and temperature and monthly values of autocovariance for precipitation, probability of a dry day, and mean duration of dry periods. The simulated meteorological data are then used as input to the HBV-model which return runoff simulations. Figure 4-1 shows the mean of the simulated and observed runoff series.
The simulated runoff series for Gaulfoss seems to agree with the observed series quite well. The simulated spring flood is however somewhat lower than observed. At Knappom the simulated runoff is too low for the spring flood, and the runoff in the winter is systematically too high. The timing of the flood is, for both drainage basins, well simulated.

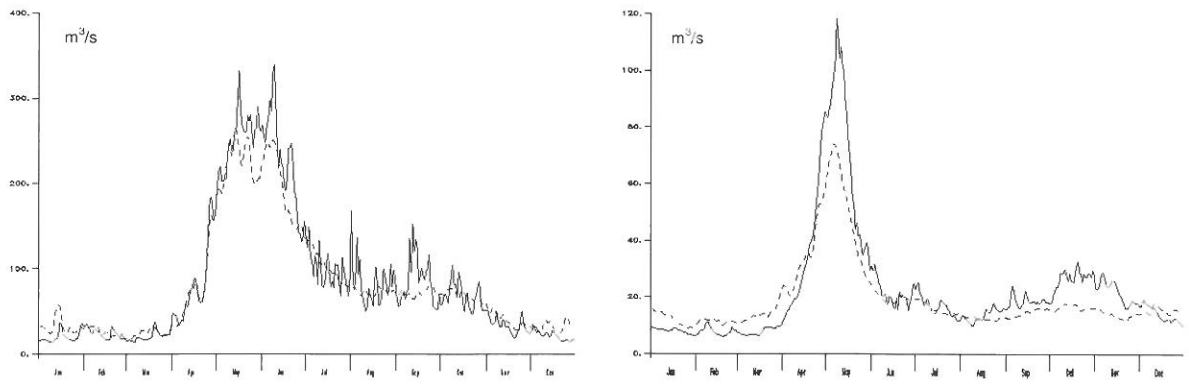

Figure 4-1: Validation of simulated runoff, Gaulfoss left and Knappom right. Solid line is daily mean of observed runoff, while dashed line is daily mean of simulated runoff.

5 DISCUSSION AND CONCLUSIONS

Despite of the apparently successful validation of the simulated meteorological data, it is obvious that the simulated runoff does not resemble observed runoff to such a degree that they can be used for flood scenario purposes. Even if the results for Gaulfoss seem reasonable, it is seen that runoff is overestimated in winter and underestimated in the melting season. This tendency is present for both drainage basins, although it is more pronounced for Knappom.
The reasons for the discrepancy between observed and simulated runoff can stem from (at least) two sources: i) The calibrated HBV model does not explain the relationship between meteorological input and simulated runoff and ii) The simulated meteorological series are not sufficiently validated. If the latter is the case, either the simulated precipitation or temperature series need further investigation.

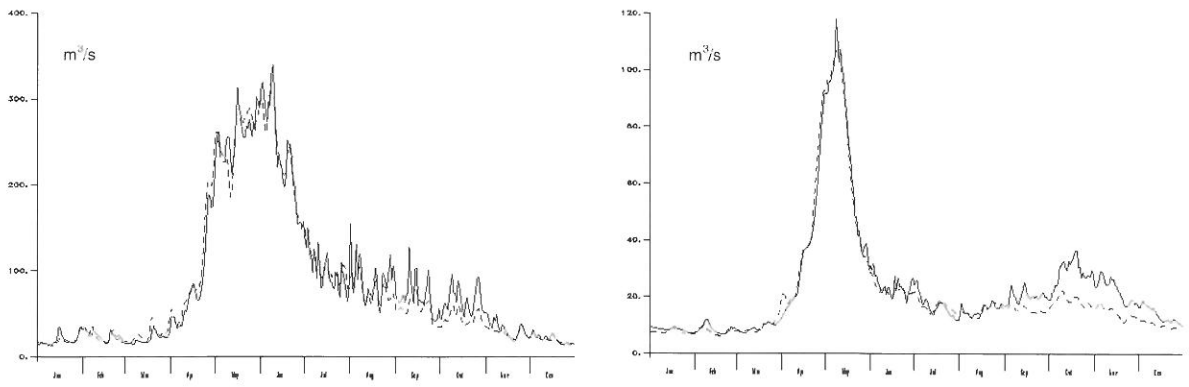

Figure 5-1: Validation of HBV-model, Gaulfoss left and Knappom right. Solid line is observed runoff and dotted line is simulated runoff.

Simulated runoff with observed meteorological data as input is shown in Figure 5-1. For both drainage basins the HBV model simulations agree very well with observed runoff with the exception of autumn rainfall events for the Knappom drainage basin, which, on the other hand, bear little relevance for spring floods scenarios. The argument i) seems, in other words, not appropriate.
Argument ii) seems thus to be a more probable cause to the observed discrepancies apparent in Figure 4-1. Since our results indicate too high runoff in the winter season, it is reasonable to assume that the error occurs in the temperature series. The simulated series consist, in principle, of deterministic daily mean and standard deviation added a random part. The random part is assumed to be normally distributed and stationary over the year. A histogram of all the standardised deviations for the 21 years of data gives us the impression that this is a reasonable assumption. If, however we choose to make a histogram of the standardised deviations for the month of March, we find that this distribution is quite heavily rightly skewed (see Figure 5-2). From a closer inspection of monthly histograms, we find that the histograms of the temperature deviations are rightly skewed for all the (cold) winter months.

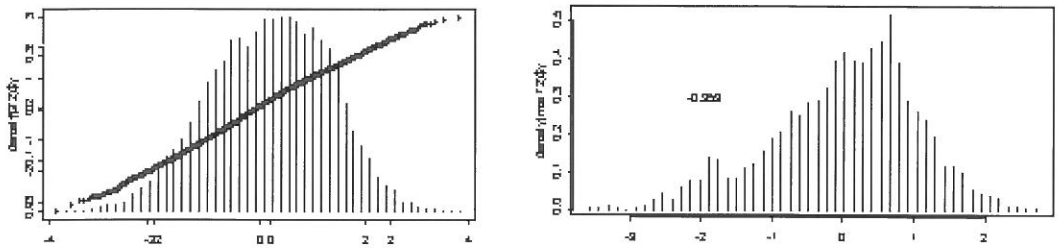

Figure 5-2: Standardised temperature deviations of the Knappom drainage basin for the whole year (left) and for the month March (right).

An effect of this feature is that too many warm days during winter are simulated which, in turn, will give too high winter runoff and too low snow reservoir at the onset of the melting season. The snow melt flood will consequently be systematically underestimated. A consistent explanation to the observed discrepancy between observed and simulated runoff values is thus found in the modelling procedure of the temperature. In order to introduce the possibility of rightly skewed temperature deviations, Gumbel (minimum) deviates were simulated as standardised deviations for months in which the coefficient of skew was less than –0.1 for the historical values. This strategy was carried out despite of the implicit violation of the assumption of normally distributed deviations in autoregressive modelling. Figure 5-3 shows the results of the new modelling procedure of temperature for both drainage basins. Compared to Figure 4-1, we observe significant improvements. The simulated winter low-flow agree more with observed values, and the simulated spring flood has increased and is closer to the observed. There is, however, still some potential for improvement of the simulation model. The spring flood and rainfall floods in autumn seem still to be underestimated, and it can be observed that the annual volume of water is not correctly estimated for the two drainage basins.

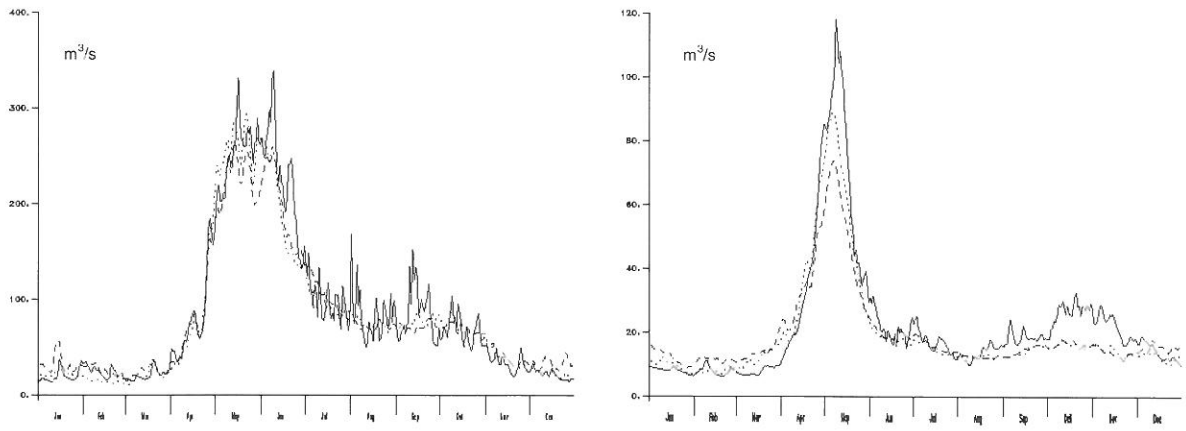

Figure 5-3: Validation of simulated runoff with Gaulfoss left and Knappom right. Solid line is observed runoff, while dashed line is simulated runoff with normal temperature deviations and dotted line is simulated runoff with Gumbel temperature deviations.

A system primarily for producing spring flood scenarios has been put forward, consisting of a precipitation and temperature generator (the Randomised Bartlett-Lewis Rectangular Pulse Model and an autoregressive temperature model) together with a rainfall-runoff model (the HBV model). The synthetic time series of discharge were improved when rightly skewed temperature deviations were introduced in the temperature model. The system is still, however, not of an operative quality and further analysis will be carried out in order to isolate possible errors in the modelling framework.

REFERENCES

Bergstrøm, S. (1976): Devlopment and Application of a conceptual Runoff Model for Scandinavian Catchments. Report RH07, Swedish Meteorological and Hydrological Institute, Norrkøping

Bergstrøm, S. (1992): The HBV model - its structure and applications. Report. RH4, Swedish meteorological and Hydrological Institute, Norrkøping

Cameron, D. et al. (2001): Flood frequency estimation by continuous simulation (with uncertainty). Continuous river flow simulation: methods, application and uncertainties. National meeting of the British Hydrological Society at the Centre for Ecology and Hydrology, Wallingford, 5'th July.

Lamb, R.L. (1999): Calibration of a conceptual rainfall-runoff model for flood frequency estimation by continuous simulation, Water Resour. Res. 35, 3103-3114, Washington, DC

Onof, C. (2000): A precipitation and temperature generator for the Nordic climate. Norwegian water resources and energy directorate, report, Oslo

Onof, C., Weather, H.S. (1993): Modelling of British rainfall using a random parameter Bartlett-Lewis Rectangular Pulse Model. J. Hydrol. 149, 67-95, Amsterdam

Onof, C. et al. (1994): Note on the analytical expression of the inter-event time characteristics for Bartlett-Lewis type rainfall models. J. Hydrol. 157, 197-210, Amsterdam

Sælthun, N-R. (1996): The "Nordic" HBV model. Publication No. 07, Norwegian water resources and energy directorate, Oslo

FLOOD DISCHARGE ESTIMATION USING STORAGE FUNCTION METHOD (CASE STUDY: THE LESTI RIVER BASIN, INDONESIA)

Tri Budi Prayogo[1], Gatot Eko Susilo[2]

[1] Lecturer at Fakultas Teknik Jurusan Pengairan (Water Resources Engineering Department), Universitas Brawijaya Malang, Jl. MT. Haryono 167 Malang, Indonesia 65145, didid72@yahoo.com

[2] Graduate student in Civil Engineering Dept. Memorial University of Newfoundland, Box 29 Faculty of Engineering and Applied Science MUN, St. John – Newfoundland, Canada A1B 3X5, susilo@engr.mun.ca

SUMMARY

The study aims to present a rainwater-flood discharge transformation process using storage function model, a method that considers a watershed as a storage that can temporary retain and store rainwater before the rainwater becomes river discharge. The model was built by using conceptual relationship among watershed parameters affecting the function of the watershed as the rainwater storage. The Lesti River Basin, in the East Java Province, Indonesia has been chosen for the study. Rainfall and discharge data for the year 1992 to year 1994, collected from rainfall gauge and hydrometric stations located on the basin were used in this study. The model was calibrated using time series rainfall and discharge data in hourly basis of September 23, 1992. Five events of floods occurred in different day and time between 1992 and 1994 were used for verification process. Results indicated that the Lesti River Basin has potential ability in storing rainwater. The maximum runoff coefficient of the basin was found 34%. The method has represented the rainwater-flood discharge transformation process very well on the Lesti River Basin. The comparison between calculated and observed discharges demonstrated less than 10% of average of mean error. The weakness of the method is its complexity in trial and error in calibration process. This causes the modeling process to be time consuming. Computer programming is necessary to assist in calibration and verification of the model.

Keywords: storage function method, rainwater-flood discharge transformation

1 INTRODUCTION

Indonesia, as many developing countries, usually has high rates of population growth. With the rapid increase in population, the decrease in quality and quantity of natural resources are often found in this area. Natural disaster such as flood and forest fire always come almost every year and causes big damage.
Water management sometimes became difficult project due to the complexity of problems, limitation of data, and the conflicts of interests in water allocations. Flood is one of the biggest problems in many areas in Indonesia. Thousands of acres of agricultural fields are damaged, and farmers loose their crops every year because of the floods. In the beginning of 2002, Jakarta, the capital of Indonesia was shut down for all activities also because of flood. Efforts to control the flood had been directed by the Government of Indonesia since long ago. Some calculation methods have been used to determine discharges in Indonesia for flood estimation. These methods generally built based on empirical approaches. Nakayasu, Snyder, and GAMA I are the examples of hydrograph calculation methods that are most frequent used in Indonesia. Non-hydrograph method, such as empirical formula of Weduwen, Melchior, Hasper, and Rational method, are also frequently used especially for watersheds that have limitation of rainfall data. In the late time, some discharge calculation methods based on river routing procedures have been developed to achieve better discharge calculation for Indonesian watersheds.
This paper is presenting study with aim to apply a method of rainwater-flood discharge transformation using storage function method. The Lesti River Basin, in the East Java Province, Indonesia has been chosen for the study.

2 STORAGE FUNCTION MODEL

Storage function method is a rainfall-runoff transformation method that uses the relationship between storage and direct runoff in the watershed as a function of distance and time. This method was introduced by Kimura (1961) and applied for the first time in the Japanese watershed. Storage function method can be accurately applied in the watersheds with area between 10 to 1000 km^2. For applica-

tion in the larger watersheds or longer channel, the area of study can be divided into several smaller areas or several sections of channel.
In common hydrologic models, rainfall is the primary factor and initial factor in runoff generation process in a watershed. Rainfall falling onto a watershed will produce runoff either surface runoff or subsurface runoff. Some of rainwater will be retained in the watershed depression storage and infiltrate to the unsaturated soil zone, and the others will flow as surface runoff on the surface of watershed and filling the main river. If the ability of watershed in retaining water is in maximum condition, the watershed is considered saturated area and all rainwater will flow as surface runoff. Discharge produced in the outlet of the watershed is usually a result of river routing.
In the storage function model, the storage capacity or the ability of a watershed in storing or retaining rainwater is the important factor to analyze. The basic concept of this method is that storage function of a watershed is considered an exponential function of direct runoff (Q):

(1) $$S = kQ^p$$

where, S is the storage of a watershed or channel (m^3), Q is direct runoff (m^3/s), and k and p is constant. The value of k and p can be derived from trial and error process involving rainfall time series data, flow time series data, and watershed area.
Flood discharge estimation in the watershed using storage function method requires two types of data: watershed characteristic data and time series data of rainfall and river discharge. The first step of the procedures is to prepare a pair of historical time series rainfall data (R) and time series discharge data (Q) of the same day. Combined with the data of watershed area (A), Q is transferred into q, a discharge variable as a function of Q and A, given as:

(2) $$q = \frac{3.6Q}{A}$$

Sometimes, the rainfall did not directly produce discharges in the watershed. Based on this condition, it is necessary to find the time difference between the initial time of rainfall and initial time of surface runoff stimulated by the rainfall. The time different furthermore is called lag_t. Trial and error processes have to be conducted for this purpose. Lag_t equal to 0 may be able to be used as an initial lag_t for trial and error. Lag_t equal to 0 means that the rainfall is directly producing surface runoff in the watershed at the same time of initial rainfall.
Using the time series data and the lag_t, the calculated storage capacity of the watershed can be derived as a function of lag_t, R, and q:

(3) $$S = \phi(lag_t, R, q)$$

When S series is obtained, the next step is to plot the relationship between q and S in the logarithmic graph form with q as an absis and S as an ordinat. If the graph indicated linear relationship, the procedure can be continued to the next step. The next step of the procedures is to find the constant k and p. Constant of k is defined as the slope of the graph ($\tan\alpha$) while p is the value of S when q is equal to 0. Using these constants, the equation explaining relationship between S and Q, as described in the equation 1, can be formed. In case the relationship is not linear, the trial and error process must be repeated using different lag_t until linear relationship between q and S obtained.
Since S is obtained, the graph explaining relationship between discharge at time t_i (q_{ti}) and storage capacity of the watershed at time t_i (S_{cti}) can be derived. Storage capacity of the watershed is formulated as:

(4) $$S_{ct_i} = S_{t_i} - \frac{q_{ti}}{t_i}$$

From the graph, equation for q as a function of S_{cti} can be obtained. This equation is used for calculating simulated q for every t_i. Other graph explained relationship between cumulative of simulated and cumulative observed q is furthermore formed to find the value of watershed runoff coefficient (f_1) and rainfall depth that makes the watershed becomes saturated (R_{sa}). f_1 is defined as the slope of the graph ($\tan\beta$) and has value between 0 and 1.
In the certain t_i, there will be a deviation between cumulative simulated and cumulative observed q. t_i of the deviation is equal to 45 degrees is taken as the time when the surface of watershed starts to be

saturated for the first time. Rainfall depth occurs at that time is considered R_{sa}. Before the R_{sa} is obtained, the calculation of the discharge in the outlet of the watershed is calculated using equation as a function of storage and time. The calculation given as:

(5) $$Q_{t_i} = \frac{1}{3.6} f_1 R_{rt} A - \frac{S_{t_i}}{t_i}$$

where Q_{ti} is the amount of water produced in the watershed outlet at t_i (m^3/hour), f_1 is the runoff coefficient of the watershed, R_{rt} is the average of rainfall at t_i and t_{i-1}(mm), A is watershed area (km^2), and S is the watershed storage (m^3).
After the R_{sa} is obtained, the rainfall is directly transformed into discharge in the outlet of the watershed and calculated as:

(6) $$Q_{t_j} = \frac{1}{3.6} f_1 R_{rt} A$$

Total discharge is the summation of discharge before and after R_{sa}. The validity of the model is tested by comparing the total discharge to the observed discharge for every t_i. If the required R^2 is obtained, the model has to be used to verify other flood events. If the model performance is good for other flood events, the model can be considered able to represent the behavior of the watershed in responding rainfall. Contrarily, if the required R^2 is not obtained either for calibration and verification processes, the trial and error have to be repeated until valid k and p are obtained. The flowchart of discharge calculation procedures in the model is presented in Appendix 1.

3 STUDY AREA

The Lesti River Basin is the sub-watershed of The Great Brantas River Basin located in East Java Province, Indonesia. Administratively, the Lesti River Basin is located in the Malang district. The basin is located in the upstream part of the Bantas River Basin. Total drainage area measured at the Automatic Water Level Recording (AWLR) on the Tawang Rejeni is 379 km^2. The main streamflow in this watershed is 32.8 km. The average slope of area is about 0.0459 with runoff coefficient about 0.62. The Lesti River Basin is a radial basin with land cover dominated by forest and agriculture areas. Small area of residences is in the basin, mainly in the downstream part.

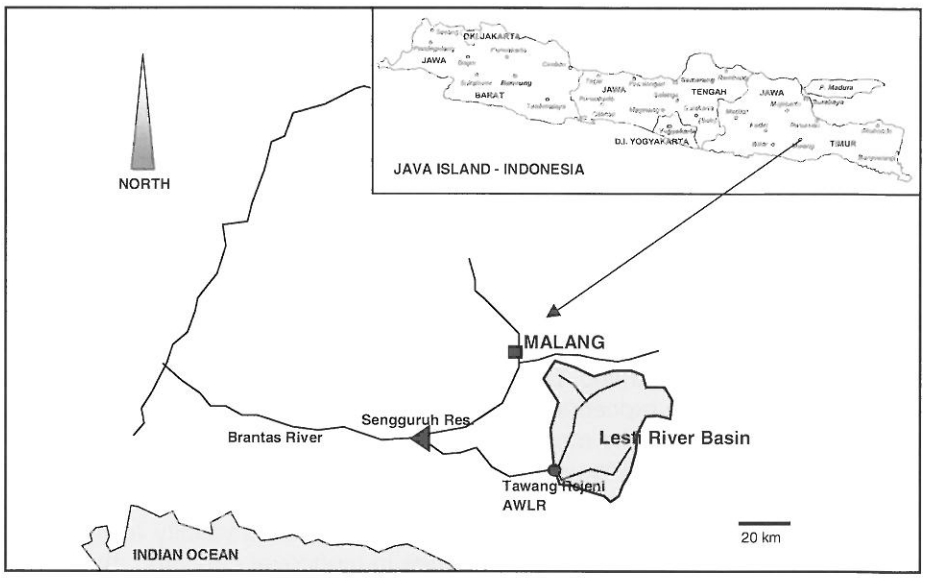

Figure 3-1:
Study Area.

There is a reservoir in the downstream part of the basin. The Sengguruh reservoir is used for hydropower generator, flood control purpose, and water supply control for Karangkates reservoir, the biggest reservoir in the Brantas River Basin. The basin is also an important part of Flood Forecasting

Warning System (FFWS) of the Brantas River. Water resources management of The Lesti River Basin recently is directed by the Perusahaan Umum Jasa Tirta I, a government company handling water resources management for the Great Brantas River Basin.
To support water resources management in the basin, Perusahaan Umum Jasa Tirta I located 6 rain gauge stations. These stations are Poncokusomo station, Dampit station, Ampelgading station, Turen station, Tangkil station, and Rejeni station. The hydrometic station, AWLR Tawangrejeni, records realtime flow data and sends directly the data to the central office of Perum Jasa Tirta I.

4 RESULT AND DISCUSSION

The method was applied to model flood discharge in the Lesti River Basin using data of the year 1992 to year 1994, obtained from rainfall gauge and hydrometric station located on the basin. Six events of floods have been used for calibration and verification process. Time series of discharge data in hourly basis of September 23, 1992 has been used for model calibration. Verification is applied to five events of floods occurred in different day and time between 1992 and 1994. Time series data for every flood event consists of 24 hours time series data for discharge and rainfall. Discharge data was obtained from AWLR Tawangrejeni and the rainfall data is an average of data from several raingauge stations in the basin.
Using trial and error method on data for calibration, the value of lag_t, and the relationship between S and Q for the basin has been found. From the experiment, lag_t of 2.5 hour is found. This means that time different between initial surface runoff in the outlet and initial rainfall falling in the basin is 2.5 hours. Constant of k and p derived from the trial and error is about 4.0 and 0.6 respectively. Furthermore, the relationship of S and Q can be explained as:

(7) $$S = 4.0Q^{0.6}$$

Based on this result, the graph for calculating simulated q for every t*i* is developed. Graph explained relationship between cumulative of simulated and cumulative observed q is furthermore formed to find the value of watershed runoff coefficient (f_1) and rainfall depth that makes the watershed becomes saturated (R_{sa}). Based on the graph, the value of f_1 is found approximately 0.30 while the average value of R_{sa} is about 18mm. Total calculated discharge finally obtained based on the value of f_1 and R_{sa} and compared to the observed discharge. The hydrograph comparison, presented in Appendix 2, shows that the mean error produced is about 3.64%.
Equation 7 furthermore is applied to five flood events for verification process. Result indicates that f_1 produced are between 0.03 and 0.34. The values of R_{sa} are varied based on the depth and distribution of rainfall in every rainfall event. However, the saturated condition of watershed has never been found. The fact about the values of f_1 and R_{sa} indicates that the basin is having strong ability in storing rainwater. The fact also tells that the basin is generally able to store 70% rainwater in every rainfall event and release the rest 30% as surface runoff. This circumstance is not surprising due to the land cover of the Lesti River Basin that is dominated by forest and agriculture areas. Residential area that exists in the downstream of watershed does not give significant contribution for surface runoff generation due to the small area and the position of this region in the basin. As final result, hydrograph comparison has been developed using observed and calculated hydrograph. The comparison between calculated and observed hydrograph demonstrated mean of error between 3% and 8%.
This circumstance can be interpreted that the method has modeled the rainwater-flood discharge transformation process very well on the Lesti River Basin. However, it is necessary to note that modeling runoff behavior in a watershed using storage function method is not easy to do. The trial and error process in the model is complicated and time consuming. Due to this condition, it is necessary to develop the method that can be used for simplifying the procedure and reducing time used in modeling. The use of computer programming is compulsory to assist the modeler calibrating and verifying the model.
Equation 1 explaining S, Q, k, and p relationship is very empirical relationship, in the sense that the equation can change any time based on the characteristics of the basin. For basins with rapid change in landcover condition, the model must be checked every year to guarantee its validity in modeling runoff behavior in the basin. Conversely, for basins with slow change in landcover condition, the model can be checked every 3 to 5 year.
At present, storage function method is used to predict flood discharge for short period such as day discharges or half-day discharges. The application of the method for modeling discharges either flood discharge or low discharge for longer period may be interesting to do in order to find more comprehensive simulation of runoff behavior in the watershed. For watersheds that have long rainfall and

discharge time series in hourly basis, the application of storage function method can be undertaken to simulate weekly, biweekly, or monthly discharges.

5 CONCLUSIONS

Flood discharge estimation using storage function method for the Lesti River Basin has been analyzed. Results indicated that storage constant k and p for the basin are 4.0 and 0.6 respectively. Results also indicated that the Lesti River Basin has strong ability to store the rainfall water falling on the basin. Based on the equations formed in the application, the maximum runoff coefficient of the basin was found to be about 34%. The model has represented the rainwater-flood discharge transformation process very well on the Lesti River Basin. The comparison between calculated and observed hydrograph demonstrated less than 10% deviation. However, to do modeling runoff behavior in a watershed using storage function method is not easy. The trial and error process in the model is complicated and time consuming. Development of a method that can be used for simplifying the procedure of trial and error and reducing time used in modeling is urgently needed. The use of computer programming is compulsory to assist the modeler calibrating and verifying the model.
The model must be checked to guarantee the validity of the model. The model must be checked every year for basins with rapid change in landcover condition. For basins with slow change in landcover condition, the model may be checked every 3 to 5 year. Finally, the application of the method for modeling discharges either flood discharge or low discharge for longer period may be interesting to do in order to find more comprehensive simulation of runoff behavior in the watershed.

REFERENCES

Department of Public Work of the Republic of Indonesia. (1974): Rainfall and Runoff Relationship and Flood Design. Directorate General of Water Resources. Department of Public Work of the Republic of Indonesia. Jakarta - Indonesia.

Department of Public Work of the Republic of Indonesia. (1976): Rivers. Directorate General of Water Resources. Department of Public Work of the Republic of Indonesia. Jakarta - Indonesia.

JICA. (1989): Study on Kelantan River Basin Wide Flood Mitigation. Government of Malaysia Workshop for Storage Function. Kelantan - Malaysia.

Kyu, Lee Jong. (1995): An Application of Fuzzy Control to Modified Storage Function Model. Flood Estimation and Water Resources Development Seminar. Penang. Malaysia.

Montarcih, Lily. (1992): Kalibrasi Parameter Hidrograf Satuan Sintetik Nakayasu di DAS Pengganjing. Seminar Article. Lombok - Indonesia.

Montarcih, Lily. (1997): Perbandingan Hidrograf Satuan Sintetis Gama I, Snyder, Nakayasu, dan FSR untuk SubDAS Amprong. Fakultas Teknik Jurusan Pengairan Universitas Brawijaya. Malang - Indonesia.

Prayogo, T. B. (1999): The Study of Parameter Determination of Storage Function Method in the Lesti River Basin. Master Thesis. Fakultas Teknik Jurusan Pengairan Universitas Brawijaya. Malang - Indonesia.

Soemarto, C. D. (1995): Hidrologi Teknik. Penerbit Erlangga. Jakarta - Indonesia.

Sosrodarsono, Suyono. 1983: Hidrologi Untuk Pengairan, Pradya Paramitha, Jakarta.

Suguira, K. (1977): Rivers, Kolombo Plan, Srilangka.

Suhartanto,Ery. (1997): Perbandingan Hidrograf Satuan Sintetis Gama I, Snyder, Nakayasu, dan FSR untuk SubDAS di Wilayah Sungai Brantas. Fakultas Teknik Jurusan Pengairan Universitas Brawijaya. Malang - Indonesia.

Yoon, Kang Hoon. (1995): A Study on the Parameter Estimation of the Storage Function Model For the Nangdong River Basin. Flood Estimation and Water Resources Development Seminar. Penang - Malaysia.

APPENDIX

Appendix 1: Flowchart of discharge calculation using storage function method.

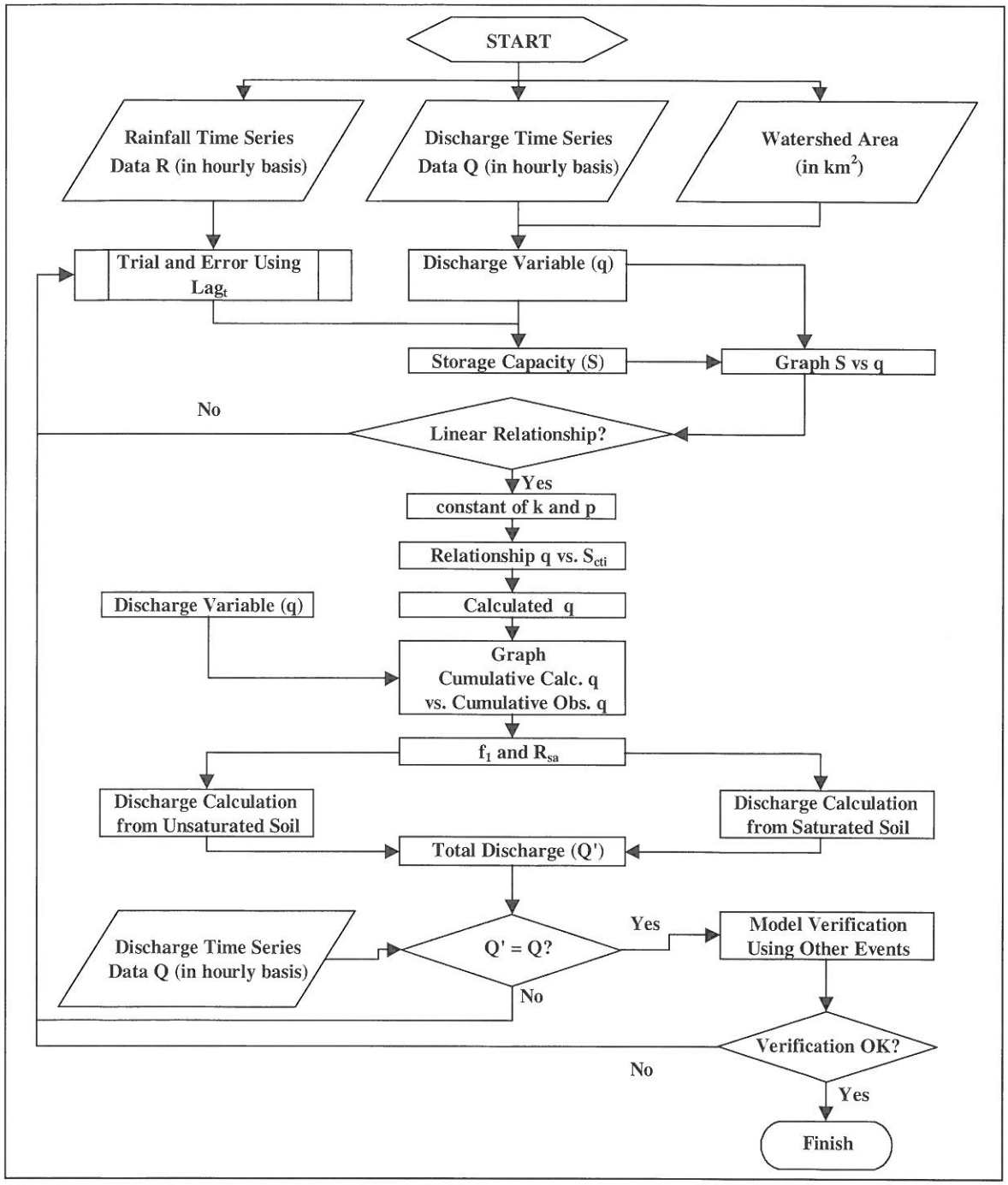

Appendix 2: Examples of hydrograph comparison of the Lesti River Basin as result of the application of storage function method.

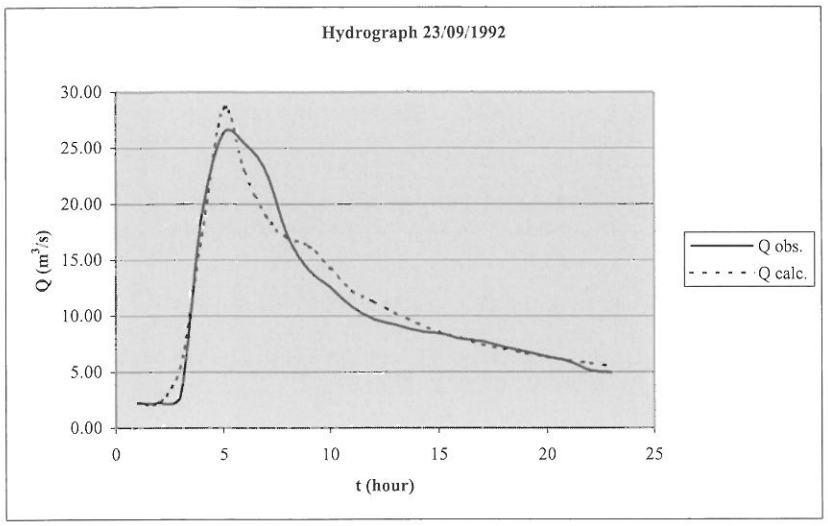

23/09/1992		
t	Q obs.	Q calc.
1	2.24	2.24
2	2.24	2.24
3	2.78	5.32
4	19.00	17.19
5	26.29	28.48
6	25.43	22.93
7	22.91	18.86
8	17.18	16.98
9	14.14	16.24
10	12.58	14.23
11	10.83	12.29
12	9.73	11.24
13	9.20	10.31
14	8.69	9.37
15	8.44	8.54
16	7.95	8.01
17	7.71	7.45
18	7.25	7.05
19	6.79	6.66
20	6.36	6.3
21	5.93	6.02
22	5.13	5.76
23	4.94	5.5

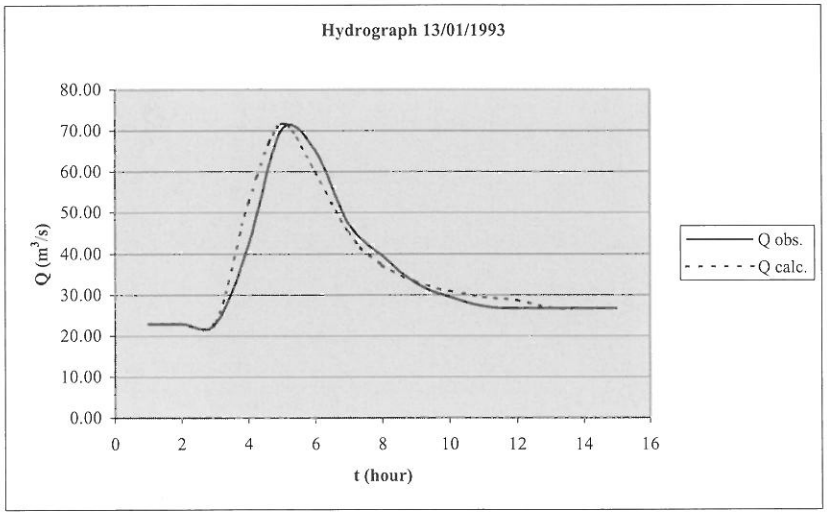

13/01/1993		
t	Q obs.	Q calc.
1	22.95	22.91
2	22.95	22.92
3	22.95	23.13
4	42.22	52.43
5	70.12	71.67
6	65.28	59.71
7	47.38	45.14
8	39.48	37.26
9	32.74	33.21
10	29.48	30.92
11	27.16	29.42
12	26.74	28.67
13	26.74	26.73
14	26.74	26.73
15	26.74	26.73

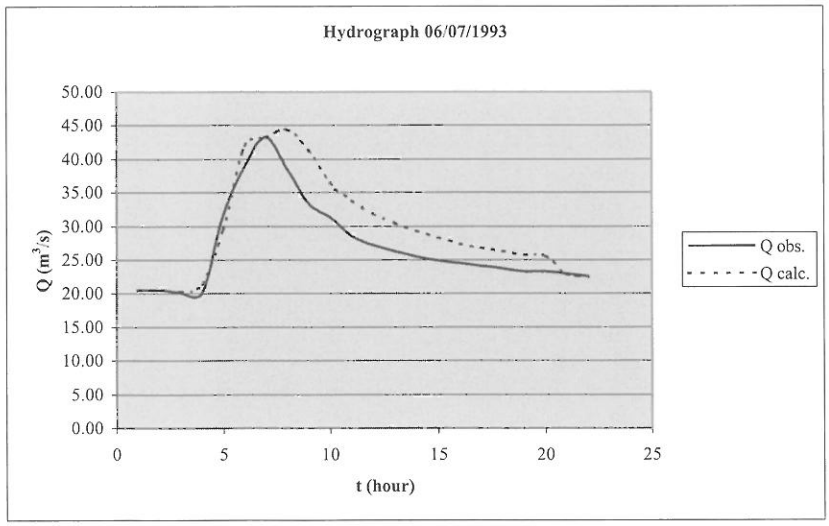

06/07/1993		
t	Q obs.	Q calc.
1	20.53	20.52
2	20.53	20.52
3	20.11	20.24
4	20.11	21.43
5	31.80	29.58
6	38.96	42.04
7	43.27	43.25
8	38.43	44.41
9	33.27	41.18
10	31.38	36.44
11	28.53	33.91
12	27.16	31.81
13	26.32	30.47
14	25.48	29.31
15	24.95	28.31
16	24.53	27.37
17	24.11	26.81
18	23.69	26.28
19	23.27	25.76
20	23.27	25.59
21	22.95	22.91
22	22.53	22.51

THE GREAT 2001 FLOOD IN GOLESTAN PROVINCE, IRAN: CAUSES AND CONSEQUENCES

Forood Sharifi, Bahram Saghafian, Abdoulrasoul Telvari

Soil Conservation and Watershed Management Research Center.13445-1136 Tehran, Iran
Sharifi@scwmrc.com, Saghafian@scwmrc.com / telvari@scwmrc.com

SUMMARY

The worst flooding event of Golestan province, Iran, in over two centuries claimed over 300 lives after a weekend of heavy rains and brought about a devastating disaster in the province of Golestan. The objective of this study was to identify the causes of the Great 2001 Flood and debris flow occurrence in flooded area located north of Iran and to analyse the runoff mechanism of this event. Considering that the area was still vulnerable to flooding, a series of site investigation activities were carried out to identify the hazardous factors and to propose mitigating measures. The preliminary evaluation indicates that the existance of bare soil in the basin, moveable material, steep slopes, high rainfall intensity, deterioration of pasture and forest lands, and inappropriate agriculture and development practices were the main factors for occurrence and the extent of the disaster. Due to the potential of flooding and debris flow events in future, some countermeasures also proposed.

Keywords: Flood, Debris flow, Iran, Golestan.

1 INTRODUCTION

Beginning late evening on 10 August 2001 and continuing into the next day, an exceptionally heavy rainfall covered large areas in north and northeastern Iran (including Golestan Province) which has gone through a persistent three year drought period. The rainstorm sparked a flood in the streams and rivers in the Mother-Soo river basin. The powerful flood traversed the basin, devastating essentially everything in its path. Trees as tall as 20 meters, road guards and road asphalt, large boulders, houses, automobiles, and human beings were removed and carried downstream by the flood into the Golestan Dam reservoir. The flood claimed a total of 300 dead and missing. Many of the missing people were presumed to be the tourists staying overnight in the Golestan forest. In addition to the death toll, thousands were left without homes; some 10,000 people were evacuated to safety during the three-day deluge. The total number of people directly affected by the floods in the region was estimated to be more than 217,000. A number of key bridges and over 194 km of roads were entirely washed away or hardly hit. The direct damage was estimated at $75 million dollars. However, official government reports put the total damage at over $400 million dollars (Sharifi and Mahdavi, 2001). In addition, some 387 villages were affected and 4,000 buildings sustained heavy damage. The floodwaters submerged some 10,000 ha of forest and pastureland and over 15,000 ha of valuable farmland. The water logging caused malaria and diarrhea to break out partially in the affected areas. Water supply of 84 villages and five towns, 300m of gas pipelines, and 130 vehicles were washed away and 6000 live stocks were lost. And last but not least, approximately 10% of Golestan dam reservoir was filled with sediment only after two years of operation.
After the flood, roads remained impassible in many spots as bulldozers and emergency workers worked frantically to clear mud, debris, and logs from major roads to provide minimum access to the local towns and villages in the province. Meanwhile, many people in the affected areas remained stranded and isolated as the floodwaters cut residents from the rest of the areas.

2 HISTORICAL FLOODS IN IRAN

In many regions in Iran runoff and flooding is produced from as little as 9 mm of rainfall (in some cases only with 10 minutes rainfall duration) over a small catchment of 50 sq. km and sometimes causes considerable loss of life and properties (an example of this flood occurred in 1997 in Masuleh city and 50 people were killed). Drought and flooding are two familiar terms in the Iranian climatic conditions. For this reason, the utilization of floodwaters and harvesting of rain waters have traditionally been practiced through flood spreading, ground water recharge systems, and recharge ponds by ancient Iranians (Sharifi and Ghafouri, 1997). Such systems have been constructed to store floodwaters as a means of combating droughts in the coming years.
In the last 50 years, about 3700 events of flooding have been reported; among them some 53% occurred during the last 10 years. During the last 20 years, the number and the peak of flood events and its damages have increased (Sharifi and Heydarian, 1999). Table 2-1 gives a summery of the flood events in the past 50 years showing an increasing trend (Sharifi and Mahdavi, 2001).

Table 2-1: Number of major flood events during period of 1951-2001 in Iran.

Period (yr)	Number of flood events	Percent (%)	% increase over (1951-69) period
1951-69	195	5.3	100
1961-70	233	6.3	120
1971-80	431	11.6	220
1981-90	904	24.4	460
1991-95	1020	27.6	520
1996-01	917	24.6	470
Total	3700	100	-

3 DESCRIPTION OF THE GOLESTAN REGION

The dominant climate in Iran is characterized as arid and semi-arid. However, the northern part of the country along the southern Caspian Sea coastline enjoys Mediterranean precipitation regime. The precipitation decreases from west to east in the 400-1900 mm range. The Golestan province is located on eastern part of the Caspian Sea coast and lies between (53, 48) to (56, 30) E longitude and (36, 35) to (38,15) N latitude. The flooded Mother-Soo basin, located in the Golestan province, is one of the six basins draining into the Caspian Sea. The Mother-Soo river ends up into the Golestan dam reservoir constructed in 1999, having 90 million cubic meter capacity. The climate of this area is characterized by mild temperature and above-country-average annual rainfall of approximately 450 mm. The Mother-Soo river basin (Figure 3-1), drains 2,188 sq. km in area and stretches about 100 km in length with a 5% average longitudinal slope. The basin may be divided into three distinctive parts. Medium pasture and bare lands cover the upper part of the basin, whose area is 1,100 sq. km. The upper basin area is believed to have been mostly covered by forest in the distant past. The middle part of basin includes a dense protected forest declared as a national park. This area is 700 sq. km. In the forested part of the basin, the river valley is relatively narrow and steep. The lower part of the basin is mixed farm and rangeland, including large cotton and potato fields, with an area of 388 sq. km. The hillsides in this area are relatively bare because of overgrazing and dryness. Overgrazing has caused compaction of the soil and widespread sheet erosion. Land use map of the basin is shown in Figure 3-1.

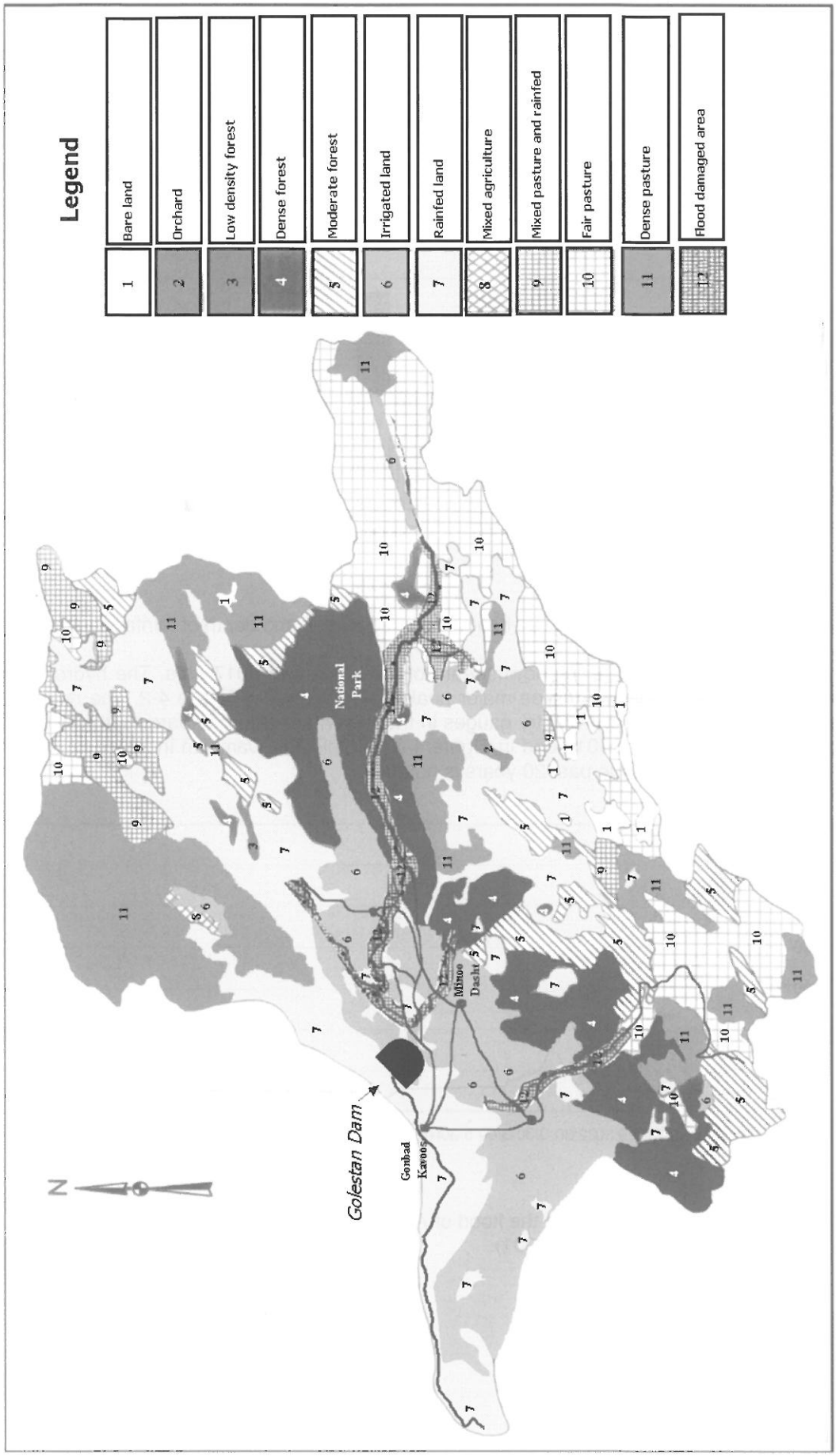

Figure 3-1: An over view of Mother-Soo catchment.

4 HYDRO-CLIMATOLOGICAL ASPECTS OF THE FLOOD

A total depth of 150 mm rainfall was recorded on the date of the flood in Dasht village located upstream of the basin. The rainfall intensity early in the first hour of rainstorm was recorded at 50 mm/hr, followed by 11 hours of continuous light rainfall of 9 mm/hr in intensity. The maximum observed 24-hr rainfall depths at the existing rain gauges are compared with the depths of rainfall corresponding to the August 2001 flood in Figure 4-1. In all rain gauges, except Galikosh, the rainfall depth of August 2001 exceeded those of historical recorded events.

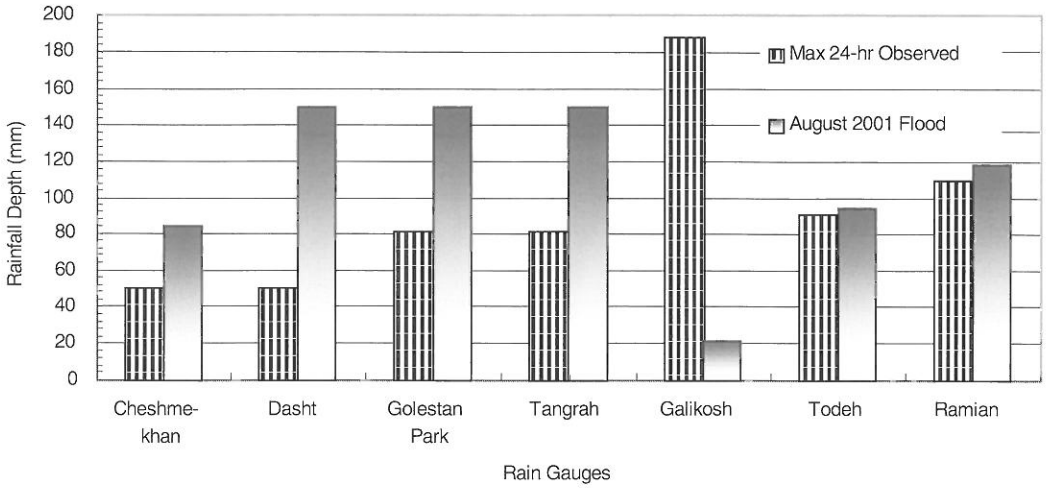

Figure 4-1: Comparison of maximum 24 hours observed rainfall and depth of rainfall caused the flood.

The peak discharge recorded at the downstream of the basin was 3017 cms. The hydrograph of the flood event at Golestan Dam with three major peaks is presented in Figure 4-2. The recorded maximum peak discharges at the hydrometry gauges in the region are also compared with the peak values corresponding to the August 2001 flood in Figure 4-3. In Golestan Dam, an increase of 7.5 times the maximum value observed in the past 20 years is noted.

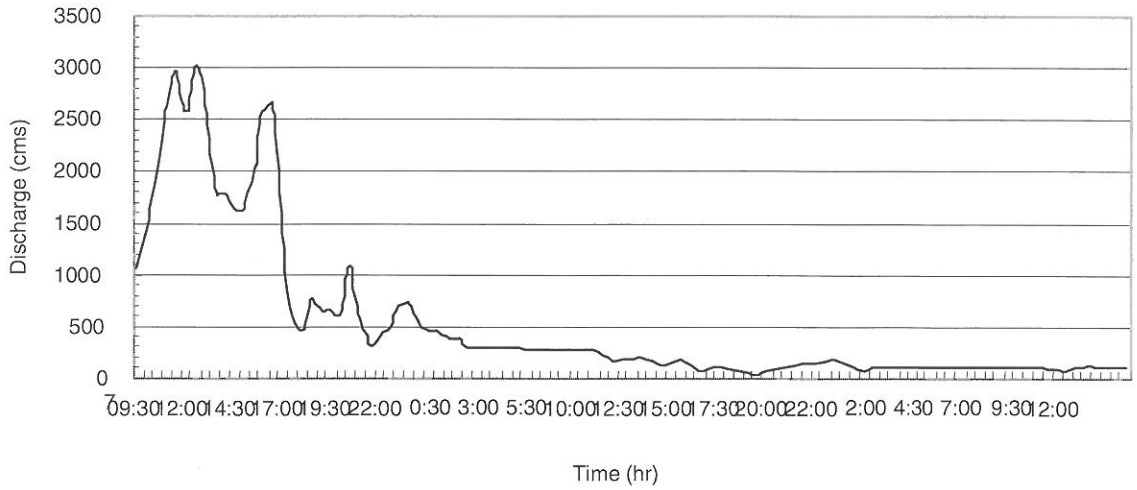

Figure 4-2: The inflow hydrograph of the flood of August 2001 at Golestan Dam (start date is August 11, 2001).

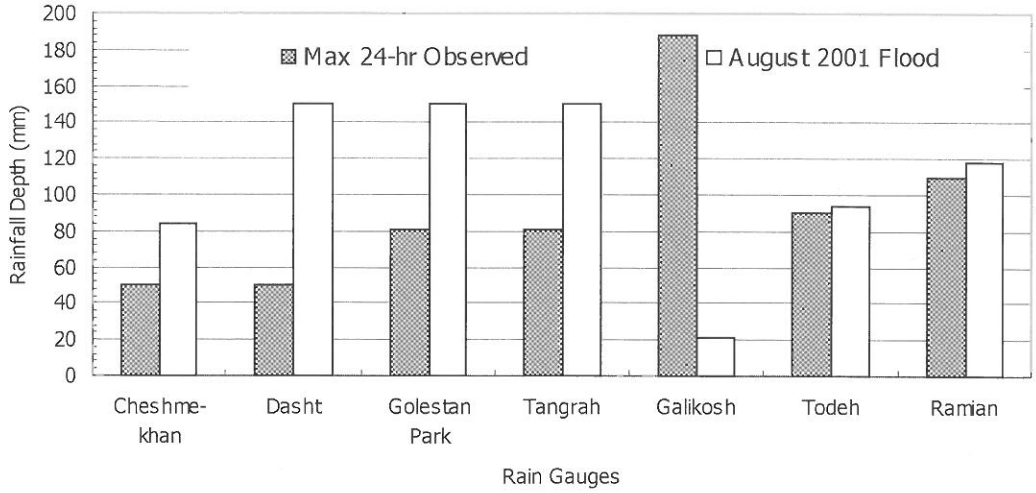

Figure 4-3: Comparison of peak values of flood 2001 with maximum observed peak discharges.

The flood height was 10 to 15 meters while passing through the middle subbasin area of Golestan National Park with a valley width varying from 100 to 300 meters. In Tangrah, at the end part of the middle forested sub-basin, the flow depth of 5 to 8 meters with a width of 400 meters inundated the area. Figure 4-4 present an image of the region after the night of flood 2001.

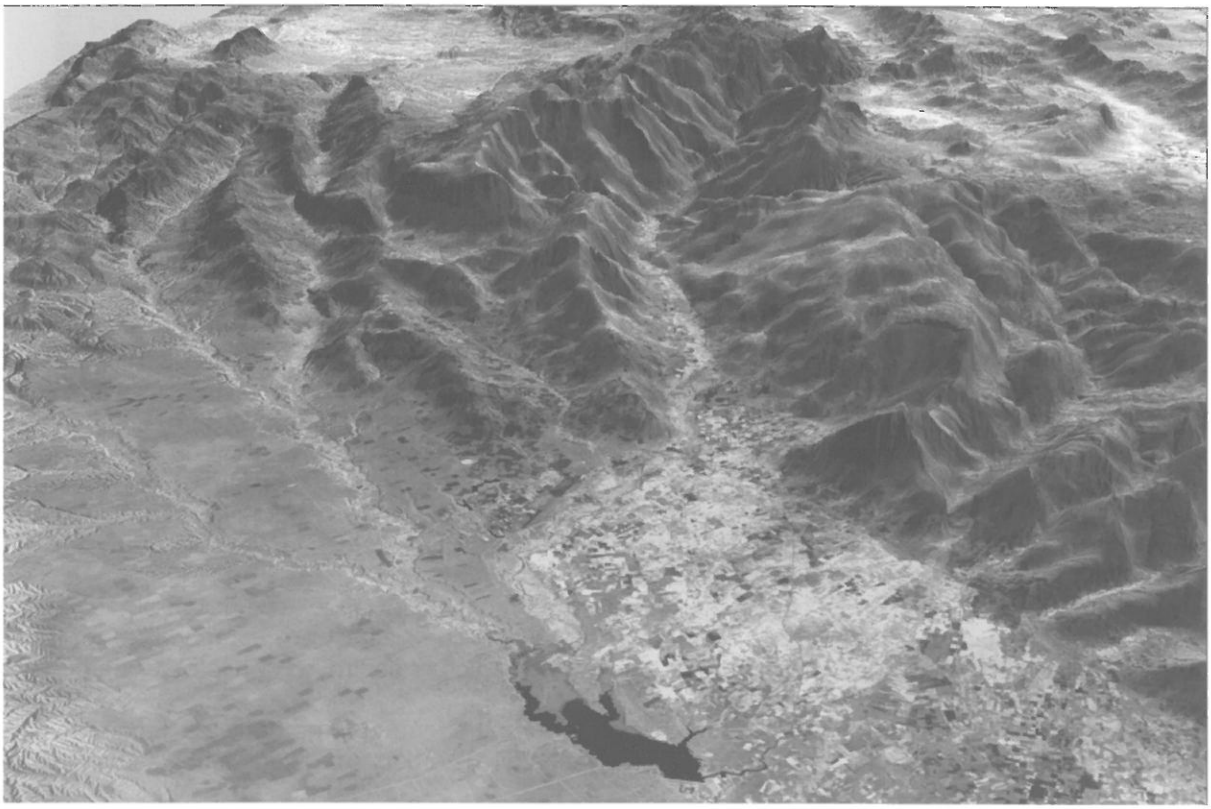

Figure 4-4: The image of the region after the night of flood 2001.

There is not very large stone in the riverbed. Diameter of most stones along the stream was about 30-50cm in maximum. Other material of riverbed is silt. It became hard and cracked after drying up.
In downstream, the traces of the flood could be seen in the form of large particle settlement and then sedimentation of fine materials. Even the more finer materials were washed away and carried to the dam reservoir.
Small streams carries various amount of geo materials. In the area of study, such streams in the upper sub basin with relatively uniform steep gradient and critical flow carried high concentrations of such materials. In this situation, even small streams heavily laden with soil result in a fluid mass of sizable

transporting power quite disproportionate to stream size. These powerful flows commonly followed pre existing drainage ways (Figure 4-5). Their unusually high density current increased its power. Moreover presence of boulder and driftwood blocked the main channel, caused the overflow through the main stream in very short period of time. Accurate measurements of accumulated deposit are necessary to further study the potential of future devastating flood.

Figure 4-5: Heavy vehicle buried by debris flow.

5 INVESTIGATION OF FLOOD CAUSES

Rainfall depths reported in excess of 150 mm in just 12 hours triggered the August 2001 flood. Over 129 million m^3 of flood volume and 12 million tons of eroded rich soil entered Golestan Dam reservoir. On the top of this, a huge volume of logs and timber was seen floating in the reservoir covering an area of 40 ha. The authors assessed the causes and extent of the flood damage in a preliminary investigation after onsite visit of the affected region. While the primary factor must have been the unusually high rainfall intensity, other factors include locally-narrow valley bottom along the flood path, blockage of road bridges by debris and driftwood, and flood waves released after collapse of some small earth dam and bridges (Figures 5-1 and 5-2).

There were six small earth dams constructed just upstream of Dasht village. The height of the largest dam, built in 1984, was 15 m with a crest length of 400 m. The dams were damaged 20 to 100% during the flood. The right side of the largest dam was completely destroyed, while other parts were eroded deeply and riprap rocks were lost.

In downstream area, the signs of the flood could be seen in the form of large particles. Fine materials were easily washed away and carried into the dam reservoir. The deposited sediment was as high as 4 m in some areas upstream of dam site.

The height of sediments are about 1.5 m on the area where is extended in 35 km length with a width of about 300 meters (Figure 5-3). The height of sediment deposition around the Tangrah area was about 100-150 cm (Sharifi and Mahdavi, 2001).

Due to the high precipitation, morphologic aspects of the mountain area and high density of population, the catchment has faced with large scale of natural disasters. The slope of hillsides and the streams are high. Even though upper part sub basin area is about 20 percent, but it can be considered to be the main debris flow producing area.

Slope of upper part sub basin produced a high-density current, which enabled the flood to erode and carry more debris, and prepared ideal condition for debris flow occurrence. The slope of lower sub basin is relatively uniform over the stream length.

Figure 5-1: Fine sediment carried by flood blocked the water way.

Figure 5-2: Bridge damaged by debris flow.

As a result, when the steep slope valley-in upper part sub basin carry a lot sediments in the steep part of watercourse they will be settled when the slope decreases. In upper part sub basin along the stream, the slopes are steep and uniform. And that doesn't result in sedimentation in the river stream and consequently, sediment density constantly increases along the river course. This fact can be clearly seen in flood event disaster on August 2001. Although high precipitation and the steep slopes are the main factors in causing debris flow, but clearly can be claimed if there was little moveable material and the soil of basin and slopes were stable, the disaster would have not been happened. Range land degradation and overgrazing| are important factors in intensifying conditions.

There are large quantity of boulders and large stones left along stream networks. These stones caused debris flow, (also these derbies and stones will play the same role in the next flood disaster). Field investigation just after the disaster along river from the most upstream to the Golestan dam site revealed that on the upper land where the land use is mainly pastures, a lot of surface and massive land slides happened on hilly sides and river sides.

Figure 5-3: Mixture of fine and coarse logs and sediment deposited in the water way.

6 CONCLUDING REMARKS AND LESSONS LEARNED

Many parts of Iran potentially face similar hazards in future and lessons must be drawn from the past and present disasters in order to take adequate and appropriate preventive measures against such hazards. For example, only two years ago, Neka city in northern Iran, in Mazandaran province, the experienced a similar type of flooding Though, the recommended countermeasures for prevention of such hazards elsewhere in the country were gone unheeded.
The extent, magnitude, and timing of floods and debris flow occurrence is primarily dependent on formation of the rainstorms. In many cases, there is sufficient time lead before the outbreak of floods, Thus, the establishment of a weather forecasting and warning systems is required to save as many people lives as possible. The hydro-climatological data collection system must also be improved in the context of a flood waning system.
The property damages are mainly due to the inundation by water and mud. Debris flow has proved to have a very high destructive energy. The direct hit by debris flow should be prevented by all means, as it destroys everything in its way. The SABO dams are known to prevent the occurrence of such disasters and to prevent direct hit by debris flow. The debris flow can be trapped if the slope of river is less than %10 and gentler than 50% of the original river slope or when the width is extended to 2-3 times the former width. A screen check dam is a suitable structure to damp the energy of debris flow. Formation of driftwood control guidelines and introducing various control works using steel structures or sediment trap pockets should also be considered in similar situations.
The flood countermeasures must be environmentally acceptable as well. In this regard, improving vegetation cover is known as an effective practice in flood control.
Apart from the serious problem directly related to property damage and loss of lives caused by debris flow, the possibility of desertification in the fragile land in semi-dry region is other important issue, which must have received due attention.

The relation between debris flow and rainfall can help in the forecast process. A research study may be conducted to introduce a threshold rainfall depth and duration for debris flow occurrence in the regional condition. Establishment of bench mark for measurement of topographical changes and measurement of volume of sediment, and measurement of soil erosion. Installation of supersonic, automatic water gauges and current meters to collect continues flow data. Also, establishment of data communication system with fiber optic cable enables monitoring of flood out break. (observation equipment). Using echo sounder to meat water depth to reservoir depth.
The worrying deterioration of basin natural resources, especially the vegetation cover, should be addressed with proper watershed management practices Reforestation planning must start and appropriate agricultural practices to be introduced to the farmers. In addition, a survey of the environmental conditions at the damaged areas is necessary.
The drawing up of basin-wide development plans, clearly indicating the priorities to be assigned to various development activities, including undertaking of reclamation activities, construction of flood control dams, provision of bank and river protection and implementation of other flood control works with a hazard map providing information on the probability of landslides in vulnerable areas where human settlements exist; and the development of supporting information systems for environmentally sound watershed management together with a mapping system to make practices more specific to the prevailing environmental conditions, which should be available to all organizations concerned.

REFERENCES

Hashemi Tabatabaei, S., and Sharifi, F. (2001): Debris Flow Disasters In Historic Town "Masuleh" In Gilan Province-Iran. International Symposium on Landslide Risk Mitigation and Protection of Cultural Heritage, 21-25 Jan. 2002, Kyoto-Japan, pp245.

Regional Water Board Division (2001): Report on Hydrological Aspects of Golestan Flood, Regional water board, Iran, Golestan Province Report pp22, Tehran-Iran (in Persian).

Sharifi, F. and Ghafouri, A.M. (1997) Flood Spreading in Iran- An Integrated Approach, J. Rain Drop (ICRCS), June 1997, Series 2. Volume 7.

Sharifi F. and A. Hydarian, A. (1999): On the Natural Resources Management Strategy in Iran, Regional Workshop on Traditional Water Harvesting Systems, Tehran-Iran, UNESCO pp. 354.

Sharifi, F. and Mahdavi, M. (2001): Investigating Causes of Summer Flooding on North-east of Golestan-Iran, Technical Report, Deputy of Watershed Management-Iran, pp. 30, Tehran-Iran (in Persian).

Watershed Management Division (2001): A Report on Golestan Flood, Watershed Management-Golestan Province, Iran, Report pp15, Tehran-Iran (in Persian).

THE HIGH INTENSITY RAINFALL DESIGN SYSTEM: HIRDS

Craig S. Thompson

National Institute of Water and Atmospheric Research, PO Box 14-901 Wellington, New Zealand,
c.thompson@niwa.co.nz

SUMMARY

HIRDS is a computer-based procedure for estimating design rainfalls in New Zealand. First developed in 1992, it was based around an established method of rainfall frequency analysis. This high intensity rainfall design system has been revised and updated (1) to incorporate the large increase in available rainfall data, and (2) by using robust analysis techniques associated with regional frequency analysis. The components of regional frequency analysis involve the mapping of an index (median annual maximum) rainfall with thin-plate smoothing splines, and regional rainfall growth curves that are ratios of the T-year rainfall depth to the index rainfall and were developed from a GEV distribution. Results of the HIRDS update and revised estimates of design rainfalls will be made available to users via the internet at www.niwa.co.nz.

Keywords: New Zealand, high intensity rainfall, regional frequency analysis, GEV/PWM, mapping with splines

1 INTRODUCTION

HIRDS (High Intensity Rainfall Design System) (Thompson, 1992) is a procedure for estimating rainfall frequency at any point in New Zealand. Such procedures have two purposes: the estimation of rainfall depths for design purposes, and the assessment of the rarity of observed rainfalls. HIRDS was based on a rainfall frequency analysis by Tomlinson (1980). This method has been the basis of rainfall frequency analysis for over 20 years in New Zealand. The usual approach is to fit a statistical distribution to the rainfall maxima to describe the properties and frequency of how often a specified event occurs. Tomlinson's method is also an example of a regional approach to frequency analysis: an established method especially in the hydrological literature (Cunane, 1988; Hosking, Wallis, 1997). Regional frequency analysis uses data from sites within a suitably defined "region" to estimate the design variable, whether it be rainfall or river flows, at each site. A benefit of a regional analysis approach is that design rainfalls at single sites can be severely affected by short-data records with a large uncertainty in their estimates, whereas combining these data usually leads to a reduction in uncertainty and more reliable estimates. Tomlinson treated New Zealand as a single "homogeneous region".
In this study, design rainfalls for New Zealand have been revised and updated. Apart from incorporating additional data held by the National Institute of Water and Atmospheric Research (NIWA) and New Zealand territorial authorities, the revision of HIRDS used robust estimation techniques through the use of probability weighted moments (PWM) (Hosking, Wallis, 1993). The revision also addresses the issue of representing New Zealand as a single region through a "region of influence" approach (Burn, 1990). The resultant design rainfalls at any location within New Zealand will become available in July 2002 as a subscription service on NIWA's web site.
The approach taken in the HIRDS regional frequency analysis is an index-rainfall procedure. The procedure involved the mapping of an index-rainfall, and the derivation of a regional growth curve that relates the rainfall depth at different average recurrence intervals, ARI, to the index-rainfall.

2 DATA

Rainfall records were extracted from NIWA's Climate Database and Water Resources Archive. Annual maximum rainfalls at each site, to the end of 2000, were extracted from monthly maxima for 10 standard durations from 10 minutes to 72 hours. A total of 2375 sets of data covering New Zealand were available for further analysis, of which there were 682 from recording raingauges covering the full 10 durations and 1693 from raingauges, read daily at 9am, covering the 1 to 3 day period. This fixed duration raingauge data was converted to the estimated 24, 48 and 72-hour values (i.e. unconstrained to end at 9am) by multiplying by 1.14, 1.07 and 1.04 respectively.
Annual maximum series at each site were used if each annual value came from a year with at least 11 months of records, and if there were at least 10 years of records in each series. However in

mountainous regions (above 500m), where there are few gauges, the minimum record length was relaxed to 5 years. Outliers in the annual maximum series were retained, as they tend to have only a small effect on the design rainfalls if efficient parameter estimation methods (e.g. maximum likelihood or probability weighted moments) are used to fit frequency distributions (Cunane, 1989). Table 2-1 provides details of the data series analysed using the above criteria.

Table 2-1: Details of annual maximum rainfall series used in HIRDS revision.

Duration	10m-12h	24-72h
Number of sites	~435	~1810
Average length of record (y)	16.5	28.7
Percent sites above 500m	35	18

A total of 205,000 station-years of data were available, comprising of 71,000 station-years of recording data and 134,000 station-years of manual daily data. When compared to 19,500 station-years of data used by Tomlinson (1980), a huge increase in data quantities has occurred in the intervening 20 or so years between design rainfall analyses, resulting largely from increases in the networks operated by the various New Zealand agencies.

3 REGIONAL RAINFALL FREQUENCY ANALYSIS

3.1 Identification of Regions: Regions of Influence

In regional frequency analysis, the index-rainfall procedure can be written as $X_i(T) = \mu_i\{x(T)/x(I)\}$. $X_i(T)$ is the rainfall estimate for the T-year rainfall event at site i, μ_i is the index rainfall, chosen to be a relatively common event, such as the mean or median, that can be reliably estimated from the data, and $x(T)/x(I)$ is a dimensionless rainfall frequency growth curve common to every site in the region. The method assumes that locations within some defined region can be combined in such a way as to produce a single rainfall growth curve that can be used anywhere in that region (Hosking, Wallis, 1997). All sites within the region are expected to have similar frequency distributions, but the implied assumption of homogeneity is seldom satisfied exactly. However, the combining or pooling of data from many sites can provide reliable and robust estimation of regional growth curves, especially at large recurrence intervals (Reed et al., 1999). Several research papers explore ways of identifying homogeneous regions (see Potter, 1987 for a summary of regionalisation techniques). More recently, a variation to regionalisation is that "a region of influence" can be defined at each rainfall site, and avoids boundary problems associated with fixed regions (Acreman, Wiltshire, 1987; Burn, 1990; Reed et al., 1999). This approach also recognises that each site can be surrounded by stations having similar statistical attributes to the site of interest.
In this HIRDS revision, a region of influence approach was used, and sites were selected isotropically within a 60km radius from the site of interest. The limit is a compromise between the possibility of selecting sites from a different rainfall climate and, the inclusion of too few sites and with it a higher likelihood of less reliable estimation. Rainfall growth curves for each site were subsequently derived from a frequency analysis of the combined data.

3.2 Index Variable - Mapping the Median Annual Maximum Rainfall

In HIRDS, the index rainfall was taken to be the median annual maximum rainfall. The median has an annual exceedance probability of 0.5 corresponding to an ARI of two years. The median is used in preference to the mean or some other location parameter, since it is not usually affected by the skewness of the distribution or by the presence of outliers. The minimum length of 10 years (5 years in the mountains) ensures, that at most locations, the median is reasonably well estimated.
Design rainfalls from a regional frequency analysis perspective require maps of median rainfall in conjunction with regional growth curves. The mapping of median rainfall involved fitting thin-plate smoothing splines as implemented by ANUSPLIN (Hutchinson, 1995; 2000). The spline is a surface that is fitted to spatially distributed data with some error assumed at each data point, so that the surface can be smoother than if the data fitted exactly. The thin-plate smoothing spline for n data values at site x_i (Hutchinson, Gessler, 1994) is

(1) $$z(x_i) = f(x_i) + \varepsilon(x_i) \quad i = 1,...,n$$

where $f(x_i)$ is an unknown smooth function to be estimated from the observations $z(x_i)$ (i.e. the median annual maximum rainfall), ε_i are the zero mean random errors with a common variance σ^2. The $z(x_i)$ normally represent geographic position in two, three or more dimensions.
The function $f(x_i)$ is estimated by minimising

(2) $$\sum_{i=1}^{n}[z(x_i) - f(x_i)]^2 + \lambda J_m(f)$$

where $J_m(f)$ is a roughness penalty of the spline function f, defined in terms of mth order partial derivatives and λ is the smoothing parameter. The value of the smoothing parameter is a compromise between surface variability and closeness of fit to the data. It is often chosen by the method of generalised cross validation (GCV) (Hutchinson, 1995; 2000) in which each site is omitted in turn from the estimation of the fitted surface. This is repeated for a range of smoothing parameter values and the value that minimises the predictive error is selected to give the optimum smoothing. However in many climatological data sets, which have few data and are noisy, using the GCV criterion can result in unrealistically smooth maps with unacceptably large differences between the data and spline surface. To address this Zheng and Basher (1995) manipulated the signal to error properties of the data and spline fit and found that enforcing a global signal to error ratio (a diagnostic measure available from the spline fitting process) provides a useful and intuitive procedure for understanding and controlling the fitting. The larger the signal to error ratio is, the closer the fitted surface passes through the data, and the smaller the error of the fitted values, although robust spline fits in data sparse areas are more likely when the ratio is no more than one (Hutchinson, Gessler, 1994). However, the final selection of the ratio is left to user (pers. comm. Hutchinson, 2001), to allow for their expertise and prior knowledge of the characteristics of the data being fitted.
Surfaces of median annual maximum rainfall were fitted with a trivariate thin-plate spline, with the three independent variables being longitude, latitude and elevation above sea level. The trivariate spline of rainfall allows for a continuous spatially varying dependence on elevation, and is well suited to applications over complex terrain as is found in New Zealand, and can provide a robust method of surface fitting meteorological data from moderately sparse data networks. Correctly specifying elevation units is critical to the performance of thin-plate splines (Hutchinson, 1995); as a rule the elevation scaling should be 100 times the horizontal scale. With position coordinates of latitude and longitude, elevations should be in kilometres.
All 10 durations were initially fitted using the GCV to optimise the fitted surface, but in the final implementation only four (10 minute, 1 hour, 24 hour and 72 hour) were mapped with ANUSPLIN and a 0.05° latitude/longitude digital elevation model. The orography at each grid-point is averaged over 0.15° radius, since the effect of terrain on precipitation is influenced by the scale at which the orography is resolved (Daly et al., 1994; Thompson et al., 1997; Hutchinson, 1998). The four surfaces were all fitted with a 4:1 signal to error ratio to maintain a consistency between the fitted surfaces. Using the GCV criterion did lead to inter-duration inconsistencies at sites where historical data did not exist.
ANUSPLIN also allows the median annual maximum rainfall to be transformed before a spline surface is fitted. By applying a square-root transformation to rainfall data Hutchinson (1998) found (1) the fitted surface errors reduced by about 10 percent over the untransformed data, and (2) the estimated standard errors in the back-transformed fitted values can be calculated directly and are positively correlated with the rainfall. The estimate of the standard error of the fitted surface is (Hutchinson, 1998)

(3) $$se(X^2) = 2s(X^2 + s^2/2)^{0.5}$$

where X is the transformed median rainfall, and s is the model standard error computed from the error covariance matrix of the spline. The second term is negligible except when X is near zero or when s^2 is relatively large. Fitted surfaces of the estimated standard error of median annual maximum rainfall were computed for the four index durations (10 minute, 1 hour, 24 hour and 72 hour). Standard error maps are useful in identifying which sites have the largest uncertainty associated with their expected value.

However, this standard error calculation is not the level of uncertainty associated with the median annual maximum rainfall, only the error associated with the fitted surface. To estimate the standard error of the median annual maximum rainfall at any location in New Zealand, including those sites that have no historical data, an assumption is made that the mapped value is also an appropriate estimate of the at-site median rainfall. The standard error of median annual maximum rainfall, X_2, is estimated empirically from a linear regression between the logarithm of var(X_2)) and the logarithm of X_2, such that:

$se(X_2) = [\exp(1.8\log(X_2) - 4.5)]^{0.5}$ (R^2 = 0.92). The standard error increases monotonically as the median rainfall increases.

Figure 3-1a presents the spatial pattern of the 24 hour median annual maximum rainfall over New Zealand. The strong influence of New Zealand's orography on the rainfall pattern is noticeable in that the largest values are found in the mountainous regions, and more especially on the western sides where moisture laden mid-latitude westerlies are forced to rise over the mountain chains to release precipitation. In contrast, the eastern coasts and inland regions to the lee of the mountains of both islands generally have the smallest rainfalls.

A map of the standard error of the fitted median annual maximum rainfall for 24 hour is given in Figure 3-1b. As expected, the standard errors are greatest in the high rainfall areas, which are also in locations having few data points. For New Zealand as a whole, the standard error is about 5 percent of the median rainfall.

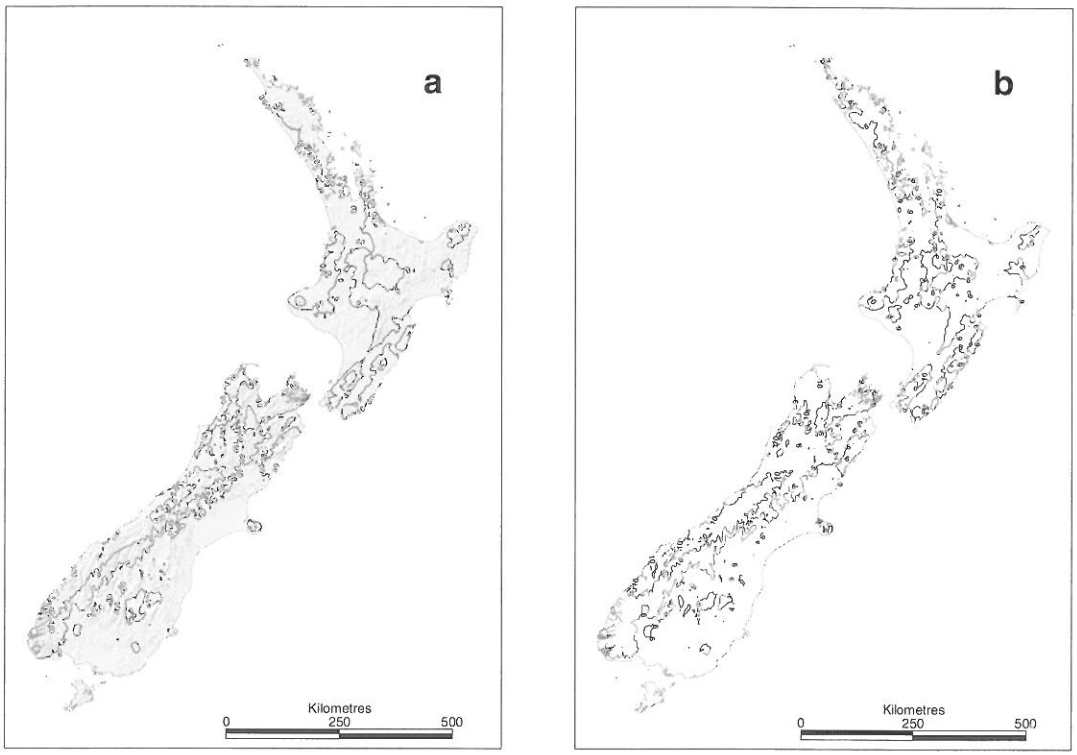

Figure 3-1: Spatial pattern of [a] 24 hour median annual maximum rainfall (contour intervals 40 80 160 and 320 mm) and [b] standard errors (contour intervals 4, 6 and 10 mm), over New Zealand. The underlying hill shading patterns in [a] shows the dominant terrain features for New Zealand.

In design situations, where the at-site median rainfalls ($X_{2(site)}$) are available in addition to the spline estimated rainfalls ($X_{2(map)}$), it is possible to get a pooled estimate. Assuming these estimates are normally distributed and have variances var($X_{2(site)}$) and var($X_{2(map)}$) respectively, then the pooled rainfall estimate (Kuczera, 1983) is

(4) $$X_{2(pool)} = sX_{2(site)} + (1-s)X_{2(map)}$$

where s is a shrinkage factor given by

(5) $$s = \mathrm{var}(X_{2(map)}) / (\mathrm{var}(X_{2(site)}) + \mathrm{var}(X_{2(map)}))$$

It can be seen from the above relation that as the variance of the fitted surface grows relative to the at-site variance, the pooled estimate "shrinks away" from the mapped estimate to the at-site value. The variance of the pooled estimated is the product of s and var($X_{2(site)}$). While pooling leads to more precise inference (Kuczera, 1983), the pooled variance is always smaller than the at-site estimate.

3.3 Development of Regional Growth Curves

The other component in the regional frequency relation is the rainfall growth curve. Growth curves are standardised and dimensionless and enables the estimation of extreme rainfalls of any specified ARI relative to the median rainfall. Inverse cumulative distribution functions are the basis of growth curves (Schaeffer, 1990), and a three-parameter generalised extreme value distribution (GEV) combined with probability weighted moment estimation (PWM) of its parameters is a widely used in regional frequency analysis. In terms of the T-year rainfall event, the inverse cumulative distribution functions of a GEV are

(6) $$x(T) = U + a[1 - (-\ln(1 - 1/T))^k / k] \qquad k \neq 0$$

(7) $$x(T) = U - a[\ln(-\ln(1 - 1/T))] \qquad k = 0$$

where U is the mode (or location), a is the dispersion or scale parameter and k is the shape parameter. For $k = 0$, the GEV distribution reduces to the usual "Gumbel" distribution. In the above equations, the part of the GEV function inside the square brackets is also known as the "reduced variate", Y_T. Parameters of a regional GEV distribution are estimated from the first three PWMs by the method of regionally averaged standardised probability weighted moments (Wallis, 1980). All data from within the region of influence are used, where each site's contribution to the regional estimate is weighted in proportion to its record length. Full details of method of regionally weighted PWMs and the subsequent estimation of the parameters of GEV distributions can be found in Hosking et al. (1985) and Cunane (1989).

If a dimensionless regional growth curve relative to the index rainfall is $x(T)/x(2)$, then after substitution with reduced variates in (6) or (7), the rainfall growth curve becomes (pers. comm. Woods, 2001)

(8) $$g(T) = x(T)/x(2) = \frac{a/U}{1 + (a/U)Y_2}(Y_T - Y_2) + 1$$

Regional growth curves depend directly on a/U and, k through the reduced variate term. a/U varies over New Zealand from about 0.2 to 0.5 (see Figure 3-2a below). The growth curves are more sensitive to a/U than to the shape parameter; the larger a/U becomes, the larger the magnitude of the growth curve relative to the median and vice versa. Moreover, a/U which is the ratio of dispersion (or standard deviation) to the mode can be thought of being like a "coefficient of variation". In regions where there are low coefficients of variations, a small degree of regional inhomogeneity does not severely impact on the application of regional frequency analysis methods (Cunane, 1989). The same could be said of a/U as used in this study.

3.3.1 Maps of a/U and k

Thin-plate splines were fitted to the values of a/U and k for the standard durations. Diagnostic output from ANUSPLIN indicated that both parameters were largely independent of site elevation and depend only on geographical position, with the fitted surfaces containing large signal to error characteristics. A map of the spatial pattern for a/U and k for a duration of 24 hours is given in Figure 3-2. In Figure 3-2a, the variation of a/U over New Zealand shows that values of a/U are generally lower in western areas of both islands and in southern New Zealand where rainfalls tend to be high and reliable. Highest values of a/U are in the eastern regions of both islands where rainfalls are lowest and the coefficient of variation is also large. The spatial pattern of the regional shape parameter k is shown in Figure 3-2b. For most of New Zealand k is less than zero, but there are areas, especially in the west of both islands where $k \geq 0$. This pattern over the country is similar to that produced by Pearson and Henderson's (1998) at-site analysis of the GEV shape parameter.

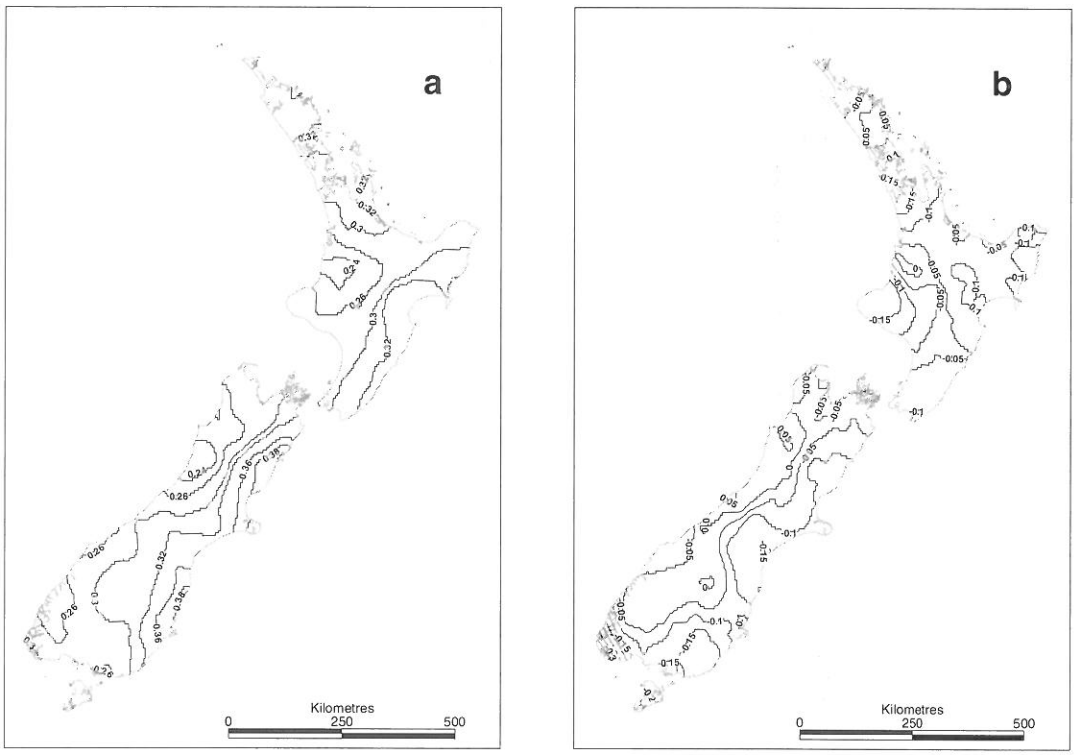

Figure 3-2: Spatial distribution of regional parameters of [a] a/U (contour intervals in steps of 0.02 from 0.24 to 0.40), and [b] shape parameter k (contour intervals in steps of 0.05 from -0.35 to 0.1) of the GEV distribution fitted to New Zealand annual maximum 24 hour rainfalls.

Mean values of a/U and k with duration over New Zealand is presented in Table 3-1. a/U decreases as the duration increases up to 6 hours, but from 24 hours remains relatively constant. This temporal variation may be a reflection of the dominant processes driving the precipitation regimes: from short-duration intense convective showers to the longer-duration less intense frontal rainfalls. Up to six hours, the modal precipitation is increasing at a faster rate than its associated variability, and hence a decline in a/U. From 24 hours the rate of change in the individual parameters is about the same. For the shape parameter k, there is a general increase in the value of k with increasing duration, with a near "Gumbel type" distribution (i.e. $k = 0$) from 6 hours. Large negative shape parameter values occur at for short duration's as (1) large outliers may be present at some sites, and (2) as noted earlier, the annual maximum data series are shorter than for the longer durations. At individual sites, there is however considerable variation in the parameters, from the mean state for New Zealand.

Table 3-1: Variation with duration of GEV distribution parameters, averaged over New Zealand.

Duration	10m	20m	30m	1h	2h	6h	12h	24h	48h	72h
a/U	0.331	0.316	0.305	0.280	0.259	0.255	0.270	0.305	0.308	0.305
k	-0.172	-0.163	-0.153	-0.148	-0.118	-0.053	-0.046	-0.080	-0.073	-0.065

3.3.2 Standard Errors of the Regional Growth Curves

Standard errors associated with the regional growth curves have been derived using the bootstrap percentile method (Faulkner, Jones, 1999). Bootstrapping is based on random resampling many times from a set of data, with the chosen datum being returned to the sample for further reselection. Given the parameters a/U and k, an annual maximum series of 100 observations is simulated from a GEV distribution for subsequent bootstrapping. Samples, randomly chosen, are selected and the remaining data are used to derive the regional growth curve in the usual way over a range of ARI. Resampling is repeated many times and the residual of each new growth curve from the original is retained. The residuals are ranked, and on the assumption of a standard normal distribution, the 17th or 85th percentile provides an estimate of the standard error of the growth curve. Ranked residuals were often skewed, and so the standard error was calculated from the larger of the two percentiles. Standard errors associated with the regional growth curves appear to be quite small: for an average recurrence interval of 100 years the error is about one to two percent of the regional growth curve.

4 ESTIMATION OF STANDARD ERRORS OF DESIGN RAINFALL, X_T

Standard errors associated with the design rainfalls are estimated in HIRDS. At any site, the design rainfall for a specified ARI of T-years is $X_T = \mu g(T)$, where μ is the median annual maximum rainfall and $g(T)$ is the regional growth curve. Provided the two constituent parts of the design rainfall relation are independent, the standard error of X_T is (Kendal and Stuart, 1969; McKerchar and Pearson, 1989)

$$se(X_T) = \left\{ [g(T)]^2 \operatorname{var}(\mu) + (\mu)^2 \operatorname{var}(g(T)) + \operatorname{var}(\mu) \operatorname{var}(g(T)) \right\}^{1/2} \quad (9)$$

Arising from the independence assumption the third term is not usually significant, especially as the variance of the regional growth factor is negligible.

5 AT-SITE DESIGN RAINFALLS

In the previous sections, regional frequency analysis methods were presented to estimate design rainfalls at any location within New Zealand. At the time of writing (April 2001) these procedures are being incorporated into a revised HIRDS (High Intensity Rainfall Design System) software package for a subscription service available from NIWA's web site at www.niwa.co.nz. The user supplies geographic coordinates and the HIRDS program produces a table of design rainfalls in a depth-duration-frequency format. A sample output for Queenstown New Zealand (45.033°S, 168.667°E) is shown in Table 5-1. Estimates of design rainfall and their associated standard errors are given.

Table 5-1: HIRDS output: design rainfalls and standard errors for Queenstown, New Zealand.

HIRDSV2 - High Intensity Rainfall Design System

Queenstown: Latitude 45.033S Longitude 168.667E

	Duration									
ARI(y)	10m	20m	30m	60m	2h	6h	12h	24h	48h	72h
2.0	3.6	5.7	7.5	11.8	16.7	28.9	40.9	57.8	68.0	74.8
10.0	5.7	8.6	11.0	16.8	23.3	39.2	54.5	75.6	89.6	99.0
20.0	7.1	10.6	13.4	20.0	27.5	45.6	62.8	86.3	102.7	113.7
30.0	8.2	12.1	15.2	22.4	30.7	50.3	68.8	94.0	112.1	124.3
40.0	9.1	13.4	16.7	24.4	33.3	54.2	73.7	100.3	119.9	133.0
50.0	10.0	14.5	18.0	26.2	35.5	57.6	78.0	105.8	126.6	140.6
60.0	10.8	15.5	19.3	27.8	37.6	60.6	81.9	110.7	132.6	147.3
70.0	11.5	16.5	20.4	29.3	39.5	63.4	85.4	115.1	138.0	153.5
80.0	12.2	17.4	21.5	30.7	41.2	65.9	88.7	119.2	143.1	159.2
100.0	13.5	19.1	23.5	33.2	44.5	70.7	94.6	126.6	152.3	169.6
125.0	15.1	21.1	25.7	36.1	48.2	75.9	101.2	134.9	162.5	181.2
150.0	16.5	22.9	27.9	38.8	51.5	80.8	107.2	142.4	171.8	191.7

Queenstown: Standard errors (mm)

2.0	0.3	0.5	0.7	1.0	1.5	2.6	3.1	4.1	4.7	5.1
10.0	0.6	0.9	1.2	1.5	2.3	3.7	4.7	6.4	7.4	8.0
20.0	0.7	1.1	1.4	1.9	2.7	4.2	5.4	7.4	8.5	9.2
30.0	0.8	1.3	1.6	2.1	3.0	4.5	5.8	8.0	9.2	10.0
40.0	0.9	1.4	1.8	2.3	3.3	4.7	6.1	8.5	9.8	10.6
50.0	1.0	1.6	1.9	2.4	3.5	4.8	6.3	8.9	10.3	11.2
60.0	1.1	1.7	2.0	2.6	3.7	5.0	6.5	9.2	10.7	11.6
70.0	1.2	1.8	2.1	2.7	3.9	5.1	6.7	9.6	11.0	12.0
80.0	1.2	1.9	2.2	2.8	4.1	5.2	6.8	9.9	11.4	12.4
100.0	1.3	2.1	2.3	3.1	4.4	5.4	7.1	10.5	11.9	13.0
125.0	1.5	2.3	2.5	3.4	4.8	5.7	7.4	11.2	12.6	13.8
150.0	1.6	2.5	2.7	3.6	5.2	5.9	7.6	11.8	13.2	14.6

5.1 Rarity of Observed Rainfall Events

Design rainfalls are an important tool for assessing the frequency of extreme events, and are used in analyses by meteorologists and hydrologists, as well as in the insurance industry in assessing the risks and hazards associated with these rare events. In Table 5-2, some recorded extreme rainfalls in New Zealand are compared to their estimated average recurrence intervals as determined from the HIRDS regional frequency analysis. The two short duration events occurred in the North Island of New Zealand and for the recorded amounts had expected ARI's well in excess of the 150 years given by the HIRDS tabular output. For the longer duration storms, these occurred in the same catchment at different times in the alpine region of the South Island. Their ARI are not as extreme as the shorter period storm totals.

Table 5-2: Average Recurrence Intervals (ARI) of Extreme rainfall Events in New Zealand

Duration	Amount (mm)	ARI (years)	Location
10 min	34	300	Tauranga (37.667°S 176.200°E)
1 hour	109	>>500	Leigh (36.267°S 174.800°E)
12 hour	473	80	Colliers Creek (42.991°S 170.995°E)
24 hour	682	150	Colliers Creek

6 CONCLUSIONS

In this revision of high intensity rainfalls in New Zealand, a large increase in data has become available since maps were last prepared in 1980 as implemented in HIRDS in the early 1990s. The method used in this HIRDS update of design rainfalls is based on the widely used technique of regional frequency analysis and involved the mapping of an index (the median annual maximum) rainfall together with regional growth curves that are common to every site within a prescribed region. Each site is considered as a unique region, thus avoiding boundary and transition problems associated with fixed regions.

The mapping of the index rainfall involved fitting a trivariate thin-plate spline to longitude, latitude, and site elevation. This type of spline allows for the local variations in terrain to be incorporated into the spline relationships, and a robust fit is achieved by transforming the median annual maximum rainfall

before fitting the spline. An immediate consequence of this transformation is that the standard errors of the fitted surfaces are proportional to the square root of the median rainfall.
The regional growth curves were derived using a generalised extreme value distribution combined with probability weighted moment estimation. The rainfall growth growths depended directly on the GEV parameters a/U and k, with a/U having a larger influence on the growth of design rainfall relative to the median than does k. Design rainfalls for any site are simply the product of the index rainfall and the regional rainfall growth curve.
Procedures described in this paper are being incorporated into a revised HIRDS software package and design rainfalls will be available by July 2002 on NIWA's web site at www.niwa.co.nz.

ACKNOWLEDGEMENTS

This work was funded by the New Zealand Foundation for Research, Science and Technology. The Regional Councils provided rainfall data, and the assistance of Kathy Walter, Kevin McGill and Stuart Burgess in extracting high intensity rainfall data from NIWA's archives are gratefully acknowledged. The maps were prepared by Jason Keys.

REFERENCES

Acreman, MC., Wiltshire, SE. (1987): Identification of regions for regional flood frequency analysis, (abstract), EOS, Trans. AGU, 68, 1262. Washington D.C.

Burn, DH. (1990): Evaluation of regional flood frequency analysis with a region of influence approach, Water Resour. Res., 26, 2257-2265. Washington D.C.

Cunane, C. (1988): Methods and merits of regional flood frequency analysis. J. Hydrol., 100, 269-90. Amsterdam.

Cunane, C. (1989): Statistical distributions for flood frequency analysis. World Meteorological Organization, Operational Hydrology Report No 33. Geneva.

Daly, C. et al. (1994): A statistical-topographic model for mapping climatological precipitation over mountainous terrain. J. Appl. Meteorol., 33, 140-158. Boston.

Faulkner, DS. (1999): Flood Estimation Handbook Volume 2: Rainfall frequency estimation. Institute of Hydrology. Wallingford.

Faulkner, DS., Jones, DA. (1999): The FORGEX method of rainfall growth estimation III: examples and confidence intervals, Hydrol. & Earth Sys. Sci., 3, 205-212. Katlenburg-Lindau.

Hosking, JRM. et al. (1985): Estimation of the general extreme value by the method of probability weighted moments. Technometrics, 27, 251-261. Alexandria.

Hosking, JRM., Wallis, JR. (1993): Some statistics useful in regional frequency analysis. Water Resour. Res., 29 271-281. Washington D.C.

Hosking, JRM., Wallis, JR. (1997): Regional frequency analysis. Cambridge University Press. Cambridge.

Hutchinson, MF. (1995): Interpolating mean rainfall using thin plate smoothing splines. Int. J. Geographical Information Systems, 9, 385-403. London.

Hutchinson, MF. (1998): Interpolation of rainfall data with thin plate smoothing splines: II Analysis of topographic dependence. J. Geographic Information and Decision Analysis, 2, 168-185. London.

Hutchinson, MF. (2000): ANUSPLIN Version 4.1 User Guide. Centre for Resource and Environmental Studies. The Australian National University. Canberra.

Hutchinson, MF., Gessler, PE. (1994): Splines-more than just a smooth interpolator. Geoderma, 62, 45-67. Amsterdam.

Kendall, MG., Stuart, A. (1969): The advanced theory of statistics. Volume 1, Distribution theory. (Third edition). Charles Griffin and Co. London.

Kuczera, G. (1983): Effect of sampling uncertainty and spatial correlation on an empirical Bayes procedure for combining site and regional information. J. Hydrol., 65, 373-398. Amsterdam.

McKerchar, AI., Pearson, CP. (1989): Flood frequency in New Zealand. Hydrology Centre Publ. No 20, Division of Water Sciences, Department of Scientific and Industrial Research. Christchurch.

Pearson, CP., Henderson, RD. (1998): Frequency distributions of annual maximum storm rainfalls in New Zealand. J. Hydrol. (NZ), 37, 19-33. Christchurch.

Potter, KW. (1987): Research on flood frequency analysis: 1983-1986. Rev. Geophys., 25,113-118. Washington D.C.

Reed, DW. et al. (1999): The FOREGEX method of rainfall growth estimation II: Description. Hydrol. & Earth Sys. Sci., 3, 197-203. Katlenburg-Lindau.

Schaeffer, MG. (1990): Regional analysis of precipitation annual maxima in Washington State. Water Resour. Res., 26, 119-131. Washington D.C.

Tomlinson, AI. (1980): The frequency of high intensity rainfall in New Zealand, Part I. Water and Soil Tech. Publ. 19. Ministry of Works and Development. Christchurch.

Thompson, CS. (1992): HIRDS (Manual and software). National Institute of Water and Atmospheric Research. Wellington.

Thompson, CS. et al. (1997): Estimating long-term annual precipitation in a mountainous region from a diagnostic model. Int. J. Climatol., 17 997-1007. Reading.

Wallis, JR. (1980): Risk and uncertainties in the evaluation of flood events for the design of hydrologic structures. Seminar on Extreme Hydrological Events-Floods and Droughts. Erice. Italy, 33pp.

Zheng, X., Basher, RE. (1995): Thin-plate smoothing spline modelling of spatial climate data and its application to mapping South Pacific rainfalls. Mon. Wea. Rev., 123. 3086-3102. Boston.